GEOCHEMISTRY OF DOLOMITIZATION AND Zn-Pb MINERALIZATION IN THE RATHDOWNEY TREND, IRELAND

Sally Louise Eyre

A thesis submitted for the degree of Doctor of Philosophy of the University of London



September 1998

Royal School of Mines,
Imperial College of Science Technology and Medicine,
London, SW7 2BP.

BIBL. LONDIN. UNIV.

ABSTRACT

GEOCHEMISTRY OF DOLOMITIZATION AND Zn-Pb MINERALIZATION IN THE RATHDOWNEY TREND, IRELAND

Petrographic evidence indicates that ore-stage sulphides at the Lisheen and Galmoy deposits are hosted by a dolomite matrix breccia (D2) which postdates regional dolomitization and lithification of the Waulsortian Limestone. Sulphides principally occur as replacements of clasts and breccia matrix and as open-space filling forms. The abundance of collomorphic and dendritic textures suggests precipitation from highly supersaturated solution.

Sulphur isotope ratios indicate that Lower Carboniferous seawater acted as the source of sulphate for precipitation of barite ($\delta^{34}S$ ~18‰). Ore-stage sulphides in the deposits ($\delta^{34}S$ -4 to -20‰) were precipitated from sulphur produced by open-system bacterial reduction of this seawater sulphate source. Late ore-stage sulphides, commonly proximal to inferred 'feeder' faults in the deposits and the dominant source of sulphur in the prospects, have higher $\delta^{34}S$ values in the range 0 to +10‰. Intermediate $\delta^{34}S$ compositions of -10‰ and -12‰ typical of major ore zones at Lisheen and Galmoy respectively, may be the result of mixing of these two sulphur sources.

$\delta^{13}C$ and $\delta^{18}O$ data exhibit a trend toward isotopically lighter compositions with time (-1‰ $_{PDB}$ and 19‰$_{(SMOW)}$ respectively) away from regional Waulsortian dolomite compositions suggesting progressively decreasing exchange between mineralizing fluids and host rock.

Fluid inclusion data support mixing between a moderate temperature (160-210 C), moderate salinity (9-15 wt% NaCl eq.) fluid with a low temperature brine as a principal mineralization mechanism. Fluid mixing is less evident in the prospects. Through time the hydrothermal system evolved from mixing-dominated to a system dominated by flow of the higher temperature end-member. A low temperature (80-140°C), high salinity (22.5-29.0 wt% NaCl eq.) fluid of MVT affinity infiltrated the Lisheen deposit at a late stage, postdating the main mineralizing event.

Pb isotopic ratios of galenas provide evidence in support of a basement contribution to the mineralizing systems. The results of this research best fit a model involving deeply circulated fluids which derived metals and a minor sulphur component from the Lower Palaeozoic basement. These fluids mixed with a shallow sulphur-bearing brine at the depositional site. The timing of mineralization is constrained to post-late Chadian.

ACKNOWLEDGEMENTS

I am indebted to my supervisors Dr Jamie Wilkinson and Dr Chris Stanley for their complete support and enthusiasm during this research, and to the late Dr Dave Johnston, who was the inspiration behind a very well defined project. The research was funded by an Imperial College Scholarship, with field support from the Natural History Museum and Rio Tinto Finance and Exploration Plc.

I would like to acknowledge Minorco Services Ireland Ltd., Arcon International Resources Plc., Rio Tinto Finance and Exploration Plc., Minco Ireland, and Ennex International Plc., for allowing me to sample core material from around the southern Irish Midlands. I would like to thank senior geologists John Elmes, Mike Lowther, Andy Bowden, Dave Blaney, John Colthurst, and Mike Bowland for facilitating my sampling programme at the various study areas. Particular thanks must go to Pat Redmond, who advised me well during my initial sampling visit to Lisheen, and for the numerous discussions that followed. I would also like to thank Paul Moran for helping me with the CAD drawings on site at Lisheen.

I would like to thank the various people at Imperial College, the Natural History Museum, and Scottish Universities Research and Reactor Centre for the technical support and analytical expertise offered; Adrian Boyce, Tony Fallick, John Spratt, Terry Williams, Chris Hayward, and Ben Williamson. I would especially like to thank Liz "just one more sample" in rock preparation.

I am grateful to the students of Trinity College, Dublin for their hospitality, particularly Niall and Mark C. Special mention must go to Calum Murray in Glasgow who supported me during a difficult period in my final year. Jay Gregg was the perfect host in Missouri, and organized a fantastic field trip to the Fletcher Mine at Vibernum. I would like to acknowledge my friends at Imperial, the crew in room 3.19, Sarah, Matt, Mark, Sean, Andy and Helen. Student No.1 Sarah, looked after me well on my arrival at Imperial. Special thanks go to Jim and Matt, great friends and great training partners! Thanks also to the Southside contingent, Marcus, Barney, Gypsy, Dave, Richard, Barry, Louise, Jamie, and Dick - I owe many drinks.

A very special thanks to my Mum, Dad, and Gran who have given me such immense support and an incredible incentive to succeed during my years of study - and to Nik, my soul mate. I dedicate this thesis to the four of them.

CONTENTS Page

CHAPTER 1: INTRODUCTION AND REVIEW

1.1 INTRODUCTION 22

1.2 EXPLORATION HISTORY OF 'IRISH-TYPE' Zn-Pb DEPOSITS 22

1.2.1 Exploration Background 22
1.2.2 Modern Geochemical and Geophysical Exploration Techniques 26

1.3 RESEARCH RATIONALE 27

1.3.1 Dolomitization and Mineralization: a key relationship 27
1.3.2 Research Objectives 28

1.4 BACKGROUND AND PREVIOUS WORK 28

1.4.1 MVT and Sedex Deposits - Characteristics and Mechanisms of Formation 29
1.4.2 Characteristics of 'Irish-type' Zn-Pb deposits 30
1.4.3 Genesis of 'Irish-type' Zn-Pb deposits 32

1.4.3a Sediment Dewatering/Compaction Models 34
1.4.3b Gravity/Topographic Driven Fluid-Flow 35
1.4.3c Density-Driven Convection 37

1.5 SIGNIFICANCE OF RESEARCH - TESTING THE HYPOTHESES 40

1.5.1 Research Methodology 40

1.5.1a Cathodoluminescence and Reflected Light Microscopy 40
Expected Results - contribution to research objectives 42
1.5.1b Electron Microprobe Analysis 42
Expected Results - contribution to research objectives 43
1.5.1c Stable Isotope Analysis (Sulphur) 44
Expected Results - contribution to research objectives 44
1.5.1d Stable Isotope Analysis (Carbon, Oxygen) 45
Expected Results - contribution to research objectives 45
1.5.1e Radiogenic Isotopes (Lead) 45
Expected Results - contribution to research objectives 46
1.5.1f Fluid Inclusion Microthermometry 46
Expected Results - contribution to research objectives 46

1.6 SUMMARY 47

CHAPTER 2: GEOLOGY

2.1 INTRODUCTION 49

2.2 PRE-CALEDONIAN BASEMENT 49

2.3 CALEDONIAN OROGENY **50**

2.4 ORTHOTECTONIC AND PARATECTONIC CALEDONIDES **50**

2.4.1 Orthotectonic Belt 50
2.4.2 Paratectonic Belt 51

2.5 UPPER PALAEOZOIC **52**

2.5.1 Late Caledonian deformation 52
2.5.2 Lower, Middle and Upper Devonian 53
2.5.3 Lower Carboniferous (Courceyan Stage) 54

2.5.3a Regional Stratigraphic Setting 55
2.5.3b Basal Red Beds 56
2.5.3c Navan Group (Mixed Beds) 56
2.5.3d Ballysteen Limestone (ABL) 57
2.5.3e Waulsortian Facies 58

2.5.4 Lower Carboniferous (Chadian to Brigantian Stages) 59
2.5.5 Lower Carboniferous Extension 60

2.6 VARISCAN OROGENY **60**

2.7 GEOLOGY OF THE RATHDOWNEY TREND DEPOSITS AND PROSPECTS **61**

2.7.1 Lithostratigraphy 66

2.7.1a Lisheen Deposit 66
2.7.1b Galmoy Deposit 68

2.7.2 Structure 70

2.7.2a Lisheen Deposit 70
2.7.2b Galmoy Deposit 71

2.7.3 Regional Dolomitization 72

2.7.3a Lisheen Deposit 73
2.7.3b Galmoy Deposit 74

2.7.4 Hydrothermal Dolomitization 74

2.7.4a Lisheen Deposit 74
2.7.4b Galmoy Deposit 75

2.7.5 Mineralization 79

2.7.5a Lisheen Deposit 79
2.7.5b Galmoy Deposit 80

2.8 SUMMARY **81**

3.2.7c Rathdowney Trend Prospects 127
Elemental Chemistry 127

3.3 DISCUSSION **128**

3.3.1 Conclusions 131

3.4 ORE PETROGRAPHY AND MINERAL CHEMISTRY **132**

3.4.1 Lisheen Deposit 133

3.4.1a Pre Ore-Stage 134
3.4.1b Main Ore-Stage 135
3.4.1c Late Ore-stage 138
3.4.1d Post Ore-Stage 140
3.4.1e Paragenetic Summary - Lisheen Deposit 140

3.4.2 Galmoy Deposit 141

3.4.2a Pre Ore-Stage 142
3.4.2b Main Ore-Stage 142
3.4.2c Late Ore-Stage 143
3.4.2d Paragenetic Summary - Galmoy Deposit 145

3.4.3 Rathdowney Trend Prospects - Durrow 146

3.4.3a Paragenetic Summary - Durrow 148

3.5 DISCUSSION **149**

COLOUR PLATES **153-216**

CHAPTER 4: ISOTOPE STUDY

4.1 INTRODUCTION **218**

4.1.1 Aims and Objectives of the Isotope Study 219

4.2 SULPHUR **219**

4.2.1 Sample Selection and Experimental Technique 220
4.2.2 Results 220

4.2.2a Lisheen Deposit 220
4.2.2b Galmoy Deposit 224
4.2.2c Rathdowney Trend Prospects 226

4.2.3 Sulphur Isotope Geothermometry 229
4.2.4 Interpretation of Results (Sulphur) 230
4.2.5 Summary 235

4.3 CARBON AND OXYGEN **235**

4.3.1 Sample Selection and Experimental Technique 236
4.3.2 Results 236

4.3.2a Lisheen Deposit 237
4.3.2b Galmoy Deposit 241
4.3.2c Rathdowney Trend Prospects 241

4.3.3 Fluid Isotopic Composition 245
4.3.4 Interpretation of Results (Carbon, Oxygen) 246

4.4 LEAD **247**

4.4.1 Sample Selection and Experimental Technique 248
4.4.2 Results 249

4.4.2a Lisheen Deposit 249
4.4.2b Galmoy Deposit 249

4.4.3 Interpretation of Results (Lead) 252

CHAPTER 5: FLUID INCLUSION STUDY

5.1 INTRODUCTION **256**

5.1.1 Sample Selection and Experimental Technique 257
5.1.2 Fluid Inclusion Types and Occurences 258
5.1.3 Microthermometric Method 259

5.2 RESULTS **261**

5.2.1 Estimate of Composition and Salinity 261
5.2.2 Lisheen Deposit 261

5.2.2a Dolomites (Syn-, to Post Ore-Stage) 261
5.2.2b Sphalerite (Late Ore-Stage) 262
5.2.2c Calcite and Authigenic Quartz (Late to Post Ore-Stage) 262

5.2.3 Galmoy Deposit 265

5.2.3a Dolomites (Syn-, to Post Ore-Stage) 265
5.2.3b Sphalerite (Ore-stage to Late Ore-Stage) 265
5.2.3c Calcite (Post Ore-Stage) 267

5.2.4 Rathdowney Trend Prospects 267

5.2.4a Dolomites (Syn-, to Late Stage) 267
5.2.4b Sphalerite (Late Stage) 269

5.2.5 Interpretation of Results 269
5.2.6 Summary 274

CHAPTER 6: DISCUSSION

6.1 INTRODUCTION 276

6.2 REGIONAL DOLOMITIZATION 276

6.3 DOLOMITE MATRIX BRECCIA FORMATION 278

6.4 SOURCES OF MINERALIZING COMPONENTS 280

6.4.1 Sulphur 280
6.4.2 Lead 281

6.5 EVIDENCE FOR FLUID MIXING DURING MINERALIZATION 281

6.5.1 Ore Textures and Sulphur 282
6.5.2 Fluid Inclusion Data 285

6.6 MECHANISM FOR MINERALIZATION AND EVOLUTION THROUGH TIME 287

6.6.1 Syngenetic vs. Epigenetic Mineralization 287
6.6.2 Distribution and Geometry of Sulphide Bodies 288
6.6.3 Host Rock Replacement and Sulphide Deposition 288

6.7 LATE BRINE INFILTRATION 290

6.8 COMPARISON OF DEPOSITS AND PROSPECTS 290

6.9 TIMING OF MINERALIZATION 291

6.10 GENETIC MODEL 291

CHAPTER 7: CONCLUSIONS

7.1 PRINCIPAL CONCLUSIONS 294

7.2 FURTHER WORK 296

7.2.1 Further Work Proposed 296

REFERENCES 299

APPENDICES 347

APPENDIX A: SAMPLE PREPARATION TECHNIQUES 347

A1. PREPARATION OF POLISHED BLOCKS 347
Mounting, Lapping, Polishing 347
A2. PREPARATION OF POLISHED THIN BLOCKS 347

Mounting, Lapping, Polishing 347

A3. PREPARATION OF FLUID INCLUSION WAFERS 347
Mounting, Lapping, Polishing 347

A4. STAINING - DICKSON'S METHOD 348
Reagents 348
Procedure 348

APPENDIX B: ELECTRON MICROPROBE ANALYSIS - DATA 349

B1. DETECTION LIMITS - CARBONATES 349

Operating Parameters: 15kV, 15μA, 15μm 349
Operating Parameters: 15kV, 15μA, 25μm 349
Operating Parameters: 15kV, 15μA, 30μm 350

B2. DETECTION LIMITS - SULPHIDES 350

Operating Parameters: 20kV, 20nA, 1-2μm (Sphalerite) 350
Operating Parameters: 20kV, 20nA, 1-2μm (Galena) 351
Operating Parameters: 20kV, 20nA, 1-2μm (Tennantite) 352
Operating Parameters: 20kV, 20nA, 1-2μm (Pyrite) 353
Operating Parameters: 20kV, 20nA, 1-2μm (All Sulphides) 353

B3. ELEMENTAL CHEMISTRY - LISHEEN CARBONATES 354

Regional Replacement Dolomites and Carbonate Cements 354
Dolomite Matrix Breccias 355
Pink Dolomite 357
Late, Minor Vein and Vug Dolomite 358
Late, Minor Vein and Vug Calcite 358

B4. ELEMENTAL CHEMISTRY - GALMOY CARBONATES 360

Regional Replacement Dolomites and Carbonate Cements 360
Dolomite Matrix Breccias 360
Pink Dolomite 361
Late, Minor Vein and Vug Dolomite 361
Late, Minor Vein and Vug Calcite 362

B5. ELEMENTAL CHEMISTRY - RATHDOWNEY TREND PROSPECT CARBONATES 363

Regional Replacement Dolomites and Carbonate Cements 363
Dolomite Matrix Breccias 363
Pink Dolomite 366
Late, Minor Vein and Vug Dolomite 366

B6. ELEMENTAL CHEMISTRY - LISHEEN SULPHIDES 367

Sphalerite 367
Galena 372

Pyrite 375
Tennantite 377
Chalcopyrite 377

B7. ELEMENTAL CHEMISTRY - GALMOY SULPHIDES 378

Sphalerite 378
Galena 379
Pyrite 379
Tetrahedrite 380
Chalcopyrite 380

B8. ELEMENTAL CHEMISTRY - RATHDOWNEY TREND PROSPECT SULPHIDES 381

Sphalerite 381
Pyrite 382
Tetrahedrite 382
Chalcopyrite 382

B9. BACKGROUND INTERFERNCE PATTERNS 384

APPENDIX C: RESEARCH TECHNIQUES 386

C1. CATHODOLUMINESCENCE 386

Introduction 386
Basic Theory 386
Activators, Co-Activators and Quenchers 387

C2. REFLECTED LIGHT MICROSCOPY 388

Introduction 388

C3. ELECTRON MICROPROBE ANALYSIS (EMPA) 388

Introduction 388
Basic Principles 388
X-Ray Spectrometry - Detection and Measurement 389
Quantitative and Qualitative Analysis 389
X-Ray Mapping 390
Detection Limits 391

APPENDIX D: ISOTOPE DATA 392

D1. SULPHUR - Lisheen Deposit 392
D2. SULPHUR - Galmoy Deposit 396
D3. SULPHUR - Rathdowney Trend Prospects 398
D4. CARBON, OXYGEN - Lisheen Deposit 400
D5. CARBON, OXYGEN - Galmoy Deposit 402
D6. CARBON, OXYGEN - Rathdowney Trend Prospects 403
D7. LEAD - Lisheen Deposit 404
D8. LEAD - Galmoy Deposit 404

APPENDIX E: FLUID INCLUSION DATA **405**

E1. FLUID INCLUSION DATA - Lisheen Gangue 405
E2. FLUID INCLUSION DATA - Lisheen Sphalerite 408
E3. FLUID INCLUSION DATA - Galmoy Gangue 411
E4. FLUID INCLUSION DATA - Galmoy Sphalerite 412
E5. FLUID INCLUSION DATA - Rathdowney Trend Prospects Gangue 413
E6. FLUID INCLUSION DATA - Rathdowney Trend Prospects Sphalerite 414

ADDENDUM **415**

Sequence of alteration and mineralization in the Rathdowney Trend 416
Schematic illustration of the textural relationships between carbonates 417
Ternary plots showing the differences in carbonate chemistry 418

POCKET

Figure 2.6 - Borehole Locality Map, Lisheen
Figure 2.7 - Derryville zone cross-section, Lisheen

LIST OF FIGURES

Fig. 1.1 Geological map of the Irish Midlands, showing the location of ore deposits and prospects

Fig. 1.2 Rathdowney Trend prospecting licences, mineral deposits and sampling localities

Fig. 1.3 Contoured isoplumbs and basement geology of Ireland

Fig. 2.1 Geological column showing Lower Carboniferous strata and facies relationships

Fig. 2.2 Geology map of the Rathdowney Trend

Fig. 2.3 Diagrammatic cross section of the Durrow prospect

Fig. 2.4 Stratigraphic column of the Lisheen area

Fig. 2.5 Stratigraphic column of the Galmoy area

Fig. 2.6 Borehole locality map for the Lisheen deposit

Fig. 2.7 Cross section of the Derryville zone

Fig. 2.8 Borehole locality map for the Galmoy deposit

Fig. 2.9 Cross section through Galmoy orebodies

Fig. 3.1 Planar and nonplanar dolomite textures

Fig. 3.2 Frequency histogram, $CaCO_3$ (mole%) concentration in $D1_R$ dolomite

Fig. 3.3 Frequency histogram, $MgCO_3$ (mole%) concentration in $D1_R$ dolomite

Fig. 3.4 Frequency histogram, FeCO3 (mole%) concentration in $D1_R$ dolomite

Fig. 3.5 Frequency histogram, MnCO3 (mole%) concentration in $D1_R$ dolomite

Fig. 3.6 Frequency histogram, $CaCO_3$ (mole%) concentration in D2 dolomite

Fig. 3.7 Frequency histogram, $MgCO_3$ (mole%) concentration in D2 dolomite

Fig. 3.8 Frequency histogram, FeCO3 (mole%) concentration in D2 dolomite

Fig. 3.9 Frequency histogram, MnCO3 (mole%) concentration in D2 dolomite

Fig. 3.10 Frequency histogram, $CaCO_3$ (mole%) concentration in D3 dolomite

Fig 3.11 Frequency histogram, $MgCO_3$ (mole%) concentration in D3 dolomite

Fig. 3.12 Frequency histogram, FeCO3 (mole%) concentration in D3 dolomite

Fig. 3.13 Frequency histogram, MnCO3 (mole%) concentration in D3 dolomite

Fig. 3.14 Stage scan, 121/162.1 (D3 dolomite)

Fig. 3.15 Stage scan, 121/165.2 (D3 dolomite)

Fig. 3.16 Stage scan, 252/174.0 (D3 dolomite)

Fig. 3.17 Stage scan, MG63/97.2 (D3 dolomite)

Fig. 3.18 Stage scan, HC13/87.5 (D3 dolomite)

Fig. 3.19 Stage scan, DUR1/686.5 (D3 dolomite)

Fig. 3.20 Stage scan, DUR4/365.5 (D3 dolomite)

Fig. 3.21 Frequency histogram, $CaCO_3$ (mole%) concentration in D4 dolomite

Fig. 3.22 Frequency histogram, $MgCO_3$ (mole%) concentration in D4 dolomite

Fig. 3.23 Frequency histogram, $FeCO_3$ (mole%) concentration in D4 dolomite

Fig. 3.24 Frequency histogram, $MnCO_3$ (mole%) concentration in D4 dolomite

Fig. 3.25 Stage scan, RE24/1625 (D4 dolomite)

Fig. 3.26 Stage scan, HC15/200.8 (D4 dolomite)

Fig. 3.27 Frequency histogram, $CaCO_3$ (mole%) concentration in D5 dolomite

Fig. 3.28 Frequency histogram, $MgCO_3$ (mole%) concentration in D5 dolomite

Fig. 3.29 Frequency histogram, $FeCO_3$ (mole%) concentration in D5 dolomite

Fig. 3.30 Frequency histogram, $MnCO_3$ (mole%) concentration in D5 dolomite

Fig. 3.31 Covariance of FeO and MnO wt% in Lisheen dolomites

Fig. 3.32 Covariance of FeO and MnO wt% in Galmoy dolomites

Fig. 3.33 Covariance of FeO and MnO wt% in Prospect dolomites

Fig. 3.34 Co, Ni and As-rich pyrite - Lisheen

Fig. 3.35 Cd, Fe and As correlation in colloform sphalerite - Lisheen

Fig. 3.36 Cd, Fe variation in brown sphalerite (361/223.4)

Fig. 3.37 Cd, Fe variation in brown sphalerite (529/246.6)

Fig. 3.38 Fe v Cd wt% in coloured sphalerite - Lisheen

Fig. 3.39 Cd, Fe and As correlation in banded sphalerite

Fig. 3.40 Fe v Cd wt% in coloured sphalerite - Galmoy

Fig. 3.41 Cd, Fe and As correlation in Cd-rich sphalerite - Durrow

Fig. 3.42 Fe v Cd wt% in pale coloured sphalerite - Durrow

Fig. 3.43 Co, Ni and As-rich pyrite - Durrow

Fig. 3.44 Summarized paragenesis for Lisheen and Galmoy mineralization

Fig. 4.1 $\delta^{34}S‰$ of all sulphur-bearing phases in the Rathdowney Trend - mineralogy

Fig. 4.2 $\delta^{34}S‰$ of all sulphur-bearing phases in the Rathdowney Trend - location

Fig. 4.3 $\delta^{34}S‰$ of all sulphur-bearing phases in the Lisheen deposit - mineralogy

Fig. 4.4 $\delta^{34}S‰$ of all sulphur-bearing phases in the Lisheen deposit - paragenetic stage

Fig. 4.5 $\delta^{34}S‰$ of all sulphur-bearing phases in the Galmoy deposit - mineralogy

Fig. 4.6 $\delta^{34}S‰$ of all sulphur-bearing phases in the Galmoy deposit - paragenetic stage

Fig. 4.7 $\delta^{34}S‰$ of all sulphur-bearing phases in the prospects - mineralogy

Fig. 4.8 $\delta^{34}S‰$ of all sulphur-bearing phases in the prospects - mineralization style

Fig. 4.9 $\delta^{34}S‰$ of all sulphur-bearing phases in the prospects - location

Fig. 4.10 $\delta^{34}S‰$ of main ore-stage sphalerite and galena - subdivided according to ore zone

Fig. 4.11 Summary of sulphur isotope data from Irish-type ore deposits

Fig. 4.12 Frequency histogram of $\delta^{13}C$ values (‰) for all carbonate samples analyzed

Fig. 4.13 Frequency histogram of $\delta^{18}O$ values (‰) for all carbonate phases analyzed

Fig. 4.14 $\delta^{13}C$ and $\delta^{18}O$ isotopic composition of all carbonates analyzed

Fig. 4.15 $\delta^{13}C$ and $\delta^{18}O$ isotopic composition of Lisheen carbonates

Fig. 4.16 Frequency histogram of $\delta^{13}C$ values (‰) for Lisheen carbonates

Fig. 4.17 Frequency histogram of $\delta^{18}O$ values (‰) for Lisheen carbonates

Fig. 4.18 Frequency histogram of $\delta^{13}C$ values (‰) for Galmoy carbonates

Fig. 4.19 Frequency histogram of $\delta^{18}O$ values (‰) for Galmoy carbonates

Fig. 4.20 $\delta^{13}C$ and $\delta^{18}O$ isotopic composition of Galmoy carbonates

Fig. 4.21 $\delta^{13}C$ and $\delta^{18}O$ isotopic composition of prospect carbonates

Fig. 4.22 Frequency histogram of $\delta^{13}C$ values (‰) for prospect carbonates

Fig. 4.23 Frequency histogram of $\delta^{18}O$ values (‰) for prospect carbonates

Fig. 4.24 Relationship between precipitation temperature and water isotopic composition

Fig. 4.25 $^{208}Pb/^{204}Pb$ vs. $^{206}Pb/^{204}Pb$ for Lisheen and Galmoy galena samples

Fig. 4.26 $^{207}Pb/^{204}Pb$ vs. $^{206}Pb/^{204}Pb$ for Lisheen and Galmoy galena samples

Fig. 4.27 Average $^{208}Pb/^{204}Pb$ vs. $^{206}Pb/^{204}Pb$ for Lisheen and Galmoy galena

Fig. 4.28 Average $^{207}Pb/^{204}Pb$ vs. $^{206}Pb/^{204}Pb$ for Lisheen and Galmoy galena

Fig. 4.29 Average $^{207}Pb/^{204}Pb$ vs. $^{206}Pb/^{204}Pb$ for Zn-Pb deposits in Ireland

Fig. 4.30 Average $^{208}Pb/^{204}Pb$ vs. $^{206}Pb/^{204}Pb$ for Zn-Pb deposits in Ireland

Fig. 5.1 Primary and secondary inclusions in sphalerite

Fig. 5.2 Frequency histogram of all homogenization temperatures (°C) at Lisheen

Fig. 5.3 Salinity vs. Homogenization temperature of sphalerite and gangue phases at Lisheen

Fig. 5.4 Frequency histogram of homogenization temperatures (°C) in sphalerite - ore zone

Fig. 5.5 Salinity vs. Homogenization temperature in sphalerite - ore zone

Fig. 5.6 Frequency histogram of all homogenization temperatures (°C) at Galmoy

Fig. 5.7 Salinity vs. Homogenization temperature of sphalerite and gangue phases at Galmoy

Fig. 5.8 Frequency histogram of all homogenization temperatures (°C) at prospects

Fig. 5.9 Salinity vs. Homogenization temperature of sphalerite and gangue phases at prospects

Fig. 5.10 Frequency histogram of all homogenization temperatures - gangue and sphalerite

Fig. 5.11 Salinity vs. Homogenization temperature of sphalerite and gangue phases all localities

Fig. 5.12 Salinity vs. Homogenization temperature of all gangue - subdivided by location

Fig. 5.13 Salinity vs. Homogenization temperature of all sphalerite - subdivided by location

Fig. 6.1 Comparison of Lisheen and Galmoy fluids with Tynagh, Navan and Silvermines

Fig. 6.2 Comparison of Lisheen and Galmoy fluids with basement-circulated fluids

Fig. 6.3 Homogenization temperature vs. $\delta^{34}S‰$ for crystalline sphalerite

Fig. 6.4 Salinity vs. $\delta^{34}S‰$ for crystalline sphalerite

Fig. 6.5 Schematic cross-sections illustrating dolomitization and mineralization events

LIST OF TABLES

Table 3.1 Chemical composition of Lisheen $D1_R$ and $D1_C$ dolomite

Table 3.2 Chemical composition of Galmoy $D1_R$ dolomite

Table 3.3 Chemical composition of Rathdowney east and Holycross $D1_R$ and $D1_C$ dolomite

Table 3.4 Chemical composition of Lisheen D2 and D3 dolomites

Table 3.5 Chemical composition of Galmoy D2 and D3 dolomites

Table 3.6 Chemical composition of prospect D2 and D3 dolomites

Table 3.7 Chemical composition of Lisheen D4 dolomite

Table 3.8 Chemical composition of Galmoy D4 dolomite

Table 3.9 Chemical composition of Rathdowney East, Durrow and Holycross D4 dolomite

Table 3.10 Chemical composition of Lisheen D5 dolomite

Table 3.11 Chemical composition of Lisheen D5 calcite

Table 3.12 Chemical composition of Galmoy D5 dolomite

Table 3.13 Chemical composition of Galmoy D5 calcite

Table 3.14 Chemical composition of Holycross D5 dolomite

Table 4.1 Lisheen deposit - Lead isotope ratios in galena

Table 4.2 Galmoy deposit - Lead isotope ratios in galena

LIST OF PLATES

1A Waulsortian mudmound, Feltrim Quarry, Co. Dublin.

2A Partially dolomitized Waulsortian Limestone - 2447-8/34.2

2B Regionally dolomitized Waulsortian Limestone - 2447-8/13.3

3 Selective dolomitization of bryozoa in Waulsortian Limestone - 2447-8/34.2

3a Regional dolomite cement ($D1_C$) overgrowing/replacing diagenetic calcite - 121/200.5

4 Weakly zoned regional dolomite cement (D1c) - 2447-8/13.3

5 X-ray distribution map of the element Fe in (D1c) - 2447-8/13.3

6 Black matrix dolomite (D2) and regional dolomite clasts ($D1_R$) - MG99/100.6

7 D2 microveinlets cross-cutting $D1_R$ dolomite clasts - MG63/97.2

8 Dull red, non-uniform luminescent regional dolomite ($D1_R$) - 3312-2/238.5.

9A Crystalline sphalerite and galena replacing regional dolomite cement ($D1_C$) - GY382/86.5

9B Crystalline white dolomite matrix with rounded mineralized clasts - GY355/97.0

10 $D1_R$ dolomite clast hosted by a non-luminescent matrix dolomite -HC15/200.8

11A Regionally dolomitized Waulsortian Limestone - RE24/1320

11B Zebra texture dolomite - DUR2/768.7

12A D2 hydrothermal breccia dolomite - 262/129.8

12B D3 hydrothermal breccia dolomite - 121/146.8

13 D2 microveinlets cross-cutting $D1_R$ dolomite clasts - 262/153.6

14 X-ray distribution map of the element Fe and Mn in $D1_R$ and D2 dolomite - 262/153.6

15 Luminescent sphalerite replacing D2 dolomite - 121/180.5

16 D2 dolomite, displaying variable crystal size - 262/159.1

17 X-ray distribution map of the element Fe and Mn in D2 dolomite - 121/194.0

18 D2 dolomite crystals with distinct mottled cores - 121/180.5

19 D3 dolomite exhibiting 4 distinct luminescent stages - 121/162.1

20 X-ray distribution map of the element Fe and Mn in D3 dolomite - 121/162.1

21 D3 dolomite exhibiting 4 distinct luminescent stages - 121/165.2

22 X-ray distribution map of the element Fe and Mn in D3 dolomite - 121/165.2

23 D3 dolomite exhibiting 4 distinct luminescent stages - 538/185.2

24 D3 dolomite exhibiting heterogeneous luminescent core - 252/174.0

25A D2 hydrothermal breccia dolomite - MG18-18/87.5

25B D3 hydrothermal breccia dolomite with calcite and pink dolomite - MG99/100.8

26 Luminescent sphalerite replacing D2 dolomite - 3.CW

27 Luminescent D2 dolomite rhombs - MG63/97.2

28 D3 dolomite exhibiting 4 distinct luminescent stages - GY355/78.0

28a X-ray distribution map of the element Fe and Mn in D3 dolomite - MG99/100.8

29 Luminescent D3 dolomite vein - MG63/97.2

29a Calcite matrix breccia, with evidence of clast rotation - 262/120.0

29a D3 dolomite vein cross-cutting D2 and $D1_R$ dolomite clast - MG63/97.2

30A D3 dolomite cross-cutting D2 dolomite - HC15/207.0

30B Well developed dolomite breccia - Silvermines

31 Luminescent D2 dolomite rhombs - HC13/115.3

32 D3 dolomite crystal - HC13/87.8

33A D3 hydrothermal breccia dolomite - HC13/87.8

33B D3 hydrothermal breccia dolomite - RE24/1674.0

34A D3 hydrothermal breccia dolomite - DUR1/686.5

34B D3 hydrothermal breccia dolomite - DK45/294.6

35 D3 dolomite exhibiting 4 distinct luminescent stages - RE24/1729a

36 Zoned D3 dolomite and sulphide - DK45/271.6

37 Luminescent D3 dolomite - DUR1/686.5

38 Luminescent D3 dolomite overgrown by an Fe rich cement stage - DUR4/365.5

39A D2 hydrothermal breccia dolomite with vug-filling D4 dolomite - 262/152.3

39B Sub-Waulsortian carbonate veins - 121/319.2

40 Luminescent D4 pink dolomite - 262/152.3

41 D4 dolomite exhibiting distinct luminescence - RE24/1625

42 X-ray distribution map of the element Fe and Mn in D4 dolomite - RE24/1625

43 D4 dolomite exhibiting distinct luminescence - HC15/200.8

44 X-ray distribution map of the element Fe and Mn in D4 dolomite - HC15/200.8

45 Luminescent and non-luminescent sub-Waulsortian carbonate veins - 121/319.2

46 Luminescent D5 calcite vein - 121/180.5

47A Sub-Waulsortian hosted, chalcopyrite rich dolomite vein - G16-27/383.5

47B Sub-Waulsortian carbonate veins - GY333/103.3

48A D4 pink dolomite and late vug-filling calcite - RE24/1625.0

48B Chalcopyrite and tennantite bearing dolomite vein - DUR2 961.9

49A Massive fine grained pyrite, cross-cut and replaced by sphalerite and galena - 121/190.2

49B Massive fine grained sulphide - 262/159.85

50A Fine crystalline, weakly colloform pink-brown sphalerite - 121/189.3

50B Massive fine grained sulphide with disrupted colloform textures - 121/192.8

51 Colloform sphalerite with Zn-rich carbonate and concentrically zoned pyrite - 262/159.85

52A Pyrite and sphalerite incorporated into the growth zones of gangue dolomite - 416 193.6

52B Sphalerite pseudomorphously replacing barite - 325/146.20

53A Selective replacement of foramanifera - 137/134.9

53B Open-space filling euhedral galena - 402/196.0

54A Selective replacement of foramanifera by galena - 171/172.7

54B Selective replacement of ooid by sphalerite and galena - 394/164.30

55A Massive colloform iron sulphide - 420/190.7

55B Massive colloform, mixed sulphide assemblage - 394/164.30

56A Granular pyrite pseudomorphously replacing barite laths - 262/162.1

56B Pyrite/marcasite assemblage exhibiting brittle fracture - 262/159.1

57A Massive, fine grained, buff coloured sphalerite - 3245-28/30.0

57B Massive fine grained sulphide with crystalline yellow sphalerite - CW10

58A Colloform texture in ore-stage sphalerite and galena - MG18/90.0

58B Zoned crystalline sphalerite - GY382/86.0

58a Distinct CL zoning in crystalline sphalerite - GY382/86.0

58a Distinct blue-purple luminescent zone in colloform sphalerite - GY355/95.0

59A Zoned colloform pyrite cross-cut by sphalerite - 2(0134)

59B Pyrite replacing ooids - DUR1/910.0

60 X-ray distribution map of the element Fe and Cd in sphalerite - DUR1/910.0

CHAPTER 1: INTRODUCTION AND REVIEW

CHAPTER 1: INTRODUCTION AND REVIEW

1.1 INTRODUCTION

The focus of this research project is the Rathdowney Trend, a 40km long belt of carbonate rocks trending NE-SW from Abbeyleix in Co. Laois to Thurles in Co. Tipperary, southern Ireland (Figures 1.1, 1.2). The Trend is host to a number of carbonate-hosted base-metal deposits including the Lisheen Zn-Pb deposit, the largest zinc discovery in Europe for 10 years and the Galmoy deposit. An understanding of the controls of Zn-Pb mineralization and alteration is critical in order to evaluate proposed genetic models for these carbonate-hosted 'Irish-type' deposits, and to provide tools for more effective exploration within the Trend. This research concentrates on both mineralized and barren environments, with particular emphasis on the Lisheen and Galmoy deposits. Other sampling localities include the Holycross, Rathdowney East, Derrykearn and Durrow prospects (Figure 1.2).

This introductory chapter presents a review of Irish carbonate-hosted base-metal deposits. The history of the modern exploration industry in Ireland is examined and recent trends are emphasised. Research rationale and objectives are presented along with an extensive literature review. Within this background investigation, significant issues regarding deposit classification and genesis are discussed. Finally, the research methodology is outlined, illustrating the multidisciplinary approach to the study, and the expected results are considered.

1.2 EXPLORATION HISTORY OF 'IRISH-TYPE' Zn-Pb DEPOSITS

1.2.1 Exploration Background

The Lower Carboniferous carbonate-hosted Zn-Pb deposits of Ireland represent a major orefield of international importance (Figure 1.1). The deposits are stratabound to stratiform and occur in the basal Carboniferous mixed sequence of carbonates and clastic rocks (Navan Group - informal designation) or within late Courceyan Waulsortian facies and time equivalent rocks. The Navan Group is host to Europe's largest Zn-Pb mine, Outokumpu's Tara Mine at Navan, with initial reserves of up to 70 million tonnes (Mt) grading 10.1% Zn and 2.7% Pb (Ashton *et al.*, 1986). Principal deposits within the Waulsortian facies and time equivalent rocks include Tynagh (Boast et al., 1981a), Silvermines (Taylor and Andrew, 1978; Andrew, 1986a), Ballinalack (Jones and Brand, 1986) and the recently discovered Rathdowney Trend deposits, Galmoy (Doyle *et al.*,

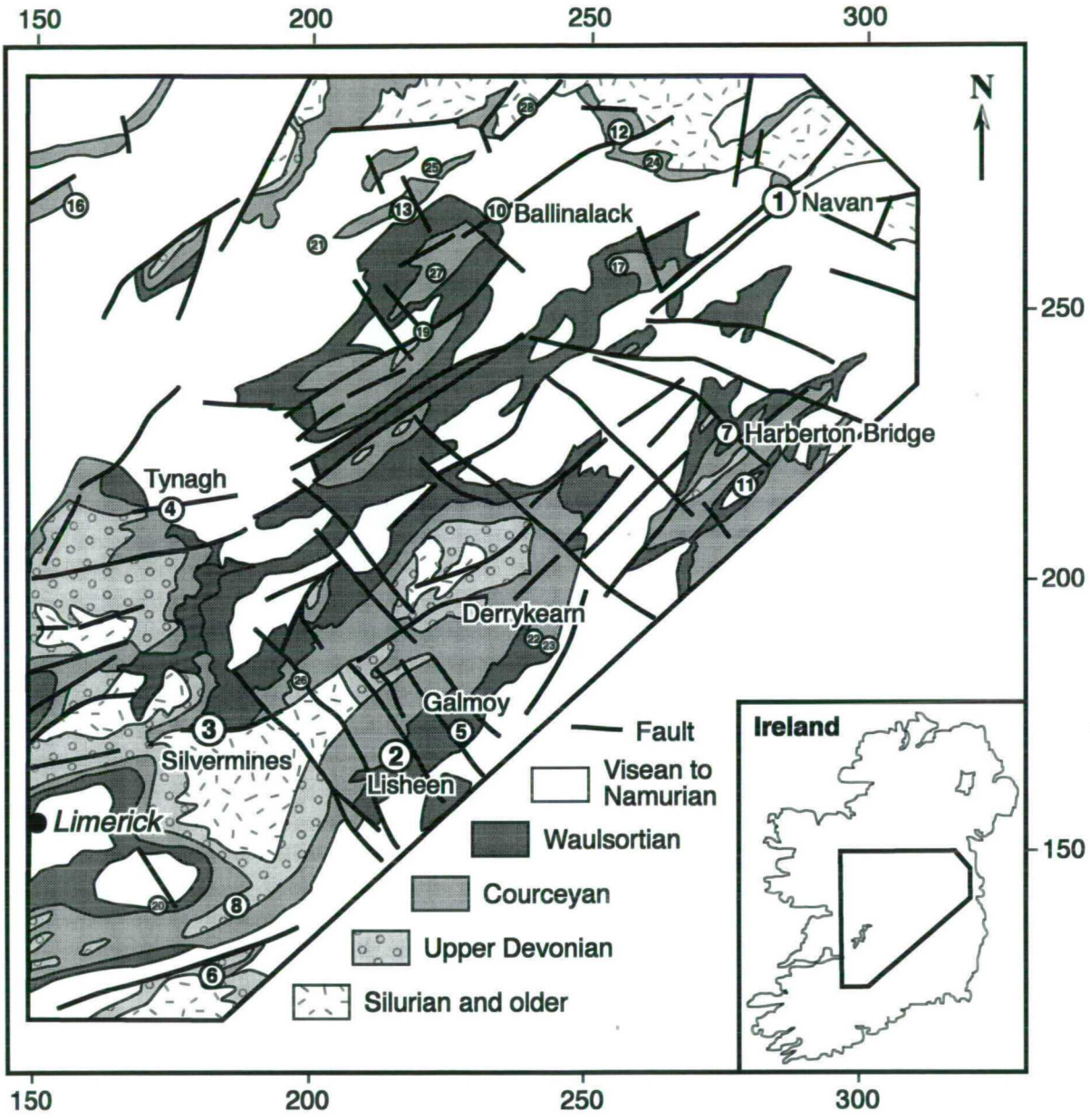
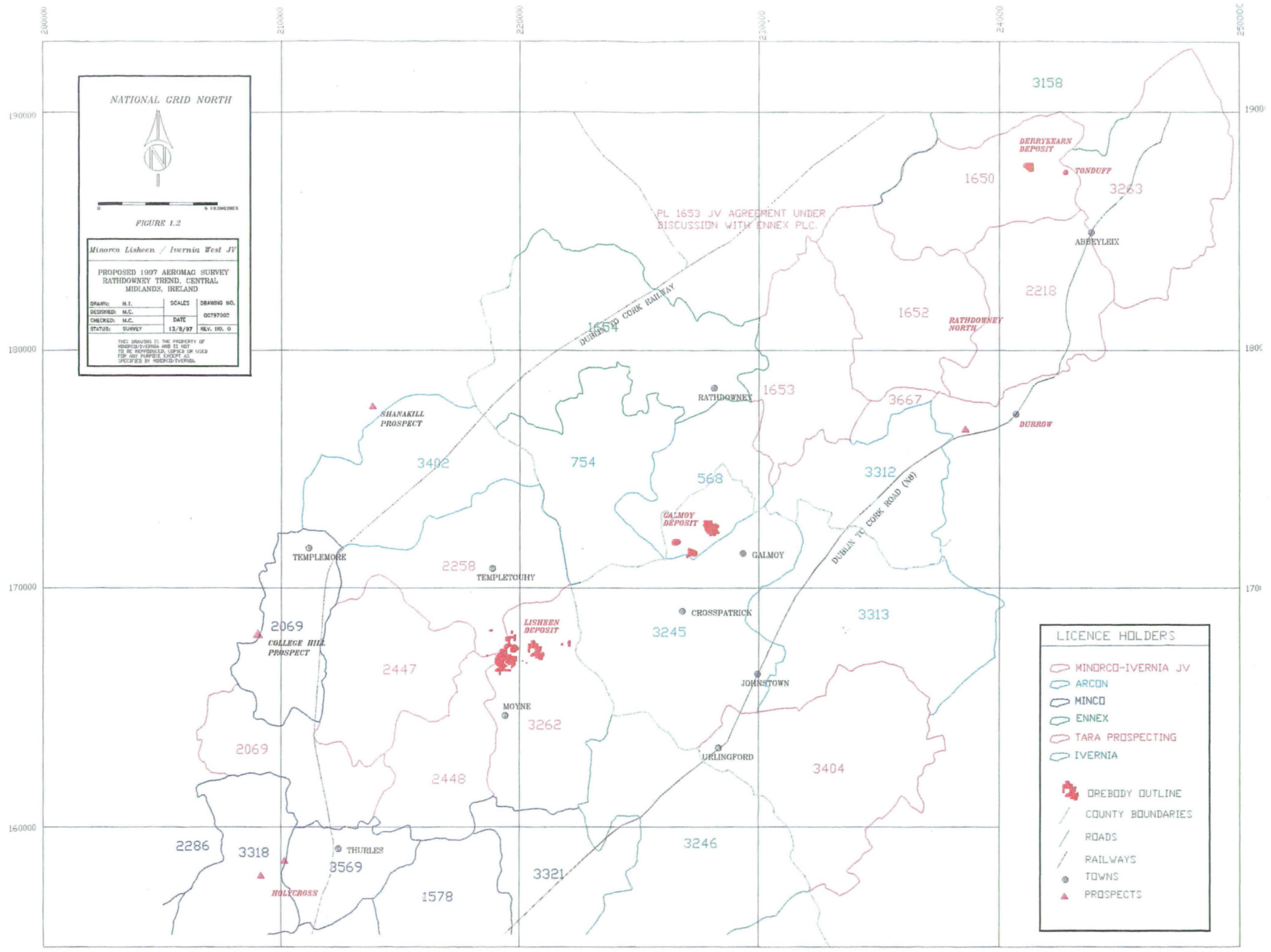


Figure 1.1 Geological map of the Irish Midlands showing the location of ore deposits and prospects. Minor prospects are: 6 - Aherlow, 8 - Gortdrum, 11 - Rickardstown, 12 - Oldcastle, 13 - Keel, 16 - Glenamaddy, 17 - Sion Hill, 19 - Moyvoughly, 20 - Carrickittle, 21 - Newtown Cashel, 23 - Tonduff, 24 - Cloonabreeny, 25 - Edgeworthtown, 26 - Clash, 27 - Moyvore, 28 - Lough Sheelin. Modified after O'Reilly *et al.* (in press).


NATIONAL GRID NORTH
FIGURE 1.2
Minorco Lisheen / Ivernia West JV
PROPOSED 1997 AEROMAG SURVEY
RATHDOWNEY TREND, CENTRAL
MIDLANDS, IRELAND
DRAWN: H.T.
DESIGNED: M.C.
CHECKED: M.C.
STATUS: SURVEY
SCALES
DATE
13/8/97
DRAWING NO.
OCT97002
REV. NO. 0
THIS DRAWING IS THE PROPERTY OF MINORCO/IVERNIA AND IS NOT TO BE REPRODUCED, COPIED OR USED FOR ANY PURPOSE EXCEPT AS SPECIFIED BY MINORCO/IVERNIA.
200000
210000
220000
230000
240000
250000
190000
180000
170000
160000
PL 1653 JV AGREEMENT UNDER DISCUSSION WITH ENNEX PLC.
DUBLIN TO CORK RAILWAY
DUBLIN TO CORK ROAD (N8)
3158
1650
3263
DERRYKEARN DEPOSIT
TONDUFF
ABBEYLEIX
2218
1652
RATHDOWNEY NORTH
1653
RATHDOWNEY
3667
DURROW
SHANAKILL PROSPECT
3402
754
568
3312
CALMOY DEPOSIT
GALMOY
TEMPLEMORE
2258
TEMPLETOUHY
CROSSPATRICK
3313
3245
LISHEEN DEPOSIT
2069
COLLEGE HILL PROSPECT
2447
JOHNSTOWN
MOYNE
3262
2069
2448
URLINGFORD
3404
2286
3318
THURLES
3569
3246
3321
HOLYCROSS
1578
LICENCE HOLDERS
MINORCO-IVERNIA JV
ARCON
MINCO
ENNEX
TARA PROSPECTING
IVERNIA
OREBODY OUTLINE
COUNTY BOUNDARIES
ROADS
RAILWAYS
TOWNS
PROSPECTS

1992) and Lisheen (Hitzman *et al.*, 1992; Shearley *et al.*, 1996). The current mineable resource at Galmoy is estimated to be 6.12Mt, grading 11.5% Zn, 1.11% Pb and 9.6% Fe. A new estimate of reserves and resources at Lisheen indicates that the orebody contains 17.7Mt, grading 13.0% Zn, 2.2% Pb and 16% Fe, with 30g/t Ag (Madden, 1996).

Production from carbonate-hosted deposits in Ireland has been known to have occurred in the Silvermines area as early as the mid-seventeenth Century (Williams and McArdle, 1978). However, it was not until Government legislation was passed in 1940, the first of several Minerals Developments Acts (1940 to 1979) that mining development began in earnest. These acts regularized the framework for mineral exploration and mining in Ireland and led to the development of a modern underground mine at the Ordovician cupriferous volcanogenic massive sulphide deposit of Avoca. Mining operations during the 1940's and 1950's were small and of modest success. Operations centred on the carbonate-hosted deposits of Silvermines, Abbeytown and Benbulben were among the deposits worked at this time (O'Brien, 1959).

The development of the Avoca mine, together with experience of working small Zn-Pb mines at Silvermines and Abbeytown, highlighted the need for mining tax revision. This was incorporated in the 1956 Finance Act. The incentive provided by this legislation, combined with the application of mineral exploration techniques developed in Canada, led to a strong revival of base-metal exploration by the late 1950s. Between 1956-1961 exploration activity was carried out over an area of about 1000 square miles. This activity culminated in the discovery of the Tynagh Zn-Pb-Cu-Ag deposit, Co. Galway, by Irish Base Metals Ltd.

The landmark discovery of Tynagh confirmed the potential of the Irish Lower Carboniferous to host substantial base-metal deposits, as well as demonstrating the applicability of modern geochemical and geophysical prospecting methods. Major Canadian-based multinational mining companies began to systematically explore Ireland, utilizing modern techniques. By 1962, an area of approximately 2000 square miles was being actively explored. Discoveries were made at Gortdrum and Silvermines, as well as numerous other minor prospects, including Ballinalack.

The period 1963-1967, however, saw no further significant finds. The 1967 Finance Act increased the incentives offered by the 1956 Act, to the extent of allowing a 20 year tax-free period on all mines brought into production before 1986. This legislation led to an increase in the number of exploration companies, working over an area of 9000 square miles (about 1/3 of the country).

The following years witnessed a further increase in exploration activity which was maintained until the end of the 1970's. The success of this period of exploration reached a zenith in 1970, with the discovery of the Navan Zn-Pb orebody by Tara Exploration and Development Co. Of the discoveries made during the period 1961-1970, mines were developed at Tynagh (1965-1981), Gortdrum (1968-1975), Silvermines (1968-1982), and Navan (1976-present).

After the discovery of the Navan deposit, the provisions of the 1967 Finance Act were severely curtailed and doubts over mineral rights ownership restricted what should have been a major expansion in exploration activity during the mid 1970's. Discoveries were made at Newton-Cashel, Tatestown, Garrycam, Boston Hill, Harberton Bridge and Oldcastle.

The early 1980's experienced a decline in the exploration for carbonate-hosted base-metal deposits in Ireland. Due to a high gold price, international exploration efforts at this time generally favoured precious metal targets. As a result, multinational companies dwindled and new junior Irish companies developed to take their place.

No further substantial deposits were discovered until 1986, when Galmoy was located within the Rathdowney Trend by Dublin-based Arcon International Resources Plc. This followed the initial discovery at Derrykearn, in 1984, of a sub-economic deposit also within the Rathdowney Trend. International focus returned to Irish base-metal exploration following the success of the mid-eighties, and interest was again heightened by the announcement of the Lisheen discovery in 1990, also within the Rathdowney Trend. This confirmed the potential of the Trend, located in the southern Irish Midlands.

1.2.2 Modern Geochemical and Geophysical Exploration Techniques

Exploration is increasingly based on the scientific understanding of the ways in which ore deposits form, particularly where concealed orebodies, typical of the Irish Midlands, are sought. Therefore, the integration of empirical and theoretical geology (genetic models), geochemistry and geophysics within a practical economic framework is fundamental in exploration strategy.

Structural control is a critical factor in the formation and location of economic mineralization in the Irish Midlands. Therefore fault information, accumulated from field mapping and reprocessed gravity and magnetic data, provides a major insight into spatial controls on mineralization and the identification of prospective fault systems. Within the Rathdowney Trend, the conceptual model

utilized during exploration involves stratabound sulphide lenses, confined to the base of dolomitized Waulsortian Limestones, bound by high-angle, mineralizing fault structures.

Geochemical prospecting centered around or near to these inferred mineralizing fault structures is perhaps one of the most significant developments in mineral exploration and was first applied in Ireland in 1959. Geochemical reconnaissance surveys led directly to the discovery of the Tynagh orebody in 1961; more recently (1990) in the Rathdowney Trend, a soil sampling program succeeded in delineating weak (150ppm) zinc values at the Lisheen prospect (Hitzman *et al.*, 1992) regardless of the target depth (~200m over most of the Trend). The use of geochemistry, coupled with widely used geophysical exploration methods in the Irish Midlands such as Induced Polarization (IP) and resistivity surveys, forms the most comprehensive exploration tool in the search for new mineral deposits. All of the main deposits within the Irish Midlands have been delineated by this methodology of integrated geochemical and geophysical prospecting techniques, coupled with increased amounts of diamond drilling. At present there is a trend to utilise airborne geophysical methods.

1.3 RESEARCH RATIONALE

1.3.1 Dolomitization and Mineralization: a key relationship

The discoveries of Lisheen and Galmoy in the Rathdowney Trend have marked a new phase in Irish base-metal exploration but, despite renewed exploration activity, new deposits are proving extremely difficult to find.

Explorationists have long recognized the importance of structural control of Irish base-metal deposits. Structural, magnetic and gravity data all indicate that the fundamental structural controls are E-NE trending basement Caledonian structures which have been reactivated in dextral transtension by NNE to NE extension during the Lower Carboniferous (Johnston *et al.*, 1996). This extension generated high permeability pathways for migrating hydrothermal fluids. These fluids were responsible for a range of alteration phenomena including the development of multiple hydrothermal dolomite generations and the precipitation of base-metal sulphides. Mineralization in the Waulsortian, intimately associated with faulting, has been recognized at Tynagh (Clifford *et al.*, 1986), Silvermines (Andrew, 1986a), Galmoy (Doyle *et al.*, 1995a), and Lisheen (Shearley *et al.*, 1996).

Within the Rathdowney Trend the host rocks are dolomitized, and the presence of dolomites is utilized as an exploration guide. The gradational contact between dolomitized and undolomitized Waulsortian facies forms a NE-SW trending regional dolomite 'front' which is sub-parallel to major basement Caledonian structures and helps to define the Rathdowney Trend (Hitzman *et al.*, 1992). The limit of complete regional dolomitization has a NE trend from Derrykearn to just south of Lisheen and corresponds to the present limits of Waulsortian facies outcrop.

Although the association between dolomitization and mineralization is well established, it is unclear whether the dolomites can be genetically linked to the ore deposits since dolomites occur throughout the Rathdowney Trend even where mineralization is absent. The location of the newly discovered deposits within the Rathdowney Trend, as well as extensive regional dolomitization sited along E-NE lineaments in the southern Irish Midlands, implies a genetic link between the two events.

A better understanding of the controls of dolomitization and mineralization particularly concerning the hydrothermal fluids responsible is therefore essential in order to improve exploration success, both in the Irish Midlands and in similar terrains elsewhere in the world. There is a critical need for well constrained data to evaluate proposed genetic models, and to provide tools for more effective exploration.

1.3.2 Research Objectives

The main objective of this research was to determine the chemical, isotopic and thermal characteristics of fluids responsible for Zn-Pb mineralization and alteration in the Rathdowney Trend, with a focus on the Lisheen deposit.

The approach was to carry out geochemical and isotopic analyses of sulphides and hydrothermal carbonates, and studies of fluid inclusions hosted by these phases. These data can be used to: (1) evaluate hypotheses regarding ore genesis, which remain controversial; (2) constrain heterogeneity in regional heat and fluid flow, within a deposit and between deposit localities; and (3) provide geochemical/isotopic tools applicable in the exploration for new deposits.

1.4 BACKGROUND AND PREVIOUS WORK

Among the ore deposit types typically hosted by sedimentary rocks are the two most important classes of Zn-Pb deposits: the sedimentary-exhalative (Sedex), 'shale-hosted' or 'sediment-

hosted' class of stratiform deposit; and the Mississippi Valley-type (MVT), or 'carbonate-hosted' class of stratabound deposit (Gustafason and Williams, 1981). Sediment-hosted stratiform deposits and MVT deposits, however, have been considered to be part of a continuum in terms of characteristics and mechanism of formation (Gustafson and Williams, 1981).

1.4.1 MVT and Sedex Deposits - Characteristics and Mechanism of Formation

MVT deposits are generally thought to have formed from large-scale fluid migration in response to convergent margin tectonism and they are particularly associated with foreland basins and foreland thrust belts (Leach and Rowan, 1986; Bradley, 1993; Bethke and Marshak, 1990; Garven and Freeze, 1984). There are four significant districts in the United States: central and east Tennessee; southeast Missouri; the Tri-state area; and the Upper Mississippi River valley. Important Canadian deposits include Pine Point (Campbell, 1967; Skall, 1975; Kyle, 1981, 1983; Krebs and MacQueen, 1984; and Rhodes *et al.*, 1984), Polaris (Kerr, 1977; Randell, 1994), Nanisivik (Olson, 1984), and Gays River (Akande and Zentilli, 1984; Ravenhurst *et al.*, 1989; Chi and Savard 1995). Sedex deposits are usually found in extensional basins where compaction-driven or density-driven fluid migration are generally evoked to move metalliferous brines to the seafloor. The most important setting for Sedex deposits is continental rift basins (Person and Garven, 1994). Examples include McArthur River, Australia (Murray, 1975); Sullivan, Canada (Hamilton *et al.*, 1983); and Meggen, Germany (Krebs, 1981).

MVT and Sedex deposits possess very different physical characteristics, such as deposit morphology, ore textures, and range of host-rock lithologies. The variation in the styles of mineralization, MVT to Sedex, relates to the lithology and diagenetic state of the host rock at the time of mineralization. MVT deposits are stratabound and typically coarse grained, whereas Sedex deposits are stratiform and normally fine grained (Sangster, 1990). The former occur exclusively in carbonate rocks; Sedex deposits also occur in carbonate rocks, but are found in almost every other type of sedimentary lithology.

The two classes also have some distinctive mineralogical and chemical characteristics. For example, although pyrite is usually the main iron sulphide associated with ore deposits of both classes, pyrrhotite is common only in deposits of the Sedex class, whereas marcasite is more common in deposits of the MVT class. Similarly, silica (usually as chert) is commonly associated with deposits of the Sedex class, but rarely with the MVT class. Metal zoning in Sedex class deposits includes a lateral and/or vertical sequence of Cu, Pb, Zn, Ba extending outward and

upward from a feeder zone (Briskey, 1986a). In MVT deposits, zoning is roughly Cu (±Ni, ±Co)-Pb-Zn-iron sulphide going up section (Briskey, 1986b).

These physical differences, as well as the mineralogical and chemical differences, are due to the different environments of ore deposition for the two deposit types. MVT deposits, which occur mostly in dolomites but also in limestones (Sangster, 1976), represent open-space filling and replacement by minerals deposited from hydrothermal solutions within porous aquifers in the subsurface. Sedex class deposits were formed on the sea floor around hydrothermal vents as sulphidic muds in a variety of sedimentary environments (Large, 1980, 1981, 1983) .

In summary, sediment-hosted stratiform deposits are distinguished from MVT deposits by an early timing of mineralization relative to deposition of host sediments, and by greater conformity with their hosts. MVT deposits formed by later replacement of lithified carbonate host-rock.

In all other features examined, however, large overlaps exist, probably reflecting the common ultimate derivation of both deposit types from fluids that emanated from or interacted with sedimentary basins (Sangster, 1990). In terms of temperature, salinity and pH, the hydrothermal fluids may have been very similar for both deposit types (Sangster, 1990).

1.4.2 Characteristics of 'Irish-type' Zn-Pb Deposits

The Irish Carboniferous base-metal deposits occupy a paradoxical position in this generally accepted classification of sediment-hosted Zn-Pb deposits, exhibiting a range of features considered diagnostic of both MVT and Sedex end-members. The Irish deposits do not fall within a single classified type, and as a result have been informally termed 'Irish-type'. It is the Navan Group, Waulsortian and Kildare-type Zn-Pb mineralization of the Central Midlands that are generally regarded as being 'Irish-type'.

Early Irish metallogenetic theorists formed two schools, the epigeneticists under Schultz (1966a), and the syngeneticists under Derry, Clark and Gillatt (1965). However, the evidence will always be contentious as syngeneticists can account for crosscutting features as replacement textures, discordant feeder zones and remobilization, while epigenetic models can justify apparently syn-sedimentary structures by selective replacement. During the 1970's the 'Irish-type' Zn-Pb deposits were classified as being of Sedex affinity (Russell, 1975; Taylor and Andrew, 1978). However, recent workers have suggested that the Irish deposits are more closely related to MVT deposits (Hitzman, 1995b; Shearley *et al.*, 1996). The deposits have also been described as

composite, or hybrid examples between MVT and Sedex end-members (Sangster, 1993), and MVT deposits in a Sedex structural setting (Sangster, 1995). Badham (1975) also suggests that the Irish Zn-Pb deposits, showing characteristics of epigenetic and syngenetic mineralization and related to Carboniferous growth faults (Russell, 1975, 1983), are transitional between the two. Hitzman and Large (1986) also occupy middle ground suggesting that the stratiform deposits are exhalative while the Waulsortian and younger deposits have MVT affinity.

This plethora of genetic classifications has complicated attempts to relate the diverse styles of mineralization within the Irish deposits. For example, the stratiform B Zone and Upper G zone of the Silvermines deposit are classified as being of the Sedex class (Taylor and Andrew, 1978). The stratiform lenses of massive barite, siderite, marcasite, pyrite, and variable amounts of base metal sulphides exhibit sedimentary characteristics (Andrew, 1995). Further, hydrothermal pyrite chimneys, partly surrounded by jasper, are proximal to the Main Fault zone (Larter *et al.*, 1981). An unusually high proportion of the sulphide in the deposit is contained within the discordant footwall zone, interpreted as the main feeder structure (Taylor and Andrew 1978; Taylor, 1984). At the Tynagh deposit, although inferred exhalative activity produced a hematite-chert iron formation, most of the ore sulphide was deposited within fractures and cavities in the host carbonate (Boast *et al.*, 1981a). Ore deposition at the Navan deposit is regarded as involving the superposition of early diagenetic mineralization on synsedimentary sulphides (Andrew and Ashton, 1982, 1985; Ashton *et al.*, 1986). The Ballinalack deposit has been described as being syndiagenetic (Jones and Bradfer, 1982). The Kildare district contains mineralization with classic MVT characteristics. The prospects are hosted in breccia bodies which range from tabular, roughly stratabound (Allenwood North) to pipe-like (Harberton Bridge) or domal (Rickardstown, Allenwood) (Andrew, 1993).

Similar associations of variable styles of base-metal mineralization have also been recognized elsewhere in the world. The McArthur Basin of northern Australia contains the huge HYC deposit, described as being Sedex (Large, 1980), whilst adjacent mineralization at Coxco, Cooley and Ridge is described as being cross-cutting, MVT-like (Walker *et al.*, 1983). Similarly, the Selwyn Basin of the Canadian and Alaskan Cordillera hosts the Sedex deposits of the Macmillan Pass area (Large, 1980; Carne and Cathro, 1982; Lydon *et al.*, 1985), while the adjacent Robb Lake and Gayna River deposits are typically described as being MVT (MacQueen and Thompson, 1978).

Comparable deposits to the Irish Carboniferous Zn-Pb deposits around the world include the Oceana deposit, Tasmania (Huston and Large, 1987); Quidong, New South Wales (McQueen,

1989); Sorby Hills, Western Australia (Hitzman and Large, 1986); Metalline Mining District, Northeastern Washington (Morton, 1993); Reocin, Northern Spain (Barbanson *et al.*, 1983); Gays River (Chi and Savard, 1995) and deposits in the Kanchanaburi Province of Thailand (Diehl and Kern 1981).

The distinctive chemical and mineralogical characteristics of 'Irish-type' carbonate-hosted Zn-Pb deposits include:

- Sphalerite and galena are the principal sulphides
- Barite is present in nearly all the deposits, ranging from a dominant phase to a minor constituent
- Fluorite is absent or very minor
- The principal ore forming fluid(s) were relatively high temperature (>150°C), metal-bearing, sulphur poor, moderately saline, and slightly acidic.
- Deposits display pre- to syn-mineralization dolomitization

The physical characteristics of 'Irish-type' carbonate-hosted Zn-Pb deposits include:

- Mineralization occurs preferentially in the local, stratigraphically lowest, non-argillaceous carbonate unit
- Mineralization occurs along, or immediately adjacent to, normal faults that appear to have formed conduits for hydrothermal fluid transport
- Deposits are stratabound - some display stratiform morphologies.
- Sulphide textures range from finely laminated to replacement of host rock to infill of solution cavities

1.4.3 Genesis of 'Irish-type' Zn-Pb Deposits

In addition to the debate as to their classification, the Irish deposits have been the subject of much discussion as to the origin of the hydrothermal fluids responsible for their formation. Both Sedex and MVT classes of ore deposit are spatially related to sedimentary basins, thus, in view of the similarities between the Irish Carboniferous Zn-Pb deposits and deposits of the Sedex and MVT classes in general, it might be expected that some variant of the basinal formation water model would also be applicable to the Irish-type deposits.

Models for the origin of the Irish-type Zn-Pb deposits must consider:

- Source of mineralizing fluids
- Source of ore forming constituents
- Precipitation mechanisms site of deposition
- Fluid pathways/migration
- Dynamics/mechanisms of fluid flow

One of the major problems in formulating genetic models for the Irish-type ore deposits is to identify those processes which are able to generate metalliferous ore solutions at temperatures of 100-250°C within sedimentary successions or within crystalline rocks of their basement, in the absence of any large magmatic body. Samson and Russell (1987) and Banks and Russell (1992) suggest that fluid temperatures had reached ~250°C at Silvermines and Tynagh. However, there is no spatial relationship between alkali basalt volcanism and mineralization in the Central Midlands. The ore metals must have been derived from the spatially associated sedimentary rocks of the South Munster and Midland Basin, and/or the basement on which these sedimentary rocks lie. The notable absence of fluorite in most of the Irish deposits may also appear to mitigate against the involvement of magmatic fluids.

There is general agreement that the hydrothermal fluids were introduced to depositional sites along normal faulting generated above major, NE trending, reactivated basement structures. Therefore, current discussions on the genesis of Irish carbonate-hosted deposits have centred on the metal source and the mechanism for hydrothermal fluid flow. Four evolutionary models have been proposed for the generation of hydrothermal fluids responsible for Irish Zn-Pb mineralization.

(1) Russell (1978) suggests the operation of a density-driven convective system where Carboniferous seawater penetrated the Lower Palaeozoic basement to depths of 10km or more, sequestering metals during hydrothermal metamorphism (Bischoff *et al.*, 1981), and returning hot mineralized fluids to the near-surface;

(2) Lydon (1986) proposes a fluid-flow system in which the ore-forming solutions are modified saline formation waters occupying the Old Red Sandstone (ORS) of the Midland Basin. In his model a combination of compaction-driven flow, a seal overlying the ORS, and very high heat flow, are responsible for delivering warm, metal rich fluids to the deposit sites;

(3) Williams and Brown (1986) propose that the fluids (and presumably dissolved metals) originated in the Midland Basin, with mineralization driven by episodic dewatering at various stages of sediment compaction. Their dewatering process includes the development of growth faults at the basin margins during extension;

(4) Hitzman and Beaty (1996) present an alternative model of basin fluid expulsion and continental scale migration through regional aquifers (e.g. ORS). In this model the Lower Carboniferous uplift of the Hercynian mountains south of Ireland provided the necessary hydrologic head necessary for the generation of hydrothermal fluids.

1.4.3a Sediment Dewatering/Compaction Models

The expulsion of contemporary connate waters to basin margins and thus to the sites of ore deposition was a widely accepted genetic mechanism for the generation of MVT deposits in North America (Garven and Freeze, 1984; Sangster, 1986). However, a direct comparison with the Irish-type deposits is inappropriate as none of the Irish basins are comparable to the sedimentary basins of the Central USA in size or geological history.

The compaction-driven expulsion model of Lydon (1986) utilises the MVT hydrologic models of Noble (1963), Jackson and Beales (1967), Sharp (1978) and Cathles and Smith (1983). Fluid is derived from sediment compaction within a rapidly filling basin such as the Dublin basin. Compaction drives pore-fluids into regional aquifers, such as the ORS or the basal Carboniferous red beds, where high heat flow promotes metal leaching of the clastic sediments. Episodic expulsion of fluids along basin margin fault zones allows these fluids to rise rapidly up-section and mineralize receptive lithologies.

Sangster (1986) has noted that dewatering commonly takes place some 30-50 Ma after basin initiation, and that this time-lag is an important aspect in the genesis of MVT deposits. This time-lag factor equates to the typical time-span of basin formation and evolution according to the MacKenzie model. In Ireland, thermal sag did not initiate until after the onset of mineralization. Thus, significant basins were not in existence at the time of the main mineralizing event (Andrew, 1991) although the tectonics which initiated basin formation may have been active (Russell, 1986).

Ore-forming fluids must be hot by the time they reach the site of deposition, yet compaction-driven flow would involve a generally cool fluid. However, a well developed basal aquifer, tectonically active regional setting, and a presumed abnormally high heat flow during the Carboniferous, could account for the high temperatures (~250°C) of hydrothermal fluids in the Irish deposits (Lydon, 1986).

Bethke (1985, 1986) and Bethke and Marshak (1990) demonstrate that the volume of fluid stored within basin sediments is not significant enough to carry the required metals to form an ore deposit. The exception is for basins with anomalously high subsidence rates. Further, the thin Carboniferous sequences (<2km) available for local dewatering in Ireland would not contain enough fluid (Andrew, 1992) or be thick enough to provide sufficient compaction to expel the fluids. Hydrologically, the compaction-driven model (Lydon, 1986) is inadequate to explain the relationships observed in Ireland (Hitzman 1995b).

1.4.3b Gravity/Topographic Driven Fluid-Flow

Hitzman and Beaty (1996) propose a foreland basin model (topographically-driven fluid-flow) which is modified after the models of Garven and Freeze (1984), Garven (1985), and Leach and Rowan (1986) for fluid flow in and around North American Mississippi Valley districts.

The model invokes the transport of formation water through the subsurface due to gravity, or topography-driven flow. In Ireland topographic relief is thought to be provided by the Variscan Orogeny. Ziegler (1989) places the thrust front approximately 250km to the south of Ireland during the Lower Carboniferous, with the Munster Basin between the northward advancing Variscan deformation front and the Midlands Basin. Fluids were driven out through the Munster Basin, in the ORS, the basal aquifer, to the complex series of basins and highs to the north. Migrating fluids would be heated either by relatively deep flow paths, or by an anomalously high heat flow caused by extension in the area of present-day Ireland. The model does not explain why the fluids travelled large distances across the Caledonian structural grain and related Lower Carboniferous faulting, without escaping from the proposed aquifer. Neither does it explain the relatively restricted nature of hydrothermal alteration in the supposed aquifer (Mallon, 1997).

This foreland basin model involving northward fluid-flow can, however, account for the early regional dolomitization patterns observed in southeastern Ireland, with limited evidence of a south to north $\delta^{18}O$ isotope gradient, suggesting a southerly source for these dolomitizing fluids (Allan *et al.*, 1992). Lewchuk and Symons (1995) have shown paragenetically that dolomitization

precedes mineralization by ~4Ma during MVT mineralizing events. In Ireland, mineralizing activity commenced isochronously during the late Courceyan Stage, contemporaneous with the onset of extensional tectonism. By the early Arundian, this mineralizing event had ceased across the orefield, approximately 4 My later (Andrew, 1991).

The red beds of the ORS are considered to provide a permeable aquifer and ultimate metal source for northerly migrating basinal fluids (Hitzman, 1995b). Sverjensky (1987) showed that basinal fluids passing through and leaching red-bed sandstones (e.g. ORS) would form Cu(Ag)-rich deposits, whereas fluids leaching a carbonate aquifer would produce Zn-Pb deposits with high Zn/(Zn+Pb) values (Sverjensky, 1984). There is a general zonation throughout Ireland, from Cu-rich deposits in the south, to Zn-rich in the southern Midlands, and Pb-rich in the north. The zonation may represent a dramatic and significant change in aquifers as fluids flowed from south to north (Sangster, 1995). However, many of these Cu-rich deposits are probably not the same age as the Zn-Pb deposits, and appear to be Variscan in age (Johnston *et al.*, 1996). Gortdrum, Aherlow, Mallow and Ballyvergin copper deposits are likely to have formed either by deep burial/metamorphic dewatering of the South Munster Basin, driven by the Variscan deformation, or by volcanic heat driven convection cells in the Asbian (Johnston *et al.*, 1996). Therefore, the apparent Cu zonation may not be real.

However, there is difficulty in modelling fluid temperatures of ≥200°C during fluid movement to the sites of mineralization using a foreland basin model (Hitzman and Beaty, 1996). Fluids must be hot by the time they reach the site of deposition. Numerical modeling by Garven *et al.* (1993) has demonstrated that an elevated geothermal gradient is required to attain the average fluid inclusion temperatures of 80-150°C at the sites of MVT-type mineralization. Therefore, there must have been enhanced hydraulic conductivity as well as either a high geothermal gradient or relatively deep circulation along the flow path.

Distances of proposed fluid flow in Ireland are less than those postulated for several North American MVT districts such as the Upper Mississippi Valley (Lydon, 1986). However, there is much resistance to the concept of fluids moving long distances in response to Variscan uplift. Age-dating of such long-range migrations elsewhere (Symons, 1995), confirms that there is a one-to-one correlation between the age of the MVT ore in a given district and the age of a major orogenic event in the nearest orogen. This correlation provides support for gravity-driven fluid-flow models in the genesis of the MVT ores (summarized in Leach and Sangster, 1993).

The gravity-driven, foreland basin, fluid-flow model presented by Hitzman (1995b) and (Hitzman and Beaty, 1986) has been examined with respect to two major factors: the timing of the Variscan Orogeny, and an apparent conflict with available Pb isotopic data. It has also been questioned whether the system could operate in the geological setting of Ireland (i.e. includes whether a regional topographic gradient existed).

Numerical models (Garven and Freeze, 1984; Hazlett and Garven, 1995) have shown that topographically-driven regional fluid-flow is unlikely in the absence of a regional topographic gradient. The results of preliminary simulations by Hazlett and Garven (1995) indicate that the Variscan Orogeny was not capable of producing a flow volume large enough to have sustained the mineralizing system in the Irish Midlands. A second simulation was constructed in which a gentle (~0.08%) south to north gradient was assigned. This resulted in much greater flow volumes. However, there is little or no evidence for significant emergence of land above sea level during the early Carboniferous, either within the sediment-starved Midland Basin region or in the region between the Midland and Munster Basins (Lewis *et al.*, 1995). The timing of Variscan deformation is not well constrained (Sevastopulo, 1981c). However, the Variscan tectonic front approaching southern Ireland may well have provided uplift of the sediments by the Westphalian (Lewis and Russell, 1995), but only after major ore deposits of the Irish Midlands had formed (Lydon, 1986). Variscan compressional structures post-date Zn-Pb mineralization all over the Irish Midlands (Johnston, 1995b).

1.4.3c Density-Driven Convection

The model first proposed by Russell (1978) calls on free convection as a fluid-flow mechanism. In this model, high heat flow associated with significant Courceyan extension drove convection of seawater through the Carboniferous and Devonian sediments and into the Lower Palaeozoic basement (Russell, 1978, 1986; Boyce *et al.*, 1983a; Samson and Russell, 1987). As the convection cells grow they 'scavenge' metals from increasingly deeper portions of the crust and the low grade metamorphic basement material underlying the deposits. Russell (1978, 1986) considered that these cells eventually reached depths of 10km or more, leading to higher temperatures and more metal-rich fluids through time. These hot, metal-rich fluids move laterally, until they encounter a vertical zone of high permeability where they ascend towards the depositional site, near to the contemporary seafloor.

Russell's model has been examined with respect to basement permeability, the driving mechanisms for convection, and isotopic evidence. Primary objections to the model revolve

around the physical difficulties of circulating large volumes of seawater necessary for the formation of the deposits to great depths through lithified basement rocks. Russell argues that the high heat flow associated with extension would provide enough energy to set up coherent convection cells. However, modern day examples of convection in rift regimes have magmatic centres that drive convection, yet no significant magmatic centres of Courceyan-Arundian age are known in Ireland. Contemporary volcanics do exist on the margins of the Shannon Trough and Dublin Basin, but the exact range in age of the rocks is uncertain (Strogen, 1995).

Basement rocks contain abundant fractures and veins proximal to the deep-seated normal 'feeder' faults (Everett *et al.*, in press), however, there is a lack of significant hydrothermal alteration beneath the deposits associated with these 'feeder' faults (Hitzman and Beaty, 1996). Hydrothermal alteration of the Kentstown granite and Lower Palaeozoic volcanics in the basement adjacent to the Navan deposits is an exception. As is the extensive alteration of the Old Red Sandstone at Silvermines (Mallon, 1997).

Pb isotope ratios provide arguably the strongest evidence of involvement of the Caledonian basement as a source for metals in the overlying Irish-type ore deposits (Russell, 1968). In addition, they suggest a role for E to NE trending basement (Caledonian) structures.

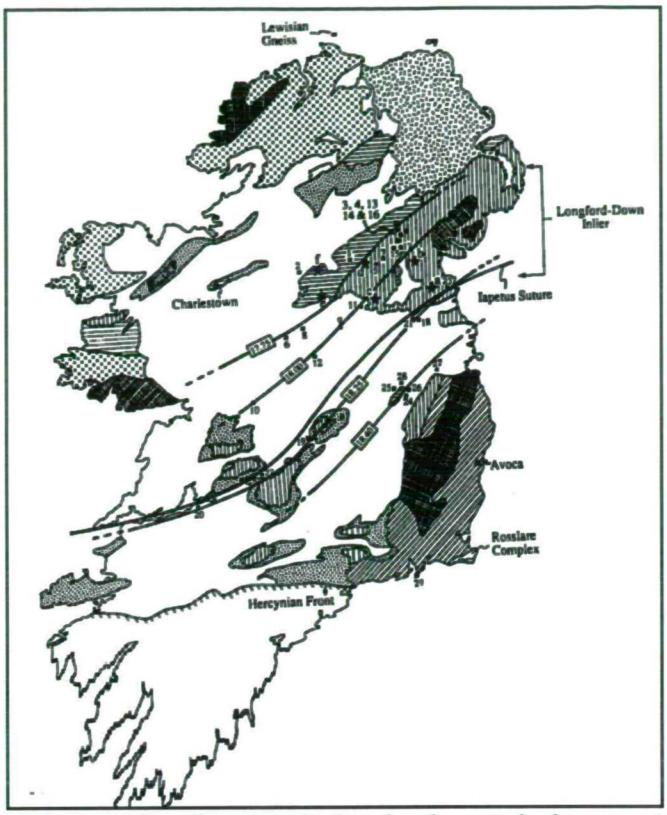


Figure 1.3 Contoured isoplumbs and basement geology of Ireland, reflecting the variation in Pb source across Ireland. (Modified after Dixon *et al.*, 1990).

The Pb isotopes reflect two sources, a less radiogenic mantle source and a more radiogenic crustal source (O'Keefe, 1986; Kennan *et al.*, 1987). The two distinct sources result in two very distinct trends. Firstly, there is a trend in $^{207}Pb/^{204}Pb$ v $^{206}Pb/^{204}Pb$ space. This trend is interpreted as a mixing line between the more radiogenic end member dominant in the southeast, and a less radiogenic end-member dominant in the northwest (Figure 1.3).

Most authors attribute the geographical variation to be a reflection of variation in the Pb source across Ireland, and note the parallelism between the contoured 'isoplumbs' and the Caledonian trend (e.g. Caulfield, 1986; O'Keefe, 1986; LeHuray *et al.*, 1987). This pattern, where trends in Pb isotopic compositions are parallel to Caledonian structures, would be consistent with the movement of mineralizing fluids along or up such structures when they were reactivated during Carboniferous times. This, together with the systematic variation in basement rocks suggests that basement is involved in sourcing Pb in the deposits.

The Pb isotopes are remarkably homogenous across the Irish Carboniferous. In addition to the Irish deposits, other carbonate-hosted deposits also have distinctively homogenous, although not necessarily uniform, lead isotope characteristics (e.g. the Alpine, Silesian and Pine Point districts) that contrast with the inhomogeneous and radiogenic characteristics of galena mineralization in the Mississippi Valley (Heyl, 1983).

Additional lead isotope data collected by Hitzman *et al.* (1992) indicate that the isoplumbs are only northeast trending in the north and west Midlands. The isoplumb pattern resulting from the additional data is permissive of the northward flow of fluids with $^{206}Pb/^{204}Pb$ values between 18.20 and 18.30 which locally acquired less radiogenic lead from the basement or basement-derived sediment (Old Red Sandstone or basal Carboniferous red beds) in the northwestern

Midlands and progressively included more radiogenic lead from Leinster Granite detritus along the edge of the Leinster Massif.

1.5 SIGNIFICANCE OF RESEARCH - TESTING THE HYPOTHESES

This thesis reports the results of a study designed to assess the chemical, isotopic and thermal characteristics of fluids associated with the development of economic mineralization and alteration at Lisheen and, to a lesser extent, Galmoy. These data are compared with similar data obtained from weakly mineralized or essentially barren environments elsewhere in the Rathdowney Trend.

As well as providing limiting constraints on mineralizing processes, these data will enable an assessment of the alternative proposed genetic models for Irish-type Zn-Pb mineralization. Increased knowledge of fluid flow characteristics throughout the Rathdowney Trend may also aid the discovery of further deposits within the trend and elsewhere within the Irish Midlands.

The research impacts on the origin of the ore forming fluids, but does not directly test one or other of the main two competing models: (1) that the fluids responsible for mineralization are deeply convected Carboniferous seawater which has interacted significantly with Lower Palaeozoic basement; or (2) are basinal fluids, expelled during Variscan tectonism, which have migrated laterally within a regional aquifer system (e.g. Old Red Sandstone).

1.5.1 Research Methodology

Sampling locations within the Rathdowney Trend (Figure 1.2) have been selected to provide a wide coverage of both economic mineralization (Lisheen and Galmoy), weakly mineralized prospects and unmineralized areas (Derrykearn, Durrow, Holycross, and Rathdowney East). A large sample suite spanning all localities has been chosen from well-constrained subsurface diamond drillcore. The suite represents a variety of Lower Carboniferous lithologies, alteration phenomena, massive and vein sulphides covering as wide a temporal and spatial distribution as possible. These samples form the basis for petrographic and geochemical analyses.

1.5.1a Cathodoluminescence and Reflected Light Microscopy

Polished thin sections were studied systematically through transmitted light microscopy and cathodoluminescence (CL). CL has many applications in the investigation of mineralization, the nature of mineralizing fluids and fluid-rock interactions (Marshall, 1988). CL is particularly suitable for revealing complex growth zones in calcite and dolomite (ore-associated gangue) cements. Correlation of these zones allows evaluation of regional diagenetic/epigenetic events and offers a framework in which to interpret large and small scale fluid flow systems.

Preliminary studies by Ebers and Kopp (1979) showed that CL petrography has possible exploration applications in MVT deposits. Differentiation between brecciated and dolomitized areas adjacent to an orebody and similar breccias which are not mineralized may be possible. Additional studies of CL cement stratigraphies have been used to document periods of extensive sulphide mineralization, dolomitization, carbonate cementation, and porosity modification that have affected carbonate rocks, sometimes of different facies and stratigraphic units, at widely scattered localities e.g. Southeast Missouri (Gregg, 1985; Voss and Hagni, 1985; Rowan, 1987), Central Appalachians (Dorobek, 1987), Illinois and Missouri (Kaufman *et al.*, 1988), Navan, Ireland (Braithwaite and Rizzi, 1997), Lisheen, Ireland (Redmond, 1997) and Tennessee (Montañez *et al.*, 1988).

The presence of regional and fault-related dolomites within the Rathdowney Trend is adopted as an empirical exploration guide. However, it is unclear whether the dolomitizing fluids can be genetically linked to the ore-forming fluids. Allan *et al.* (1992) and Hitzman (1995b) propose regional northward fluid flow of basinal brines for regional epigenetic replacement dolomites in the Irish Midlands. However, the lack of a mechanism to move sufficient volumes of fluid through a limestone has been one of the principal objections to epigenetic dolomitization models presented in the past (Morrow, 1982). Alternatively, an early diagenetic model involving seawater is proposed for this extensive type of regional dolomite by Land (1985) and Morrow (1990).

The aim of the CL study was to establish a sequence of alteration events in and around the deposits and prospects. CL properties of ore-associated dolomite at Lisheen were compared to all other deposits and prospects within the Trend. To date, there have been no published attempts to compare CL microstratigraphies in dolomite cements associated with base-metal mineralization, between deposits or in non-mineralized areas in the Rathdowney Trend.

Ore petrography was based on the study of polished blocks by reflected light microscopy, both in air and oil. Ore emplacement mechanisms, relative time relationships and the depositional

environment in which mineralization processes occurred, can be interpreted from textural evidence. The determination of ore-gangue time relationships are critical, and impact on the interpretation of isotopic and fluid inclusion analyses of pre, syn, late, and post-ore stage mineralizing and gangue phases.

Detailed ore-gangue petrographic studies have been carried out at a number of deposits in the Irish Midlands and include the following: Navan (Kucha and Wieczorek, 1984; Anderson, 1990; Ashton *et al.*, 1992; Rizzi, 1993; Anderson *et al.*, in press), Silvermines (Boyce *et al.*, 1983b; Banks, 1986; Kucha, 1989), Lisheen (Beaty *et al.*, 1991; Hitzman *et al.*, 1992; Shearley *et al.*, 1996; Redmond, 1997), Tynagh (Boast *et al.*, 1981a), Tatestown (Andrew and Poustie, 1986), Moyvoughly (Poustie and Kucha, 1986), Ballinalack (Jones and Brand, 1986) and Ballyvergin (Andrew, 1986b).

Expected Results- contribution to research objectives

If the regional dolomite can be shown to have a unique set of correlatable CL properties and geochemical characteristics of a late epigenetic dolomite formed by warm fluid(s) (Sibley and Gregg, 1987) then dolomitization by regional homogeneous fluid(s) would be indicated. However, if a variety of petrographic textures with variable geochemical signatures are observed that show no spatial or temporal trends, then it can be inferred that at least some of the regional dolomite is either early diagenetic and has been later modified by basinal fluid (Gregg, pers. comm., 1996), or that heterogeneous local effects control dolomite texture and CL. Alternatively, localized hydrological systems that are relatively isolated from one another (Russell, 1986), could be invoked.

A detailed mineral paragenesis can be established following transmitted light microscopy, CL, and reflected light microscopy of carbonate and ore sulphide phases respectively. These time relationships form the basic framework for looking at fluid chemistry, temperature, and rock geochemical evolution.

1.5.1b Electron Microprobe Analysis

Following petrographic analysis, the mineral chemistry of both carbonates and sulphides can be determined by this method. Major and trace element geochemistry will help define the nature of the mineralizing fluid(s) in the Rathdowney Trend. Using trace element distributions, particularly Fe and Mn, fluid sources and flow pathways can be determined, providing valuable tools for mineral exploration, particularly if large regions of carbonate rock are altered by mineralizing

fluids. In sulphides, trace element distributions particularly Fe, Cd in sphalerite, and As, Ni, Co, in iron sulphides may also reflect the nature of the metal-bearing fluid(s).

The level of major and trace element homogeneity (or heterogeneity) in crystals of the same generation can reflect the level of thermodynamic equilibrium that prevailed during precipitation of dolomites (Veizer, 1983). Bulk solution equilibrium (producing homogeneous cement) usually indicates slow fluid movements and direct carbonate precipitation or a system with high water-to-rock ratios (W/R). Bulk solution disequilibrium (producing heterogeneous cement) reflects conditions where thermodynamic equilibrium is not reached because surface reactions are faster than diffusion of chemical species (Veizer, 1983).

Reconnaissance studies of trace element distributions in the Bonneterre Dolomite in Southeast Missouri indicate distinct regional trends in Fe, Mn and Sr (Viets *et al.*, 1983; Buelter and Guillemette, 1988; Ramage, 1984; Ramage and Holland, 1984; Gregg and Shelton 1989). This pattern was interpreted to result from partitioning of the metals into dolomite as the fluid migrated upward from the Lamotte Sandstone. An alternative interpretation for these data is that changing depositional environments upward in the section resulted in increasingly more oxidizing conditions, and therefore less Fe^{2+} and Mn^{2+} available for incorporation into the dolomite. The Fe/Mn ratio in carbonates is a strong function of oxygen fugacity, providing a potentially useful tool for assessing spatial and temporal variations in this important parameter.

Although the major mineral assemblages of carbonate-hosted ore deposits are both simple and relatively uniform, there is commonly evidence for a zonal distribution in terms of minor elements. The importance of Ni as a minor element in sulphides of MVT mineralization is highlighted by Hagni (1976) and Hagni and Trancynger, (1977).

To date, there have been few published attempts to study trace element distributions in regionally dolomitized Waulsortian facies and fault-related dolomites in the Irish Midlands. A study of the lithogeochemical environment at Tynagh (Russell, 1975), reported elevated values of Mn around the deposit. An Irish base-metals EEC project investigated the distribution of 12 elements (Cu, Pb, Zn, Mn, Fe, As, Ni, Co, Ba, Sr, Mg and Hg) in drillcore from Tynagh, Tatestown, Gortdrum and Moate, the results of which are unavailable.

Expected Results- contribution to research objectives

Determination of trace and minor element distributions throughout the trend will be used in order to constrain heterogeneity in regional fluid flow. Additionally, covariation of these data with

isotope compositions are useful in examining the extent of, and, variation in water-rock interaction along fluid flow pathways (see below).

1.5.1c Stable Isotope Analysis (Sulphur)

Isotope data provide important constraints within which genetic models must be bound. Using stable isotope analyses it is possible to constrain the sources of components (sulphur, carbon, and water) involved in mineralizing systems. Comparison of data obtained from Lisheen and Galmoy with weakly mineralized or essentially barren environments elsewhere in the Rathdowney Trend, will help identify the key isotopic characteristics associated with the development of economic mineralization. These data will also enable an assessment of the use of isotopic measurements as an exploration tool.

Sulphur isotope studies on sulphide and sulphate minerals have been carried out at a number of Irish-type Zn-Pb deposits in order to understand the origins of the sulphur. Data are reported in the following references: Navan (Anderson *et al.*, 1989, in press; Anderson, 1990; Boyce *et al.*, 1993, 1994), Silvermines (Greig *et al.*, 1971; Coomer and Robinson, 1976; Boyce *et al.*, 1983b), Tynagh (Boast *et al.*, 1981a), Ballinalack, Keel, Moyvoughly and Tatestown (Caulfield *et al.*, 1986; Caulfield, 1986), Abbeytown (Recio *et al.*, 1988), Harberton Bridge (Gallagher *et al.*, 1992), Lisheen (Eyre *et al.*, 1996).

The major objectives of the sulphur isotope analyses were to use $\delta^{34}S$ to determine the source(s) of sulphur in the Rathdowney Trend deposits and prospects; to evaluate the relative importance of biogenic, abiogenic and mixing processes in mineralization, particularly at Lisheen and Galmoy; and to compare $\delta^{34}S$ of sulphides at Lisheen (in three spatial dimensions, plus time via mineral paragenesis) and Galmoy, with regional samples from the Rathdowney Trend.

Expected Results - contribution to the objectives

Isotopically light sulphur is indicative of biogenic activity, whilst heavier sulphur values suggest a deeper hydrothermal component. Variations in $\delta^{34}S$ both at Lisheen and Galmoy, and in prospects in the Rathdowney Trend, will indicate the relative importance of such sulphur sources and identify the components critical to the formation of economic mineralization.

1.5.1d Stable Isotope Analysis (Carbon, Oxygen)

Carbon and oxygen isotopes are useful for establishing sources of carbon, for estimating parental fluid $\delta^{18}O$, evaluating the nature and extent of fluid-rock interaction, and possibly temperature(s) of formation of hydrothermal mineral assemblages.

To date, few carbonate isotope studies have been published, even though most Irish-type deposits are hosted by carbonates. Ore-related carbonate petrography coupled with a stable carbon and oxygen isotope study was pioneered by Boast *et al.* (1981a) at Tynagh, but since then only one detailed study has been published, that at Harberton Bridge (Gallagher *et al.*, 1992), although work has also been done at Abbeytown (Recio *et al.*, 1988) and Keel (Slowey *et al.*, 1995). Preliminary data exist for regional dolomites in southeastern Ireland (Allan *et al.*, 1992; Hitzman and Beaty, 1996; Hitzman *et al.*, 1998). Isotopic studies on the basement have been published by Dixon and Rye (1991) and Everett *et al.* (1996).

The major objectives of carbonate isotope analyses were to use $\delta^{18}O$ from hydrothermal carbonates to calculate the oxygen isotopic composition of mineralizing fluid(s) as an indicator of fluid source and, in combination with $\delta^{13}C$, to evaluate temporal and spatial variations in fluid-rock interaction within mineral deposits and prospects.

Expected Results - contribution to the objectives

Relatively high $\delta^{18}O$ (fluid) indicates a fluid which has undergone extensive interaction with rocks at elevated temperatures, lower values (close to or below 0 ‰) are indicative of surface-derived water, with limited interaction. Variations in this parameter (plus $\delta^{13}C$) in space and time may be used to constrain the evolution of the mineralizing system.

1.5.1e Radiogenic Isotope Analysis (Lead)

Lead isotope ratios provide arguably the strongest evidence for involvement of the Caledonian basement as a source for metals in the overlying Irish-type ore deposits (see section 1.4.3). However, there is evidence that the systematic trend of the isoplumbs (e.g., LeHuray *et al.*, 1987) does not extend down to the Rathdowney Trend (Hitzman *et al.*, 1992; Hitzman, 1995b). Therefore, further analysis of Pb isotopic ratios in galenas from both Lisheen and Galmoy will confirm whether the significant variance in lead source established throughout the north and central Midlands extends into the south Midlands.

An extensive body of lead isotope data are available for the deposits in Central Ireland, and can be found in the following references: Greig *et al.* (1971), Boast et al. (1981b), Caulfield (1986), Caulfield *et al.* (1986), O'Keefe (1986), LeHuray *et al.* (1987). In addition there are detailed studies of Navan (Mills *et al.* 1987), and Harberton Bridge (Gallagher *et al.* 1992).

The principal objective of the lead isotope analyses is to use lead isotopic ratios to constrain sources of lead, and to identify potential basement fluid-rock interactions in the southern Irish Midlands.

Expected Results - contribution to the objectives

The analysis of Pb isotopic ratios in galenas will provide a relatively straightforward test of a local basement contribution to the mineralized system. $^{206}Pb/^{204}Pb$ isotope ratios of 18.20-18.30 are suggested from studies of the Lower Palaeozoic basement in the area. In addition, Old Red Sandstone aquifer studies indicate a higher ratio around 18.35-18.50, offering a potential test of alternative genetic models.

1.5.1f Fluid Inclusion Microthermometry

Fluid inclusion microthermometry of pre-, syn-, late and post-ore phases can be used to characterize the evolution of the hydrothermal system and to determine if one or several fluids were involved. The temperature of ore formation, salinity of fluid entrapped and potential mixing of mineralizing fluids can be assessed by this analytical technique.

The major objective of the fluid inclusion study is to determine the chemical and thermal characteristics responsible for ore-stage mineralization and dolomitization within the Trend. Data are compared with that already obtained for Silvermines (Samson and Russell, 1987), Tynagh (Banks and Russell, 1992), Abbeytown (Hitzman, 1986) and new data from Navan and Keel (Everett *et al.*, 1997).

Expected Results - contribution to the objectives

Fluid inclusion data from Silvermines (Samson and Russell, 1987) and Tynagh (Banks and Russell, 1992), are interpreted as reflecting fluid mixing of a high temperature, moderate salinity fluid and a low temperature, high salinity fluid. The presence of these fluids both at Lisheen and Galmoy would suggest they are critical to the ore-forming process, and would support a fluid mixing model.

Spatial variations in temperature and chemical composition can provide clues to pathways of fluid migration, particularly if two distinct mineralizing fluids are inferred .

1.6 SUMMARY

The chemical, isotopic, and thermal characteristics of mineralizing fluid(s) in the Rathdowney Trend are defined with the outlined multidisciplinary study. Spatial and temporal variations are compared between sampling localities. The data impact on the proposed models for the generation of ore forming fluids, but do not test the hypotheses directly. The well constrained data generated can provide tools for more effective exploration in the southern Irish Midlands.

CHAPTER 2: GEOLOGY

CHAPTER 2: GEOLOGY

2.1 INTRODUCTION

This chapter provides a geological framework in which the Irish-type Zn-Pb deposits can be placed and includes a brief overview of the stratigraphy, basin evolution and tectonic history of Ireland. Particular attention is given to the Lower Carboniferous (Courceyan Stage) of the Irish Midlands, which hosts virtually all of the major Irish-type Zn-Pb deposits. The geology of the Rathdowney Trend deposits and prospects is outlined in detail, covering lithostratigraphy, structure, dolomitization and mineralization.

The Lower Carboniferous sequence consists of the clastic Munster basin to the south with a northward thinning carbonate sequence which diachronously overlies Middle and Upper Devonian to basal Carboniferous Red Bed siliciclastics. The sequence reflects a progressive northward transgression and subsidence during the Lower Carboniferous. These Upper Palaeozoic sediments unconformably overlie the Caledonian 'basement' which comprises Lower Palaeozoic and Dalradian volcano-sedimentary sequences of varying metamorphic grade (Andrew, 1991,1993). Many distinguishing features of the Carboniferous geology result directly from influences imposed by this underlying 'basement'.

2.2 PRE-CALEDONIAN BASEMENT

Recognition of the pre-Caledonian basement has depended largely upon evidence of overprinting, for the contacts which can be seen between basement and Caledonian cover rocks are all tectonic in origin (Phillips *et al.*, 1976). In the Rosslare complex, southeast Co. Wexford, an angular unconformity is inferred between a Caledonian cover of Cambrian sediments and a basement of metasediments, amphibolite facies gneisses, in which several orogenic cycles have been identified (Winchester and Max, 1982; O'Connor *et al.*, 1988; Max and Roddick, 1989).

Precambrian crystalline basement beneath Palaeozoic cover rocks has been interpreted from seismic refraction studies across the country (Jacob *et al.*, 1985; Lowe, 1988; Lowe and Jacob, 1989), and from a limited number of radiometric age determinations and neodymium model ages in the range 1900 to 1000Ma (Sanders *et al.*, 1987; O'Connor *et al.*, 1988; Max and Roddick, 1989; Menuge and Daly, 1990; Muir *et al.*, 1994). Four quite different zones of basement have been recognized using these methods. Pre-Caledonian (Grampian) amphibolite facies gneisses

occur at Inishtrahull (Laxfordian c.1700Ma) and in North Mayo (Grenville, c.1000Ma) (Van Breeman *et al.*, 1978). Pre-Caledonian basement rock consisting of high grade metasediments crop out in the Ox Mountains and Lough Derg inlier (Phillips *et al.*, 1975; Sanders *et al.*, 1987). These basement rocks are overlain by late Precambrian and Lower Palaeozoic rocks which record the opening and closing of the Iapetus Ocean (Phillips and Sevastopulo, 1986).

2.3 CALEDONIAN OROGENY

In the late Precambrian to Mid-Devonian interval, tectonic events throughout the British Isles were controlled by the development and subsequent closure of the Iapetus Ocean (Dewey, 1969; Phillips *et al.*, 1976; Barker and Gayer, 1985). Consolidation of a landmass in the area now occupied by Ireland occurred during the Caledonian Orogeny. The orogeny records the sinistral-oblique collision of the Laurentian-Greenland (North American) and Baltica-Fennosarmatian (European) plates in the Upper Silurian through Lower Devonian. The collision marked the closure of the Iapetus Ocean and formation of the Laurussian Megacontinent (Ziegler, 1988).

Ireland lies at the southern end of this Himalayan type collision zone, termed the Iapetus Suture Zone (Phillips *et al.*, 1976) (Figure 1.3), immediately north of the intersection of this orogeny with the Proto-Tethys Ocean (Soper and Hutton, 1984). The Iapetus Suture Zone was recognised initially by an abrupt change of structural style in the Lower Palaeozoic rocks on either side of a north easterly line extending through the Solway Firth and Shannon Estuary. The suture zone extends through the vicinities of Navan and Silvermines, (Phillips *et al.*, 1976) and divides Ireland into two crustal blocks northwest and southeast Ireland, which have quite different geological histories prior to the Silurian (Phillips and Sevastopulo, 1986).

2.4 ORTHOTECTONIC AND PARATECTONIC CALEDONIDES

The Caledonides exhibit two types of structural zone (Anderton *et al.*, 1992): (1) the orthotectonic zone, displaying intense folding and low to high grade metamorphism (Phillips, 1981); (2) the paratectonic zone, displaying more simple folds and only low grades of metamorphism (Holland, 1981).

2.4.1 Orthotectonic Belt

The orthotectonic belt of northwest Ireland involved the deposition and subsequent deformation of the Dalradian Supergroup (dominantly clastic sediments). The stratigraphy of the Dalradian

Supergroup is summarized in Harris and Pitcher (1975). The high grade metamorphism and complex deformation in late Cambrian to mid-Ordovician times (Barker and Gayer, 1985) was entirely due to the early Ordovician Grampian Orogeny, with emplacement of basic and ultra basic intrusions and eruptive volcanism. The main deformation event was completed by the end of the Ordovician (Phillips, 1981).

2.4.2 Paratectonic Belt

During the Precambrian the paratectonic belt of southeast Ireland (Holland, 1981) consisted of a thick pile of marine sediments, intercalated with lava flows and extensive pyroclastics produced during long periods of Late Precambrian volcanic activity. The Celtic Orogeny at the end of the Precambrian affected a small area of rocks in southeast Ireland and was accompanied by plutonism and low to high grade metamorphism. With the exception of these small areas, only very low grade rocks are found in the south and the complexity of deformation is much less than that observed in the north (Anderton *et al.*, 1992).

The Lower Palaeozoic succession of southeast Ireland (Brück *et al.*, 1979) extends from Lower Cambrian to late Silurian (Ludlow). A widespread turbiditic deposit, the Bray Group (Van Lunsen and Max, 1975; Brück and Reeves, 1976; Tietzsch-Tyler and Phillips, 1989; O'Byrne, 1990) of probable Cambrian age, is extensively developed throughout Leinster. Younger (?) Ribband Group rocks comprise deep basinal shales (Kennan and Kennedy, 1983). Silurian rocks throughout southern Ireland are quartz rich siltstones and greywackes, with minor volcanics preserved in Dingle (Johnston, 1995a).

Southern Ireland experienced widespread volcanism in the upper Ordovician (Stillman and Williams, 1978; Brück *et al.*, 1979) associated with subduction of the oceanic crust beneath Laurentia. Volcanic activity developed in the mid-Ordovician (Llanvirn) and eventually ended in the mid-Silurian (Late Wenlock) and was most pronounced in the Leinster Basin, an area subject to rapid subsidence (Phillips and Sevastopulo, 1986). Arc volcanism (andesite-rhyolite) was most extensive in a belt extending from Arklow to Waterford and westwards to the Dingle Peninsula, whilst tholeiitic and calc-alkaline basalts erupted to form oceanic islands in the northern part of the Leinster Zone (Stillman and Williams, 1978; Stillman, 1982). Emplacement of large scale plutons was not associated with this magmatism and accompanying deformation (Anderton *et al.*, 1992). The deformational history of the rocks in the southeast is discussed by Crimes and Dhonau (1967); Crimes and Crossley (1968); Brenchley and Treagus (1970); Gardiner (1970); Gardiner and Robinson (1970); Brindley (1973); Brück (1973); Van Lunsen and Max (1975);

Brück and Reeves (1976); Brück *et al.*, (1978); Shannon (1978, 1979); and Cooper and Brück (1983).

2.5 UPPER PALAEOZOIC

2.5.1 Late Caledonian Deformation

Late Silurian to early Devonian times witnessed the end of an important chapter in the evolution of the British Isles related to the collision between the North American and European plates (Ziegler, 1988). During this time, the whole of Ireland was affected by Caledonian deformation involving metamorphism, plutonism, and widespread fracturing of the pre-Devonian basement (Phillips and Sevastopulo, 1986). At the end of the Caledonian deformation during the late Silurian to early Devonian, the shortening direction changed from north to northwest (Johnston, 1995b). Finally, Acadian deformation in the Mid-Devonian (c.395Ma) affected Lower Palaeozoic rocks either side of the suture zone and probably represents the termination of convergence of the plates (Soper *et al.*, 1987). An angular unconformity exposed between folded Lower Palaeozoic rocks and clastic rocks of uppermost Devonian or Lower Carboniferous age marks the end of the collision (Phillips and Holland, 1981).

The suture zone in the British Isles comprises a complex series of terranes bounded by NE-SW strike-slip faults on which sinistral movements of the order of 100's of kilometres took place in the late Silurian to Mid-Devonian (Gibbons and Gayer 1985; Hutton, 1987). In NW Ireland, sinistral shear zones were the dominant features and controlled the emplacement of the Donegal granites at about 400Ma (Hutton, 1982). The late to post-orogenic Leinster Granite Batholith, Newry Granodiorite and Galway Granite were also emplaced at this time (Brindley, 1969; Kennan, 1979; Plant, 1986) and likewise show some evidence of sinistral shear (Brück and Cooper, 1983; Murphy, 1989; McCaffrey, 1992, 1994).

These characteristic late Caledonian granite intrusions are widespread and found either side of the 'suture' in both the orthotectonic and paratectonic Caledonides (Plant, 1986). The granitoid complexes lie close to older (Ordovician) volcanic arcs and may have inherited feeder systems from the arcs (Phillips and Sevastopulo, 1986).

2.5.2 Lower, Middle and Upper Devonian

Following the Late Middle-Devonian (Acadian) deformation, important basins in the southwest were re-established and extensive continental clastic sedimentation resumed in the Upper Devonian (Hitzman and Large, 1986). Alluvial and fluvial red-bed siliclastics of Lower and Middle Devonian age were deposited in fault-controlled continental basins in the southwest, northwest and northeast of the country (Graham, 1983).

Sedimentation centred principally on the NE-SW trending Munster Basin, a post-orogenic intra-cratonic half-graben (Gardiner and MacCarthy, 1981) developed in response to north-south crustal tension (Naylor and Jones, 1967; Naylor *et al.*, 1981). The basin contains in excess of 7km of dominantly non-marine Devonian sediments, with the oldest known sediments being of Late Middle-Devonian age (Clayton and Graham, 1974; Russell, 1978; Higgs and Russell, 1981). The basin was bounded to the north by the Killarney-Mallow Fault which controlled sedimentation (Gardiner and MacCarthy, 1981; Price, 1988; Price and Todd, 1988; Williams *et al.*, 1989). Red, grey and green conglomerates, sandstones, siltstones and shales assigned to the Old Red Sandstone (ORS) were deposited (Gardiner and MacCarthy, 1981). The petrography of the ORS has been summarized by MacCarthy (1995). The sandstones which comprise the bulk of the ORS are usually fine to medium grained and contain from 40 to 90% quartz. The vast majority of the sandstones are quartz arenites, sublitharenites or subarkoses. The sandstones contain minor amounts of potassium and plagioclase feldspars, volcanic fragments, rock fragments, micas, chert and heavy minerals including zircon, tourmaline and apatite. The bulk of the quartz is thought to have been derived from high grade metamorphic or plutonic igneous sources. Feldspars account for less than about 5% of the rock. The sandstones are cemented by a matrix of microcrystalline sericite with variable amounts of quartz, clay, chlorite and calcite. Where sediments are red the grains are coated with haematite.

A second listric fault developed towards the end of the Devonian (Kenmare-Cork Fault) within the Munster Basin. This played a major role in controlling the deposition of some 2.5km of marine sediments during the late Devonian and Carboniferous, and separated the Munster Basin into two parts (MacCarthy, 1995). To the north of the fault, a relatively stable platform developed, while to the south lay an area of relatively deep water sedimentation known as the South Munster Basin (MacCarthy, 1995).

2.5.3 Lower Carboniferous (Courceyan Stage)

Following the earliest Devonian eustatic low stand of sea level, sea levels rose cyclically during the early Carboniferous (Vail *et al.*, 1977). A northerly directed marine transgression initiated during the early Courceyan stage ensued, resulting in the deposition of diachronous, carbonate-dominated, shallow marine sediments throughout the Irish Midlands (Clayton and Higgs, 1978). The Courceyan stratigraphic succession indicates a north to south transition from littoral and sub-littoral facies through offshore carbonate sands with intercalated argillaceous beds, to deeper water Waulsortian facies (Phillips and Sevastopulo, 1986).

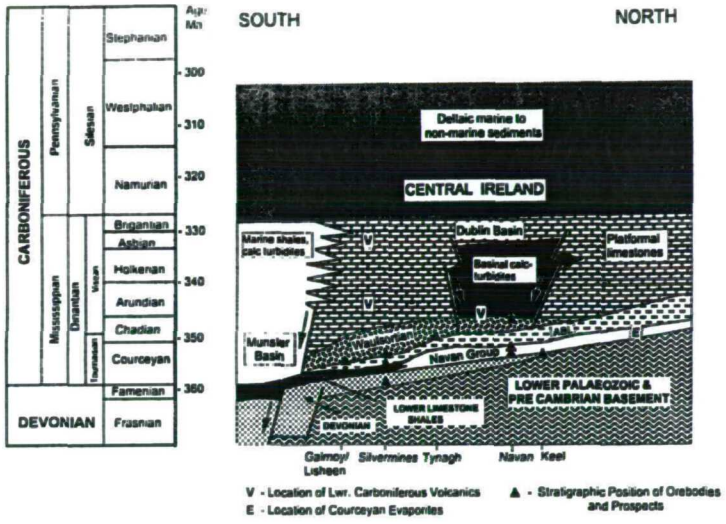


Figure 2.1 Geological column and schematic section showing Lower Carboniferous strata and facies relationships of the Irish Midlands (after Hitzman, 1995a; Andrew, 1986)

This marine transgression continued throughout the Courceyan and Chadian (Figure 2.1) with the development of a complex series of basins defined by inherited Caledonian basement structural zones (Andrew, 1993). Many features of the Lower Carboniferous geology of Ireland result directly from influences imposed by this basement (Andrew, 1993; Johnston, 1995a; Johnston *et al.*, 1996).

The Irish Zn-Pb deposits are hosted primarily by Lower Carboniferous rocks, almost all of Courceyan and Chadian age, although in a few places (e.g. Harberton Bridge) hydrothermal alteration and sulphides extend up into Arundian rocks (Johnston *et al.*, 1996). Courceyan-hosted mineralization is dominated by the Navan and Argillaceous Bioclastic Limestone (ABL or ABC) Groups (Andrew and Ashton, 1982; Philcox, 1984; Andrew, 1986b). A diagrammatic representation of the Courceyan stratigraphy of the Irish Midlands is found in Andrew (1986c).

2.5.3a Regional Stratigraphic Setting

Stratigraphic and palaeogeographical settings of the Lower Carboniferous sequences are described in detail by Sevastopulo (1981a, 1982), Philcox (1984), Strogen and Somerville (1984), Somerville and Jones (1985), Andrew (1986c), Phillips and Sevastopulo (1986), Jones *et al.* (1988), Naylor *et al.* (1989), Strogen and Jones (1990) and Somerville *et al.* (1992).

Phillips and Sevastopulo (1986) have subdivided the Irish Courceyan into four provinces based on differences in the local succession: the South Munster Basin; the Limerick Province; the Midlands Province; and the North West Province (mainly post-Courceyan).

The south Munster Basin (Naylor *et al.*, 1989) is filled with a carbonate-poor, clastic-dominated succession. Fluviatile red-beds are overlain by marine sandstones and shales. Clastic deposition continued throughout the Courceyan, with starvation of the basin later in the early Carboniferous.

Carbonate-dominated units of the Limerick Province are widespread and laterally persistent (Philcox, 1984; Somerville *et al.*, 1992) and are host to the Silvermines, Lisheen, Galmoy, Courtbrown and Tynagh deposits. Transgression occurred during the early Courceyan. The base of the sequence comprises non-marine red beds and marginal marine sandstones and shales. Overlying these are calcareous shales (Ringmoylan Shale Formation) which pass up into muddy bioclastic limestones (Ballymartin and Ballysteen Limestone Formations), these are in turn overlain by Waulsortian Limestones (Lees, 1964; Lees and Miller, 1985). Overlying the Waulsortian are either shelf, or in some areas basinal carbonates.

It should be noted that the Ballymartin Formation of Somerville and Jones (1985) is the equivalent of the Lower Ballysteen of Philcox (1984) and that the Lower Ballysteen of Somerville and Jones (1985) is equivalent to the Middle Ballysteen of Philcox (1984).

In the Midlands Province, transgression took place later, during the mid-Courceyan (Sevastopulo, 1981a; Phillips and Sevastopulo, 1986). A formal stratigraphy for the region was erected by Strogen and Jones (1990). The region is characterized by lateral facies variation, and has been divided into sub-provinces by Philcox (1984) and Strogen and Somerville (1984). A widespread Basal Red Bed lithology is overlain by a series of shallow-water micritic and oolitic limestones, collectively referred to as the Navan Group (temporally equivalent to the Ballymartin Limestone of the Limerick Province). At Navan Mine these are informally termed the Pale Beds, and these

are host to the Navan and nearby Tatestown deposits. The Pale Beds are overlain by the Argillaceous Bioclastic Limestones of the Moathill and Slane Castle Formations (lithologically equivalent to the Ballysteen Limestone). Waulsortian micrites of the Feltrim Formation overlie the Slane Castle Formation and are host to sulphides at Ballinalack and Garrycam. Overlying the Waulsortian micrites is a sequence of basinal graded calcarenites and calcisiltites of the Lucan Formation, widely referred to as the Upper Dark Limestones.

In the North West Province, much of the lower part of the Carboniferous section is made up of very shallow water sediments, lithologically equivalent to the Pale Beds, with a slightly later Courceyan to Chadian transgression.

2.5.3b Basal Red Beds

The basal portion of the shelf succession contains coarse to medium grained clastic rocks, similar in provenance to the ORS (Hitzman and Large, 1986). This clastic lithofacies, termed Basal Red Beds, thins and youngs northward (Andrew and Ashton, 1985).

These basal beds are overlain by 50-100m thick carbonate rich shales, siliciclastic sediments and argillaceous carbonates in the southern portion of Ireland (Lower Limestone Shale - informal designation (Philcox, 1984); Mellon House, Ringmoylan and Ballyvergin Formations) and mixed peritidal, carbonate, siliciclastic and locally evaporitic sediments in Central Ireland (Navan Group - informal designation, or Mixed Beds (Philcox, 1984)).

2.5.3c Navan Group (Mixed Beds)

The Navan Group is developed over some 8200 square kilometres of the east-central Midlands and thins from 400m at its maximum to 50m at its northern and southern extremities (Andrew, 1991, 1993). The group is typically 150-200m thick and generally consists of a basal, thin, upward fining terrigenous sequence that passes upward with increasing carbonate and argillite content, into pale oncolithic and birds eye micrites (Andrew, 1991, 1993). These are overlain by shallow water, high energy, calcareous sandstones, sandy and bioclastic grainstones and oolites (Andrew, 1991, 1993). The uppermost part of the Navan Group comprises mildly argillaceous calcarenites, shales and calcareous sandstones indicative of increasing water depths; the Shaley Pales of Philcox (1984). In the southern part of the country the Navan Group is poorly developed and is represented by 30-50m of argillaceous, skeletal calcareous shales and siltstones with thin oolite and sandstone shoals (Andrew, 1991, 1993). Lateral facies variations within the Navan

Group appear to have resulted from local fluctuations in shorelines and the influence of sedimentary barriers (Andrew, 1992) rather than syn-sedimentary tectonism.

The Navan Group contains the world class Tara Mine at Navan and prospects at Keel, Moyvoughly, Oldcastle and Tatestown. The Navan orebody is four times the size of the largest known Waulsortian hosted deposit, Lisheen (Hitzman *et al.*, 1992; Shearley *et al.*, 1995, 1996).

2.5.3d Ballysteen Limestone (ABL)

The Navan Group is overlain by a thick sequence of argillaceous bioclastic limestones (ABL) which ranges in thickness from 150m in the northern parts of the Midlands to greater than 2000m in the east-central Midlands and Shannon area (Andrew, 1991, 1993). The Group comprises two major Formations: the Lower Ballysteen Limestone (Shephard-Thorn, 1963; Philcox, 1984) and the Waulsortian Limestone Formation, a distinctive lithology in the Lower Carboniferous of Ireland (Sevastopulo, 1991).

The Ballysteen Limestone was deposited in a ramp environment during the early Courceyan in southern Ireland and transgressed northwards reaching the Navan area in the late mid-Courceyan (Sevastopulo, 1981a; Phillips and Sevastopulo, 1986; Ashton *et al.*, 1986). A ramp environment consists of a gently dipping depositional surface where there is no perceptible change of slope marking the boundary between shallow water shelf, and deep water basinal sediments (Archer *et al.*, 1996). The Lower Ballysteen Limestone consists of a relatively homogenous sequence of argillaceous, crinoidal and bryozoan-rich bioclastic wackestones with locally abundant dark, skeletal, calcareous shales. The uppermost portion of the Lower Ballysteen Limestone typically displays a nodular texture with pale grey, nodular mudstone lenses, several centimetres in diameter, enclosed by fossiliferous, highly argillaceous wackestones and packestones (Somerville and Jones, 1985).

Throughout the Irish Midlands, the Ballysteen Limestone is approximately 300-450m thick, but diplays marked thickening in the area north and northwest of Dublin (Sheridan, 1972). In the south it conformably overlies the Lower Limestone Shale, and in the north-central Midlands conformably overlies the Navan Group. The Ballysteen Limestone is not significantly mineralized, except at Silvermines (Andrew 1986a) where discordant sulphide zones were mined along major faults below the Waulsortian Limestone in the Lower Dolomite, a local oolitic member of the Ballysteen Limestone.

2.5.3e Waulsortian Facies

Throughout southern and central Ireland the Ballysteen Limestone is overlain by Waulsortian Limestone facies (Hitzman, 1995a). Waulsortian deposition was initiated in the mid-Courceyan along the northern edge of the South Munster Basin and transgressed northwards reaching the northern edge of the Irish Midlands by the late Courceyan (Hitzman, 1995a). Waulsortian Limestone facies deposition is not chronostratigraphic in Ireland (Hitzman, 1991a) and ranges from mid-Courceyan in the south to earliest Chadian in the northeast near Navan (Andrew and Ashton, 1985).

The Waulsortian facies comprises coalesced mudbanks which average 150-250m in thickness (Andrew, 1991). The facies consists of poorly bedded, dense, pale/medium grey micrite to calcarenite containing well developed stromatactis structures. In southern Ireland the facies is well developed with coalesced mudbanks up to 800m thick (Hitzman, 1991a). However, in the northern Midlands, the Waulsortian thins into individual knolls which are enveloped by flank facies and set within argillaceous packstones and grainstones, lithologically similar to the Ballysteen Limestone (Andrew, 1991). In the South Munster Basin, a thin sequence of shales and highly argillaceous carbonates, typical of a starved moderate to deep water basin, is laterally equivalent to the coalesced Waulsortian mudbanks of the southern Midlands (Sevastopulo, 1981a; Sleeman *et al.*, 1986).

High porosity in the Waulsortian due to an abundance of stromatactic cavities was reduced by the deposition of internal sediment and the precipitation of marine fibrous calcite (probably high magnesium calcite) cement, now seen as radiaxial fibrous calcite. These inferred marine cements can form more than 50% of the rock volume (de Brit, 1989). The early cementation probably produced the rigidity necessary to sustain the high depositional dips observed in many of the Waulsortian mudmounds (Lees, 1964; Philcox, 1971). Further studies by Lees (1964), Sevastopulo (1982) and Miller (1986) demonstrated that the Waulsortian had a complex diagenetic history and became lithified soon after deposition.

Waulsortian Limestone sequences display syn-sedimentary fault control throughout the Midlands (Hitzman, 1995a). At Silvermines, probable tectonic slump breccias within the Waulsortian suggest late Courceyan fault movement (Andrew, 1986a). At Lisheen, thickness variations and facies changes in the upper Waulsortian indicate latest Courceyan to early Chadian syn-sedimentary fault movement (Shearley *et al.*, 1995). At Tynagh (Clifford *et al.*, 1986), and

elsewhere throughout the northern Midlands, normal faults controlled the thickness and facies distribution of late Courceyan Waulsortian mudbanks (Hitzman, 1995a).

The Waulsortian facies hosts the majority of Irish Zn-Pb (Ba) deposits and prospects. The major deposits are Silvermines, Tynagh, Galmoy and Lisheen. Significant prospects include Ballinalack, Garrycam, Courtbrown and Carrickittle. Mineralization occurs primarily at, or near, the base of the Waulsortian, and consequently, this is the primary target in exploration projects in the south and west Midlands.

2.5.4 Lower Carboniferous (Chadian to Brigantian Stages)

The Waulsortian facies was succeeded in the latest Courceyan to Arundian by the deposition of shallow water shelf limestones and deeper water carbonates and argillites (Calp - informal designation or Upper Dark Limestones at Navan) (Hitzman, 1991a).

Rapid facies changes and irregular facies distribution characterize the latest Courceyan to Arundian, unlike the widespread distribution of facies during the Courceyan (Hitzman, 1991a). The late Chadian to Arundian was a period of tectonic activity with syn-depositional tilting apparent at some places (e.g. Navan; Ashton *et al.*, 1986; 1992) and extensional deformation (Johnston *et al.*, 1996). Facies distribution was largely controlled by fault-controlled basins, such as in the Dublin Basin (Andrew, 1992).

Throughout the Central Irish Midlands a series of interconnected basins developed, with north-dipping faults dominant in the south and south-dipping faults in the north (Johnston *et al.*, 1996). Sediments adjacent to these faults display rapid facies and thickness changes from the late Chadian onwards (e.g. the Tynagh Fault; Philcox, 1984). These faulting events were sometimes accompanied by chaotic breccias in the Midlands Province (Nolan, 1986, 1989; Crowe, 1986; Philcox, 1989; Pickard *et al.*, 1992) and in the NW Province (Philcox, *et al.*, 1989).

Following the mid-Arundian, basinal areas began to fill leading to a general shallowing upwards throughout the Irish shelf which continued through the Brigantian and into the Namurian, ultimately resulting in the deposition of deltaic sediments (Hitzman, 1991a).

Alkali basalt volcanic activity began in latest Chadian times and continued through to the early Arundian in the central Midlands and Co. Limerick (Strogen, 1973; Philcox, 1984; Strogen, 1995).

2.5.5 Lower Carboniferous Extension

The structural history of the Carboniferous in Ireland may be divided into Lower Carboniferous extension, and late Carboniferous to early Permian (Variscan) compression (Johnston *et al.*, 1996).

The tectonic environment of the Irish Shelf from the Late Devonian until at least the Arundian appears to have been extensional (Hitzman and Large, 1986; Hitzman, 1991a). Fault activity was most pronounced during the late Devonian and the late Courceyan to Arundian Stages (Hitzman and Large, 1986; Hitzman, 1991a). Arundian to late Asbian Stages were tectonically quiescent over most of the country (Andrew, 1993). The degree of tectonic activity during the late Courceyan to Arundian Stages varied considerably both temporally and spatially across the country, initiating in the Late Courceyan at Silvermines and Tynagh, but only in mid- to late Chadian times around Navan (Sevastopulo, 1981b; Phillips and Sevastopulo, 1986; Ashton *et al.*, 1986).

In late Courceyan times, active listric faulting (usually trending ENE to NE) initiated and became dominant under a phase of subsidence induced by crustal stretching, accompanied by high heat flow (Andrew, 1993). This tectonism resulted in a series of generally NE trending fault blocks. Geophysical evidence suggests that this tectonism followed and was controlled by pre-existing fractures in the Caledonian basement (Johnston *et al.*, 1996). The prevailing extensional tectonic regime in the early Carboniferous appears to have been a fundamental cause of the development of extensive base-metal mineralization in the Irish Midlands, with all deposits showing some degree of proximity if not direct control by listric faults of this epoch (Andrew, 1993).

2.6 VARISCAN OROGENY

The Variscan Orogeny resulted from subduction on the southern margin of the Laurussian Megacontinent and the subsequent collision between the Laurussian and Gondwana plates (Ziegler, 1988). Convergence of the plates culminated during the Lower Carboniferous in a Himalayan-type collision (Ziegler, 1988). The deformation front prograded northwards, reaching the area of present day Ireland in the Late Carboniferous (Ziegler, 1982, 1984, 1988).

The entire Devonian-Carboniferous successions of the Munster and South Munster Basins were strongly deformed during the Variscan Orogeny by a northward propagating deformation front (Gill, 1962; Naylor *et al.*, 1983; Cooper *et al.*, 1984, 1986; Johnston, 1995b), changing the local tectonic regime from extensional to compressional in the late Carboniferous to early Permian (Ford, 1987). The period of the Variscan deformation is suggested to be between 320 and 270Ma, peaking around 295Ma (Halliday and Mitchell, 1983). The resulting fold belt is part of the Rhenohercynian fold belt (Ford, 1987).

This deformation has been zoned by Gill (1962) on the basis of structural styles and trends which illustrate a northward decrease in deformation intensity. The deformation style changes across the Killarney-Mallow Fault, termed the Variscan 'front' (Gill, 1962). It does not mark an abrupt change; the strain and cleavage development decrease within a transition zone north of the 'front'.

In the southern area (Munster Basin) the rocks have undergone extensive shortening (50-60%; Ford, 1987) with large upright folds trending ENE, and are accompanied by pervasive cleavage (Johnston *et al.*, 1996). The deformation has been interpreted as being either thin-skinned and thrust-related (Cooper *et al.*, 1984, 1986), or thick-skinned and related to dextral transpression (Sanderson 1984). Deformation also resulted in inversion of many of the Carboniferous sub-basins of Central Ireland (Hitzman, 1991a).

To the north of the 'Variscan front', deformation decreases through a zone of major open folds with numerous thrusts into a 'foreland zone' of gentle folds (less than 20% shortening) and reactivated Caledonian and Courceyan-Chadian faults (Coller, 1984; Cooper *et al.*, 1984; Gill, 1962). However, evidence for dextral transpression continues northwards (Johnston, 1993; Fitzgerald *et al.*, 1994), and the importance of right-lateral strike slip movements in the Variscides has been noted by many authors (e.g. Arthaud and Matte, 1977; Badham, 1982).

2.7 GEOLOGY OF THE RATHDOWNEY TREND DEPOSITS AND PROSPECTS

The Lisheen deposit (Hitzman *et al.*, 1992; Shearley *et al.*, 1995, 1996) is located in Co. Tipperary (PL 3262), 130km southwest of Dublin and 10km northeast of Thurles. It is a stratabound-stratiform, Zn-Pb (Ag) deposit, hosted by dolomitized Waulsortian Limestone of Courceyan age (Figure 2.2). The discovery was made in April 1990 by the Chevron Mineral Corporation of Ireland - Ivernia West Plc Joint venture. The deposit is located close to the

southeastern edge of the Rathdowney Trend, a 40km long belt of carbonate rocks trending NE-SW, parallel to inferred Caledonian basement structures.

The bulk of mineralization is hosted by dolomitized Waulsortian Limestone, with subordinate mineralization hosted by the Lisduff Oolite Member of the Ballysteen Limestone (c.120m below the base of the Waulsortian) adjacent to the Killoran and Derryville Faults. These E-W trending normal faults form part of a major 40km long relay fault system which extends along the Rathdowney Trend. Argillaceous bioclastic limestones (upper part of the Ballysteen Limestone Formation) form the footwall to the Waulsortian hosted mineralization throughout most of the deposit area.

The Galmoy deposit (Doyle *et al.*, 1992; Doyle and Bowden, 1995a) is located in north Co. Kilkenny (PL 568), some 110km southwest of Dublin, and 5km northwest of Johnstown on the main Dublin-Cork road. It is a stratabound Zn-Pb deposit, hosted in Waulsortian Limestone of Courceyan age. The current mineable resource is estimated to be 6.12 Mt, grading 11.5% Zn, 1.11% Pb and 9.6% Fe; significant Ag up to 100g/t occurs in the G orebody (Lowther, pers. comm., 1998). The discovery hole was drilled in February 1986 by Conroy Petroleum and Natural Resources Plc., (now Arcon International Resources Plc.). The deposit is located in the southeast of the Lower Carboniferous Midland Basin, also on the southeastern edge of the Rathdowney Trend, approximately 10km northeast of the Lisheen deposit.

At Galmoy, the base of the ore grade mineralization coincides closely (within 1m) with the base of the dolomitized Waulsortian. Minor sub-economic mineralization does occur within the upper 5m of the underlying Upper Ballysteen Limestone as thin sphalerite veinlets in clean micrite beds. However, in the vicinity of the major ENE-trending G Fault, mineralization including replacement mineralization, is of sufficient intensity to be ore grade in places. The G fault is a significant regional fault which has been traced to the southwest. At Lisheen, it forms part of the Killoran Fault Zone, and is interpreted as a dextral transtensional fault with individual E to ENE-trending strands (Shearley *et al.*, 1996).

The Durrow prospect (PL 3688) is located in Co. Laois, approximately 12km northeast of Galmoy (Figure 2.2). Minor base metal mineralization and trace Cu mineralization is hosted by the Lisduff Oolite Member of the Ballysteen Limestone (c.150m below the base of the dolomitized Waulsortian) in the footwall of a major reverse fault (Figure 2.3). The Holycross

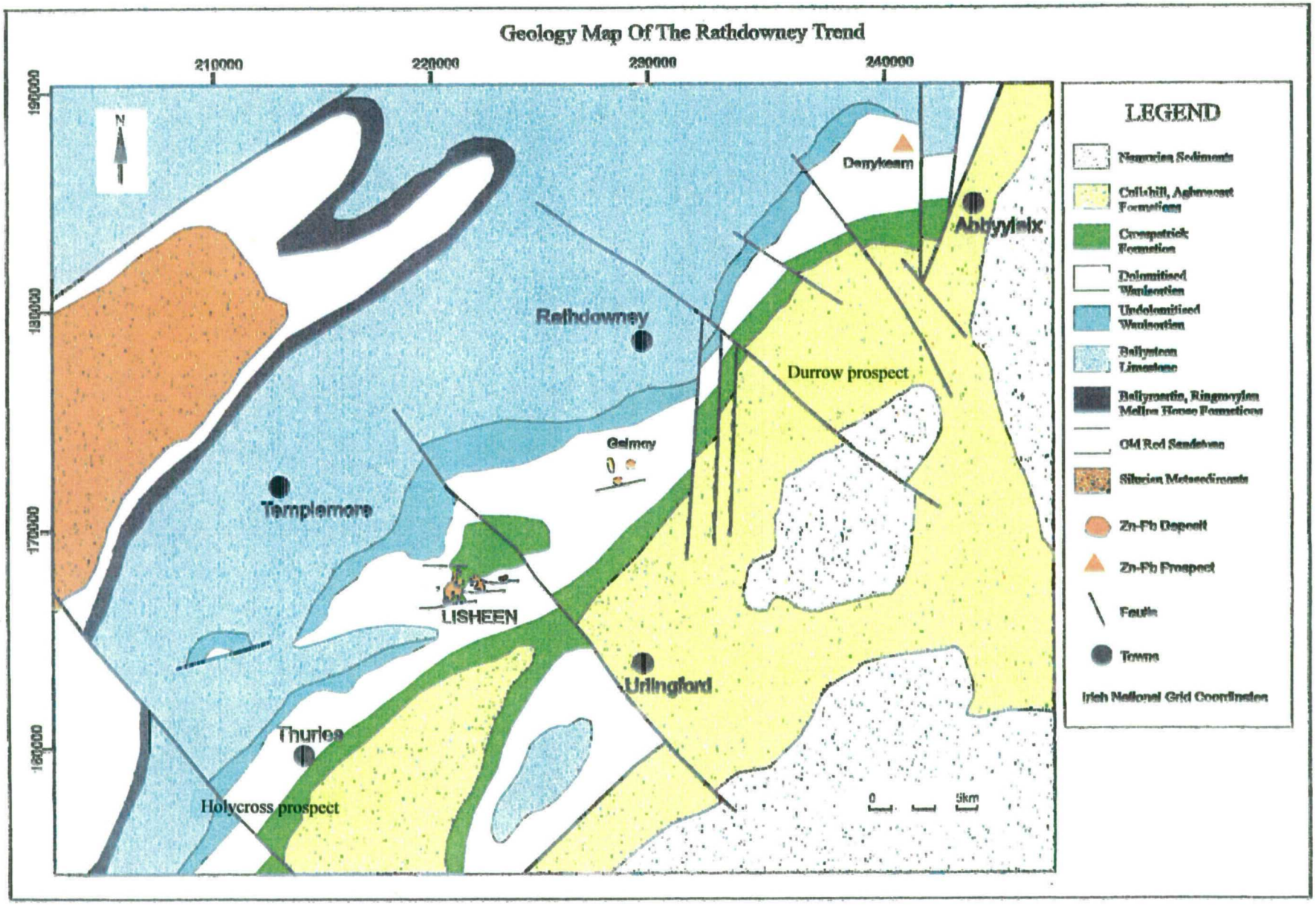


Figure 2.2 Geology of the Rathdowney Trend (modified after Redmond, 1997).

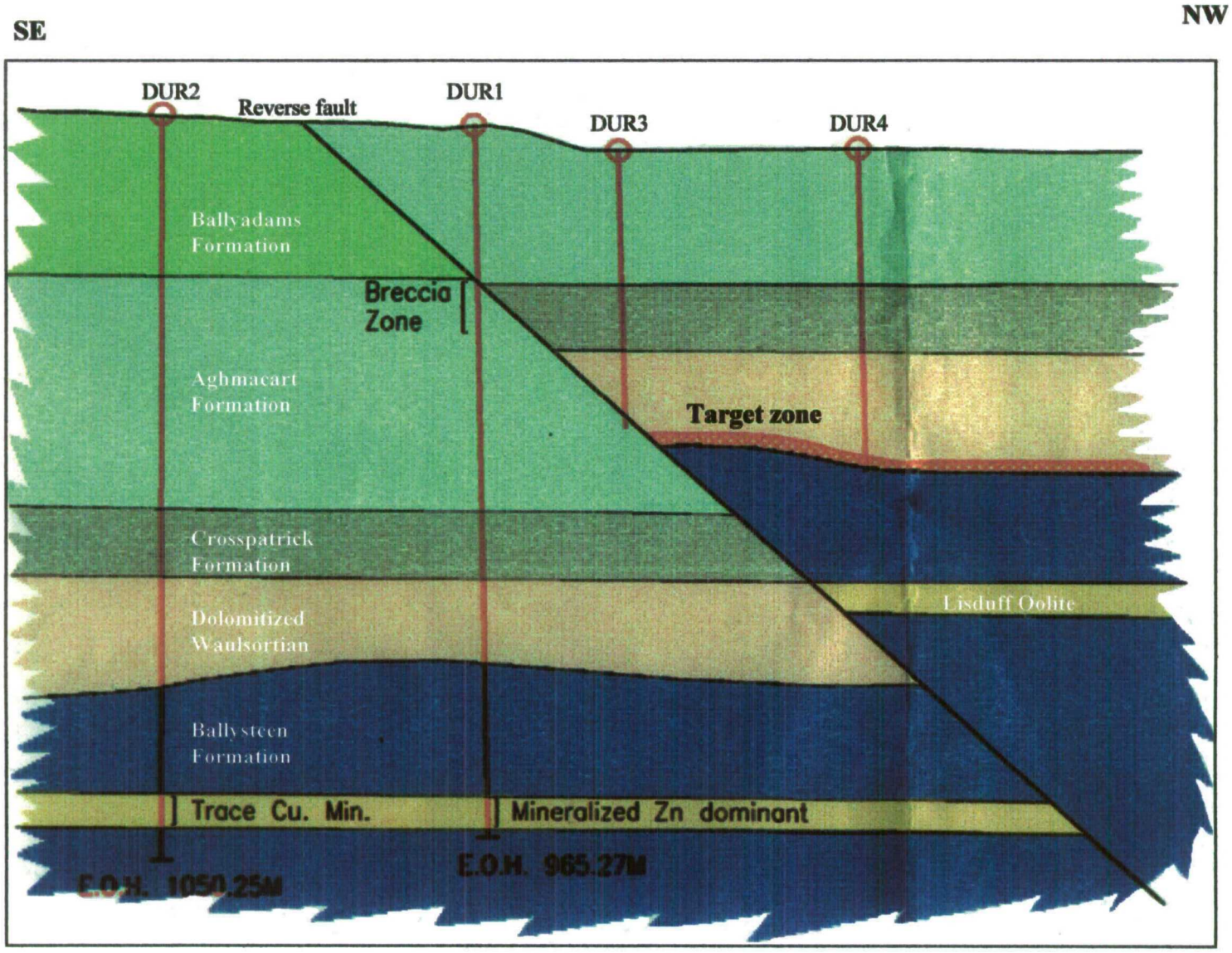


Figure 2.3 Diagrammatic cross section - Durrow prospect (scale 1:10000). Source: Rio Tinto Finance and Exploration Plc.

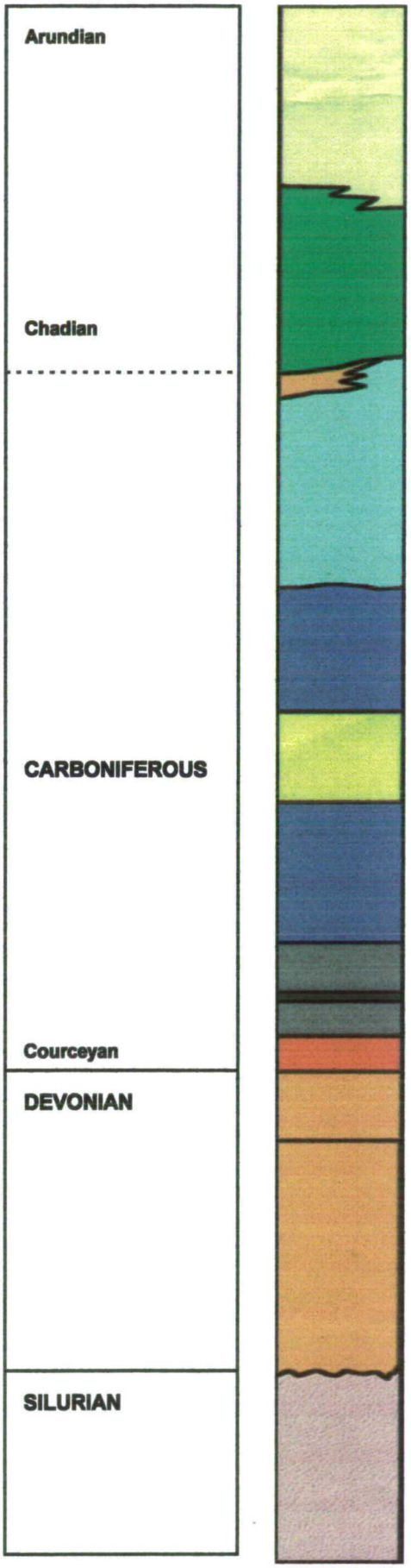


Figure 2.4 Stratigraphic column - Lisheen area
Source: CSA Ltd.

area (PL 3318, 3569) is located approximately 12km southwest of Lisheen (Figure 2.2). There is no significant mineralization in the area, however, moderate to well developed dolomite breccias do occur at the base of the dolomitized Waulsortian. Hydrothermal alteration occurs in the Rathdowney East area (PL 2218, 1652) located approximately 5km northwest of Durrow and approximately 15km northeast of Galmoy (Figure 2.2), but the area is barren of significant mineralization. Other minor prospects have been discovered further north along the Rathdowney Trend (PL 1650), including the Derrykearn prospect, Co. Laois (Johnston *et al.*, 1996).

2.7.1 Lithostratigraphy

2.7.1a Lisheen Deposit

The Lower Carboniferous succession at Lisheen (Figure 2.4) (Hitzman *et al.*, 1992; Shearley *et al.*, 1995, 1996) is similar to that recognized elsewhere in south Central Ireland (Shepherd-Thorn, 1963; Philcox, 1984; Somerville and Jones, 1985; Somerville *et al.*, 1992).

The Ballysteen Limestone, Waulsortian Limestone and Crosspatrick Formation are the main lithological units recognised in the Lisheen area. The lithostratigraphy of the area is described by Shearley (1993a). Waulsortian and Crosspatrick facies distribution are described by Kelly *et al.* (1993).

The initial transgression resulted in the deposition of a shallow water sequence of mixed carbonates and clastics (Mellonhouse Formation, 35m thick), followed by deeper water shales and limestones (Ringmoylan to Ballysteen Formations, approximately 450m thick). The transgression culminated in the deposition of Waulsortian mudmounds (170-210m thick) during late Courceyan to early Chadian times. This was succeeded by an open marine limestone shelf to ramp sequence (Crosspatrick Formation 165-175m thick) and an overlying shallow water, more restricted shelf sequence (Aghmacart Formation, greater than 200m thick), of Chadian to Arundian age.

The Ballysteen Limestone (370m), can be subdivided into three mappable members: the Lower Calcarenite Member, the Lisduff Oolite Member and the Upper Calcarenite Member. The Lower Calcarenite (130-150m thick) consists of a sequence of fossiliferous packstones and grainstones. The overlying Lisduff Oolite Member (70-80m thick) consists of well-sorted oolitic grainstones and crinoidal packstones and wackestones (Sleeman, 1990). The Upper Calcarenite Member (130-140m thick), consists of argillaceous, fossiliferous packestones with interbedded

argillaceous wackestones. The upper 20-30m of this member consists of nodular micrites with associated calcarenites and argillites. Close to the contact with the overlying Waulsortian these argillites are green (colouration probably due to hydrothermal alteration) (Shearley, 1993a). Two distinct green tuff horizons approximately 13m and 16m below the top of the unit are important marker horizons throughout the Rathdowney Trend.

The Waulsortian Limestone (170-210m thick) contact with the underlying nodular micrite unit is often gradational. The Waulsortian consists of a complex of many coalesced mudbanks, each composed of basal, core, flank and cover facies which form massive biomicrites. At Lisheen these have been affected by both regional and hydrothermal dolomitization.

The majority of the Waulsortian comprises core facies which can be divided into two sub-facies: 'Veines-Bleues' facies (Lees *et al.*, 1977) and biomicrites. The Veines-Bleues limestone is distinguished by an abundance of sparry calcite and stromatactic cavities. The biomicrite facies is composed of micrite mud with variable amounts of bioclastic debris, primarily fenestellid bryozoans and crinoids (Shearley, 1993a). There is little to no argillaceous material within the core facies.

Flank facies define the boundaries between individual mudbanks. At Lisheen the development of interbank flank facies is minor. Flank facies consist of crinoidal micrites with minor to abundant argillite laminae, which give the rock a wavy laminated texture. High dips of up to 45° are typical for the flanks of mudbanks.

The overlying cover facies at Lisheen, termed the 'Upper Wavy Laminated Unit' (10-20m) (Shearley, 1993a), is lithologically similar to the flank facies and consist of crinoidal micrites with wavy laminated textures and diagenetic chert nodules. This unit is interpreted to have been influenced by movements on the major faults and is thought to be a deeper water equivalent of the Waulsortian Limestone complex (Shearley, 1993a).

Adjacent to main faults in the Lisheen area, biomicrites typical of the upper Waulsortian Limestones pass upward and laterally into a sequence of dark grey, slightly argillaceous, disturbed, wavy laminated biomicrites which are assigned to the Upper Transition Biomicrite Unit (Shearley, 1993a). They are time equivalent to the upper 'reef' and grade laterally into normal micrite facies away from faults. Increased thicknesses (70-100m) of the Upper Transition Biomicrite Unit occur at zones of maximum displacment along the E-W trending Killoran and Derryville faults. The transitional beds are also seen to thicken towards N-S trending splay faults.

The Crosspatrick Formation (Sleeman, 1990) conformably overlies the Waulsortian and is 60-80m thick in the Lisheen area and up to 170m thick in the southeastern part of the Rathdowney Trend. In local fault controlled sags, the lowermost Crosspatrick Formation is laterally equivalent to the uppermost Waulsortian, indicating that the contact is not a time line. The Formation consists of dark, cherty, argillaceous wackestones and packstones.

2.7.1b Galmoy Deposit

The Galmoy area (Doyle *et al.*, 1992; Doyle and Bowden, 1995a;1995b) is underlain by the same Lower Carboniferous sequence which is observed in the Lisheen area. The Ballysteen Limestone, Waulsortian Limestone and supra-Waulsortian limestones (Crosspatrick, Aghmacart, Ballyadams and Clogrenan Formations; Sleeman, 1990). The Carboniferous sequence is covered by glacial deposits.

The detailed stratigraphy of the Galmoy area (Figure 2.5) has been established mainly by drilling to the top of the ORS (Doyle *et al.*, 1992). The Lower part of the Courceyan sequence is similar to that of the Limerick Province as described by Philcox (1984) and Somerville and Jones (1985).

The ORS in the Galmoy area is overlain by a thick succession of sandstones, siltstones and grey to green mudstones (20m), that correlate with the Mellon House Formation; these are in turn overlain by grey shales with siltstone beds and bioclastic silty calcarenites (Ringmoylan Formation, 22m thick). The Ringmoylan Formation is followed by silt banded shales with a distinct greenish colour (Ballyvergin Mudstone Formation, 3m thick). This is overlain by bioturbated, bioclastic and argillaceous calcarenites and unfossiliferous mudstone beds (Ballymartin Limestone Formation, 30m, thick).

The Ballysteen Limestone Formation (425m) can also be subdivided into three mappable members: the Lower Ballysteen, the Lisduff Oolite and the Upper Ballysteen. The Lower Ballysteen Limestone (170m) consists of a sequence of bioturbated argillaceous calcarenites with wisps of dark calcareous mudstone. The overlying (100m thick) Lisduff Oolite Member (Sleeman, 1990) consists of coarse, clean bioclastic and oolitic calcarenite to oolitic biosparite. The Upper Ballysteen Limestone (120m) is the equivalent facies to the Argillaceous Bioclastic Limestones (ABL) of the North Midlands. It consists of interbedded thin micrites and bioclastic, calcareous mudstones with abundant crinoids and bryozoa. The proportion of mudstone decreases upwards through the unit and a few thicker-bedded mudstones locally provide useful marker beds

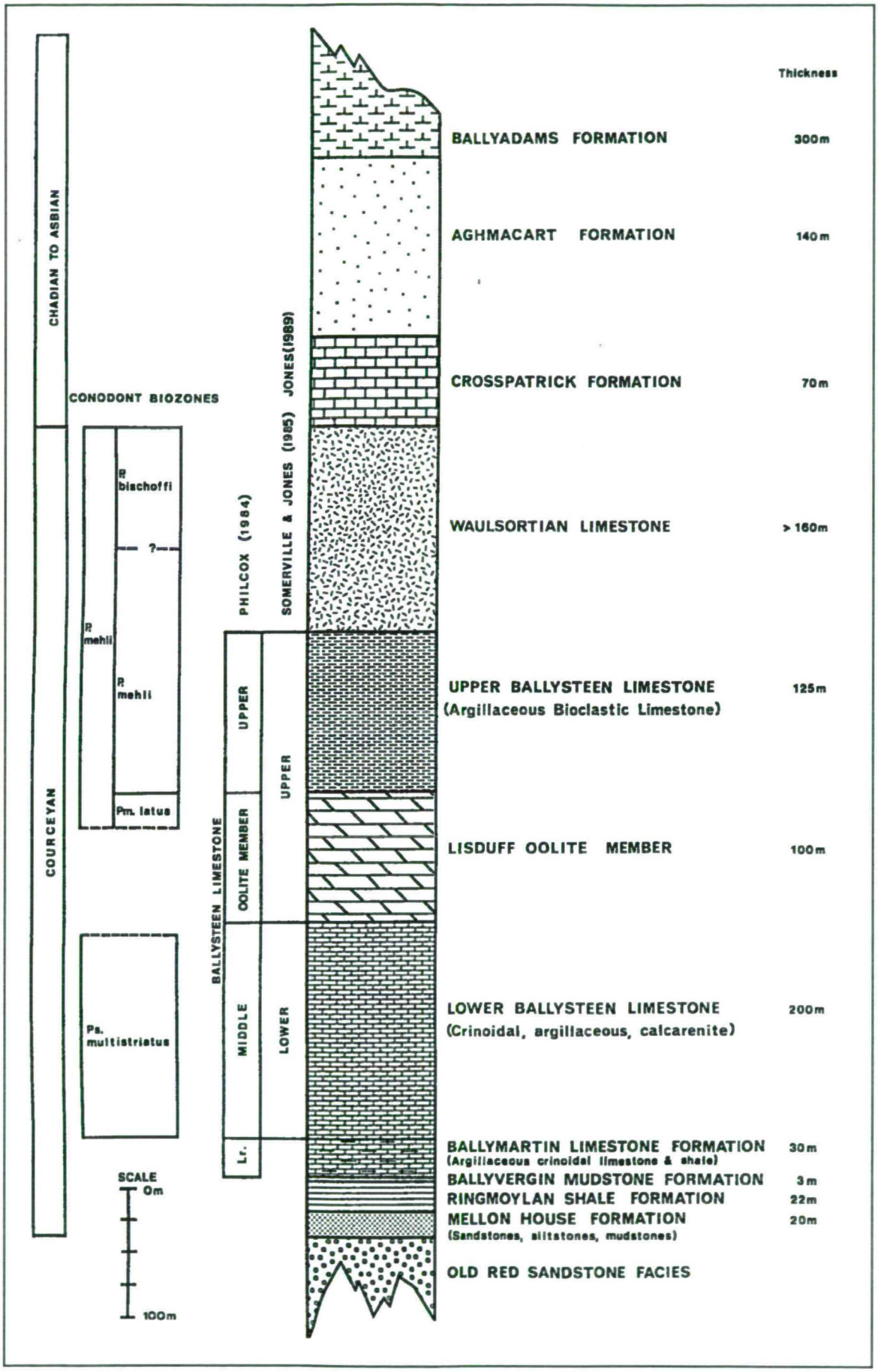


Figure 2.5 Stratigraphic column - Galmoy deposit. After Doyle *et al.*, 1992.

(Doyle *et al.*, 1992). The upper part of the Ballysteen Limestone is lithologically variable. The micrites become nodular towards the top of the unit.

The contact of the Waulsortian Limestone (180-200m thick) with the underlying Upper Ballysteen Limestone is generally sharp, and is usually marked by 50-300mm of distinctive green to green-grey mudstone (Doyle *et al.*, 1992).

Above the Waulsortian Limestone and to the southeast lies the laterally variable Crosspatrick Formation (70m) which, in the Galmoy area, consists of pale grey crinoidal calcarenites with interbedded cherts or chert nodules. The Crosspatrick Formation is overlain by the Aghmacart Formation (140m) which comprises thickly bedded, dark-grey, fine grained calcarenites and dark micrites with dispersed, matrix-supported bioclastic debris. Overlying the Aghmacart Formation is the Ballyadams Formation which is a coarse grained, light grey, bioclastic limestone with rare thin shale beds. The highest limestone formation is the Clogrenan Formation which also consists of thick bedded pale grey calcarenite but contains bands and nodules of bluish chert. These overlying Chadian to Brigantian rocks (Crosspatrick, Aghmacart, Ballyadams and Clogrenan Formations) represent a return to carbonate platform environments (Doyle *et al.*, 1992).

2.7.2 Structure

2.7.2a Lisheen Deposit

Two major ENE to E trending normal faults, the Killoran and Derryville Faults, bound the southern edge of the Lisheen deposit (Shearley *et al.*, 1993b, 1995, 1996). They exercise a primary control on the distribution of mineralized zones, dolomitization and sedimentation (Figures 2.6, 2.7). The faults dip at 45-55° to the north in the zone of maximum displacement (200m), and steepen to greater than 60° towards their termination zones. The Killoran and Derryville Faults form short fault segments (1.5km and 1km respectively) of a major 40km long relay fault system, which sub-parallels the Rathdowney Trend (Figure 2.2).

The Killoran and Derryville Faults have surface traces of 2.2 and 2km respectively. In plan view, they overlap and are separated by 350m. Within the overlap zone, displacement along the Killoran Fault decreases to the east and along the Derryville Fault displacement decreases to the west. A combined displacement of 200m is maintained throughout the overlap zone. Displacements are transferred from one fault segment to another by means of a left stepping

faulted relay ramp (Walsh and Watterson, 1989). Displacement transfer is accommodated by normal faulting and increased bed dip (Shearley *et al.*, 1996).

The hanging walls of the two major faults contain several subsidary E-W trending high angle (80-85°) normal faults (Shearley *et al.*, 1993b) which strike sub-parallel to the main structures (Shearley *et al.*, 1996). These subsidary faults have small displacements (5-25m) and occur over an area extending 1.5 to 2km to the north of the surface trace of the major faults. The hanging walls are also cut by N-S trending, sub-vertical, faults. Displacements are of the order of 10-40m (Shearley *et al.*, 1996). The faults appear to originate from the main Killoran and Derryville Faults at points of major irregularity, i.e strike/dip changes along the fault lengths. They are thought to have formed as accommodation structures during normal faulting, as a result of rapid lateral changes in displacement along the main fault zones (Shearley *et al.*, 1996). On the western side of the deposit, these faults downthrow to the east (within the overlap zone they downthrow to the west), while on the eastern side they downthrow to the west accounting for the large grabens of Supra-Waulsortian lithologies in the Lisheen area with the base of the Waulsortian downthrown in the centre of the deposit (Shearley *et al.*, 1993b).

Most of the structures are thought to have originated pre- to syn-mineralization, with both E-W and N-S structures influencing mineral distribution (Shearley *et al.*, 1993b). The structures form bounding surfaces for ore where displacements are large, and especially where more impermeable lithologies (Ballysteen Limestone) are faulted against permeable lithologies (Waulsortian Limestone) (Shearley *et al.*, 1993b). Where displacements are small, mineralization cross-cuts structures, the thicker and higher grade intersections occur on the downthrown sides of both E-W and N-S structures (Shearley *et al.*, 1993b).

2.7.2b Galmoy Deposit

Two main fault sets are recognized in the Galmoy area (Doyle *et al.*, 1992). An early ENE-trending set, and a later NNW-trending set (Figure 2.8, 2.9). Of the ENE-trending set the best known is the G fault. Drilling at the G orebody shows this fault to comprise a zone c.50m wide dipping 50-55° NNW. It is a normal fault with a vertical throw in excess of 200m, which brings the Waulsortian Limestone into contact with Lower Ballysteen Limestone (Doyle and Bowden, 1995). The G Fault forms the southern margin of the G zone orebody to the south and is considered to have been an important control on the mineralization of the G Zone orebody, forming a conduit for mineralizing hydrothermal fluids. Movement on the G Fault is considered to have been syn- to post- the mineralizing event (Doyle and Bowden, 1995). Down the dip of the

fault much of the movement appears to have been dissipated within the hanging wall by horse-tailing into bedding-slip in the Lower Ballysteen Limestone and underlying lithologies (Doyle *et al.*, 1992).

The regional dip of the Lower Carboniferous limestones is approximately 10° to the southeast, with a northeasterly regional strike. However, it is only the supra-Waulsortian rocks that consistently reflect this trend, the local dips in the deposit area are to the west in the CW orebody and to the north in the G orebody. These variations are local effects, brought about by faulting and folding (Doyle *et al.*, 1992).

The G Fault is a significant structure and if the main displacement took place around the Courceyan-Chadian boundary then this could have affected subsequent sedimentation. Evidence of a change in the sedimentary environment is observed from drilling carried out southeast and northwest of the G fault. Both the Waulsortian and the immediate supra-Waulsortian rocks thicken to the northwest (to the southeast the Waulsortian is approximately 120m thick while to the northwest it is approximately 210m; Doyle and Bowden, 1995b). To the southeast the supra-Waulsortian (Visèan rocks) consist mainly of coarse grained bioclastic calcarenites, interpreted to represent a shelf facies environment. To the northwest the Visèan rocks consist of argillaceous bioclastic limestones with fine grained calcarenites and common chert, interpreted to represent a deep water environment. In short, the area appears to straddle a regional shelf margin (shelf to the southeast) that became active in the late Courceyan to early Chadian (Doyle and Bowden, 1995a). The NNW trending faults are clearly later than the ENE faults which they offset. They appear to have some strike-slip component of movement (Doyle *et al.*, 1992).

2.7.3 Regional dolomitization

Drilling combined with research studies at Chevron Oil Field Research Company have confirmed the extent of regional dolomitization throughout the Rathdowney Trend. However, the degree of complete dolomitization throughout the Trend is still debatable. Hitzman *et al.* (1998) have recently proposed that the extent of regional dolomitization in southern Ireland affected the Lower Carboniferous Waulsortian Limestone from the Munster Basin to just south of Dublin, a total distance of ~170km.

2.7.3a Lisheen Deposit

The Waulsortian Limestone has been converted to dolomite over large areas of the Rathdowney Trend (Beaty *et al.*, 1991). The gradational contact between dolomitized and undolomitized Waulsortian forms a NE-SW trending regional dolomite 'front' which sub-parallels the major structures and helps to define the Rathdowney Trend (Hitzman *et al.*, 1992). The contact occurs approximately 2km to the northwest of Lisheen, with dolomitized Waulsortian to the southeast and undolomitized Waulsortain to the northwest (Shearley *et al.*, 1995) (Figure 2.2).

Distribution of the regional dolomite throughout the trend is assumed to be largely controlled by major structural features and the original fabric of the Waulsortian Limestone (Hitzman and Shearley 1991). The limit of complete regional dolomitization has a NE trend from Derrykearn to just south of Lisheen and corresponds to the present limits of Waulsortian facies outcrop (Hitzman and Shearley 1991). Complete dolomitization extends further west in the middle and upper portions of the Waulsortian complex than at its base and partial dolomitization extends out even further, between 2-10km (Hitzman and Shearley 1991). In the northern part of the Rathdowney Trend, the overlying Aghmacart Formation is dolomitized (Shearley *et al.*, 1996). The Waulsortian in the Silvermines area has not been subjected to regional dolomitization, unlike the Rathdowney Trend (Hitzman, 1991c).

In the Lisheen area, the entire Waulsortian complex as well as relatively non-argillaceous beds within the overlying Crosspatrick Formation are completely dolomitized (Shearley *et al.*, 1995). Regional dolomite occurs on both the hanging wall and footwall sides of the main Killoran and Derryville Faults; there is no clear spatial relationship between the regional dolomite and the normal faults locally (Shearley *et al.*, 1995). However, these normal faults controlled later hydrothermal dolomitization (Shearley *et al.*, 1995).

The regional dolomite is composed of fine to medium-grained crystalline replacive dolomite and texturally later, coarse crystalline white dolomite. The fine replacive dolomite preferentially replaces the microcrystalline components of the Waulsortian Limestone whereas the coarse white dolomite replaces the coarse grained components of the Waulsortian, such as calcite-filled stromatactis cavities and bioclasts. In partially dolomitized Waulsortian Limestone, selective replacement is controlled more by crystal size than by mineralogy (Sibley and Gregg, 1987); the micritic portion of the rock is preferentially dolomitized, whereas bioclasts, being composed of coarse calcite grains, initially resist dolomitization (Hitzman and Shearley, 1991).

The regional distribution of dolomite and a south to north $\delta^{18}O$ isotope gradient (+21‰ to +26‰ respectively) suggest a southerly source for the dolomitizing fluids (Allan *et al.*, 1992; Hitzman *et al.*, 1998). It is thought that the regional dolomite may have formed as a result of northward expulsion of pulses of heated, formation waters from a foreland basin (the Munster Basin) during the onset of the Hercynian Orogeny (Allan *et al.*, 1992). However, it has been suggested more recently that the regional dolomite may be better explained by an early diagenetic model (Gregg pers. comm., 1996).

2.7.3b Galmoy Deposit

Regional dolomitization appears to have affected, in varying degrees of intensity, most of the Waulsortian Limestone in the Galmoy area (Doyle *et al.*, 1992). The original, presumably micritic, framework of the Waulsortian is altered to medium to coarse-grained, equigranular dolomite. Veining and brecciation, filled and cemented by crystalline dolomite are associated with this style of dolomitization (Doyle *et al.*, 1992).

Regional dolomitization occurs in a zone which strikes NE-SW, with an ENE-trending dolomite 'front' occurring approximately 1km north of the Galmoy deposit, with undolomitized Waulsortian occurring northwest of the front. The contact between dolomitized and undolomitized Waulsortian Limestone is not well defined (Doyle *et al.*, 1992).

2.7.4 Hydrothermal Dolomitization

2.7.4a Lisheen Deposit

At Lisheen, the regional dolomite is cut and brecciated by significant local hydrothermal dolomitization (Shearley *et al.*, 1995). This event resulted in the formation of hydrothermal dolomite matrix breccias, termed the black matrix breccia (BMB) (Hitzman *et al.*, 1992) and the white matrix breccia (WMB) (Redmond, 1997).

The BMB is very distinctive and its recognition led to the discovery of the deposit (Hitzman *et al.*, 1992). It is best developed within the basal 20m of the regionally dolomitized Waulsortian, adjacent to the major normal faults (Hitzman, 1995b). BMB is ore-related and envelops the massive sulphide body displaying sharp contacts with the ore. It extends about 500m beyond the northern edge of the deposit, up to 200m beyond the eastern and western margins, and

approximately 10m above the sulphide lens (Shearley *et al.*, 1996). Locally, BMB is developed in the footwall Lisduff Oolite (proximal to the main faults), and is associated with subordinate mineralization (Shearley *et al.*, 1996). The lack of significant BMB in the footwall rocks of the main faults and the geometry of the dolomite body (Figure 2.7) suggests that brecciation occurred after significant movement had occurred on the main faults (Shearley *et al.*,1996).

The WMB is broadly spatially associated with the BMB, but is less well defined (Redmond, pers. comm., 1995). The WMB forms within the regionally dolomitized Waulsortian, and occurs generally above the BMB in the deposit area.

The BMB dolomite consists of a dark, fine crystalline (non-ferroan to ferroan) dolomite matrix. Well developed BMB contains 40-60% by volume angular to subrounded clasts of variable size (Shearley *et al.*, 1995). Regional dolomite clasts are most common. However, clasts of undolomitized or partially dolomitized Waulsortian also occur (Shearley *et al.*, 1995). The dark colouration of the matrix is due to crystal size, void space, argillite content and the presence of disseminated sulphides (Shearley *et al.*, 1995). The WMB consists of a white, medium to coarse crystalline dolomite matrix. Regional dolomite clasts are angular to subrounded and variable in size.

Comparable textures to those observed at Lisheen have also been described from Silvermines. However, these have been interpreted as a syn-sedimentary breccia (Taylor and Andrew, 1978; Taylor, 1984; Andrew, 1986a and 1995). Though syn-sedimentary limestone breccias are present within the Waulsortian at Silvermines and Lisheen, petrographic studies (Kucha 1989; Hitzman *et al.*, 1992; Shearley *et al.*, 1995) have demonstrated that dolomitization post-dated slumping and was replacive.

2.7.4b Galmoy Deposit

Dolomitized Waulsortian at Galmoy shows the development of a breccia which is cemented by white crystalline dolomite (Doyle *et al.*, 1992). This crystalline dolomite is texturally equivalent to the WMB at Lisheen. This interpretation is contradictory to the interpretation of the WMB at Lisheen. The breccia textures vary from fine cracks through irregular dolomite veinlets filled with crystalline dolomite to well developed breccias commonly utilizing stromatactis cavities. Vugs within this crystalline dolomite are filled by later calcite. In outcrop and near surface, the dolomite is slightly oxidized and is a pale buff colour; at depth it is unoxidized and is a light to medium grey colour (Doyle *et al.*, 1992).

This style of brecciation rarely extends into the mineralized rock matrix breccia which is texturally similar to the BMB at Lisheen. At Galmoy, this brecciation extends from above the rock matrix breccia to the top of the sub-crop. Crystalline dolomite breccias occur throughout most of the area of the regionally-dolomitized Waulsortian. It is believed that crystalline matrix breccias formed due to volume reduction caused by the regional dolomitization of the massive Waulsortian Limestone (Doyle *et al.*, 1992).

The rock matrix breccia occurs within the basal few metres of the Waulsortian at Galmoy, its distribution considered non-uniform (Lowther, pers. comm., 1998). It comprises sub-rounded to sub-angular dolomite clasts set in a dark grey, fine grained, dolomitic and apparently argillaceous matrix with rare microscopic quartz. The predominant clast lithology is a medium grey, fine-grained dolomite. The majority of clasts are ellipsoidal in shape and vary in length from 5mm to 25mm. Some of the clast boundaries suggest minor dissolution. The breccias vary from entirely clast supported to sections with only a few fine clasts. A downhole progression is seen, from clast-support through to matrix-support and finally matrix only. The general sub-parallel and sub-horizontal orientation of the long axes of the clasts suggests little rotation has occurred. The lack of mixing and rotation of the clasts suggests that the breccias did not originate as debris flows or slides or by solution and collapse (Doyle *et al.*, 1992).

The origin of the rock matrix breccia is problematic but it is suggested that the process was initiated during diagenesis and compaction of the primary Waulsortian sediment (Doyle *et al.*, 1992). It is believed that the breccias were formed *in situ* and it is possible that the mechanism which was responsible for the disruption and transformation of the incipient breccias into the rock matrix breccia was instability in the sediment pile related to early movements on the G Fault (Doyle *et al.*, 1992). Such movements may have been responsible for the introduction of dolomitizing fluids and mineralizing fluids which in turn may have enhanced the brecciation process (Doyle *et al.*, 1992).

Below and south of the G Orebody, principally in the footwall of the G Fault, beds of the Lower Ballysteen Limestone and Lisduff Oolite Member are altered to a medium to coarse-grained, equigranular dolomite. Some of the original fabric, including a faint oolitic or bioclastic texture, can be discerned. This dolomite appears in part to be associated with an intense fracture-induced brecciation, and is the host for epigenetic, fracture-filling copper-silver mineralization.

The Lisduff Oolite Member is completely dolomitized for at least 400m north of the G Fault, while the Lower Ballysteen Limestone below and Upper Ballysteen above are completely

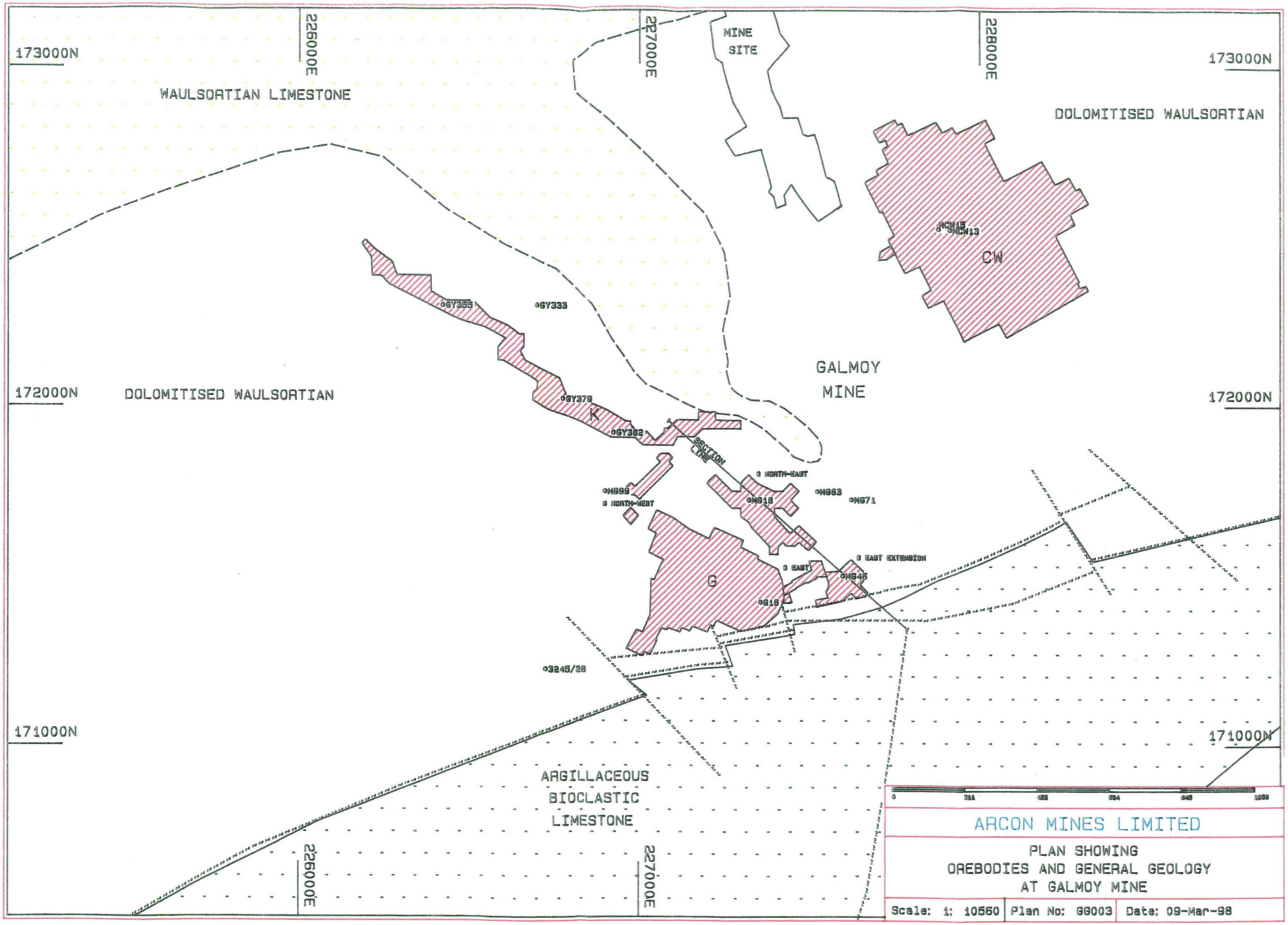

173000N
226000E
227000E
228000E
MINE SITE
WAULSORTIAN LIMESTONE
DOLOMITISED WAULSORTIAN
CW
GALMOY MINE
K
G
172000N
171000N
ARGILLACEOUS BIOCLASTIC LIMESTONE
ARCON MINES LIMITED
PLAN SHOWING
OREBODIES AND GENERAL GEOLOGY
AT GALMOY MINE
Scale: 1: 10560
Plan No: GG003
Date: 09-Mar-98
sallya.pf
SURPAC SOFTWARE INTERNATIONAL, AUSTRALIA

Figure 2.8

undolomitized (Doyle *et al.*, 1992). The Lisduff Oolite Member is not dolomitized beneath the CW orebody (Doyle *et al.*, 1992).

2.7.5 Mineralization

2.7.5a Lisheen Deposit

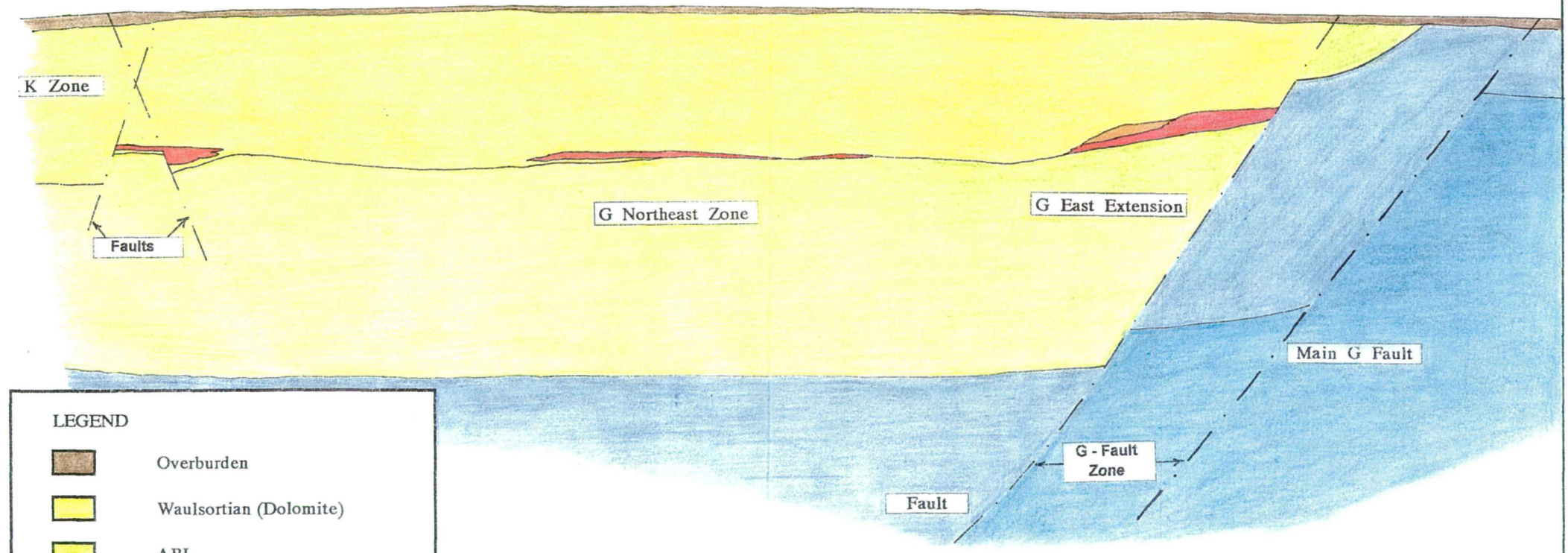
Mineralization in the Lisheen area is structurally controlled (Shearley *et al.*, 1993b) and occurs principally in the hanging wall rocks of the Killoran and Derryville Faults (Figures 2.6, 2.7). It is predominantly hosted by the dolomitized Waulsortian Limestone complex, at a depth of 170-210m (Shearley *et al.*, 1996). Subordinate mineralization is hosted by the Lisduff Oolite Member of the Ballysteen Limestone Formation adjacent to the faults, c.120m below the base of the Waulsortian (Shearley *et al.*, 1993b). The ABL (upper part of the Ballysteen Limestone Formation) forms the footwall to the Waulsortian hosted mineralization over most of the deposit area (Shearley *et al.*, 1995).

Brecciation pre-dates mineralization and is thought to have increased the permeability of the dolomitized Waulsortian and controlled the distribution of the sulphide mineralization (Shearley *et al.*, 1996). The sulphides are believed to replace both matrix and regional dolomite clasts within the breccia (Hitzman *et al.*, 1992).

The ore occurs as a series of massive to semi-massive stratiform sulphides lenses, as irregular zones of breccia/vein style mineralization and finely disseminated sulphides (Shearley *et al.*, 1995). There are three principal zones of mineralization in the deposit: Main, Derryville and North Zones (Shearley *et al.*, 1996) (Figure 2.6).

Mineralization extends 2km along the strike length of the fault system and approximately 1.5km to the north in the hanging wall (Shearley *et al.*, 1995). Individual stratabound sulphide lenses vary in thickness from <0.5m to >30m, with an average lens thickness of 5m. Mineral occurrences thicken and increase in metal grade towards a series of normal faults (Shearley *et al.*, 1993c; 1995; 1996). The thickest lenses (up to 30m) and highest grade mineralization (up to 35% Zn) (Shearley, 1993d) occur adjacent to the Killoran and Derryville Faults, suggesting that they served as major conduits for mineralizing fluids which were focussed at points of maximum displacement (Shearley *et al.*, 1996). The most extensive breccia sheets occur where the 'parent' fault changes dip (Johnston, 1995c). With increasing distance from major conduits, orebody thicknesses decrease to 3m over a horizontal distance of 120-150m (Shearley, 1993d) and the

ARCON MINES LIMITED	GEOLOGY DEPARTMENT
SECTION THROUGH SOME OF THE GALMOY OREBODIES	
Date:	9.04.98
Drawn by:	B. Balding
Checked by:	JmL 29.4.98
Scale:	1:2,500



LINE OF SECTION IS SHOWN ON PLAN No. GG003

Figure 2.9

development of BMB dolomite also decreases with distance from the major faults (Johnston, 1996).

Subsidiary ENE-E trending structures also appear to form important conduits for mineralizing solutions (Shearley *et al.*, 1993b). N-S trending faults show no evidence of having been conduits for hydrothermal fluids. Only at the intersection of these ENE and N-S structures do the N-S faults appear to act as 'feeders', and this is where the thickest and highest grade mineral intersections often occur. This pattern of faulting subdivides the orebody into a number of individual structural blocks (Shearley *et al.*, 1993b).

2.7.5b Galmoy Deposit

There are 3 principal zones of mineralization in the deposit: CW, G and K Zones (Doyle *et al.*, 1992; Doyle and Bowden, 1995a) (Figures 2.8, 2.9). Economic mineralization in each of the delineated orebodies is confined to a layer of rock matrix breccia that occurs at, or close to, the base of the dolomitized Waulsortian Limestone at an average depth of 70m, and ranging from 30m in the east to 110m in the southwest.

The CW orebody lies some 500m further north of the G fault. The average thickness of mineralization is 6m, ranging up to 16m. A pyrite-marcasite 'cap' overlies the ore in an area of approximately 100m by 50m in the east central part of the orebody. The cap is up to 4m thick, it has a sharp upper contact, and gradational lower contact with the underlying ore.

The G orebody is clearly associated with the G Fault (Doyle and Bowden, 1995a). The thickness, grade and iron content of the ore within the G orebody all increase towards the G fault. However, the average thickness is 8m, ranging up to 22m. The G orebody pyrite 'cap' is more extensive than that in the CW Zone, and measures some 150m by 100m, with a thickness of up to 5m. It has a sharp upper contact and overlies the southern part of the G orebody, close to the G Fault. The southern margin of the G orebody is truncated by the G fault, beneath which copper-silver mineralization has been intersected in a few deeper holes. The mineralization intersected beneath the G zone occurs in the dolomitized Lisduff Oolite Member and Lower Ballysteen Limestone. Vein-type copper-silver mineralization and minor Zn-Pb mineralization also occur within the footwall block of the G Fault. Higher Pb and Fe contents occur adjacent to the G fault (Bowden, pers. comm., 1997) suggesting that the fault acted as a conduit for the ore forming fluids (Doyle and Bowden, 1995a). Chalcopyrite and tetrahedrite-tennantite are the main copper minerals. Higher silver values are associated with increasing concentrations of tetrahedrite-tennantite, but

native silver may also occur as a separate phase (Doyle *et al.*, 1992). Much of the mineralization occurs as epigenetic open space filling, either in a fine-vein network or stockwork, or in small vugs.

A new zone of mineralization, G-West Zone, with an average grade of 15.15% Zn equivalent (Zn equivalent is calculated as the Zn grade plus half the lead grade) was discovered in 1996. The zone was intersected by eight drillholes approximately 250m from the G orebody. In addition, a mineralized zone adjacent to the G orebody in the east was discovered and delineated with a measured resource of over 644,000 tonnes at 22.92% Zn equivalent.

The K orebody contains a measured resource of over 1.2Mt, with an average grade of 14.01% Zn equivalent. Intersected widths and grades are similar to both the CW and G orebodies. The K orebody is located 750m northwest of the G orebody. A new open ended zone of mineralization was discovered within the Templetouhy Bog region, 6km southwest of the Galmoy mine, with a resource in excess of 300,000 tonnes grading 12.16% Zn equivalent.

2.8 SUMMARY

The Lower Carboniferous of Ireland consists of a clastic basin to the south with a northward thinning carbonate sequence underlain by thin basal red beds. The sequence reflects progressive northward transgression and subsidence during the Lower Carboniferous. Many of the features of Carboniferous geology result from the influences imposed by the underlying basement. The NE-SW trending Rathdowney Trend (defined by the gradational contact between dolomitized and undolomitized Waulsortian Limestone) is sub-parallel to inferred major basement Caledonian structures. Mineralization, accompanied by hydrothermal dolomitization, is structurally controlled and occurs principally in the hanging wall rocks of the major faults hosted by tabular, stratabound breccia sheets within dolomitized Waulsortian Limestone of Courceyan age. Subordinate mineralization often occurs in the Lisduff Oolite Member of the Ballysteen Limestone Formation.

CHAPTER 3: PETROLOGY

CHAPTER 3: PETROLOGY

3.1 INTRODUCTION

Subsurface diamond drill core samples formed the basis for petrographic and geochemical investigations. The sample suite chosen represents a variety of Lower Carboniferous lithologies, alteration phenomena, massive and vein sulphides covering as wide a temporal and spatial distribution as possible throughout the Rathdowney Trend.

Carbonate petrography was based on the study of polished thin sections. The sections were studied systematically through transmitted light microscopy (TrL) and cathodoluminescence (CL); paired photomicrographs record permanent images of luminescent characteristics. The thin section off cuts were stained with mixed Alizarin Red S and potassium ferricyanide solution to discriminate between calcite and dolomite minerals. Ore petrography was based on the study of polished blocks by reflected light microscopy, both in air and oil. Chemical characterization of carbonate and ore minerals was carried out using electron microprobe analysis (EMPA). All sample preparation techniques and a summary of analytical methodology is presented in Appendix A. Electron microprobe data are presented in Appendix B. Basic theory, and instrument parameters for CL, reflected light microscopy and EMPA are presented in Appendix C.

3.1.1 Cathodoluminescence

Common minerals (calcite, dolomite, quartz) and some ore minerals (e.g. sphalerite) exhibit CL which reflects variations in the properties of the fluids responsible for deposition. Complex sequences of precipitation and/or dissolution events can be recorded by variation, often extremely subtle in nature, in the CL characteristics of gangue calcite and dolomite. Applications of CL to carbonate-hosted Pb-Zn deposits of the Mississippi Valley-type have been described in detail by Sommer (1972b), Meyers (1974, 1978), Ebers and Kopp (1979), Frank *et al.* (1982), Frank and Lohmann (1987), Gregg and Hagni (1987), Kopp *et al.* (1987), Rowan (1987), Ghazban *et al.* (1994), Thompkins *et al.* (1994), Wallace *et al.* (1994). In Ireland, applications of CL to carbonate-hosted Zn-Pb deposits have been described by Redmond (1997) and Gregg (1997). Hayward (1998) provides an extensive review of CL applications in ore geology, in particular its use in carbonate-hosted Pb-Zn deposits. These ore-related applications, particularly in the

exploration and understanding of carbonate-hosted Pb-Zn deposits may be summarized as follows:

- Correlation of stratigraphic horizons, alteration zones or cement crystallization sequences between boreholes, mines or districts
- Relative timing of mineralizing events
- Determination of diagenetic histories through the identification of events (e.g. cementation, mineral growth, dissolution, compaction) in optically continuous carbonate growth
- Interpretation of mineral deposit development and history
- Identification of changes in the physicochemical properties of fluids
- Interpretation of fluid transport paths and mechanisms

3.1.2 Reflected Light Microscopy

Reflected light microscopy is a standard tool used for examination of opaque and translucent ore and gangue minerals (Craig and Vaughan, 1981). Mineral textures and intergrowths provide information which can be used to interpret a series of equilibrium states which represent different conditions in time or space, and which may allow identification of processes of ore formation (Barton, 1970). Determination of ore-gangue associations are critical to understanding ore emplacement mechanisms and relative time relationships in carbonate-hosted Pb-Zn deposits. As already discussed in Chapter 1, the origin of Irish Zn-Pb ore deposits remains controversial, and theories ranging from syngenetic to wholly epigenetic mineralization have been propounded by many workers in recent years. The paragenetic relationships between carbonate cements and opaque sulphide minerals have been worked out for the southeast Missouri MVT deposits (Voss *et al.*, 1989) by employing reflected light microscopy together with CL and transmitted light microscopy. This method of study is discussed by Gregg and Karakus (1991).

3.1.3 Electron Microprobe Analysis

EMPA is a technique for chemically analyzing small selected areas of solid samples, in which X-rays are excited by a focused electron beam (Reed, 1996). In addition to optical microscopy and X-ray diffraction, EMPA provides compositional information which assists mineral identification. EMPA is ideally suited to the determination of the composition of coexisting phases in rock, from which information such as temperature and pressure of formation can be derived. The high spatial resolution of the technique enables chemical zoning within mineral grains to be studied in detail.

The mineral chemistry of both carbonates and sulphides in the present study have been determined by EMPA. Elemental chemistry provides useful data for distinguishing between different types of dolomite. Major and trace element geochemistry provide information about fluid geochemistry, and might possibly indicate the direction of fluid flow during dolomitization and mineralization.

Applications of EMPA to carbonate-hosted Pb-Zn deposits have been described by Savard (1996) who studied the Gays River Formation of the Lower Windsor Group in the vicinity of the Gays River Zn-Pb deposit. Gregg and Shelton (1989), and Buelter and Guillemette (1988) describe in detail the chemical composition of epigenetic dolomite associated with Pb-Zn mineralization of the Viburnum Trend, southeast Missouri.

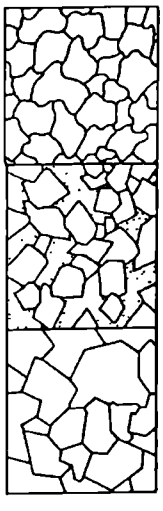
3.2 CARBONATE PETROGRAPHY AND MINERAL CHEMISTRY

Textural, mineralogical, and petrographic relationships of carbonates in the Rathdowney Trend have been determined by CL, transmitted light petrography, and electron microprobe analysis. The determination of diagenetic histories through the record of events preserved in successive precipitation and dissolution episodes, forms a stratigraphic sequence of cement zones which can be observed, interpreted and correlated rapidly with CL. If the cement zones are correlatable, a homogeneous regional groundwater flow system may be inferred in the Rathdowney Trend. Alternatively, localized hydrothermal systems may be more likely if regional correlation is not possible.

A number of processes have been proposed to account for the dolomitization of limestone (Morrow, 1982). These can be divided into two groups: (1) early diagenetic processes, typically involving modified or unmodified seawater (Adams and Rhodes, 1960; Hsü and Siegenthaler, 1969; Badiozamani, 1973; Folk and Land, 1975; Saller, 1984); and (2) late diagenetic or epigenetic processes, commonly involving Mg-rich, basin derived fluids (Zenger, 1983; Gregg, 1985; Machel and Mountjoy, 1986; Hardie, 1987). These processes may be distinguished by textural and chemical characteristics. In Ireland, textures within the Waulsortian host rocks depict a complex sequence of carbonate diagenesis (Lees, 1964; Philcox, 1984; Miller, 1986). Diagenetic fabrics include compaction, cementation and complete replacement. The sequence of diagenetic events within the Waulsortian sediments has a major impact on its potential as a host for mineralization and as a conduit for mineralizing fluids. Thus it is important to be able to identify these stages in order to understand controls on the localization of mineralization.

Dolomite textures have been classified according to the scheme of Sibley and Gregg (1987). The classification scheme is descriptive of textures that develop as a result of the kinetics of dolomite nucleation and growth. The two major divisions in the classification are based on: (1) crystal size distribution - unimodal or polymodal; and (2) crystal boundary shape - planar or non-planar. Planar textures are further subdivided into euhedral (e) or subhedral (s). The textural features are controlled by the mineralogy of the precursor (low- or high-Mg calcite or aragonite), the availability of dolomite nucleation sites, and the degree of saturation of the circulating solution with respect to the carbonate being replaced (Sibley, 1982). This classification scheme is largely descriptive, but carries genetic implications because crystal size distribution is controlled by both nucleation and growth kinetics, and boundary shape is controlled by growth kinetics (Sibley and Gregg, 1987).

The standard cement terminology of Gillies (1987) assists the communication and comparison of CL results. A cement stage is defined as a package of cement with definite and recognizable CL characteristics, mineralogy, chemistry and crystal habit bounded by a disconformity (stages are designated by upper case letters). A zone is the smallest scale cement division visible within the stage or sub-stage, and usually has homogeneous CL characteristics. Four categories are used to define luminescence intensity: *non-luminescence, dull luminescence, moderate luminescence* and *bright luminescence.*



Nonplanar: closely packed anhedral crystals with mostly curved, lobate or otherwise irregular intercrystalline boundaries. Preserved crystal-face junctions are rare and crystals often have undulatory extinction in cross polarized light.

Planar-e (euhedral): most dolomite crystals are euhedral rhombs;crystal-supported with intercrystalline area filled by another mineral or porous.

Planar-s (subhedral): most dolomite crystals are subhedral to anhedral with straight, compromise boundaries and many crystal-face junctions Low porosity and/or low intercrystalline

Figure 3.1 Planar and nonplanar dolomite textures. Modified after Sibley and Gregg (1987).

Analyses of major and trace elements were performed by electron microprobe (wavelength-dispersive) on each dolomitization stage (1-5) for all sampling locations (see Appendices B3,4,5). Spatial and temporal variations were examined, with particular emphasis on the elements Fe and Mn. The detection limits of $FeCO_3$ and $MnCO_3$ are 0.12 mole% (578ppm) and 0.08 mole% (382ppm) respectively, for a beam diameter of 15μm; 0.21 mole% (1012ppm) and 0.11 mole% (526ppm) for a beam diameter of 25μm; and 0.14 mole% (675 ppm) and 0.06 mole% (287ppm) for a beam diameter of 30μm (see Appendix B1). It should be noted that some of the Fe and Mn values reported in the following tables are below the limit of quantitative determination. The elements Sr and Na were largely undetectable, therefore

they have been omitted from the summary tables which follow. For Mg, Ca, Mn, and Fe, the standards used were periclase, calcite, manganese and iron, respectively. High totals are common for carbonate analyses; the minerals break down releasing CO_2, which results in a relative increase in the CaO content. Further, instrumental factors such as beam current drift, and poor spectrometer calibration may cause low or high totals.

3.2.1 Regional Dolomites and Carbonate Cements (Stage 1)

The Waulsortian Limestone has been converted to dolomite over large areas of the Rathdowney Trend (Beaty *et al.*, 1991). The gradational contact between dolomitized and undolomitized Waulsortian forms a NE-SW trending regional dolomite 'front' (see Chapter 2, section 2.3.6). Near to this gradational contact, partially dolomitized Waulsortian is common (Plates 2A, 3A and B). The regional dolomite is composed of a fine to medium crystalline grey dolomite and coarse crystalline white dolomite cement (Plate 2B).

3.2.1a Lisheen Deposit

The regional fine crystalline grey dolomite ($D1_R$) at Lisheen consists of closely packed crystals, 20-100μm in size, displaying a polymodal, nonplanar texture (Plate 2A). The dolomite preferentially replaces microcrystalline components of the Waulsortian limestone and original depositional fabrics are generally destroyed. The dolomite exhibits a dull red, homogeneous luminescence (Plate 2B).

The regional coarse crystalline white dolomite cement ($D1_C$) consists of subhedral to euhedral saddle dolomite crystals 500-5000μm in size. The crystals have curved faces and display a distinct sweeping extinction pattern. The dolomite can be classified as having a polymodal, planar (e) texture. The cement occurs in vugs within the regional fine grey dolomite and preferentially replaces the coarse grained components of the Waulsortian Limestone, such as (high Mg) calcite-filled stromatactis cavities and bioclasts (Plate 3). The vugs often exhibit internal sediment of silt size, at the base of the stromatactic cavities (Plate 2B). The original depositional fabrics are generally preserved, a feature which has been related to the crystal size and mineralogy of the precursor limestone (Sibley, 1982; Bullen and Sibley, 1984). $D1_C$ overgrows or partly replaces diagenetic calcite within a Waulsortian Limestone lens from within the deposit (Plate 3a). The intercrystal spaces created by the network of euhedral saddle dolomite crystals is often infilled by later calcite spar.

$D1_C$ exhibits a dull to moderate, red, weakly zoned luminescence and displays concentric growth zoning (Plates 4A and B). This weak zoning is due primarily to variations in Fe content as demonstrated by X-ray maps (Plate 5A). Quantitative point analysis shows that the non-luminescent zones correspond to high $FeCO_3$ values of up to 0.71 mole%.

Elemental Chemistry

$D1_R$ at Lisheen is non-stoichiometric (Figures 3.2, 3.3, 3.4, 3.5) and contains from 54.59 to 58.30 mole% $CaCO_3$, with an average of 56.77 mole%. The $D1_R$ dolomites are weakly bimodal: one population ranges from 54.5 to 56.5 mole% $CaCO_3$; the second population ranges from 56.5 to 58.5 mole% $CaCO_3$. The $FeCO_3$ content of $D1_R$ ranges from below detection to 0.29 mole%, and $MnCO_3$ from below detection to 0.11 mole% (Table 3.1). D1c at Lisheen is non-stoichiometric and is distinctly more Fe-rich than $D1_R$.

Sample	Carb	No. of Analyses	STDEV ($CaCO_3$)	Average Mole% $CaCO_3$	STDEV ($MgCO_3$)	Average Mole% $MgCO_3$	STDEV ($FeCO_3$)	Average Mole% $FeCO_3$	STDEV ($MnCO_3$)	Average Mole% $MnCO_3$
2447-8 13 3	$D1_C$	29	0 68	54 65	0.67	42 65	0 28	0 32	0 05	0 05
262/153 6	$D1_R$	16	0 71	55 40	0 81	43 49	0.07	0 07	0 03	0 03
121 31.4	$D1_R$	22	0 61	57 50	0 51	43 77	0 09	0 06	0 03	0 03
297 183.3	$D1_R$	6	0.53	57 41	0.60	43.46	0 05	0 07	0.03	0 03

Table 3.1 Chemical composition of Lisheen regional fine crystalline grey dolomite ($D1_R$) and coarse crystalline white dolomite cement ($D1_C$)

3.2.1b Galmoy Deposit

The regional fine crystalline grey dolomite ($D1_R$) at Galmoy displays a polymodal, nonplanar texture, as at Lisheen, and exhibits variable luminescence characteristics. $D1_R$ clasts within sample MG99/100.6 consist of small (10-100μm), closely packed crystals which exhibit a mottled moderate, red - orange luminescence (Plate 6), whilst dolomite clasts within sample MG63/97.2 exhibit a dull red, much more homogeneous luminescence (Plate 7). In sample 3312-2/238.5, the regional fine replacive dolomite consists of closely packed crystals, 50-300μm in size, which exhibit a dull to bright red, non-uniform 'blotchy' luminescence with turbid cores displaying a bright luminescence (Plate 8).

The regional coarse crystalline white dolomite cement ($D1_C$) at Galmoy has a polymodal, planar (e) texture, again very similar to Lisheen. $D1_C$ consists of coarse crystalline, interlocking euhedral dolomite crystals (300-2000μm) within fine crystalline grey dolomite. $D1_C$ occurs in vugs within the regional fine grey dolomite. Sample GY382/86.0 is associated with minor, later sphalerite, and galena mineralization (Plate 9A). Internal sediment of silt size also occurs at the

base of the stromatactis cavities in the Galmoy area (Plate 9A). $D1_C$ exhibits a moderate red, weakly zoned luminescence, slightly less pronounced than the zonation observed at Lisheen.

Elemental Chemistry

$D1_R$ at Galmoy is non-stoichiometric (Figures 3.2, 3.3, 3.4, 3.5), and contains from 57.82 to 62.04 mole% $CaCO_3$, with an average of 59.31 mole% $CaCO_3$ (calcium rich dolomite). The $D1_R$ dolomite is strongly bimodal, with one population being highly non-stoichiometric (60.5 to 62.5 mole% $CaCO_3$), and a second non-stoichiometric population (57.5 to 59.0 mole% CaCO3). The $FeCO_3$ content of $D1_R$ ranges from 0.08 mole% to 0.68 mole%, with a mean of 0.37 mole%. $MnCO_3$ ranges from below detection to 0.28 mole% with a mean of 0.08 mole% (Table 3.2).

Sample	Carb	No. of Analyses	STDEV ($CaCO_3$)	Average Mole% $CaCO_3$	STDEV ($MgCO_3$)	Average Mole% $MgCO_3$	STDEV ($FeCO_3$)	Average Mole% $FeCO_3$	STDEV ($MnCO_3$)	Average Mole% $MnCO_3$
MG63 97.2	$D1_R$	8	0.62	58.05	0.52	41.94	0.39	0.50	0.09	0 07
MG99/100.6	$D1_R$	7	1.80	60.57	1.35	39.58	0.09	0.23	0.07	0 08

Table 3.2 Chemical composition of Galmoy regional fine crystalline grey dolomite ($D1_R$)

3.2.1c Rathdowney Trend Prospects

The regional fine crystalline grey dolomite ($D1_R$) in the Rathdowney Trend prospects displays a polymodal, nonplanar texture similar to both Lisheen and Galmoy (e.g. Plate 10A). A fine, dark grey crystalline dolomite clast in sample HC15/200.8 is composed of a mosaic of small, closely packed anhedral crystals (50-300μm) which exhibits a moderate red-orange, non-uniform luminescence. This clast is hosted by a non luminescent, matrix dolomite, which clearly post-dates the clast (Plate 10B).

The regional coarse crystalline white dolomite cement ($D1_C$) in the Rathdowney Trend prospects can be classified as having a polymodal, planar (e) texture, as at Lisheen and Galmoy. $D1_C$ consists of coarse (300-2000μm) crystalline, interlocking euhedral dolomite, which exhibits a moderate red, weakly zoned luminescence. The dolomite cement occurs in vugs replacing calcite-filled stromatactis cavities which, in sample RE24/1320, have flat bottoms and irregular, digitate tops (Plate 11A). White, saddle dolomite crystals also occur in irregularly shaped vugs, as a component of striped zebra dolomites (Plate 11B) in the Durrow prospect. These 'zebra texture' dolomites represent classic Waulsortian 'reef' textures (Blaney pers. comm., 1995).

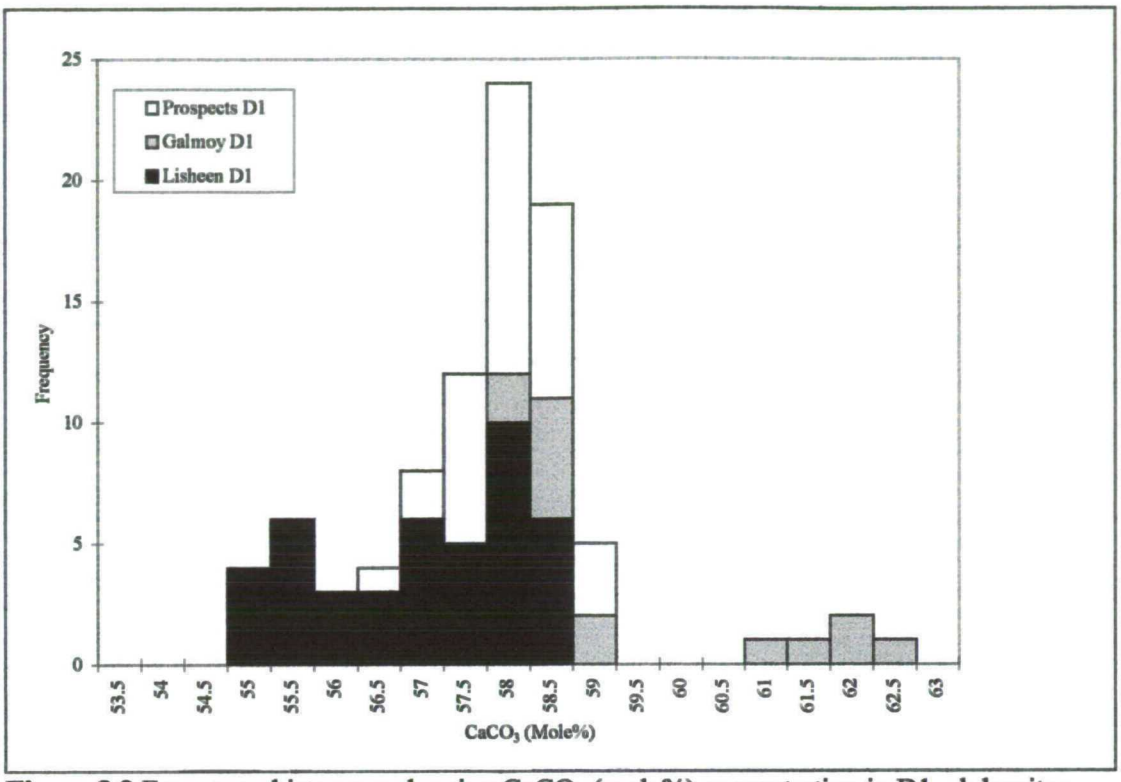


Figure 3.2 Frequency histogram showing $CaCO_3$ (mole%) concentration in $D1_R$ dolomites.

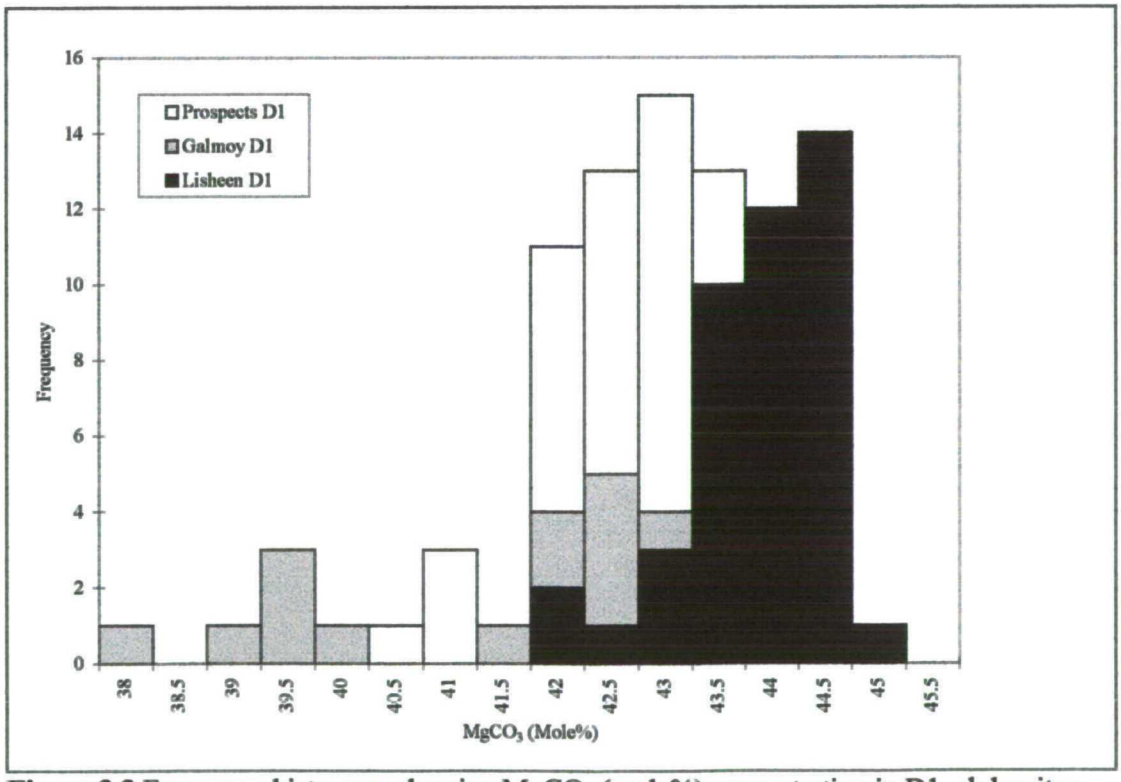


Figure 3.3 Frequency histogram showing $MgCO_3$ (mole%) concentration in $D1_R$ dolomites.

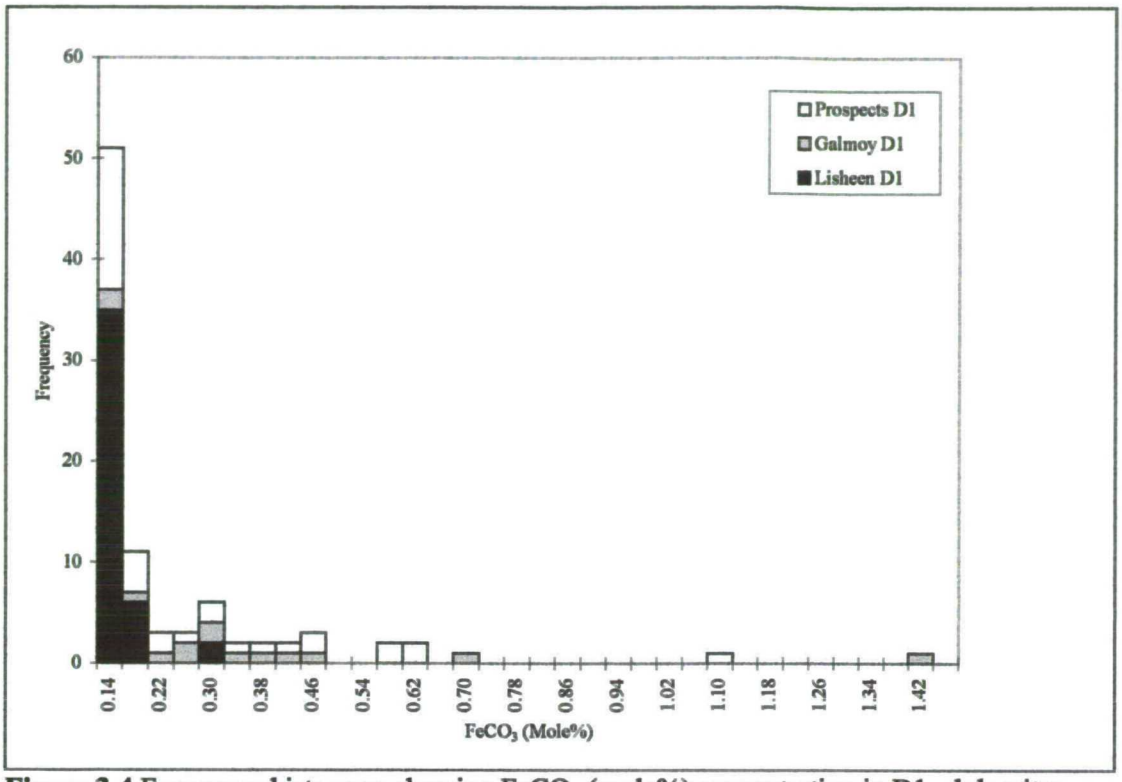


Figure 3.4 Frequency histogram showing $FeCO_3$ (mole%) concentration in $D1_R$ dolomites.

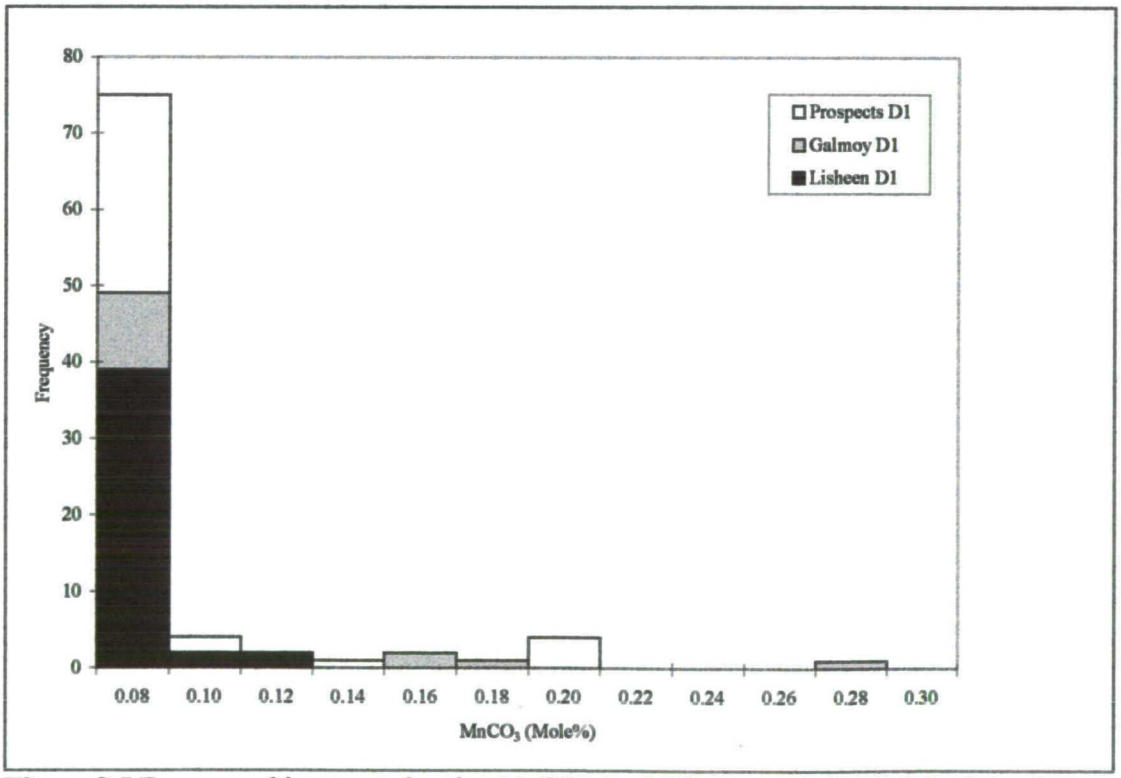


Figure 3.5 Frequency histogram showing $MnCO_3$ (mole%) concentration in $D1_R$ dolomites.

Elemental Chemistry

$D1_R$ at Rathdowney East and Holycross prospects is non-stoichiometric (Figures 3.2, 3.3, 3.4, 3.5), and contains from 56.29 to 58.71 mole% $CaCO_3$, with an average of 57.81 mole% $CaCO_3$ The $FeCO_3$ content of $D1_R$ ranges from below detection to 1.07 mole%, with a mean of 0.26 mole%, and $MnCO_3$ ranges from below detection to 0.21 mole% with a mean of 0.06 mole% (Table 3.3).

Sample	Carb	No of Analyses	STDEV ($CaCO_3$)	Average Mole% $CaCO_3$	STDEV ($MgCO_3$)	Average Mole% $MgCO_3$	STDEV ($FeCO_3$)	Average Mole% $FeCO_3$	STDEV ($MnCO_3$)	Average Mole% $MnCO_3$
RE24 1625	$D1_R$	10	0 88	57 93	0 67	41 73	0 15	0 42	0 08	0 08
RE24 1320	$D1_R$	10	0.51	57 66	0 33	42 85	0 06	0 08	0 03	0 04
RE24 1320	$D1_C$	11	0 41	58 10	0 40	42 97	0 04	0 06	0 04	0 04
HC5 122 9	$D1_R$	14	0 39	57 84	0 76	42.05	0 28	0 27	0 07	0 07

Table 3.3 Chemical composition of Rathdowney East and Holycross regional fine crystalline grey dolomite ($D1_R$) and coarse crystalline white dolomite cement ($D1_C$)

3.2.2 Interpretation of Results (Stage 1)

Timing of dolomitization as determined from petrography indicates that precipitation of the regional fine crystalline grey dolomite ($D1_R$) and coarse white dolomite cement ($D1_C$) post-date Waulsortian Limestone deposition and early Mg rich calcite cements but pre-date mineralization.

$D1_R$ replacement dolomites display polymodal, nonplanar, anhedral dolomite mosaics which represent the final product of dolomitization, with total destruction of original depositional fabrics. Waulsortian Limestone close to the dolomite front is only partially dolomitized, and some depositional fabrics are preserved as a function of selective replacement. The formation of these closely packed, anhedral dolomite crystals may involve a relatively long diagenetic history (Carozzi, 1993). However, in some cases they can form very fast (Gregg *et al.*, 1992). Nonplanar boundaries are characteristic of growth at elevated temperatures (>50°C) and/or high supersaturation (Sibley and Gregg, 1987). $D1_C$ dolomite cements are interpreted to have replaced marine cements (Pickard, 1996), with preservation of the original depositional fabric. In the present study $D1_C$ dolomite has been observed replacing high Mg calcite, presumed to be of early marine origin. $D1_C$ dolomite is interpreted as being a textural variant of $D1_R$ dolomite, but is also chemically different suggesting it probably formed slightly later than the $D1_R$ dolomite. The dull to moderate, weakly zoned luminescence of $D1_C$ dolomite cement, together with its higher Fe content probably reflect variably reducing conditions at the time of its precipitation. Under reduced conditions, Mn and Fe are both in the 2+ oxidation state and both can substitute for Ca,

leading to a dull, partially quenched CL (Carpenter and Oglesby, 1976; Frank *et al.*, 1982; Tucker and Wright, 1990).

On the basis of petrographic evidence and elemental data the pre-ore dolomites are interpreted as involving both early and late diagenetic or epigenetic dolomitizing fluids. The dull red, uniform to non-uniform 'blotchy' luminescence of $D1_R$ probably reflects partial replacement of older dolomite rather than formation *via* direct growth from solution. The bimodal distribution of $CaCO_3$ (mole%) compositions in $D1_R$ dolomites at the Lisheen and Galmoy deposits probably reflects the original chemistry of the dolomite modified by later alteration by D2 dolomitizing fluids. Late diagenetic alteration of ancient dolomites may significantly mask the original chemistry of these rocks (Land, 1980). For example, platform carbonates of the Bonneterre and Davis Formations (southeast Missouri) have undergone both early and late diagenetic dolomitization (Gregg and Shelton, 1990).

3.2.3 Dolomite Matrix Breccias (Stage 2 and 3)

Regional dolomite in Waulsortian Limestone at Lisheen, Galmoy, and Silvermines is cut by texturally distinct dolomite which form large bodies spatially associated with 'feeder' faults. These dolomite bodies are distinguished from earlier regional dolomites by their characteristic breccia textures. This dolomite takes two forms. The first occurs as a distinctive black crystalline dolomite forming a matrix, often with minor sulphides, to brecciated Waulsortian clasts, best developed adjacent to major normal faults and at the base of the Waulsortian complex (see Chapter 2, section 2.6.4). This is considered to be ore-related. The texture, combined with the dark colouration has led various workers to refer to this rock type as dolomite breccia (Silvermines: Andrew, 1986a); rock matrix breccia (Galmoy: Doyle *et al.*, 1992); and black matrix breccia (Lisheen: Hitzman *et al.*, 1992). Dolomite breccias with a distinctive white crystalline matrix also cut regional dolomite in Waulsortian Limestone at Lisheen and Galmoy. The spatial distribution of this dolomite breccia is less well defined but is interpreted to form large bodies which envelop the rock matrix and black matrix breccias (Redmond, pers. comm., 1997). This rock type is referred to as crystalline dolomite breccia (Galmoy: Doyle *et al.*, 1992); or white matrix breccia (Lisheen: Redmond, 1997).

3.2.3a Lisheen Deposit

At Lisheen black matrix breccias consist of angular to subrounded clasts of Waulsortian cemented by a fine grained (20-50μm) crystalline dolomite matrix (D2), displaying a polymodal,

planar - (e) texture (Plate 12A). This dolomite matrix appears black or dark grey in drillcore, probably due to the fine grain size, crystal habit and high porosity. The clasts are mostly regionally dolomitized Waulsortian, but undolomitized limestone clasts are also occasionally observed. The clasts range in size from ~0.5mm to >1m (Shearley *et al.*, 1995) with an average diameter of ~3cm. They are mainly matrix supported, display sharp contacts with the D2 matrix and rarely show evidence of significant rotation. Rarely, similar breccias with a calcite matrix have been observed in the Lisheen area (Plate 29a).

D2 dolomite is intimately associated with ore mineralization (Plates 13, 14, 15) with sulphides replacing first matrix and, ultimately, also clasts (section 3.5). D2 microveinlets are common but can normally only be seen under CL cross-cutting $D1_R$ dolomite clasts (Plate 13B). The D2 dolomite exhibits a bright to moderate, orange-red, non-uniform luminescence (Plates 13, 15). The variable luminescence is a result of predominantly dull red luminescent dolomite clasts and rhombs (approximately 50-250μm in size) which have Fe/Mn poor cores, Fe/Mn rich rims and occur in a fine crystalline, more brightly luminescent Mn-rich (630ppm), Fe-poor matrix (Plate 17). Coarse, weakly zoned, red luminescent, rhombic D2 dolomite crystals in sample 262/159.1 (Plate 16) occur in a finer, variable luminescent matrix. In sample 121/180.5, D2 dolomite crystals display mottled cores exhibiting dull to moderate red luminescence, overgrown by planar, dull to non-luminescent oscillatory zoned dolomite with late bright red luminescent infilling dolomite (Plate 18). These crystals are unusually coarse for D2 dolomite, and therefore may have been syntaxially overgrown by D3 dolomite.

The WMB dolomite (D3) consists of white, coarse (500-900μm) saddle dolomite and subhedral to euhedral interlocking dolomite crystals exhibiting a unimodal, planar - (s) texture (Plate 12B). D3 dolomite is predominantly an open space growth form and is texturally similar to the regional $D1_C$ The coarse dolomite rhombs commonly have cloudy cores and clear outer rims and are relatively clear of fluid inclusions, although some growth zones contain inclusions. The D3 dolomite forms the cement to a breccia of angular to sub-angular, grey clasts of regionally dolomitized Waulsortian (Plate 12B). The clasts are generally more angular than those observed in D2 dolomite, and occasionally display dark, fine crystalline tops (Plate7B). Clast size is highly variable and ranges from approximately 1mm to ~10cm, with an average clast diameter of approximately 3cm. D3 dolomite veinlets are common and cross-cut clasts and there is evidence of minor clast movement and rotation reflected by the orientation of the 'dark tops' (Plate 12B).
The CL characteristics of D3 dolomite cement are very distinct. It exhibits alternating moderate to bright luminescent stages, including a pronounced yellow zone. Sample 121/162.1 consists of 4 concentric growth stages: B, C, D and E (Plates 19, 20). Cement stage B consists of moderate

red, homogeneous luminescent crystal cores; these are overgrown by a thick, mottled dull red luminescent cement stage C. Cement stage D is characterized by alternating bright red-orange to moderate red luminescence zones, followed by a prominent bright yellow zone. Stage E consists of complex fine, dull to moderate red oscillatory zones. Sample 121/165.2 also consists of cement stages B, C, D and E (Plates 21, 22). A similar sequence of growth stages is observed in sample 538/185.2, with a pronounced yellow-orange zone (~30μm thick) in stage D (Plate 23). Sample 252/174.0 (Plate 24) exhibits a bright orange-red, heterogeneous luminescent core, and an alternating bright-dull-bright red zoned outer rim. The bright, distinct yellow zone at the boundary between the luminescent core and outer rim displays a ragged outer edge. Small occurrences of the yellow zone on a different crystal face indicate that the boundary marks a dissolution event, suggesting the zone may have been partially dissolved.

D3 dolomite cements which exhibit these CL properties are commonly located within the ore zones and are close to major and minor faults. Samples 121/162.1 and 121/165.2 are proximal to the major Killoran Fault in the Main zone. Sample 538/185.2 is located in Main zone, approximately 800m north of the Killoran Fault; it is proximal to F14, a subsidary E-W trending fault. Sample 252/174.0 is located in the north of Derryville zone and is not proximal to a fault. Variation of these properties with depth has not been evaluated in this study. However, Redmond (1992) has concluded that the number and thickness of these zones increase downhole within the Lisheen deposit and also increase laterally, moving inward from the edges of the Lisheen system. The observed variation in luminescence of the yellow zone in cement stage D, supports the suggestion that the thickness and intensity of these zones increases laterally, towards the source of mineralizing/dolomitizing fluids. The brightest zone D seems to be in samples from borehole 121 located in Main zone.

Elemental Chemistry

D2 dolomites at Lisheen are non-stoichiometric (Figure 3.6, 3.7, 3.8, 3.9) and vary chemically from 54.22 to 61.40 mole% $CaCO_3$, with an average of 57.82 mole% $CaCO_3$. They show a bimodality with one population ranging from 54.22 to 56.81 mole% $CaCO_3$ and the second ranging from 57.27 to 61.40 mole% $CaCO_3$. The $FeCO_3$ content of D2 dolomites ranges from below detection to 1.29 mole%, with a mean of 0.21 mole%, and $MnCO_3$ from below detection to 0.24 mole % (Table 3.4). There is a striking difference with D3 dolomite which shows much simpler, unimodal compositions.

D3 dolomites at Lisheen are non-stoichiometric (Figures, 3.10, 3.11, 3.12, 3.13), and vary chemically from 54.83 to 60.35 mole% $CaCO_3$, with an average of 57.73 mole% $CaCO_3$ The

$FeCO_3$ content of D3 dolomites ranges from below detection to 1.29 mole%, with a mean of 0.13 mole%. $MnCO_3$ ranges from below detection to 0.11 mole% (Table 3.4).

The prominent bright yellow luminescent zone (40-50μm thick) in stage D (sample 121/162.1) is characterized by Fe, Mn and Sr concentrations of 1787, 465 and 507ppm respectively (Plate 20), as shown by a stage scan across the crystal (Figure 3.14). In sample 121/165.2 a similar yellow zone (50-80μm thick) occurs in stage D, with Fe and Mn values up to 8550 and 2400ppm respectively (Plate 22). Sr concentrations of up to 1606ppm were also detected in this sample (Figure 3.15). The Fe/Mn ratio for the yellow luminescent zone in cement stage D is 3.83 and 3.55 for samples 121/162.1 and 121/165.2 respectively. Cement stages B, C in sample 121/162.1 are characterized by Fe and Mn compositions of 1011 and 387ppm respectively, as shown by the stage scan (Figure 3.14). The Fe/Mn ratio is 2.6. For sample 121/165.2, cement stages B and C are characterized by Fe compositions of up to 466ppm. The Fe/Mn ratio is 2.7. A stage scan across sample 252/174.0 (Figure 3.16) displays significant trace element variations between the alternating bright-dull-bright red zoned outer rim and bright orange-red, heterogeneous luminescent core. The boundary between the two zones is characterized by anomalous Fe, Mn and Sr concentrations of 4430, 2091 and 592ppm respectively. The boundary can clearly be seen under CL. The Fe/Mn ratio for this partially luminescent zone is 2.12.

Sample	Carb	No. of Analyses	STDEV ($CaCO_3$)	Average Mole% $CaCO_3$	STDEV ($MgCO_3$)	Average Mole% $MgCO_3$	STDEV ($FeCO_3$)	Average Mole% $FeCO_3$	STDEV ($MnCO_3$)	Average Mole% $MnCO_3$
262/153 6	D2	17	1.17	55 43	0.81	43 10	0.14	0 19	0 05	0 04
262/152 3	D2	9	0 96	57 83	0 56	43.20	0.15	0 18	0 03	0 05
262/129.8	D2	10	0 82	57 98	0 53	42 04	0 33	0.37	0 07	0 07
259/222.0	D2	10	1.06	57.90	0 61	43 23	0 04	0.07	0.04	0.05
413/100.5	D2	16	1.04	59 98	0.58	40.19	0.10	0.22	0.04	0 05
538 185 2	D3	25	0.88	57.73	1.08	43.73	0.10	0 09	0 03	0 04
252/174 0	D3	19	1 06	58 24	1 01	42 43	0 33	0.19	0 03	0 09
297/183.3	D3	10	0 74	58.24	0 49	43.74	0.08	0.09	0.03	0 03
121 162.1	D3	49	1.00	56.69	1.1	43.54	0 16	0.14	0.01	0 06

Table 3.4 Chemical composition of Lisheen black matrix breccia (D2) and white matrix breccia dolomites (D3).

3.2.3b Galmoy Deposit

The rock matrix breccia (referred to hereafter as black matrix breccia) consists of a dark, very fine (20-50μm) crystalline dolomite matrix (D2), displaying a polymodal, planar - (e) texture similar to Lisheen. The breccia contains approximately 50-65% by volume sub-angular to sub-rounded clasts of medium grey regional dolomite ranging from 5 to 25mm in size. Sample MG18/87.5 contains sub-rounded dolomite clasts (Plate 25A). The clasts are noticeably more rounded than those commonly seen in the Lisheen black matrix breccias (compare Plate 12B);

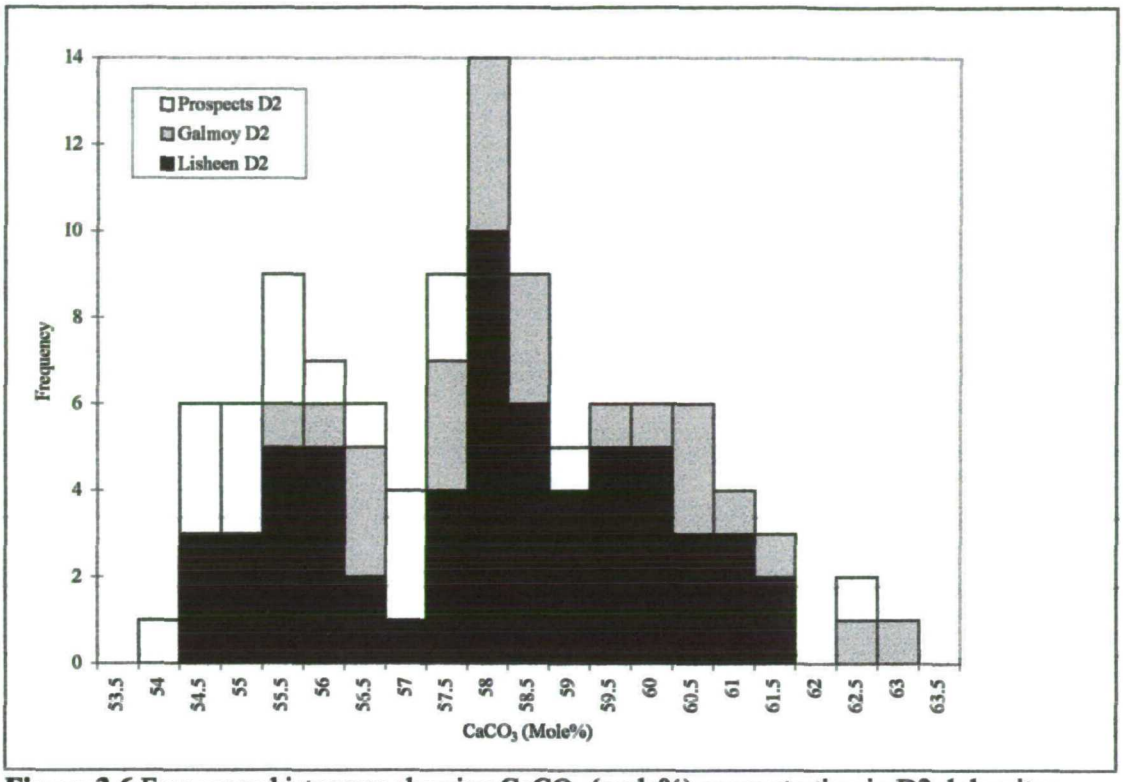


Figure 3.6 Frequency histogram showing $CaCO_3$ (mole%) concentration in D2 dolomites.

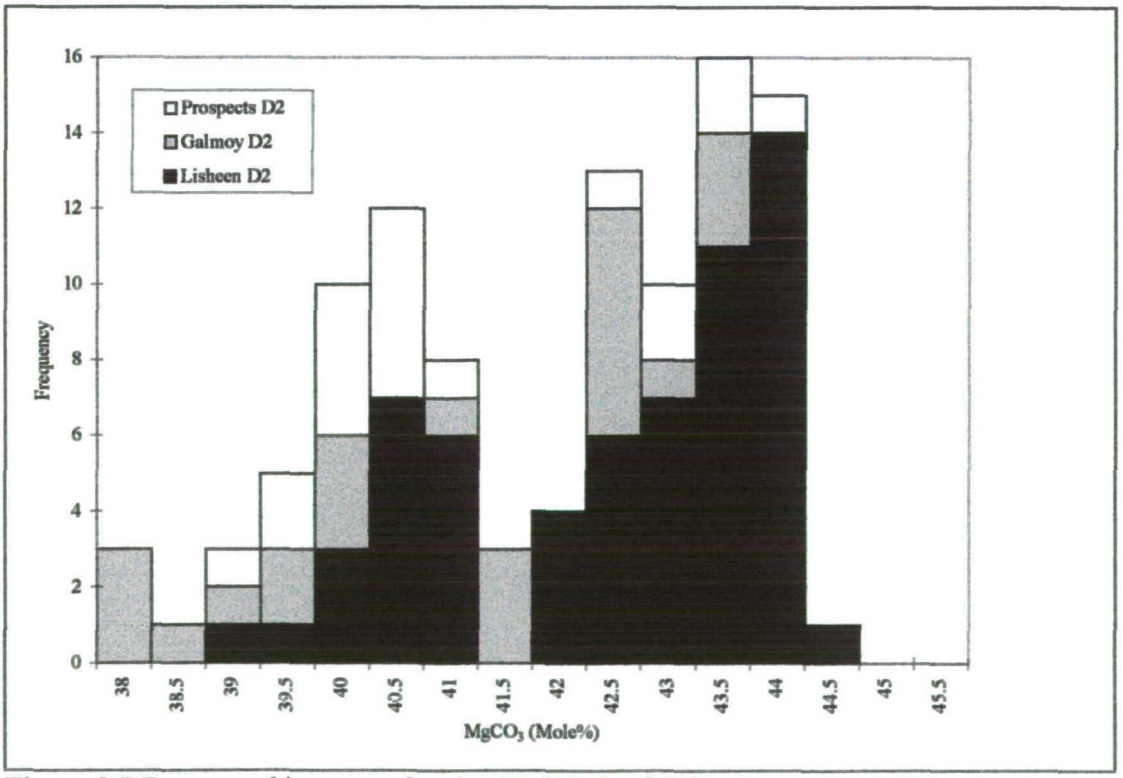


Figure 3.7 Frequency histogram showing $MgCO_3$ (mole%) concentration in D2 dolomites.

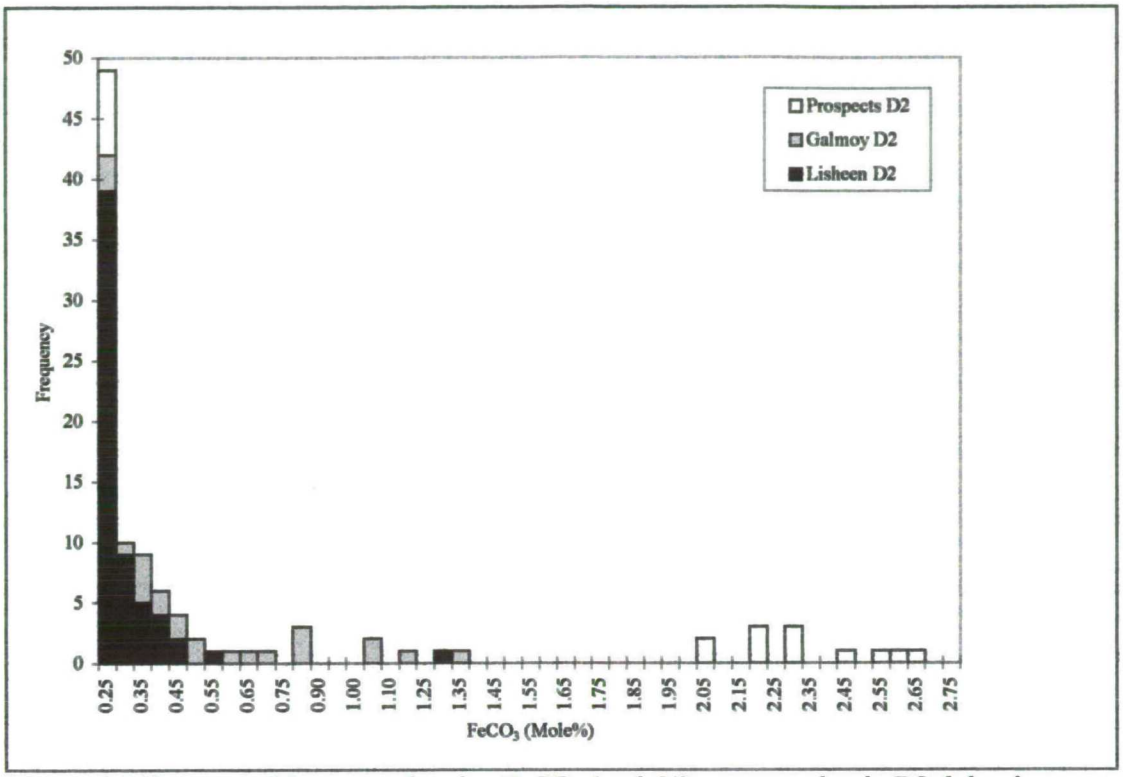


Figure 3.8 Frequency histogram showing $FeCO_3$ (mole%) concentration in D2 dolomites.

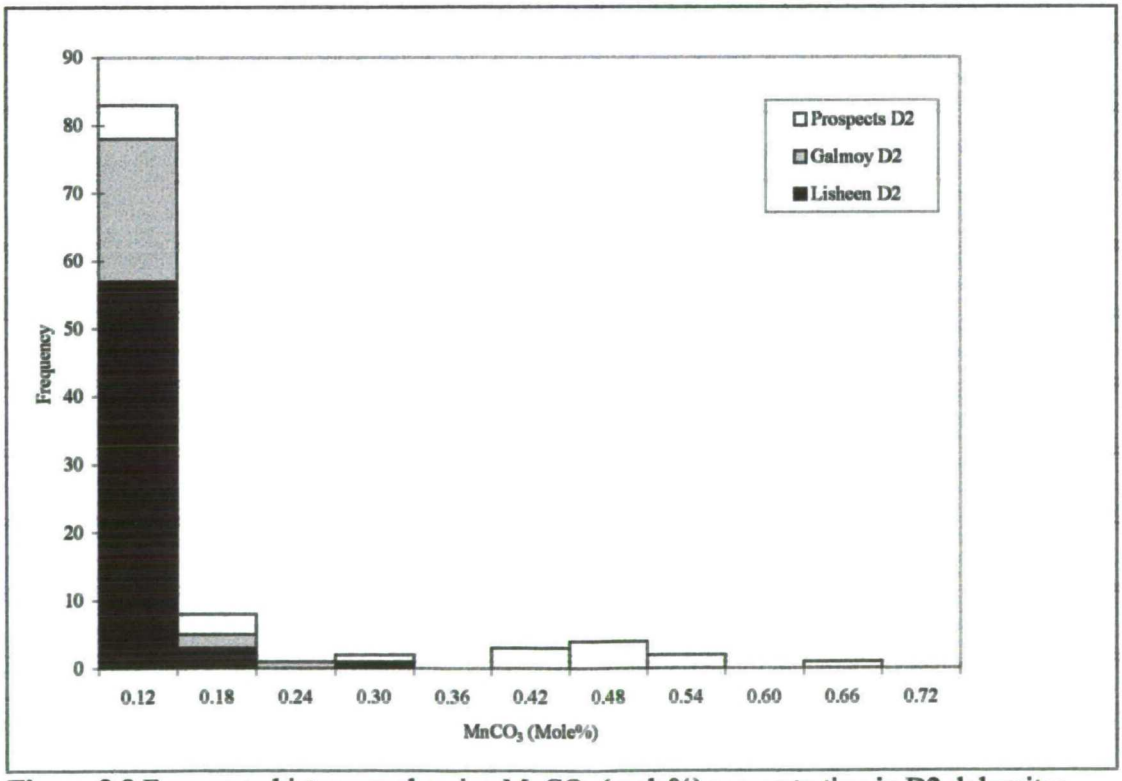


Figure 3.9 Frequency histogram showing $MnCO_3$ (mole%) concentration in D2 dolomites.

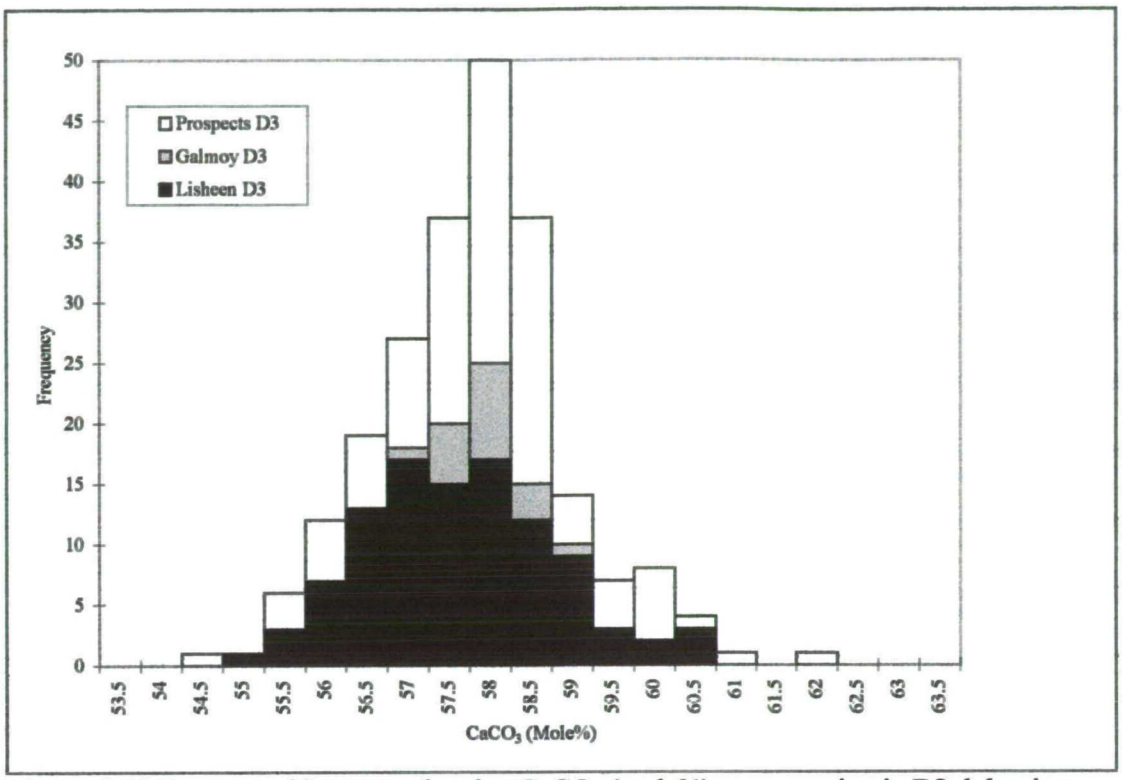


Figure 3.10 Frequency histogram showing $CaCO_3$ (mole%) concentration in D3 dolomites.

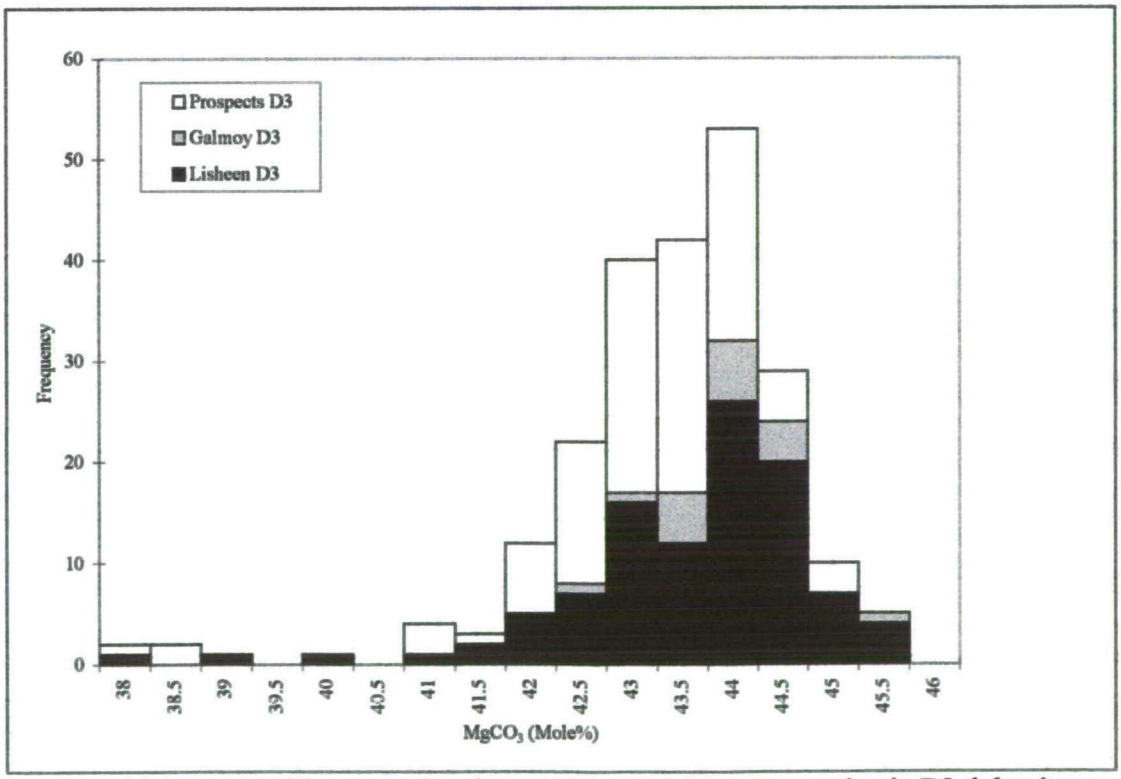


Figure 3.11 Frequency histogram showing $MgCO_3$ (mole%) concentration in D3 dolomites.

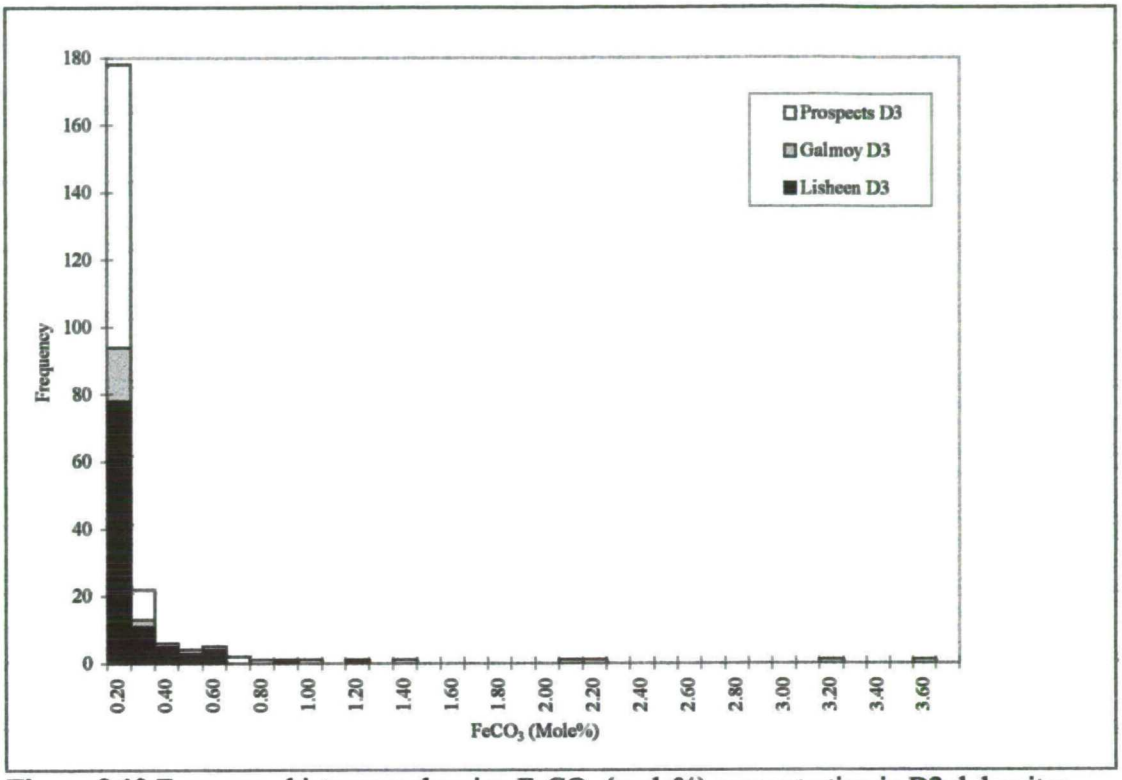


Figure 3.12 Frequency histogram showing $FeCO_3$ (mole%) concentration in D3 dolomites.

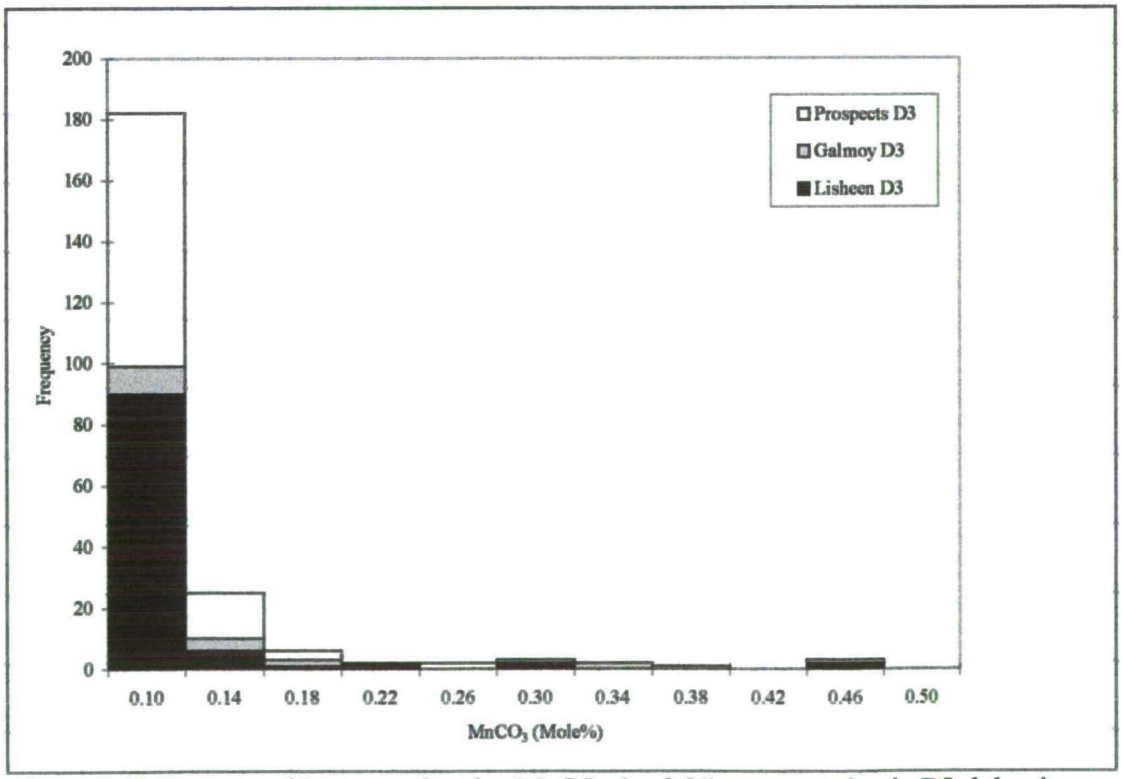


Figure 3.13 Frequency histogram showing $MnCO_3$ (mole%) concentration in D3 dolomites.

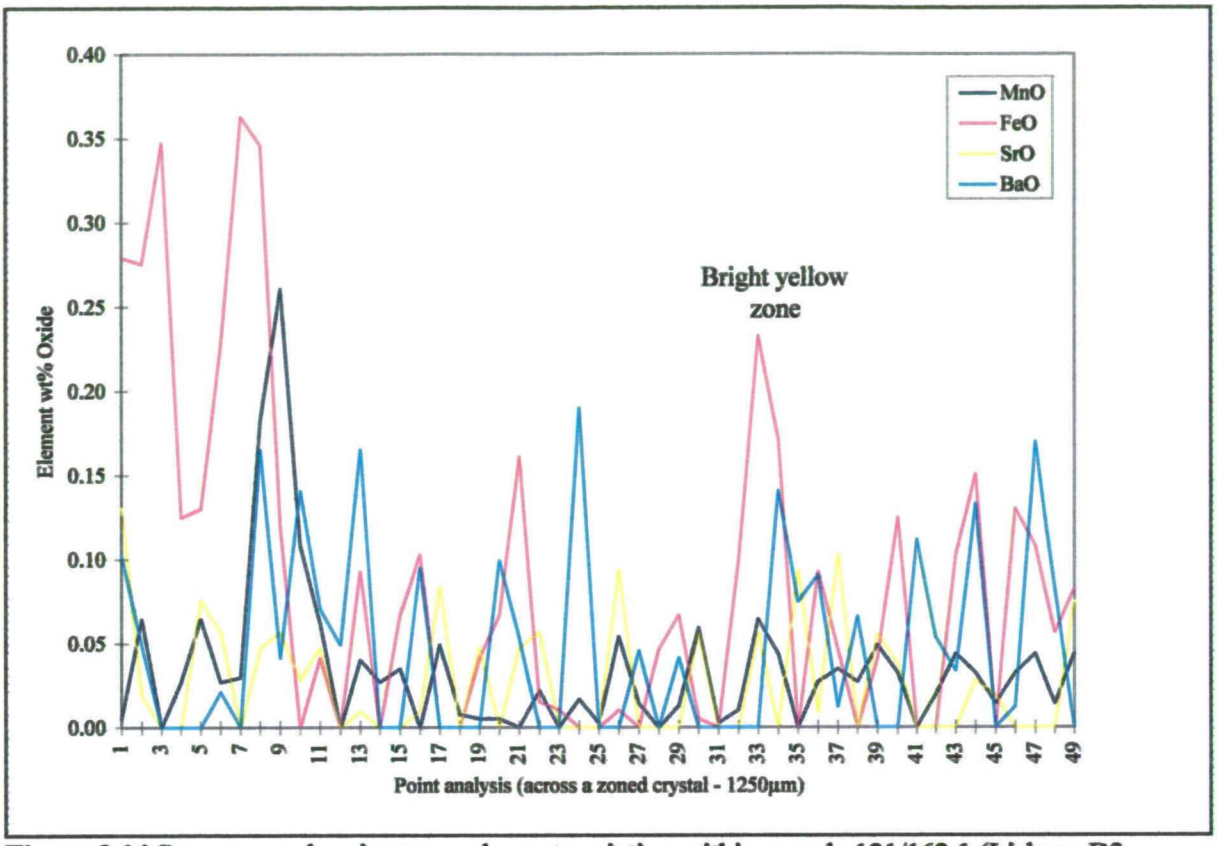


Figure 3.14 Stage scan, showing trace element variation within sample 121/162.1 (Lisheen D3 dolomite).

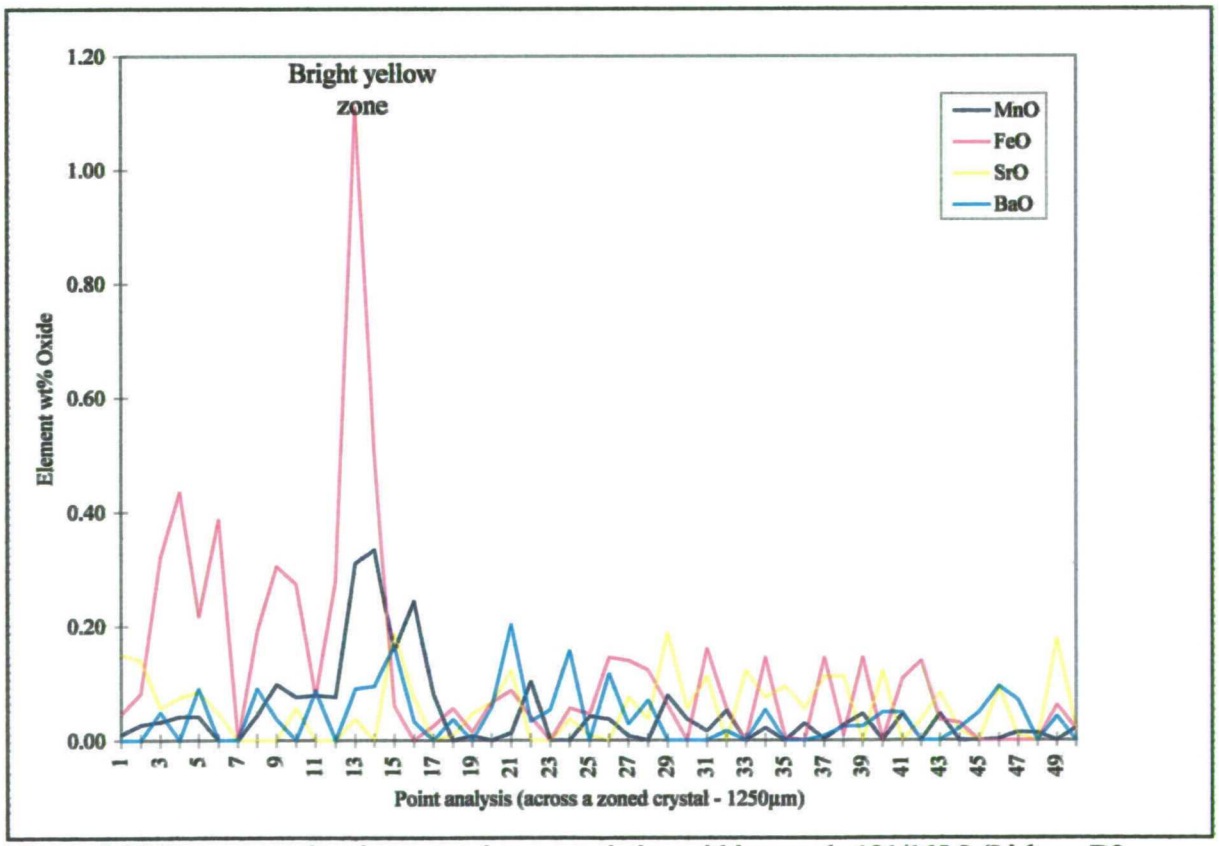


Figure 3.15 Stage scan, showing trace element variation within sample 121/165.2 (Lisheen D3 dolomite).

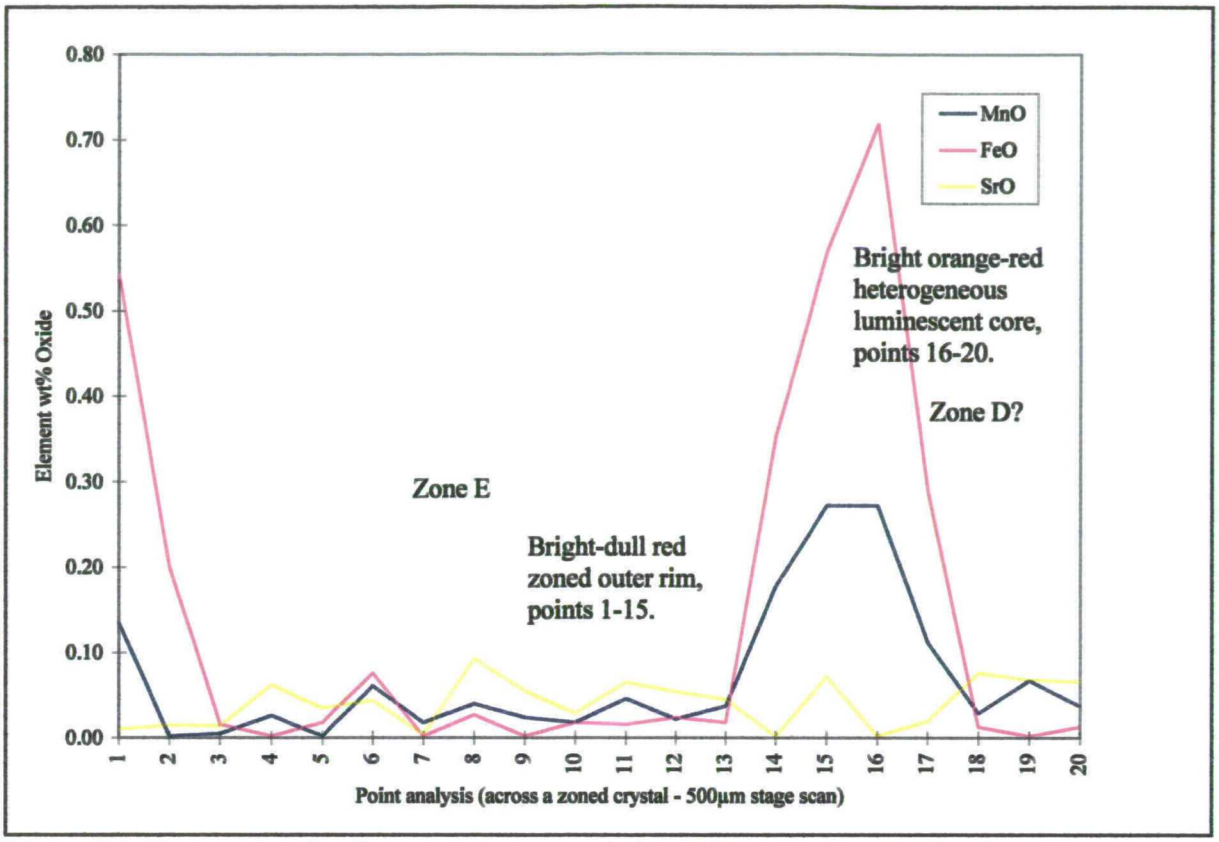
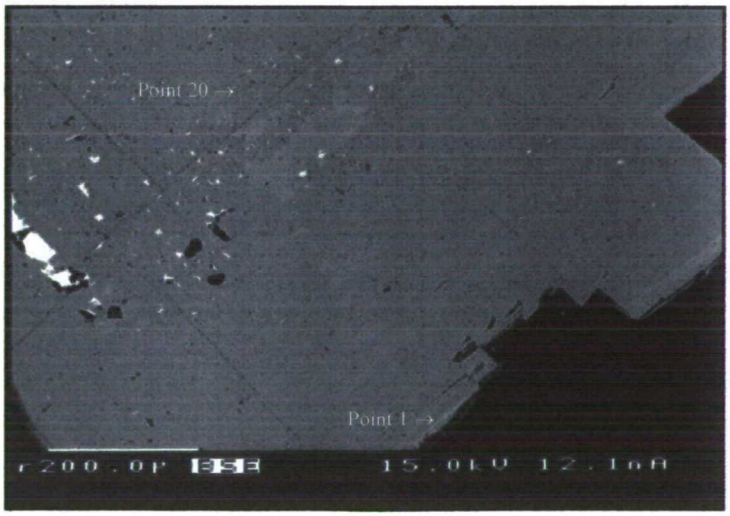


Figure 3.16 Stage scan, showing trace element variation within sample 252/174.0 (Lisheen D3 dolomite). Traverse of points shown below on back-scattered electron image of D3 crystal.



however, sometimes paler, larger, and more angular clasts of dolomite do occur. Many of the sub-rounded clasts display embayed edges, and are partly replaced by D2. In a down-hole progression, breccias vary from entirely clast-supported through matrix-supported to sections with only a few clasts. More than 95% of the clasts are dolomitized (Lowther, pers. comm., 1998). D2 is intimately associated with ore mineralization (Plate 26) with non, dull and brightly zoned luminescent sphalerite replacing D2 dolomite (section 3.5). The occurrence of rare, cross-cutting crystalline dolomite veinlets suggests that the black matrix breccia is postdated by the crystalline dolomite breccia (Doyle *et al.*, 1992).

D2 dolomite exhibits a bright to dull, orange-red, non-uniform luminescence (Plates 6, 7). The variable luminescence is characterized by dull red luminescent, euhedral dolomite rhombs (approximately 40 -160μm in size), displaying minor oscillatory zoning set in a brighter, mottled fragmentary matrix. The dolomite rhombs are matrix supported and are partially replaced by the finer grained brighter luminescent matrix (Plate 6B). D2 dolomite microveinlets, similar to those observed at Lisheen, display bright orange-red luminescence and are observed cross-cutting $D1_R$ dolomite clasts (Plate 7B). Euhedral dolomite rhombs (approximately 35-100μm in size) in sample MG63/97.2 (Plate 27) exhibit moderate red luminescent cores and bright luminescent rims. These luminescent properties probably reflect Fe/Mn poor cores, and Fe/Mn rich rims similar to D2 dolomites at Lisheen (compare Plate 17). There seems to be increased luminescence of $D1_R$ at the contact with D2 dolomite in sample MG63/97.2 (Plate 27).

The crystalline dolomite breccia (referred to hereafter as white matrix breccia) is mostly confined to the massive Waulsortian unit and consists of a matrix of white, coarse (500-800μm), subhedral to euhedral dolomite (D3) displaying unimodal, planar (s) texture as at Lisheen. D3 dolomite is predominantly an open space growth form and is texturally similar to the regional $D1_C$, with cloudy centred cores and clear-rimmed rhombs common throughout (Plate 28A). D3 dolomite generally contains approximately 35-55% by volume angular to sub-rounded, grey clasts of regionally dolomitized Waulsortian, of highly variable size. Clast rotation is minimal. Some sub-rounded mineralized clasts are present (Plate 9B), clearly indicating that the white matrix breccia dolomite event was syn -to post the main ore-related dolomitizing stage. Crystalline white dolomite veinlets in sample MG63 97.2 cross-cut D2 dolomites (Plates 29 and 29a.) and $D1_R$ dolomite clasts, indicating that the D3 dolomite is later than the D2 dolomitizing event. The D3 dolomite in sample GY355/97 is overgrown by pink dolomite (D4) (Plate 9B). The crystalline matrix is predominantly white, with minor D4 dolomite cement. Occasionally, vugs within this crystalline matrix of D3 and D4 dolomite cements are filled by late calcite spar.

The D3 cement at Galmoy exhibits alternating moderate to bright luminescence stages - including a pronounced yellow zone in stage D similar to that observed in the Lisheen D3 dolomite (compare Plates 19 and 28). Sample GY355/78 consists of approximately 4 concentric growth stages designated B, C, D, and E. However, the yellow luminescent zone (10μm thick) is much less pronounced and notably thinner than the observed yellow zones in the Lisheen D3 dolomites. The white crystalline dolomite vein in sample MG63/97.2 displays dolomite cement stages A, B, C, D and E (Plate 29). Cement stage A displays bright, yellow-orange, luminescence either side of a fracture; this is followed by cement stages B and C characterized by a moderate red luminescence with yellow luminescent inclusions. Cement stage D is characterized by a bright red-orange, uniform luminescence, but there is no yellow zone. Stage E is Fe-rich, and consequently displays non to dull red luminescence.

Elemental Chemistry

D2 dolomite at Galmoy is non-stoichiometric (Figures 3.6, 3.7, 3.8, 3.9), and varies chemically from 55.01 to 62.59 mole% $CaCO_3$, with an average of 58.90 mole% $CaCO_3$. The D2 dolomites are bimodal, one population is highly non-stoichiometric and ranges from 59.00 to 62.59 mole% $CaCO_3$. The second population ranges from 55.01 to 58.5 mole% $CaCO_3$. These populations are very similar to Lisheen D2 dolomite. The $FeCO_3$ content of D2 dolomites ranges from below detection to 1.32 mole%, with a mean of 0.66 mole%. $MnCO_3$ content ranges from below detection to 0.20 mole% with a mean of 0.12 mole%. (Table 3.5).

D3 dolomites at Galmoy are non-stoichiometric (Figures 3.10, 3.11, 3.12, 3.13) and vary chemically from 56.50 to 62.59 mole% $CaCO_3$, with an average of 57.60 mole% $CaCO_3$. The $FeCO_3$ content of D3 dolomites ranges from below detection to 0.24 mole%, with a mean of 0.04 mole%. $MnCO_3$ ranges from below detection to 0.33 mole%, with a mean of 0.11 mole% (Table 3.5).

Fe, Mn and Sr concentrations of up to 1166, 1549 and 507ppm respectively have been detected in sample MG99/100.8 (Plate 28a A, B). This D3 dolomite displays a pronounced Fe, Mn rich zone, approximately 50-100μm thick.

The prominent bright yellow-orange luminescent cement stage A, either side of the fracture in sample MG63/97.2 (Plate 29) is the earliest vein phase and is characterized by high K values. A scan across this vein (Figure 3.17) shows that between points 21 and 29 there is a positive correlation between K and Fe. This correlation can be observed again, between points 42 and 48 representing the other vein margin. Cement stages B and C are characterized by average Fe and

Mn compositions of 5985 and 1859ppm respectively and there is a positive correlation between Fe and Mn within these stages (points 31 to 40). The Fe/Mn ratio for the moderate red luminescent cement stage with yellow luminescent inclusions is 3.2, similar to the Fe/Mn ratio calculated for the yellow luminescent zone in cement stage D for Lisheen D3 dolomites.

Sample	Carb	No. of Analyses	STDEV ($CaCO_3$)	Average Mole% $CaCO_3$	STDEV ($MgCO_3$)	Average Mole% $MgCO_3$	STDEV ($FeCO_3$)	Average Mole% $FeCO_3$	STDEV ($MnCO_3$)	Average Mole% $MnCO_3$
MG99 100 6	D2	9	2.25	60 28	0 87	38 83	0 36	0 56	0 06	0 08
MG63/97.2	D2	8	1.96	58 81	1.42	40.33	0 67	1.00	0.14	0 24
5.	D2	10	0 90	57 62	0.65	42 49	0.17	0.42	0.02	0 05
GY355 97.0	D3	9	0.68	57 53	0.63	44 13	0 03	0.02	0 04	0 04
MG99 100 8	D3	10	0.41	57.67	0.49	43.35	0.09	0.07	0 01	0.18
MG63/97 2	D3	21	1.62	58 30	1.33	40 25	0 36	0 57	0 11	0 15

Table 3.5 Chemical composition of Galmoy black matrix breccia (D2) and white matrix breccia dolomites (D3).

3.2.3c Rathdowney Trend Prospects

Similar, localized, ore-related dolomitization events which produced well developed dolomite matrix breccias at both Lisheen and Galmoy were probably responsible for the formation of weak to moderately well developed dolomite matrix breccias at the Holycross, Rathdowney East, Durrow and Derrykearn prospects. The occurrence of coarse crystalline white dolomite veinlets (D3?) cross-cutting poorly developed black matrix dolomite (Plate 30) suggests that the coarse crystalline white dolomite is syn - to post the black matrix breccia dolomitization event observed in the prospects, comparable with Galmoy.

The black matrix breccia dolomite (D2) at Holycross comprises a dark, crystalline matrix composed of euhedral dolomite rhombs (40-200μm), displaying a polymodal, planar - (e) texture.

The dolomite matrix consists of notably more euhedral dolomite rhombs than D2 dolomites observed at Lisheen and Galmoy. The D2 dolomite exhibits moderate red, non-uniform luminescent cores and bright red luminescent outer rims (Plate 31).

The coarse crystalline white dolomite (referred to hereafter as D3 dolomite) consists of white, coarse (400-800μm) subhedral to euhedral, crystalline dolomite displaying unimodal, planar (s) texture. Cloudy centred cores and clear-rimmed rhombs are common throughout (Plate 32). The D3 dolomite cements angular to sub-rounded clasts of pale and dark grey dolomitized Waulsortian ($D1_R$) (Plates 33 and 34). The prospect breccias appear more matrix supported, with more rounded clasts than deposit breccias. Clast to matrix ratio is highly variable. Clast sizes are variable ranging from approximately 1mm to 6cm. The rounded pale grey clasts in sample

DUR1/686.5 (Plate 34A) are porous and have diffuse rims, the dark grey clasts are less porous and have sharper non-diffuse rims.

The D3 dolomite cement in the prospects exhibits alternating moderate to bright luminescence stages, including the pronounced yellow zone observed in the Lisheen D3 dolomite (Plate 35,36). However, the yellow luminescent zone (5-10μm thick in sample RE24/1729a, and 20-40μm thick in sample 45/271.6) of stage D is much less pronounced and notably thinner, than the observed yellow zones in the Lisheen D3 dolomites (compare Plates 19, 21, 23, and 35, 36). The distinctive yellow zone of stage D is present in Rathdowney East (RE24/1729) and Derrykearn (45/271.6) samples, the yellow zone is not present in Holycross and Durrow D3 dolomite samples (Plates 32, 37, and 38). However, a bright red-orange luminescent zone is present in DUR1/686.5, and a bright red-orange luminescent zone which is overgrown by a late Fe rich zone is present in DUR4/365.5. The luminescence characteristics of Rathdowney East (sample RE24/1729) are comparable to Galmoy, sample GY355/78 (compare Plates 35 and 28).

Elemental Chemistry

D2 dolomite at the Holycross prospect is non-stoichiometric (Figures 3.6, 3.7, 3.8, 3.9), and varies chemically from 53.90 to 62.36 mole% $CaCO_3$, with an average of 55.76 mole% $CaCO_3$. The range in $CaCO_3$ composition is large, however, two populations can be defined. One population ranges from 54.0 to 55.5 mole% $CaCO_3$, the second population ranges from 56.5 to 57.5 mole% $CaCO_3$. The $MgCO_3$ composition clearly shows two populations. The $FeCO_3$ content of D2 dolomite ranges from below detection to 2.61mole%, with a mean of 1.18 mole%, and $MnCO_3$ from below detection to 0.60 mole % with a mean of 0.24 mole% (Table 3.6).

D3 dolomite at all the Rathdowney Trend prospects is non-stoichiometric (Figures 3.10, 3.11, 3.12, 3.13), and varies from 54.83 to 61.92 mole% $CaCO_3$, with an average of 57.55 mole% $CaCO_3$, and a modal composition of 58.0 $CaCO_3$ mole%. The $FeCO_3$ content in D3 dolomites ranges from below detection to 3.55 mole%, with a mean of 0.18 mole%. $MnCO_3$ ranges from below detection to 0.44 mole%, with a mean of 0.06 mole% (Table 3.6).

Stage scans across Holycross (HC13/87.5) and Durrow (DUR1/686.5, DUR4/365.5) samples (Figures 3.18, 3.19, 3.20), show trace element variations across weakly zoned crystals. Sample HC13/87.5 (Plate 32) exhibits a bright red-orange, mottled luminescent core, and an alternating dull to moderate red luminescent finely oscillatory zoned rim. The trace elements Fe, Mn and Sr are all below detection in the luminescent core. A dull red luminescent outer zone, approximately

100μm thick is characterized by Fe and Sr compositions of 622 and 676ppm respectively. Mn is below detection.

The bright red luminescent zone in sample DUR1/686.5 (Plate 37) is characterized by Fe and Mn concentrations of 1244 and 387ppm respectively. The Fe/Mn ratio is 3.2, which is virtually the same as for D3 dolomites at Lisheen (samples 121/162.1 and 121/165.2) and Galmoy (sample MG63/97.2). The bright red-orange luminescent zone in sample DUR4/365.5 (Plate 38) which is overgrown by an Fe rich zone is approximately 100 to 500μm thick and is characterized by Fe, Mn and Sr values up to 8006, 1704 and 423ppm respectively. The Fe/Mn ratio is 4.7, higher than in DUR1/686.5, and in Lisheen and Galmoy samples. The Fe rich zone which overgrows the bright red-orange luminescent zone is characterized by Fe, Mn and Sr compositions of 17100, 2091, and 507ppm respectively. The zone is non-luminescent, probably a function of the very high Fe/Mn ratio, 8.15.

Sample	Carb	No. of Analyses	STDEV ($CaCO_3$)	Average Mole% $CaCO_3$	STDEV ($MgCO_3$)	Average Mole% $MgCO_3$	STDEV ($FeCO_3$)	Average Mole% $FeCO_3$	STDEV ($MnCO_3$)	Average Mole% $MnCO_3$
HC13 115 3	D2	8	1.96	57 84	1 46	42 68	0 05	0 07	0 05	0 07
HC3569-2/293	D2	12	0.78	54 96	0.51	39.86	0.19	2.29	0.11	0 42
DUR1 686 5	D3	13	0 79	56 05	0 67	42.13	0 03	0 04	0 03	0 04
DUR4 365 5	D3	18	0 92	57.02	1.71	42.49	1 08	0 58	0.14	0.10
45/294 6	D3	8	0 31	58 08	0 35	44 07	0 10	0 11	0.05	0 06
45/273.0	D3	20	1 09	58 09	1 22	42 40	0.46	0 16	0 05	0 06
HC13 87 5	D3	19	0 62	57.69	0 64	43 53	0 06	0 07	0 04	0 06
RE24 1674a	D3	12	0 53	57 78	0 52	43 38	0 61	0 25	0 08	0 05
RE24/1718 0	D3	12	0 69	58 12	0 51	43 56	0 07	0 04	0 04	0 05

Table 3.6 Chemical composition of Rathdowney Trend Prospect black matrix breccia (D2) and white matrix breccia (D3) dolomites.

3.2.4 Interpretation of Results (Stage 2 and 3)

3.2.4a Timing of Dolomitization

Timing of dolomitization as determined from petrography indicates that precipitation of both the D2 and D3 dolomites post-dates the regional $D1_R$ and $D1_C$ dolomites. D2 predates the mineralization event, the timing of D3 is less conclusive. However, D3 is interpreted as probably being syn- to post the mineralization event. D3 is principally a breccia matrix, whilst $D1_C$ occurs in vugs and veins within $D1_R$ Generally white dolomite in $D1_R$ clasts truncated by D2 dolomite can be texturally interpreted as being $D1_C$ Occasionally, occurrences of white dolomite within $D1_R$ clasts cannot be unequivocally interpreted as such.

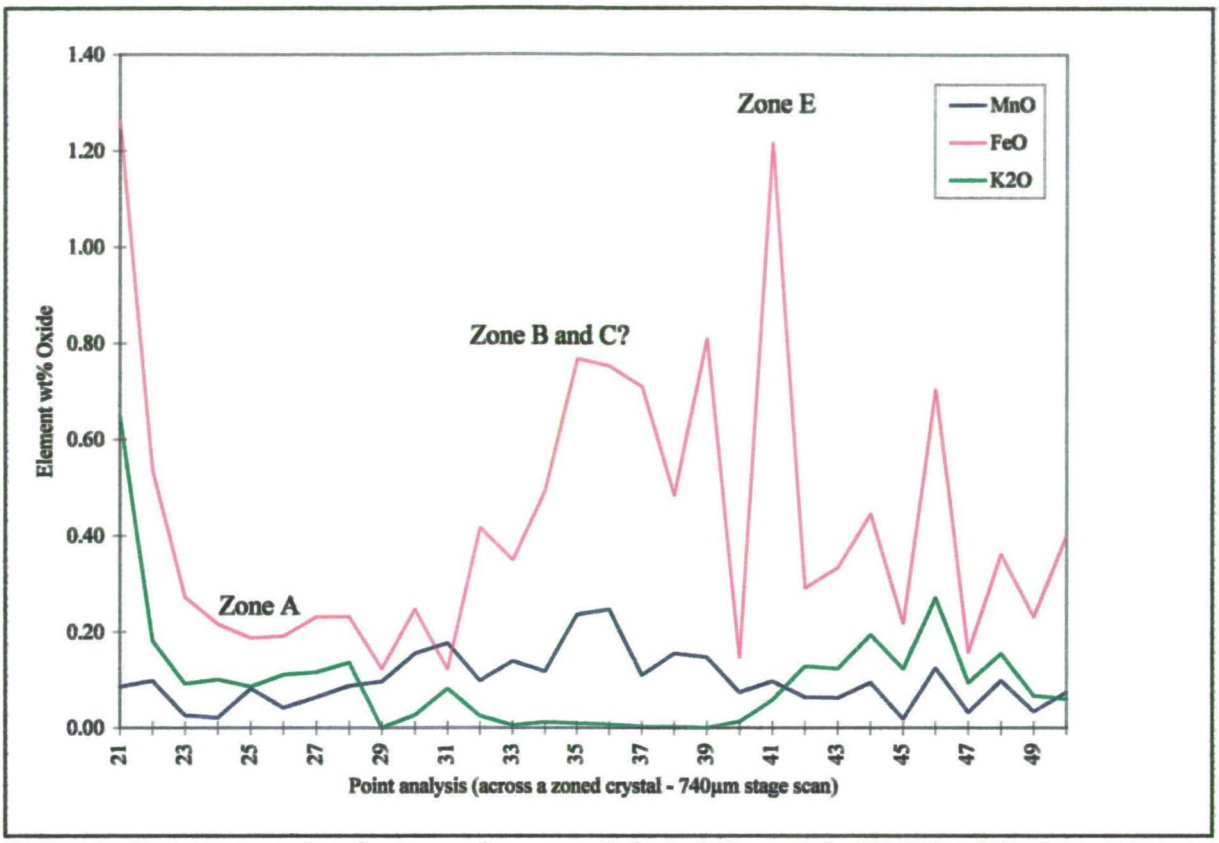


Figure 3.17 Stage scan, showing trace element variation within sample MG63/97.2 (Galmoy D3 dolomite).

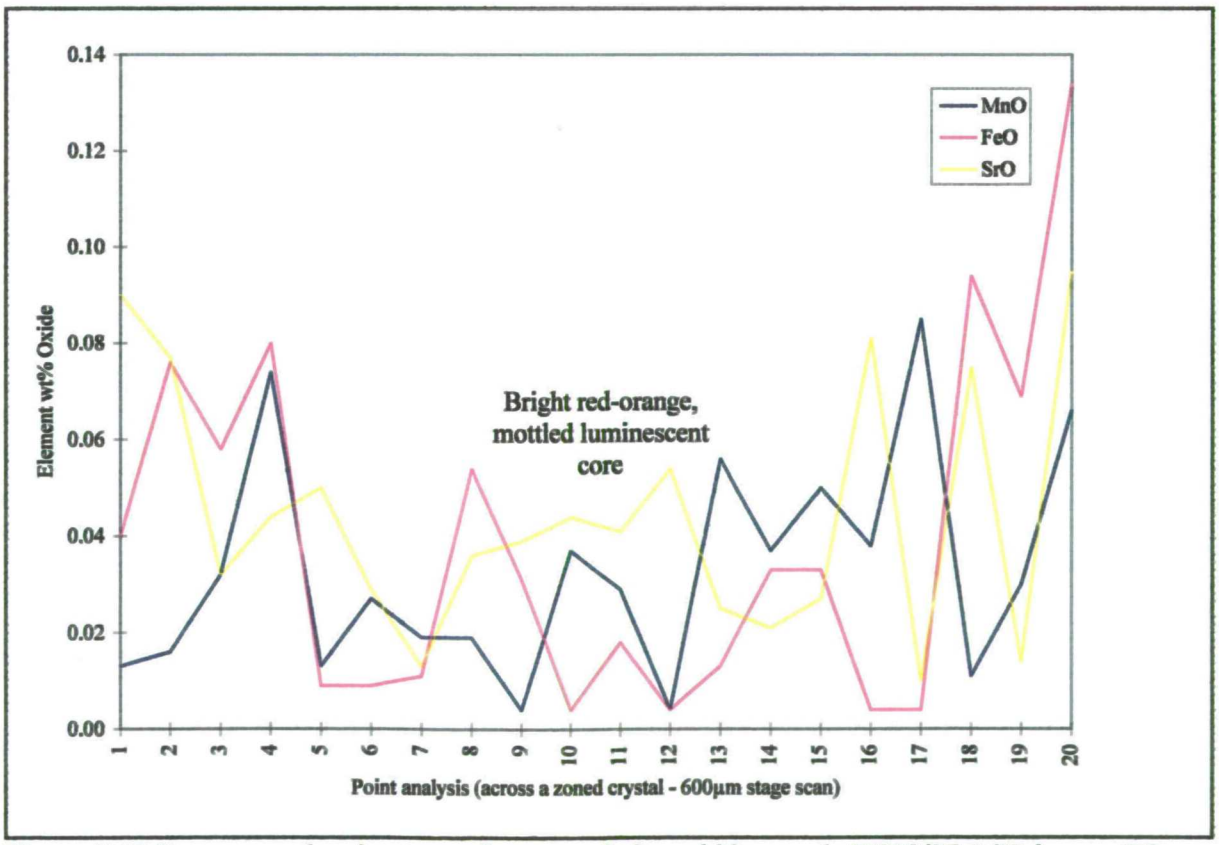


Figure 3.18 Stage scan, showing trace element variation within sample HC13/87.5 (Holycross D3 dolomite).

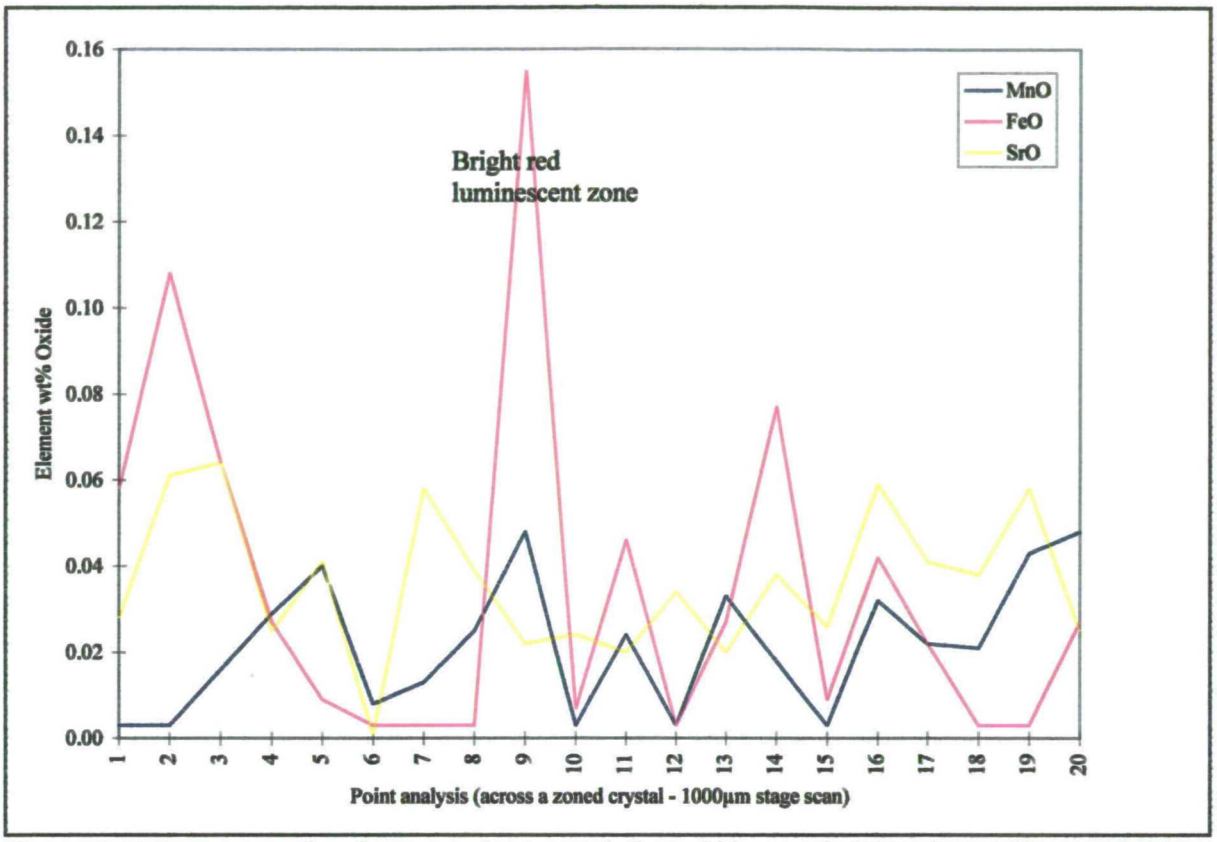


Figure 3.19 Stage scan, showing trace element variation within sample DUR1/686.5 (Durrow D3 dolomite).

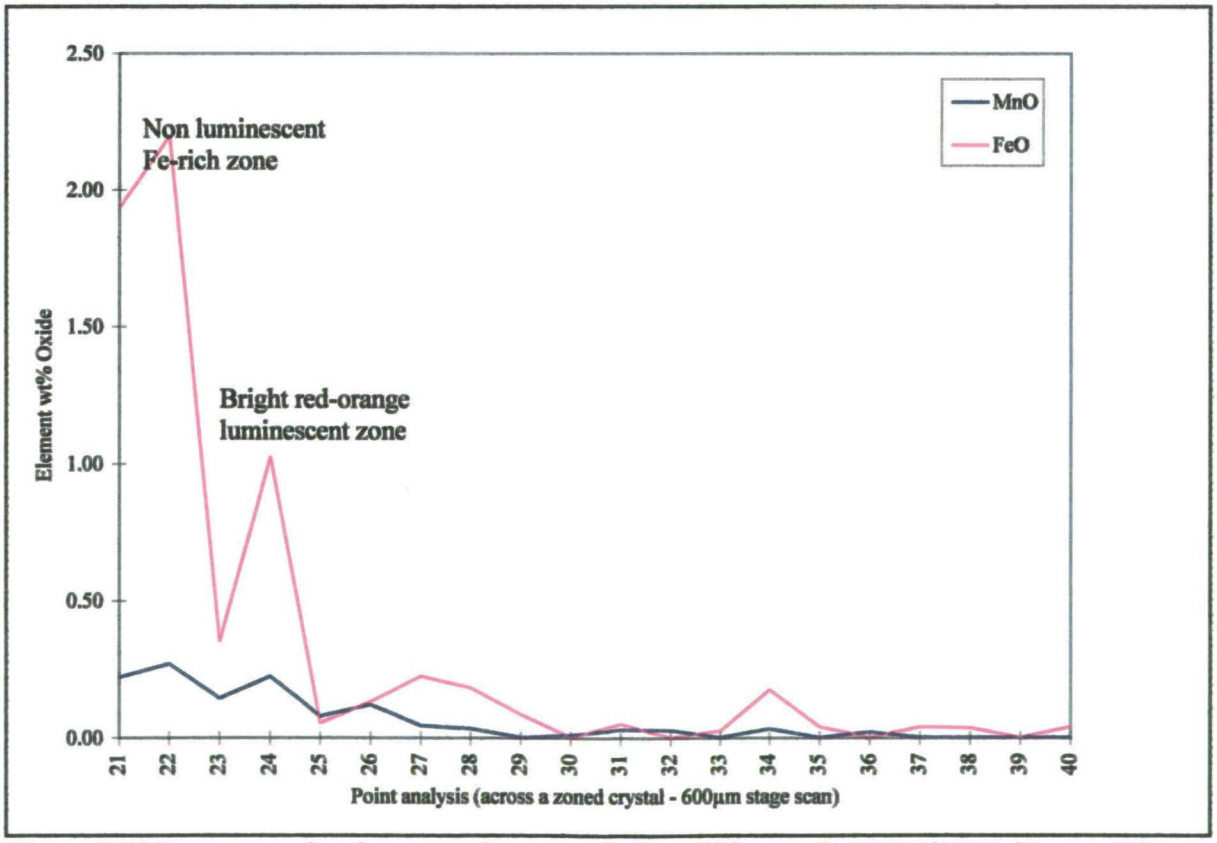


Figure 3.20 Stage scan, showing trace element variation within sample DUR4/365.5 (Durrow D3 dolomite).

The D2 and D3 dolomites at Lisheen have been interpreted by Redmond (1992) as being time equivalent, precipitating from the same fluid. Hitzman (1995b) suggested that both D2 dolomite and sulphide mineralization may have formed synchronously, precipitating from the same hydrothermal fluid. However, D2 dolomite is largely replaced by sulphide mineralization. D2 is interpreted to have formed by microfracturing and partial replacement, while the D3 dolomite is predominantly an open space growth form. However, from cross-cutting relationships the D3 dolomite is interpreted to at least in part post date the D2 dolomite at Lisheen, Galmoy, and Rathdowney Trend prospects.

3.2.4b Comparison of Dolomite Chemistry

Textural similarities exist between D2 dolomites at Lisheen and Galmoy. However, D2 dolomites from the prospects show a number of differences, particularly a more euhedral dolomite rhomb matrix. Compositionally, differences exist between the deposits and Rathdowney Trend prospects. The deposits generally show higher Mg concentrations, whilst the prospects tend to display elevated Fe and Mn concentrations. D2 dolomites at both Lisheen and Galmoy are highly non-stoichiometric compared with D2 dolomites at the prospects. The $CaCO_3$ (mole%) composition of D2 dolomites at both Lisheen and Galmoy exhibit a bimodal distribution, which may reflect the analysis of some small, unrecognized regional dolomite clasts present in the matrix. The compositions support this; the lower $CaCO_3$ (mole%) population and higher $MgCO_3$ (mole%) population (Figures 3.6, 3.7) respectively, are similar to those for regional dolomite (Figures 3.2, 3.3). Alternatively, the D2 dolomite could be interpreted as consisting of two distinct dolomitizing stages. A good example of this is evident in Plates 16 and 17, which shows two texturally and chemically distinct phases. Fine crystalline dolomite rhombs within the matrix are composed of Fe/Mn poor cores and Fe/Mn rich outer rims at both Lisheen and Galmoy; at the prospects, the fine crystalline euhedral dolomite rhombs do not exhibit this compositional zoning.

The Fe/Mn ratio in D2 dolomites from Lisheen and Galmoy is notably higher than the Fe/Mn ratio in D3 dolomites. The Fe/Mn ratio in D2 and D3 dolomites from the prospects show no obvious relationships, however the D2 dolomites in the prospects mainly contain higher $MnCO_3$ (mole%) concentrations than either Lisheen or Galmoy D2 dolomites. The Fe/Mn ratio is greatest in D2 dolomites from Galmoy; and least in the D3 dolomites. The variations in Fe/Mn ratios are primarily due to Fe variations. The Fe content is always higher in D2 dolomites than D3 dolomites.

The dark colouration of the D2 dolomite matrix is thought to be due to small crystal size, void space, argillite content, presence of sulphides or a combination of these (Shearley *et al.*, 1995). Crowley (1986) has demonstrated that very small amounts (<0.1%) of organic matter are capable of causing darkening in carbonate rocks. The D2 dolomite contains between 0.01 and 0.1% more total organic carbon (TOC) than Waulsortian Limestone or regional dolomite (Walton, 1992). This suggests that disseminated organic carbon may contribute to the dark colour of the matrix, but is not necessarily a primary cause. Analysis of TOC in the D2 dolomite has not been carried out in this study.

D3 dolomite consists of coarse subhedral to euhedral interlocking crystals which display unimodal, planar (s) textures. Unimodal size distributions can result from a single nucleation event on homogeneously distributed nucleation sites combined with uniform growth rates (Sibley and Gregg, 1987). Cloudy centred cores and clear outer rims may develop when initial dolomitizing fluids are saturated with respect to low-Mg calcite and therefore minute crystals of it can be included in early rhomb centres. Later, as diagenetic fluids become undersaturated with low Mg calcite, dolomite zones may be free of such inclusions (Sibley, 1980). The $CaCO_3$ (mole%) composition of D3 dolomite exhibits a unimodal distribution in both deposits and prospects. The $MnCO_3$ (mole%) content of D3 dolomites is generally higher than D2 dolomites, with the exception of the prospects D2 dolomite. The Fe/Mn ratio is higher in prospect D3 dolomite than either Lisheen or Galmoy.

3.2.4c D3 Cement Stratigraphy

Ebers and Kopp (1979) have highlighted several important points associated with the application of cement microstratigraphy (see Appendix C1). Correlation of cement zones should not be attempted unless 3 prominent zones are observed. The prominent yellow zone in cement stage D should only therefore be correlated if the surrounding zones are also similar. The cement stages B,C and D can be correlated in most cases. The major assumption associated with the use of regional cement microstratigraphy in correlation is that each of the cement zones identified is regionally time-correlative, rather than being diachronous.

The D3 dolomite shows consistent and comparable luminescence patterns. Cement stages B, C, D and E, record a progressive history of the growth of the D3 dolomite cement. Formation of the individual zones suggests that the cement stages represent growth from a fluid medium that was changing in composition rather than as a result of grain growth through recrystallization.

Cement stages B and C are characterized by a uniform to non-uniform moderate red, luminescent core with occasional bright luminescent inclusions. Cement stage D is characterized by a bright red-orange luminescent zone, with a distinctive yellow luminescent zone. The final zone, E is characterized by alternating dull to non luminescent zones. This pattern of moderate, bright, dull to non luminescence is typical of cement precipitated from increasingly reducing pore waters in the course of basin subsidence (Bruckschen *et al.*, 1996). At high oxidizing potentials, Mn is in the 3+, or 4+ state, and Fe is in the 3+ state. These ions are strongly excluded from the carbonate lattice and the characteristic CL is not produced. At somewhat lower oxidation potentials, the Mn is reduced to Mn^{2+} and can substitute for Ca^{2+}. However the Fe remains in the 3+ state and is not incorporated as a quencher. The resulting luminescence intensity is high. Cement stage D is characterized by high Mn concentrations, and may represent such a dolomite, precipitated from slightly reduced meteoric or marine porewaters modified by shallow burial. At even more reducing conditions, Mn and Fe are both in the 2+ state and both can substitute for Ca, leading to a dull, partially or totally quenched CL. Cement stage E is characterized by relatively high Fe concentrations and could on this basis be interpreted as a relatively deep burial cement. Machel (1996) adds a note of caution for the use of CL in the interpretation of solution pH, Eh, salinity and temperature, which has become quite common in applications of carbonate CL. Machel (1996) suggests most interpretations of CL of diagenetic carbonates are based on oversimplifying assumptions that include the popular application of pH, Eh diagrams, inferences that cements are correlatable over tens to hundreds of kilometres, and determination of fluid chemistries from Mn^{2+} and Fe^{2+} concentrations in carbonates. Machel (1996) advises the integration of CL with other analytical methods including isotopic and fluid inclusion studies (Chapters 4 and 5).

Distinct luminescent cement stages and zones in the D3 dolomites correspond with distinct compositional zones. Luminescent intensity of the bright yellow zone in cement stage D is controlled by the Fe/Mn ratio in the zone, and not by the absolute concentrations of either cation. These absolute concentrations are highly variable within various samples throughout the Rathdowney Trend. The Fe/Mn ratio remains relatively constant in D3 samples, cement stages and zones in the deposits, but is notably higher in most of the prospect cement stages and zones. Fe/Mn ratios of between 3.2-3.8 are characteristic of cement stage D in the deposits and in the bright red luminescent zone in Durrow. Higher Fe/Mn ratios of between 4.0-4.7 are characteristic of cement stage D in the remaining prospects, Rathdowney East and Holycross. Fe/Mn ratios of between 2.1-2.7 are characteristic of cement stages B, C in Lisheen; higher Fe/Mn ratios are characteristic of the prospects. The lack of Sr precludes a marine cementation origin for D3 dolomite.

The distinct yellow zone in cement stage D can be correlated throughout the Rathdowney Trend with similar brightly luminescent zones observed in D3 dolomites at Lisheen, Galmoy, Rathdowney East, and Derrykeam. However, the yellow luminescent zone is missing in D3 dolomites at Holycross and Durrow. However, the bright red luminescent zone in the Durrow sample has a similar Fe/Mn ratio as the bright yellow zone in the Lisheen samples.

The thickness and luminescence intensity of the yellow zone in the Lisheen deposit is interpreted by Redmond (1997) to increase laterally towards a source of mineralizing/dolomitizing fluids. This systematic variation in thickness and luminescent intensity would also be expected to occur in the Galmoy deposit; however, this has not been observed, probably due to the much smaller sample suite analyzed.

3.2.4d Origin of the Breccias

D2 and D3 dolomites are interpreted as having formed largely in areas of complete regional dolomitization at Lisheen, Galmoy and the Rathdowney Trend prospects. At Silvermines, however, the breccias are particularly well developed where early regional dolomitization was relatively weak (Hitzman, 1995b).

At Lisheen and Galmoy the D2 dolomites have been described as *in situ* hydrothermal dolomite breccias by Hitzman *et al.* (1992) and Doyle *et al.* (1992). Hitzman *et al.* (1992) interpret the breccia as having formed by hydraulic fracturing and brecciation, with subsequent *in situ* alteration of dolomitized Waulsortian Limestone. The fine crystalline matrix is thought to have formed by the dissolution and recrystallization of large crystals (>200μm) in the regional dolomite clasts. However, during surface energy driven recrystallization large crystals grow at the expense of small crystals (Ostwald ripening; Gregg, 1996), therefore the recrystallization of larger crystals to smaller crystals (20-50μm) is unlikely. Evidence from this study suggests that the D2 dolomite partially replaces regional dolomite clasts and remnant regional dolomite crystals in the matrix. At Galmoy, the origin of the D2 dolomite is interpreted by Doyle *et al.* (1992) to have initiated during diagenesis and differential compaction of the primary Waulsortian sediment, resulting in lithified nodular textures. These textures may be considered an initial form of *in situ* brecciation, disrupted further by instability in the sediment pile related to early movements on the G Fault. Some workers favour a synsedimentary origin (particularly at Silvermines) related to growth faulting, followed by further tectonic and/or chemical brecciation during dolomitization (Taylor and Andrew, 1978; Taylor, 1984; Andrew, 1986a; Andrew, 1995).

However, more recent petrographic studies of the Silvermines and Lisheen breccias have demonstrated that dolomitization post-dated slumping and was replacive (Kucha, 1989; Hitzman *et al.*, 1992; Beaty *et al.*, 1992; Shearley *et al.*, 1995, 1996).

Johnston (1995c) and Johnston *et al.* (1995) cite the numerical modelling of fluid flow in fractured rock masses of Sanderson and Zhang (1997) to suggest a possible mode of formation for the dolomite matrix breccias. The modelling suggests that changes in the stress state of a rock mass can result in a sudden transition from diffuse flow through fracture networks to a highly localized flow generated by the opening of 'pipes' where fractures intersect. Modelling further demonstrates that a normal fault zone with a throw as small as 1m can give a massive increase in fluid flow in the hangingwall (typically increased by several orders of magnitude at least). This leads to zones of enhanced or 'pipe' flow which will be localized at specific sites depending on localized stress and geometry. Johnston (1995c) proposes that the breccias are the product of fault related processes, with extensive breccia sheets occurring where the 'parent' fault changes dip. Contrasting rheological behaviour of the massive Waulsortian Limestone with the more ductile sub-Waulsortian argillaceous bioclastic limestones resulted in differential hangingwall subsidence. Displacement continued in the hangingwall beneath the Waulsortian, opening a wedge shaped dilatant zone into which the overlying rocks collapsed (Johnston, 1995c). Under conditions of small differential stresses, such a geometry could result in the generation of extensive, tabular, shallowly dipping zones of dilation without requiring fluid overpressuring (Johnston *et al.*, 1995).

The lack of mixing and rotation of the clasts in D2 dolomite at Lisheen and Galmoy suggests that the breccias did not originate as debris flows or by major solution collapse. However, minimal clast rotation in later D3 dolomites suggests a mode of formation under different conditions. Morrow (1982) concludes that breccias formed by solution and collapse are usually accompanied by the introduction of coarsely crystalline white dolomite, which cements the clasts. At Galmoy, the D3 dolomites have been interpreted as being formed due to volume reduction caused by the regional dolomitization of the massive Waulsortian Limestone (Doyle *et al.*, 1992) effectively syn-regional dolomitization ($D1_R$). However, the D3 dolomite has been shown in this study to postdate D2 dolomite, which postdates regional dolomitization.

3.2.5 Pink Dolomite (Stage 4)

Pink-white vuggy dolomitization occurs commonly as a cement in Waulsortian facies, but may occur through much of the Carboniferous (up to Asbian) and also in the underlying Lower

Palaeozoic basement (Andrew, 1993). The pink dolomite is often accompanied by later coarse, euhedral, calcite cement, which occupies vuggy porosity possibly created during introduction of the dolomite.

3.2.5a Lisheen Deposit

The pink dolomites at Lisheen are widespread and occur in all zones (Plate 39A). Samples 138/225.0 and 515/173.0 are from Main zone, and are proximal to the Killoran fault. They are both Waulsortian-hosted. D4 dolomite in sample 515/173.0 post-dates amber coloured crystalline sphalerite. Sample 318/450.5 is Lower Ballysteen-hosted and also from Main zone, but is proximal to a N-S trending normal fault in the hanging wall of the Killoran fault. Late, euhedral, vug fill calcite (D5 Calc) post-dates the dolomite (Plate 39B).

D4 dolomite consists of coarse (500-5000μm) crystalline, pink saddle dolomite. The crystals have curved faces, and distinct luminescence characteristics (Plate 40). D4 dolomite cement sometimes overgrows D3 dolomite cement stages B, C, D and E. D4 exhibits alternating moderate to bright orange - red, and dull to non, red luminescence stages. Late Fe rich zoning is characteristic of the late D4 dolomite cement.

Elemental Chemistry

D4 dolomites at Lisheen are non-stoichiometric (Figures 3.21, 3.22, 3.23, 3.24), and vary from 55.68 to 60.39 mole% $CaCO_3$, with an average of 56.36 mole% $CaCO_3$. The $FeCO_3$ content of pink dolomite ranges from below detection to 2.05 mole% with a mean of 1.56 mole%. $MnCO_3$ content ranges from 0.18 to 0.49 mole%, with a mean of 0.35 mole%. (Table 3.7).

Sample	Carb	No of Analyses	STDEV ($CaCO_3$)	Average Mole% $CaCO_3$	STDEV ($MgCO_3$)	Average Mole% $MgCO_3$	STDEV ($FeCO_3$)	Average Mole% $FeCO_3$	STDEV ($MnCO_3$)	Average Mole% $MnCO_3$
138/225.0	D4	10	0 48	56 41	0.22	42 37	0.17	1.67	0 07	0 36
318 450.5	D4	10	0 29	56 41	0 66	42 80	0.13	1.35	0 07	0 30
515 173.7	D4	10	1 25	57 53	0.97	41.62	0.31	1 09	0 10	0 35

Table 3.7 Chemical composition of Lisheen pink dolomite (D4).

3.2.5b Galmoy Deposit

At Galmoy, the D4 dolomite was observed in the Waulsortian hosted sample GY355/97 overgrowing D3 dolomite cement (Plate 9B). The D4 dolomite consists of subhedral to euhedral, interlocking crystals (500-800μm in size) displaying a unimodal, planar (s) texture.

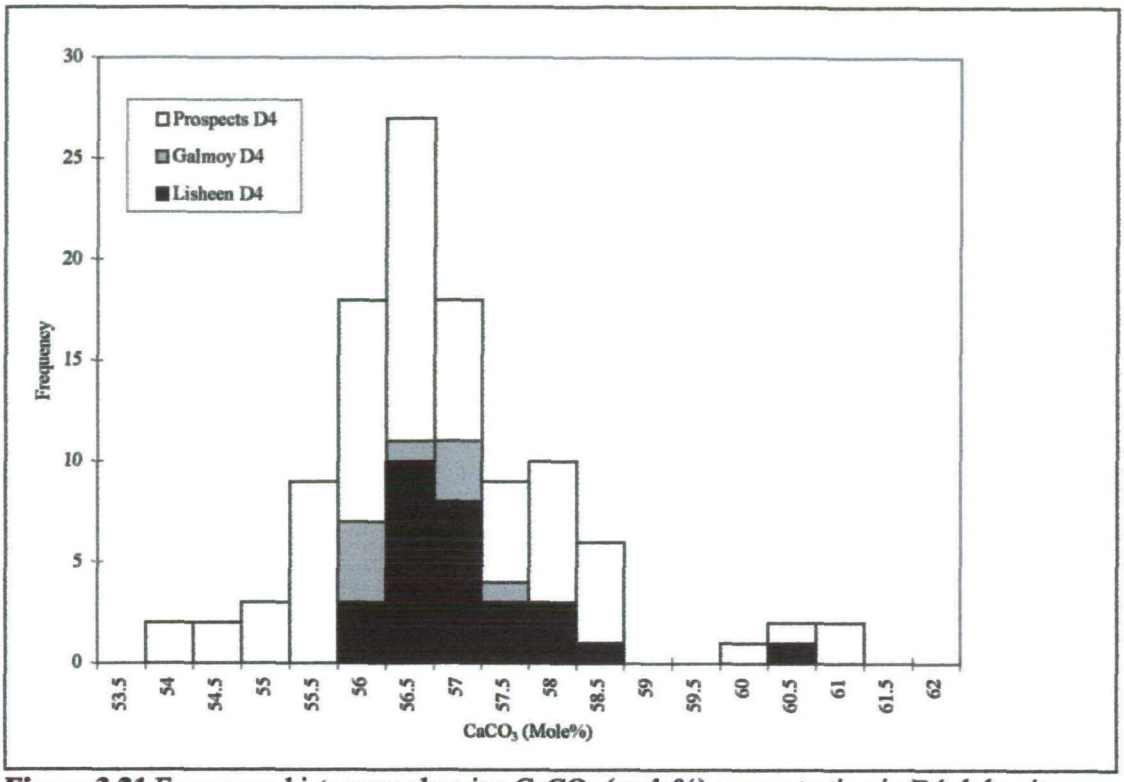


Figure 3.21 Frequency histogram showing $CaCO_3$ (mole%) concentration in D4 dolomites.

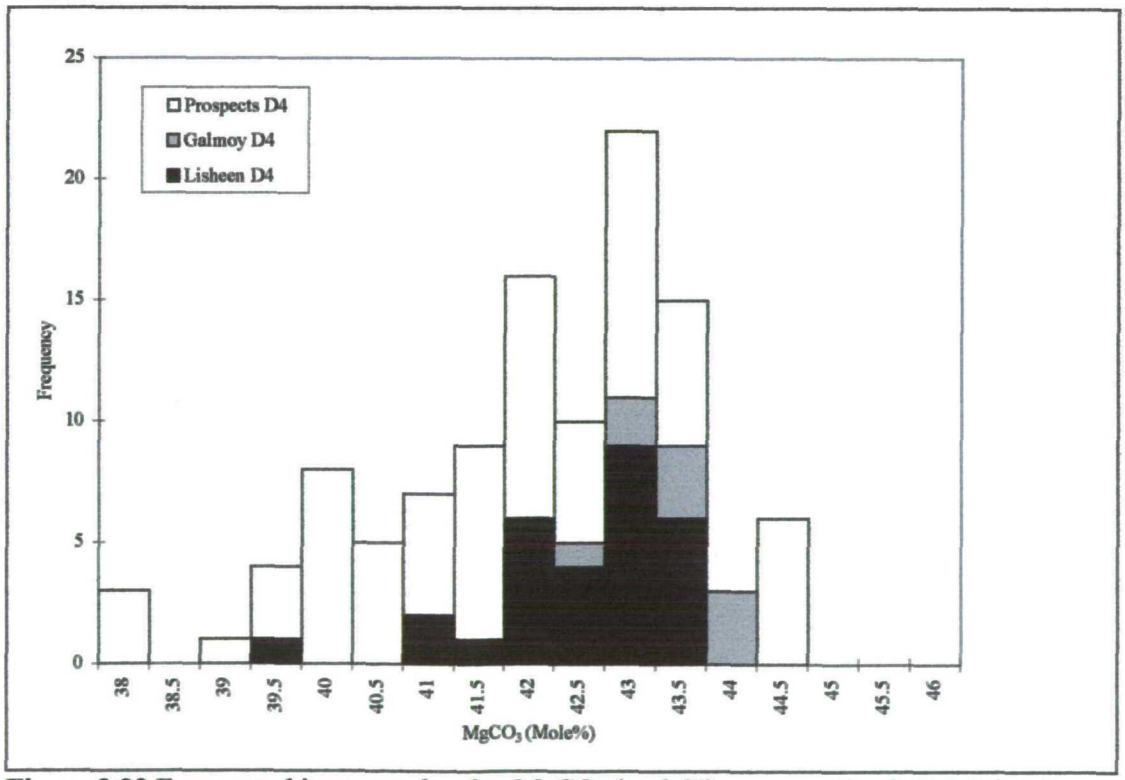


Figure 3.22 Frequency histogram showing $MgCO_3$ (mole%) concentration in D4 dolomites.

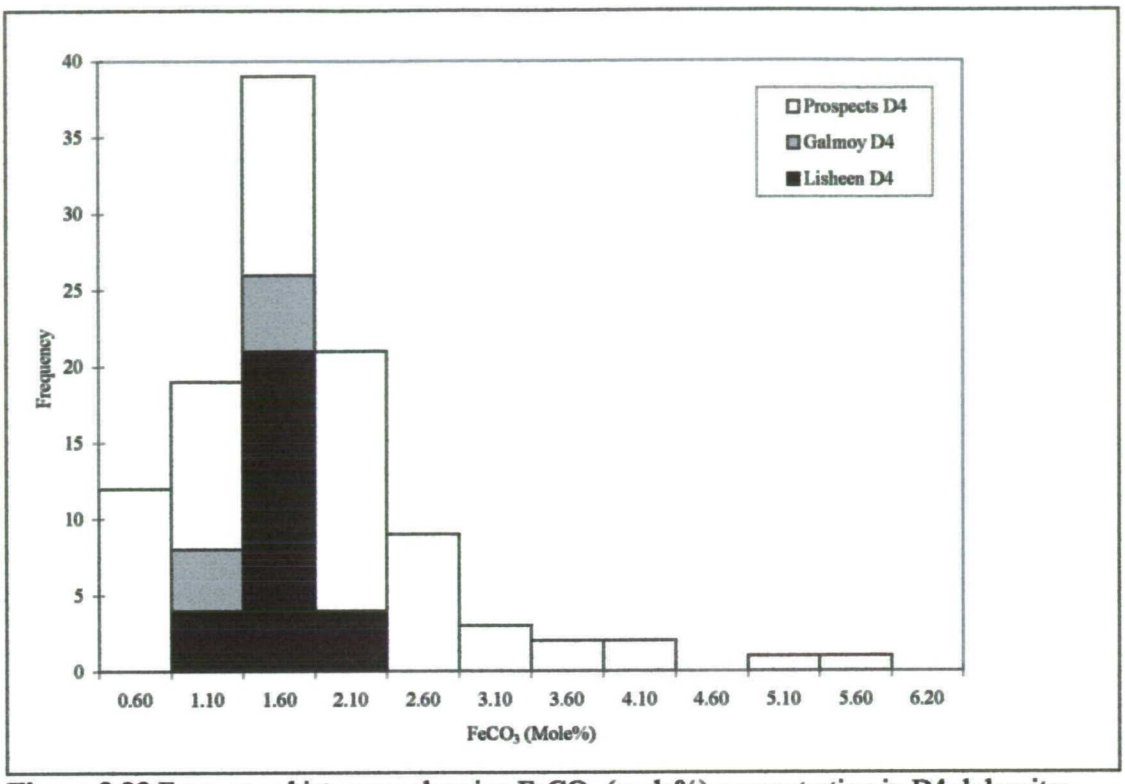


Figure 3.23 Frequency histogram showing $FeCO_3$ (mole%) concentration in D4 dolomites.

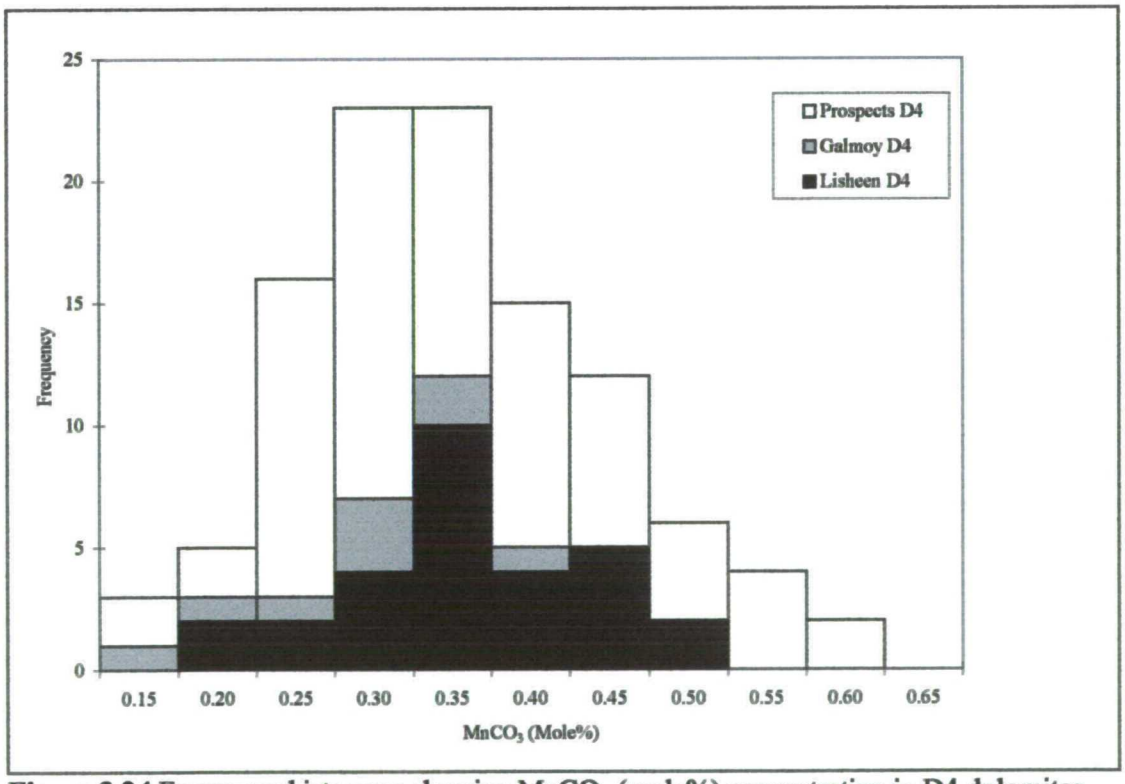


Figure 3.24 Frequency histogram showing $MnCO_3$ (mole%) concentration in D4 dolomites.

Elemental Chemistry

The D4 dolomite at Galmoy is non-stoichiometric (Figures 3.21, 3.22, 3.23, 3.24), and varies chemically from 55.63 to 57.34 mole% $CaCO_3$, with an average of 56.30 mole% $CaCO_3$. The $FeCO_3$ content of D4 dolomite ranges from 0.71 to 1.32 mole% with a mean of 1.06 mole%. $MnCO_3$ content ranges from 0.15 mole% to 0.38 mole%, with a mean of 0.27 mole% (Table 3.8).

Sample	Carb	No. of Analyses	STDEV ($CaCO_3$)	Average Mole% $CaCO_3$	STDEV ($MgCO_3$)	Average Mole% $MgCO_3$	STDEV ($FeCO_3$)	Average Mole% $FeCO_3$	STDEV ($MnCO_3$)	Average Mole% $MnCO_3$
GY355 97.0	D4	10	0.54	56 30	0 50	43 19	0 18	1.06	0.08	0.27

Table 3.8 Chemical composition of Galmoy pink dolomite (D4).

3.2.5c Rathdowney Trend Prospects

D4 dolomites occur at all the prospects. However, only samples from Rathdowney East (Plate 48), Durrow, and Holycross have been analysed. The samples are all Waulsortian-hosted apart from DUR 2/960.8, which is hosted by the Lisduff Oolite Member.

D4 dolomites consist of coarse (500-5000μm) crystalline, pink saddle dolomite. The crystals have curved cleavage traces and very distinct luminescence properties. D4 dolomite cement exhibits alternating moderate to bright orange - red, dull to non, red luminescence stages, and a pronounced late cement stage characterized by Fe rich zoning (Plates 41, 42, 43, 44). The late cement stage F displays alternating dull red to very bright orange-yellow luminescence zones. These luminescent properties are observed in D4 dolomites at both Holycross and Rathdowney East prospects and the similarity between them is striking. The prominent cement stage F of D4 dolomite post-dates a dissolution event (Plate 44A).

Elemental Chemistry

D4 dolomites at Rathdowney East and Durrow prospects are non-stoichiometric (Figures 3.21, 3.22, 3.23, 3.24), and vary chemically from 53.75 to 60.60 mole% $CaCO_3$, with an average of 57.20 mole% $CaCO_3$ The $FeCO_3$ content of pink dolomite ranges from below detection to 5.16 mole% with a mean of 0.77 mole% $FeCO_3$ The $MnCO_3$ content ranges from below detection to 0.55 mole%, with a mean of 0.29 mole%. (Table 3.9).

Stage scans across Rathdowney East (RE24/1625) and Holycross (HC15/200.8) samples (Figures 3.25, 3.26) show very distinct and remarkably similar trace element variations across the strongly

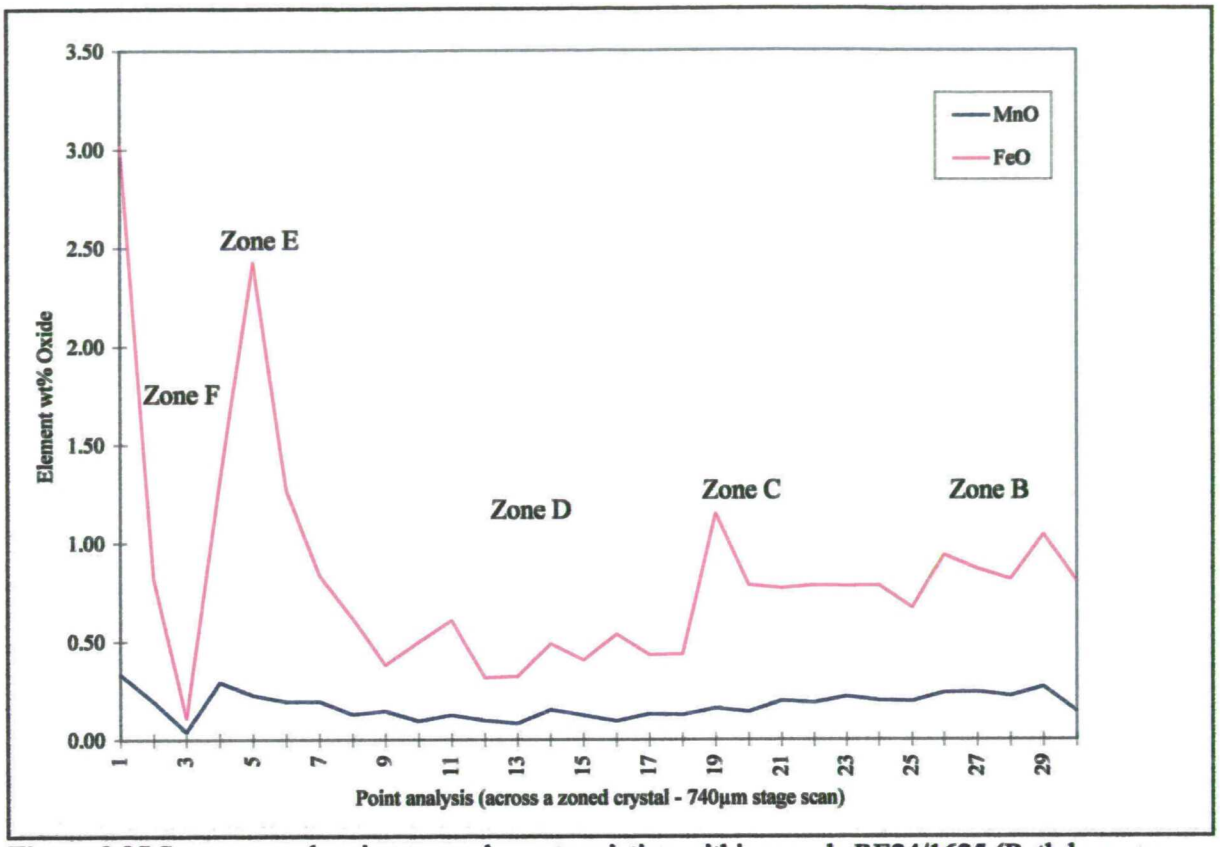
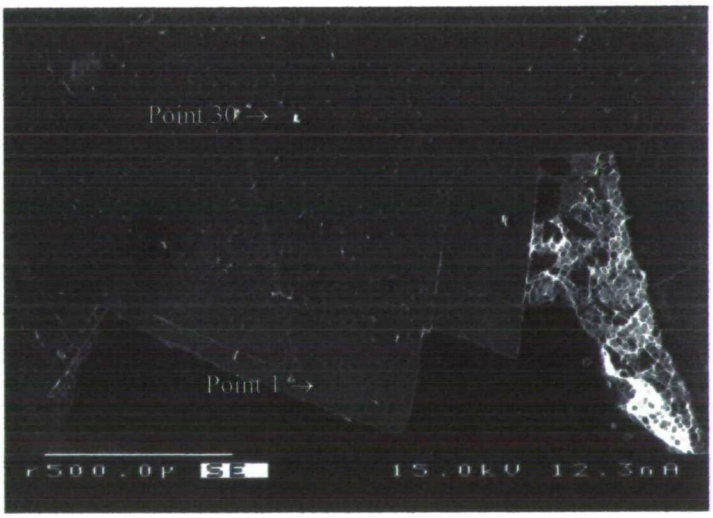


Figure 3.25 Stage scan, showing trace element variation within sample RE24/1625 (Rathdowney East D4 dolomite). Traverse of points shown below on secondary electron image of D4 crystal.



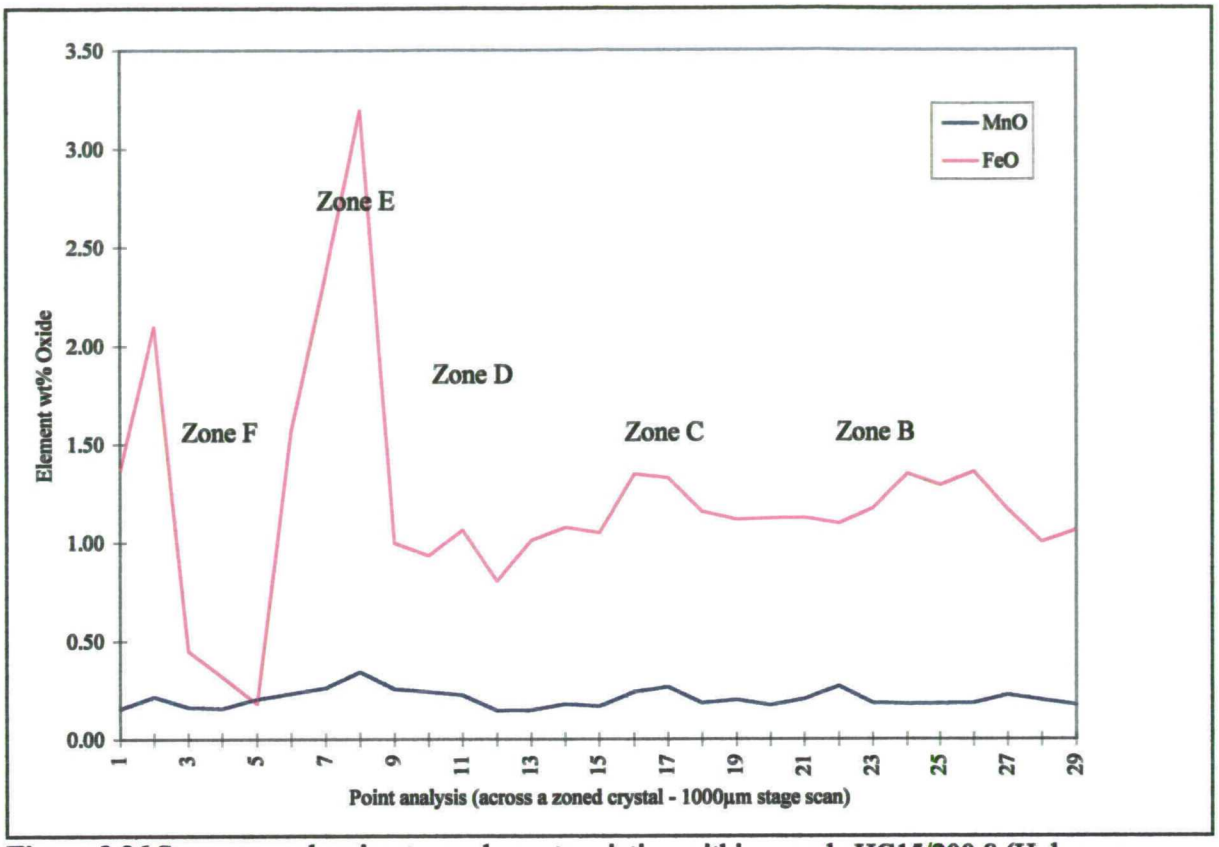
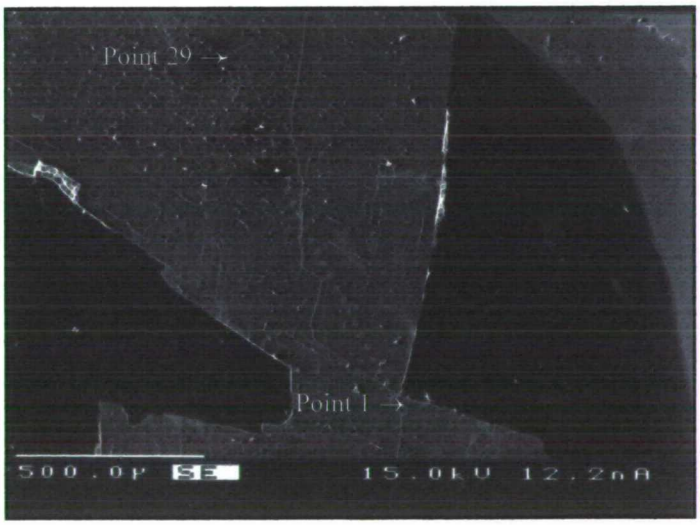


Figure 3.26 Stage scan, showing trace element variation within sample HC15/200.8 (Holycross D4 dolomite). Traverse of points shown below on secondary electron image of D4 crystal.



zoned D4 dolomite crystals. Sample RE24/1625 exhibits a bright to moderate red-orange, mottled luminescent core with yellow-orange luminescent inclusions, defined as cement stages B,C (Figure 3.25). This cement stage consists of Fe and Mn values up to 6452 and 1626ppm respectively. The Fe/Mn ratio for cement stages B and C is 3.95. Sr is below detection. Cement stage D (~300μm thick), which displays a bright red, very weakly zoned luminescence is characterized by Fe and Mn compositions of 3809 and 929ppm respectively. The Fe/Mn ratio for cement stage D is 4.1. Sr is below detection. Cement stages E and F are very strongly zoned. The sequence of zones can be defined under CL (Plate 41) and by production of an X-ray distribution map (Plate 42). The cement stages exhibit alternating dull to non, and bright orange-yellow, bright yellow, moderate red and non luminescent zones. The Fe and Mn concentrations in the dull to non luminescent zone are 23475, and 2556ppm respectively. The Fe/Mn ratio is 9.2. Fe and Mn concentrations in the bright orange-yellow zone are 6374 and 1549ppm respectively with an Fe/Mn ratio of 4.1. Fe and Mn concentrations of the bright yellow zone are 855, and 310ppm respectively with an Fe/Mn ratio of 2.75. The Fe, Mn concentrations of the dull zone are 18889 and 1781ppm respectively. The Fe/Mn ratio is 10.6.

Sample HC15/200.8 (Plate 43) exhibits very similar properties to RE24/1625. The cement exhibits a bright to moderate red-orange, mottled luminescent core with yellow-orange luminescent inclusions (cement stage B). Cement stage C is typified by a moderate red luminescence. The Fe, Mn concentrations of cement stages B and C are 9095 and 1549ppm respectively with an Fe/Mn ratio of 5.85. Cement stage D (~100μm thick) displays a very weakly zoned bright red luminescence with Fe and Mn values up to 7773, and 1859ppm respectively. The Fe/Mn ratio is 4.2. Cement stages E and F post-date these earlier cements and a dissolution event, and are characterized by distinct Fe zoning (Plate 44). The cement stages exhibit alternating dull, bright orange-yellow, bright yellow, dull to moderate red and non luminescent zones. The Fe and Mn concentrations of the dull to non luminescent zone are 16324 and 1704ppm respectively, with an Fe/Mn ratio of 9.58. Fe and Mn concentrations of the bright orange-yellow zone are 3498 and 1239ppm respectively. The Fe/Mn ratio is 2.74. The Fe and Mn values of the bright yellow zone are 1399 and 1626ppm respectively, with an Fe/Mn ratio of 0.88. The dull to moderate luminescent zone is characterized by Fe and Mn values of 12204 and 1781ppm respectively. The Fe/Mn ratio is 6.85. The non luminescent zone contains Fe and Mn concentrations of 24874 and 2633ppm respectively, with an Fe/Mn ratio of 9.41.

In summary, the striking characteristics of D4 dolomite are (1) elevated Fe, Mn over all previous dolomite stages; (2) consistent Mn content irrespective of zoning; (3) very strong Fe zoning. Fe

variations control CL in D4 dolomite and is shown by Plates 41 and 42 which show an inverse relationship between Fe content and luminescence intensity.

Sample	Carb	No of Analyses	STDEV ($CaCO_3$)	Average Mole% $CaCO_3$	STDEV ($MgCO_3$)	Average Mole% $MgCO_3$	STDEV ($FeCO_3$)	Average Mole% $FeCO_3$	STDEV ($MnCO_3$)	Average Mole% $MnCO_3$
RE24 1625	D4	28	1 13	56.50	1 46	41 82	0 96	1 40	0 11	0 29
DUR2/960 8	D4	9	0 48	57 74	0 64	43 73	0 31	0 15	0 07	0 29
HC15/200 8	D4	26	1 51	56 72	1 25	40 83	0 93	1 89	0 08	0 33
HC3569-2/293	D4	9	0 47	54 49	0 45	39 75	0 34	2 80	0 04	0 50

Table 3.9 Chemical composition of Rathdowney East, Durrow, and Holycross pink dolomite (D4).

3.2.6 Interpretation of Results (Stage 4)

Timing of dolomitization as determined from petrography indicates that precipitation of D4 saddle dolomite post-dates ore-related D2 and D3 dolomites and ore-stage mineralization. The D4 dolomite is thought to represent a late-stage dewatering event (Andrew, pers. comm., 1995) probably related to post-compressional relaxation in late Variscan times (Andrew, 1993). Saddle dolomite is assumed to be a good geothermometer, indicating burial temperatures between 50° and 150°C (Radke and Mathis, 1980; Kretz, 1992). It also commonly appears to be a product of chemical compaction and thermochemical sulphate reduction, consistent with a relatively high temperature of formation from hypersaline brines (Machel, 1987).

D4 dolomites generally contain higher Fe and Mn concentrations than D1, D2 or D3 dolomites. Anomalous Fe and Mn values occur at Holycross. Fe/Mn ratios in the prospect D4 dolomites are generally greater than Fe/Mn ratios at Lisheen or Galmoy, but they vary widely between zones. The higher Fe concentration in D4 dolomite suggests that the late dolomitizing fluids were either more Fe rich, or that different redox conditions existed at the time of deposition. The dissolution surface between cement stages D and E identified in the CL zones probably coincides with a significant change in the fluid chemistry (also reflected by a change to higher and more variable Fe content).

D4 dolomite displays zonations due to high iron concentrations, which are well expressed in cathodoluminescence. The Fe concentration primarily controls the CL; Mn concentrations remain fairly consistent irrespective of luminescence zoning. Cement stage F is characterized by very pronounced zoning, 5 alternating zones are clearly distinguished petrographically and compositionally, and are comparable and correlatable between Rathdowney East and Holycross, suggesting that a homogeneous regional groundwater flow system is responsible for the formation of D4 dolomite.

3.2.7 Late, Minor Vein and Vug Dolomite and Calcite (Stage 5)

Late, minor vein and vug filling phases include mineralized and unmineralized ferroan and non-ferroan dolomite and calcite. These late phases predominantly post-date main ore-stage mineralization.

The relative timing of these phases is difficult to determine with certainty. Unmineralized, vug filling calcite spar is clearly late and post-dates D4 dolomite cement. Late vug-filling dolomite and calcite mostly post-dates crystalline sphalerite precipitation, though in some cases gangue carbonate precipitation is interpreted to have been coeval with sphalerite precipitation. Therefore some of these late carbonates are unlikely to post-date D4 dolomite cement, and were probably formed during the waning phase of mineralization.

3.2.7a Lisheen Deposit

In sample 121/319.2, a ferroan dolomite vein is cross-cut by a late calcite and quartz vein (Plate 39B). The ferroan dolomite is non-luminescent; the calcite vein exhibits bright, orange-yellow luminescence (Plate 45). Both calcite and dolomite cross-cut black matrix breccia dolomite in sample 121/180.5 (Plate 46). Late, mineralized calcite and dolomite vugs are hosted by both Waulsortian and Ballysteen units. These late carbonate phases do not exhibit zoned cement stages under cathodoluminescence.

Calcite matrix breccias (Plate 49) consist of sub-angular to sub-rounded clasts of Waulsortian in a matrix of coarse crystalline calcite. The calcite matrix breccia, sample 262/120.0, contains clasts of Waulsortian wavy laminated facies. The orientation of the wavy argillite wisps within the central clast provides good evidence of clast rotation. The calcite matrix breccias have been interpreted as post-dating all other breccia types (Kelly *et al*, 1993).

Elemental Chemistry

Late, minor vein and vug dolomites (D5 Dol) at Lisheen are non-stoichiometric (Figures 3.27, 3.28, 3.29, 3.30), and vary chemically from 57.24 to 60.57 mole% $CaCO_3$, with an average of 58.23 mole% $CaCO_3$. The $FeCO_3$ content in late, minor vein and vug dolomite ranges from below detection to 15.40 mole%, and $MnCO_3$ content ranges from below detection to 1.26 mole% (Table 3.10).

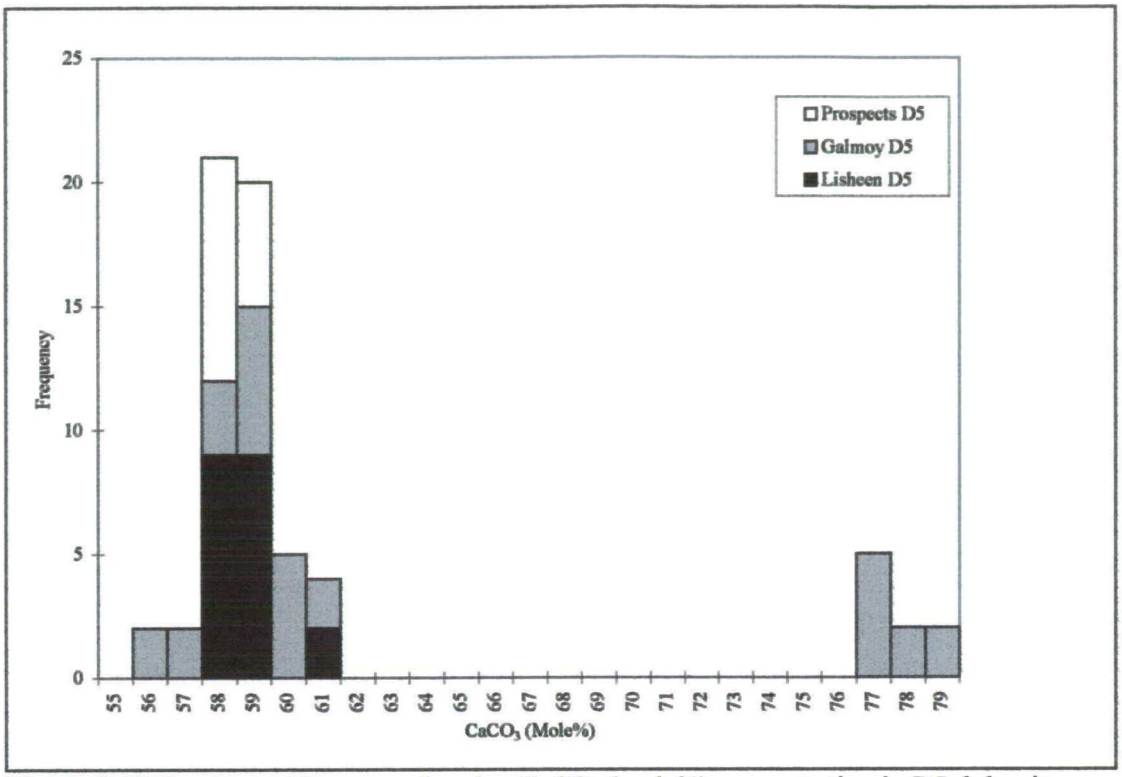


Figure 3.27 Frequency histogram showing $CaCO_3$ (mole%) concentration in D5 dolomites.

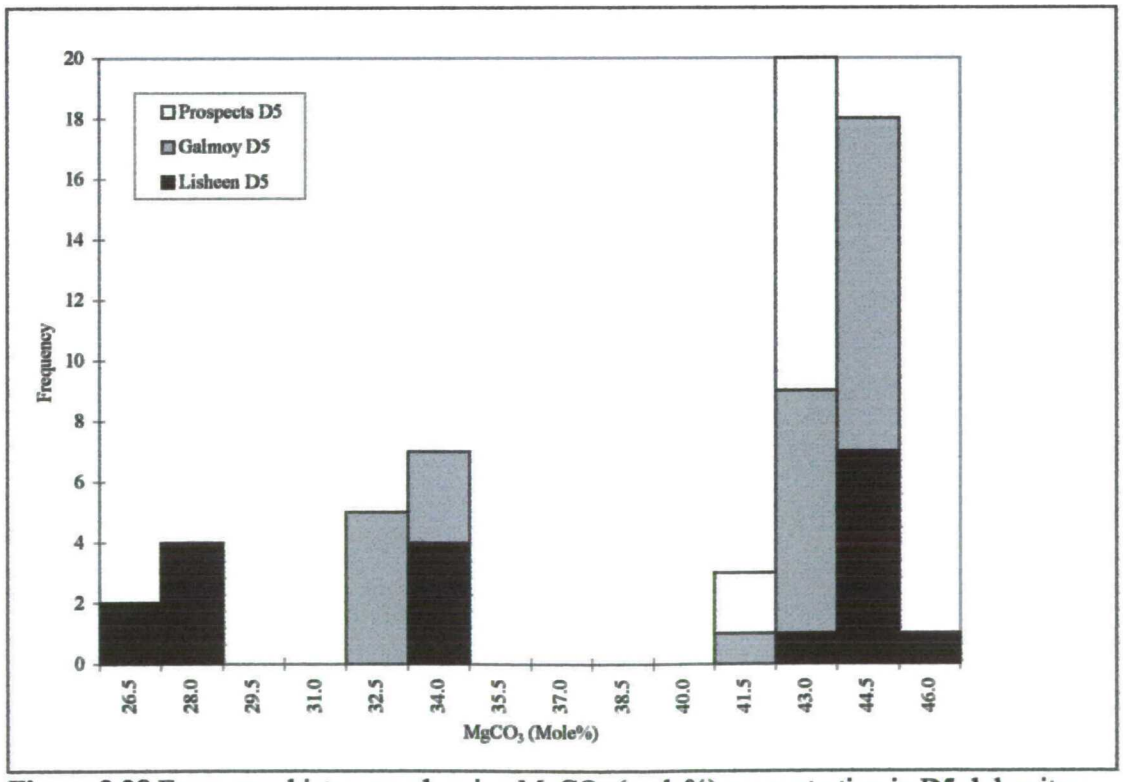


Figure 3.28 Frequency histogram showing $MgCO_3$ (mole%) concentration in D5 dolomites.

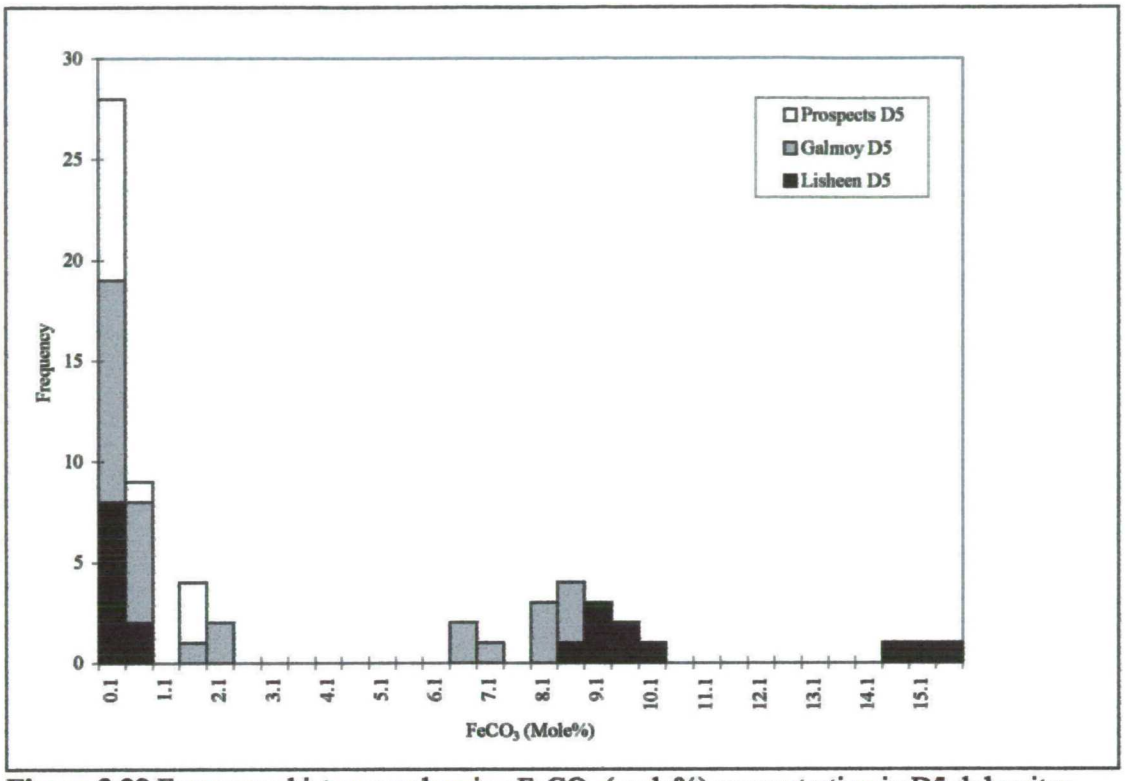


Figure 3.29 Frequency histogram showing $FeCO_3$ (mole%) concentration in D5 dolomites.

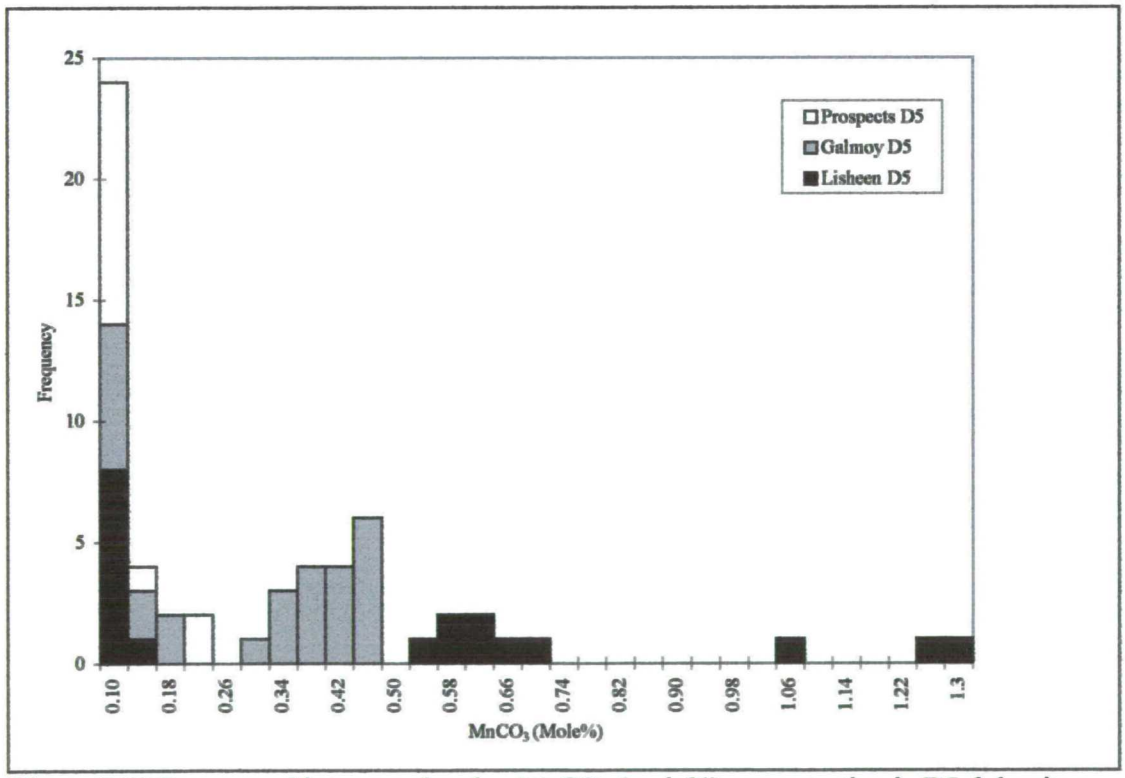


Figure 3.30 Frequency histogram showing $MnCO_3$ (mole%) concentration in D5 dolomites.

A late ferroan dolomite/ankerite vein in sample 121/319.2 is non-stoichiometric, and varies chemically from 57.16 to 60.06 mole% $CaCO_3$ with a mean of 58.10 mole% $CaCO_3$. The Fe content is higher ranging from 8.28 to 15.40 mole%, with a mean of 10.82 mole%. The $MnCO_3$ content in this vein ranges from 0.52 to 1.26 mole%, with a mean of 0.77 mole % (Table 3.10, 3.11).

Sample	Carb	No of Analyses	STDEV ($CaCO_3$)	Average Mole% $CaCO_3$	STDEV ($MgCO_3$	Average Mole% $MgCO_3$	STDEV ($FeCO_3$)	Average Mole% $FeCO_3$	STDEV ($MnCO_3$)	Average Mole% $MnCO_3$
121 319 2	D5 Dol	10	0 86	58 10	2 75	30 81	2 85	10 82	0 29	0 77
517/205 0	D5 Dol	8	1 05	58 23	0 75	43 80	0 05	0 05	0 04	0 05

Table 3.10 Chemical composition of Lisheen Late, minor vein and vug dolomite (D5).

D5 Calc in the Lisheen area mostly post-dates crystalline sphalerite precipitation (e.g. samples 514/182.5, 457/212.6, 451/139.10, 095/335.0, 529/246.6), though in some cases gangue carbonate precipitation is interpreted to have been coeval with sphalerite precipitation (e.g. 449/95.5 and 463/173.0). Generally, syn-sphalerite calcites have elevated Mg relative to post-mineralization calcites. The calcite vein in sample 121/319.2 post-dates a mineralized ferroan dolomite vein. The calcite spar in sample 318/450.0 clearly post-dates D4 dolomite, and is unmineralized. The samples are hosted by both Waulsortian and Ballysteen facies. The trace element concentrations of Fe and Sr are below detection for Waulsortian hosted D5 Calc veins and vugs. Fe and Sr concentrations for Ballysteen hosted D5 Calc veins and vugs range from 0.07 to 0.81 wt%, and 0.05 to 0.14 wt% respectively.

Sample	Carbonate	No. of Analyses	Average Weight% Mg	Average Weight % Mn	Average Weight % Fe	Average Weight % Sr
121 319.2	D5 Calc	10	0 08	0 05	0 09	0 05
318/450 5	D5 Calc	10	0 07	-	-	-
514 182 5	D5 Calc	9	0 05	-	-	-
449/95 5	D5 Calc	10	0 21	0 07	0 28	-
457/212 6	D5 Calc	10	0 27	0 04	-	-
463 173.0	D5 Calc	10	0.18	0 07	0.81	0 14
095 335 0	D5 Calc	9	0 05	0 08	0 07	0 06
451 139 10	D5 Calc	11	0 13	0 13	0 05	-
529/246 6	D5 Calc	10	0 17	0 05	0 07	0 10

Table 3.11 Trace element composition of Lisheen late, minor vein and vug calcite (D5 Calc).

3.2.7b Galmoy Deposit

At Galmoy, late dolomite and calcite veins are common. Sample G16-27/383.5 (Plate 47A) is a Lower Ballysteen hosted, chalcopyrite-bearing dolomite vein (5-7mm thick). The sample is located close to the G fault, which forms the southern margin of the G orebody. A vertical carbonate vein (12mm thick) in sample GY333/103.3 (Plate 47B) is complex, with an early

calcian dolomite phase postdated by sphalerite-bearing calcite, which in turn is postdated by a minor pyrite-bearing calcite vein. This vein is also hosted within the Ballysteen, and is located east of K orebody.

Elemental Chemistry

Late, minor vein and vug dolomites (D5 Dol) at Galmoy are non-stoichiometric (Figures 3.27, 3.28, 3.29, 3.30), and vary chemically from 55.58 to 64.62 mole% $CaCO_3$, with an average of 58.29 mole% $CaCO_3$. The $FeCO_3$ content of late, minor vein and vug dolomite ranges from below detection to 1.97 mole%, with a mean of 0.42 mole%. $MnCO_3$ ranges from below detection to 0.40 mole%, with a mean of 0.2 mole%. A calcian dolomite (>30mole% $MgCO_3$) vein in GY333/103.3 varies from 76.55 to 78.37 mole% $CaCO_3$ with an average of 77.24 mole%. The $FeCO_3$ content of this late phase ranges from 6.18 to 8.42 mole%, with a mean of 7.59 mole%. $MnCO_3$ composition varies from 0.32 to 0.45 mole%, with a mean of 0.40 mole% (Table 3.12, 3.13).

Sample	Carb	No. of Analyses	STDEV ($CaCO_3$)	Average Mole% $CaCO_3$	STDEV ($MgCO_3$)	Average Mole% $MgCO_3$	STDEV ($FeCO_3$)	Average Mole% $FeCO_3$	STDEV ($MnCO_3$)	Average Mole% $MnCO_3$
GY333 103 3	D5 Dol	9	0 65	77.24	0.5	32 31	0 85	7 59	0 05	0.40
G16-27/383.3	D5 Dol	10	1 14	57.08	0.89	42.82	0 83	0 62	0 04	0 36
5.	D5 Dol	8	0 60	59.48	0.73	42 72	0 05	0 07	0 05	0 08

Table 3.12 Chemical composition of Galmoy late, minor vein and vug dolomite (D5 Dol).

Sample	Carbonate	No of Analyses	Average Weight% Mg	Average Weight % Mn	Average Weight % Fe	Average Weight % Sr
GY333 103 (Pts 11-20)	D5 Calc	10	0 10	0 07	0 26	-
GY333 103 (Pts 21-30)	D5 Calc	10	0 16	0.09	0 23	-

Table 3.13 Trace element composition of Galmoy late, minor vein and vug calcite (D5 Calc).

3.2.7c Rathdowney Trend Prospects

Sample HC5/122.9 is the only late vein phase sampled from the prospects and comes from Holycross. The mineralized white dolomite vein is host to cream and amber coloured sphalerite, galena and pyrite.

Elemental Chemistry

The minor dolomite vein at Holycross is non-stoichiometric (Figure 3.27, 3.28, 3.29, 3.30), and varies chemically from 56.74 to 59.62 mole% $CaCO_3$, with an average of 57.93 mole% $CaCO_3$.

The $FeCO_3$ content ranges from below detection to 1.24 mole%, with a mean of 0.31 mole%. $MnCO_3$ ranges from below detection to 0.34 mole%, with a mean of 0.12 mole% (Table 3.14).

Sample	Carb	No of Analyses	STDEV ($CaCO_3$)	Average Mole% $CaCO_3$	STDEV ($MgCO_3$)	Average Mole% $MgCO_3$	STDEV ($FeCO_3$)	Average Mole% $FeCO_3$	STDEV ($MnCO_3$)	Average Mole% $MnCO_3$
HC5 122 9	D5 Dol	13	0 94	57 93	1 31	42 15	0 50	0 31	0 10	0 12

Table 3.14 Chemical composition of Holycross minor dolomite vein (D5).

3.3 DISCUSSION

On the basis of petrography, CL characteristics, elemental chemistry and spatial distribution, five dolomitization stages have been recognized in the Rathdowney Trend: (Stage 1) regional fine crystalline replacive grey dolomite, and regional coarse crystalline white dolomite cement; these dolomites occur throughout the Rathdowney Trend and pre-date ore mineralization; (Stage 2) black matrix breccia dolomite; (Stage 3) white matrix breccia dolomite; these dolomites are fault related, occur within the deposit areas. D2 is intimately associated with ore mineralization; (Stage 4) regional pink dolomite; common throughout the Irish Midlands; (Stage 5) late, minor dolomite and calcite phases.

All the dolomites studied are highly non-stoichiometric. Dolomite is a difficult mineral to form because of the precise Ca-Mg ordering required (Goldsmith, 1959) and its formation is accomplished more readily if the crystallization rate is very slow or if solutions are dilute, with few interfering ions (Folk and Land, 1975). The Mg, Ca, CO_3 ions within an ideal dolomite crystal, exhibit an ordered 3-layered arrangement with planes populated entirely by Mg ions alternating with CO_3 ions and planes of Ca ions in the sequence Mg-CO_3-Ca-CO_3. Natural crystals however, often depart significantly from this ideal composition. Dolomites with the highest Fe and Mn concentrations generally correspond to the least stoichiometric dolomites, because Fe and Mn preferentially occupy Mg lattice sites. Further, dolomites which are non-stoichiometric are generally less well ordered than 'ideal' dolomite, through the occurrence of Ca ions in the Mg sheet or Mg ions in the Ca sheet of the dolomite structure. Dolomite is not stoichiometric in most modern environments. Slow growth from dilute solutions, possibly aided by elevated temperatures and an abundance of Mg^{2+} ions in the dolomitizing fluids, would result in near stoichoimetric dolomite (Tucker, 1988). The near-stoichiometry of dolomites is interpreted as reflecting burial conditions (Zenger and Dunham, 1988).

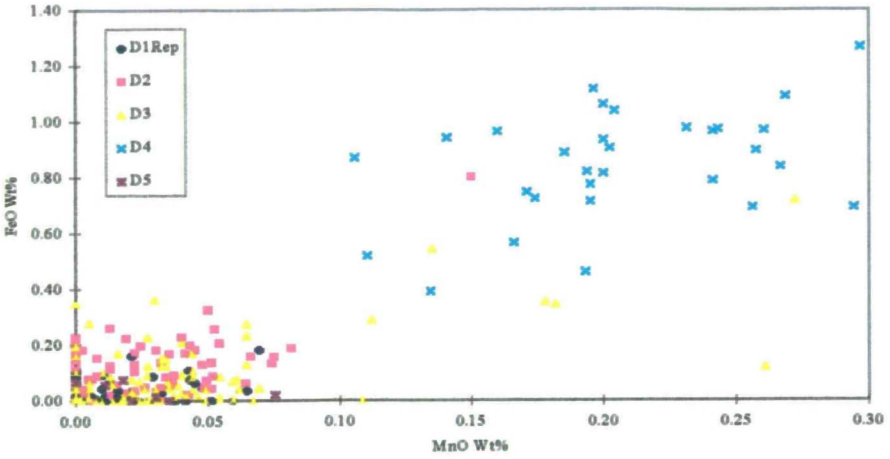


Figure 3.31 Covariance of FeO and MnO wt% in Lisheen Dolomites

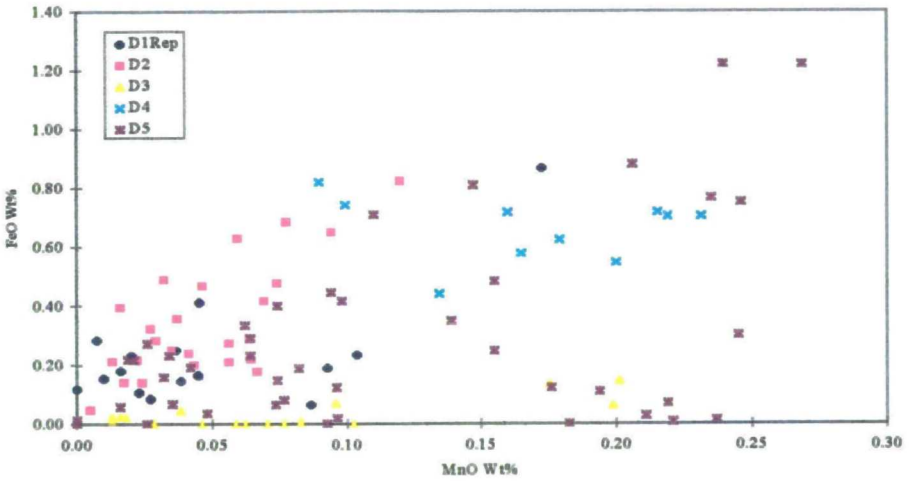


Figure 3.32 Covariance of FeO and MnO wt% in Galmoy Dolomites

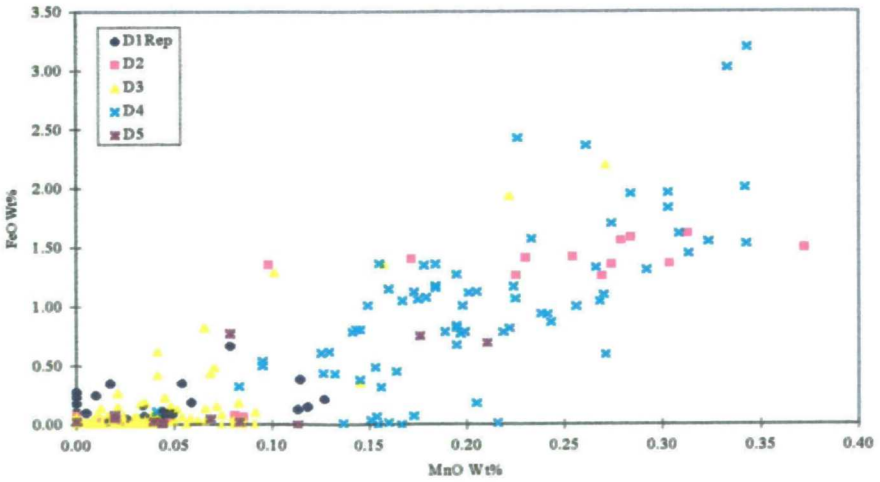


Figure 3.33 Covariance of FeO and MnO wt% in Prospect dolomites

There is a general trend of increasing Fe and Mn through time in each of the dolomite stages (D1-D5) (Figures 3.31, 3.32, 3.33). This trend is seen in all the sample localities throughout the Rathdowney Trend. However, there is a noticeable difference between the two mineral deposits, Lisheen and Galmoy, and the prospects. A higher variance in Fe compositions, and generally higher values in all prospect dolomites (D1-D5) is evident. Fe and Mn compositions are significantly higher in D2 prospect dolomite than in the deposits. This trend could be a useful tool in exploration. Generally, the Fe/Mn ratio in D2 deposit dolomite is higher than the Fe/Mn ratio in D3 deposit dolomite. The Fe/Mn ratio in D3 and D4 prospect dolomites is higher than in the deposits. Fe and Mn concentrations are much higher in D4 dolomites in all sample areas than D1, D2, or D3. Land (1980), and Veizer (1983) have indicated that Fe tends to be enriched in later diagenetic dolomites, especially those formed from saline formation waters. D4 dolomite post-dates ore-related D2 and D3 dolomite and is interpreted as coinciding with a significant change in the depositional environment.

There are no systematic variations in dolomite trace element content which might indicate the direction of fluid flow during dolomitization.

Dolomitization models based on the circulation of normal or slightly modified seawater are favoured for large scale dolomitized sequences. It is thought that the D1, pre-ore, regional dolomite may have originally formed as a result of pulses of heated, marine derived formation waters, possibly from a foreland basin to the south of the carbonate shelf during the onset of the Hercynian Orogeny (Allan *et al.*, 1992; Shearley *et al.*, 1996). However, these dolomites were probably later modified locally by epigenetic dolomitizing/mineralizing fluid(s) responsible for the development of D2 and D3 dolomites. As a result of this modification the original depositional chemistry of these regional dolomites is indistinct, and dolomitization models for the formation of D1 pre-ore, regional dolomite cannot be easily constrained. This impacts on the proposed model of Allan *et al.* (1992) for regional dolomite in Southern Ireland where the evidence for a marine water/ burial origin is based on $\delta^{18}O$ analyses.

More recent studies of carbonate cements by Braithwaite and Rizzi (1997) at Navan, and Redmond (1997) at Lisheen, confirm that local correlation of cement zonation within individual ore deposits is possible. In this study, comparable luminescent patterns of cement sequences have been identified in D3 dolomite cements throughout the Rathdowney Trend. The detailed CL study of dolomites at Navan by Braithwaite and Rizzi (1997) reveal three principal stages of dolomite precipitation, each stage reflecting several changes in the character of the dolomitizing fluids. The Stage 2 dolomite at the Navan deposit displays similar CL properties to the D3

dolomite cement at the Lisheen deposit. Both are characterized by a bright orange-yellow zone; at Navan this zone consists of up to 7 subzones. The bright Stage 2 zones are principally found within the centre of the massive dolomite, decreasing towards the margins of the body. This lateral variation in stage/zone thickness and luminescence intensity was first observed by Redmond (1992) at the Lisheen deposit.

A preliminary study of fluid flow, dolomitization and mineralization of Lower Carboniferous rocks in the Irish Midlands has been initiated by Somerville *et al.* (1997). The study aims to determine whether or not replacement dolomites and associated open-space-filling dolomite (and calcite) can be linked genetically to a regional hydrological system throughout the Irish Midlands (e.g. Gregg and Shelton, 1989). Preliminary petrographic and CL analysis (Gregg *et al.*, 1997) confirms the existence of well-defined and variable cement statigraphies in both epigenetic dolomite and calcite cements. However, large scale correlation of cement zonations has not yet been attempted (Gregg, pers. comm., 1998).

3.3.1 Conclusions

- Five dolomitization stages have been identified in the Rathdowney Trend; pre-ore regional dolomites, $D1_R$ and $D1_C$; syn- to post-ore dolomite matrix breccias, D2 and D3; post-ore pink dolomite, D4; and late- to post-ore, minor vein and vug dolomites, D5.

- The dolomites are all highly non-stoichiometric, this is typical of dolomites not usually associated with slow growth from dilute solutions normally associated with burial conditions.

- The original chemistry of $D1_R$ dolomite at Lisheen and Galmoy has been modified by later epigenetic dolomitizing/mineralizing fluid(s) responsible for the formation of D2 and D3 dolomites.

- Fe and Mn concentrations generally increase with time from the earliest pre-ore dolomites to the post-ore dolomites. Elevated Fe and Mn concentrations commonly occur in prospect dolomite.

- The Fe concentration is nearly always higher in D2 dolomites than D3 dolomites.

- The distinct yellow zone in D3 dolomite is generally correlatable throughout the Rathdowney Trend.

- Lateral variation in thickness and luminescence intensity of the distinct yellow zone in D3 dolomite has been observed in the Lisheen deposit.

- In D3 dolomite, luminescence intensity is controlled by the Fe/Mn ratio and not by the absolute concentration of either cation. In D4 dolomite, however, luminescence is controlled primarily by high Fe variations.

- A dissolution surface between D3 and D4 dolomite marks a significant change in the dolomitizing/mineralizing fluid(s) chemistry.

- Comparable and correlatable zonations in D4 dolomite between Rathdowney East and Holycross prospects indicate a homogeneous regional groundwater flow system at this stage.

3.4 ORE PETROGRAPHY AND MINERAL CHEMISTRY

Detailed textural and petrographic relationships at Lisheen, Galmoy, and Durrow have been determined from a study of polished blocks and thin sections. Textural characterization and paragenesis of the Lisheen ore deposit is well constrained, following detailed petrographic examination of a large number of samples. For Galmoy and Durrow, the sample suite was much smaller. With the exception of crystalline sphalerite associated with late stage dolomite veining in the Holycross prospect, only minor disseminated sulphides (mostly pyrite) are present in the remaining prospects.

Determining the time relationship between sulphide mineralization and host carbonate is critical to understanding the formation of the 'Irish-type' ore deposits. Early timing of mineralization relative to deposition of the host sediment and greater conformity with the host rock distinguishes sediment hosted stratiform deposits from MVT deposits, which are formed by later replacement of lithified carbonate host rocks.

Sphalerite (ZnS) and galena (PbS) are the principal ore minerals in a relatively simple mineral assemblage which also consists of abundant iron sulphides. Chalcopyrite ($CuFeS_2$), arsenopyrite (FeAsS), bornite (Cu_5FeS_4) and tetrahedrite-tennantite ($Cu_{12}(As,Sb)_4S_{13}$), Pb-Sb sulphosalts such as boulangerite ($Pb_5Sb_4S_{11}$) and Pb-As sulphosalts including jordanite ($Pb_{14}As_6S_{23}$) are present in minor amounts.

For simplicity, mineralization has been classified into four stages: pre-ore stage, main ore-stage, late ore-stage, and post ore-stage. The ore-stages are defined in terms of mineralogy, texture and chemistry. Common textural types include disseminated, colloform banded, massive replacement, vein and vug-filling ores.

Analyses of major and trace elements were performed by electron microprobe (wavelength-dispersive) on a variety of sulphides (Appendices B6,7,8). For Zn, Pb, Cu, Mn, Cd, Ni, Co, Sb, and Ag the standards used were pure (i.e. 100%) element standards. For Fe, As, Hg, Bi, and S the standards used were troilite, gallium arsenide, mercury telluride, bismuth telluride and troilite respectively. The elements Ga, Ge, and In were largely undetectable.

Different element lists were set up for the individual analyses of sphalerite, galena, pyrite, and tennantite-tetrahedrite minerals (Appendix C3). The element list for pyrite was also employed to analyze chalcopyrite. Detection limits for the major and trace elements differ slightly for separate analyses of sphalerite, galena, pyrite and tennantite-tetrahedrite (Appendix B5).

Potential background interference patterns (Appendix B9) between As, Sb, Ag, and Bi, S, Pb have been examined using the software programme "Virtual WDS". The As line indicates a second order peak overlap with Sb. The elements Bi, S, and Pb show significant interference, most notably a Pb line which occurs beneath the main Bi peak. Peak interference between Cd and Ag has also been identified; however, analyses of Cd will only be affected if significant amounts of Ag are present. The elements Ga and Zn show significant interference, Ga values below 0.2wt% are not real. Tl and S also show serious interference patterns.

3.4.1 Lisheen Deposit

Mineralization at Lisheen occurs within 30m of the base of the Waulsortian, forming single and multiple stratiform zones separated by D2 dolomite. The massive orebodies display sharp contacts with the dolomites. Sulphides are also present in the Lisduff Oolite Member, both in the footwall and hangingwall of the Killoran and Derryville faults. Sulphides within the Lisduff Oolite in the footwall of the Killoran fault zone have generally similar ore textures and paragenetic relationships to ore zones within the Waulsortian. Hanging wall sulphide zones within the Lisduff Oolite are distinctive both texturally and mineralogically.

Sulphides are generally fine to medium grained (Plate 49); coarse crystals are only present in the later stages of sulphide precipitation. They commonly occur as thin veins and veinlets; disseminations; massive orebodies; stylolites; coarse vug fillings; rim cements; colloform bands; and interporosity fill.

3.4.1a Pre Ore-Stage

Minor disseminated pyrite occurs in $D1_R$ dolomite and around the margins of $D1_R$ clasts within D2 dolomite breccias (Plate 39). The earliest sphalerite and pyrite mineralization occurs as infill of intergranular D2 dolomite porosity with fine grained pyrite occurring interstitial to the fine grained sphalerite. The pyrite is granular in appearance and is composed of polycrystalline aggregates of anhedral to euhedral crystals a few microns in size. This granular pyrite predates a subsequent extensive iron sulphide mineralization phase which comprises large, euhedral, equant pyrite grains with approximately 120° interfacial angles, often enclosing aggregates of early fine grained, non-colloform sphalerite (e.g. 262/159.1).

The first phase of significant sphalerite mineralization resulted in the formation of a very fine crystalline, weakly colloform, pale pink-brown sphalerite (Plate 50A). This sphalerite preferentially occurs in the D2 dolomite matrix.

The most extensive iron sulphide mineralization event postdates the earliest non-colloform and weakly colloform pink-brown sphalerite, but predates the main sphalerite-galena ore-stage. The iron sulphide mineralization contains minor inclusions of galena, sphalerite and gangue (Plate 55). Pyrite is the earliest and dominant iron sulphide, and is overgrown by pyrite-marcasite growth bands with marcasite becoming more abundant in successive growth bands, (Plate 55A). Marcasite occurs as alternating bands with pyrite in colloform masses, elongate radiating laths intergrown with pyrite, and as coarse subhedral pyrite-marcasite associations. Small pyrite spheroids (0.001-0.01mm in diameter) probably acted as nuclei for subsequent overgrowths leading to the development of commonly colloform banded pyrite, a significant textural component of massive iron sulphide. Sphalerite, galena, and gangue dolomite occasionally occur as discrete bands within the banded iron sulphides, or as isolated crystals along particular iron sulphide growth bands (Plate 55B). Galena often occurs as small colloidal spheres within massive iron sulphide. Radial coxcomb textures are less common, but are well developed in the Lisduff Oolite adjacent to fault zones. Fine grained granular pyrite, and subhedral pyrite-marcasite associations pseudomorphously replace elongate laths of barite (Plate 56A). Pyrite locally replaces ooids in the Lisduff Oolite; relict ghost textures are preserved. Framboids are a minor

component of the iron sulphides. The framboids tend to occur in isolation or as small clusters, particularly in proximity to major E-W trending faults (275/175.5). They are commonly overgrown by later, massive pyrite.

Cataclastic textures in pyrite and marcasite probably formed in response to faulting in the Main and Derryville zones. Pyrite is infilled/replaced along fractures by sphalerite (Plate 56B) and also by ore-stage galena.

The iron sulphides are arsenian, with concentrations up to 5.21 wt% As (431/205.70). A strong negative correlation exists between Fe and As in this As-rich pyrite-marcasite assemblage (r = -0.99).

3.4.1b Main Ore-Stage

A complex mixed sulphide precipitation event followed the early deposition of sphalerite and iron sulphides. It is characterized by the precipitation of ore-stage sphalerite, galena and minor chalcopyrite, arsenopyrite, tennantite, gangue dolomite and barite, with coeval precipitation suggested by mutual growth boundaries. This main phase of mineralization resulted in the progressive replacement of both D2 dolomite matrix and $D1_R$ clasts in the BMB (Plate 49 and 50). Relict clasts can be observed in the massive sulphides which are predominantly hosted in zones that were occupied by black matrix breccias.

The most significant and abundant colloform sphalerite at Lisheen (Plate 51) occurs in aggregates within massive mixed sulphides and consists of well defined colour zonations that range from pale cream to dark brown. Colloform sphalerite in sample 262/159.1 (Derryville zone) consists of 40 distinct zones with approximately 70 sub-zones. Cd, Fe and As variations across the zones are identified by a stage scan (Figure 3.35). A weak negative correlation exists between Cd and Fe (r = -0.5). In sample 400/205.65 (North zone) a finely zoned yellow colloform sphalerite contains up to 1.95 wt% Fe (mean = 0.37 wt%), yellow to grey coloured colloform sphalerite contains up to 0.12 wt% Fe (mean = 0.06 wt%), and orange-brown colloform sphalerite contains up to 2.84 wt% Fe (mean 0.63 wt%). Galena occurs with these distinctly zoned colloform sphalerites. The colloform sphalerites contain up to 0.24 wt% Ag, 0.47 wt% Cd, and 0.60 wt% As. Distinct zones of pyrite, gangue dolomite, and Zn rich carbonate also occur in the colloform sphalerite (sample 262/159.85). The Zn rich carbonate is highly granular. Often pyrite occurs as small concentrically zoned grains within the colloform sphalerite (Plate 51). Dolomite rhombs are hosted within

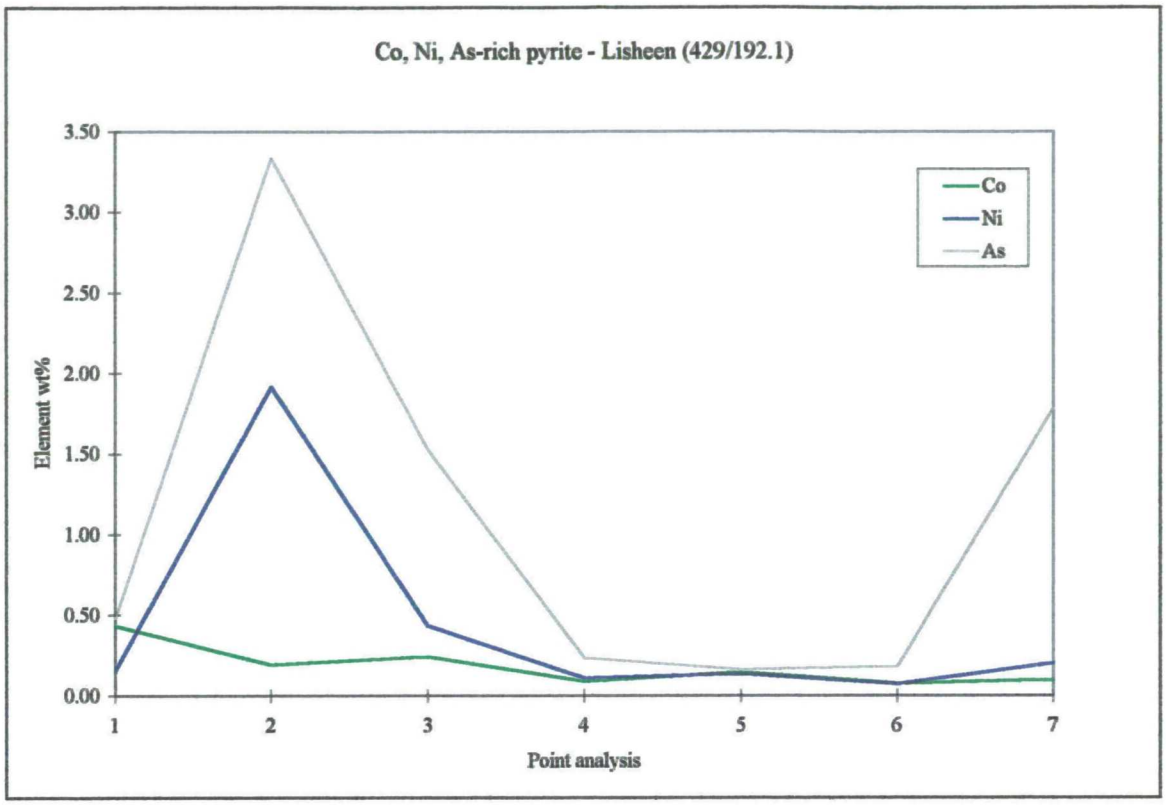


Figure 3.34 Ballysteen hosted, Co, Ni and As-rich pyrite - Main zone, Lisheen.

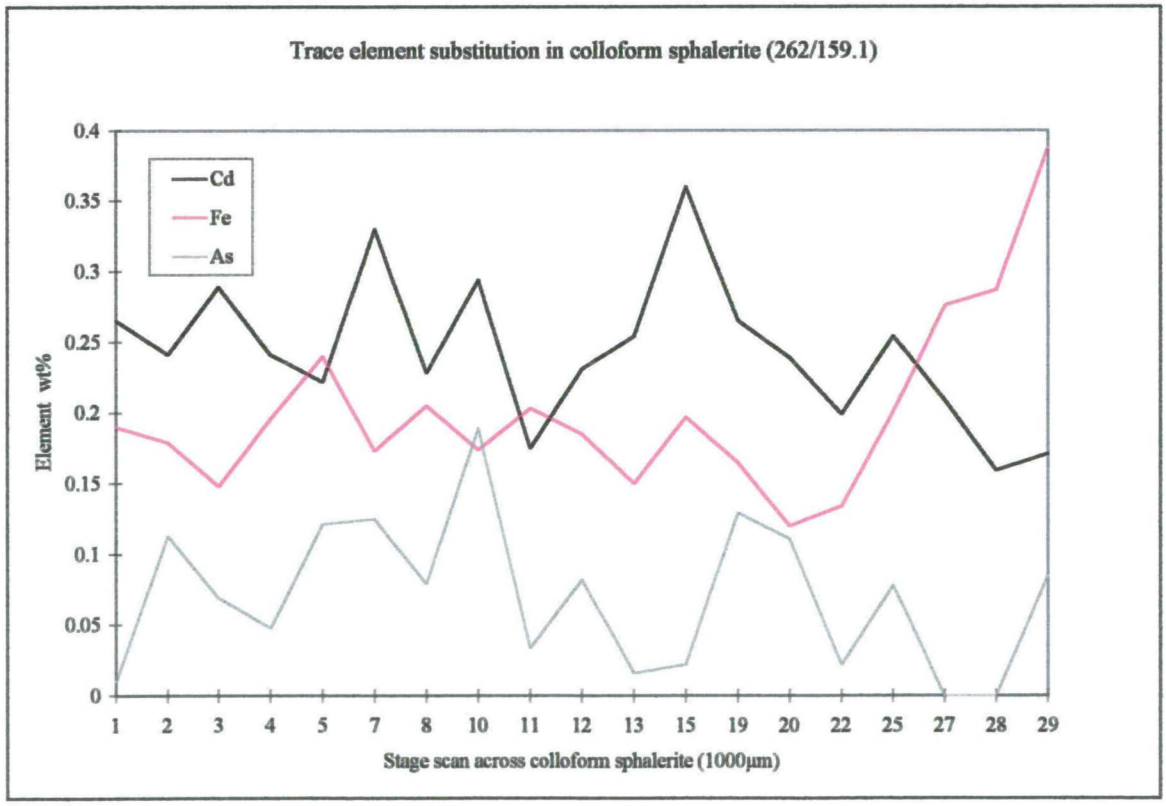


Figure 3.35 Cd, Fe and As correlation in colloform sphalerite - Derryville zone, Lisheen.

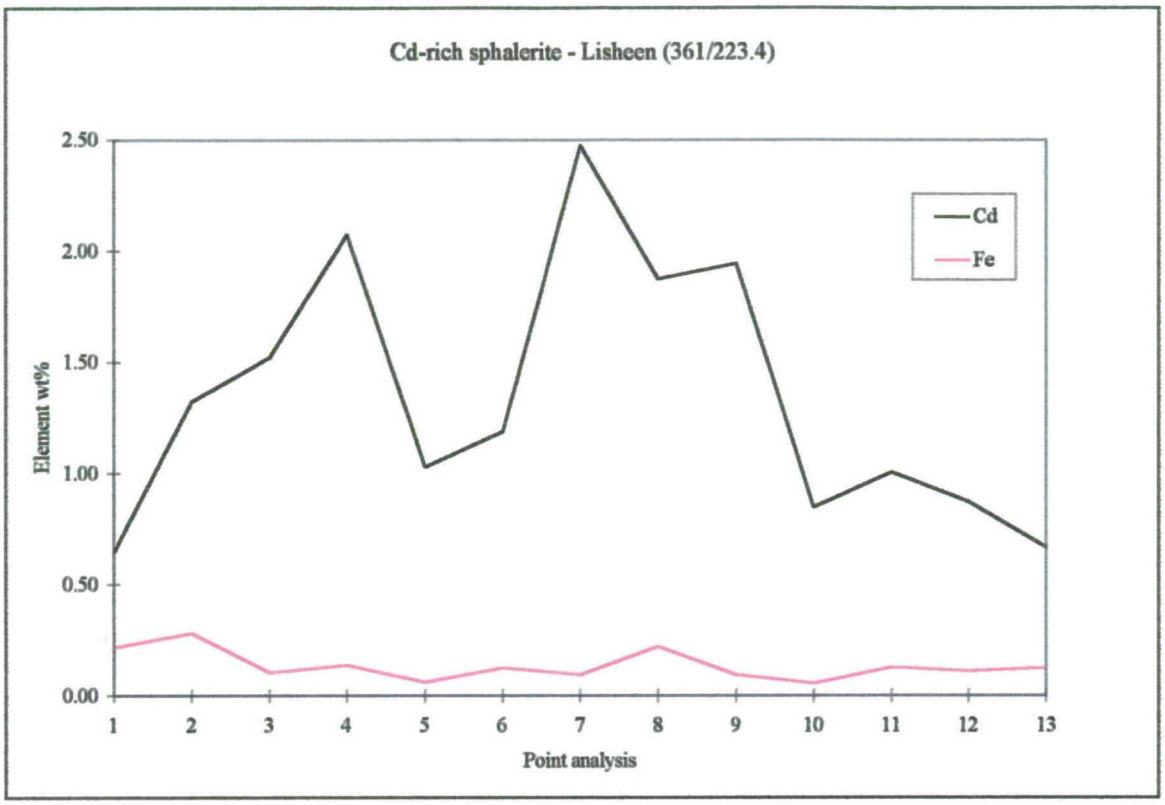


Figure 3.36 Ballysteen hosted, Cd-rich, crystalline brown sphalerite - Bog zone, Lisheen.

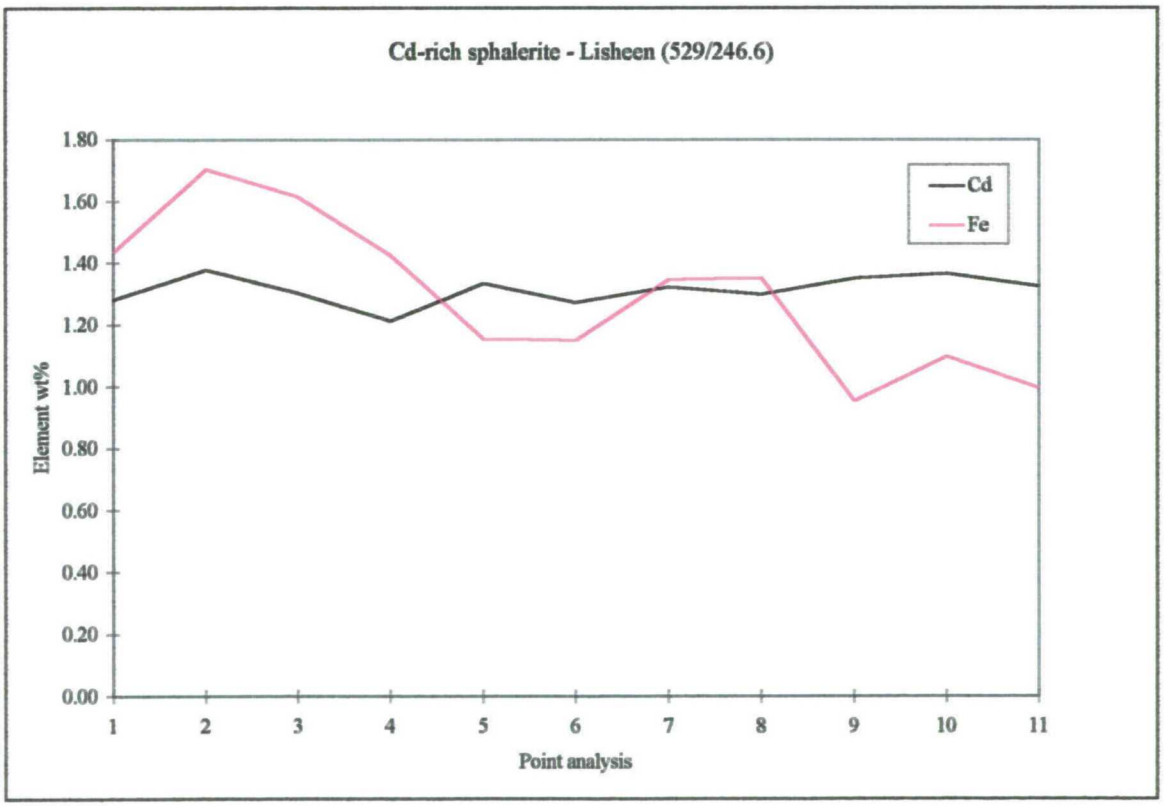


Figure 3.37 Lisduff Oolite hosted, Cd-rich brown sphalerite - Bog zone, Lisheen.

colloform sphalerite (416 193.6) and early pyrite and sphalerite are incorporated into the growth zones of the dolomite rhombs (Plate 52A). The colloform sphalerite is locally broken and rotated.

Massive fine grained sphalerite is unzoned. Sphalerite intergrowths with pyrite are common. Ore-stage sphalerite and galena are generally intergrown, but galena is often replaced by the latest sphalerite phase. Fe and Cd concentrations in fine grained ore-stage sphalerite are generally less than 0.5 wt%, lower than typically observed in the colloform sphalerite. Sphalerite replaces dolomite rhombs (121/192.8a) and partially replaced rhombs commonly contain inclusions of sphalerite and galena. Sphalerite bow tie textures in pyrite (sample 121/192.8a), and elongate laths of sphalerite in a mixed assemblage of pyrite and galena may be pseudomorphs after early barite (Plate 52B). There is no consistent temporal relationship between sphalerite and pyrite in the main ore stage. Selective replacement of microfossils by sphalerite is also common (Plate 53A). Sphalerite also forms rims on pyrite grains (pyrite is also observed to form rims on sphalerite grains) and occurs as small veinlets cross-cutting and replacing pyrite (Plate 49A).

Ore-stage galena is predominantly replacive. Replacement textures include caries textures, where galena replaces D2 dolomite. Selective replacement of microfossils and ooids is also common (Plate 54). The relict ooid textures preserved indicate deformation prior to mineralization. Ooids do not generally deform under burial conditions, but may do as a result of tectonic activity. This indicates mineralization occurred after a certain amount of faulting. There is no evidence of post-depositional deformation within galena. Relatively uncommon open space textures include skeletal and dendritic growths, similar to those described from Navan (Anderson *et al.* in press).

Galena is abundant in zones proximal to the Killoran and Derryville faults. Tennantite inclusions occur within galena sampled from Main zone, proximal to the Killoran fault (sample 121/192.8). Galena inclusions are also found within tennantite. The Pb-Sb sulphosalt boulangerite ($Pb_5Sb_4S_{11}$) is also associated with galena.

The chemical composition of galena at Lisheen is relatively homogeneous. Massive ore-stage galena commonly contains up to 0.34 wt% Bi. However, Bi compositions in Lisduff Oolite hosted ore-stage galena are below detection. Ag concentrations of up to 0.19 wt% are only present in samples (095/335.0, 431/199.65) located proximal to 'feeder' faults.

Chalcopyrite, arsenopyrite, tennantite and barite are also most abundant near the Killoran and Derryville faults, especially within the footwall Lisduff Oolite. Tennantite commonly occurs as irregular inclusions in Lisduff Oolite hosted galena, chalcopyrite and sphalerite. The tennantite is

characterized by up to 3.91 wt% Zn, 5.63 wt% Fe and 0.32 wt% Ag. Tennantite (sample 121/192.8) inclusions in Waulsortian hosted, euhedral galena occur in isolation and are especially abundant near grain boundaries and growth planes. The tennantite is characterized by higher Zn (up to 8.55 wt%), lower Fe (<1.72 wt%), and lower Ag (<0.24 wt%) concentrations. Massive chalcopyrite (235/167.0) occurs in the footwall Lisduff Oolite of Main Zone. It is distinguished by As compositions up to 0.73 wt% (mean = 0.16 wt%). Minor chalcopyrite (361/223.4) in the Bog zone Lisduff Oolite is characterized by lower As compositions up to 0.11 wt% (mean = 0.07 wt%). Minor disseminated, euhedral arsenopyrite rhombs occur in ore-stage galena, proximal to fault zones (431/209.20, 275/175.5).

The Co, Ni concentrations in ore-stage, and late pyrite are often below detection, however, in samples where the concentrations are above the level of detection the Co/Ni ratio is always <1.0. A positive correlation exists between Ni and As (r = 0.89) in a Co, Ni, and As-rich pyrite (429/192.1) with concentrations up to 0.44, 1.92, and 3.34 wt% respectively (Figure 3.34). These samples are located very close to the major Killoran fault.

Barite was probably deposited both prior to and during the main period of sulphide mineralization. Early sulphides, in particular pyrite-sphalerite replace barite. However, later precipitation of barite with the complex mixed sulphide assemblage cross-cuts earlier pyrite-sphalerite assemblages. Ore-stage sulphides pseudomorphously replace barite (Plate 52B). Barite can easily be mistaken for gangue carbonate under reflected light. It has a prismatic habit and forms in radiating patterns which produce cracks. It has a greater reflectance than calcite but this is dependent on orientation (Criddle, pers. comm., 1996).

3.4.1c Late Ore-Stage

Coarse crystalline sphalerite and euhedral galena crystals are generally restricted to late stage fracture-fill mineralization and are often associated with late vug-filling D5 dolomite and calcite cements (Plate 53B). The sulphides are usually early relative to the gangue carbonate cement they are associated with. The galena is often post-dated by the late sphalerite, which forms a distinct rim cement around the galena. Occasionally the galena co-precipitates with the sphalerite. Concentrically zoned pyrite grains occur within these late sphalerite rims. There is no significant trace element content in late euhedral, fracture-fill galena.

Coarse crystalline sphalerite (1-7mm in size) is not very common. Nearly all the coarse sphalerite samples studied have come from the latest infill drilling project, covering all major mineralized

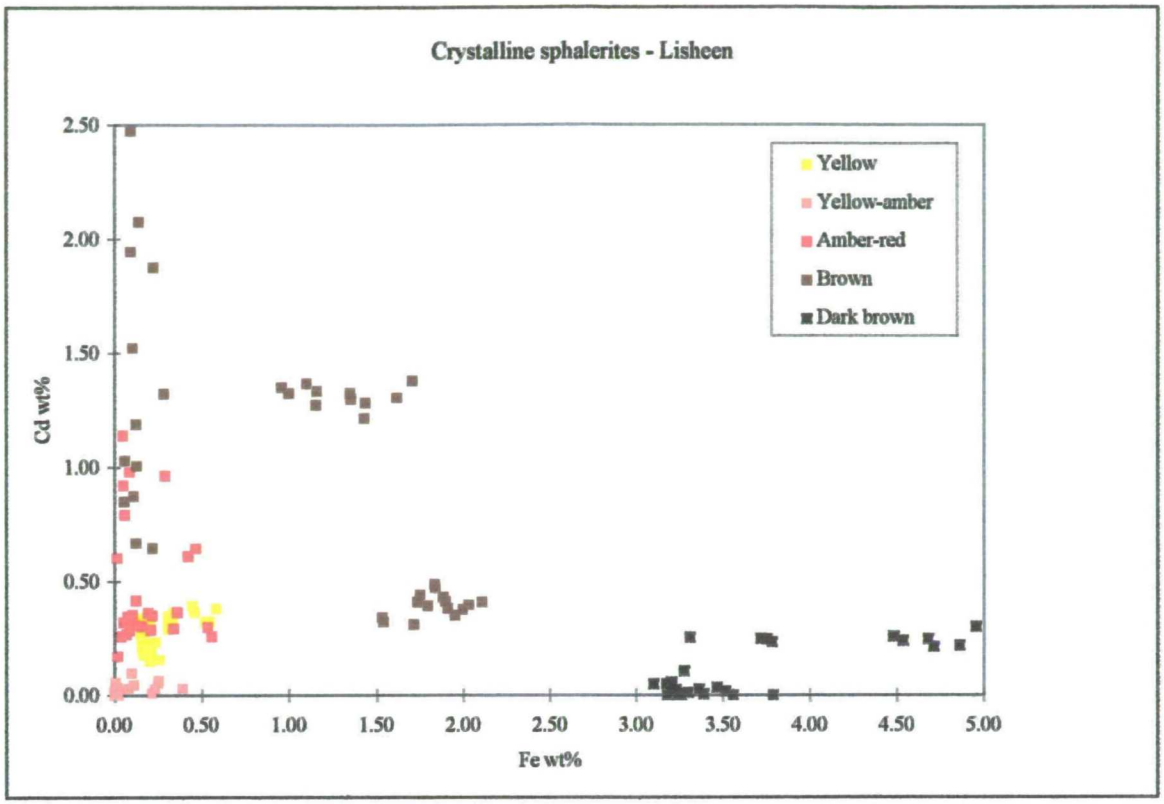


Figure 3.38 Fe wt% (x-axis) v Cd wt% (y-axis) in crystalline coloured sphalerites.

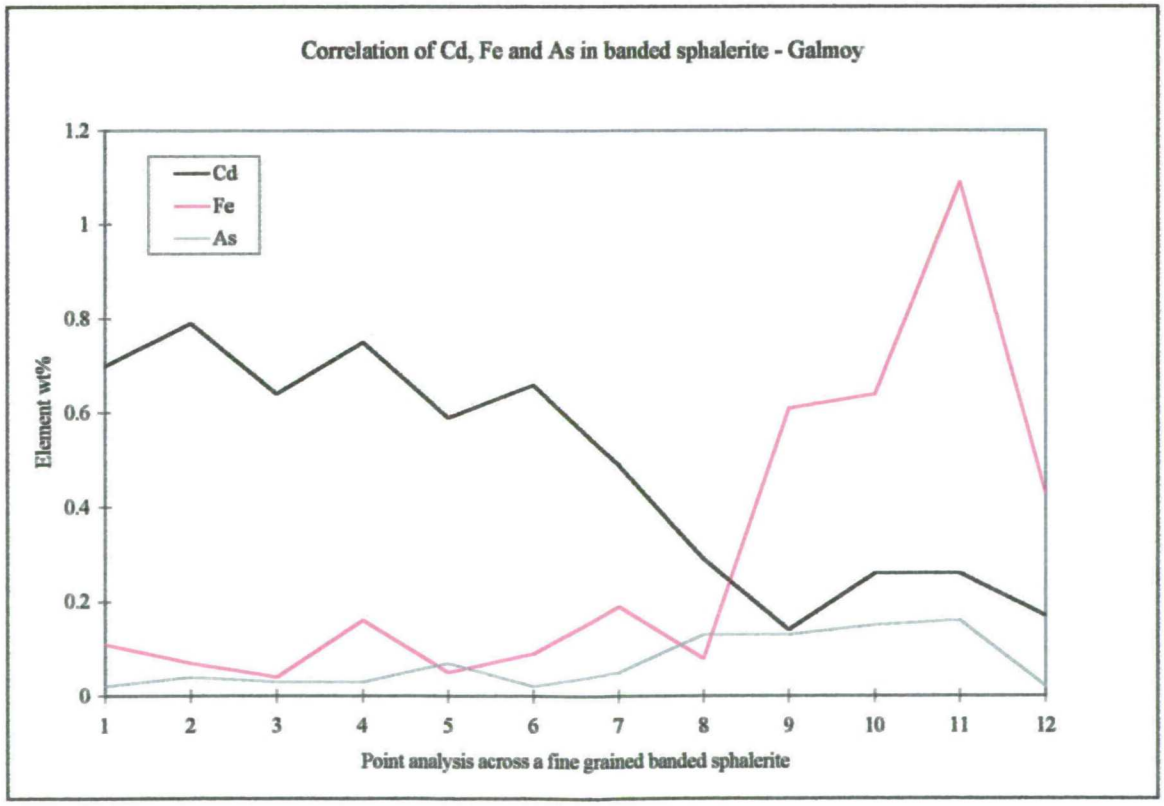


Figure 3.39 Correlation of Cd, Fe and As in banded sphalerite - K zone, Galmoy.

zones. The coarse sphalerite crystals contain an abundance of workable fluid inclusions, unlike the fine grained replacive sphalerite or finely zoned colloform sphalerites. Colour is extremely variable, ranging from yellow, through amber to dark brown. The dark brown crystalline sphalerites are generally more iron rich than the yellow sphalerites, and contain up to 4.96 wt% Fe. The Fe content of yellow and amber sphalerites is generally <0.5 wt%. Cd compositions are highly variable. Sub-Waulsortian hosted brown sphalerites from the faulted Bog zone are notably Cd-rich (Figures 3.36, 3.37). Yellow sphalerite contains up to 0.34 wt% Cd, amber sphalerite contains up to 1.14 wt% Cd, and brown sphalerite contains up to 2.48 wt% Cd. Brown to dark brown sphalerites are generally located within the Ballysteen Limestone; these show an antipathetic relationship between Fe and Cd (Figure 3.38). The yellow-amber crystalline sphalerite is commonly located within the Waulsortian. Ag compositions in dark brown sphalerite are below detection; however, the amber-yellow Waulsortian hosted sphalerites contain up to 0.12 wt% Ag. All these sphalerites are generally more iron rich and contain lower As (usually < 1.0 wt%) than the earlier colloform sphalerites.

3.4.1d Post Ore-stage

Sulphides which post-date the waning stages of mineralization are considered post-ore stage. These sulphides often occur with pink dolomite, which has been shown petrographically to post-date the main mineralization event. These post-ore sulphides may have been remobilized from earlier deposition, however, this is difficult to ascertain.

3.4.1e Paragenetic Summary - Lisheen Deposit

Early sulphide precipitation into intercrystalline voids in D2 dolomite was succeeded by early replacement of the host D2 dolomite by fine grained sphalerite and pyrite. This was followed by the deposition of significant iron sulphide, containing minor amounts of sphalerite, galena and gangue dolomite and barite. Ore-stage mineralization involved the precipitation of a complex mixed sulphide assemblage. Early colloform sphalerite was succeeded by massive replacive mineralization, which consisted predominantly of sphalerite and galena associations with minor amounts of chalcopyrite, arsenopyrite and tennantite. The waning stages of mineralization are recorded in the late veins and vugs filled with coarse crystalline, euhedral sulphides and late carbonate cements.

A general sequence of deposition is: (1) pre-sulphide carbonate; (2) early sphalerite and pyrite; (3) extensive iron sulphide precipitation with minor sphalerite, galena, and gangue; (4) mixed

sulphide assemblage, including ore-stage sphalerite and galena; (5) late sphalerite and galena; (6) late carbonate. Pyrite and sphalerite show some evidence of coeval formation in stage (3).

Fe and Cd concentrations are highly variable in late-ore stage, crystalline sphalerite. Brown, Fe and Cd rich sphalerites are generally sub-Waulsortian hosted and proximal to inferred 'feeder faults'. Yellow-amber coloured crystalline sphalerites contain lower Fe, variable Cd and higher Ag concentrations than the brown coloured crystalline sphalerites, and is commonly located within the Waulsortian. Fe and Cd concentrations in the main-ore stage colloform, and fine grained sphalerites are generally less variable and much lower.

The Fe concentration appears to correlate with colour in these late-ore crystalline sphalerites. In most cases Fe-rich sphalerites are brown to dark brown in colour. However, this colour correlation may also be partly dependent on the concentration of Cd as well.

The highest Ag concentrations up to 0.32 wt% occur in tennantite inclusions within the footwall oolite hosted galena and are higher than the Ag concentrations in both colloform sphalerite and ore-stage galena. The chemical composition of ore-stage galena at Lisheen is relatively homogeneous, although occasionally elevated Bi concentrations exist. However, tennantite inclusions within ore-stage galena are characterized by higher Zn concentrations than the footwall oolite hosted tennantite inclusions.

As concentrations >2.5 wt% in iron sulphides commonly occur proximal to the major Killoran and Derryville fault zones.

3.4.2 Galmoy Deposit

Mineralization at Galmoy occurs at, or close to, the base of the Waulsortian, at an average depth of 70m. Ore-stage mineralization is principally confined to the D2 dolomite but, sulphides also occur in the dolomitized Lisduff Oolite Member and Lower Ballysteen Limestone beneath the G zone in the hanging wall of the G fault. Vein-type Cu-Ag mineralization also occurs in the footwall of the major G Fault (Plate 47A). The general paragenesis is similar to that observed at Lisheen.

3.4.2a Pre-Ore Stage

Minor disseminated pyrite is common in $D1_R$ dolomite and around the margins of $D1_R$ clasts. Early pyrite, sphalerite and galena occur as fine grained disseminations within D2 breccia matrix dolomite. Granular aggregates of subhedral pyrite commonly enclose early sphalerite grains. The earliest phase of significant sphalerite mineralization is buff coloured and occurs as fine grained disseminations and cross-cutting veinlets.

Massive intergrown iron sulphides, predominantly pyrite and marcasite, form pyrite 'caps' which overlie the CW and G orebodies. This extensive iron sulphide event is thought to have formed either by complete replacement of unbrecciated dolomite or by infill of a large cavity (Doyle *et al.*, 1992). The iron sulphide mineralization event probably pre-dates the main sphalerite-galena ore-stage event.

3.4.2b Main-Ore Stage

The earliest ore-stage sphalerite is normally fine grained, and occasionally displays banding. This banded sphalerite is usually accompanied by euhedral galena. Minor pyrite rims observed around these euhedral galenas contain up to 1.36 wt% As. Co and Ni are below detection. However, galena typically occurs as massive ores. Small inclusions of the earliest formed sphalerite are enclosed in massive galena which is usually intergrown with ore-stage sphalerite. Colloform textures are also sometimes displayed by ore-stage galena which rhythmically alternates with sphalerite (Plate 58A). Early pyrite is replaced by these ore-stage sulphides. Zoned colloform pyrite occurs in high grade ore zones, and is post-dated by sphalerite veins (Plate 59A).

High grade ore sphalerite is commonly fine grained, however, in some zones the latest ore-forming sphalerites exhibit fine crystalline textures (Plate 57). These crystalline sphalerites contain workable fluid inclusions.

The sphalerite at Galmoy is generally Fe poor. Massive, fine grained ore-stage sphalerite contains up to 0.57 wt% Fe (mean = 0.38 wt%), 0.3 wt% Cd (mean = 0.25 wt%) and 0.25 wt% Ag. This fine grained, high-grade ore also contains up to 0.14 wt% As, and 0.17 wt% Cu. Fine crystalline ore-stage sphalerite contains up to 0.64 wt% Fe (mean = 0.46 wt%), 0.22 wt% Cd (mean = 0.1 wt%) and 0.12 wt% Ag. Cd and As compositions in these sphalerites are generally <0.3, and <0.1 wt% respectively. Banded, fine grained sphalerite contains slightly higher Fe concentrations, up to 1.09 wt% Fe (mean = 0.51 wt%) and 0.79 wt% Cd (mean = 0.49 wt%). The Fe-rich sphalerite

bands correlate with elevated As concentrations of up to 0.16 wt% (Figure 3.39) with a correlation coefficient of 0.71. A negative correlation exists between Cd and Fe (r = -0.7) and Cd and As (r = -0.69).

Chalcopyrite and galena mineralization occurs in the Ballysteen Limestone beneath the G zone in the footwall of the G fault. The mineralization occurs as open-space fill, in carbonate veins and as fine cross-cutting veinlets. Tetrahedrite inclusions are abundant in the galena. The inclusions are characterized by up to 7.51 wt% Zn, 1.05 wt% Fe, 0.51 wt% Ag and 0.11 wt% Hg. Small isolated Pb-Sb sulphosalt inclusions, probably of jordanite ($Pb_{14}As_6S_{23}$), occur within the tetrahedrite inclusions. The chalcopyrite contains up to 0.14 wt% As, 0.06 wt% Co, and 0.06 wt% Ni.

The chemical composition of galena at Galmoy is relatively homogenous. Massive ore-stage galena commonly contains up to 0.31 wt% Bi, similar to massive ore-stage galena at Lisheen. Euhedral galena associated with banded sphalerite appears to contain up to 0.14 wt% Cd, and 0.15 wt% Ag. However, the high concentration of Cd may be due to interference as a result of the higher Ag concentrations in the galena.

3.4.2c Late Ore-Stage

Open-space filling euhedral galena is common, and is normally post-dated by the latest stages of sphalerite mineralization, which involve the deposition of coarse crystalline sphalerite in vugs and veins. The sphalerite crystals often exhibit distinct colour zonation, ranging from brown to yellow (Plate 58B). In CL these zones exhibit distinct luminescence. The brown sphalerite is often non-luminescent, but pronounced yellow and turquoise zones occur in the pale yellow to colourless sphalerites (Plate 58a, A). These late crystalline sphalerites also contain workable fluid inclusions. Minor colloform sphalerite occurs around the edge of late carbonate vugs. In CL this sphalerite also exhibits distinct luminescence, most notably a purple luminescent zone within green-yellow luminescent sphalerite (Plate 58a, B). The distinct turquoise and purple luminescent zones are also seen in colloform sphalerite at Navan (pers. comm., Wilkinson 1998).

The late coarse crystalline sphalerite contain up to 3.48 wt% Fe (mean = 1.44 wt%) in the brown coloured zones. The yellow to colourless zones contain up to 2.16 wt% Fe (mean = 0.65 wt%) (Figure 3.40). Cd concentrations in these late crystalline sphalerites are higher than in the ore-stage sphalerites but are lower than observed in the crystalline sphalerites at Lisheen. The crystalline sphalerites contains up to 0.12 wt% Ag. Late, vug-hosted galena contains up to 0.18 wt% Bi, and 0.12 wt% Ag.

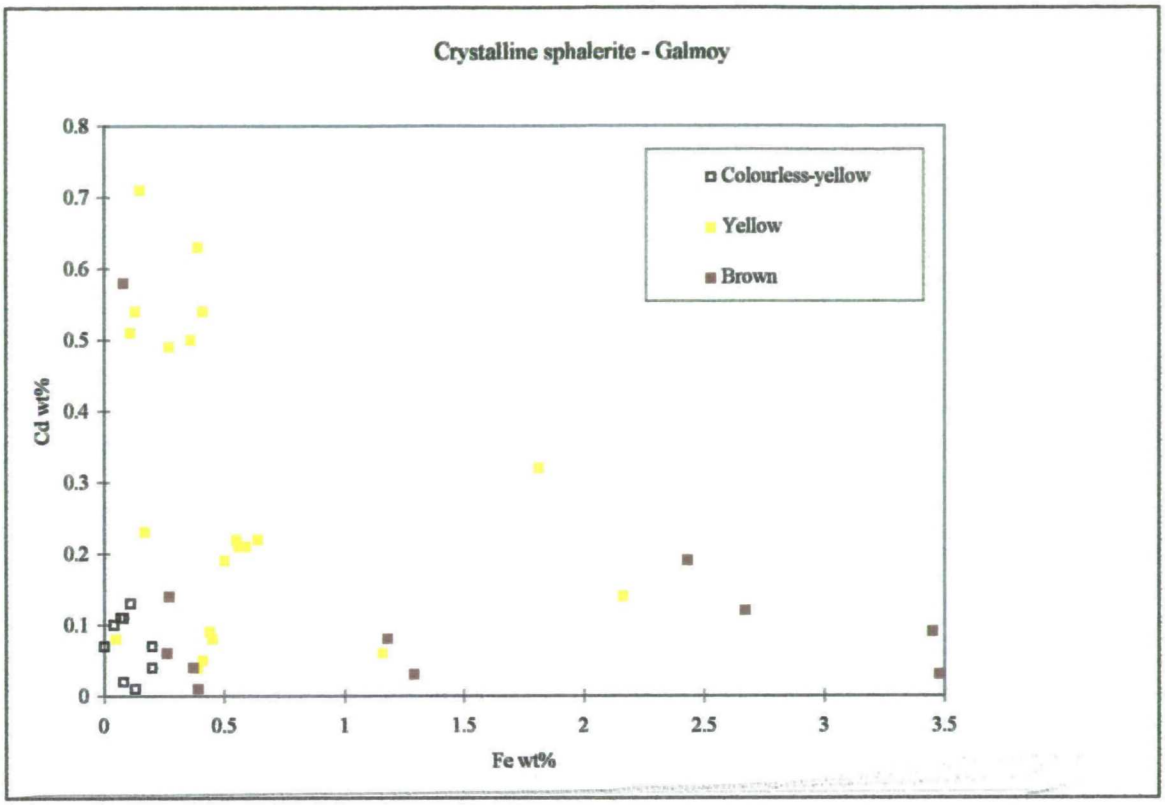


Figure 3.40 Fe wt% (x-axis) v Cd wt% (y-axis) in crystalline coloured sphalerites.

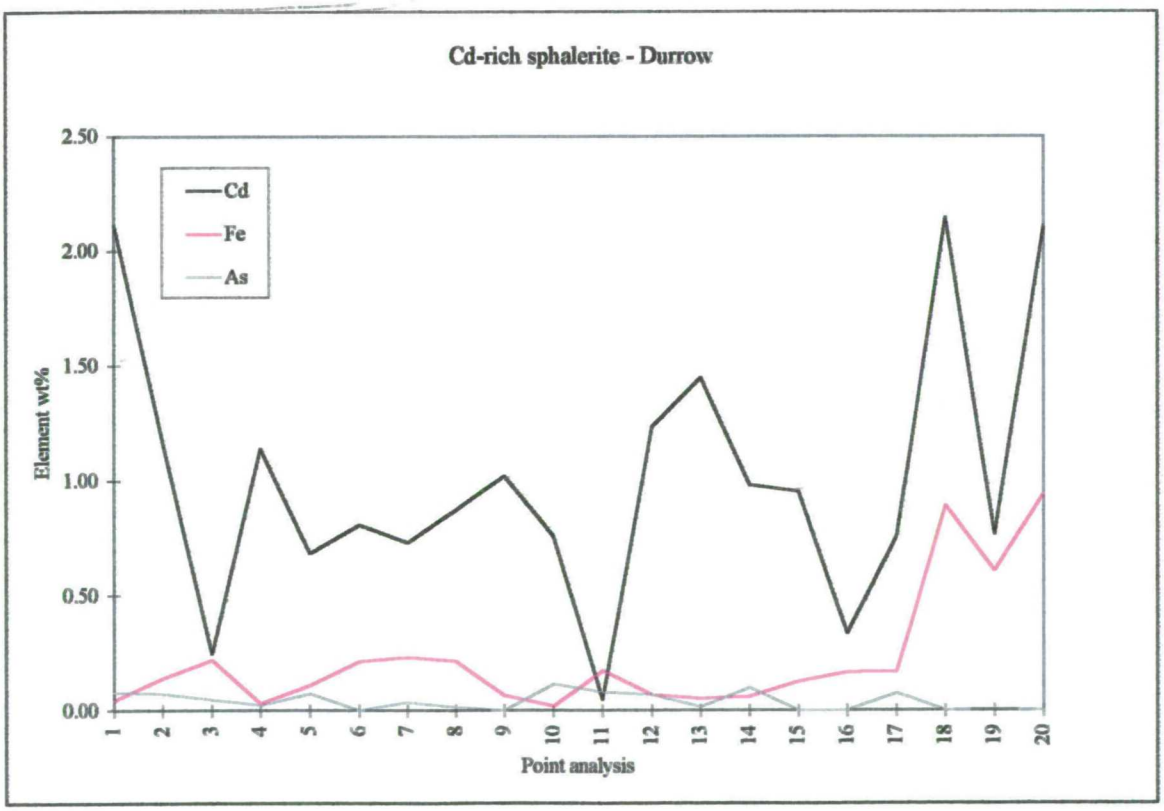


Figure 3.41 Lisduff Oolite hosted, Cd-rich sphalerite - Durrow (1/910).

3.4.2d Paragenetic Summary - Galmoy Deposit

The ore paragenesis at Galmoy is broadly similar to Lisheen (Figure 3.44). However, the sequence of ore deposition in the Galmoy deposit is less well constrained due to the examination of a much smaller sample suite.

A general sequence of deposition is: (1) pre-sulphide carbonate; (2) early pyrite and sphalerite; (3) Pyrite and marcasite; (4) ore-stage sphalerite and galena; (5) late sphalerite and galena; (6) late carbonate.

Brown crystalline sphalerites are generally more Fe-rich than the colourless to yellow coloured sphalerites, and contain up to 3.48 wt% Fe. Fe concentrations in yellow coloured sphalerite are much higher than for yellow crystalline coloured sphalerites analyzed at Lisheen with concentrations up to 2.16 wt% . In general the Cd concentrations are much lower for both brown and yellow crystalline sphalerites in the Galmoy deposit compared to the highly variable Cd concentrations seen in the Lisheen deposit. However, at Galmoy the Cd concentrations in the yellow sphalerite are more variable than in the brown sphalerites.

Fine grained ore-stage sphalerite contains up to 0.25 wt% Ag, similar to ore-stage colloform sphalerites in the Lisheen deposit. Ag concentrations in galena of 0.15 wt% are lower than concentrations in the Lisheen deposit, which contain up to 0.19 wt%. Ag concentrations of up to 0.12 wt% in the crystalline sphalerites are the same for crystalline yellow sphalerites at Lisheen.

Anomalously high trace element concentrations exist in banded sulphides from K zone. Cd and Fe concentrations up to 0.79 and 1.09 wt% occur in fine grained sphalerite, and high As concentrations of up to 1.36 wt% occur in pyrite.

Tetrahedrite inclusions within the footwall hosted galena beneath the G fault contain similar concentrations of Zn and Fe as the tennantite inclusions in hosted in galena at Lisheen. However, the tetrahedrite at Galmoy contains twice as much Ag, up to 0.51 wt% and Hg concentrations of up to 0.11 wt%.

3.4.3 Rathdowney Trend prospects - Durrow

Mineralization at Durrow occurs within the uppermost part of the Lisduff Oolite Member. The mineral assemblage consists of pyrite, chalcopyrite, sphalerite and tetrahedrite. Gangue minerals include dolomite, calcite, ferroan calcite, ferroan dolomite and minor quartz. There is a marked difference in mineralogy between the two boreholes sampled, DUR1 and DUR2.

In borehole DUR1, the dolomitized oolite consists of a fine sparry white dolomite matrix, which contains trace amounts of pyrite, sphalerite and galena. Minor sphalerite (red to brown in colour) and pyrite occurs above the Lisduff Oolite in the ABL. Pale brown sphalerite is associated with late stage dolomite veining in dolomitized Aghmacart Formation. In borehole DUR2, the dolomitized oolite is cut by late dolomite veining which contains trace amounts of pyrite, chalcopyrite, tetrahedrite and sphalerite. Fine grained pyrite disseminations occur throughout the dolomitized Waulsortian; textural evidence indicates that it is early and possibly of diagenetic origin.

Early sphalerite occurs as fine grained replacements of the sparry dolomite matrix in the Lisduff Oolite. Later pale yellow sphalerite replaces pyrite along fractures (Plate 59B) and characteristically contains up to 2.92 wt% Cd, 0.20 wt% Hg, 0.12 wt% As, 0.26wt% Ga, and is low in Fe (<1.0 wt% Fe) (Figures 3.41, 3.42). There is no correlation between Fe and Cd in the Durrow sphalerite. The Cd displays sector zoning in the sphalerite crystals (Plate 60). Late, vein and vug filling crystalline sphalerite is present but uncommon. The Cd, Ga and Hg content of these low Fe sphalerites is worthy of note, being much higher than similar sphalerite at Lisheen and Galmoy.

Early pyrite occurs as fine grained disseminations in the matrix dolomite. Later pyrite forms subhedral to euhedral crystals, locally replacing ooids in the Lisduff Oolite (Plate 59). Relict ghost textures are well preserved. Later, coarse pyrites, contain inclusions of dolomite and sphalerite, display evidence of brittle fracture and sphalerite commonly replaces pyrite around these fractures (Plate 59B). However, large euhedral pyrite grains enclose fine grained sphalerite. Pyrite framboids, veins, fracture fills, and stylolites are minor textural forms.

Unlike the massive iron sulphides at Lisheen and Galmoy, the pyrite at Durrow contains low concentrations of As (<0.15 wt%). Co and Ni are generally below detection. An exception is a late vein-hosted pyrite in DUR2 which contains up to 2.13 wt% As (mean = 0.20 wt%), 3.02 wt% Cu (mean = 0.74 wt%), 0.64 wt% Ni (mean = 0.10), and 0.23 wt% Co (mean = 0.07 wt%).

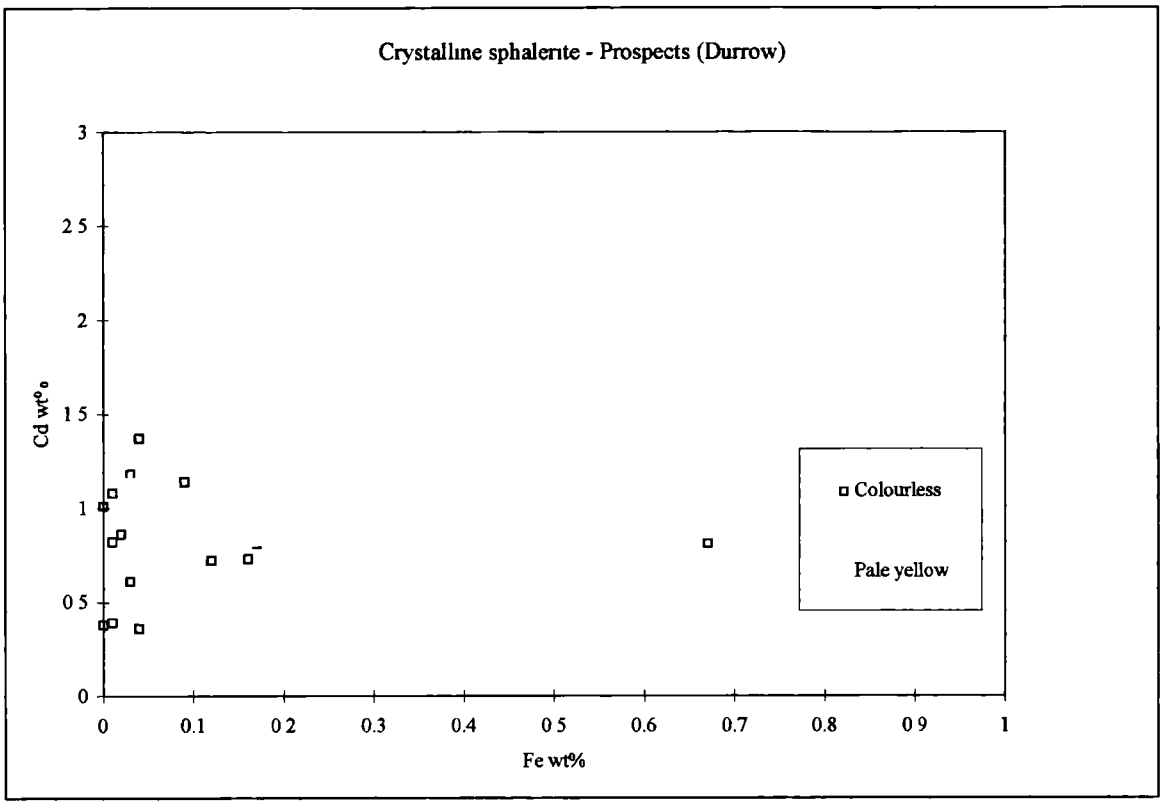


Figure 3.42 Fe wt% (x-axis) v Cd wt% (y-axis) in crystalline, pale coloured sphalerite.

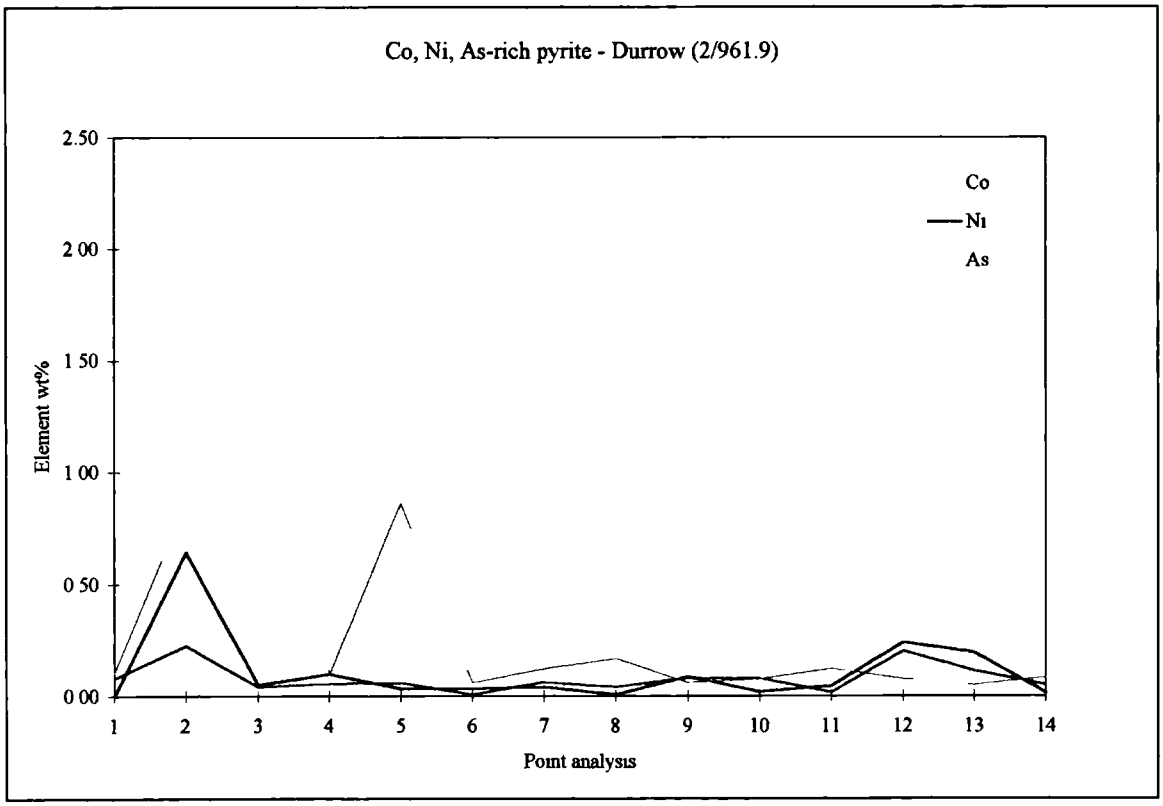


Figure 3.43 Lisduff Oolite hosted, Co, Ni and As-rich pyrite - Durrow (2 961.9).

Co and Ni in this sample (2/961.9) exhibit a positive correlation (r = 0.85) (Figure 3.43). The Co/Ni ratio is <1.0, similar to ore-stage and late pyrite at Lisheen.

A mixed sulphide assemblage of tetrahedrite, chalcopyrite, and pyrite occurs in late dolomite veins. Tetrahedrite occurs mostly as subhedral to anhedral grains in coarse crystalline ferroan dolomite with abundant chalcopyrite and pyrite intergrowths. Minor sphalerite inclusions occur within chalcopyrite. The tetrahedrite contains higher As, Hg, Fe, and lower Zn and Ag concentrations than late tetrahedrite at Galmoy. Chalcopyrite contains up to 0.20 wt% As (mean 0.07 wt%), this is similar to the As content of massive chalcopyrite at Lisheen, also hosted within the Lisduff Oolite Member.

3.4.3a Paragenetic Summary - Durrow

The general characteristics of sulphides at Durrow show general similarities with the late ore-stages at Galmoy and Lisheen. Late stage, cross-cutting Cu-rich veins are minor. Trace element contents however, are distinctive particularly elevated Hg, Cd, and Ga.

A general sequence of deposition is: (1) pre-sulphide carbonate; (2) Early sphalerite and pyrite; (3) pyrite; (4) sphalerite; (5) Late, mixed assemblage of tetrahedrite, chalcopyrite, and pyrite.

Colourless to pale yellow crystalline sphalerites in the Durrow prospect are notably more Cd rich than at Lisheen and Galmoy, but contain much lower Fe concentrations (<1.0 wt%). The sub-Waulsortian hosted sphalerites also contain Ga and Hg concentrations of up to 0.26 and 0.2 wt% respectively. Ga is below detection in all of the sphalerites at Lisheen and Galmoy. Hg has not been analyzed for in the deposit sphalerites, except for a single colloform sphalerite sample in the Derryville zone, Lisheen where concentrations up to 0.21 wt% were detected.

Vein-hosted tetrahedrite at the Durrow prospect contains lower Ag concentrations than tetrahedrite inclusions at the Galmoy deposit - but, higher Ag concentrations (up to 0.29 wt%) than tennantite inclusions at the Lisheen deposit. The tetrahedrite also contains lower Zn than both the tetrahedrite and tennantite at the deposits. However, Hg is much higher at the prospect with up to 1.3 wt%. Hg is largely undetectable in the tetrahedrite and tennantite at the deposits. As concentrations in the tetrahedrite at both prospect and Galmoy are similar (~3 to 5 wt%).

Pyrite at Durrow is As poor, unlike the arsenian iron sulphides at Lisheen and Galmoy with concentrations generally less than 0.15 wt%. Late vein-hosted pyrite is the exception with As concentrations as high as 2.13 wt%.

3.5 DISCUSSION

Mineralization in the Lisheen and Galmoy deposits and Durrow prospect exhibit a complex variety of ore textures which are best interpreted principally in terms of open-space infill and replacement. Much of the ore-stage mineralization at Lisheen and Galmoy formed by replacement of the D2 and $D1_R$ dolomite in the BMB zones.

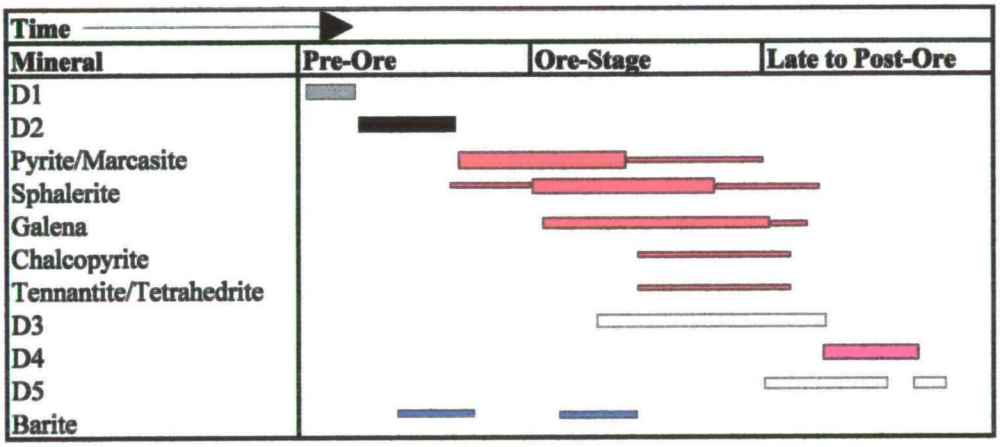


Figure 3.44 Summarized paragenesis for Lisheen and Galmoy mineralization.

The D2 dolomite is the most susceptible to mineralization, probably due to its high permeability and porosity which allowed easy access by hydrothermal fluids. Initial sulphide precipitation occurred in pore space; further mineralization led to the complete replacement of both matrix and clasts. Relict clasts can be detected in the massive ores at Lisheen. The latest stages of ore deposition in the deposits occurred as fracture-fill type mineralization in the fully lithified Waulsortian. Layered sulphides are rarely observed and are probably the result of replacement of a laminated precursor or are infillings of geopetal cavities by fine grained sulphides such as observed at Navan (Anderson *et al.* in press).

The ore paragenesis at Lisheen is broadly similar to Galmoy (Figure 3.44). Pre-ore stage massive iron sulphides overlie the orebodies at both Lisheen and Galmoy and have also been described at Tynagh (Derry *et al.*, 1965; Boast *et al.*, 1981a). This iron sulphide event was followed by the precipitation of a mixed sulphide assemblage, including ore-stage sphalerite and galena. Clear

changes in the mineral assemblage at Lisheen and Galmoy in time and space indicate significant changes in the property of the mineralizing fluid(s).

The sphalerite at Lisheen and Galmoy is generally Fe poor, the values obtained from electron microprobe analysis are normally less than 3 wt% Fe. At Durrow the Fe values are even lower and normally less than 1 wt% Fe. Late crystalline sphalerites at Lisheen occasionally contain up to 5 wt% Fe. The Fe concentration does generally correlate with colour in crystalline sphalerites at Lisheen. However, Craig and Vaughan (1981) state that the correlation of Fe with colour banding is supposedly unreliable if the Fe content is less than 5%. At Galmoy where the Fe concentrations are lower, correlation is less conclusive.

Cd concentrations in crystalline sphalerites at Lisheen are variable, but generally higher in the brown coloured sphalerites, whilst at Galmoy Cd concentrations are much lower in both brown and yellow sphalerites. Crystalline 'honeyblende' sphalerite occurs at Keel, where it forms a matrix replacement of the quartz-pebble conglomerate adjacent to fault zones. This crystalline sphalerite is Cd rich, as are nearly all the sphalerite varieties, commonly containing >1.0 wt% Cd (Slowey, 1986; Slowey et al., 1995). Lattice-bound Hg has also been identified in the sphalerites (Watling, 1972). Cd-rich zoning and concentrations of up to 0.2 wt% Hg are a feature of the pale to colourless sphalerites at Durrow.

Colloform textures are often cited as evidence for initial formation by colloidal deposition. Roedder (1968) has suggested that many colloform sphalerites in Pb-Zn ores grew as tiny fibrous crystals projecting into a supersaturated ore fluid. However, textures such as this can also be produced by recrystallization of colloidal precipitates (Wilkinson, pers. comm., 1998). Either way, the texture is indicative of rapid precipitation from a highly supersaturated solution. Small sphalerite spheroids (0.015mm) at Lisheen probably acted as nuclei for subsequent overgrowths resulting in abundant zoned colloform textures. These main ore-stage textures reflect the depositional process. Rapid supersaturation due to fluid mixing is one of the most effective ways of forming these classic textures. Dendritic textures in galena at the Navan deposit are interpreted as indicating rapid precipitation caused by the mixing of a metal bearing fluid with a second fluid at the site of ore deposition (Anderson, 1990; Anderson *et al.*, in press). The presence of two fluids was proposed initially by Anderson and MacQueen (1982). Dendritic forms of galena have also been observed in the Lisheen deposit. Conversely, late to post ore-stage sulphides are mostly euhedral crystal forms interpreted as having precipitated at low degrees of supersaturation. Therefore, fluid mixing was probably not occurring during the waning stages of mineralization. This suggests that the process of deposition may have evolved with time from a two fluid system

to a one fluid dominant system. Precipitation from a single fluid may be caused either by a drop in solubility (due to temperature drop, fluid-rock interactions *etc.*) if the ore-forming metal was transported together with reduced sulphur (Sverjensky, 1981). Anderson (1975) pointed out that if the metals and reduced sulphur were transported together in a single fluid, the fluid must be very acidic.

The zoning in colloform sphalerite is due to major and minor element substitutions, in particular Fe. Other substitutions include Hg, Cd, Ag, Tl, In, As, Cu, and Mn. Cd, Fe and As appear to be the most significant element substitutions in the colloform sphalerites at Lisheen. Zoning can also be attributed to changes in the rate of growth (Ramdohr, 1980). Each zone represents some change in the ore fluid or the conditions of precipitation, evident from the inclusion of minor dolomite and pyrite rich zones in colloform sphalerite at Lisheen. According to Andrew (1991) the colour variations in colloform sphalerite reflect admixed colloidal carbonate or argillaceous matter as opposed to the lattice Fe content. From this study the Fe content appears to control the colour of the crystalline sphalerites, however the Fe-rich brown sphalerites are nearly always hosted in the argillaceous sub-Waulsortian. Most sphalerites observed in Lower Palaeozoic hosted veins are brown to dark brown. Sphalerite at the Navan deposit exhibits colour variations similar to those observed in the Lisheen deposit.

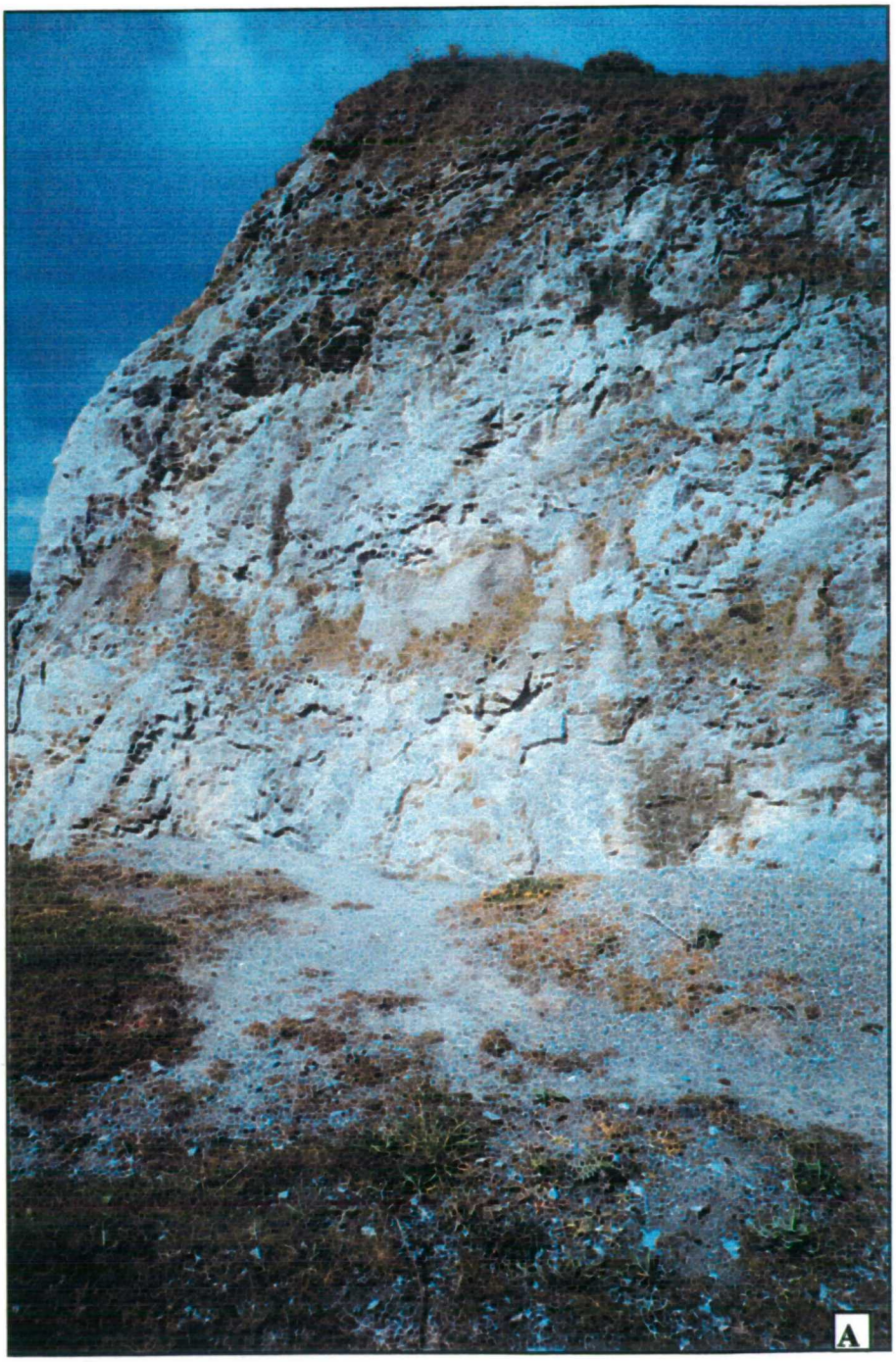
The high Ag values in colloform sphalerites suggests that Ag possibly occurs in solid solution in sphalerite and not in galena. The principal source of silver, however, is the tennantite-tetrahedrite minerals. The occurrence of tennantite inclusions within galena, probably indicates a relatively high temperature of formation. Commonly, Cu-, As-rich and Ag-, Sb-poor tennantite-tetrahedrites are deposited proximal to the hydrothermal source of the mineralizing fluids (e.g Goodell and Petersen, 1974; Wu and Petersen, 1977; Hackbarth and Petersen, 1984). Galena is capable of solid solution with a variety of silver minerals at high temperature but at moderate temperatures can not accommodate more than 0.1 wt% silver in its structure (Ramdohr, 1980). Argentiferous galena is homogenous when there is less than 0.1 wt% Ag; more than 0.1 wt% and silver minerals occur as minute blebs 1-2 microns in diameter and oriented in the planes of the galena, precipitated from solid solution during cooling (Ramdohr, 1980). One of the chief Ag minerals formed in this way is tetrahedrite (Nissen and Hoyt, 1915; Roedder, 1968).

Arsenic variations in the iron sulphides at Lisheen and Galmoy probably reflect colloform growth banding in both pyrite and marcasite. Concentrations >2.5 wt% commonly occur proximal to the major fault zones at Lisheen. Low Co/Ni values obviate a volcanogenic origin for the pyrite ore, normally characterized by higher Co/Ni values (>5 but more often >10) than those attained by

sedimentary or hydrothermal pyrites (Bralia *et al.*, 1979). Recrystallization textures in pyrite are present, but not common.

The proposed occurrence of Bornite in the Lisheen deposit (pers. comm., Hitzman 1996) has not been substantiated during detailed ore microscopy of samples in this study. However, it has been identified in hand specimen.

Plate 1.



A. Feltrim Quarry, Co. Dublin: A Waulsortian mudmound with high depositional dips.

Plate 2.

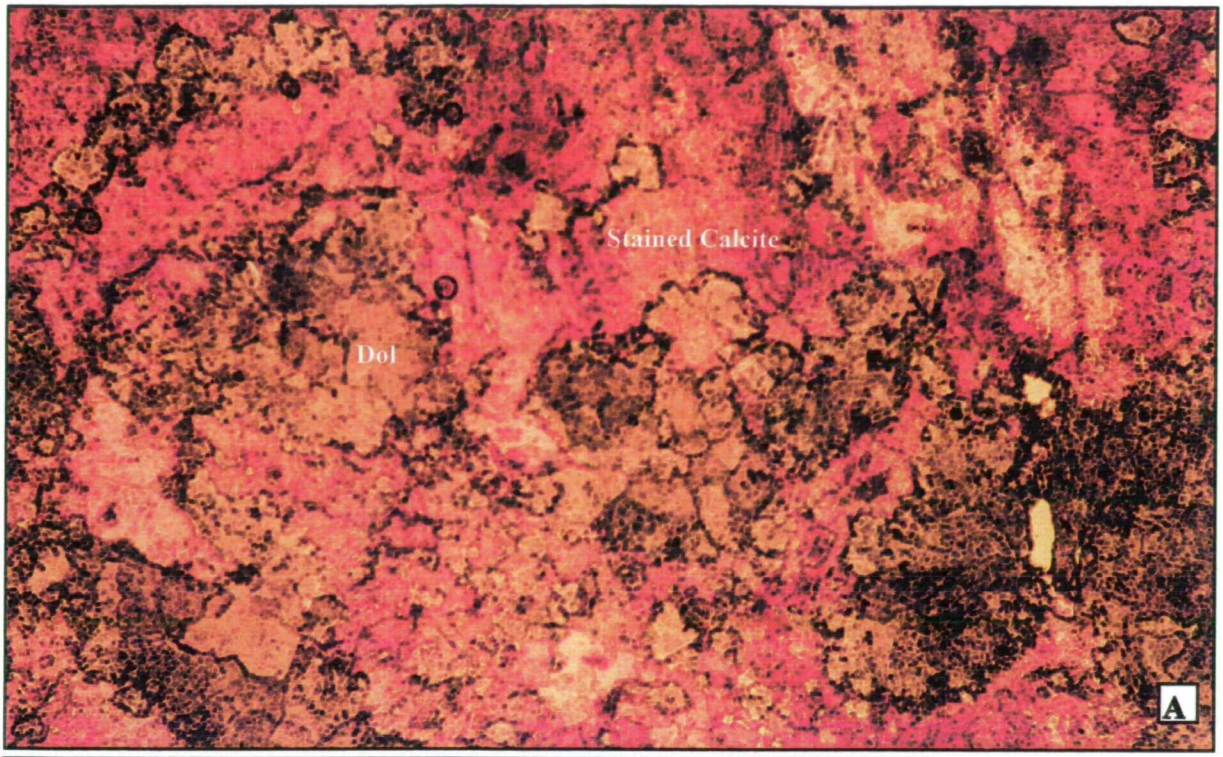


A. Lisheen: Partially dolomitized (Dol)Waulsortian Limestone (Lst) with abundant bryozoa.

B. Lisheen: Regional fine crystalline grey dolomite ($D1_R$) and regional coarse crystalline white dolomite cement ($D1_C$) from outside the deposit area. Well developed stromatactis structures.



Plate 3.



A. Lisheen, 2447-8/34.2: Transverse section of Bryozoa skeletal microstructure in partially dolomitized (Dol) Waulsortian Limestone, close to the regional dolomite front. Dolomitized areas are not stained.
B. The original high Mg calcite precursor is preferentially dolomitized with good fabric retention.

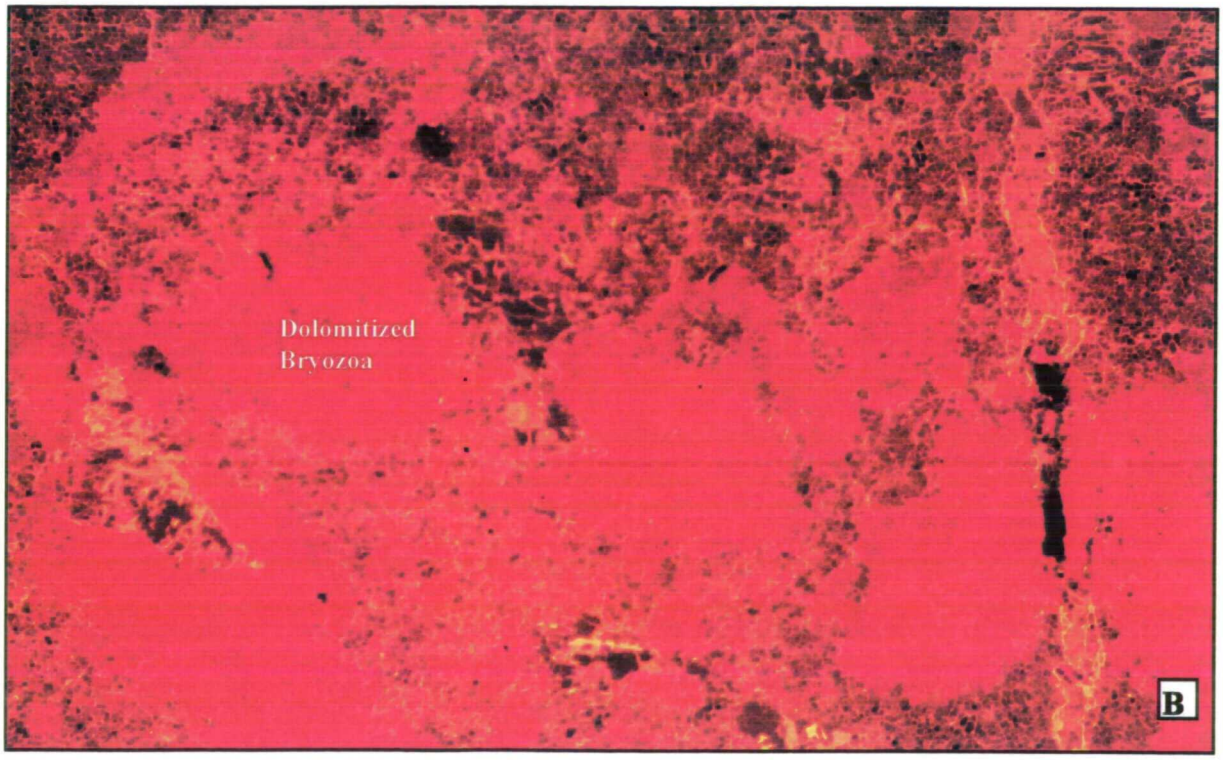
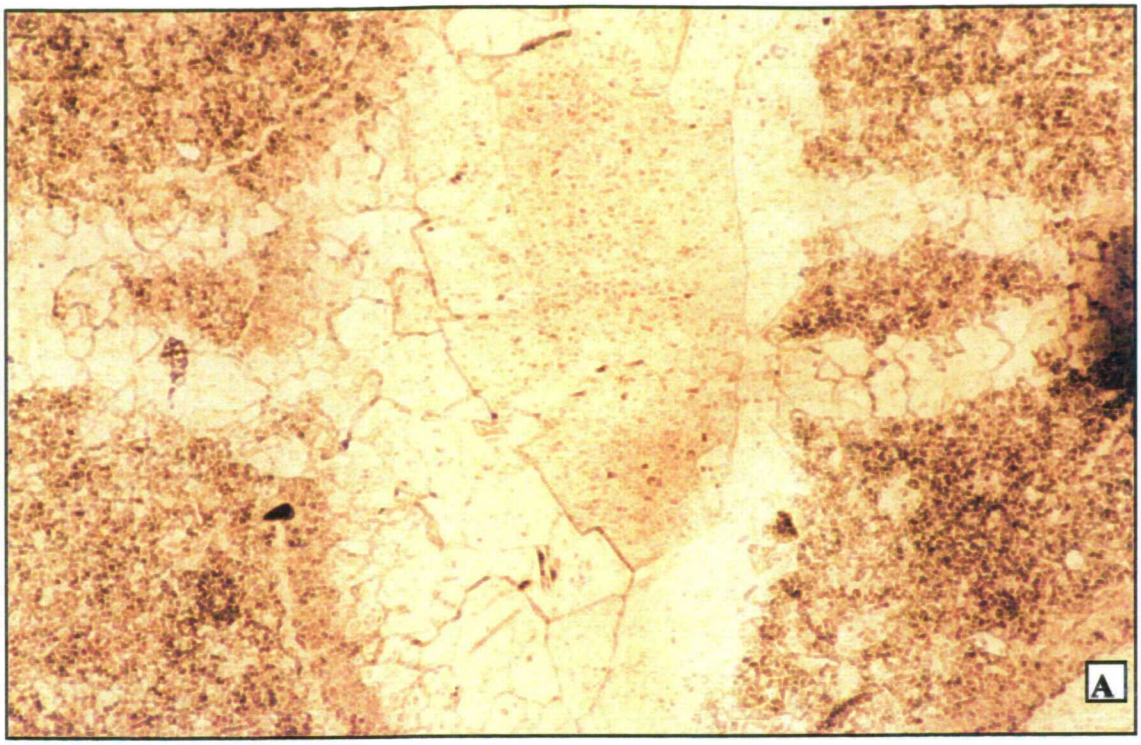


Plate 3a.



A. Lisheen, 121/200.5: Photomicrograph (TrL) of $D1_C$ overgrowing/partly replacing diagenetic calcite.

B. A late Fe-rich calcite vein changes mineralogy as it cross-cuts different precursors. Long axis of photomicrograph = 1250μm.

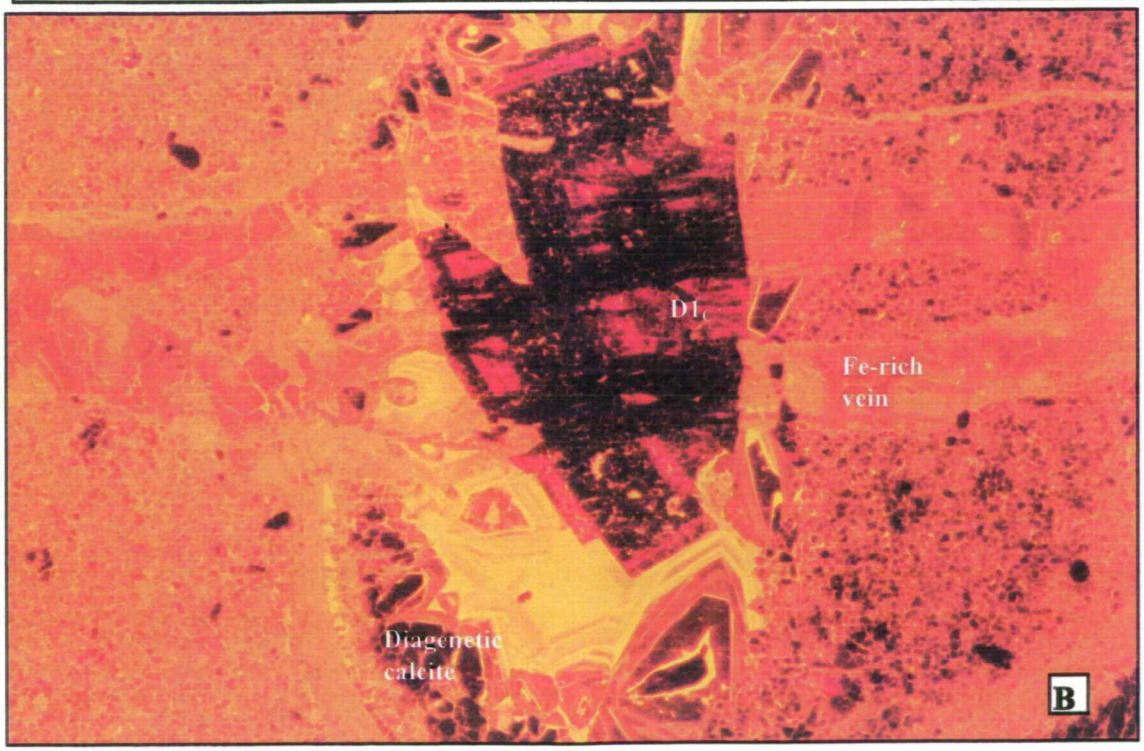
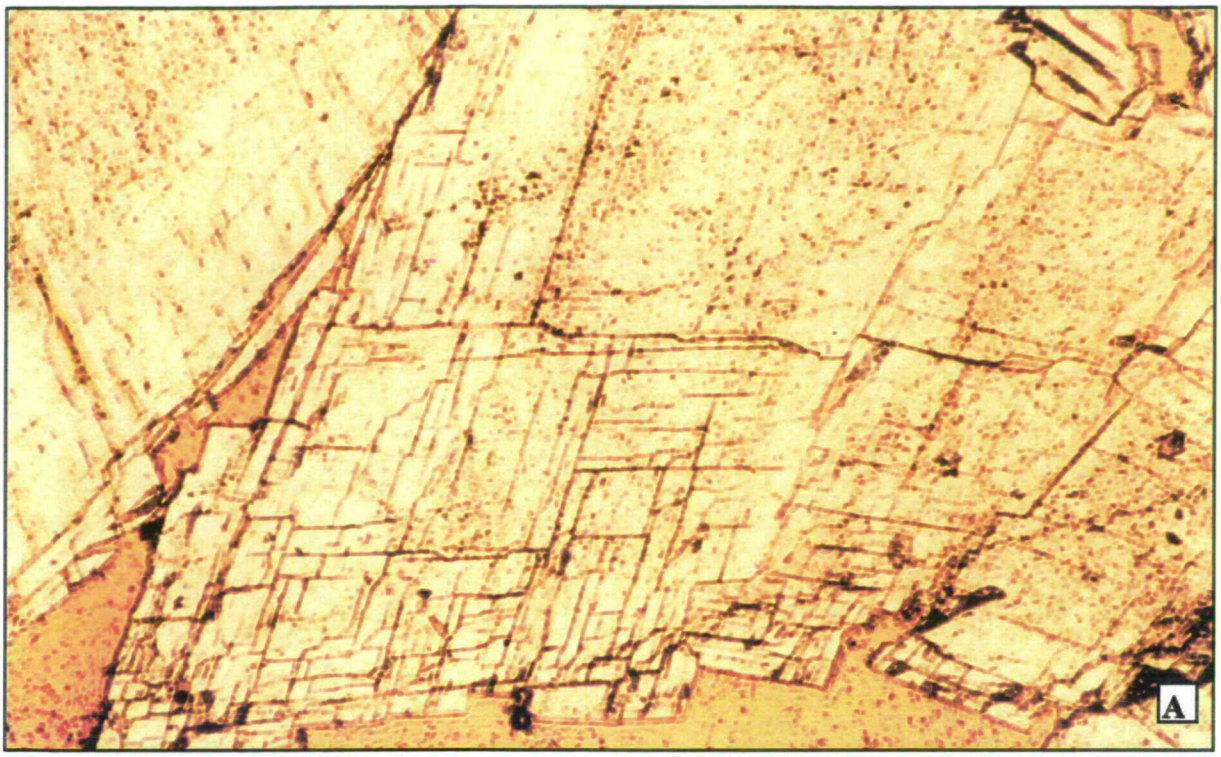


Plate 4.



A. Lisheen, 2447-8/13.3: Photomicrograph (TrL) of regional coarse crystalline white dolomite cement $D1_C$.

B. $D1_C$ dolomite exhibits a dull to moderate red, weakly zoned luminescence. Zoning is primarily due to variations in Fe. Long axis = 1250μm.

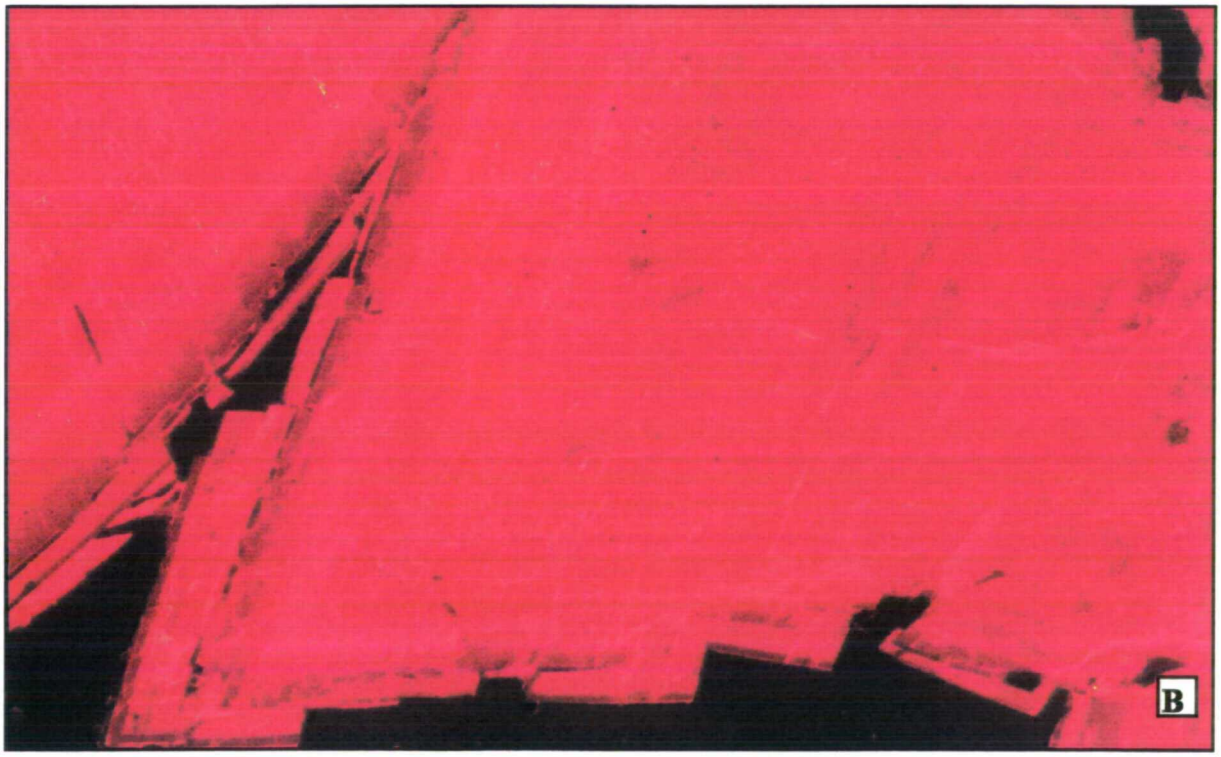
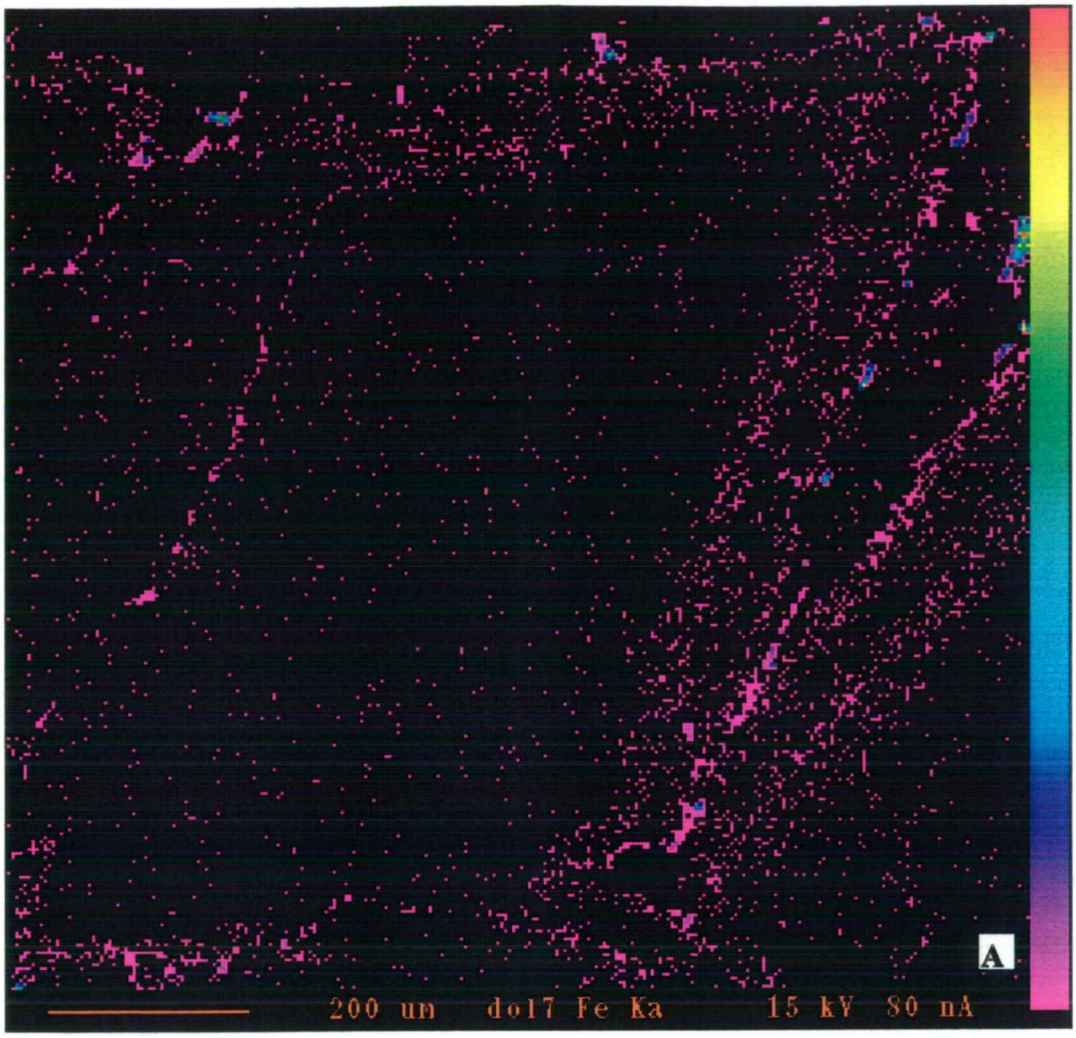
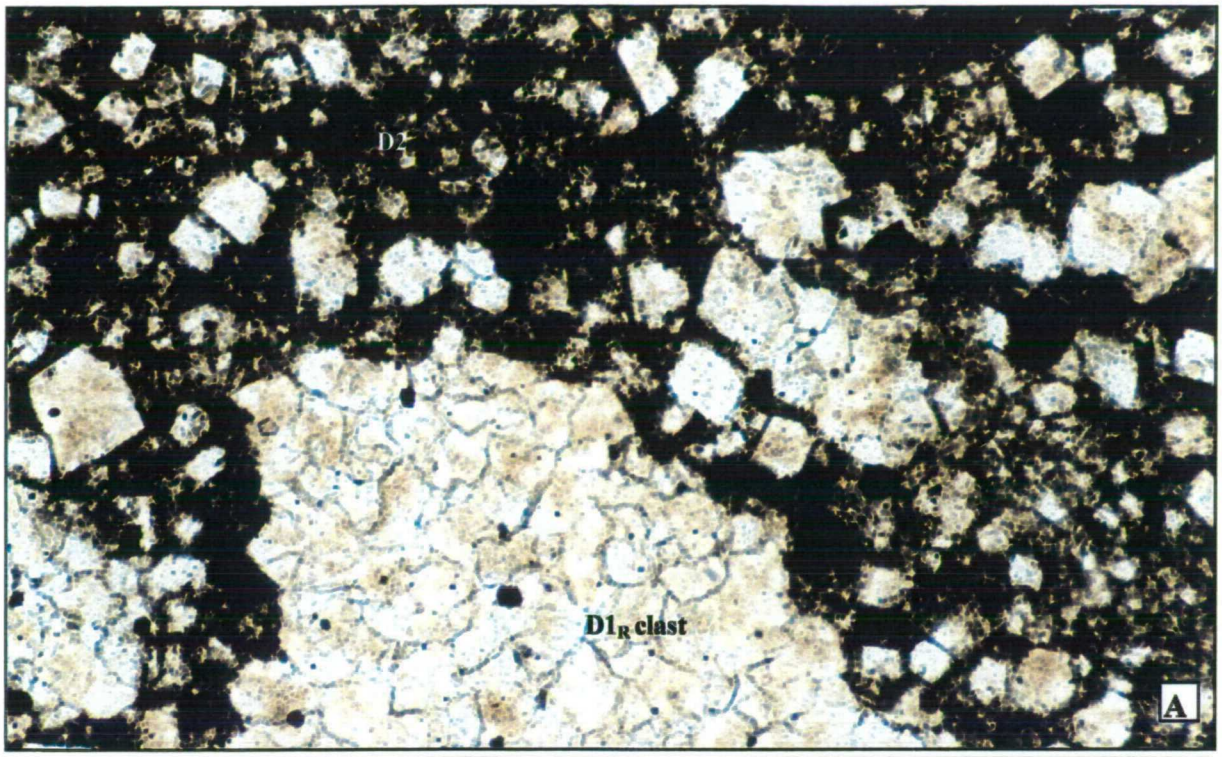


Plate 5.



A. Lisheen, 2447-8/13.3: X-ray distribution map of the element Fe in $D1_C$ dolomite.

Plate 6.



A. Galmoy, MG99/100.6: Photomicrograph (TrL) of D2 dolomite matrix and $D1_R$ dolomite clasts.
B. The bright orange-red luminescent matrix (D2) post-dates and partially replaces dull red, zoned (D2) dolomite rhombs. The $D1_R$ dolomite clast exhibits a moderate, red-orange luminescence. Long axis = 1250μm.

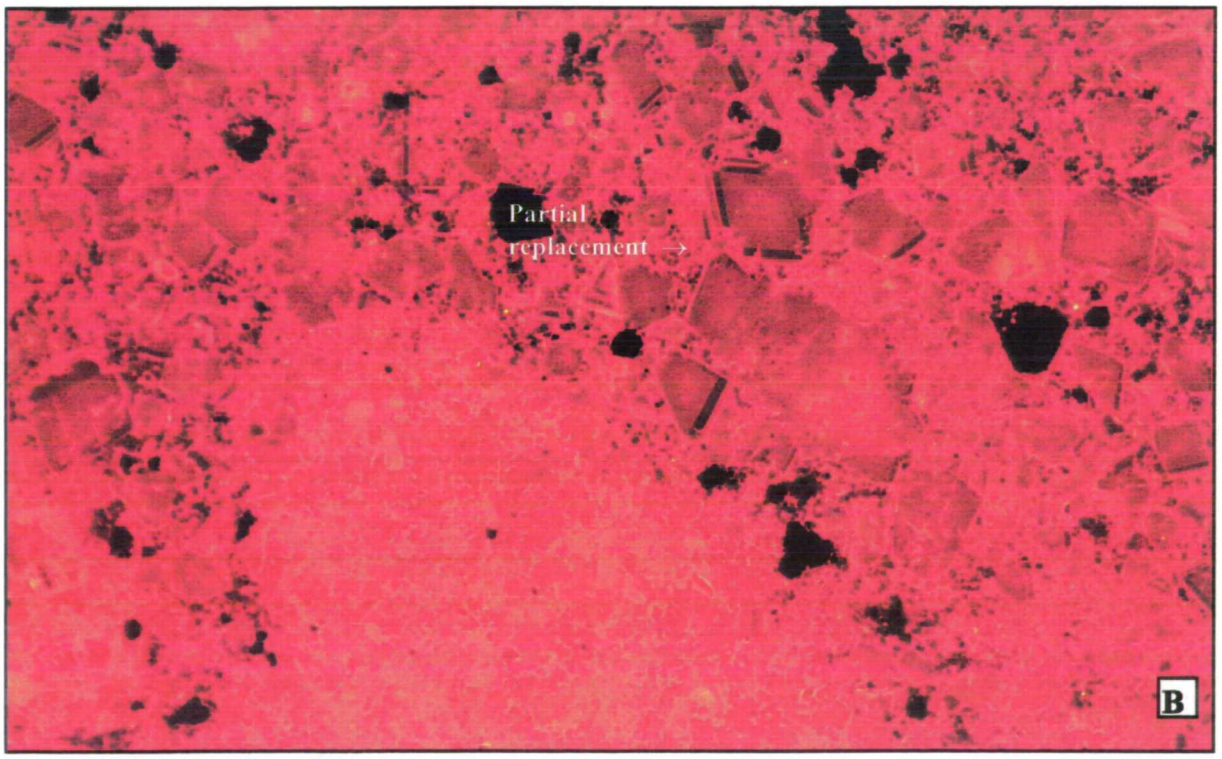
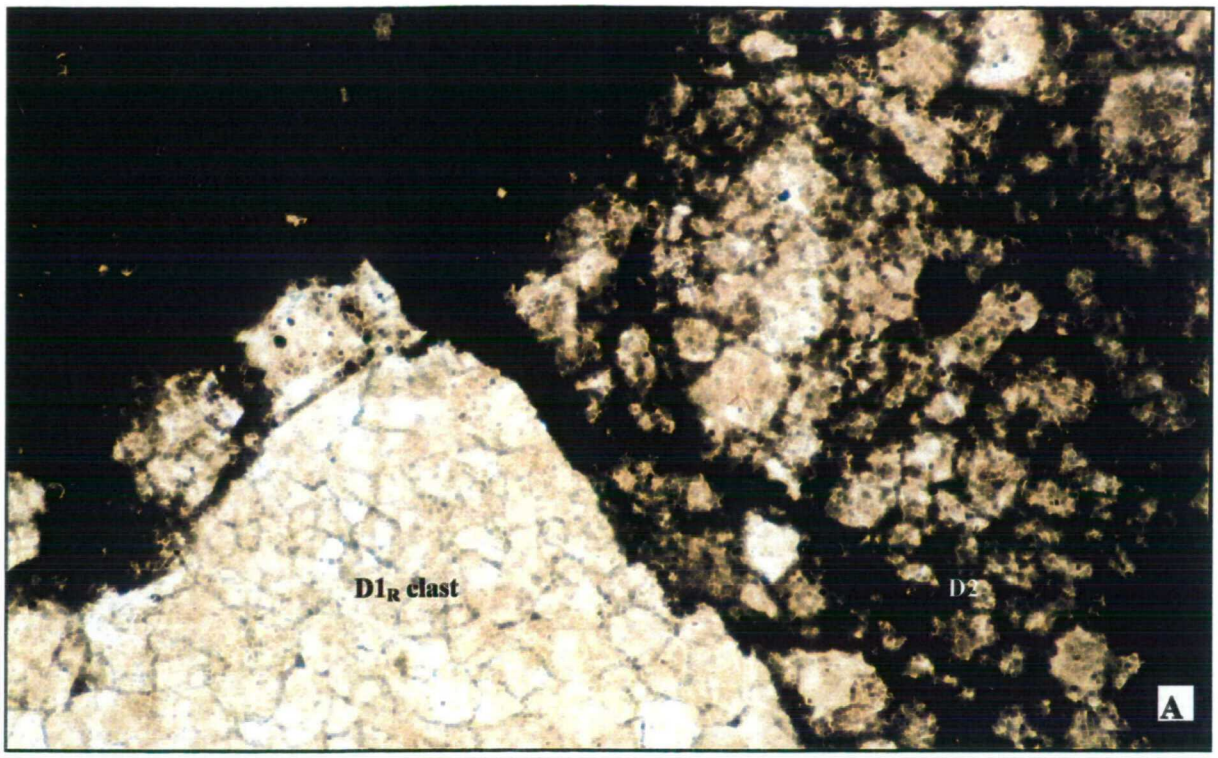


Plate 7.



A. Galmoy, MG63/97.2. Photomicrograph (TrL) of D2 dolomite matrix and $D1_R$ dolomite clast.
B. D2 dolomite exhibits a bright to moderate, orange-red luminescence. D2 dolomite microveinlets cross-cut $D1_R$ dolomite clasts, which exhibit a dull red, homogeneous luminescence. Long axis = 1250μm.

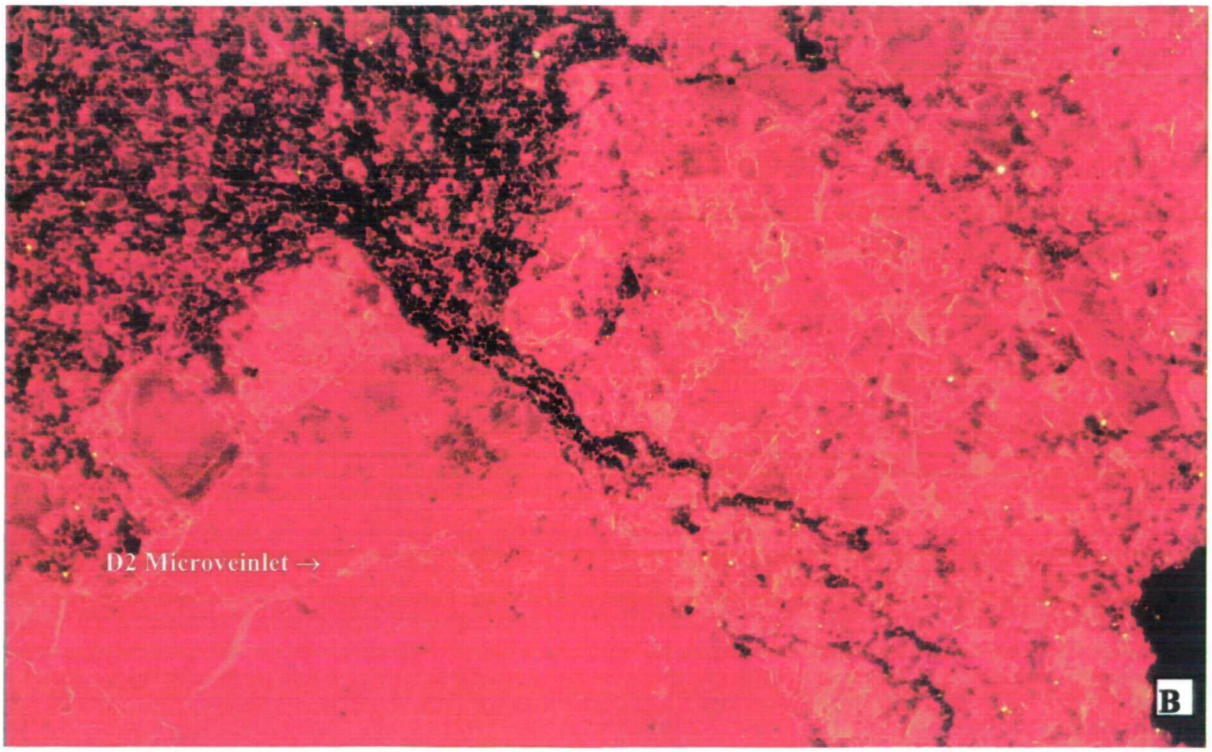
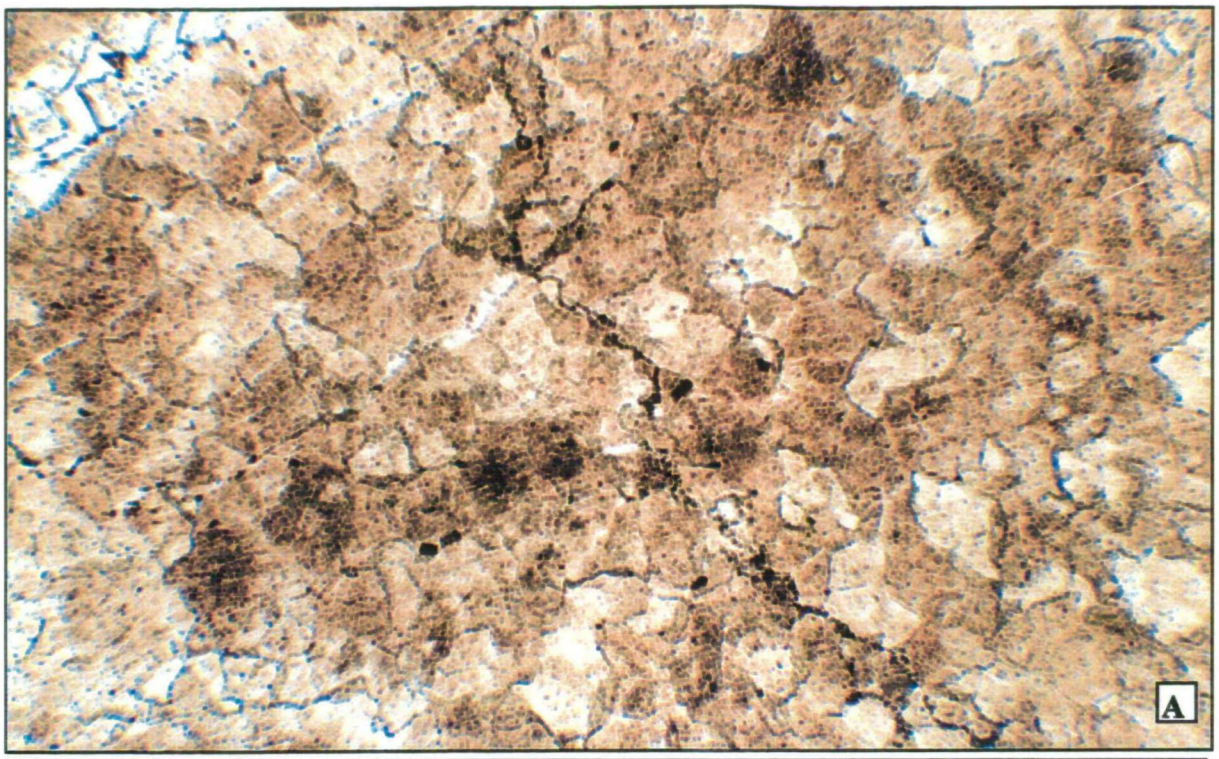


Plate 8.



A. Galmoy, 3312-2/238.5: Photomicrograph (TrL) of regional fine crystalline dolomite $D1_R$.

B. $D1_R$ dolomite exhibits a dull red, non-uniform luminescence. A bright red, luminescent microveinlet cross-cuts the $D1_R$ dolomite. Long axis = 3000μm.

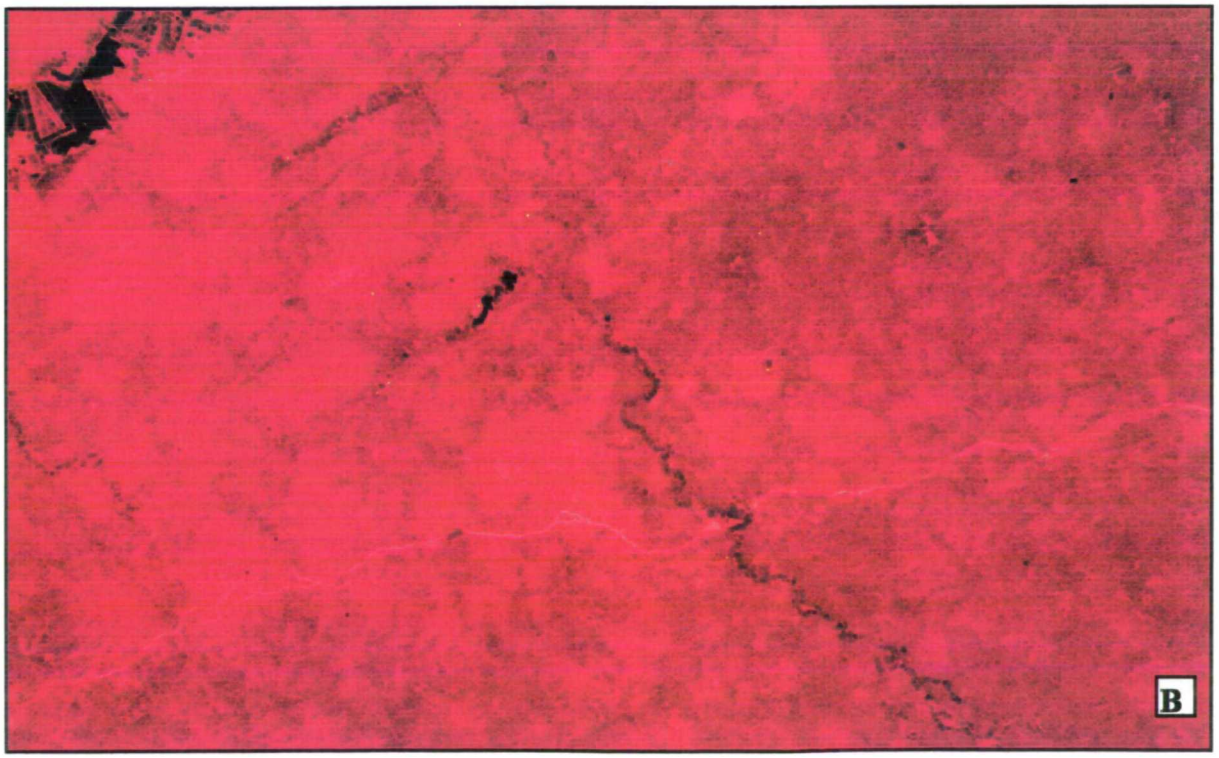


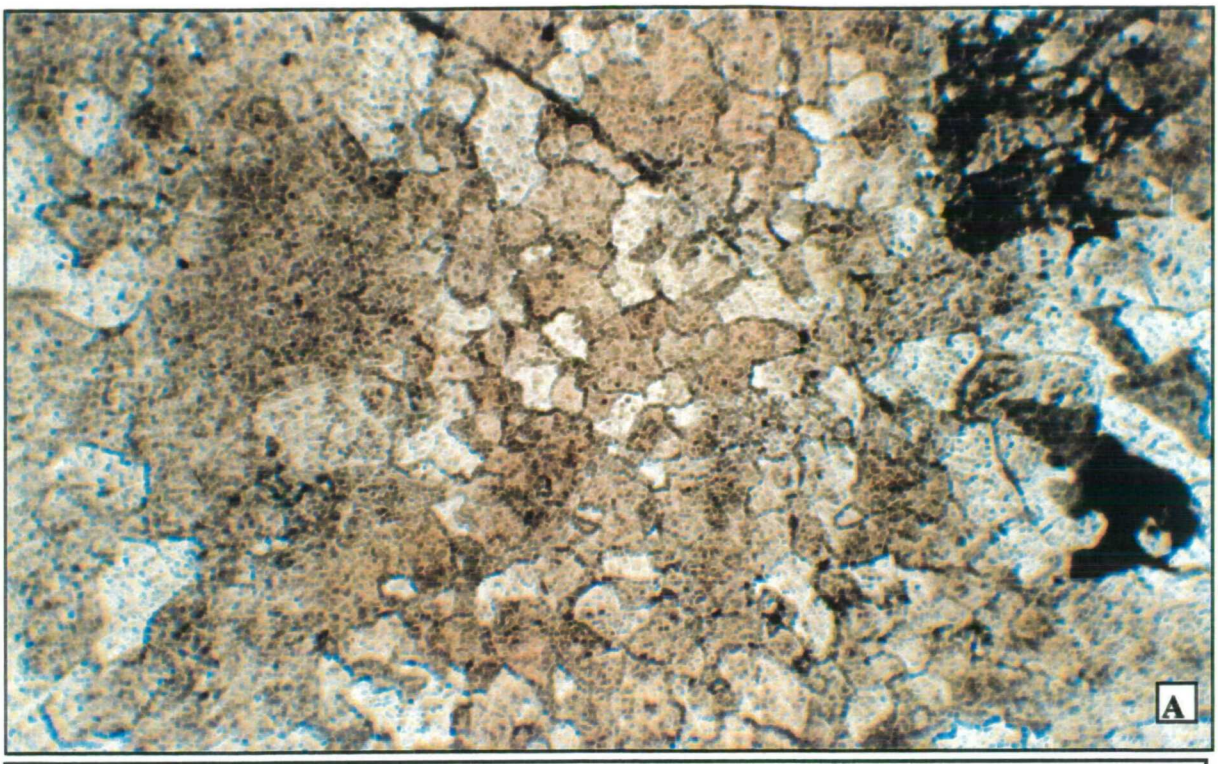
Plate 9.



A. Galmoy, K orebody: Fine crystalline sphalerite and minor galena replace regional coarse white dolomite cement ($D1_C$). Stromatactis cavities are preserved in places.
B. Galmoy, K orebody: White matrix breccia dolomite (D3) overgrown by minor pink dolomite (D4). Crystalline dolomite matrix contains rounded mineralized clasts.



Plate 10.



A. Holycross, HC15/200.8: Photomicrograph (TrL) of a fine dark grey crystalline dolomite clast ($D1_R$).

B. The clast exhibits a moderate red-orange, non-uniform luminescence. The clast is hosted by a non-luminescent matrix dolomite, which clearly post-dates the clast. Long axis = 3000μm.



Plate 11.



A. Rathdowney East: Medium grey, regional fine crystalline grey dolomite ($D1_R$) and poorly developed coarse white dolomite cement ($D1_C$). Moderate stromatactis development.
B. Durrow: Medium to dark grey dolomite with, laminated coarse crystalline white dolomite - 'Zebra texture'.



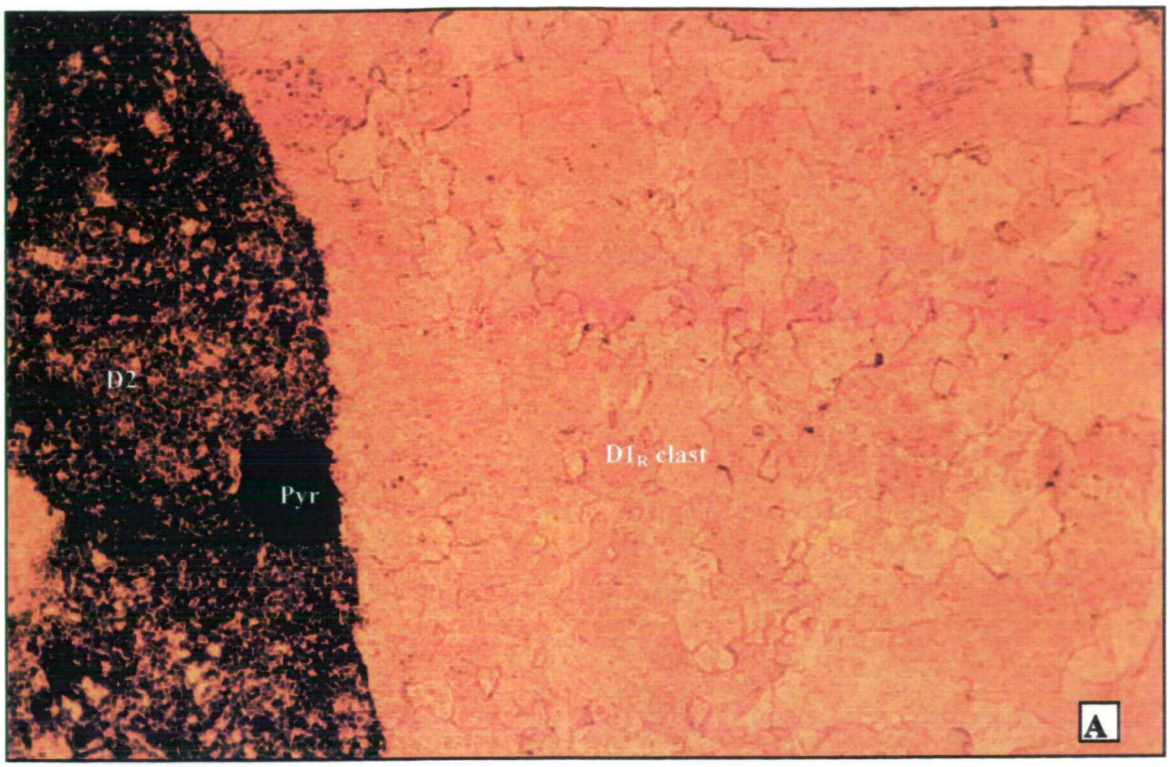
Plate 12.



A. Lisheen: Well developed black matrix breccia dolomite (D2) with large angular clasts of $D1_R$ dolomite. Disseminated pyrite in D2 dolomite matrix.
B. Lisheen: Well developed white matrix breccia dolomite (D3) with angular to sub-rounded clasts of $D1_R$ dolomite. Clasts have dark fine crystalline dolomite 'tops'.



Plate 13.



A. Lisheen, 262/153.6: Photomicrograph (TrL) of D2 dolomite, and a $D1_R$ dolomite clast.
B. The D2 dolomite exhibits a bright to moderate, orange-red, non-uniform luminescence. D2 microveinlets fracture and post-date the $D1_R$ dolomite clast, which exhibits a dull red luminescence. Long axis = 1500μm.

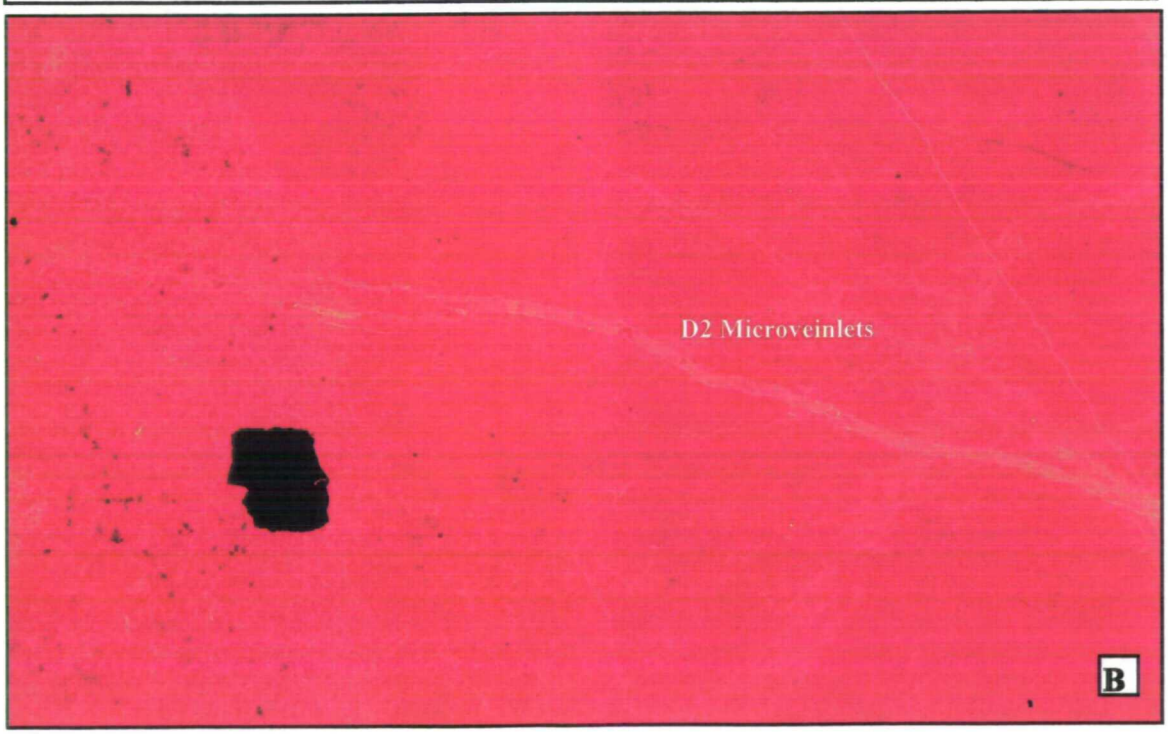
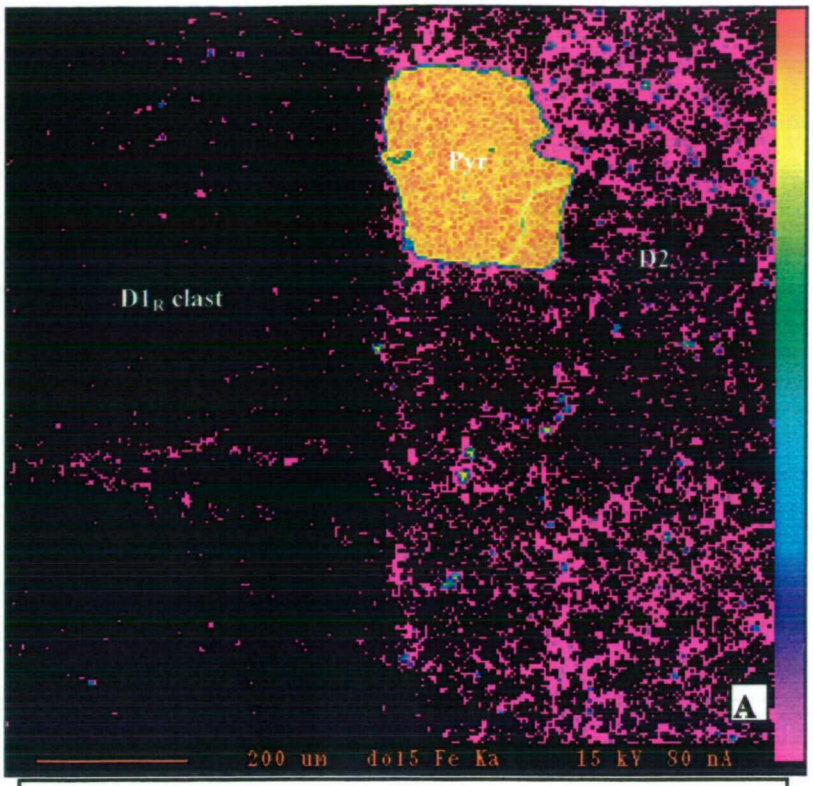


Plate 14.



A. Lisheen, 262/153.6: X-ray distribution map of the element Fe in $D1_R$ and D2 dolomite.
B. Lisheen, 262/153.6: X-ray distribution map of the element Mn in $D1_R$ and D2 dolomite.

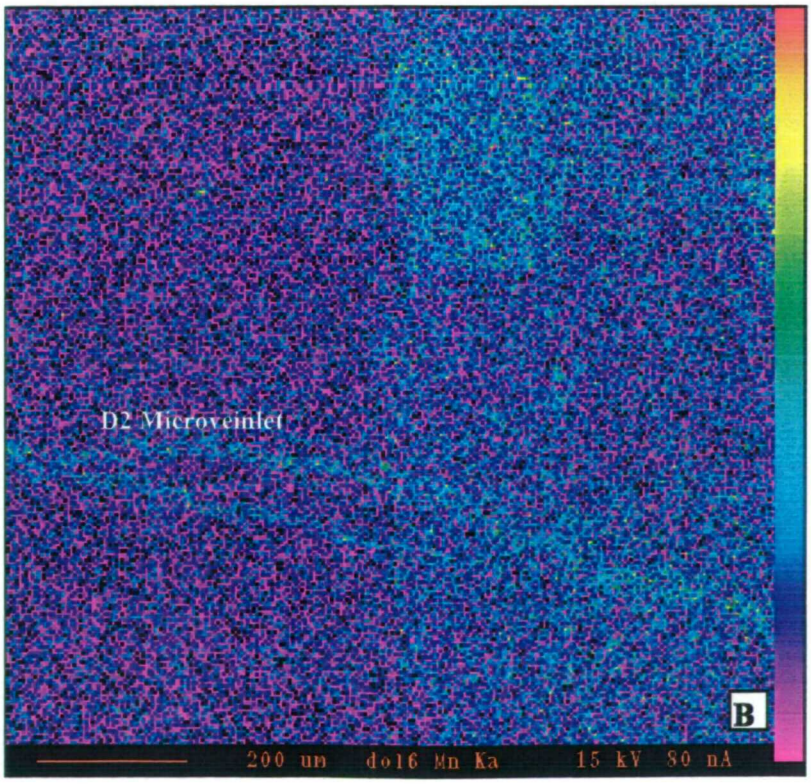
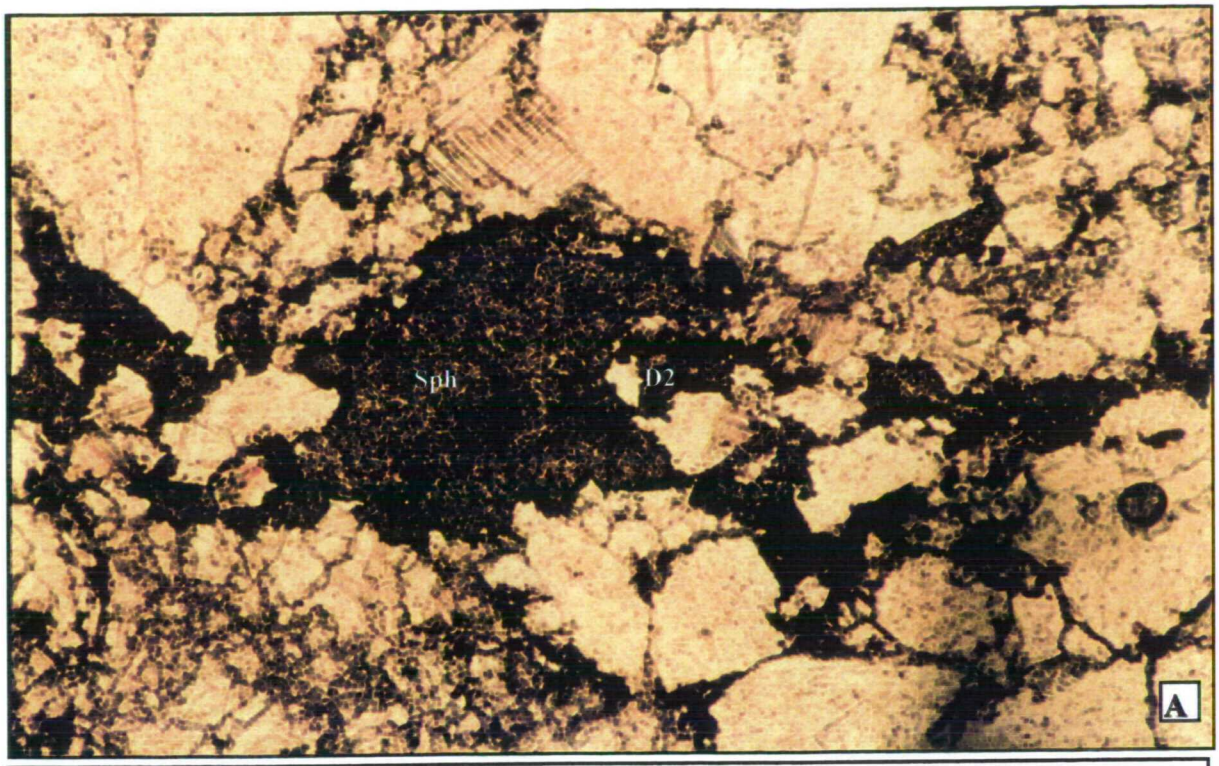


Plate 15.



A. Lisheen, 121/180.5: Photomicrograph (TrL) of sphalerite replacing D2 dolomite.

B. D2 dolomite exhibits bright to moderate orange-red, non-uniform luminescence. Sphalerite exhibits non to dull, yellow luminescence. Long axis = 2500μm.

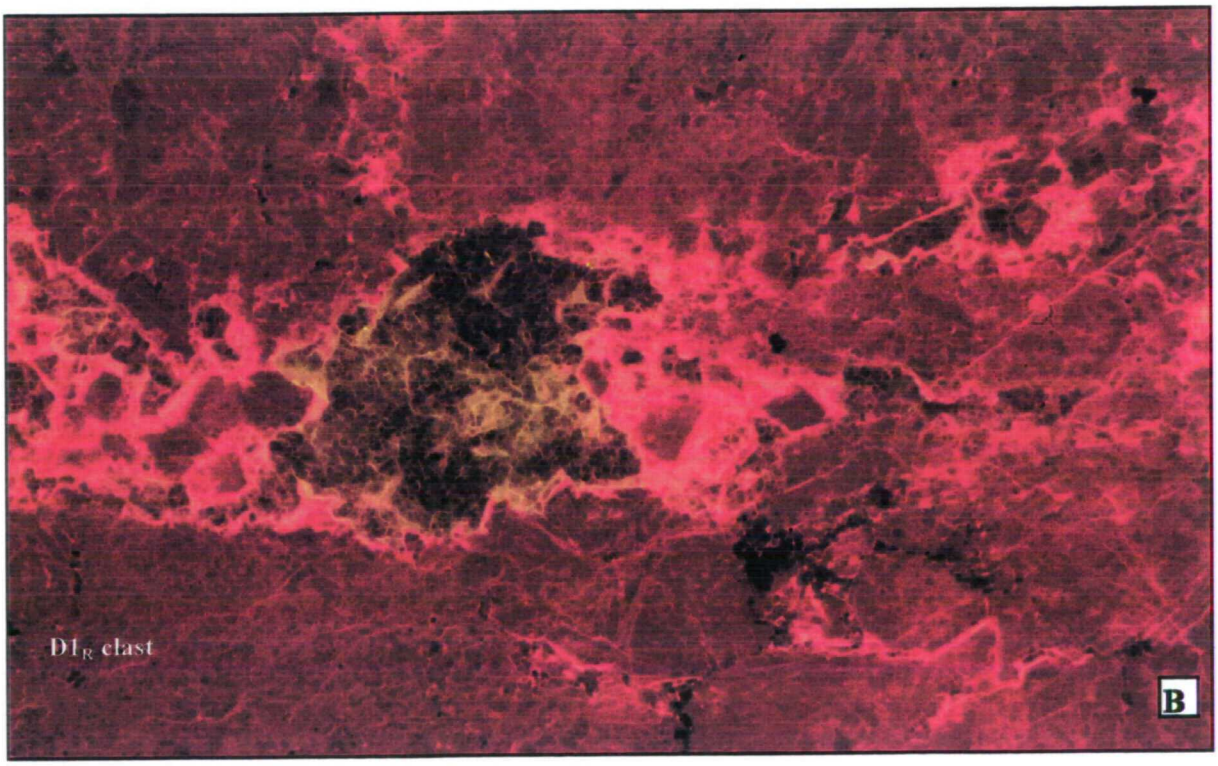
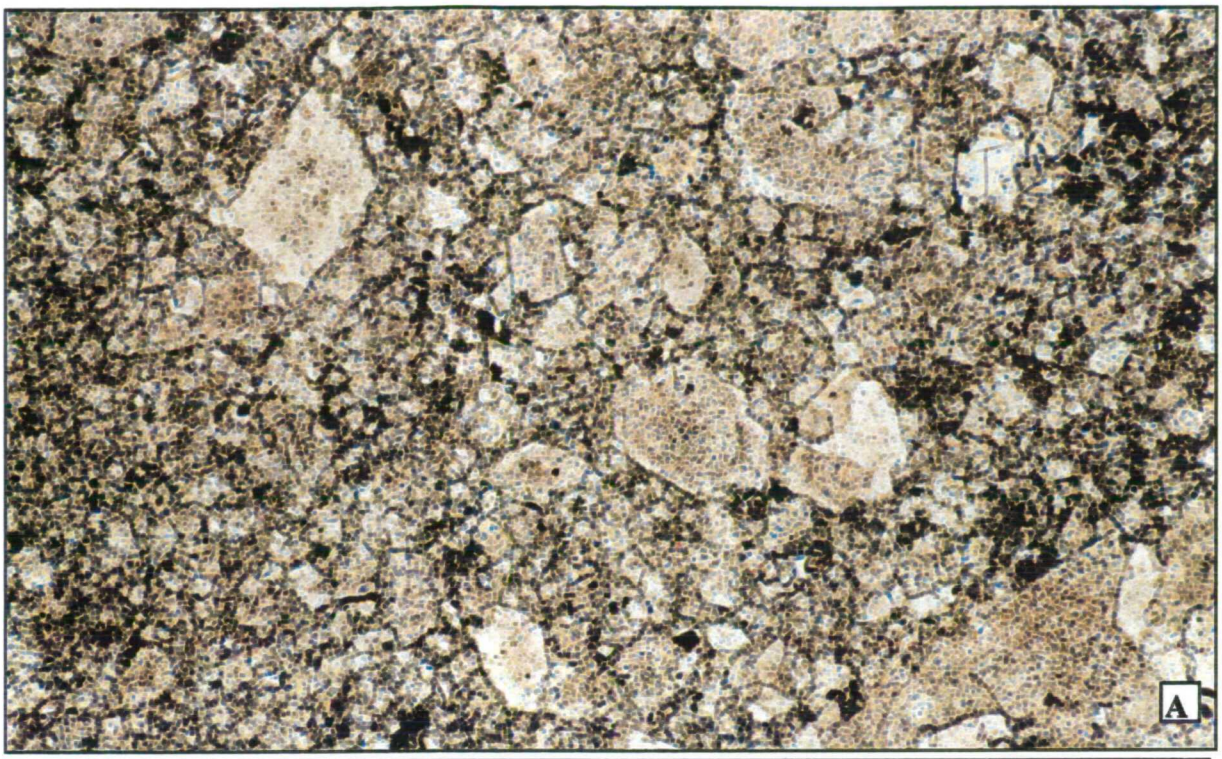


Plate 16.



A. Lisheen, 262/159.1: Photomicrograph (TrL) of D2 dolomite, which displays variable crystal sizes (30-250μm).
B. D2 dolomite exhibits variable, bright to moderate orange-red luminescence. Long axis = 1250μm.

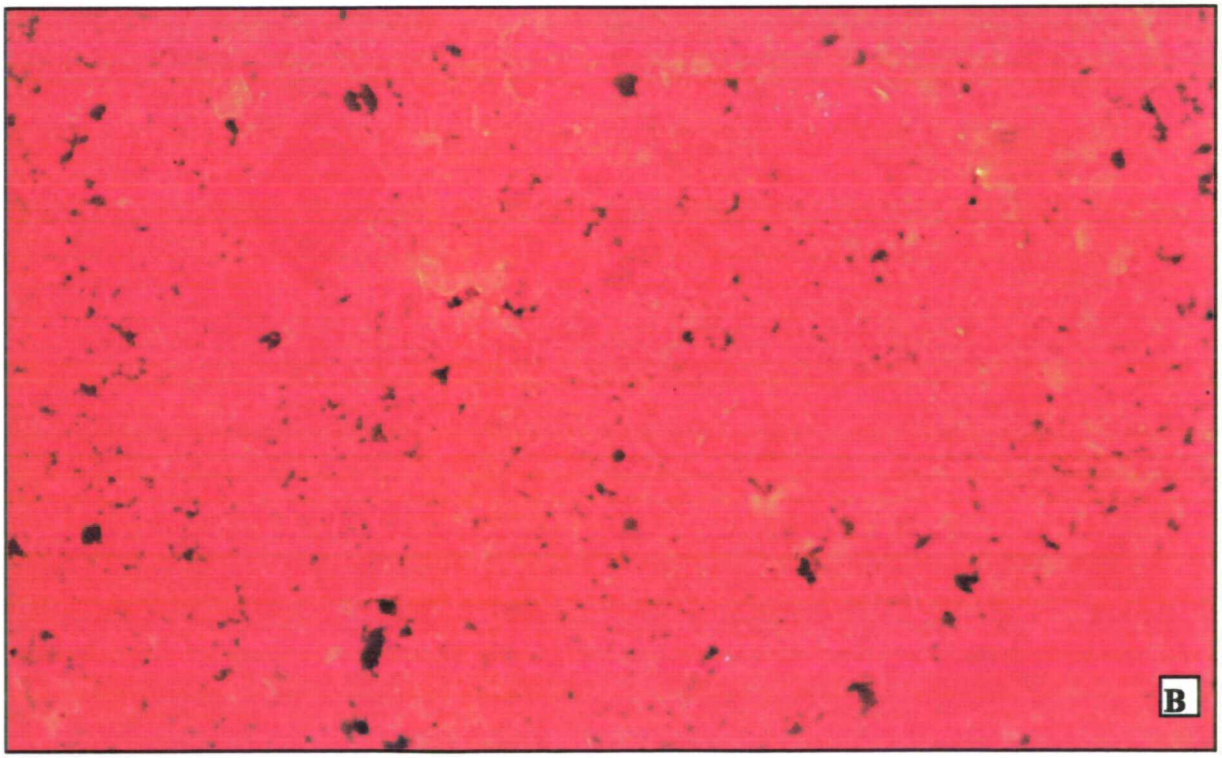
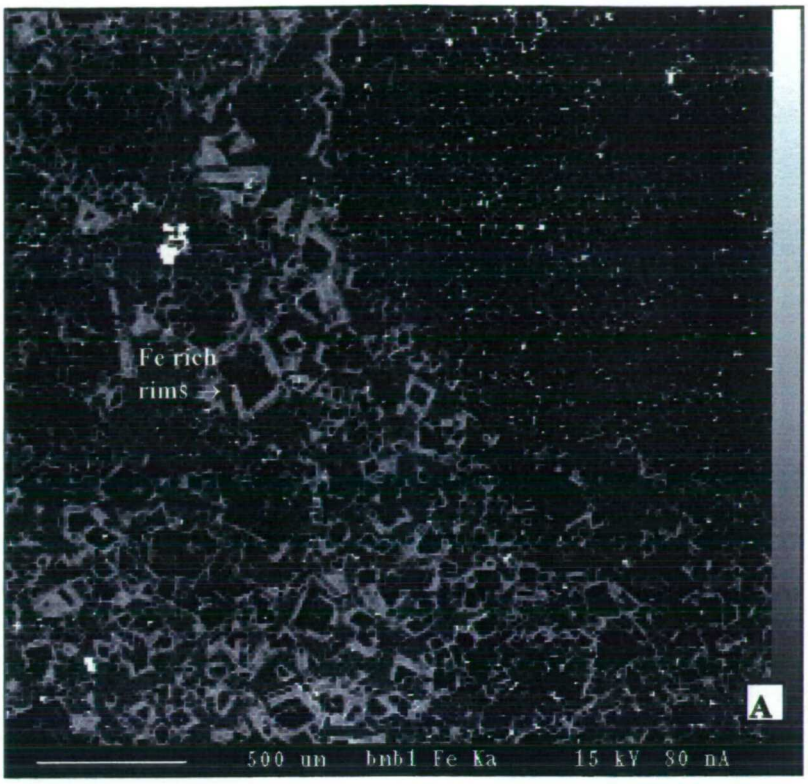


Plate 17.



A. Lisheen, 121/194.0: X-ray distribution map of the element Fe in D2 dolomite.
B. Lisheen, 121/194.0: X-ray distribution map of the element Mn in D2 dolomite.

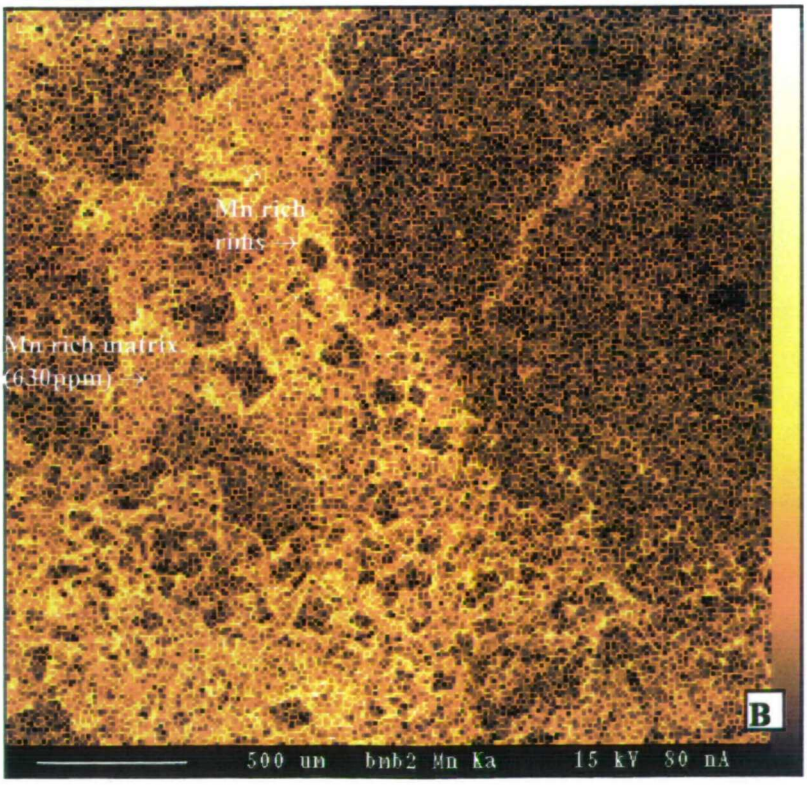
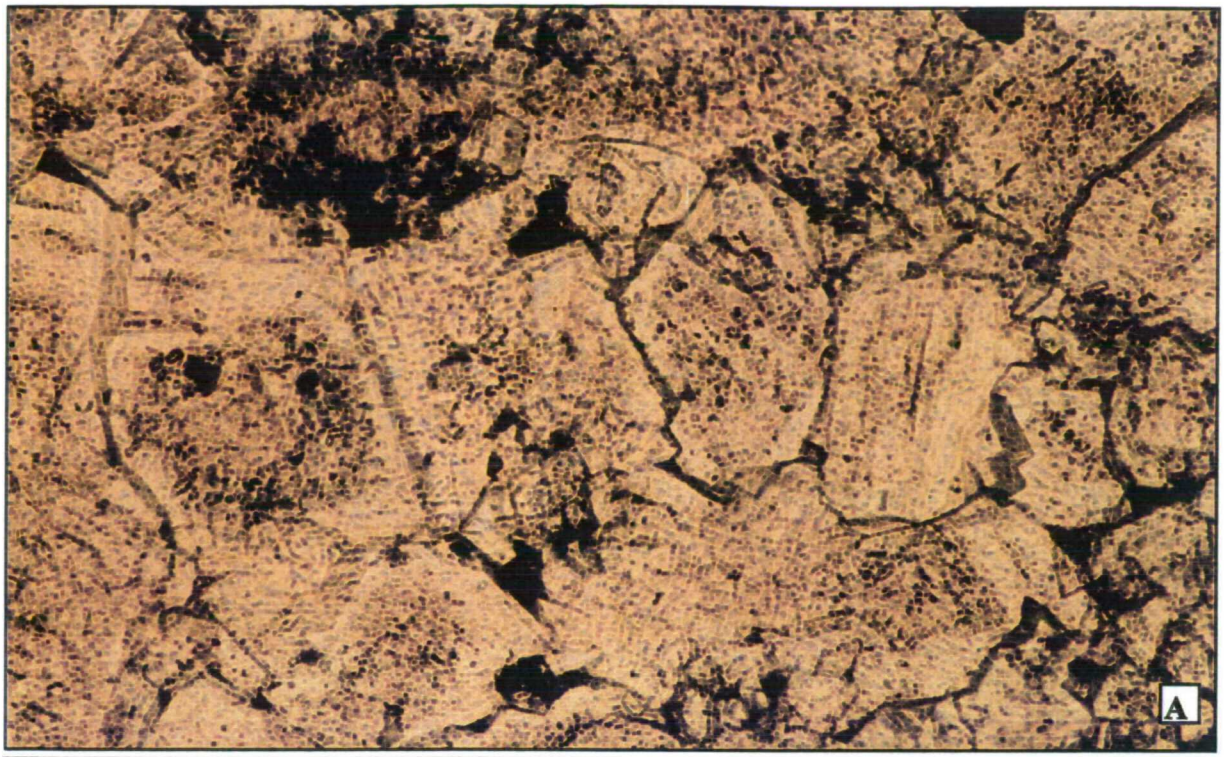


Plate 18.



A. Lisheen, 121/180.5: Photomicrograph (TrL) of D2 dolomite crystals (250-300μm in size).
B. Crystals display in detail mottled cores exhibiting dull to moderate red luminescence, overgrown by planar, oscillatory zoned dolomite with late, bright red luminescent infilling dolomite. Long axis = 1250μm.

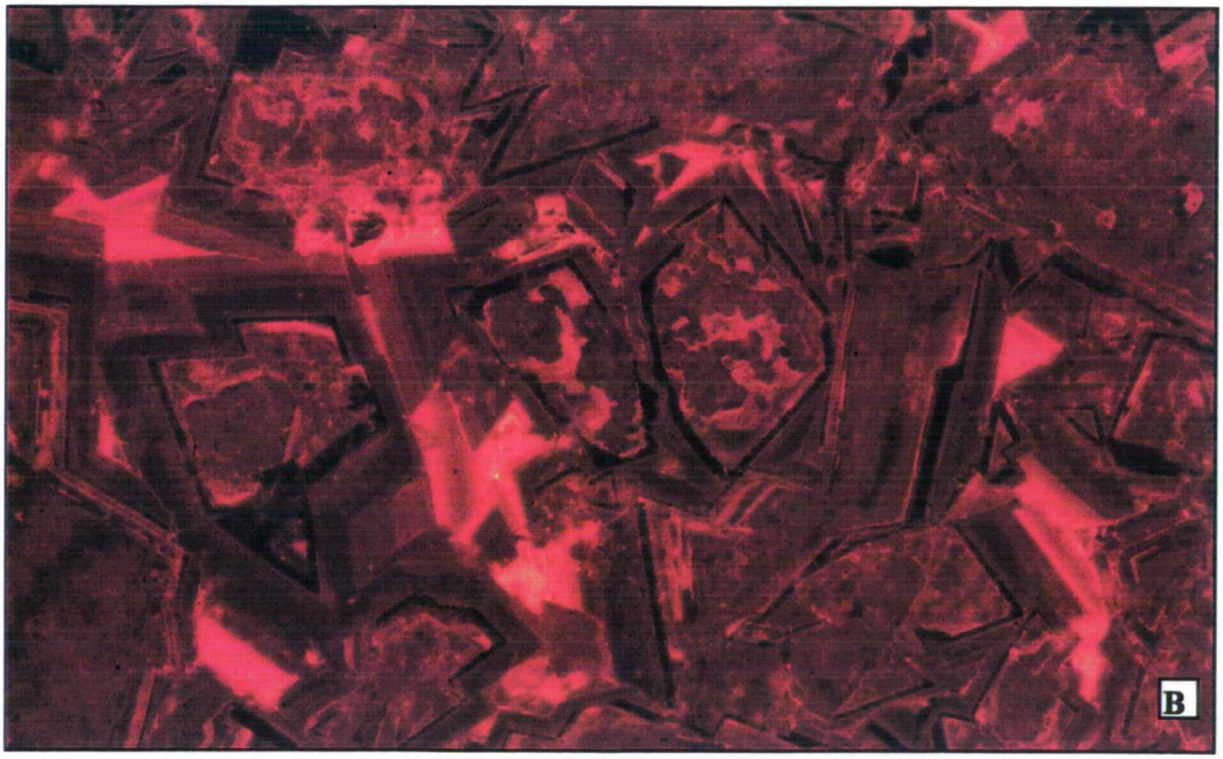
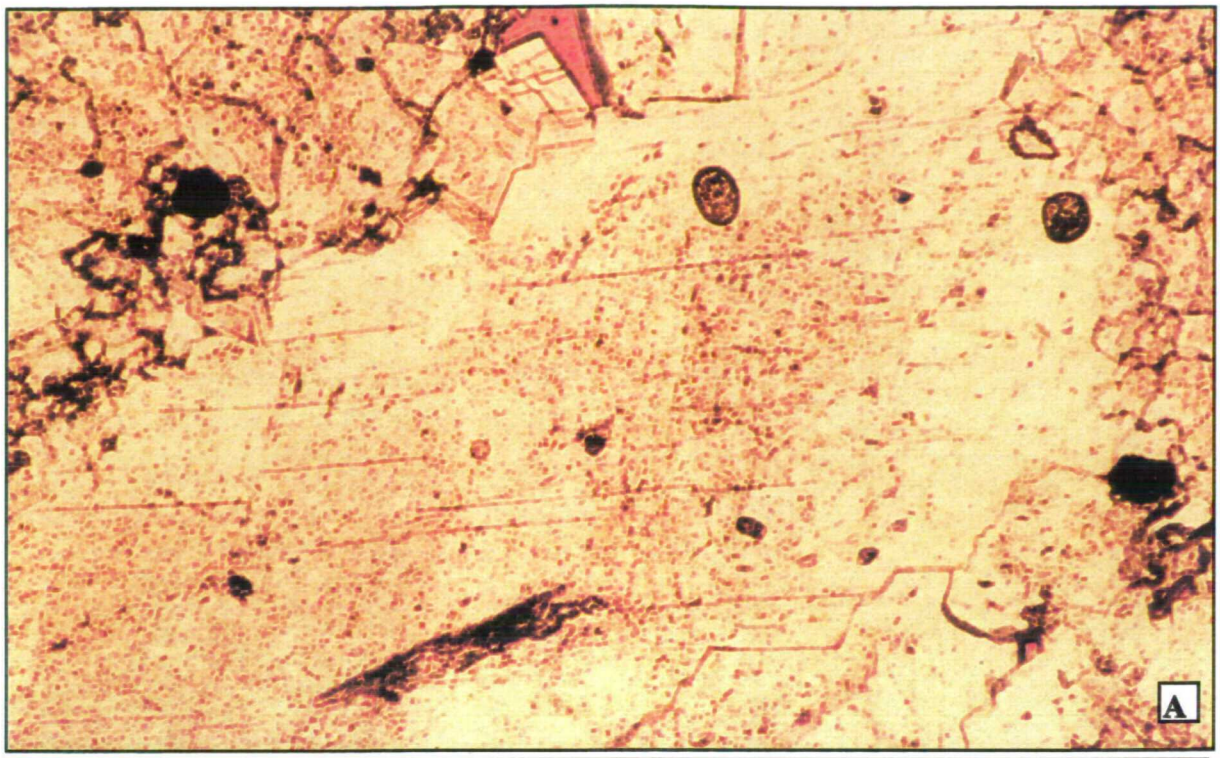


Plate 19.



A. Lisheen, 121/162.1: Photomicrograph (TrL) of D3 dolomite crystal, displaying cloudy cores and clear outer rims.

B. D3 dolomite exhibits 4 distinct alternating moderate to bright luminescent stages; B, C, D and E. Cement stage D is characterized by a pronounced yellow zone in stage D. Long axis = 1250µm.

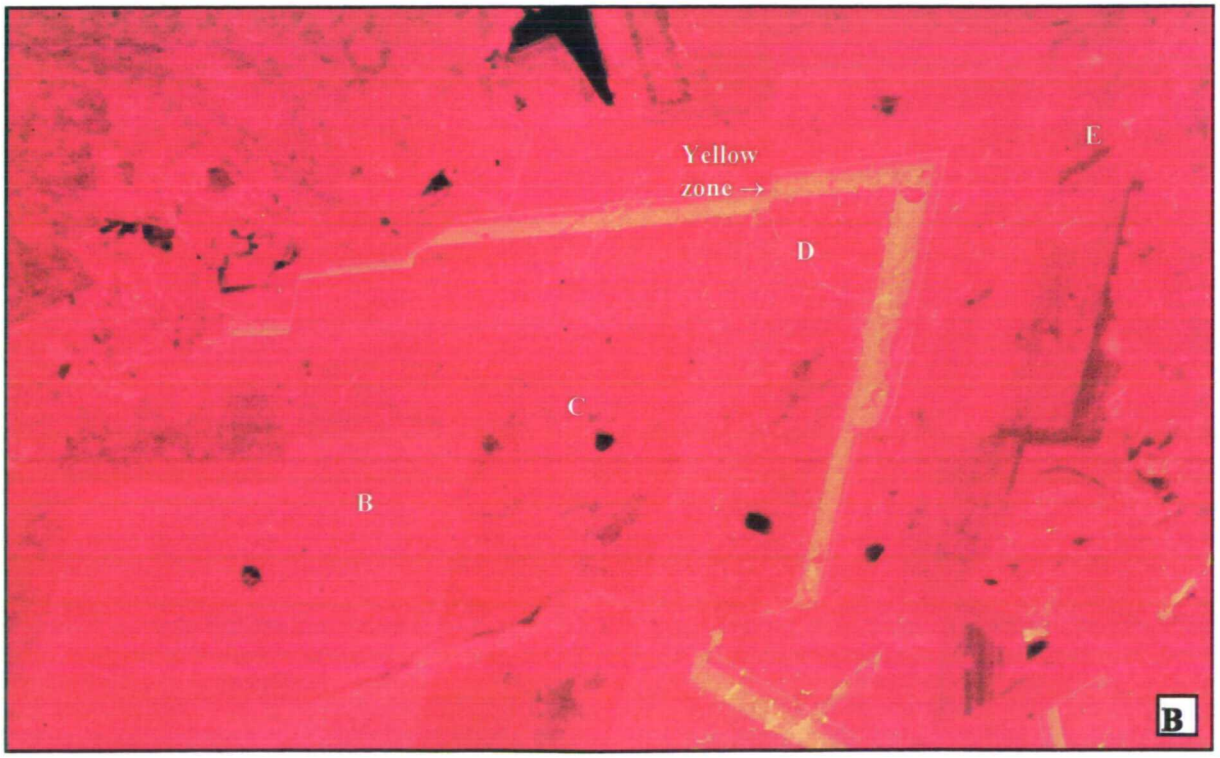
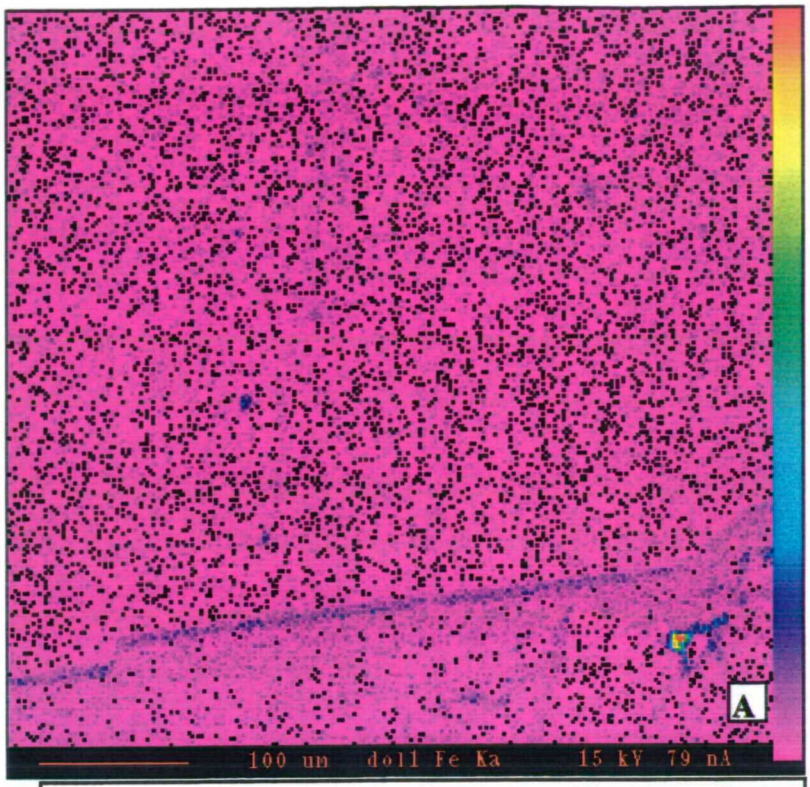


Plate 20.



A. Lisheen, 121/162.1: X-ray distribution of the element Fe in D3 dolomite.
B. Lisheen, 121/162.1: X-ray distribution of the element Mn in D3 dolomite.

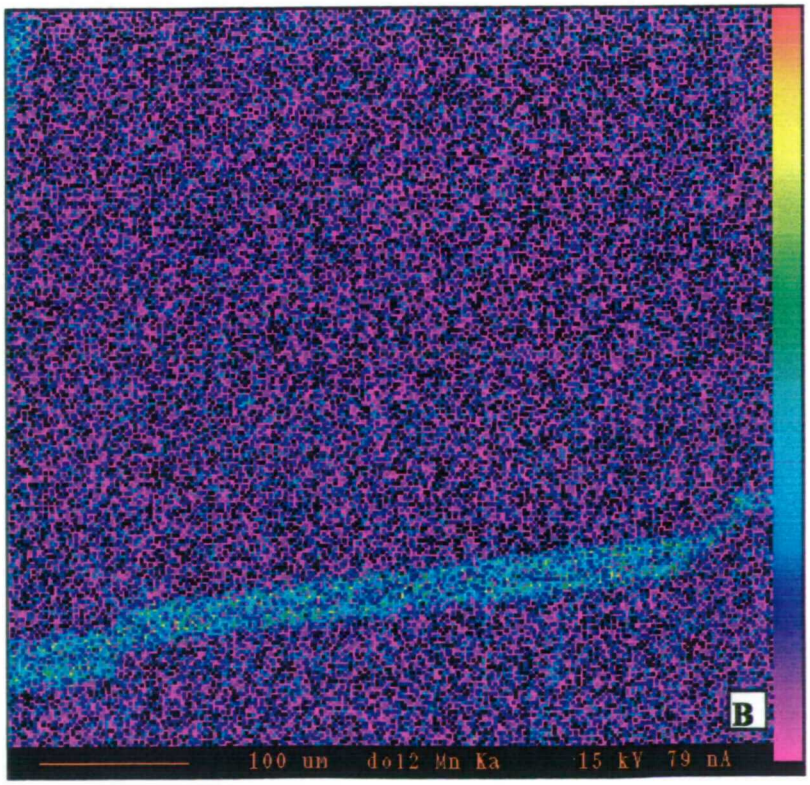
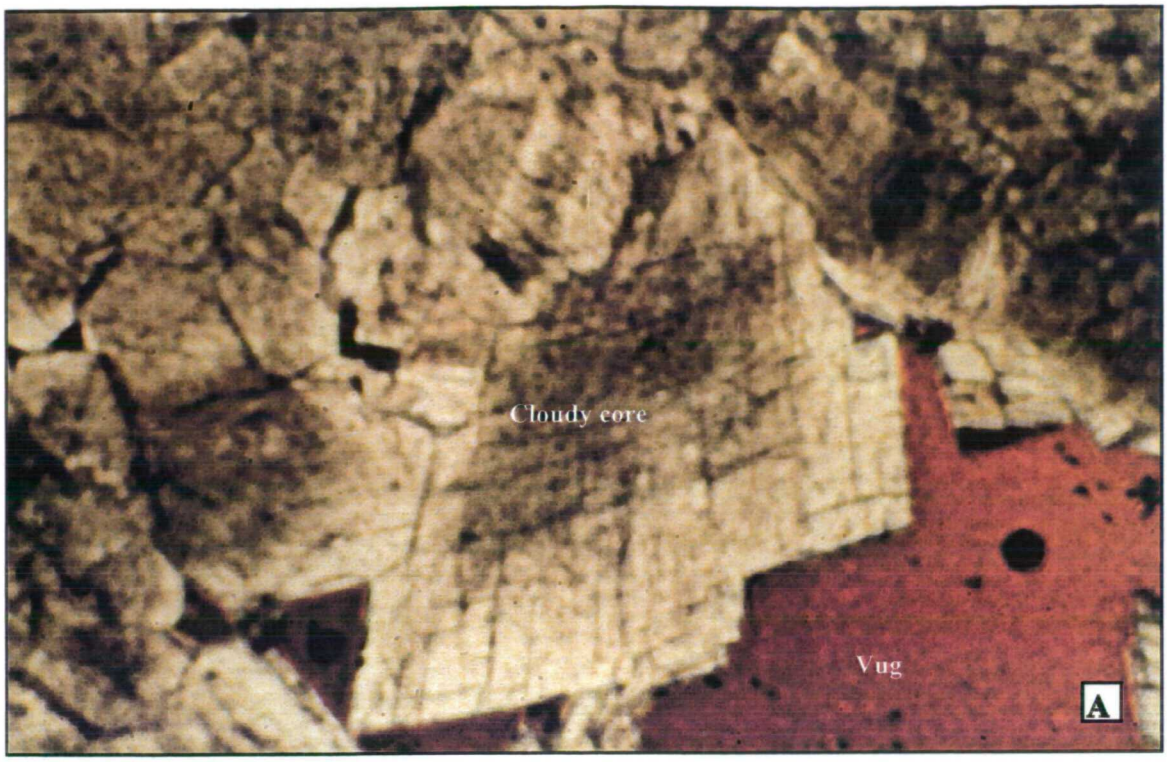


Plate 21.



A. Lisheen, 121/165.2: Photomicrograph (TrL) of D3 dolomite, displaying cloudy cores and clear outer rims.

B. D3 dolomite exhibits 4 distinct alternating moderate to bright luminescent stages; B, C, D and E. Cement stage D is characterized by a yellow zone in stage D. Long axis = 1500μm.

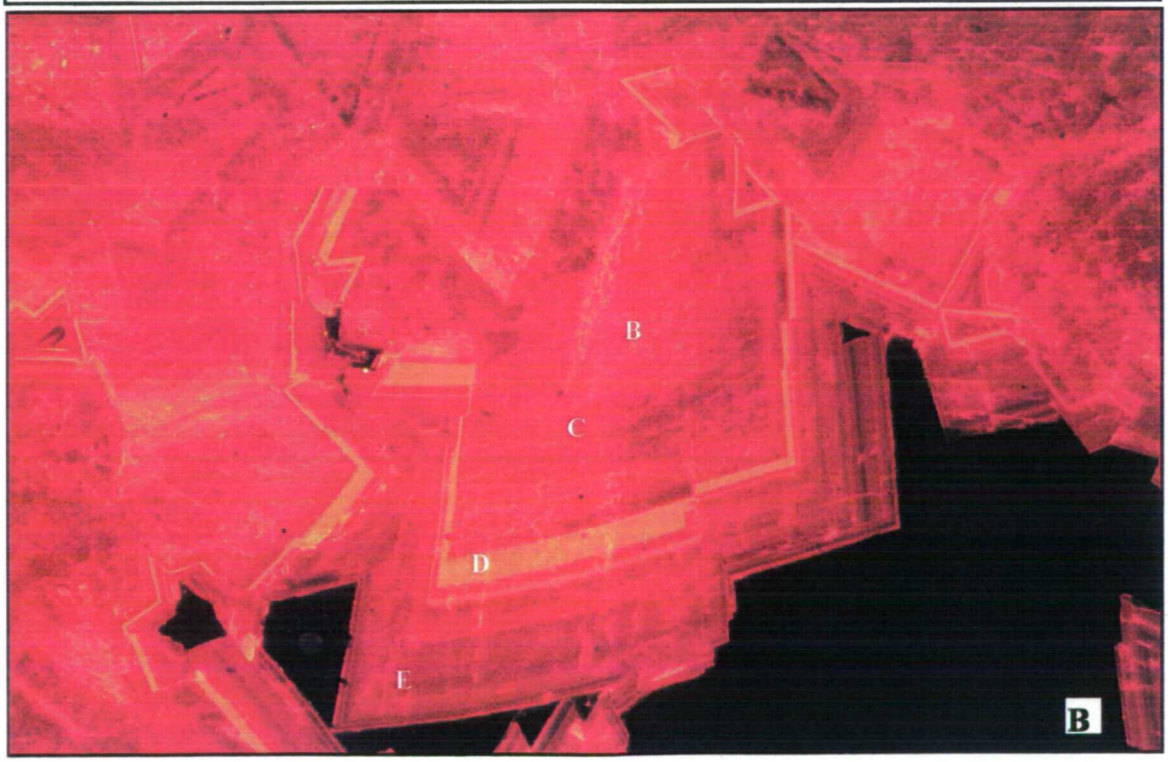
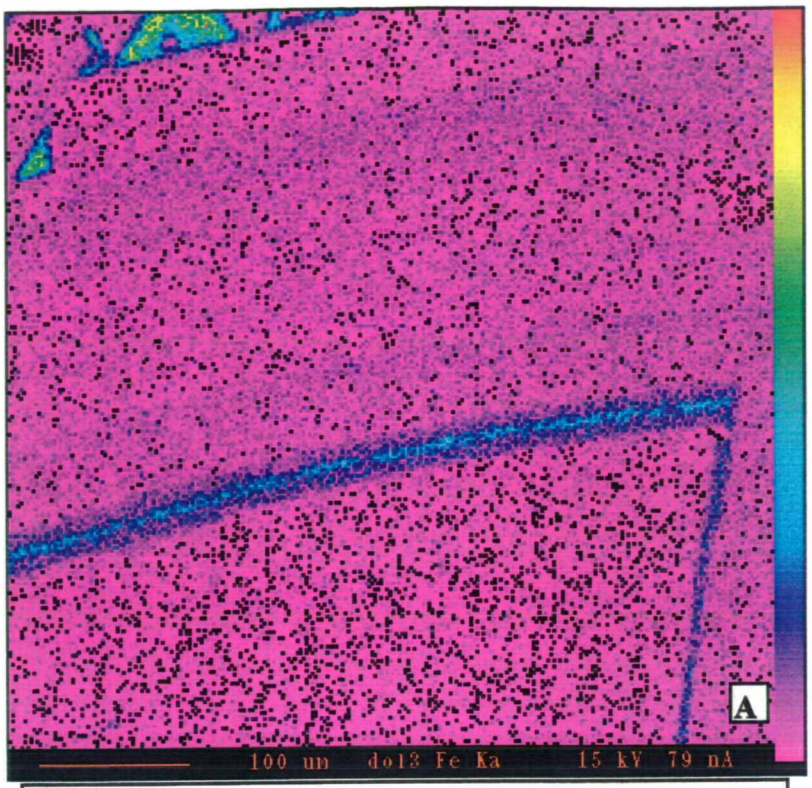


Plate 22.



A. Lisheen, 121/165: X-ray distribution map of the element Fe in D3 dolomite.
B. Lisheen, 121/165.2: X-ray distribution map of the elements Fe (yellow), Mn (blue), and Sr (pink) in D3 dolomite.

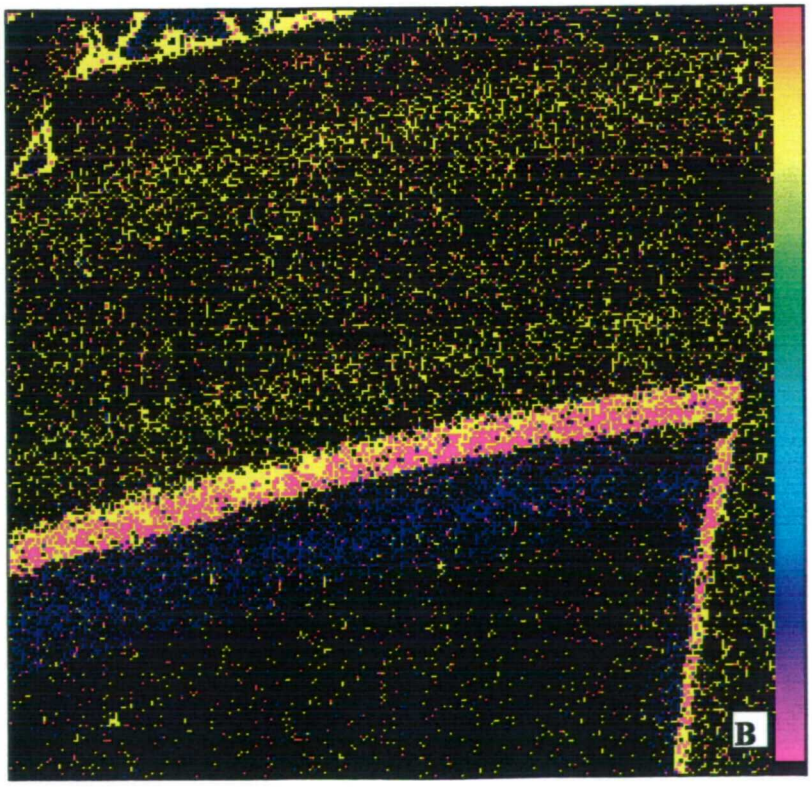
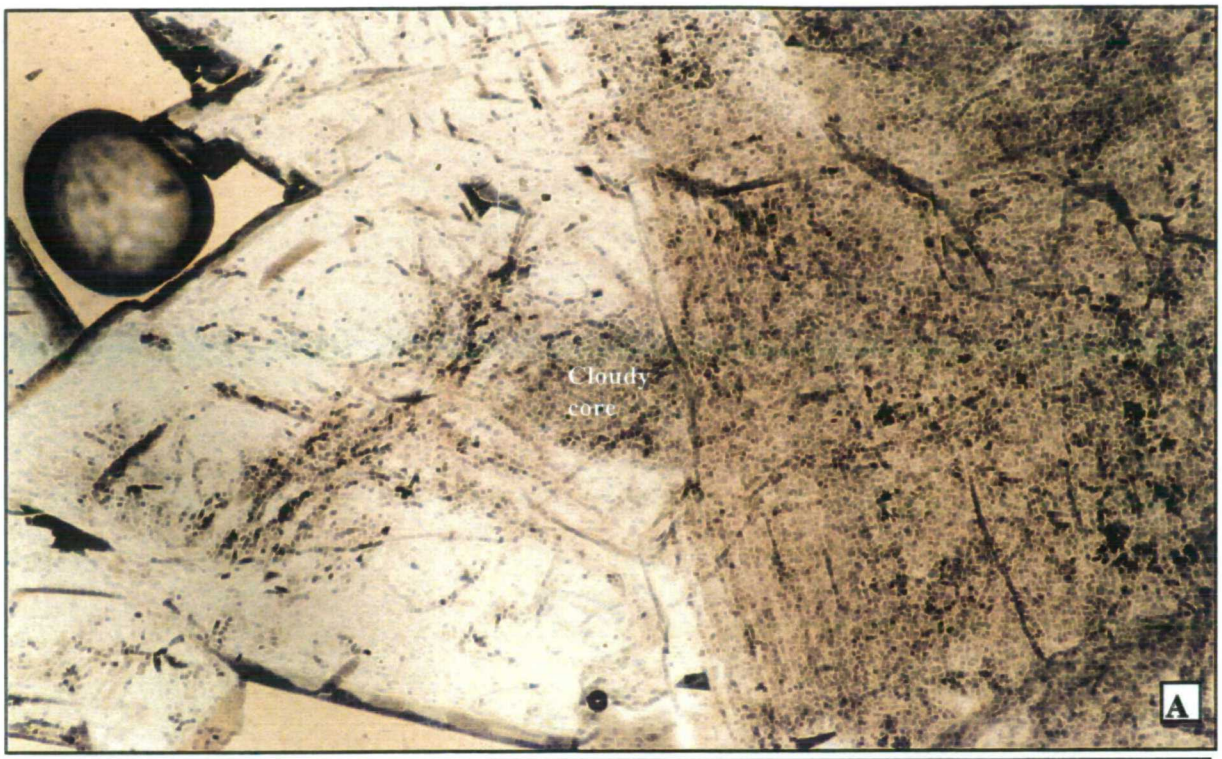


Plate 23.



A. Lisheen, 538/185.2: Photomicrograph (TrL) of D3 dolomite crystal, displaying a cloudy core and clear outer rim.

B. The D3 dolomite exhibits 4 distinct cement stages; B, C, D, and E. The pronounced yellow-orange luminescent zone is present in cement stage D. Long axis = 1250μm.

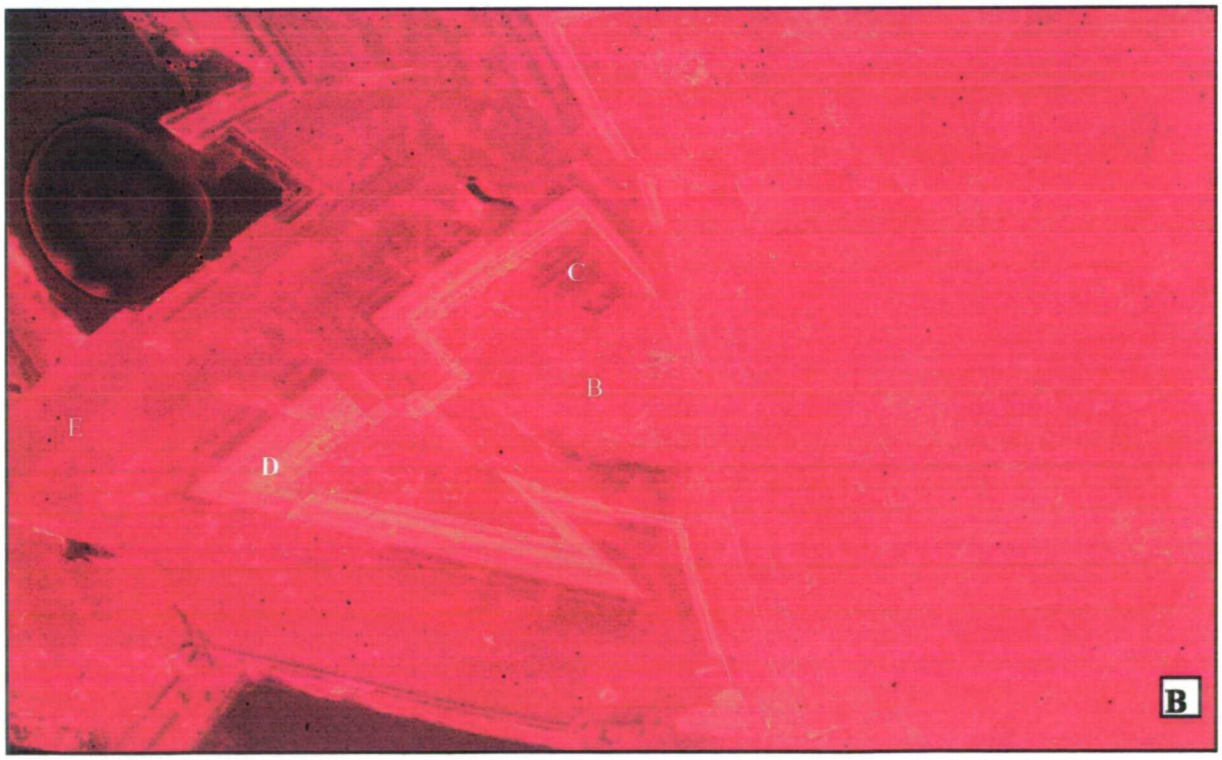
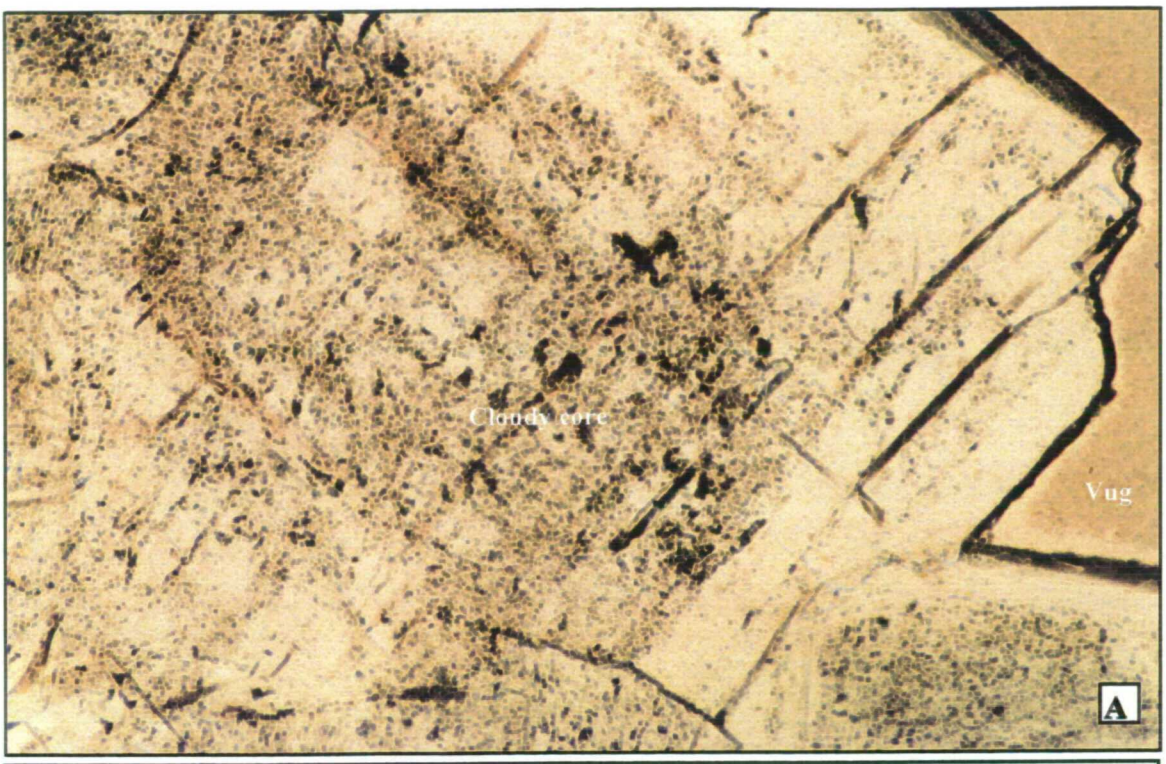


Plate 24.



A. Lisheen, 252/174.0: Photomicrograph (TrL) of D3 dolomite crystal.
B. D3 dolomite exhibits alternating bright-dull-bright red, zoned outer rim (cement stage E) and bright orange-red, heterogeneous luminescent core (cement stage B, C). The distinct yellow zone in cement stage D is only partially formed. Long axis = 1250μm.

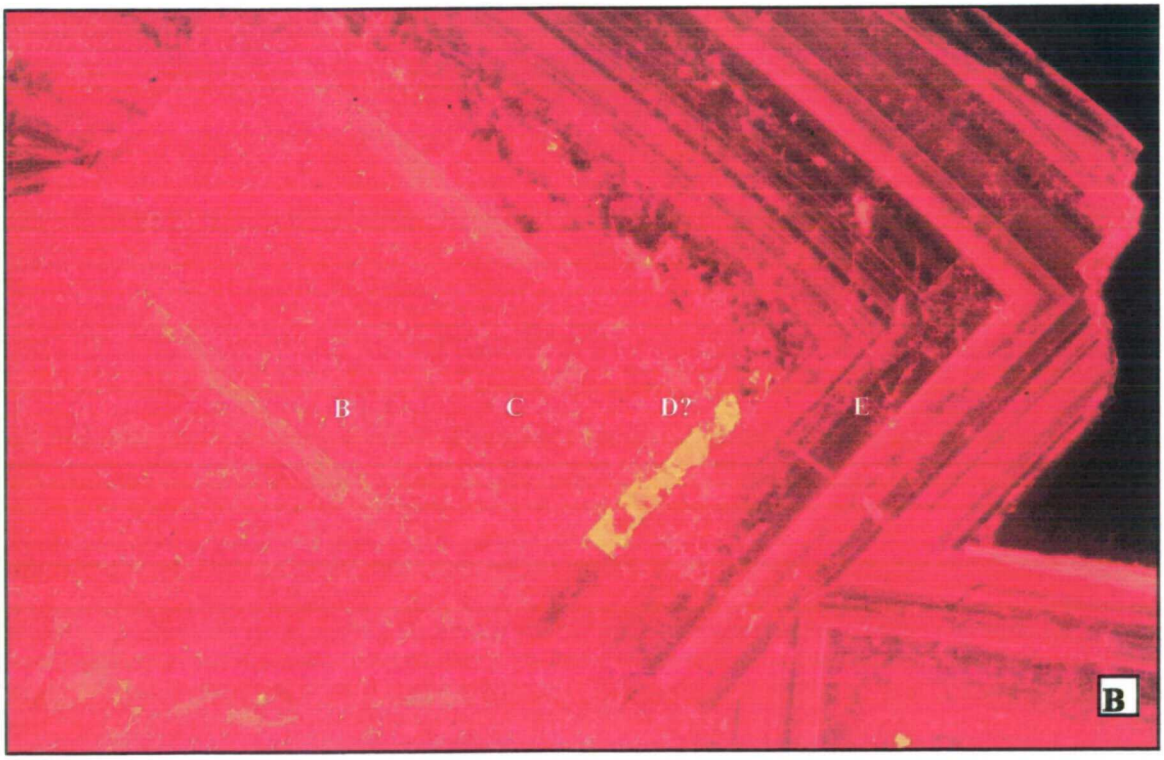


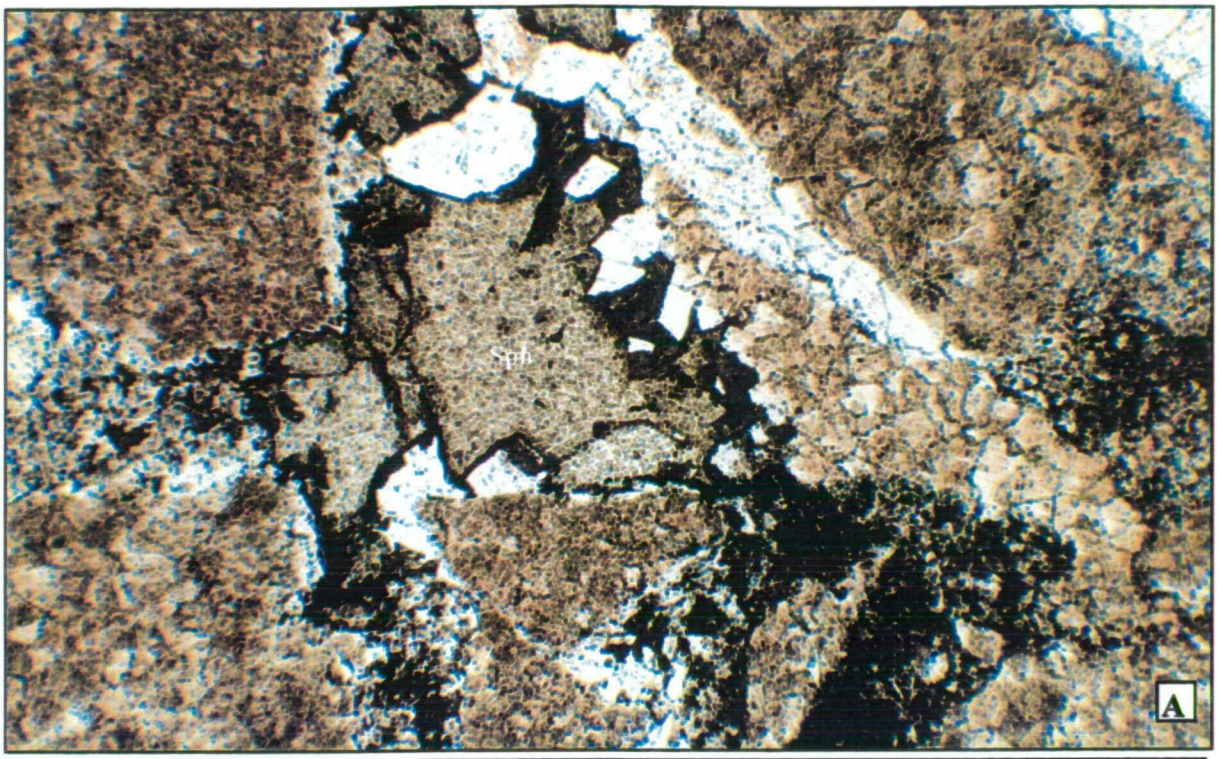
Plate 25.



A. Galmoy, G-NE orebody: Moderately developed black matrix breccia dolomite (D2) with angular to sub-rounded clasts of $D1_R$ dolomite.
B. Galmoy, West of G orebody: Moderately developed white matrix breccia dolomite (D3) with late pink dolomite (D4) and calcite (D5 Calc).



Plate 26.



A. Galmoy, sample 3, CW orebody: Photomicrograph (TrL) of sphalerite replacing D2 dolomite.
B. D2 dolomite exhibits bright to moderate orange-red luminescence. $D1_R$ dolomite clasts display non to dull red, homogeneous luminescence. Sphalerite exhibits alternating non, dull and brightly luminescent zones. Long axis = 3000μm.

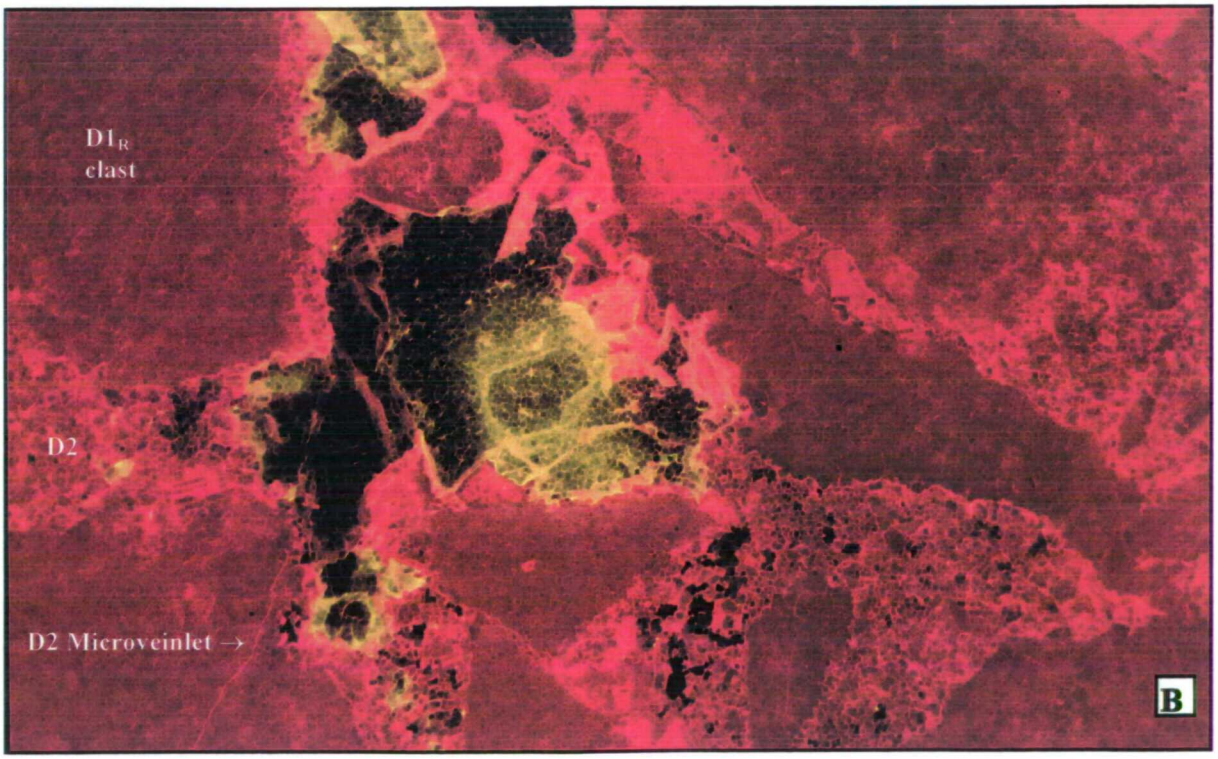
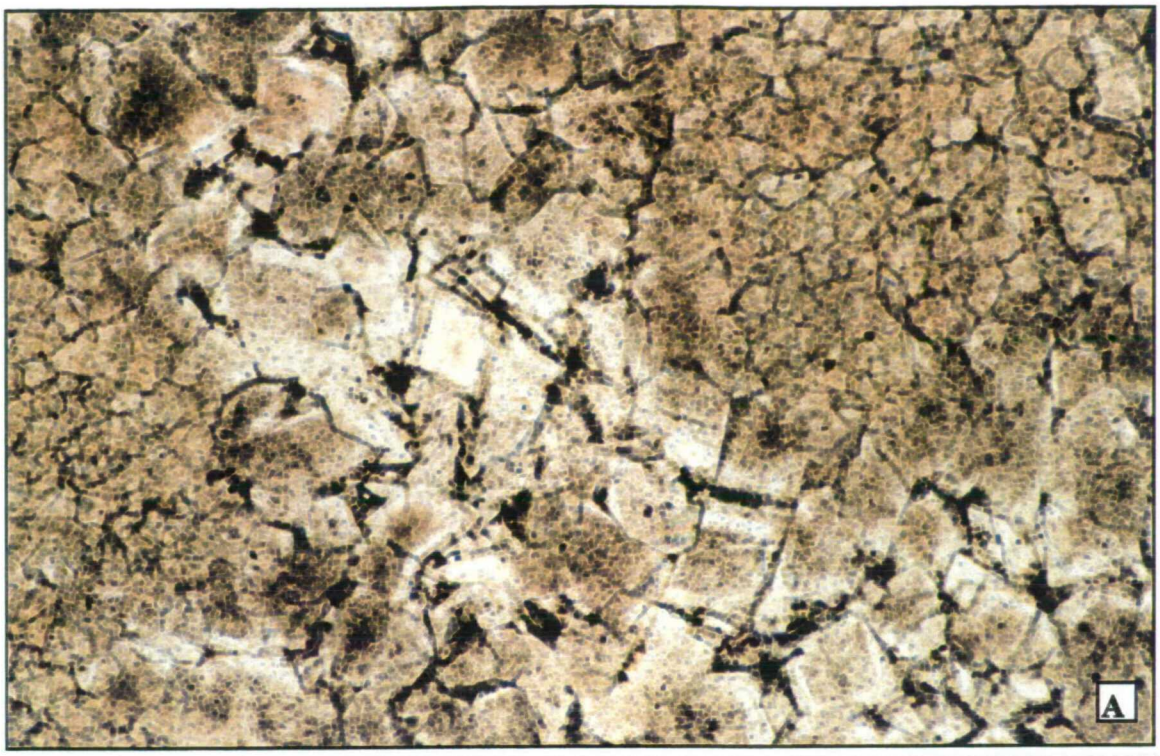


Plate 27.



A. Galmoy, MG63/97.2: Photomicrograph (TrL) of D2 dolomite rhombs.

B. D2 dolomite rhombs exhibit moderate red luminescent cores, and bright orange-yellow luminescent rims. Long axis = 1250μm.

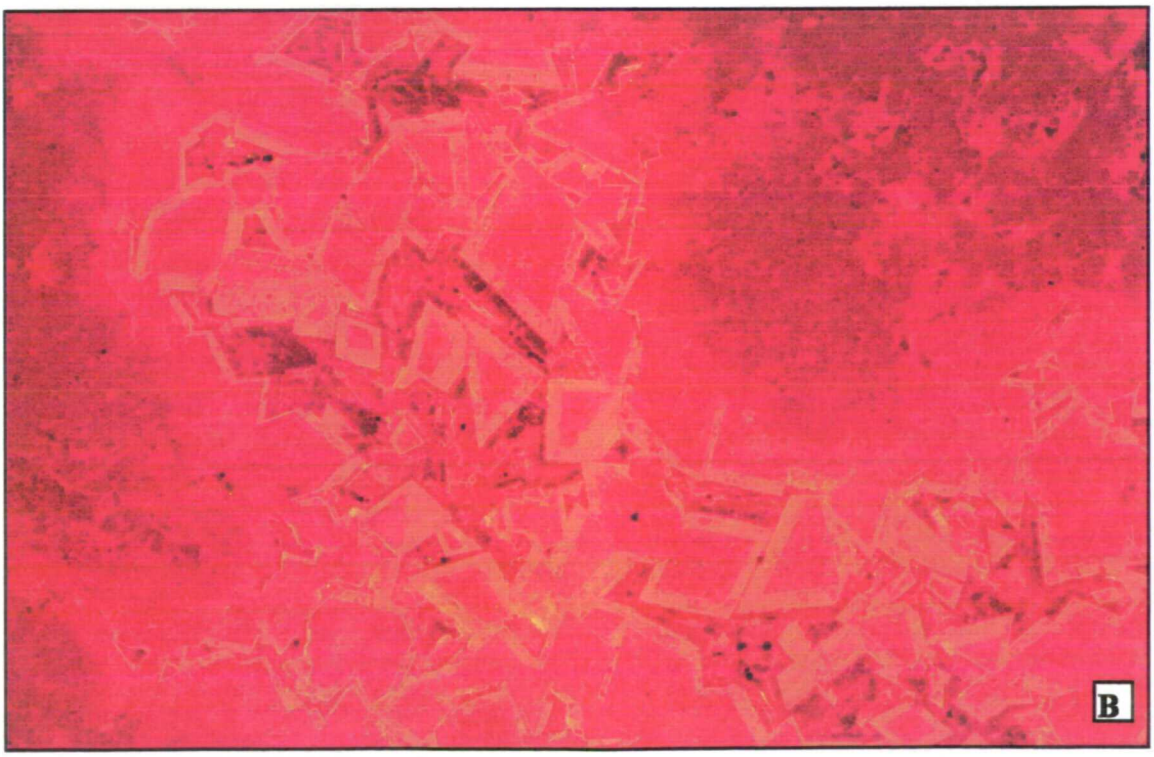


Plate 28.



A. Galmoy, GY355/78.0: Photomicrograph (TrL) of D3 dolomite.

B. D3 dolomite exhibits alternating moderate to bright luminescent stages B, C, D, and E. The distinct yellow zone of cement stage D is approximately 10μm thick. Long axis = 3000μm.

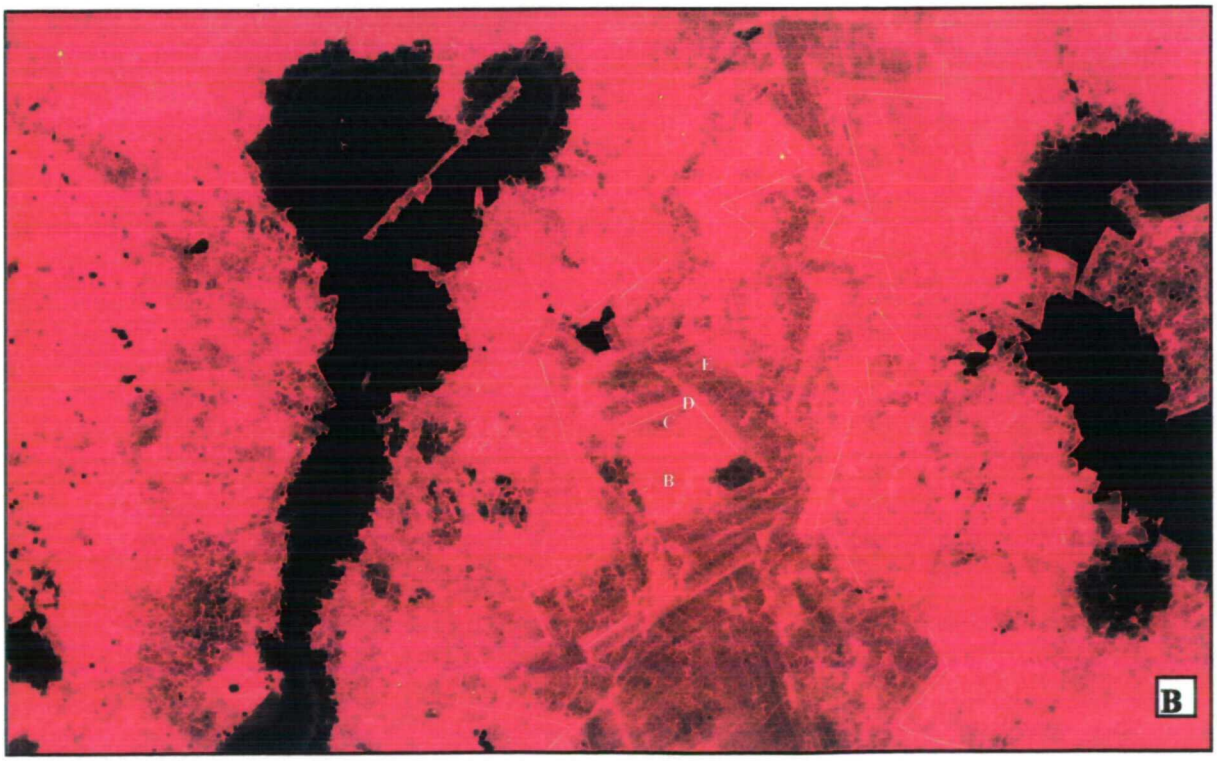
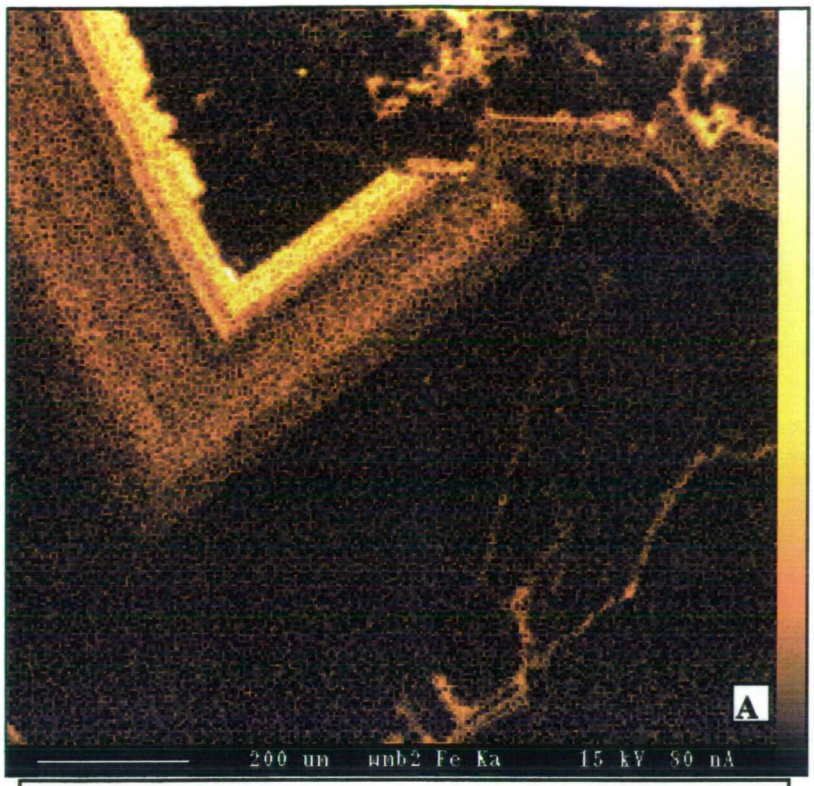


Plate 28a.



A. Galmoy, MG99/100.8: X-ray distribution map of the element Fe in D3 dolomite.
B. Galmoy, MG99/100.8: X-ray distribution map of the element Mn in D3 dolomite.

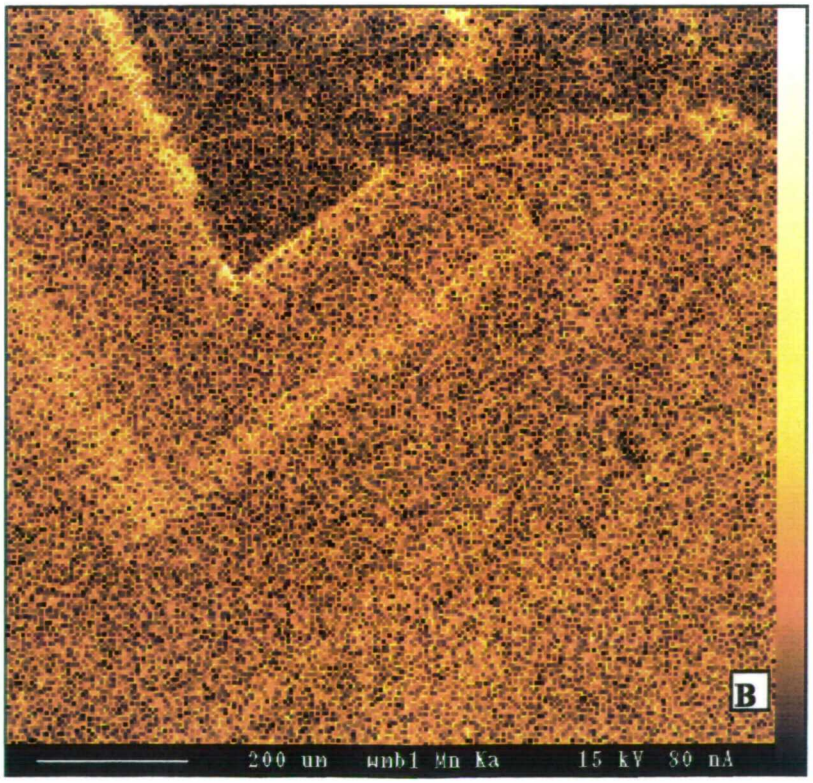
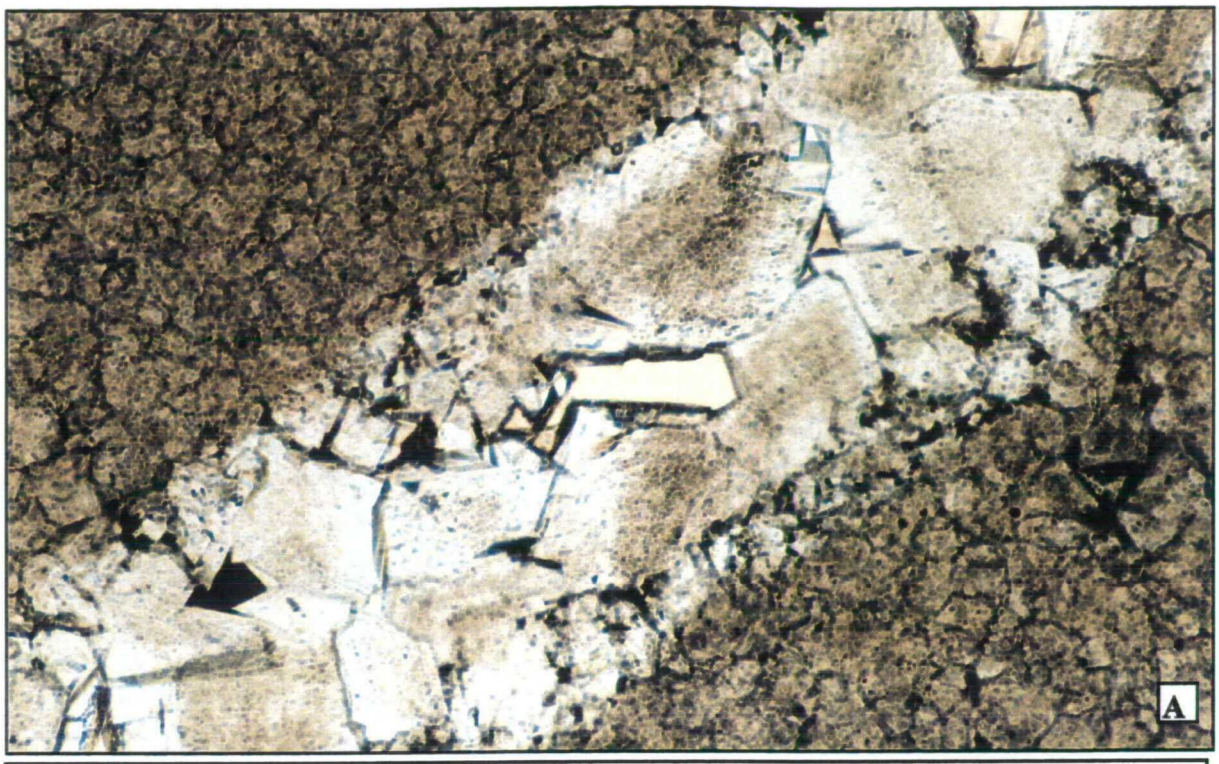


Plate 29.



A. Galmoy, MG63/97.2: Photomicrograph (TrL) of D3 dolomite vein, cross-cutting $D1_R$ clast.
B. The D3 dolomite vein exhibits cement stages A, B, C, D, and E. The cement stages are characterized by alternating bright yellow-orange, moderate red, bright red-orange, and non to dull red luminescence respectively. Long axis = 1250μm.

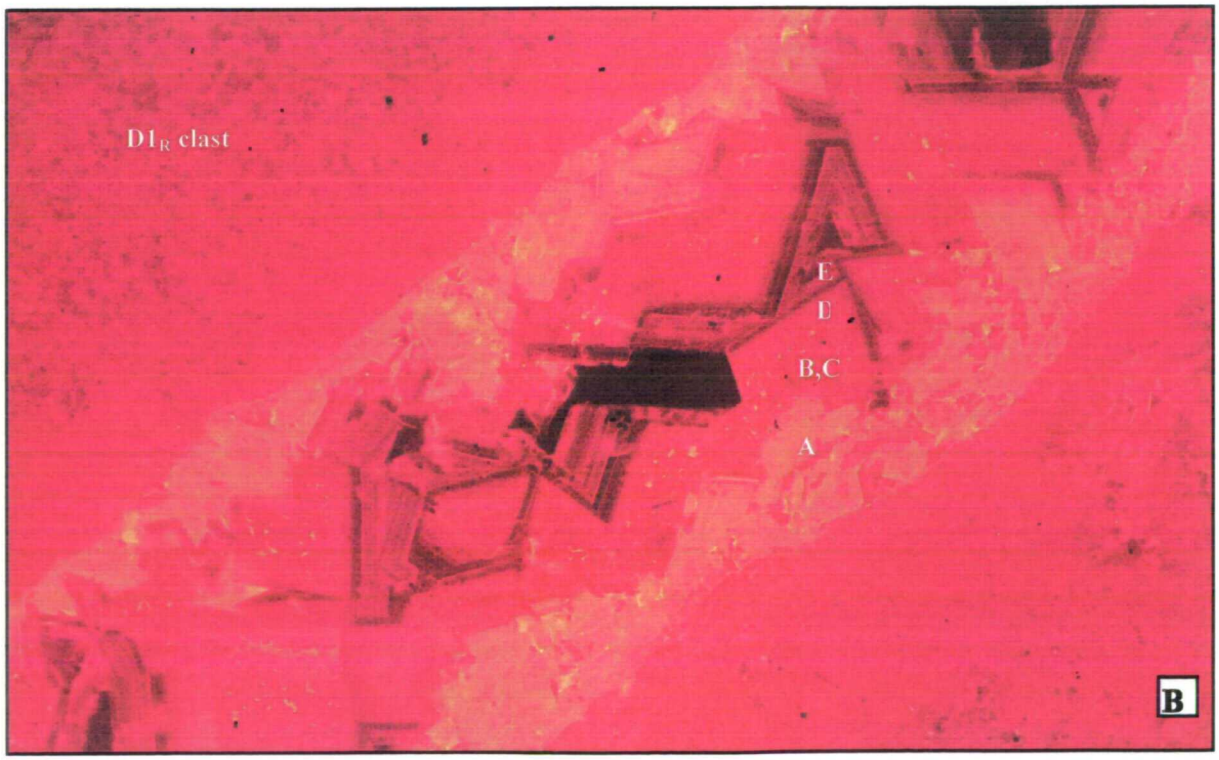


Plate 29a.



A. Lisheen, 262/120.0: Calcite matrix breccia, with sub-rounded clasts of Waulsortian wavy laminated facies. Orientation of wavy argillite wisps in the clast provides good evidence of clast rotation.
B. Galmoy, MG63/97.2: Crystalline white D3 dolomite vein post dates D2 and $D1_R$ dolomite.



Plate 30.

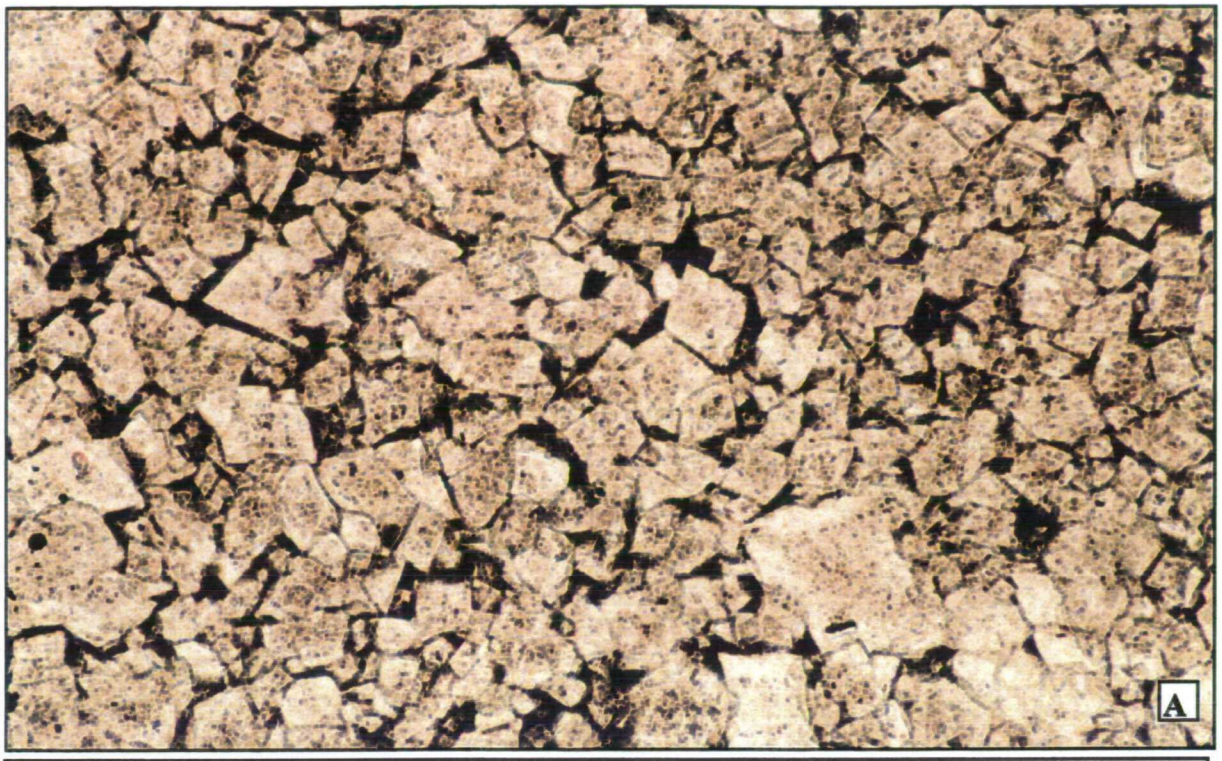


A. Holycross: Crystalline white dolomite (D3?) post-dates poorly developed D2 dolomite.

B. Silvermines: Well developed dolomite breccia (D2), with sub-rounded ferroan calcite clasts.



Plate 31.



A. Holycross, HC13/115.3: Photomicrograph (TrL) of D2 euhedral dolomite rhombs.

B. D2 dolomite rhombs exhibit moderate red, non-uniform luminescent cores and bright red luminescent outer rims. Long axis = 1250μm.

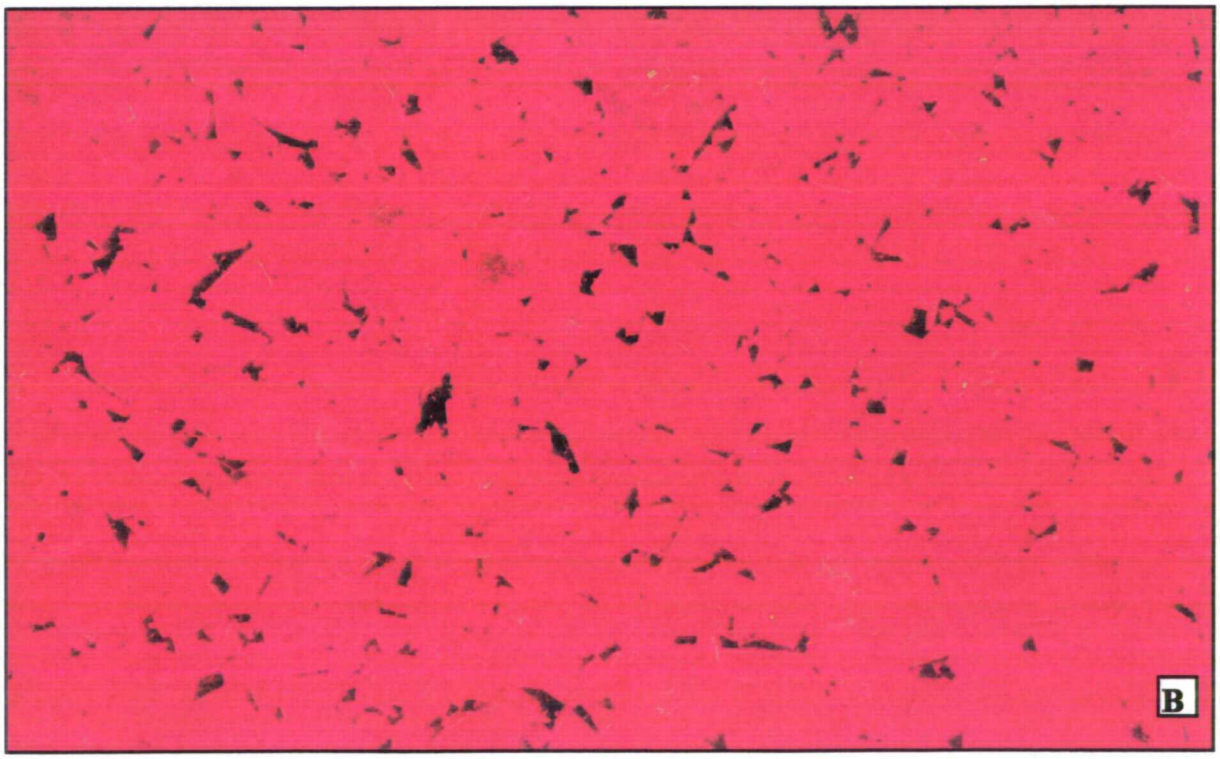


Plate 32.



A. Holycross, HC13/87.8: Photomicrograph (TrL) of a D3 dolomite crystal. The dolomite crystal consists of a cloudy centred core and clear outer rim.
B. The dolomite crystal exhibits a bright red-orange, mottled luminescent core and an alternating dull to moderate red luminescent outer rim. Long axis = 1250µm.

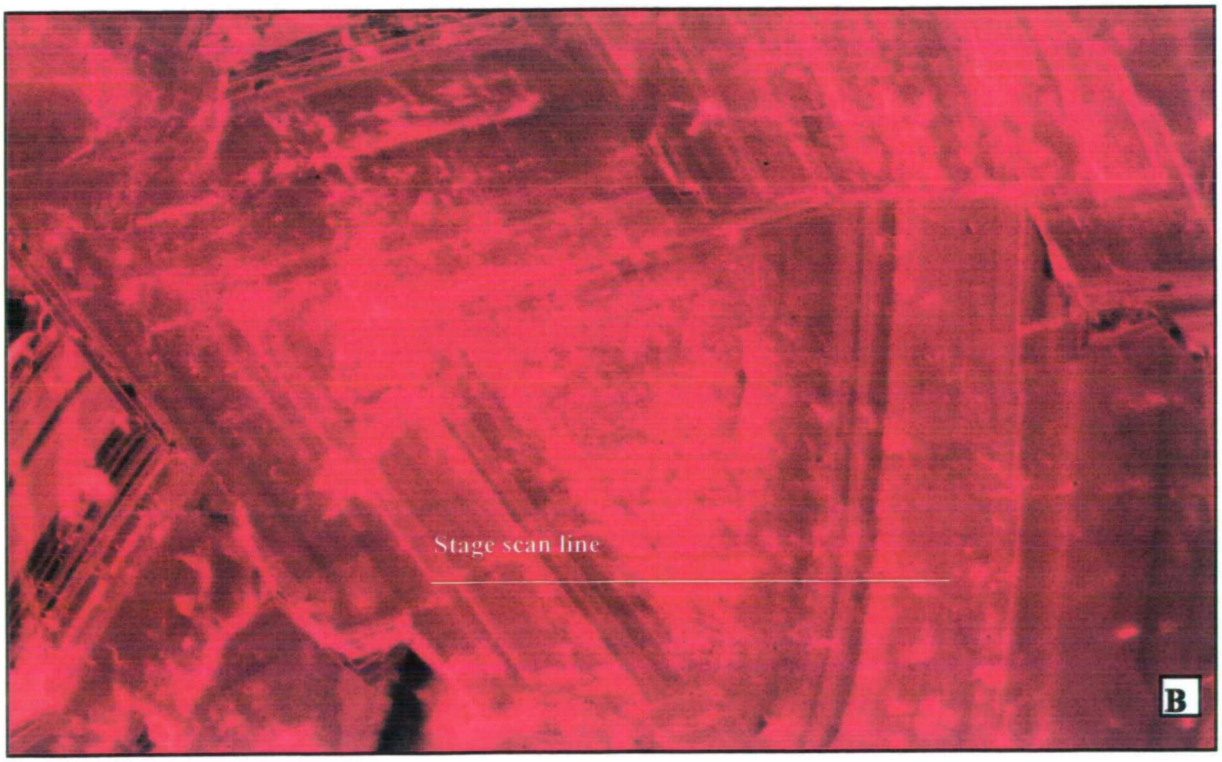


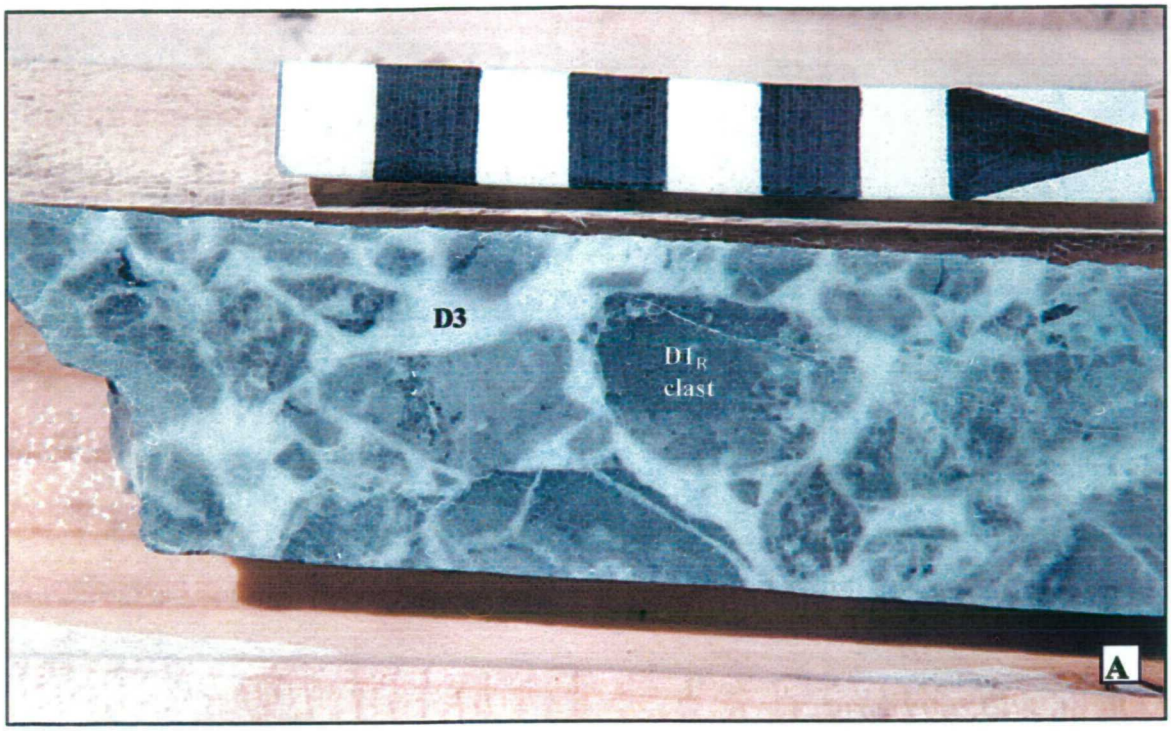
Plate 33.



A. Holycross: Well developed crystalline white matrix breccia dolomite (D3) with sub-rounded, dark grey dolomitized clasts.
B. Rathdowney East: Well developed crystalline white matrix breccia dolomite (D3) with moderately sorted, and sub-angular small clasts.



Plate 34.

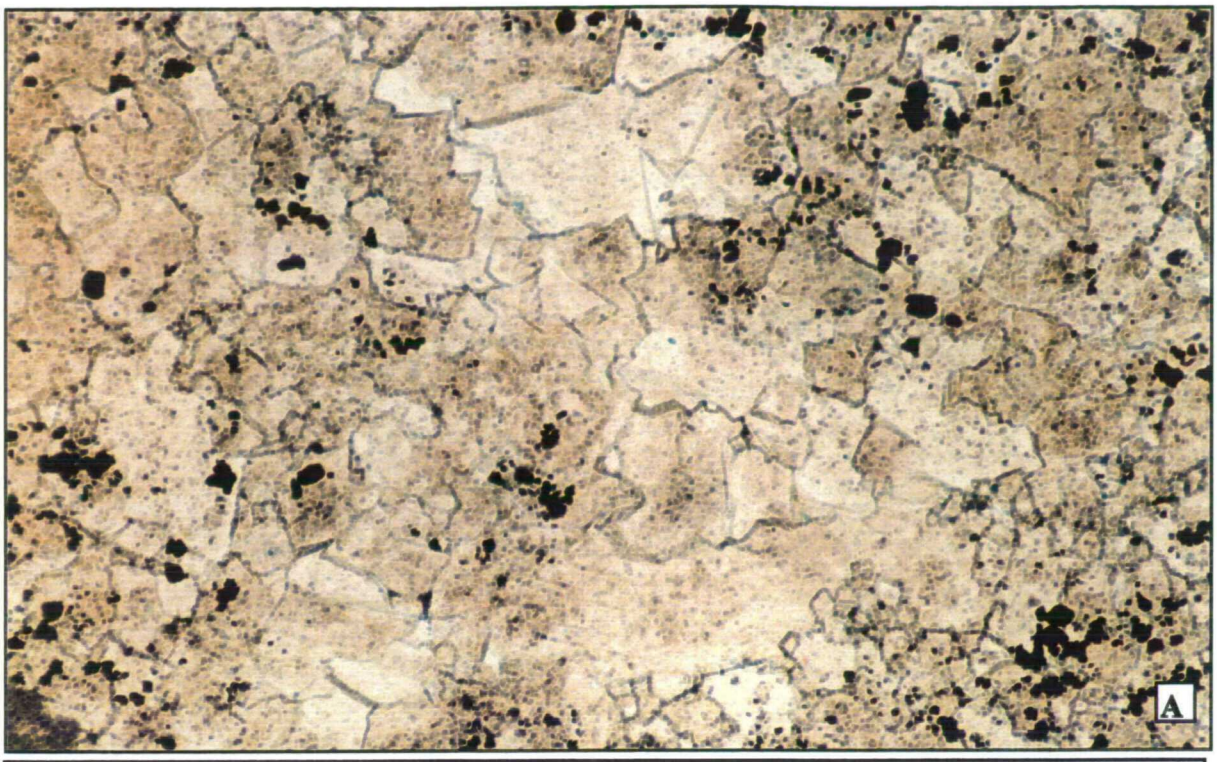


A. Durrow, DUR1/686.5: White matrix breccia dolomite (D3), with sub-rounded clasts of $D1_R$ dolomite.

B. Derrykearn, 45/294.6: White matrix breccia dolomite (D3), with sub-angular to sub-rounded clasts of $D1_R$ dolomite. Late dolomite veinlets cross-cut matrix and clasts.



Plate 35.



A. Rathdowney East, RE24/1729a: Photomicrograph (TrL) of D3 dolomite and disseminated sulphides associated with fine grained D2? dolomite.

B. D3 dolomite exhibits 4 distinct alternating luminescent stages B, C, D, and E. The yellow luminescent zone is present in cement stage D. Long axis = 1250µm.

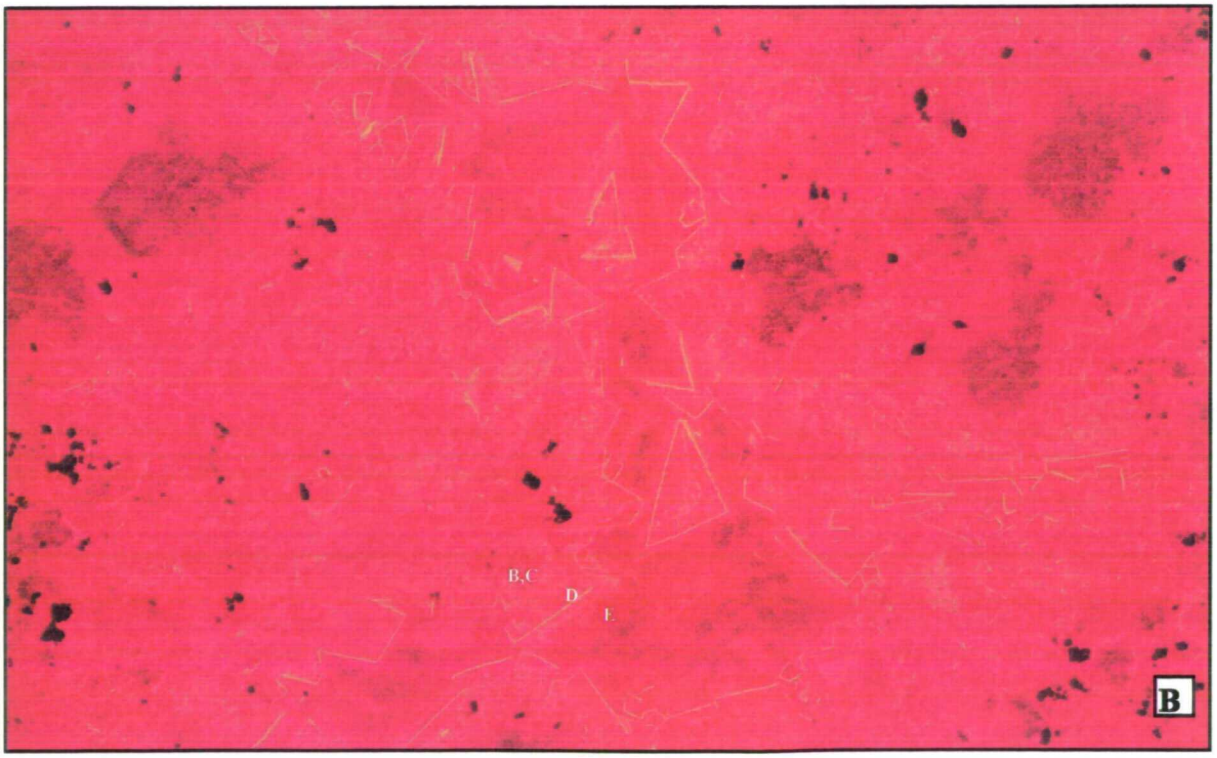
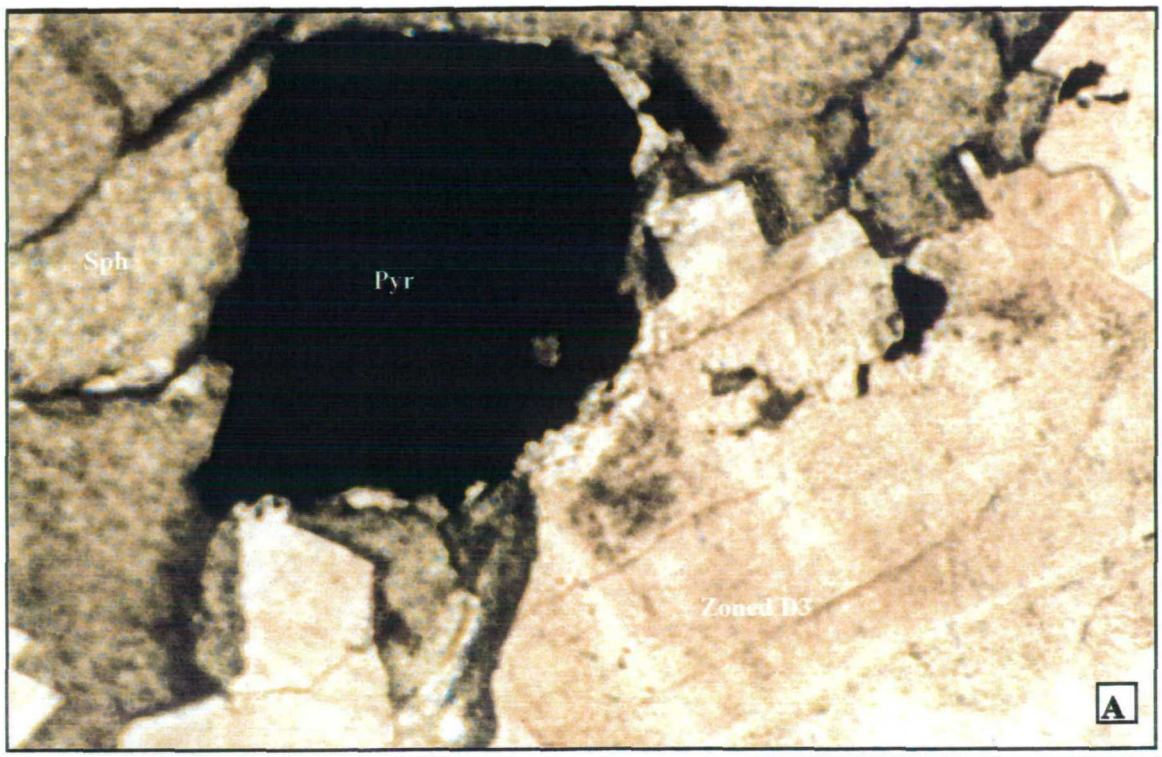


Plate 36.



A. Derrykearn, 45/271.6: Photomicrograph (TrL) of zoned D3 dolomite and sulphide mineralization.
B. Zoned D3 dolomite exhibits alternating moderate to bright luminescent stages B, C, and D. The yellow zone is present in cement stage D. Long axis = 1250μm.

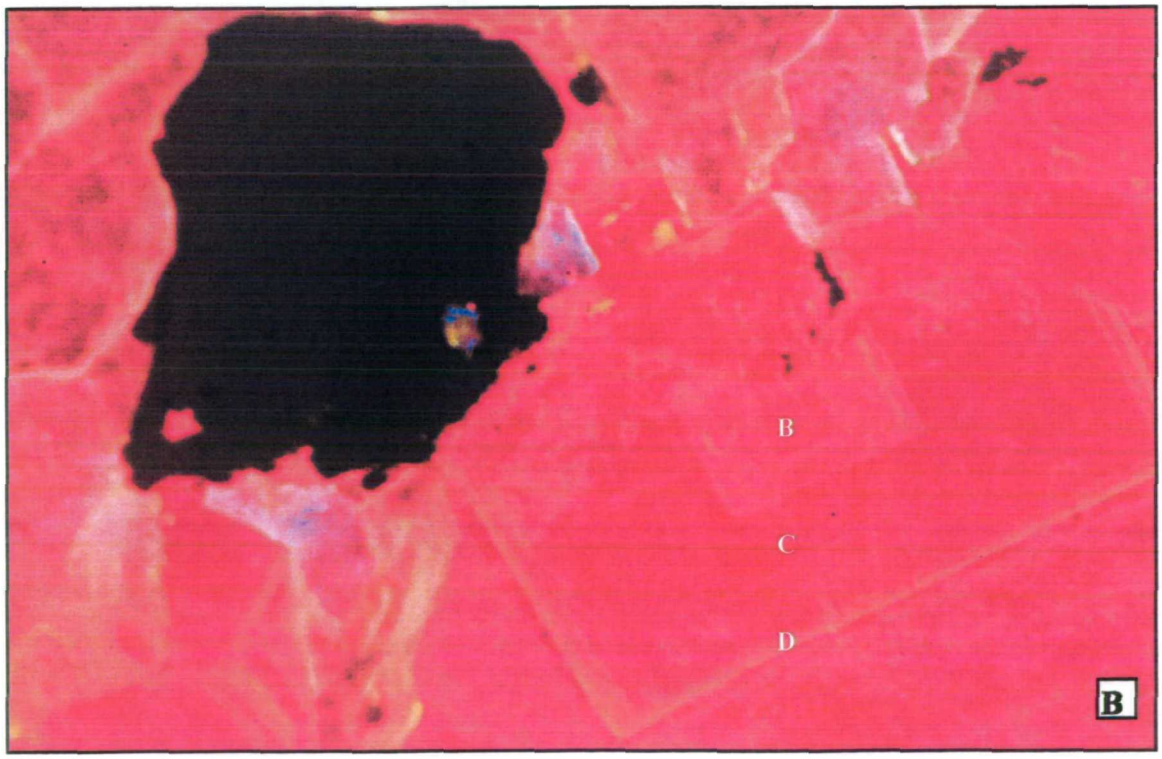
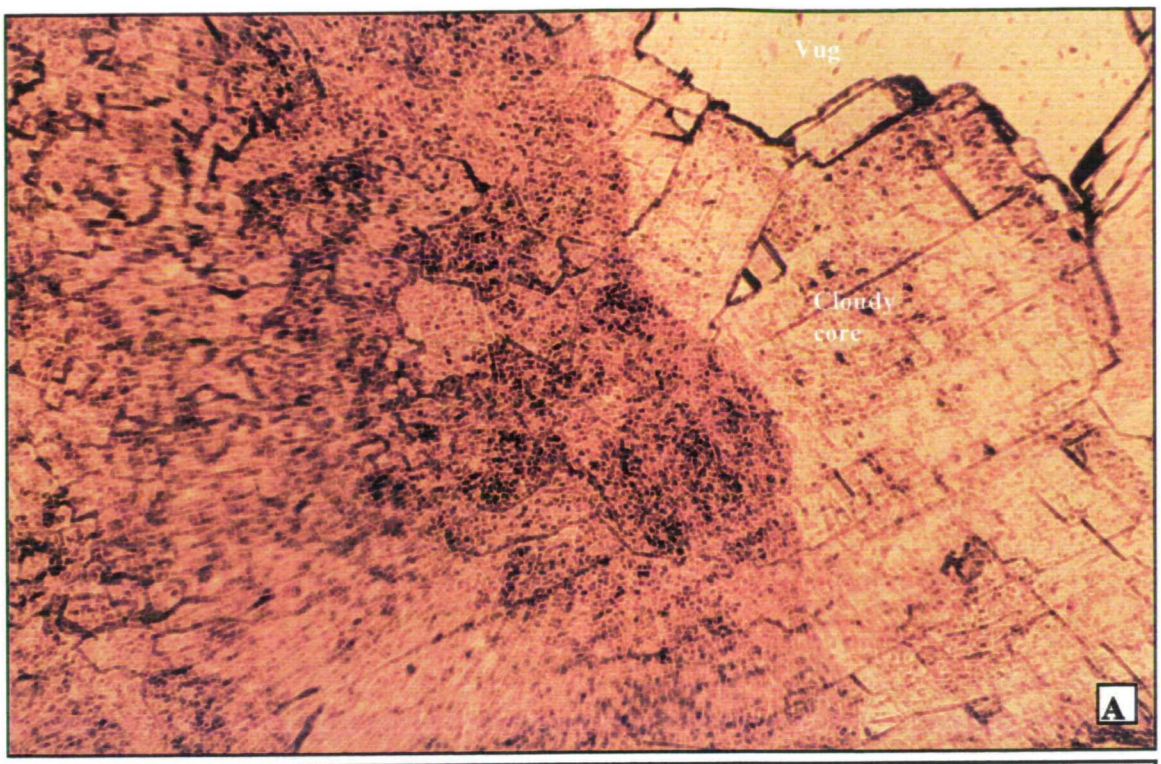


Plate 37.



A. Durrow, DUR1/686.5: Photomicrograph (TrL) of D3 dolomite.

B. D3 dolomite exhibits alternating non to dull, and bright red luminescent zones. The distinct yellow zone of cement stage D is missing. Long axis = 2500µm.

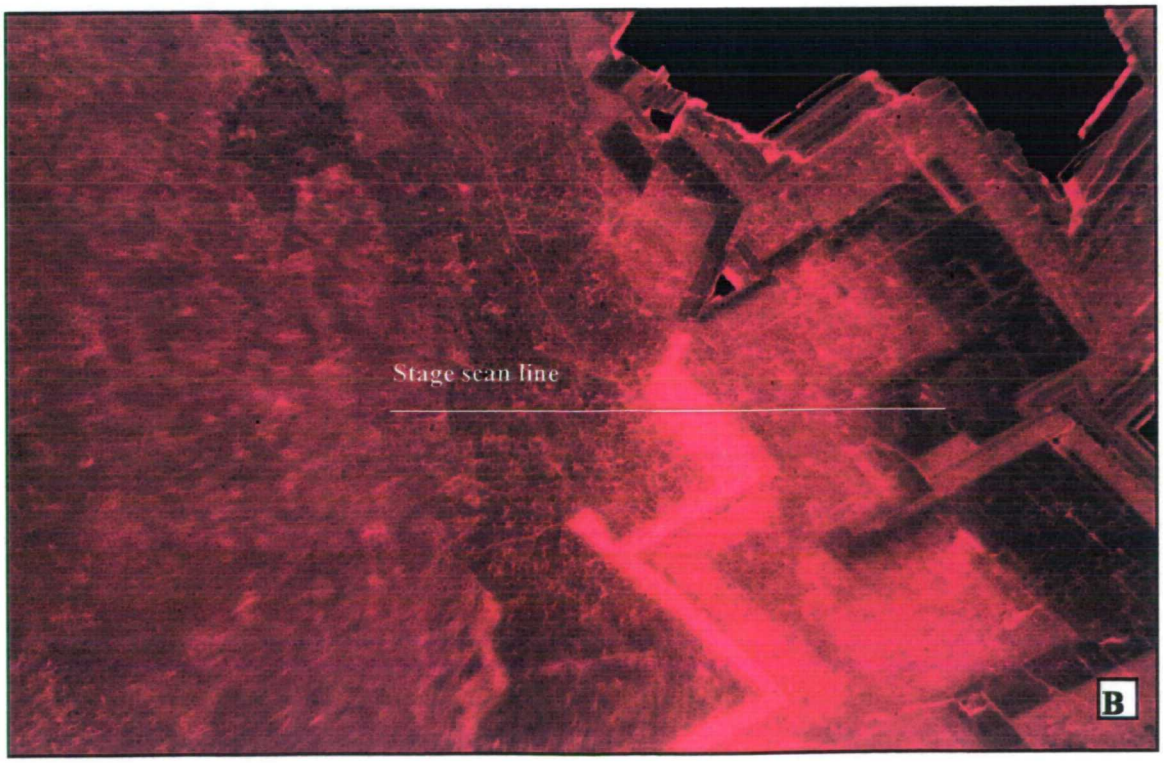


Plate 38.

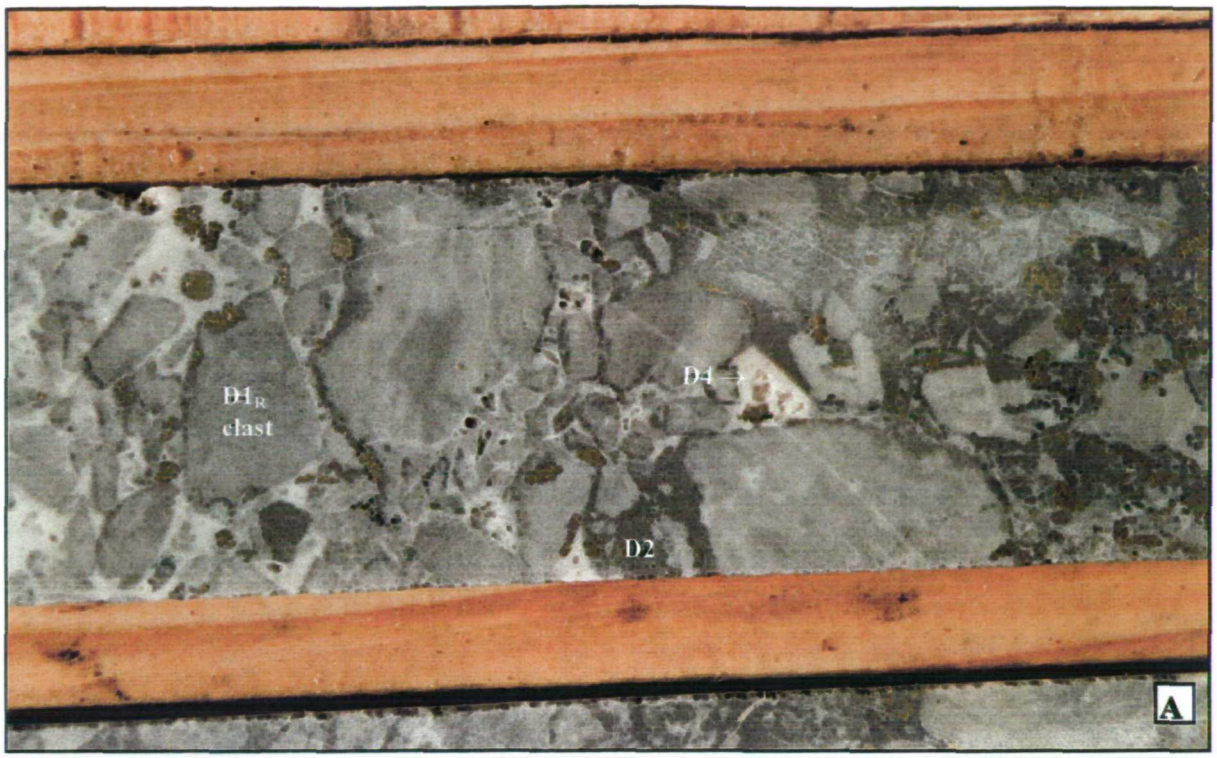


A. Durrow, DUR4/365.5: Photomicrograph (TrL) of D3 dolomite.

B. The D3 dolomite exhibits a bright red-orange luminescent zone which is overgrown by a late Fe rich cement stage. Long axis = 3000μm.



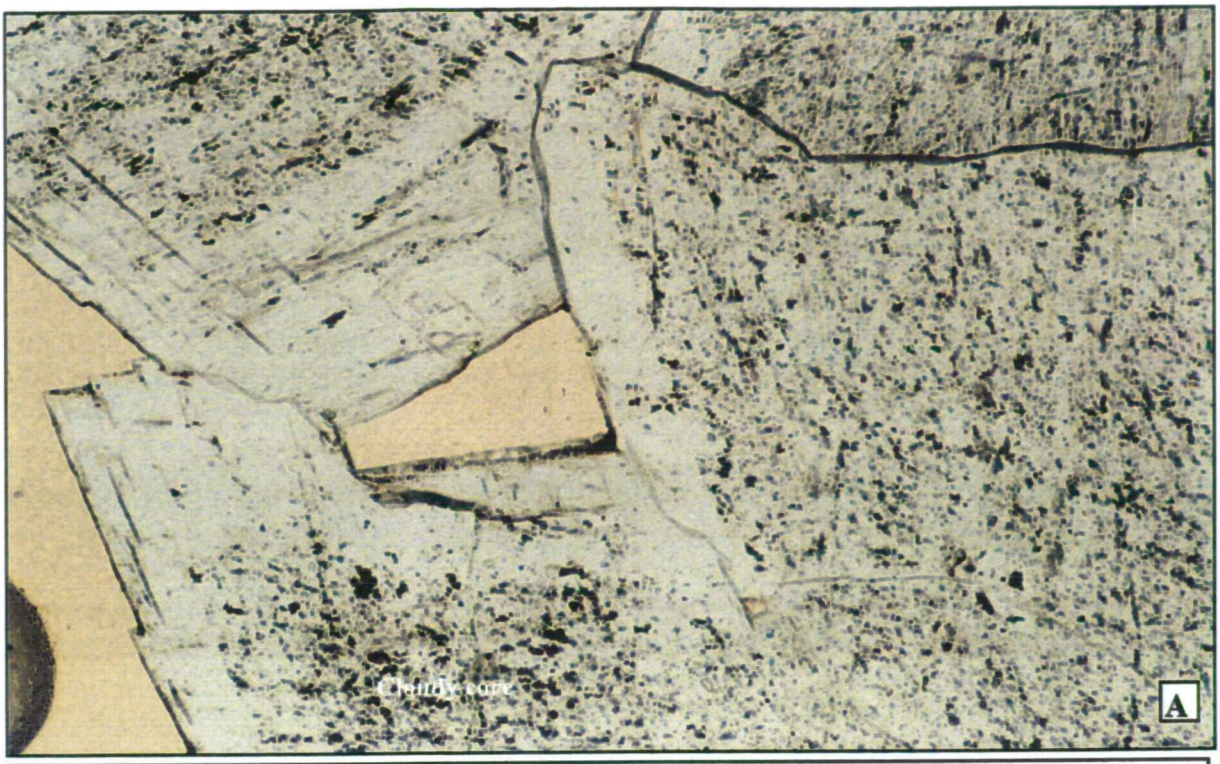
Plate 39.



A. Lisheen, 262/152.3: Well developed D2 dolomite, with $D1_R$ dolomite clasts and late vug-filling and cross-cutting D4 dolomite. Sulphides replace both matrix and clasts.
B. Lisheen, 121/319.2: Sulphide bearing ferroan dolomite vein (D5 Dol) is cross-cut by a late calcite vein (D5 Calc), with small euhedral quartz crystals.



Plate 40.



A. Lisheen, 262/152.3: Photomicrograph (TrL) of D4 dolomite crystals, with curved cleavage traces.

B. The D4 dolomite exhibits a moderate to bright orange-red luminescent core, and dull to non red, luminescent outer rim. Long axis = 1250µm.

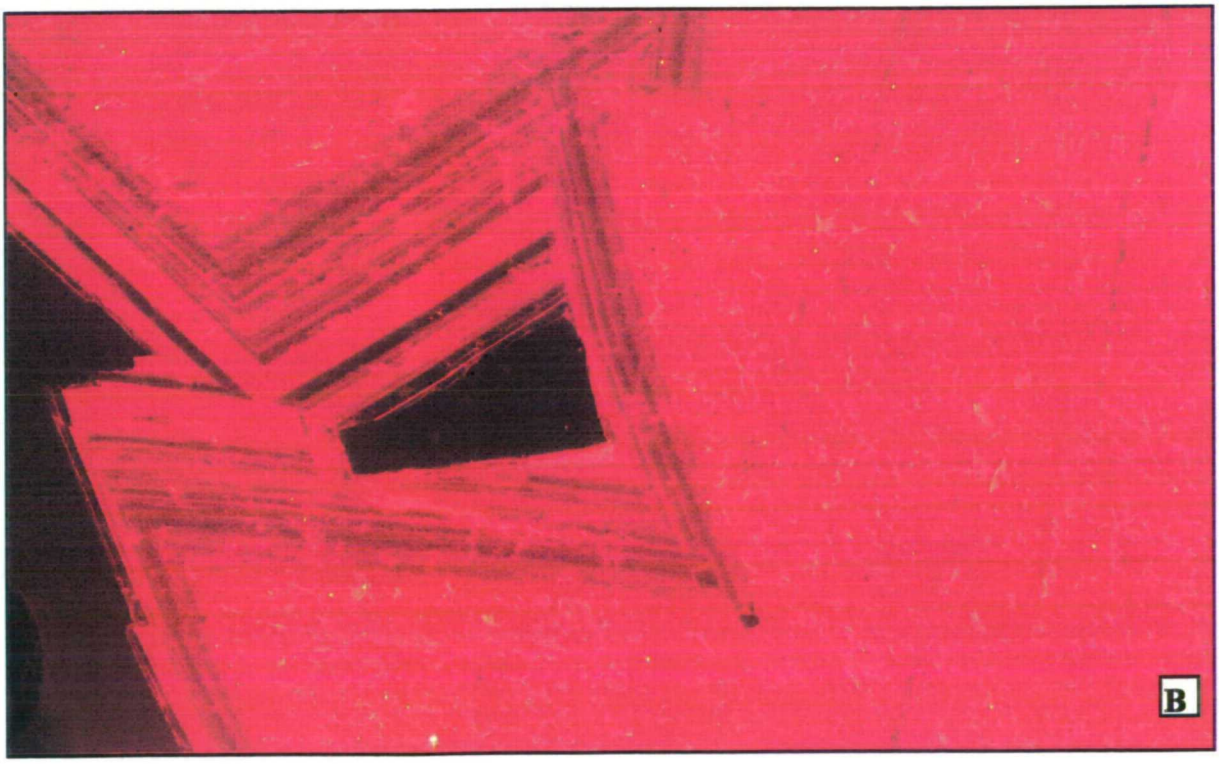
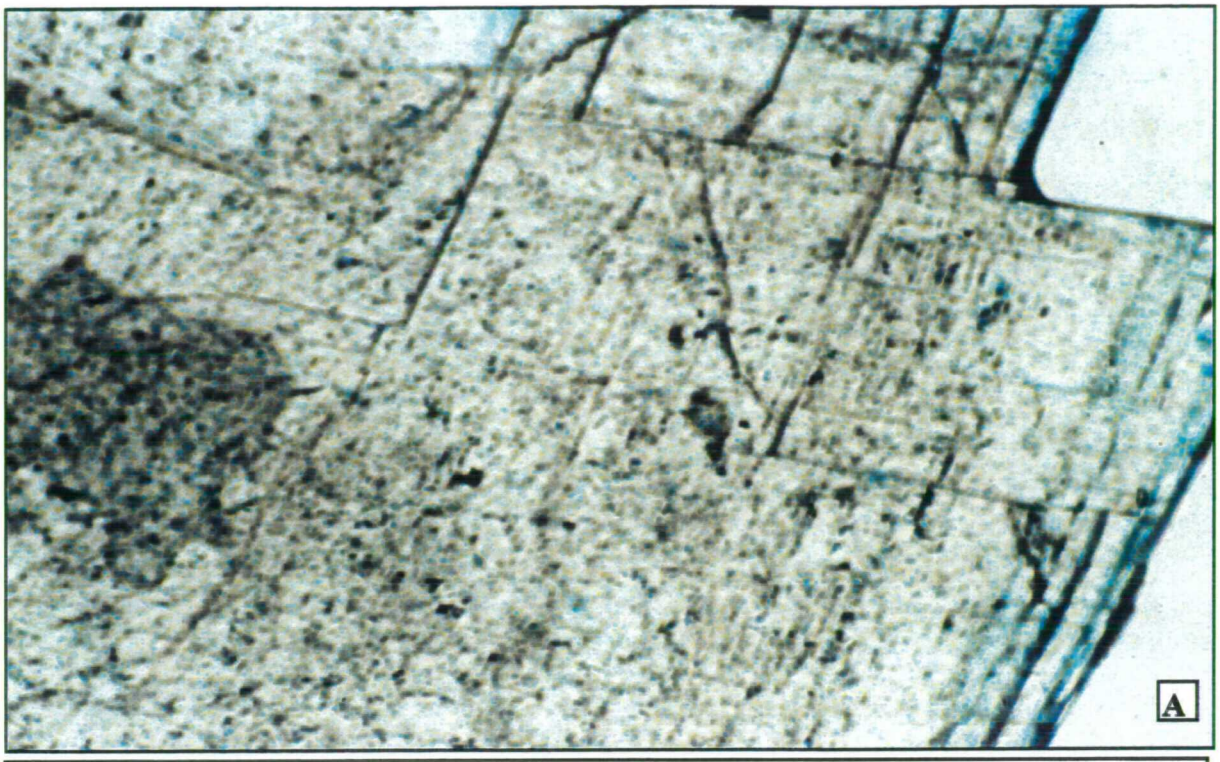


Plate 41.



A. Rathdowney East, RE24/1625: Photomicrograph (TrL) of a D4 dolomite crystal.
B. The D4 dolomite exhibits alternating bright, moderate, dull, and non luminescence cement stages; B, C, D, E, and F. Cement stage F is characterized by Fe, Mn rich zoning. Long axis = 1250µm.

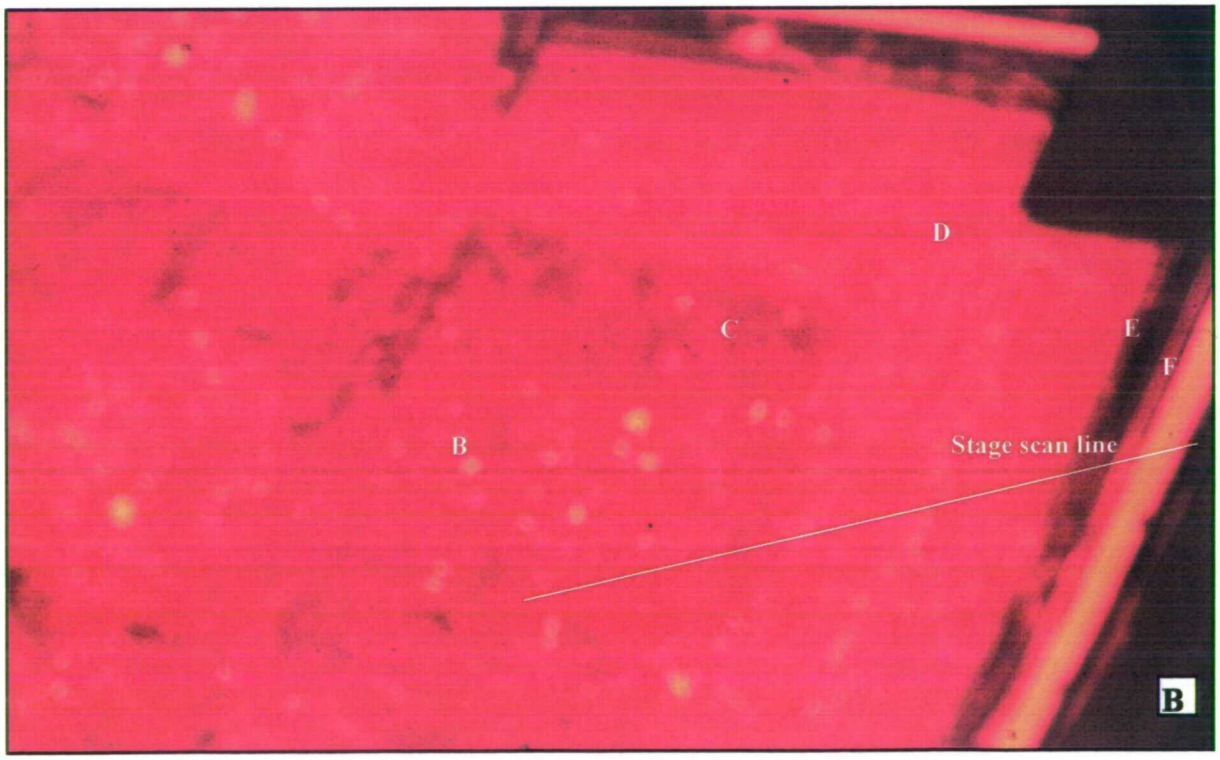
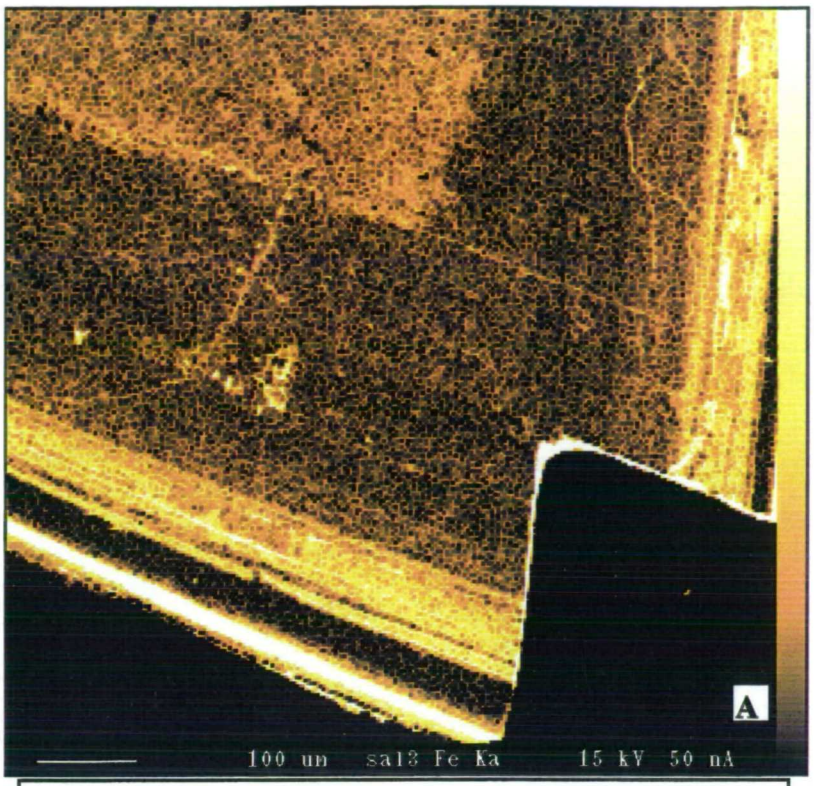


Plate 42.



A. Rathdowney East, RE24/1625: X-ray distribution map of the element Fe in D4 dolomite..
B. Rathdowney East, RE24/1625: X-ray distribution map of the element Mn in D4 dolomite.

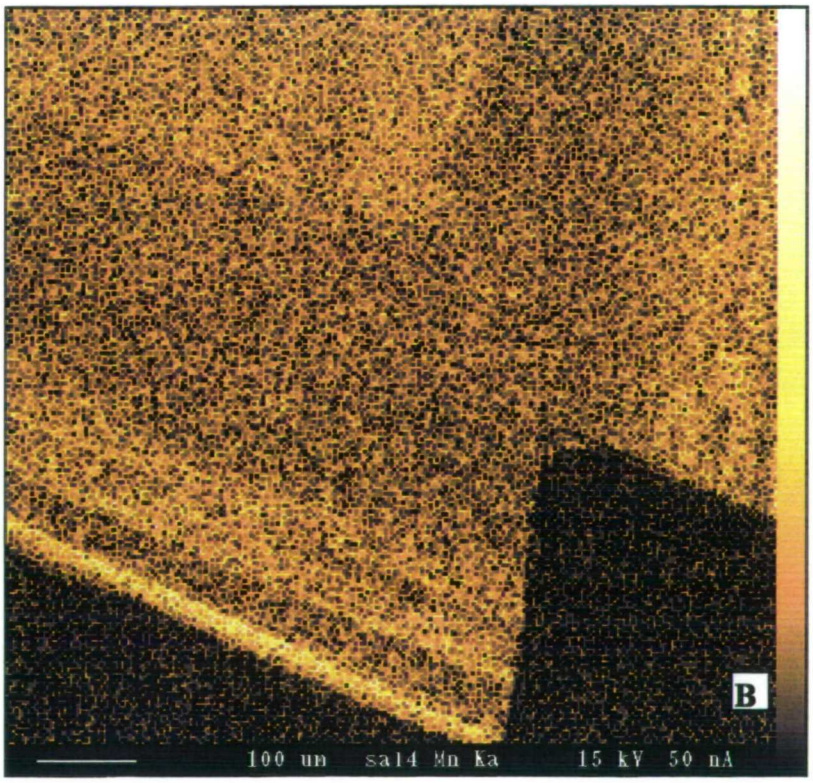
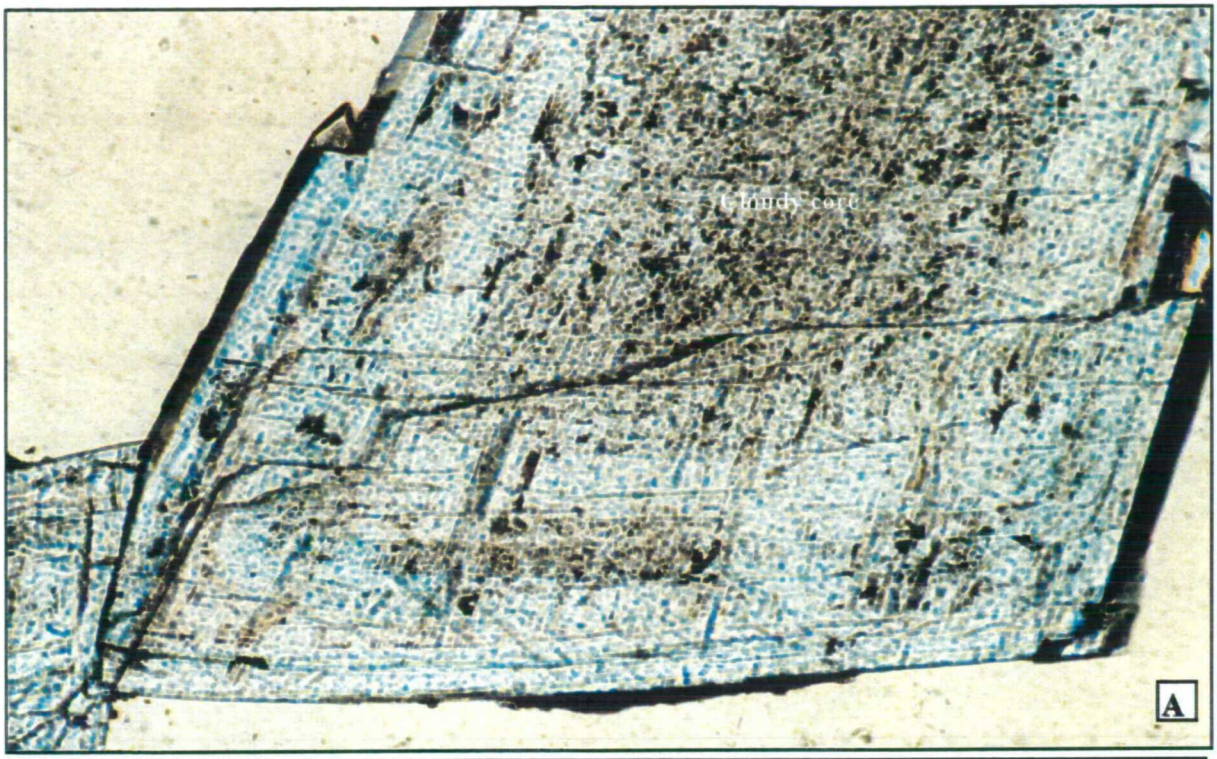


Plate 43.



A. Holycross, HC15/200.8: Photomicrograph (TrL) of D4 dolomite crystal.
B. D4 dolomite crystal exhibits alternating bright, moderate, dull and non luminescent cement stages; B, C, D, E, and F. Cement stage F is characterized by Fe, Mn rich zoning. Long axis = 1250µm.

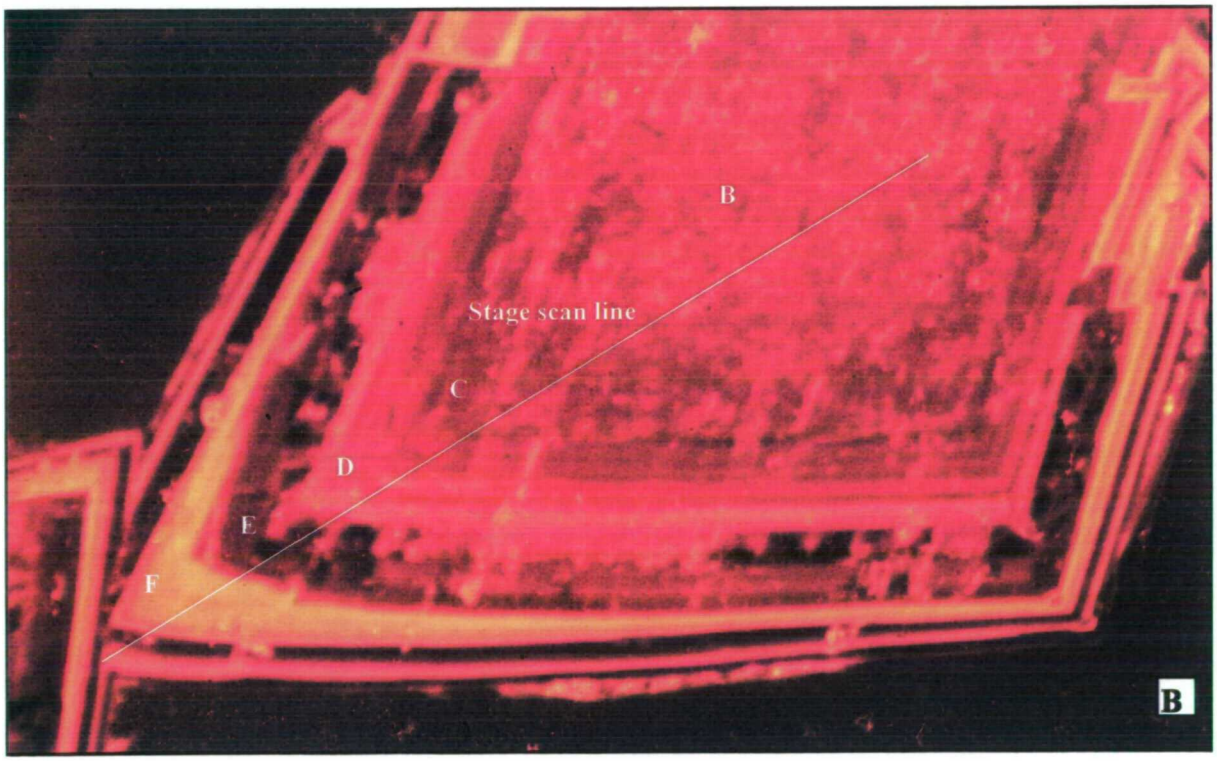
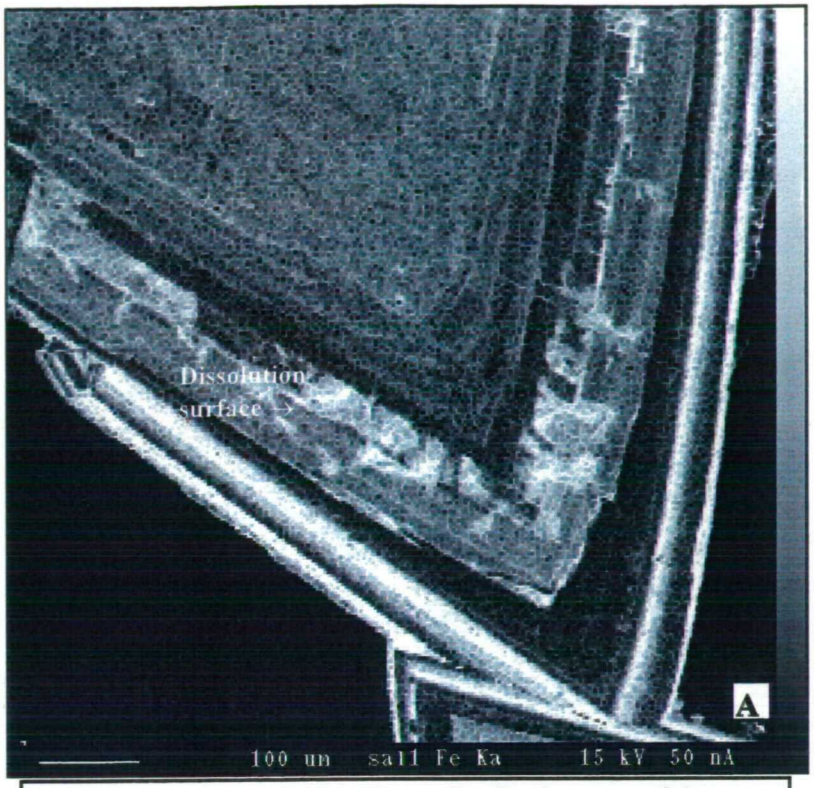


Plate 44.



A. Holycross, HC15/200.8: X-ray distribution map of the element Fe in D4 dolomite.
B. Holycross, HC15/200.8: X-ray distribution map of the element Mn in D4 dolomite.

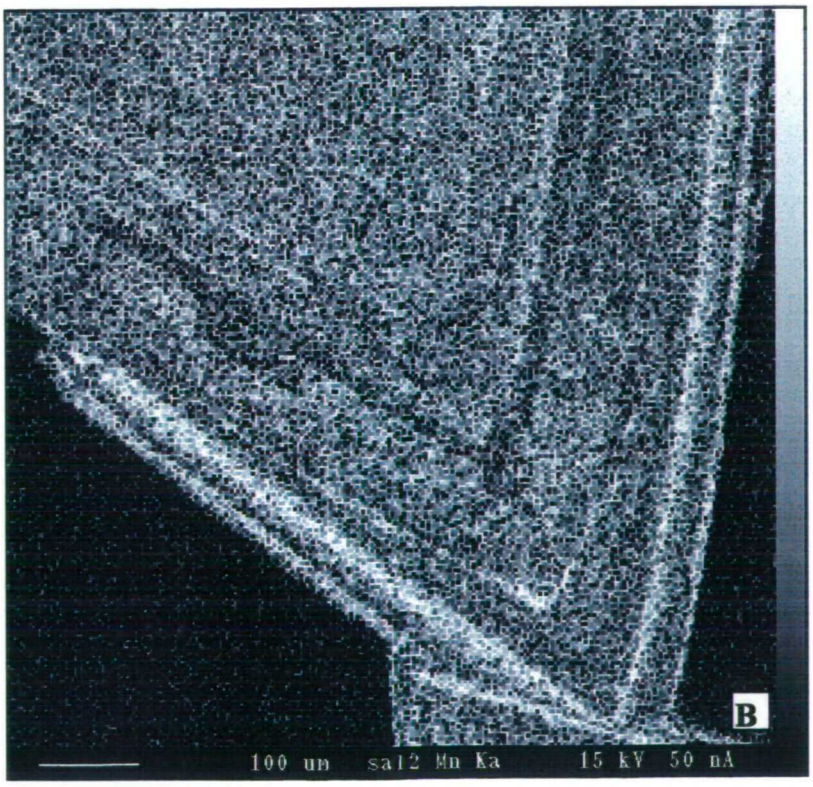
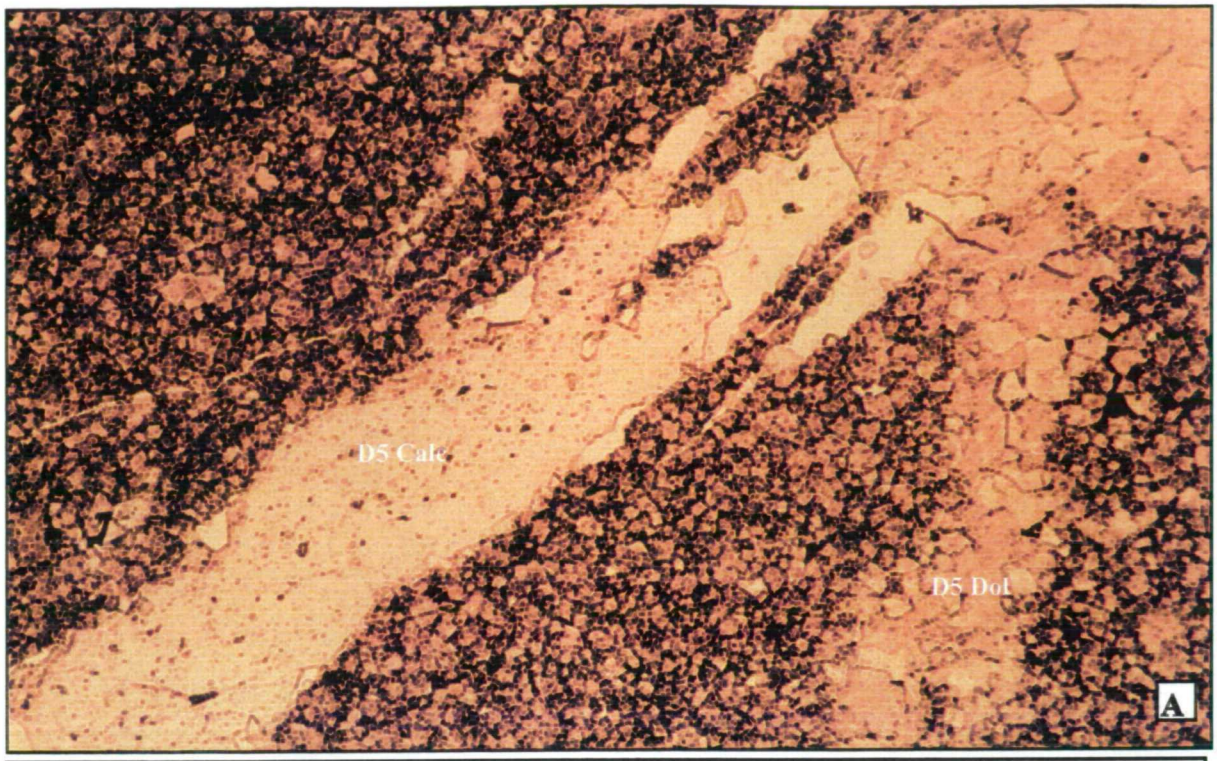


Plate 45.



A. Lisheen, 121/319.2: Photomicrograph (TrL) of a late ferroan dolomite vein (D5 Dol) cross-cut by a later calcite vein (D5 Calc).
B. The calcite vein exhibits bright, orange-yellow luminescence, the ferroan dolomite is non luminescent. Long axis = 1500μm.

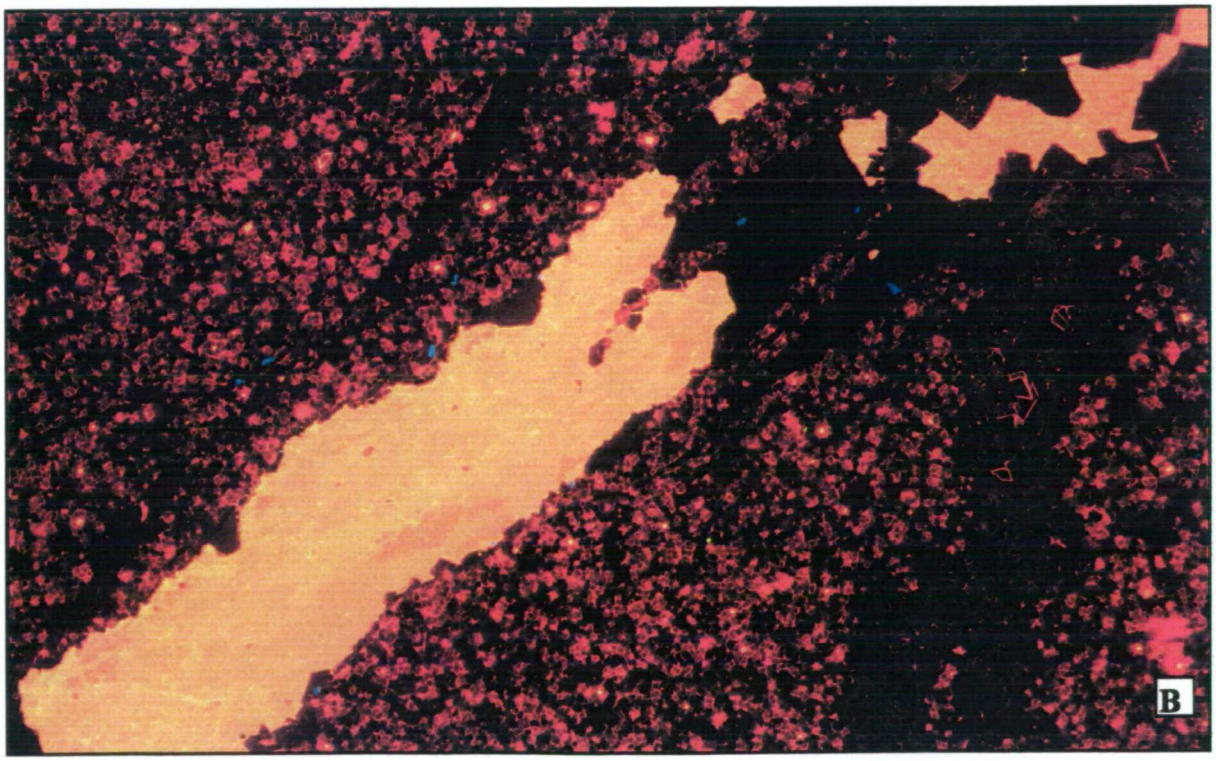
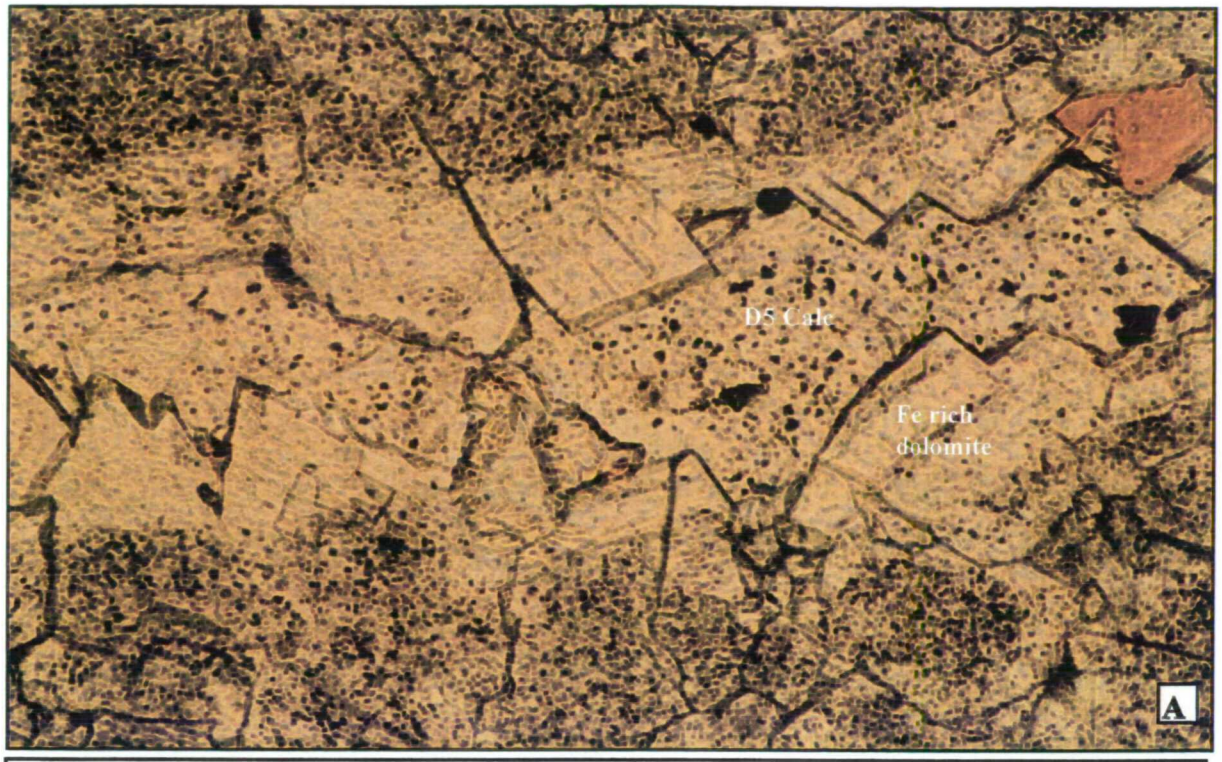


Plate 46.



A. Lisheen, 121/180.5: Photomicrograph (TrL) of late stage calcite (D5 Calc) post-dating an Fe rich dolomite vein. Both calcite and dolomite post-date D2 dolomite.
B. The calcite exhibits bright yellow luminescence, the dolomite vein displays dull red luminescent zones. Long axis =1250μm.

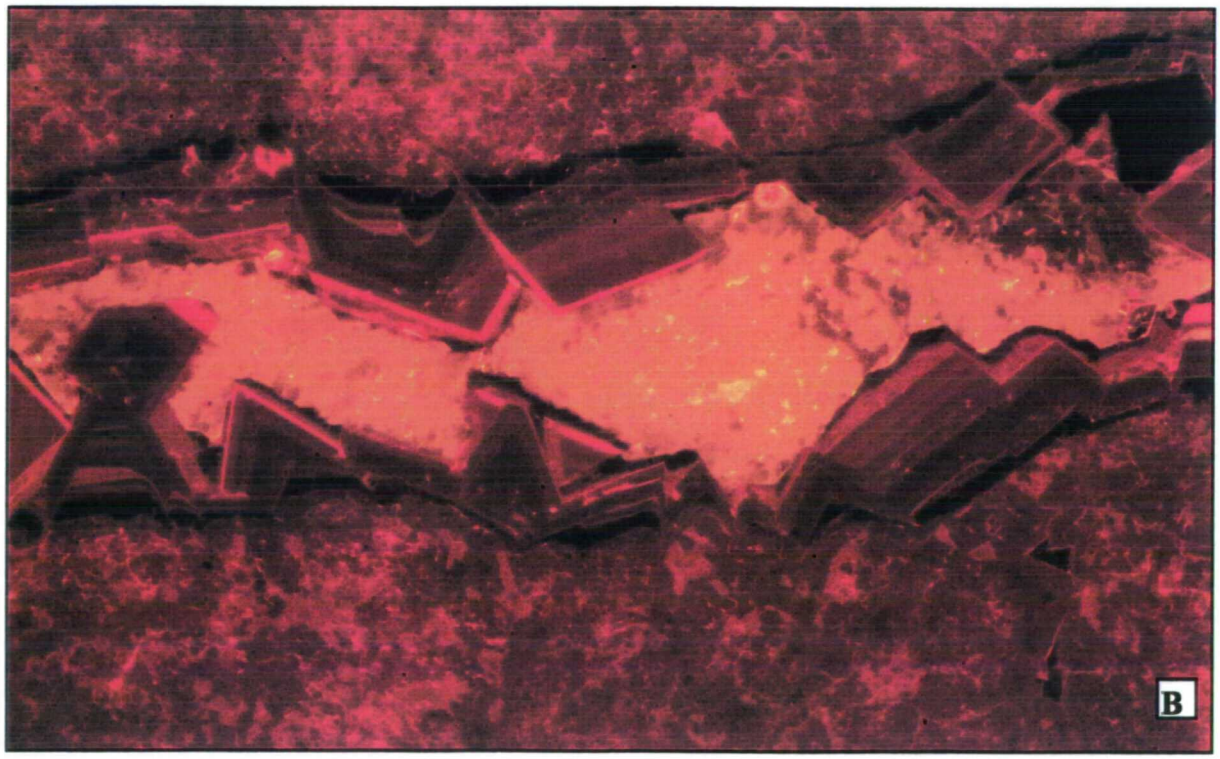


Plate 47.



A. Galmoy, G orebody. Chalcopyrite rich dolomite vein hosted within the Lower Ballysteen.

B. Galmoy, G orebody. Complex late carbonate veins. An early calcian dolomite is post-dated by a sphalerite bearing calcite vein, which is cross-cut by a minor pyrite bearing calcite vein.



Plate 48.



A. Rathdowney East: Abundant crystalline D4 dolomite with late vug fill calcite (D5 Calc).

B. Durrow, 2/961.9: Chalcopyrite and tennantite bearing dolomite vein (D5 Dol) hosted by dolomitized oolite. Disseminated pyrite associated with even later dolomite vein.

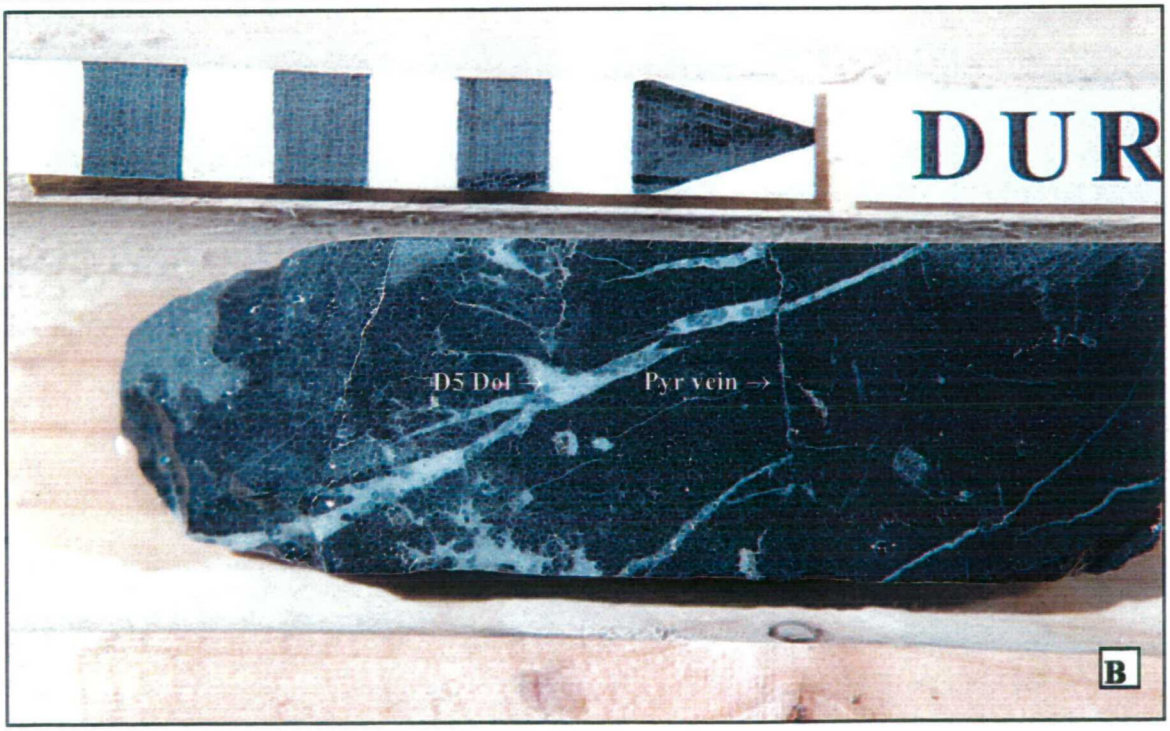


Plate 49.



A. Lisheen, 121/190.2: Massive fine grained pyrite, cross-cut and replaced by later sphalerite and galena, Main zone.

B. Lisheen, 262/159.85: Massive fine grained sulphide, Derryville zone.



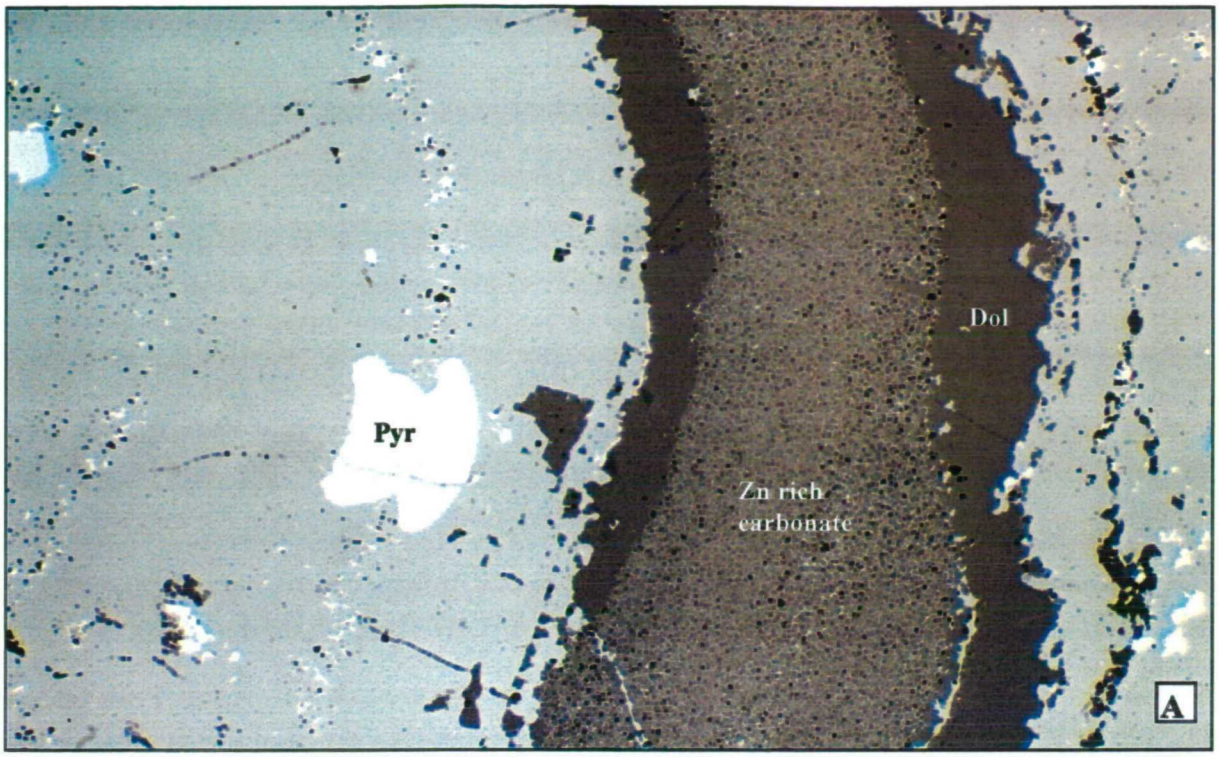
Plate 50.



A. Lisheen, 121/189.3: Fine crystalline, weakly colloform pink-brown sphalerite in poorly developed D2 dolomite.
B. Lisheen, 121/192.8: Massive fine grained sulphide, with disrupted colloform textures.



Plate 51.



A. Lisheen, 262/159.85 (Reflected light): Colloform sphalerite, with concentrically zoned pyrite, granular Zn rich carbonate and dolomite.

B. Lisheen, 262/159.85 (Crossed Nicols): Colloform sphalerite, with concentrically zoned pyrite, granular Zn rich carbonate and dolomite. Long axis of photomicrograph = 1400µm.

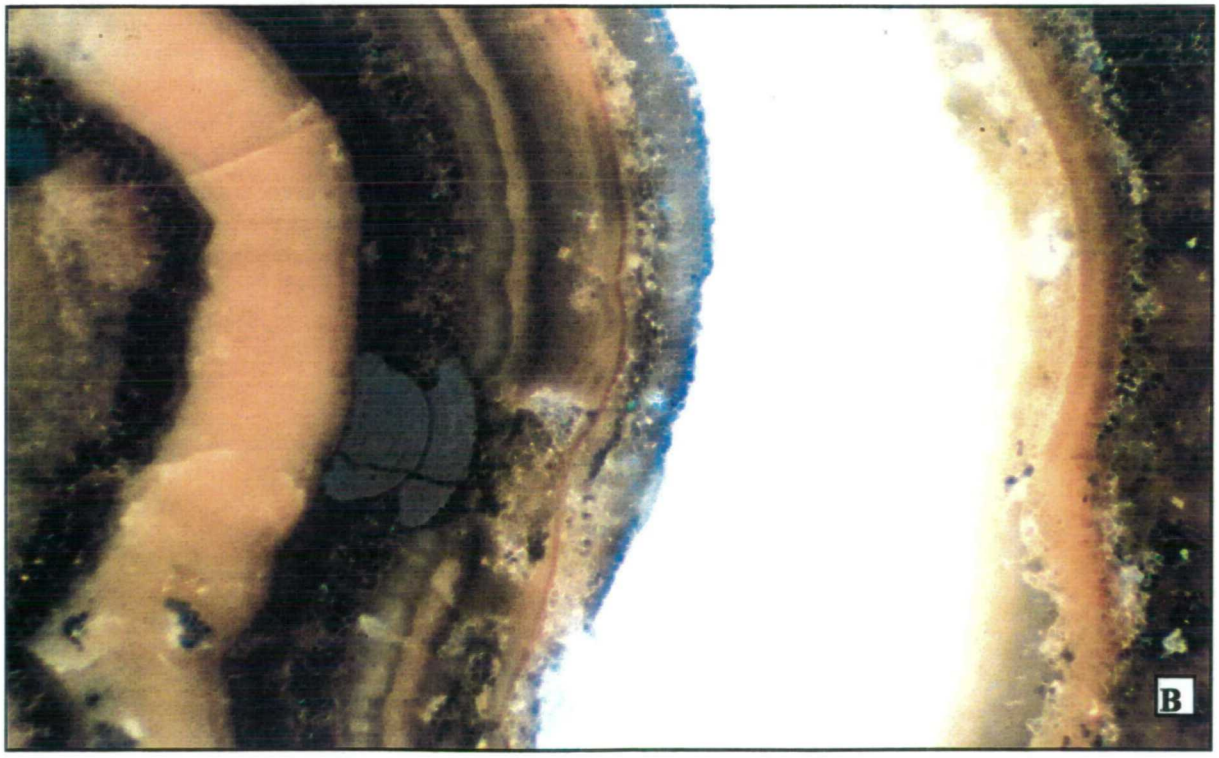
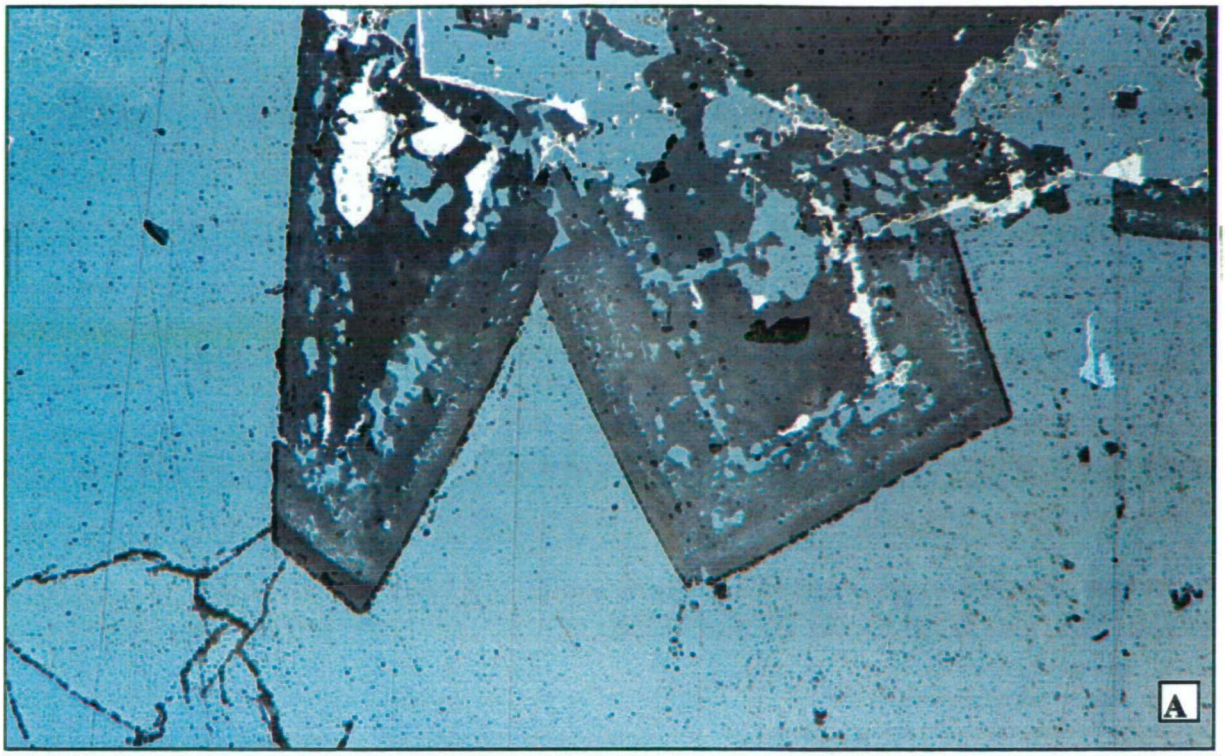


Plate 52.



A. Lisheen, 416/193.6: Early formed pyrite and sphalerite incorporated into the growth zones of gangue dolomite rhombs. The rhombs occur within a paragenetically later colloform sphalerite.
B. Lisheen, 325/146.20: Mixed sulphide assemblage with sphalerite pseudomorphously replacing barite. Long axis of photomicrograph A. = 700μm, B. =1400μm.

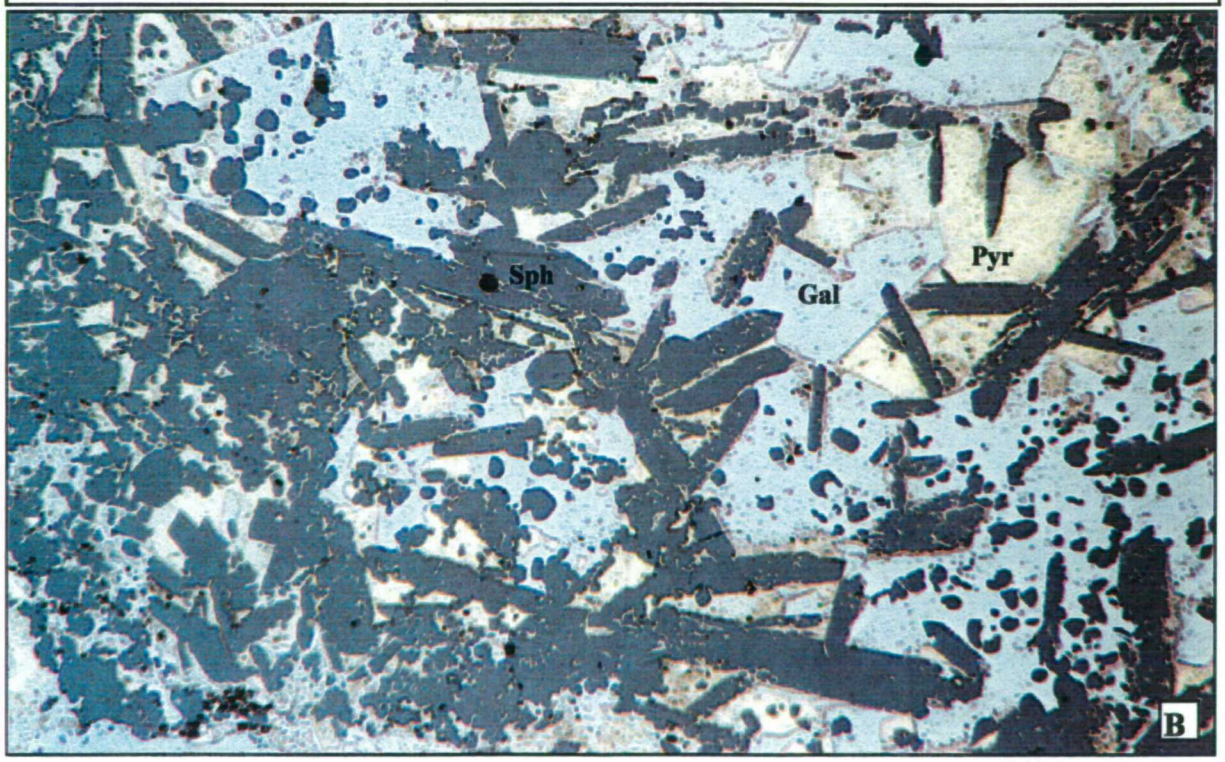
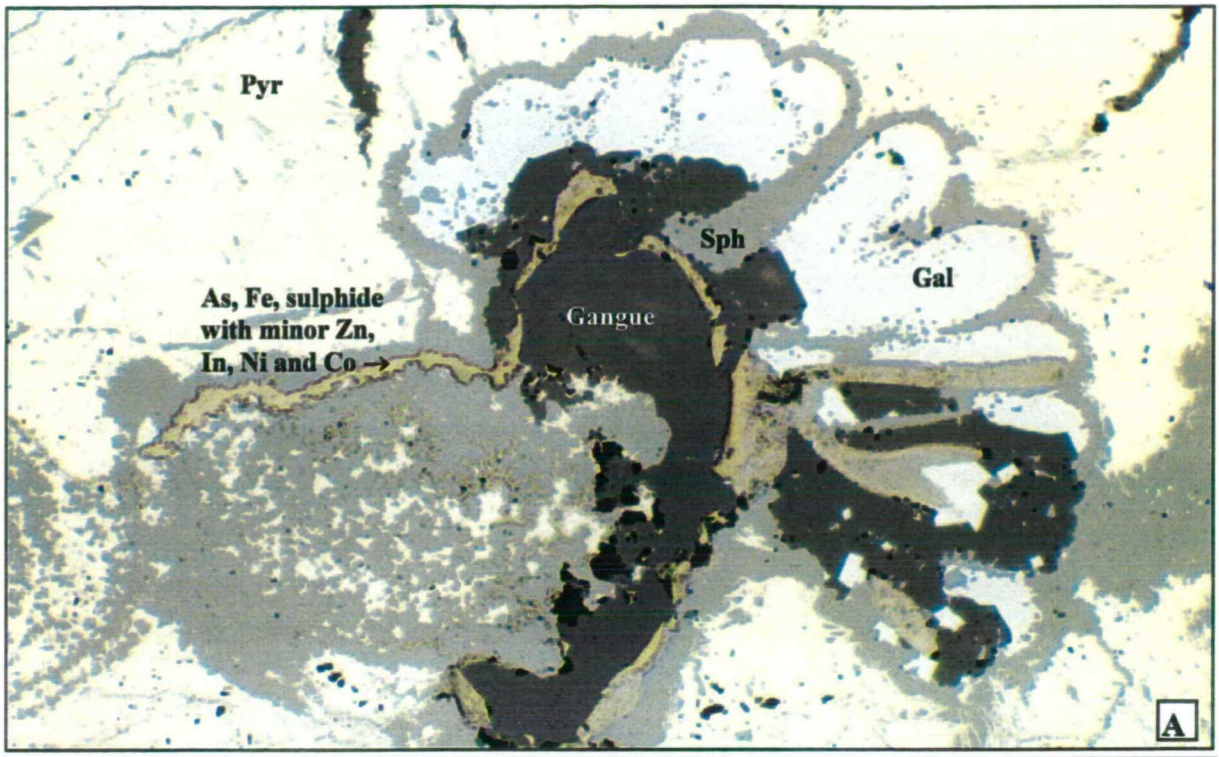


Plate 53.



A. Lisheen, 137/134.9: Selective replacement of foraminifera (Endothyrid). Long axis of photomicrograph = 1400μm.

B. Lisheen, 402/196.0: Open-space filling euhedral galena, post-dated by concentrically zoned pyrite, late sphalerite and gangue carbonate. Long axis of photomicrograph = 2800μm.

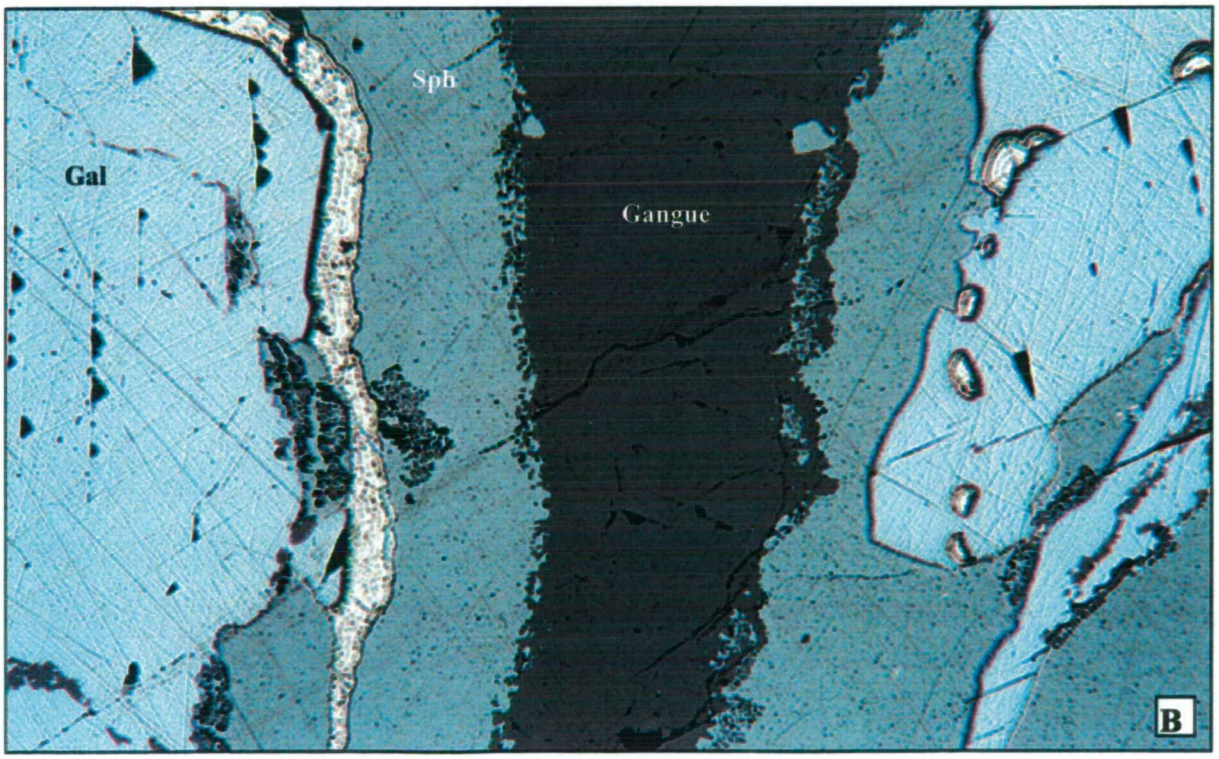
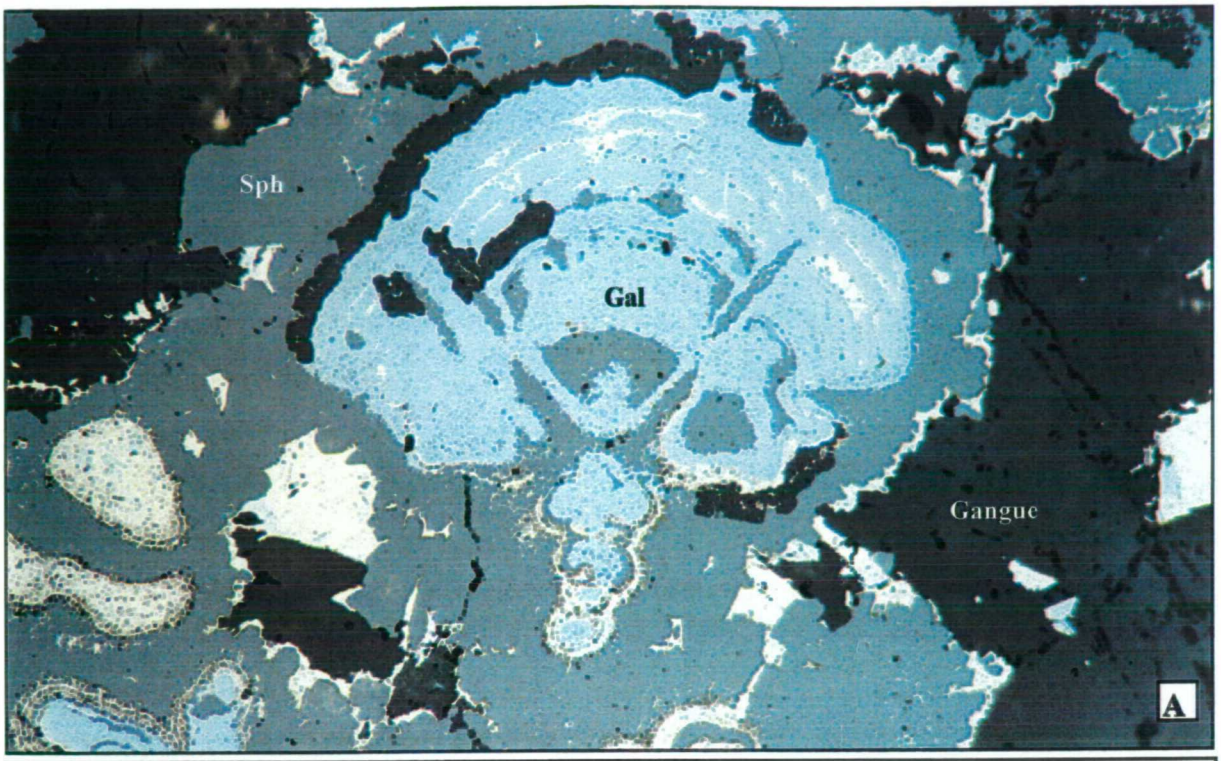


Plate 54.



A. Lisheen, 171/172.7: Selective replacement of foramanifera by galena. Long axis of photomicrograph = 700µm.
B. Lisheen, 394/164.30: Selective replacement of ooid by sphalerite and galena. Long axis of photomicrograph = 1400µm.

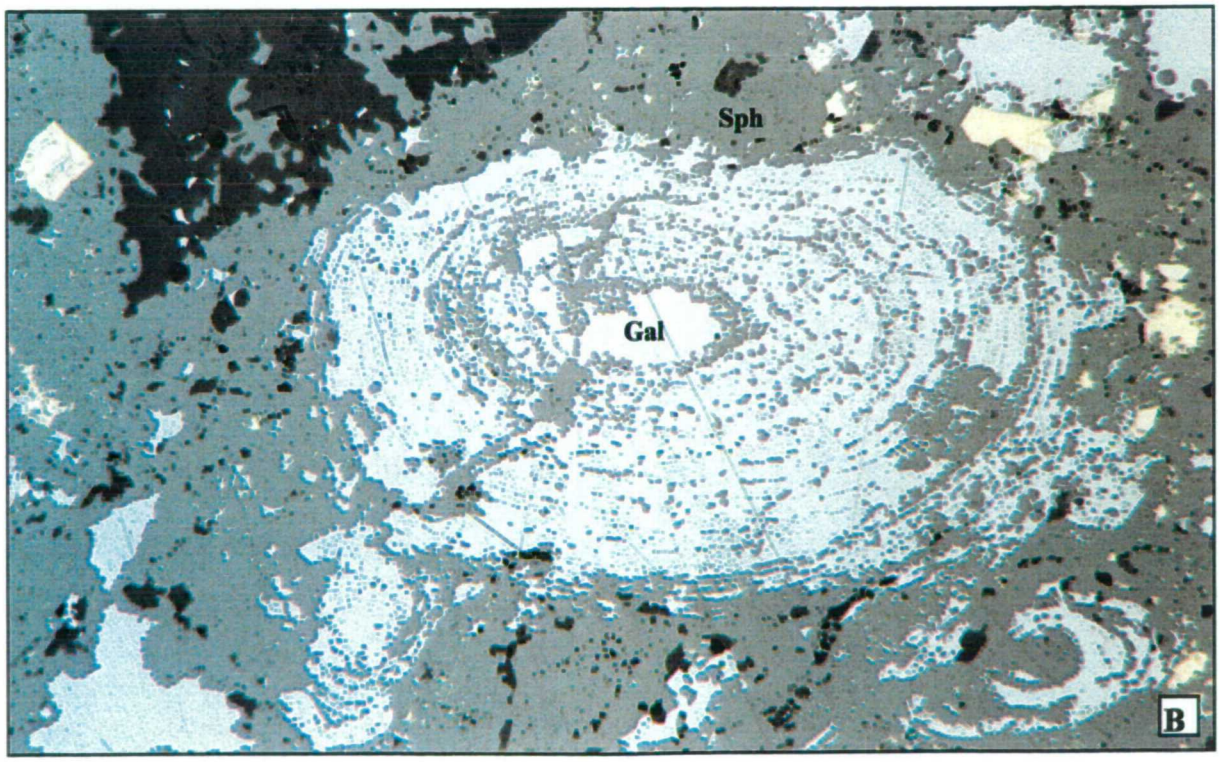
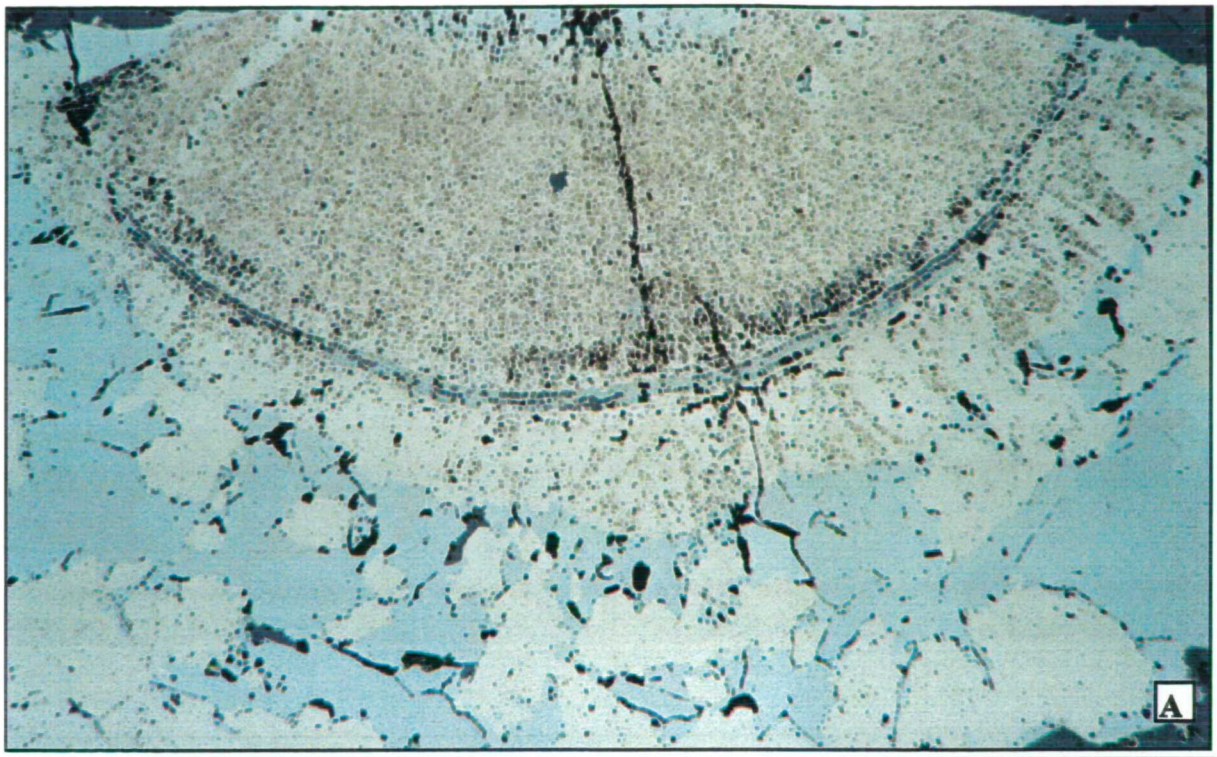


Plate 55.



A. Lisheen, 420/190.7: Massive colloform iron sulphides. Pyrite with minor gangue and sphalerite inclusions overgrown by subhedral pyrite, marcasite. Long axis of photomicrograph = 700μm.
B. Lisheen, 394/164.30: Massive colloform, mixed sulphide assemblage. Pyrite pre-dates ore-stage sphalerite and galena. Long axis of photomicrograph = 2800μm.

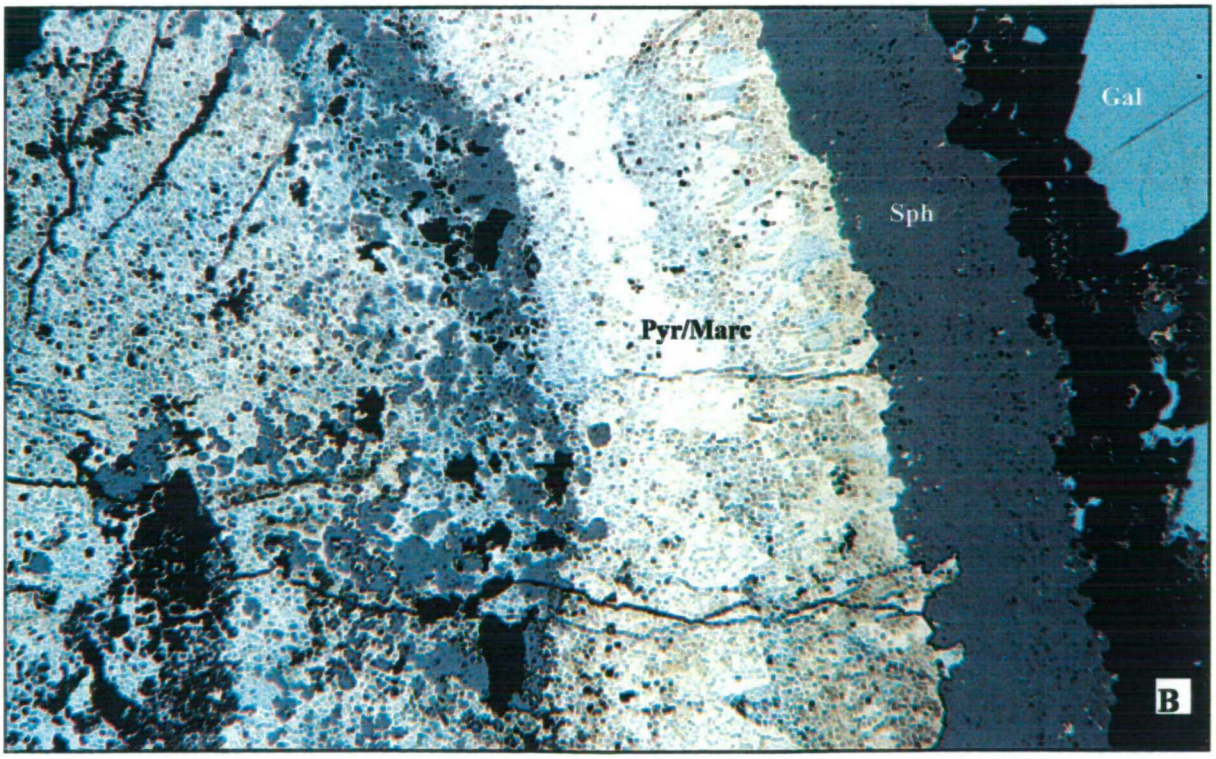
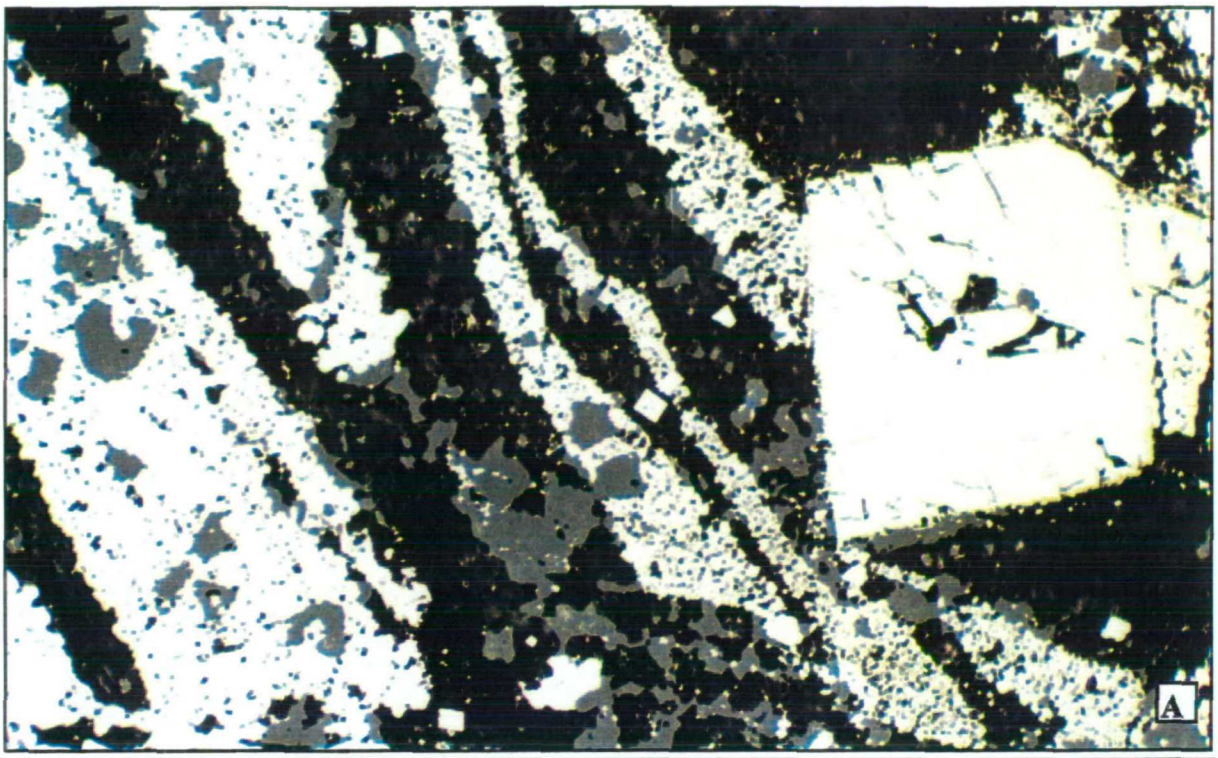


Plate 56.



A. Lisheen, 262/162.1: Fine grained granular pyrite pseudomorphously replacing elongate barite laths. Long axis of photomicrograph = 700μm (in oil).

B. Lisheen, 262/159.1: Massive pyrite-marcasite exhibiting brittle fracture and cataclasis. Pyrite is replaced along fractures by later sphalerite. Long axis of photomicrograph = 700μm (in oil).

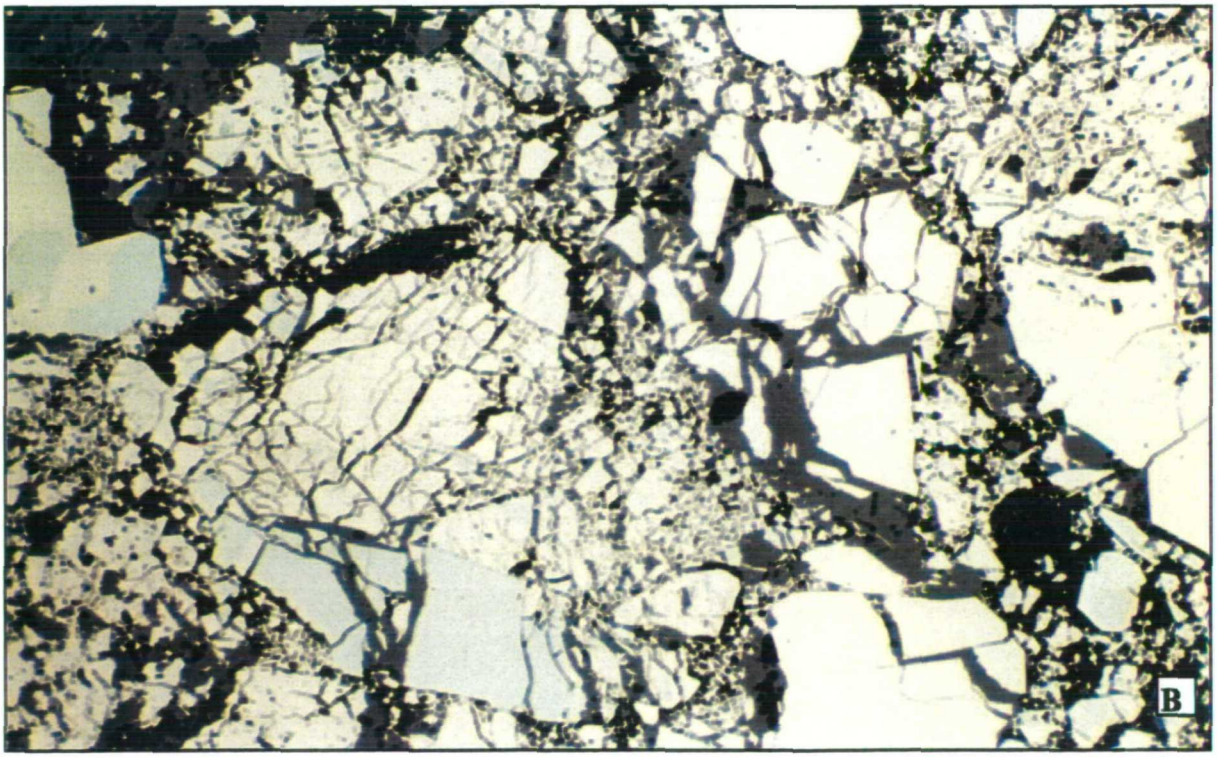


Plate 57.



A. Galmoy, G West orebody: Massive fine grained buff coloured sphalerite.
B. Galmoy, CW orebody, CW10: Massive fine grained sulphide with coarse crystalline yellow sphalerite and euhedral galena. Sample = 12cm long.

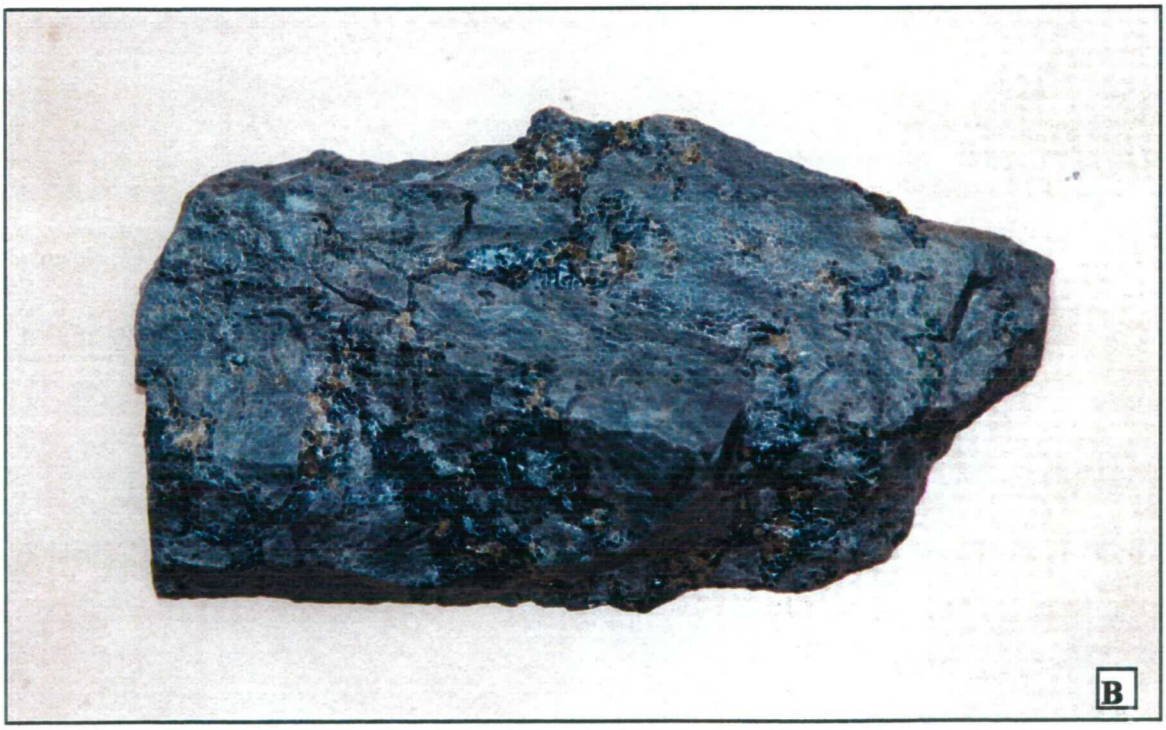
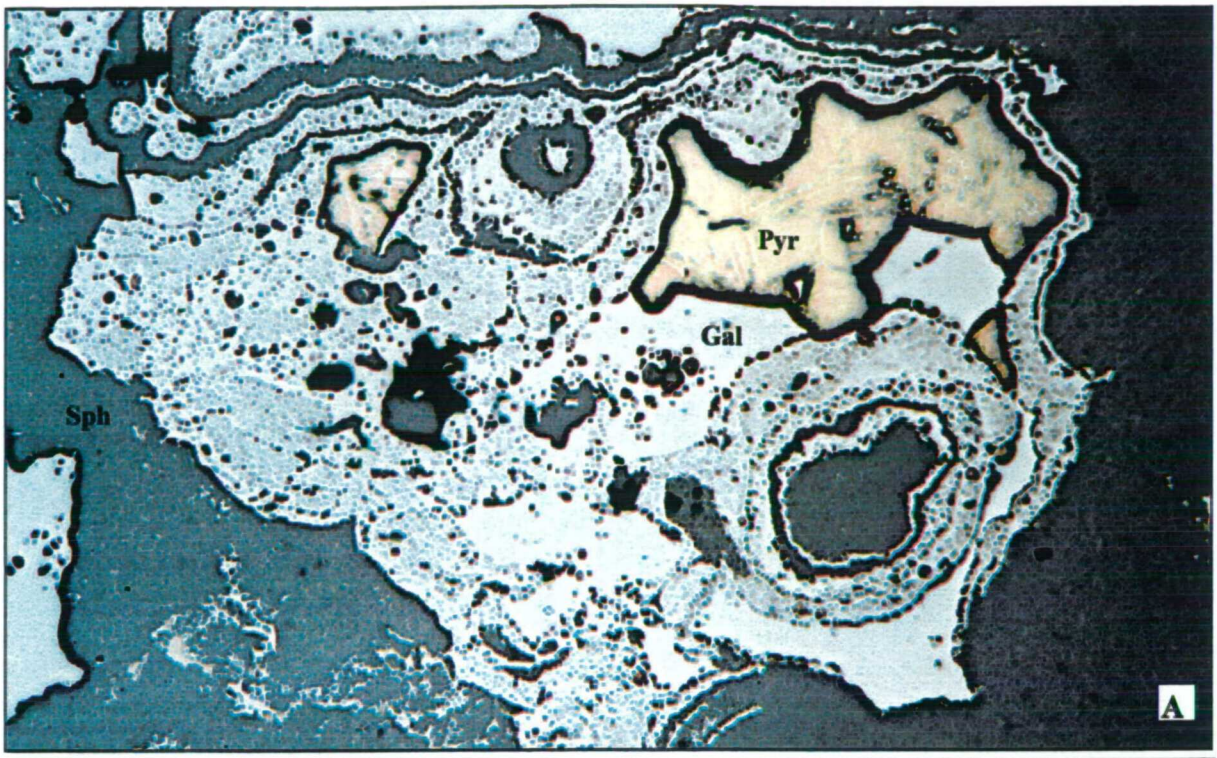


Plate 58.



A. Galmoy, G North-East orebody, MG18/90.0: Colloform textures displayed by ore-stage sphalerite and galena. Long axis of photomicrograph = 2800μm.

B. Galmoy, K orebody, GY382/86.0: Zoned crystalline sphalerite. Long axis of photomicrograph = 1400μm.

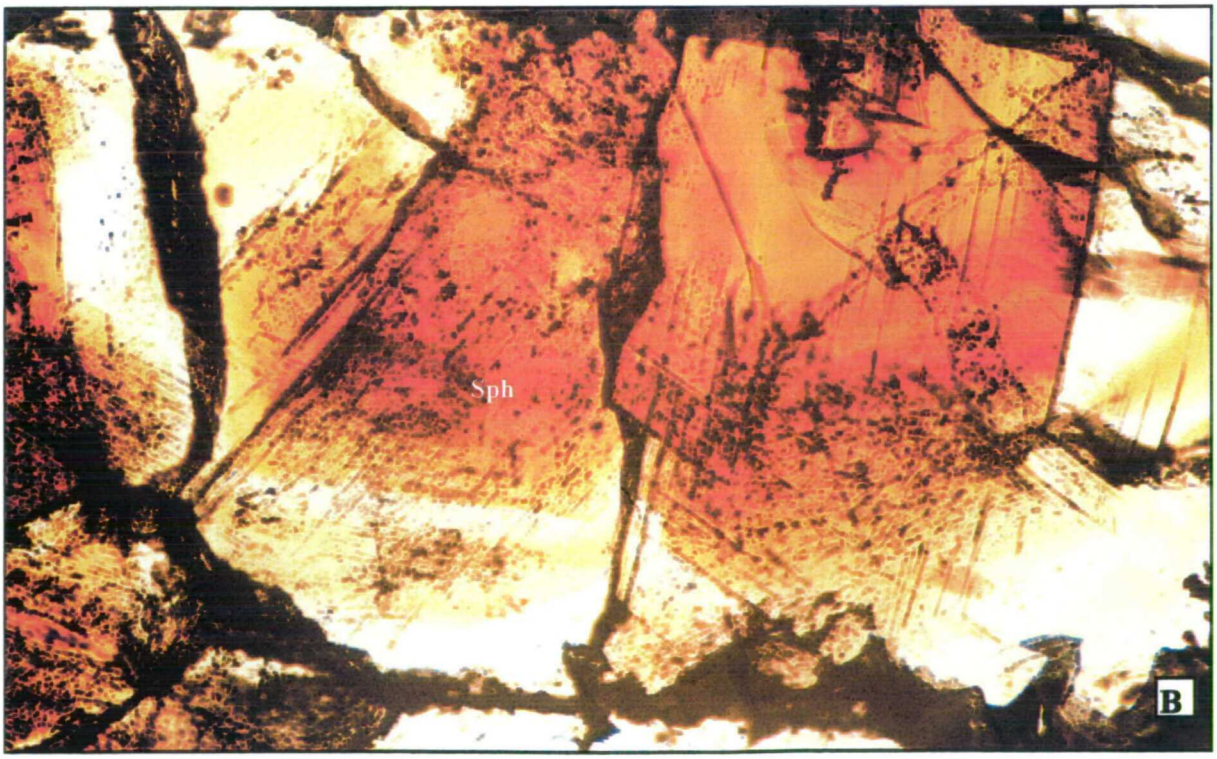
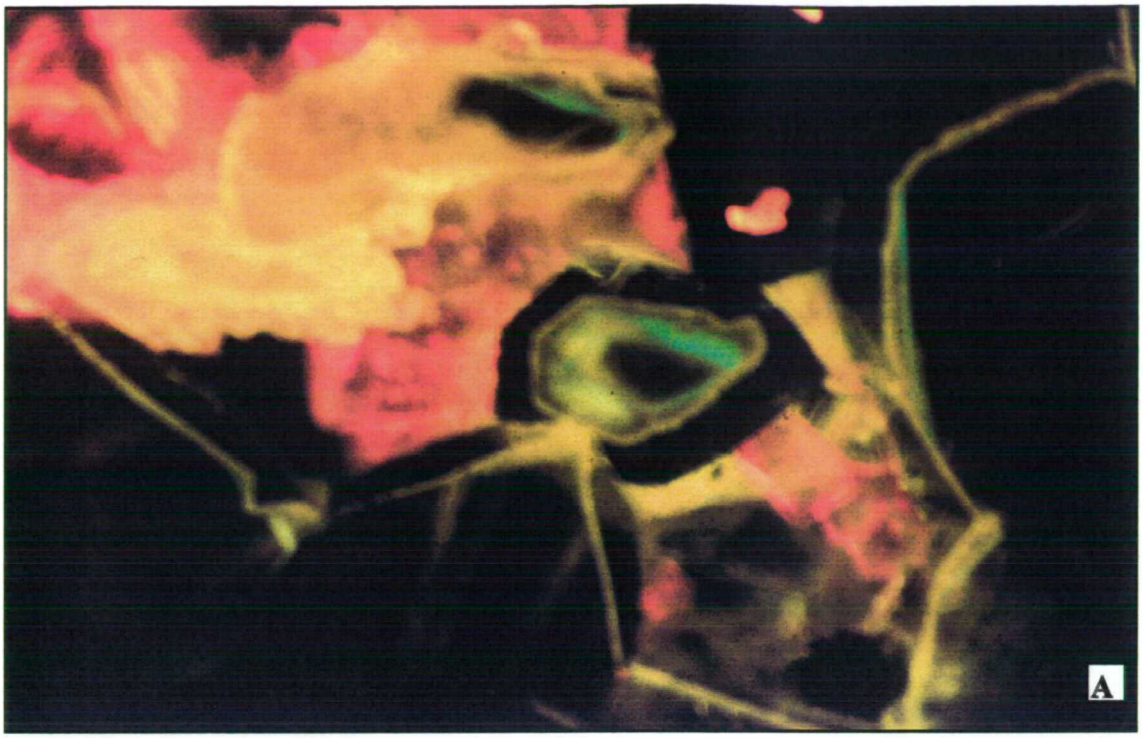


Plate 58a.



A. Galmoy, GY382/86.0: Distinct CL zoning in crystalline sphalerite.

B. Galmoy, GY355/95.0: Distinct blue-purple luminescent zone in late colloform sphalerite. Long axis of photomicrograph = 1250μm.

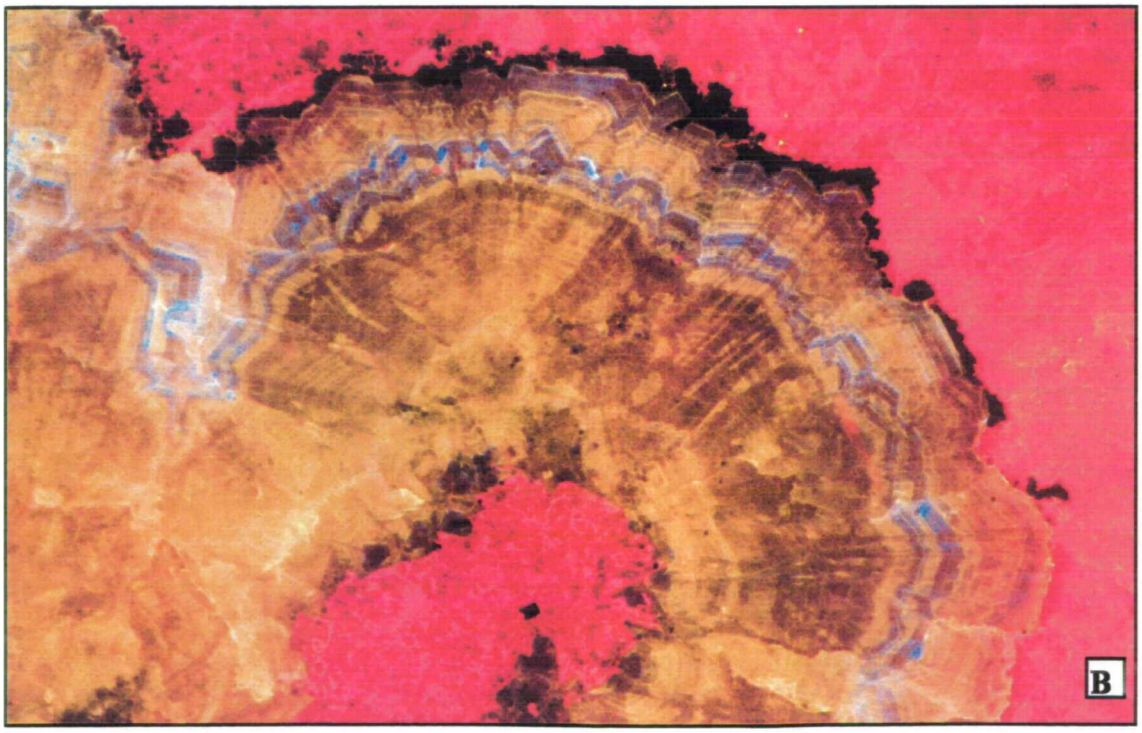
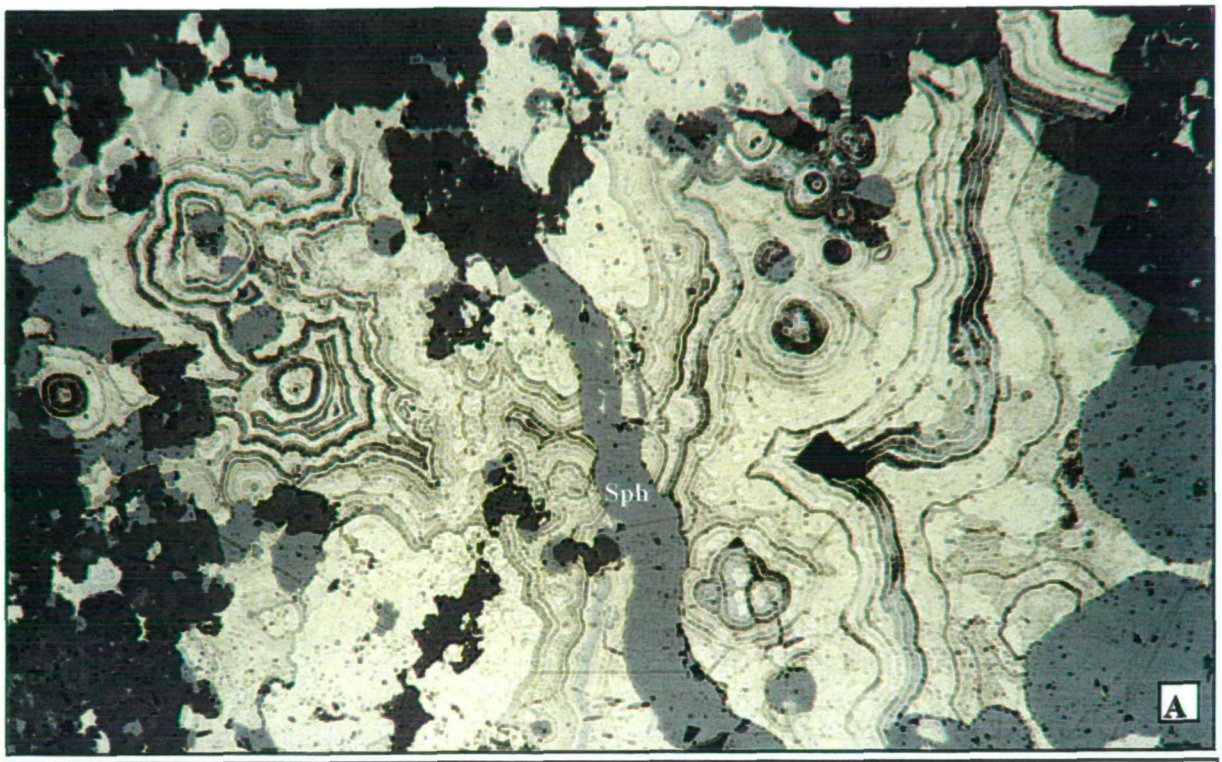


Plate 59.



A. Galmoy, CW orebody, 2(0134): Zoned colloform pyrite cross-cut by sphalerite. Long axis of photomicrograph = 700µm.

B. Durrow, DUR1/910.0: Subhedral pyrite locally replaces ooids, sphalerite replaces pyrite along fractures. Long axis of photomicrograph = 1400µm.

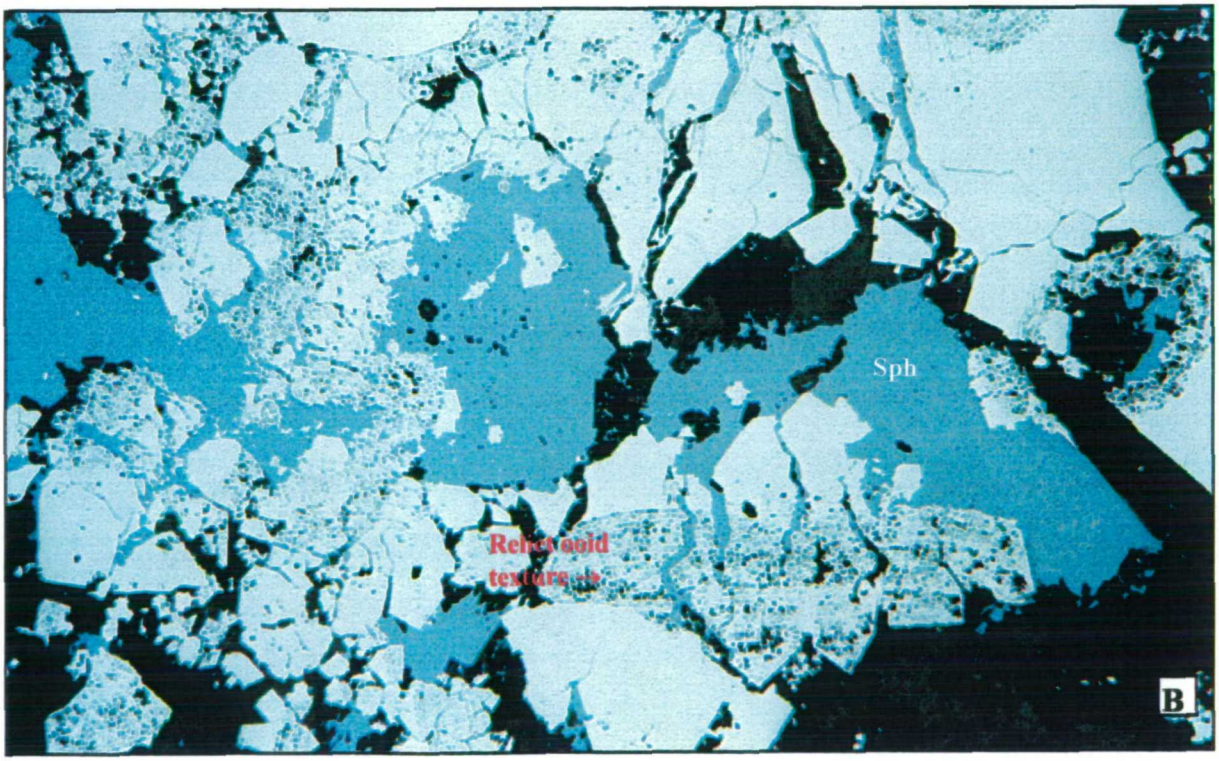
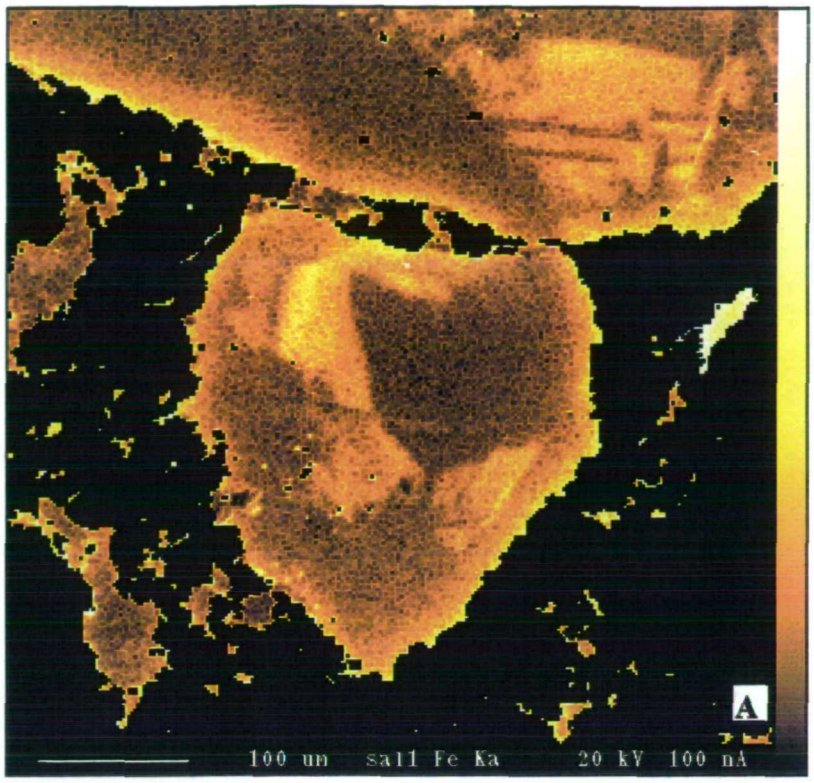
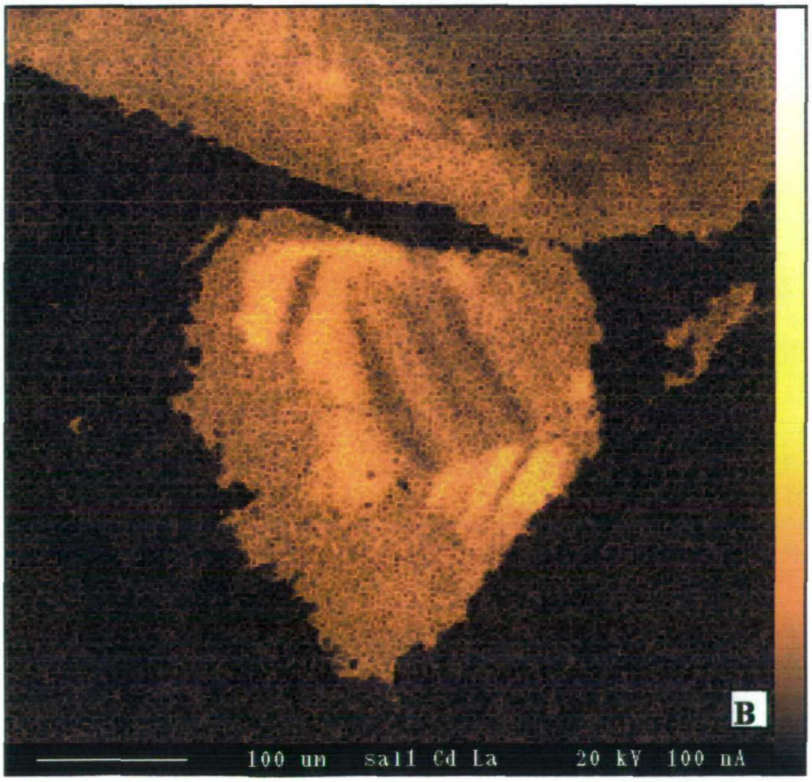


Plate 60.



A. Durrow, DUR1/910.0: X-ray distribution map of the element Fe in sphalerite.
B. X-ray distribution map of the element Cd in sphalerite.



CHAPTER 4: ISOTOPE STUDY

CHAPTER 4: ISOTOPE STUDY

4.1 INTRODUCTION

Stable isotopes are useful because, unlike radiogenic isotopes, isotope ratios of an element are not a function of time or the chemical behaviour of the element and the distribution of the isotopes between different phases is primarily a function of temperature. Stable and radiogenic isotope work on carbonate-hosted mineral deposits in Ireland has proved to be a unifying feature in ore genetic studies (Gallagher *et al.*, 1992). Using stable isotope analyses it is possible to constrain the source(s) of components (sulphur, carbon, water) and also the geometry of the mineralizing systems. Using radiogenic lead isotope analyses it is possible to constrain the source(s) of lead and also the timing of mineralization.

Interpretation of isotope data for sulphur and carbon bearing species is complicated by the wide range of oxidation states these can occur as in nature. For example sulphur exists in the -2 valence state in sulphides (e.g. ZnS, H_2S), but the +6 valence state in sulphates (SO_4^{2-}); carbon occurs in the -4 valence state in organic compounds (CH_4), or the +4 valence state in carbonates (CO_3^{2-}). There are many different mechanisms (biological and chemical) that control these different redox states and large equilibrium fractionation effects exist between the oxidized and reduced species, with a tendency towards enrichment of the heavier isotopes e.g. ^{34}S and ^{13}C in compounds with higher oxidation states. In addition, significant kinetic fractionation effects are often associated with redox reactions, particularly with reduction (Ohmoto, 1986). As a result, variations in isotopic composition of hydrothermal systems may occur due to changes in temperature, pressure, pH, and fugacity. Precipitation of minerals may also remove a significant amount of C and S from the fluid phase, resulting in some of the temporal isotopic variations that are seen in many ore deposits.

Conventional techniques were employed for determining S, C, and O isotopic compositions. Relatively large sample sizes (e.g., 5-10mg) of sulphide and carbonate minerals were required in order to generate yields >10μmol of SO_2 and CO_2 Individual sulphide, carbonate and lead samples were drilled out of core samples with a dentist-type drill. Repeat analyses on split samples were carried out for some sulphides. Separation of a single mineral phase representing a specific time in the growth history was difficult because of the relatively large quantity of sample required. Thus, individual cement zones within dolomites, and zones within sulphides have not been analyzed in the course of this isotope study.

4.1.1 Aims and Objectives of the Isotope Study

The major objectives of the sulphur isotope study were to: (1) determine the source(s) of sulphur in the Rathdowney Trend deposits and prospects; (2) to evaluate the relative importance of biogenic, abiogenic and mixing processes in mineralization, particularly at Lisheen and Galmoy; and (3) to compare $\delta^{34}S$ of sulphides at Lisheen (in three spatial dimensions, plus time via mineral paragenesis) and Galmoy, with regional samples from the Rathdowney Trend. Variations in $\delta^{34}S$ both at Lisheen and Galmoy, and in prospects in the Rathdowney Trend, should indicate the relative importance of different sulphur source(s) and hopefully identify the components critical to the formation of economic mineralization.

The major objectives of the carbon and oxygen isotope study were to: (1) constrain the origin of $\delta^{13}C$ in gangue dolomite and calcite; (2) use $\delta^{18}O$ from hydrothermal carbonates to calculate the oxygen isotopic composition of mineralizing fluid(s) as an indicator of fluid source; and (3) in combination with $\delta^{13}C$, to monitor temporal and spatial variations in fluid-rock interaction, both within the deposits and for comparison with regional samples from the Rathdowney Trend prospects.

The objective of the lead isotope study was to use lead isotopic ratios to confirm or refute the general geographic variation in lead isotope ratios observed in the deposits and evaluate potential sources for lead in the southern Irish Midlands. $^{206}Pb/\ ^{204}Pb$ isotope ratios of 18.20-18.30 are characteristic of Pb from the Lower Palaeozoic basement in the area; conversely, studies of the ORS indicate a higher ratio of 18.35 -18.50.

4.2 SULPHUR

Applications of sulphur isotopes in ore deposit research address issues such as source, transport, and precipitation mechanisms. The source of sulphur in low temperature base-metal mineralizing hydrothermal systems has important implications for modelling of ore-forming processes. It is still not clear whether metals and reduced or oxidized species are commonly carried in the same brine, or whether metal sulphide precipitation occurs because of the later addition of H_2S or other S species (Anderson, 1975; Sverjensky, 1984).

4.2.1 Sample Selection and Experimental Technique

A total of 188 analyses on 90 core samples were carried out in this study. Sulphur isotope data (Appendices D1,2,3) have been collected from a range of sulphides in the Rathdowney Trend, including early disseminated, main ore-stage, and texturally later vein hosted and vug fill mineralization (Figures 4.1, 4.2). Pyrite, galena and sphalerite constitute the bulk of the data, with limited data from chalcopyrite and tennantite group minerals.

Sulphur was extracted as SO_2 from sulphides by fusing samples (5-10mg) under vacuum at 1076°C in a Cu_2O (200mg) matrix (Robinson and Kusakabe, 1975). Sulphur was extracted as SO_2 from sulphates following the method of Coleman and Moore (1978). SO_2 was analyzed on a VG SIRA II mass spectrometer to obtain values of $\delta^{66}SO_2$, which were converted to $\delta^{34}S$. Standard correction factors were then applied (e.g. Craig, 1957). Results are given in standard $\delta^{34}S$ ‰ notation relative to the Cañon Diablo troilite (CDT) international standard. Reproducibility based on full replicate analyses of internal laboratory standards (CP1, Z40), and an international standard (NBS 123), was ±0.2 ‰ (1σ).

4.2.2 Results

Sulphur isotope data are presented in frequency histograms. Frequency histograms of $\delta^{34}S$‰ (CDT) are subdivided according to mineralogy, paragenetic stage, mineralization style, and location for Lisheen and Galmoy deposits, and Rathdowney Trend prospects.

4.2.2a Lisheen Deposit

A total of 119 analyses were carried out on 53 core samples from Lisheen. Main, Derryville, North, and Bog Zone ore was sampled in detail in order to constrain spatial variations in $\delta^{34}S$. Pyrite, sphalerite, and galena sulphides constitute the bulk of the isotope data, with limited data from chalcopyrite and barite (Appendix D1).

$\delta^{34}S$ values at Lisheen range from -44.1 to 11.8‰, with a mean value of -13.7‰ (Figures 4.3, 4.4). Main ore-stage sulphides (Figure 4.4) always have negative $\delta^{34}S$ values and fall dominantly within the range -4 to -20‰, with a modal value of -10‰.Very low $\delta^{34}S$ values in the range -30 to -44‰ are only observed in pre ore-stage disseminated pyrite. Late ore-stage vein-hosted and vug fill sulphides fall within the range -20 to +12‰, whilst post ore-stage sulphides fall within the

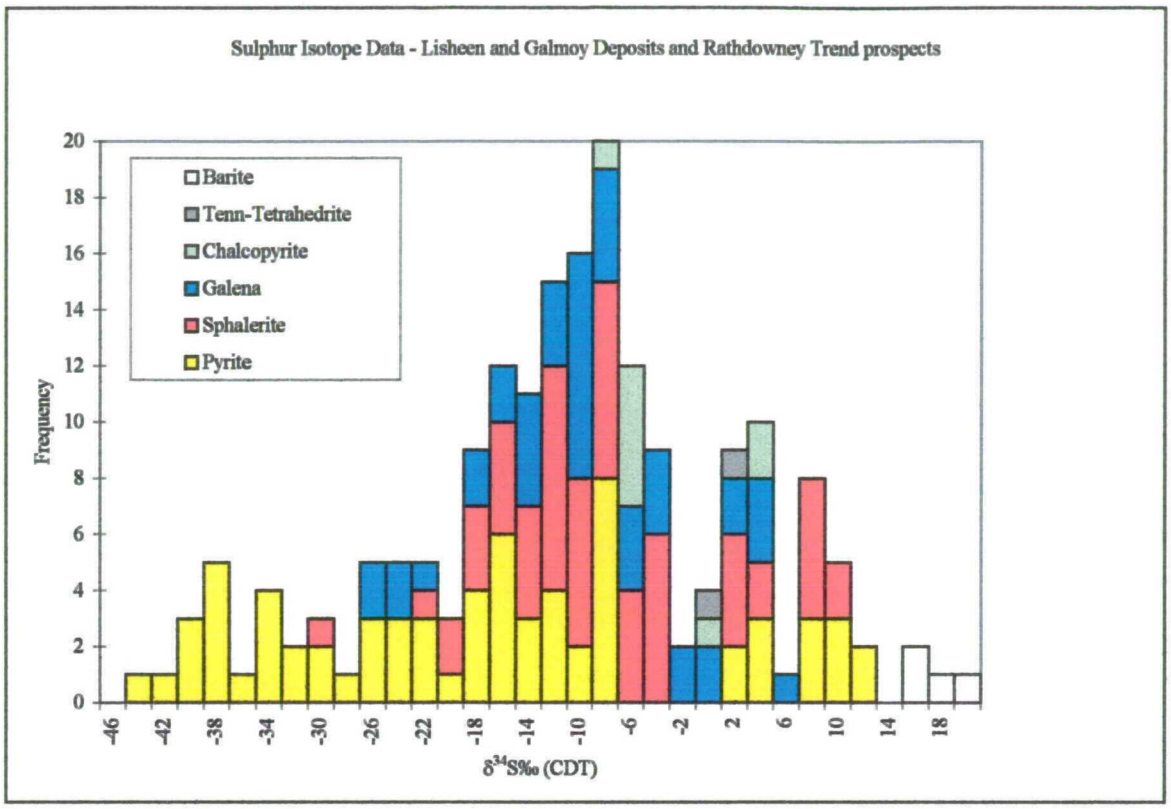


Figure 4.1 Frequency histogram of $\delta^{34}S$ (‰) of all sulphur-bearing phases in the Rathdowney Trend subdivided according to mineralogy.

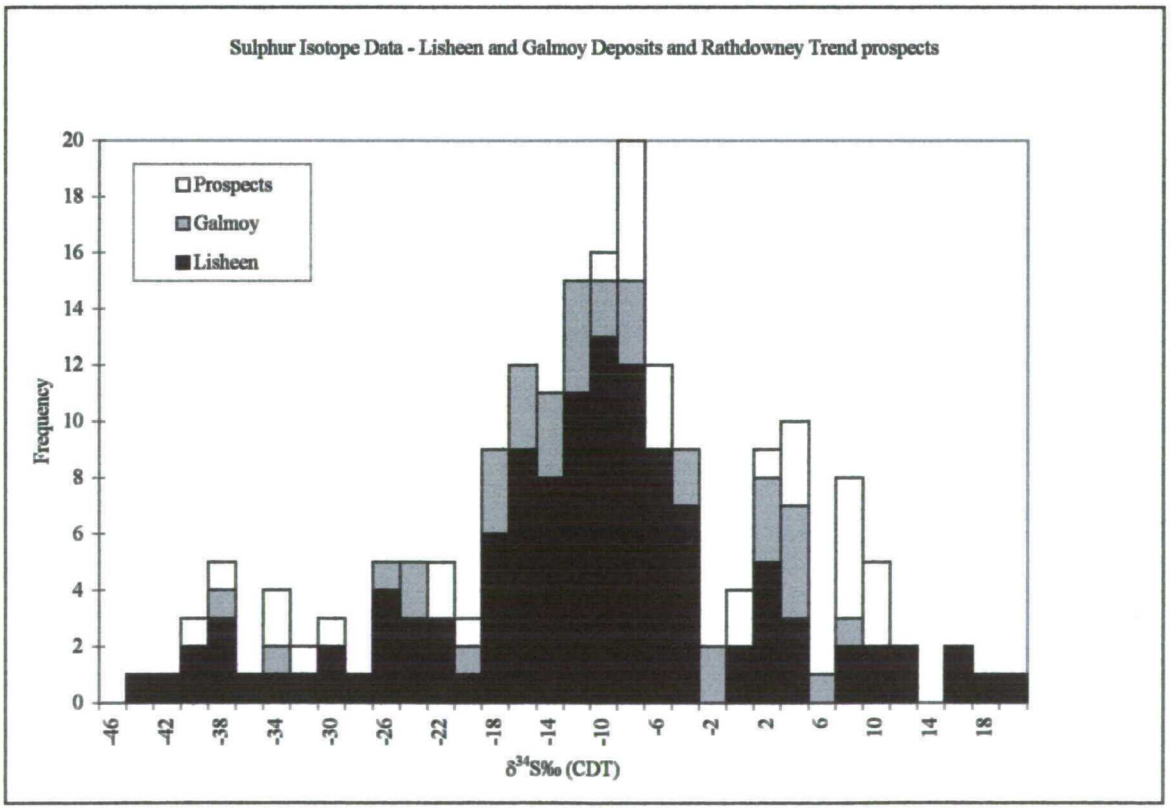


Figure 4.2 Frequency histogram of $\delta^{34}S$ (‰) of all sulphur-bearing phases in the Rathdowney Trend subdivided according to location.

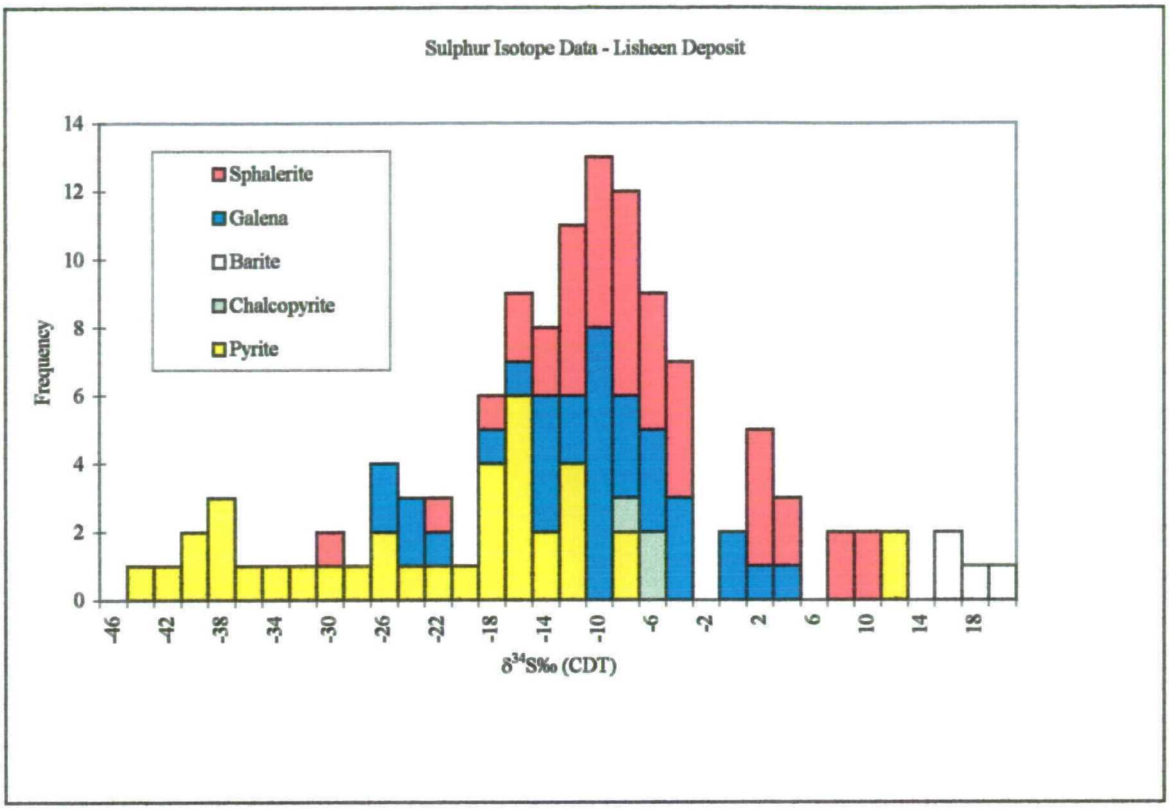


Figure 4.3 Frequency histogram of $\delta^{34}S$ (‰) of all sulphur-bearing phases in the Lisheen deposit subdivided according to mineralogy.

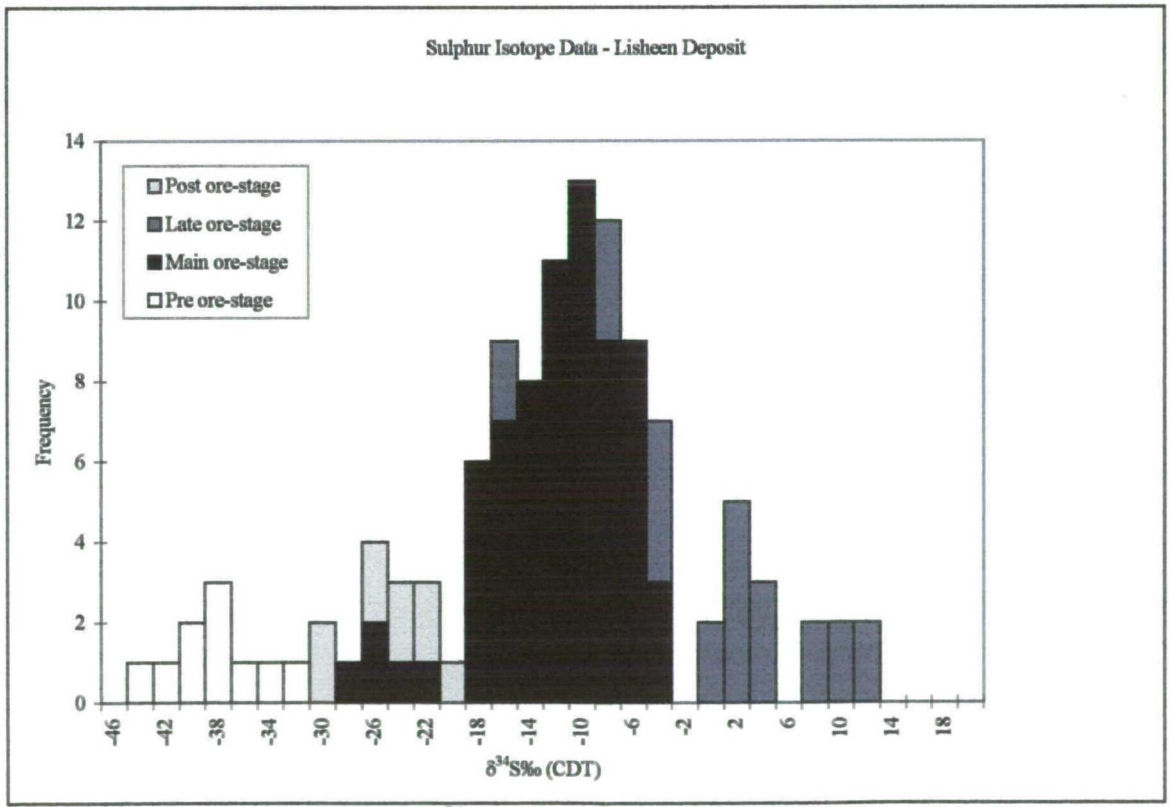


Figure 4.4 Frequency histogram of $\delta^{34}S$ (‰) of all sulphur-bearing phases in the Lisheen deposit subdivided according to paragenetic stage.

range -20 to -32‰. In general the more negative $\delta^{34}S$ values occur in Waulsortian hosted sulphides, and higher $\delta^{34}S$ values occur lower in the stratigraphy in other host lithologies such as the Ballysteen Formation and Lisduff Oolite Member.

Sphalerites (n – 41) have a mean $\delta^{34}S$ value of -7.9‰ ± 8.5‰ (1σ) similar to those of galena, and fall within the range -31.5 to 8.6‰. Ore stage sphalerites (n = 25), however, have a mean $\delta^{34}S$ value of -11.1‰ ± 3.8‰. A coarse (~ 6mm) crystalline, vein-hosted, dark brown sphalerite exhibits an anomalously low $\delta^{34}S$ value -31.5‰. This sphalerite is associated with a white dolomite vug (galena is also present) hosted within the base of the Waulsortian and proximal to a fault zone. The fault zone is cross-cut by minor sphalerite veinlets. Another coarse crystalline, vein hosted dark brown sphalerite exhibits the anomalously high $\delta^{34}S$ value of +8.6‰. This sphalerite is associated with a calcite vug hosted within the upper calcarenite member of the Ballysteen Formation. Late vein-hosted sphalerite associated with dolomite generally exhibits negative $\delta^{34}S$ values, conversely late vein hosted sphalerite associated with calcite generally exhibits positive $\delta^{34}S$ values.

Galenas (n = 34) have a mean $\delta^{34}S$ value of -11.7‰ ±7.5‰, and fall within the range -26.8 to +3.2‰. Ore stage galenas (n = 22), have a mean $\delta^{34}S$ value of -11.2‰ ± 3.3‰. Galena hosted by the Lisduff Oolite Member and intergrown with fine grained sphalerite features the most positive $\delta^{34}S$ value of +3.2‰. The most negative $\delta^{34}S$ value, -26.8‰, comes from vein-hosted galena associated with tennantite at the base of Waulsortian-hosted massive sulphide in the Derryville Zone.

Pyrites (n = 37) have a mean $\delta^{34}S$ value of -22.4‰ ±13.3‰, and fall within the range -44.1 to +11.8‰. Ore stage pyrites (n = 24), have a mean $\delta^{34}S$ value of -20.1‰ ± 7.1‰. Disseminated pyrite hosted by well developed hydrothermal D2 dolomite exhibits the most negative $\delta^{34}S$ value of -44.1‰, whereas carbonate vein-hosted pyrite from within the upper calcarenite member of the Ballysteen formation displays the highest $\delta^{34}S$ value of +11.8‰.

Barite intergrown with sulphides in the Derryville Zone (n = 2) has positive $\delta^{34}S$ values of 18.1 and 17.2‰ (repeat values of the a single sample). Barite sampled from the Main Zone (n = 2) exhibits lower positive $\delta^{34}S$ values (possibly contaminated) of 14.3 and 14.5‰ (repeat values of a single sample).

4.2.2b Galmoy Deposit

A total of 37 analyses on 19 core samples were carried out from Galmoy. Pyrite, sphalerite, and galena constitute the bulk of the data, with limited analyses of chalcopyrite (Appendix D2).

Most $\delta^{34}S$ values at Galmoy are also negative (Figure 4.5, 4.6). Sulphides in the Galmoy deposit have a mean $\delta^{34}S$ similar to Lisheen sulphides of -11.2‰, for a range of -39.9 to +6.4‰. Main ore-stage sulphides nearly always have negative $\delta^{34}S$ values and fall dominantly within the range -4 to -20‰, with a modal value of -12‰. Very low $\delta^{34}S$ values in the range -24 to -40‰ are observed in pre ore-stage disseminated pyrite. Late ore-stage vein-hosted and vug fill sulphides have positive $\delta^{34}S$ values in the range 0 to +8‰.

Sphalerites (n = 15) have a mean $\delta^{34}S$ value of -12.2‰ ± 7.0‰, and fall within the range -20.3 to +6.4‰. Ore stage sphalerites (n = 14), have a mean $\delta^{34}S$ value of -13.6‰ ± 4.9‰, lower than ore stage sphalerites in the Lisheen deposit. A late vug filling, coarse crystalline zoned sphalerite exhibits an anomalously high $\delta^{34}S$ value of +6.4‰. The lowest $\delta^{34}S$ value of -20.3‰ comes from fine grained sphalerite hosted within the Ballysteen formation.

Galenas (n = 10) have a mean $\delta^{34}S$ value of -5.2‰ ± 8.9‰, and fall within the range -19.6 to +5.8‰. Ore stage galenas (n = 6), have a mean $\delta^{34}S$ value of -10.6‰ ± 7.2‰, similar to ore stage galenas in the Lisheen deposit. A late, vug filling subhedral galena exhibits the highest $\delta^{34}S$ value of +5.8‰. This galena co-exists with the crystalline sphalerite which also displays an anomalously high $\delta^{34}S$ value. The most negative $\delta^{34}S$ value, -19.6‰, comes from massive fine grained galena intergrown with sphalerite and pyrite.

Pyrites (n = 10) have a mean $\delta^{34}S$ value of -18.6‰ ±14.2‰, and fall within the range of -39.9 to +0.8‰. Ore stage pyrites (n = 5) exhibit highly variable $\delta^{34}S$ values, however the mean $\delta^{34}S$ value of -6.8‰ ± 7.3‰ is markedly higher than ore stage pyrites from the Lisheen deposit. One anomalously high $\delta^{34}S$ value (+0.8‰) is exhibited by banded pyrite which coexists with banded sphalerite and galena. Shale-hosted botryoidal pyrite-marcasite from CW orebody exhibits the lowest $\delta^{34}S$ value of -39.9‰.

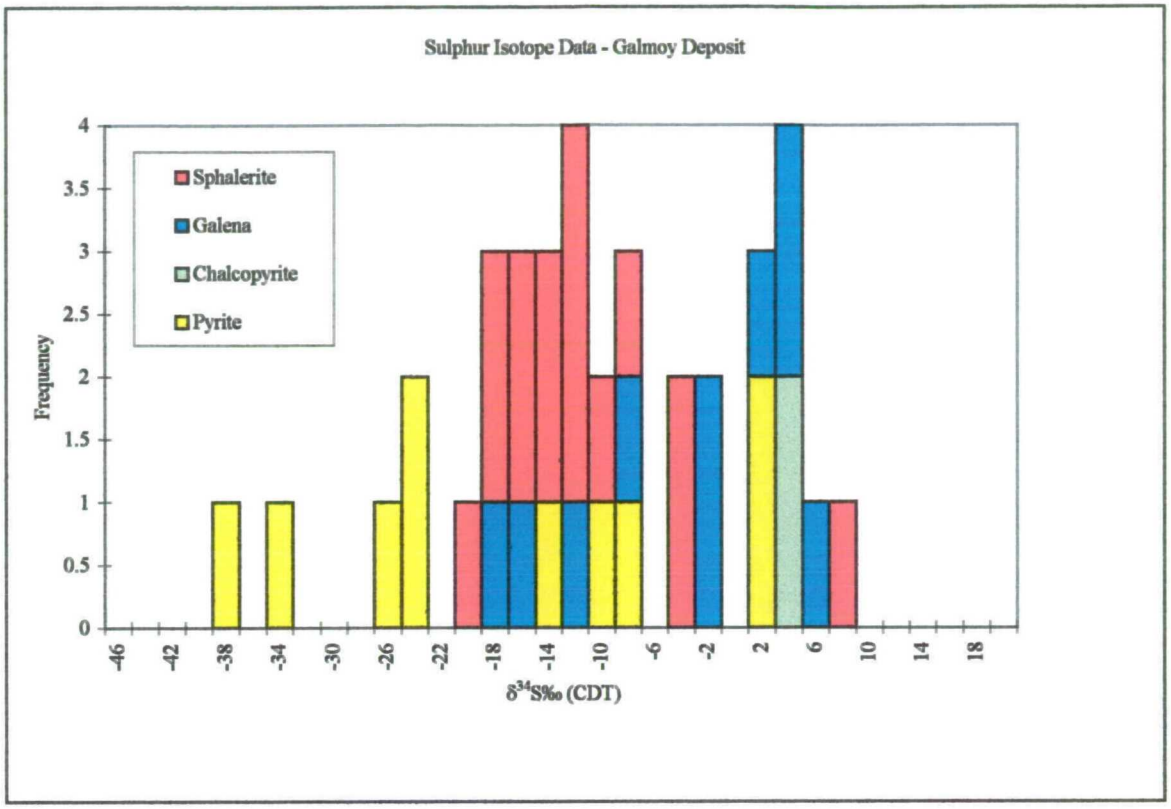


Figure 4.5 Frequency histogram of $\delta^{34}S$ (‰) of all sulphur-bearing phases in the Galmoy deposit subdivided according to mineralogy.

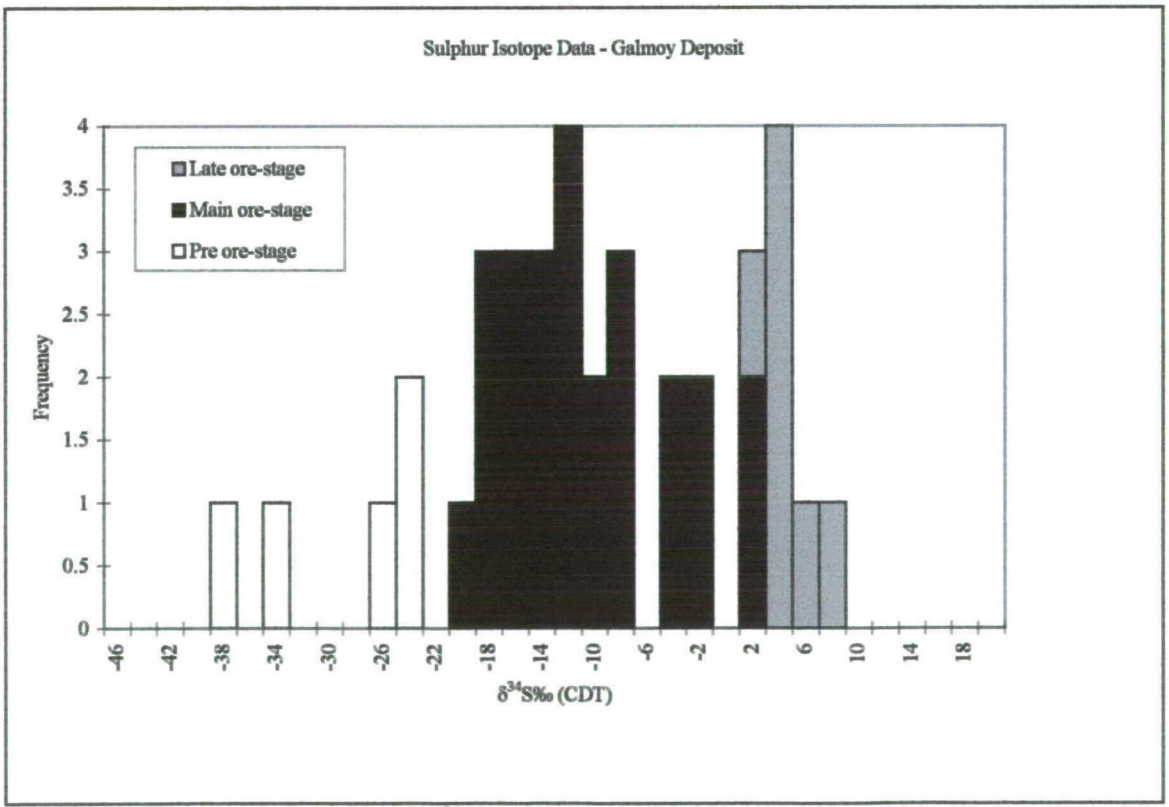


Figure 4.6 Frequency histogram of $\delta^{34}S$ (‰) of all sulphur-bearing phases in the Galmoy deposit subdivided according to paragenetic stage.

4.2.2c Rathdowney Trend Prospects

A total of 32 analyses on 18 core samples were carried out from Rathdowney Trend prospects in the course of this study. Pyrite constitutes the bulk of the data, with limited results from chalcopyrite, sphalerite and tennantite-tetrahedrite (Appendix D3).

The prospects exhibit both negative and positive $\delta^{34}S$ values (Figures 4.7, 4.8) with a mean $\delta^{34}S$ of -9.1‰, for a range of -40.1 to +8.6‰. Massive sulphides have negative $\delta^{34}S$ values and fall dominantly within the range -8 to -24‰, similar to main ore-stage mineralization at Lisheen and Galmoy. Vein-hosted and vug fill sulphides commonly have positive $\delta^{34}S$ values in the range 0 to +10‰, similar to vein-hosted and vug fill sulphides in the Lisheen deposit. However, negative $\delta^{34}S$ values in the range -2 to -8‰ also occur. Very low $\delta^{34}S$ values within the range -30 to -42‰ are only observed in early disseminated pyrite. These low $\delta^{34}S$ values are typical of pre ore-stage disseminated pyrite at Lisheen and Galmoy.

Derrykearn, Rathdowney East and Holycross sulphides are Waulsortian hosted, whereas at Durrow, sulphides are hosted within the Lisduff Oolite Member. Sulphides in the Durrow prospect, (n = 13) have a mean $\delta^{34}S$ value of -7.7‰. At the Derrykearn prospect, sulphides (n = 9) show a wide range with populations at ~ -20, -10 and +8‰. Sulphides in the Rathdowney East prospect (n = 5) have a mean $\delta^{34}S$ value of -36.2‰. In the Holycross prospect, sulphides (n = 5) exhibit a bimodal distribution with ~ -30 and +10‰ populations (Figure 4.9).

Pyrites (n = 23) have a mean $\delta^{34}S$ value of -11.3‰ ± 17.5‰, and fall in the range -40.1 to +8.6‰. Pyrite at the Derrykearn, Durrow, and Holycross prospects exhibits a range of positive $\delta^{34}S$ values which range from +3.0 to +8.6‰. Negative $\delta^{34}S$ values in the range -8.6 to -22.9‰ occur only in pyrite at Derrykearn and Durrow, and perhaps significantly are from massive pyrite. A third population of pyrite is observed at Rathdowney East and Holycross which exhibits very low $\delta^{34}S$ values between -31.4 and -40.1‰. Replacive sphalerite mineralization at Durrow is characterized by a negative $\delta^{34}S$ value of -20.4‰, whilst vein hosted sphalerite at Holycross exhibits a positive $\delta^{34}S$ value of +8.5‰. Chalcopyrite at Durrow is characterized by $\delta^{34}S$ values in the range -0.3 to +7.9‰.

4.2.3 Sulphur Isotope Geothermometry

Sulphur isotope geothermometry has been extensively utilized in ore deposit studies. Theoretical and experimental studies indicate that isotope exchange reactions among cogenetic sulphide minerals and ore forming fluids may achieve equilibrium and that the temperature of equilibration can be estimated from $\Delta^{34}S$ values of coexisting sulphides (Ohmoto and Rye, 1979). Sphalerite-galena and pyrite-galena mineral pairs are suitable geothermometers. Equilibrium fractionation factors are primarily a function of temperature, but successful application of sulphur isotope thermometry depends also on the following conditions: (1) both mineral phases were formed in equilibrium; (2) no isotopic exchange took place between mineral phases, or between a mineral phase and a fluid phase after the formation of the minerals; and (3) pure mineral phases can be separated for isotopic analysis. Alternatively, if the temperature of precipitation of sulphides can be constrained independently sulphur isotope fractionation can be used to test for the degree of isotopic equilibrium between apparently cogenetic sulphides. This provides evidence for the nature of the sulphide precipitation process.

The equilibrium fractionation factor ($\Delta_{sp\text{-}gn} = (0.74/T^2 \times 10^6)$) between sphalerite-galena mineral pairs is based on data from many ore deposits (Czamanske and Rye, 1974; Kamilli and Ohmoto, 1977; Robinson and Ohmoto, 1973; Allmandinger and Ohmoto, (unpublished data); Landis and Rye, 1974; Sasaki and Krouse, 1969; Sasaki, 1974; McLimans, 1977). Assuming sphalerite and galena precipitated in isotopic equilibrium, sphalerite would yield $\delta^{34}S$ values approximately 3.0, 4.0, and 5.0‰ greater than galena at 200, 150 and 100°C respectively. If pyrite and galena were precipitated in equilibrium, pyrite would yield $\delta^{34}S$ values approximately 4.0, 6.0, and 8.0‰ greater than galena at 200, 150 and 100°C respectively (Sakai, 1968). These figures are based on experimental and theoretical data.

Isotope fractionations between apparently co-existing sphalerite and galena in the Lisheen deposit range from +3.0 to +8.3‰ and indicate that isotopic equilibrium was probably not established, particularly in the late, vein hosted mineral pairs. In most cases pyrite is nearly always out of isotopic equilibrium with galena. The sphalerite-galena pair in sample 451/139.0 shows a noticeable deviation from equilibrium with a $\Delta_{sp\text{-}gn}$ value of 8.3‰ giving a calculated temperature of 25°C, an unrealistic value geologically since fluid inclusions in calcite from the same sample indicate temperatures of ≥200°C.

Isotope fractionations between apparently co-existing sphalerite and galena in the Galmoy deposit range from less than 1.0 to 7.1‰, also suggestive of sulphur isotopic disequilibrium. In sample 10CW, a sphalerite-galena pair with a $\Delta_{sp\text{-}gn}$ value of 3.2‰ gives a calculated temperature of 207°C, this is an unrealistic temperature since fluid inclusions in sphalerite from the sample indicate temperatures of ≥140°C.

Banded galena, sphalerite and pyrite in the Galmoy deposit (sample GY355/95.0) are similar to the banded sulphides in the Lisheen deposit (sample 431/205.70, see above). These banded sulphides exhibit different $\delta^{34}S$ values, but the fractionation between each of the pairs is virtually the same. Assuming isotopic equilibrium, the observed fractionation between sphalerite and galena would imply a precipitation temperature of 270°C. Given the maximum estimated temperatures from fluid inclusions of ~230°C, this would suggest that the sulphides were not precipitated in isotopic equilibrium.

4.2.4 Interpretation of Results (Sulphur)

In many stratabound and stratiform base metal deposits, aqueous (seawater) sulphate is considered to be a major source of sulphur (Ohmoto and Goldhaber, 1997). Seawater sulphate is fixed through a variety of mechanisms as sulphides in ore deposits. However, the mechanisms of sulphate reduction are problematic considering the low to moderate temperatures of formation of these deposits (Ohmoto *et al.*, 1990). Sulphate reduction has been produced experimentally by two mechanisms: first, by sulphur-reducing bacteria at temperatures generally less than 100°C; and second, by reduction with ferrous iron or organic matter at temperatures above ~250°C.

Bacteriogenic sulphate reduction (BSR) at temperatures below 100°C has been shown by many workers (e.g., Coomer and Robinson, 1976; Caulfield *et al.*, 1986) to be a viable mechanism, providing of course that environmental conditions are suitable for bacterial development. The most common sulphur-reducing bacteria are of the genus *Desulfovibrio* (Ohmoto *et al.*, 1990). Recently evidence has come to light that suggests the upper limit for microbial activity may extend higher than 100°C (e.g., Jørgenson *et al.*, 1992) and perhaps to temperatures as great as 120° (Elsgaard *et al.*, 1994), but the heat tolerant bacteria responsible appear to be rare and are not normally active in basinal environments (Kiyosu and Krouse, 1990). This upper temperature limit to bacterial sulphate reduction places an important constraint on the direct involvement of these organisms in hydrothermal processes. Various environmental parameters that influence the rate of bacterial sulphate reduction, including bacterial species, population, pH, salinity, nutrients

and trace metal contents have been reviewed by many investigators (e.g., Chambers and Trudinger, 1979; Berner, 1984, 1985; Postgate, 1984; Skyring, 1987; Ohmoto *et al.*, 1990; Trudinger, 1992). The optimum pH for growth is near neutrality. The bacteria can tolerate an extremely wide range of salinity from fresh waters up to halite saturation (Postgate, 1984).

All sulphate-reducing bacteria are obligate anaerobes. Most of the seafloor is oxygenated, therefore the bacteria may be become active only in environments where anoxic conditions are created by decomposition of organic matter. The two principal environments are below the water-sediment interface in normal marine sediments or in euxinic water bodies.

Bacteria split oxygen from sulphate ions and excrete H_2S which is enriched in ^{32}S relative to the original sulphate. The extent of isotope fractionation during the reduction of the sulphate ion is due to the different rates at which S-O bonds are broken. Harrison and Thode (1958) and Kaplan and Rittenberg (1964) report the fractionation of up to 27‰ and 46‰ respectively obtained in the laboratory. However, isotope fractionation in nature is more extensive than suggested by most laboratory experiments. Bacteriogenic fractionation is primarily governed by the conditions under which the bacteria operated, even the type of bacteria can influence the fractionation (Kaplan and Rittenberg, 1964; Goldhaber and Kaplan, 1975)

Inorganic thermochemical sulphate reduction (TSR) has often been cited as the source of large accumulations of H_2S gas in carbonate reservoirs (Orr, 1974). The mechanism of thermochemical sulphate reduction probably involves an initial key step in which SO_4^{2-} reacts with H_2S to form elemental sulphur, followed by reduction of the elemental sulphur by organic matter (Orr, 1974). However, the specific reactions operative in these environments, or experimental analogues at moderate to low temperatures, have not been identified until relatively recently. Krouse *et al.* (1988) presented combined petrographic, gas composition and isotopic evidence from the Palaeozoic foothill reservoirs of western Canada which suggested that thermochemical sulphate reduction occurred at temperatures between 90° and 175°C with light hydrocarbon gases serving as reducing agents. The most compelling evidence in support of TSR in this system did not come from the sulphur isotope data (which only showed a ≈7‰ fractionation between H_2S and anhydrite) but came from the decrease in $\delta^{13}C$ values of the associated light hydrocarbon gases present (Krouse *et al.*, 1988). This case study suggested that the recognition of processes such as TSR from $\delta^{34}S$ values alone may be difficult without supporting data from the reducing phase.

4.3.3 Fluid Isotopic Composition

The $\delta^{18}O_{(H2O)}$ value of fluids which would have been in equilibrium with the various dolomite and calcites have been calculated over a range of temperatures (Figure 4.24) using the fractionation factors of Friedman and O'Neil (1977). In the absence of precise temperature constraints, such plots can be used to estimate the isotopic composition of fluids which could have been responsible for dolomite and calcite precipitation. However, in the present study, fluid inclusion homogenization temperatures are available for most of these phases which can be used as a precipitation temperature constraint (Chapter 5). It should be noted that these values strictly represent minimum formation temperatures (see 5.1.3), therefore estimates of $\delta^{18}O_{(H2O)}$ will also be minima.

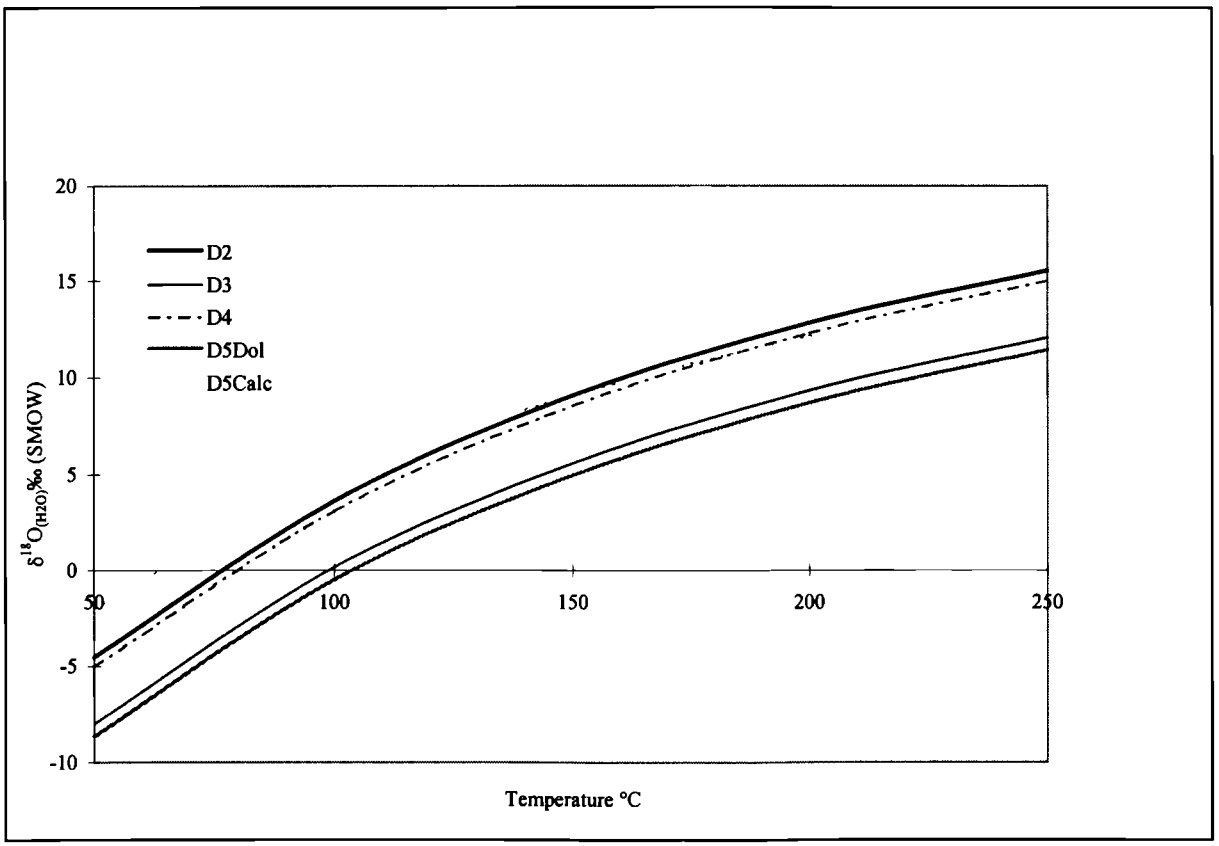


Figure 4.24 Curves illustrating the relationship between precipitation temperature and water isotopic composition for average dolomite and calcite compositions.

No workable fluid inclusions were obtained from D2 dolomite in the fluid inclusion study (Chapter 5), therefore the temperature of formation of D2 dolomite in the Rathdowney Trend is unknown. However, Wilkinson and Earls (in prep) have measured primary fluid inclusion homogenization temperatures of 150-220°C in black dolomite matrix breccia from the west

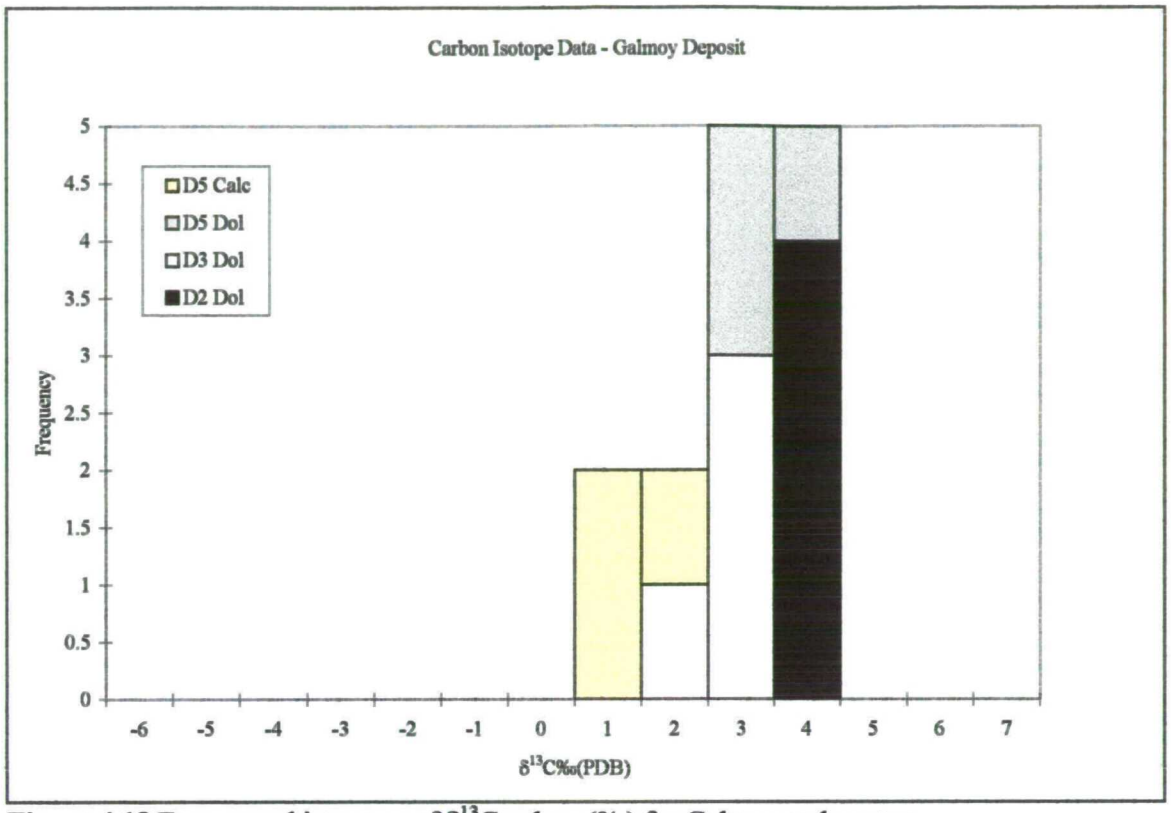


Figure 4.18 Frequency histogram of $\delta^{13}C$ values (‰) for Galmoy carbonates.

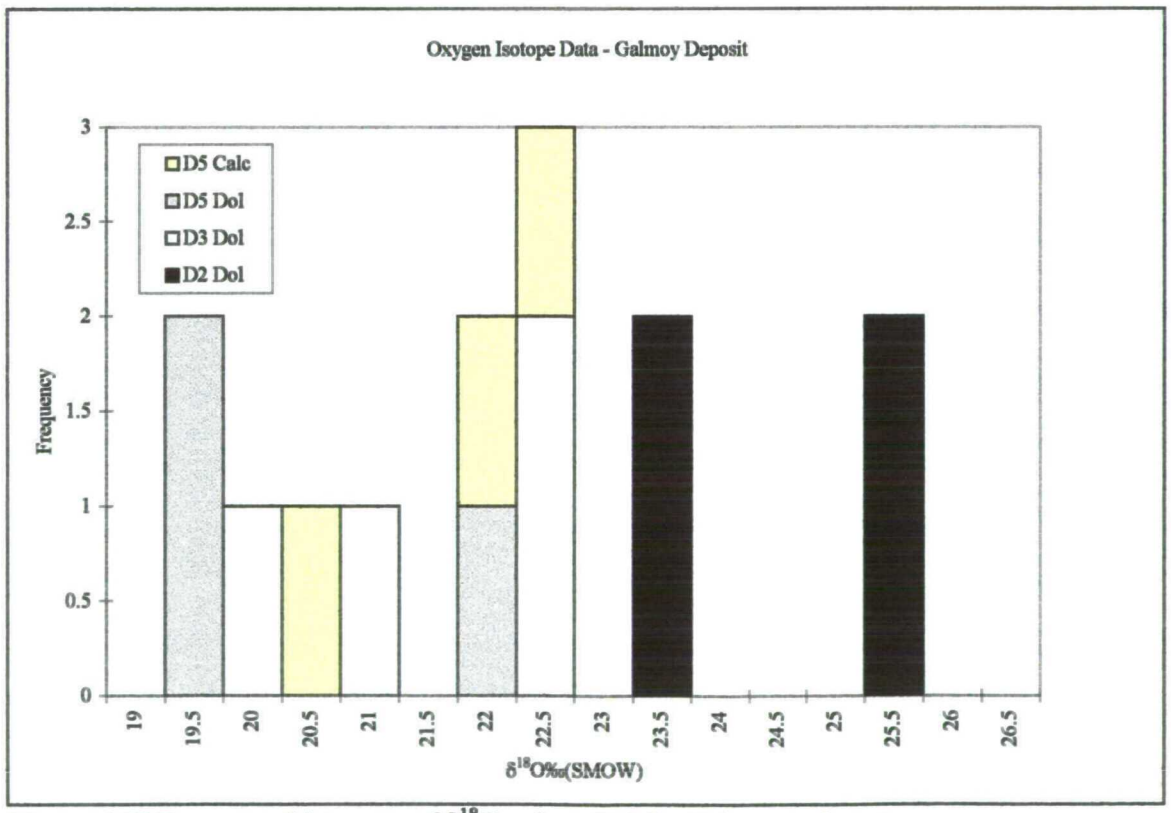


Figure 4.19 Frequency histogram of $\delta^{18}O$ values (‰) for Galmoy carbonates.

The attractiveness of the non-biogenic pathways of sulphate reduction as a mechanism for H_2S generation is that it is the only presently recognized mechanism for providing an isotopically heavy sulphur in low-temperature, kinetically controlled systems (Ohmoto and Goldhaber, 1997).

Sulphur isotopic characteristics of syngenetic and diagenetic sulphide minerals and organic sulphur in sediments are controlled primarily by three parameters: (1) initial $\delta^{34}S$ value of aqueous sulphate; (2) the kinetic isotopic fractionation factor during bacterial sulphate reduction; and (3) the open or closed nature of the system with respect to SO_4^{2-}. The rate of bacterial sulphate reduction is most affected by temperature, increasing by 2 orders of magnitude from 0°C to 40°C, and by the availabilty of oxidizable organic substrates, that is, digestible foods. The open or closed nature of a system with respect to SO_4^{2-} is determined by the relative rates of sulphate supply compared to sulphate reduction.

The $\delta^{34}S$ value of Lower Carboniferous seawater sulphate declined with time from about +17 to +22‰ at the beginning of the Carboniferous to about +14 to +17‰ at the beginning of the Late Carboniferous (Claypool *et al.*, 1980). Two measured barite values of 17.2 and 18.1‰ in the Lisheen deposit suggest barite deposition for these samples involved essentially unmodified Carboniferous marine sulphate. This is comparable with virtually all $\delta^{34}S$ values of barite from the Irish deposits which fall in the range +15 to +23‰. If a +18‰ value for barite at Lisheen is taken as being the isotopic composition of Lower Carboniferous seawater sulphate at the time of mineralization, then ore-stage sulphides are isotopically lighter by 22 to 38‰ with respect to coexisting sulphate. Such depletions in $\delta^{34}S$ are typical of kinetic fractionation induced during bacterial reduction of the sulphate source. $\delta^{34}S$ values ($\delta^{34}S$ -30 to -44‰) of early disseminated pre-ore sulphides (iron sulphides) commonly hosted in BMB are isotopically lighter by 48 to 62‰ with respect to seawater sulphate. They are also consistent with bacteriogenic reduction of Lower Carboniferous seawater sulphate, although the mechanism of achieving the additional fractionation is not well understood (Boyce, pers. comm., 1996). A similar, almost exclusively pyrite component of low $\delta^{34}S$ is also noted at Silvermines (Boyce *et al.*, 1983b; Boyce, 1990) and in pyrtite/marcasite in the 2-1 lens at Navan (Anderson *et al.*, in press). At Navan it has been suggested that environment of bacteriogenic reduction in the Boulder Conglomerate and immediately underlying Pale Beds was more oxidizing in proximity to the Lower Carboniferous sea, relative to the deeper Pale Beds, resulting in additional fractionation (through re-oxidation of reduced sulphur species, followed by further bacteriogenic reduction) and predominant deposition of iron sulphides.

The textural evidence that much of the iron sulphides and some base-metal sulphides near fluid conduits replace earlier sulphides suggests that the sulphur in the post ore-stage sulphides ($\delta^{34}S$ -20 to -32‰) was derived from early sulphides as well as from sulphate reduction.

The lack of evidence in the Lisheen and Galmoy area for substantial quantities of evaporites makes it unlikely that bacteriogenic reduction of evaporites could have provided the quantities of bacteriogenic sulphur invoked in the formation of the deposits.

Sulphur isotopic values for the majority of ore-stage sulphides in the Rathdowney Trend are strongly negative, incorporating biogenic sulphur. The range (-4 to -20‰) and mode (-10‰ for Lisheen, -12‰ for Galmoy) of ore-stage sulphides in the Rathdowney Trend deposits are typical of all other producing deposits in Ireland (Figure 4.11) including Navan (Anderson *et al.*, 1989; Anderson, 1990, Anderson *et al.*, in press; Boyce *et al.*, 1993, 1994), Silvermines (Greig *et al.*, 1971; Coomer and Robinson, 1976; Boyce *et al.*, 1983b), and Tynagh (Boast *et al.*, 1981a).

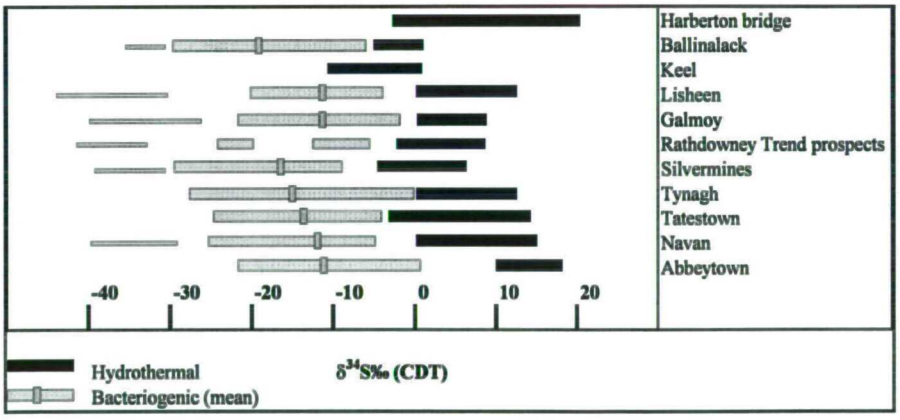


Figure 4.11 Summary of sulphur isotope data from Irish-type ore deposits. Data from Abbeytown (Recio *et al.*,1988; Hitzman *et al.*,1988), Navan (Anderson *et al.*, 1989; Anderson, 1990; Anderson *et al.*, in press) Boyce *et al.*, 1993; 1994), Keel, Moyvoughly, Ballinalack and Tatestown (Caulfield *et al.*, 1986), Tynagh (Boast *et al.*, 1981a), Silvermines (Coomer and Robinson, 1976; Boyce *et al.*, 1983b), Lisheen, Galmoy, and Rathdowney Trend prospects Rathdowney Trend prospects (this study), Harberton Bridge (Gallagher *et al.*, 1992).

The dominant bacteriogenic component in the Rathdowney Trend deposits, implies that local circulation must have either transported reduced sulphur to the site of ore deposition, or introduced sulphate for *in situ* bacterial reduction. Anderson (1983) noted that the amount of bacteriogenic sulphur in an economic Zn-Pb deposit is too great to have been present in a static fluid prior to introduction of the metals, and it is essential to have a continuous supply of reduced sulphur to the metals to produce the quantities of ore observed. This could be achieved by continuous *in situ* reduction of sulphate at the site of mineralization. However, the environmental conditions at the site of ore deposition may not be suitable for bacterial development. The upper limit for BSR, is empirically determined by the temperature above which almost all sulphate

reducing bacteria cease to metabolize (Machel, 1987; Orr, 1974). Therefore bacteriogenically derived sulphur in the Rathdowney Trend deposits is most likely to have been transported to the site of ore deposition.

The heavy isotope values principally found in late ore-stage sulphides proximal to fault zones, are interpreted to be from a separate source of sulphur from the bacteriogenic supply. The two most likely candidates for the isotopically heavy component are: (1) thermochemical reduction of Lower Carboniferous seawater sulphate or sulphate transported with the metals, by organic matter or hydrocarbons at the site of ore deposition; (2) a component of hydrothermal sulphide transported with the metals. In either case an abiogenic process is implicated.

The reduction of seawater sulphate is improbable since the distribution of the $\delta^{34}S$ is not that expected of thermochemical sulphate reduction (Boyce pers. comm., 1996). Therefore, a hydrothermal component of H_2S transported with the metals is invoked. This distinct sulphur source is recognized in many of the Irish deposits (e.g., Coomer and Robinson, 1976; Boast *et al.*, 1981a; Caulfield *et al.*, 1986; Anderson *et al.*, in press).

Regarding the source of the hydrothermal sulphide, the absence of igneous activity contemporaneous with the mineralization and the isotopic composition itself are inconsistent with an igneous origin. An alternative origin proposed by Anderson *et al.* (1989) is the release of sulphur from diagenetic sulphides during hydrothermal metamorphism as aqueous fluids convect within the underlying Lower Palaeozoic rocks. In a detailed study of the Lower Palaeozoic-hosted pyrite below the Navan deposit, Boyce *et al.* (1994) suggest that hydrothermal sulphur is leached from diagenetic pyrite in the Lower Palaeozoic rocks.

Following detailed analysis of $\delta^{34}S$ with depth and proximity to major faults in the Main, Derryville, North, and Bog Zones, it can be concluded that variation of $\delta^{34}S$ within the Lisheen deposit is generally not systematic (Figure 4.10). However, the heavy sulphur component is principally found in late ore-stage sulphides proximal to fault zones.

Isotopic fractionation between sphalerite-galena mineral pairs at Lisheen and also Galmoy, where the minerals are intergrown and interpreted texturally as having been precipitated in equilibrium, in general indicate isotopic disequilibrium. Apparent disequilibrium relationships may be due to impure mineral separates, the selection of uncontemporaneous phases, or more likely the fact that they precipitated together but in isotopic disequilibrium. Pyrite is nearly always out of isotopic equilibrum with galena, even where they apparently co-precipitated. This is not surprising given

mineral and the aqueous carbonate species and the relative abundance of carbon species in the fluid (Ohmoto and Rye, 1979). Previously published work indicates that in low pH saline brines, HCO_3^- will be the dominant carbon species (Hanor 1994).

Carbon and oxygen isotope systematics of the Irish deposits are less well defined than for sulphur. Only Tynagh (Boast *et al.*, 1981a), Abbeytown (Recio *et al.*, 1988; Hitzman *et al.*, 1988) and Harberton Bridge (Gallagher *et al.*, 1992) have been studied in any detail. Preliminary studies have been carried out at Keel and Garrycam (Slowey *et al.*, 1995)

4.3.1 Sample Selection and Experimental Technique

A total of 64 analyses on 52 core samples were carried out in this carbon, oxygen isotope study (Appendices D4,5,6). Carbon and oxygen isotope data have been collected from a range of carbonates in the Rathdowney Trend, including ore-related and post-ore dolomites and calcites. Pre-ore regional dolomites have generally not been analyzed.

CO_2 was liberated from carbonate minerals by dissolution in 100% phosphoric acid (Craig, 1957; Swart *et al.*, 1991). CO_2 gas for analysis was extracted from calcite and dolomite by reaction with phosphoric acid *in vacuo* at 25°C for a minimum of 3 hours, and at 100°C for a minimum of ~12 hours, in the manner described by McCrea (1950) and Rosenbaum and Sheppard (1986) respectively. The resultant CO_2 was analyzed on a VG-SIRA 10 mass spectrometer. Results are given in standard $\delta^{13}C‰$ notation relative to the PDB standard for carbon, and $\delta^{18}O‰$ notation relative to the SMOW standard for oxygen. Reproducibility based on full replicate analyses of an internal laboratory standard (SMII) was ±0.04‰ (1σ) for $\delta^{18}O$, and ±0.02‰(1σ) for $\delta^{13}C$.

4.3.2 Results

Carbon and oxygen isotope data are presented in frequency histograms and scatter plots. Frequency histograms of $\delta^{13}C$ and $d^{18}O$ are subdivided according to paragenetic stage, i.e., D1, D2, D3, D4, D5 and location (Figures 4.12, 4.13, 4.14).

Unaltered Waulsortian micrite and associated diagenetic calcites were not analyzed in this study, therefore for comparison the isotopic compositions of unaltered Waulsortian micrite provided by Boast *et al.* (1981a) are used. Carbon isotope compositions display a narrow range from 3.1 to 4.1‰, with a mean of 3.8‰. The $\delta^{18}O$ (SMOW) values range from 22.2 to 28.1‰, with a mean

of 26.3‰. These values are similar to those from other studies of unaltered Waulsortian limestone in the southern Irish Midlands (Hitzman *et al.*, 1998). The isotopic compositions of regional Waulsortian dolomite from the Lisheen area (Hitzman *et al.*, 1998) display a range of carbon values from 3.2 to 4.1‰. The $\delta^{18}O$ (SMOW) values range from 22.2 to 26.0‰.

4.3.2a Lisheen Deposit

A total of 41 analyses on 33 core samples were carried out in the course of this study, 23 analyses on ore-related and post-ore dolomites, and 18 analyses on syn- to post-ore calcites (Appendix, D4). Values for $\delta^{13}C$ in dolomite and calcite mineral phases range from -5.79 to 6.29‰. Corresponding $\delta^{18}O$ values range from 19.29 to 26.27‰ (Figures, 4.15, 4.16, 4.17).

The mean $\delta^{13}C$ and $\delta^{18}O$ values for D2 dolomite are 4.26‰ ± 1.36‰, and 24.64‰ ± 1.81‰ respectively. These values are higher than the corresponding values in D3 dolomite which have mean $\delta^{13}C$ and $\delta^{18}O$ values of 2.43‰ ± 0.19‰ and 20.67‰ ± 0.32‰ respectively. This relationship is also seen at the Galmoy Deposit. $\delta^{13}C$ and $\delta^{18}O$ data for regional $D1_C$ dolomite outside the Lisheen deposit are similar to D3 dolomite with values of 2.70‰ and 21.50‰ respectively. D4 dolomite generally displays higher $\delta^{18}O$ values than those observed in D3 dolomite, however, $\delta^{13}C$ values are very similar. This relationship is also observed in the prospects. The mean $\delta^{13}C$ and $\delta^{18}O$ values for D4 dolomite are 2.03‰ ± 0.37‰ and 23.74‰ ± 0.93‰ respectively.

The $\delta^{13}C$ value of late D5 dolomite is generally lower and more variable than the $\delta^{13}C$ value of D2, D3, and D4 dolomite with a mean value of 1.15‰ ±1.68‰, and a range between -1.30 and 2.67‰. The $\delta^{13}C$ values are generally lower when the dolomites are associated with sulphides. The $\delta^{18}O$ value of D5 dolomite is less variable than $\delta^{13}C$. The mean $\delta^{18}O$ value of D5 dolomite is 20.47‰ ± 0.65‰, with a range between 19.37 and 21.05‰, similar in isotopic composition to the ore-related D3 dolomite.

The $\delta^{13}C$ value of D5 calcite is lower than the $\delta^{13}C$ value of D5 dolomite, with a mean value of 0.22‰ ± 0.82‰. Isotopically distinct late, vug-filling calcite which clearly post-dates D4

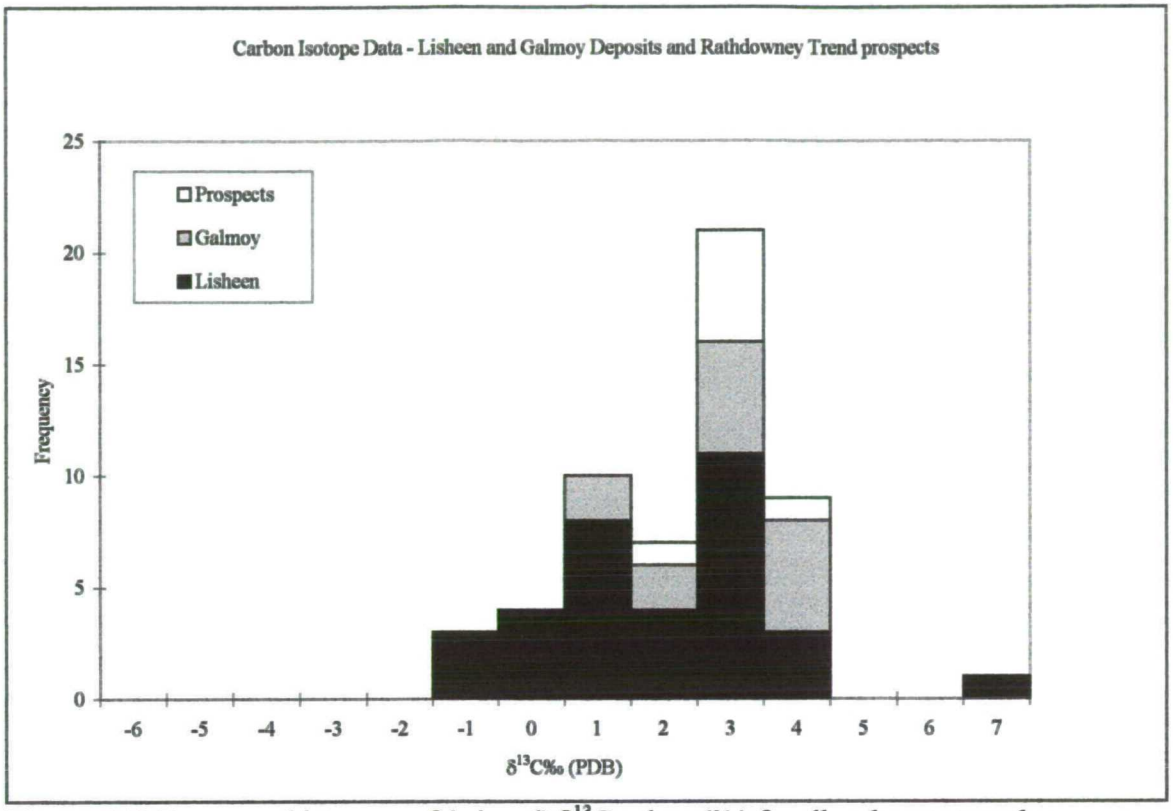


Figure 4.12 Frequency histogram of (mineral) $\delta^{13}C$ values (‰) for all carbonate samples analyzed.

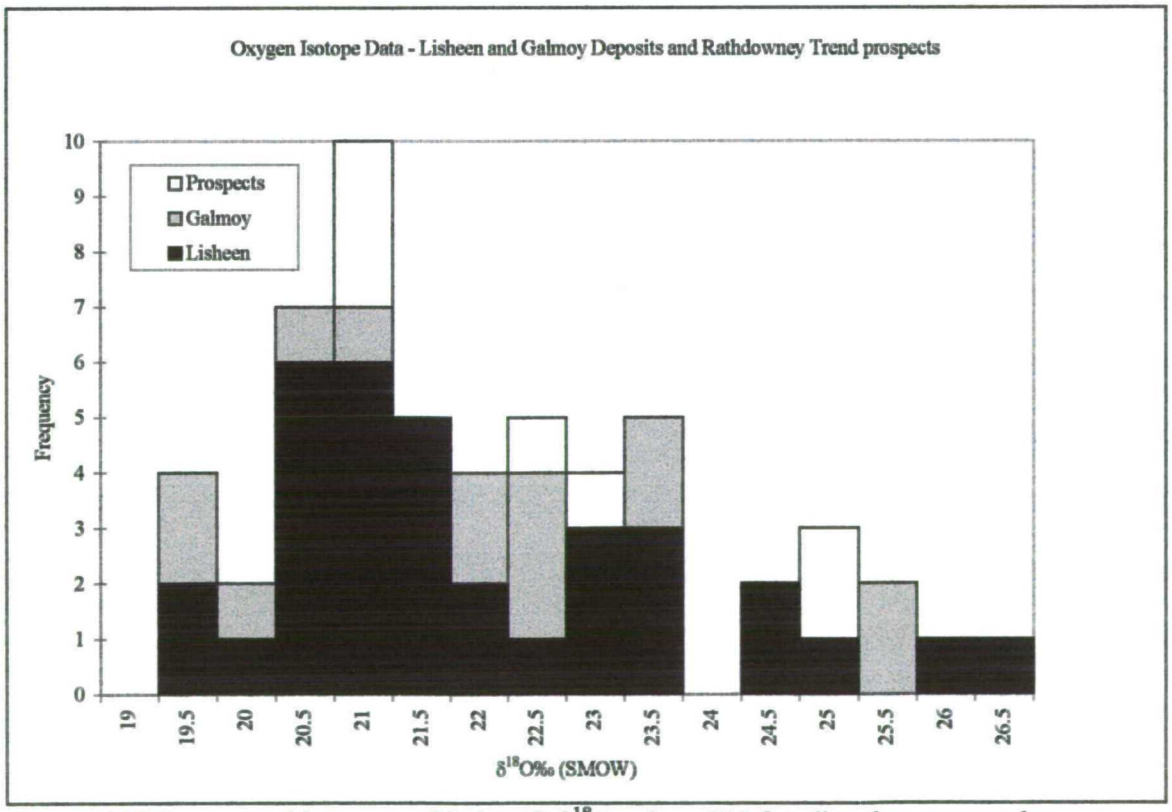


Figure 4.13 Frequency histogram of (mineral) $\delta^{18}O$ values (‰) for all carbonate samples analyzed.

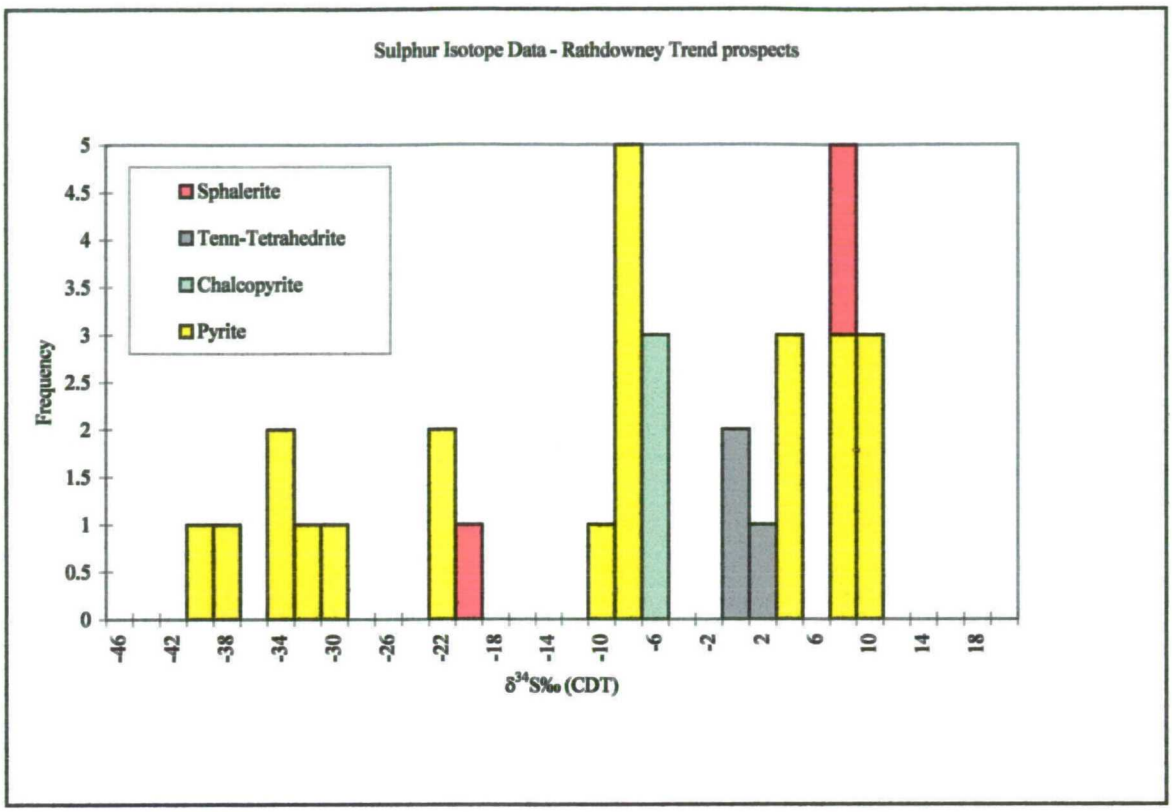


Figure 4.7 Frequency histogram of $\delta^{34}S$ (‰) of all sulphur-bearing phases in the Rathdowney Trend prospects subdivided according to mineralogy.

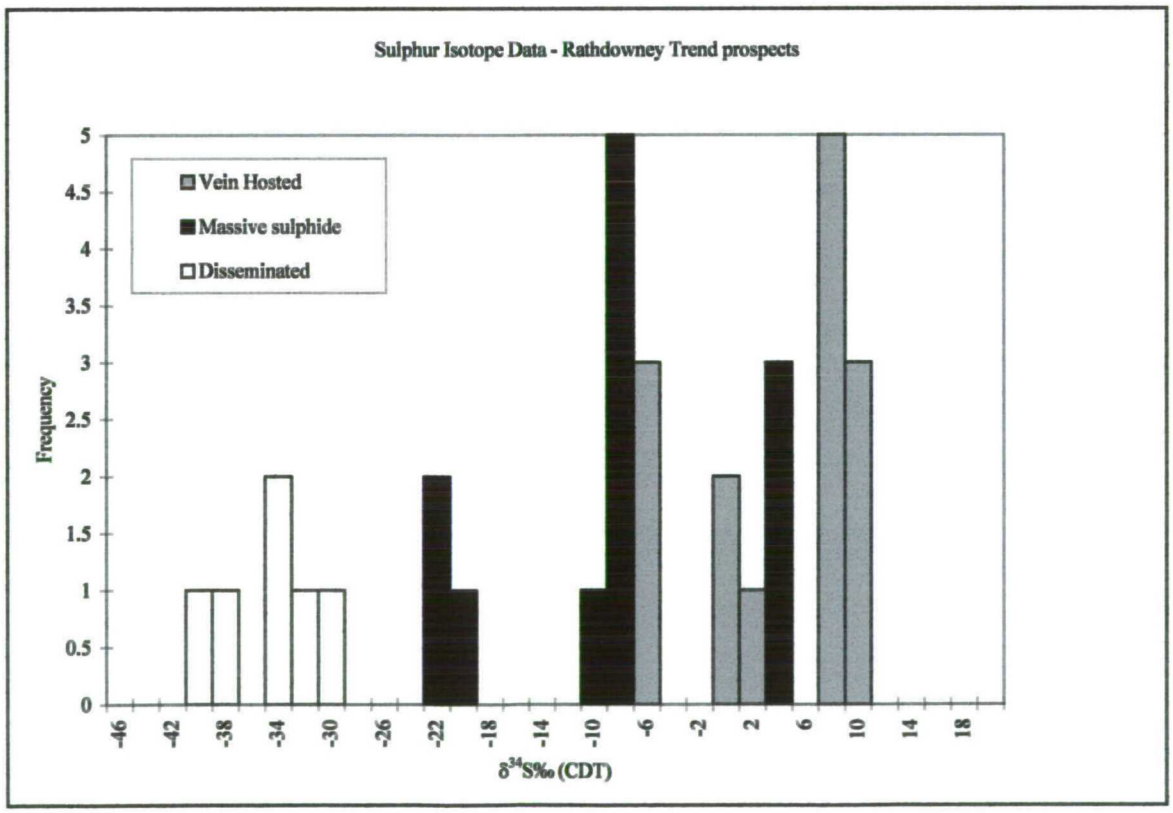


Figure 4.8 Frequency histogram of $\delta^{34}S$ (‰) of all sulphur-bearing phases in the Rathdowney Trend prospects subdivided according to mineralization style.

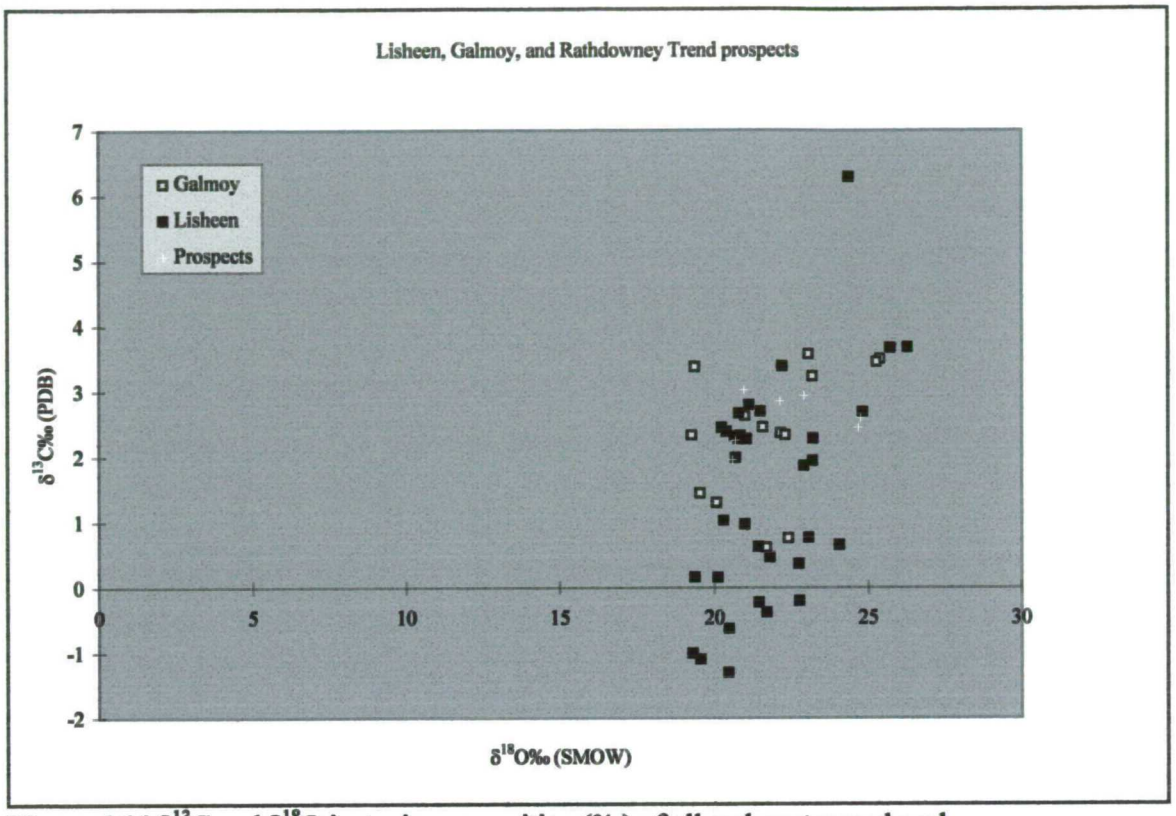


Figure 4.14 $\delta^{13}C$ and $\delta^{18}O$ isotopic composition (‰) of all carbonates analyzed.

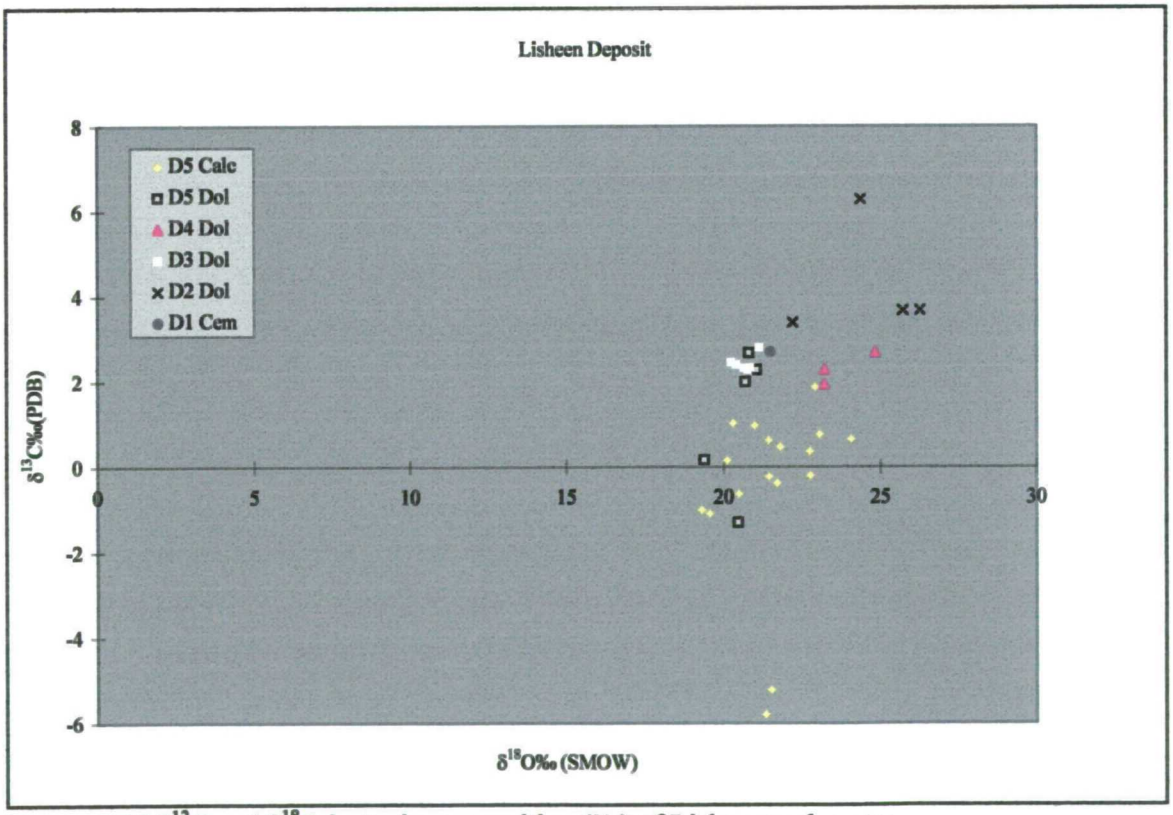


Figure 4.15 $\delta^{13}C$ and $\delta^{18}O$ isotopic composition (‰) of Lisheen carbonates.

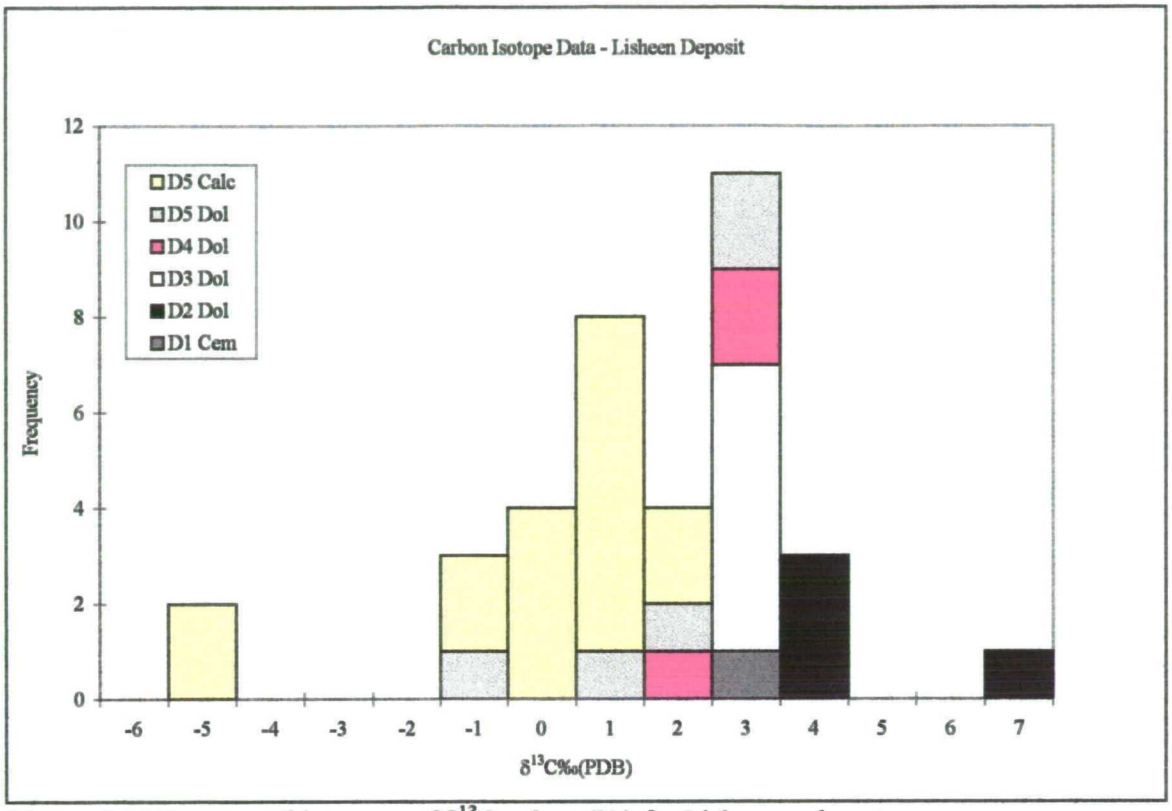


Figure 4.16 Frequency histogram of $\delta^{13}C$ values (‰) for Lisheen carbonates.

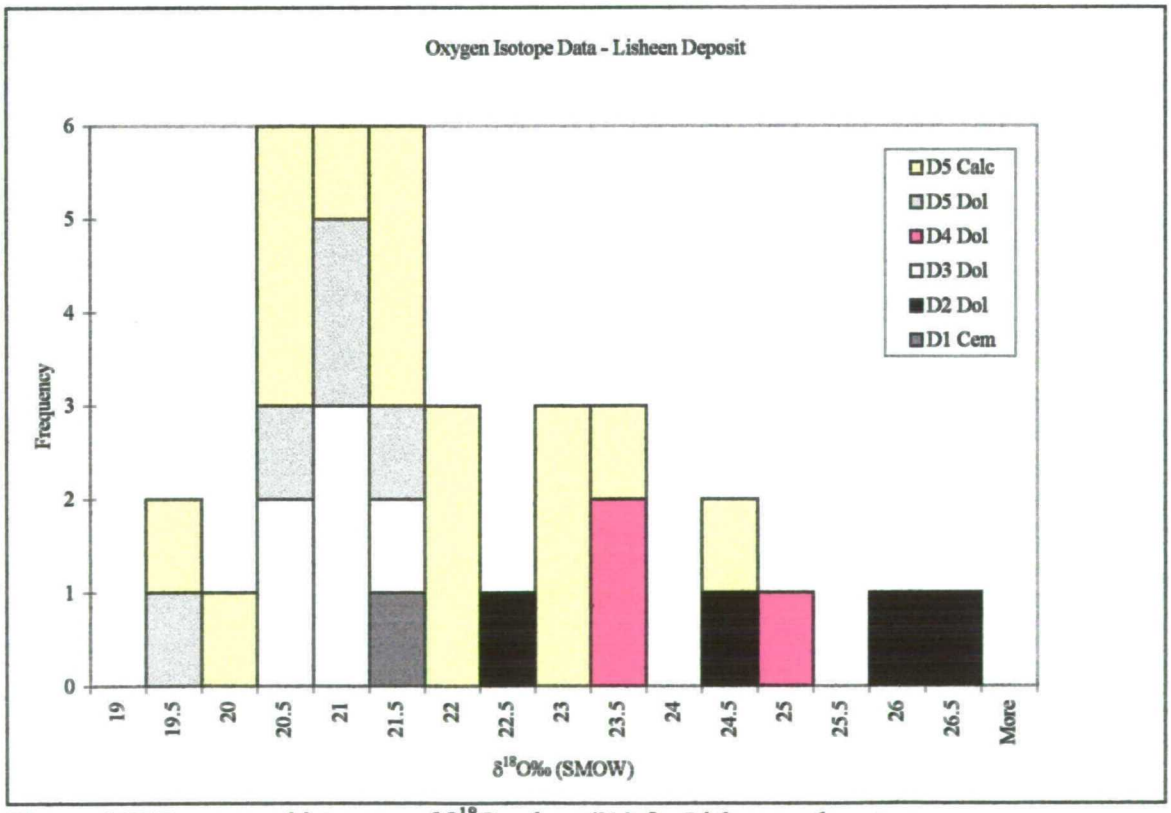


Figure 4.17 Frequency histogram of $\delta^{18}O$ values (‰) for Lisheen carbonates.

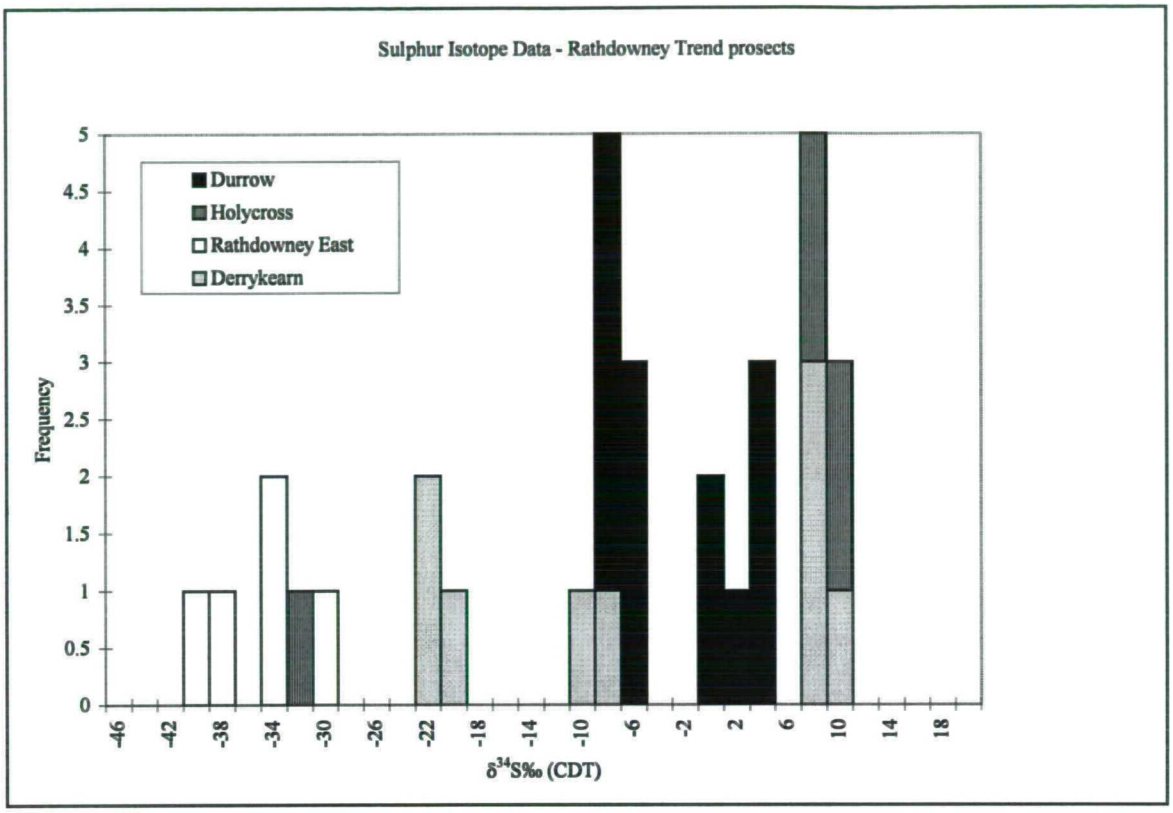


Figure 4.9 Frequency histogram of $\delta^{34}S$ (‰) of all sulphur bearing phases in the Rathdowney Trend prospects subdivided according to location.

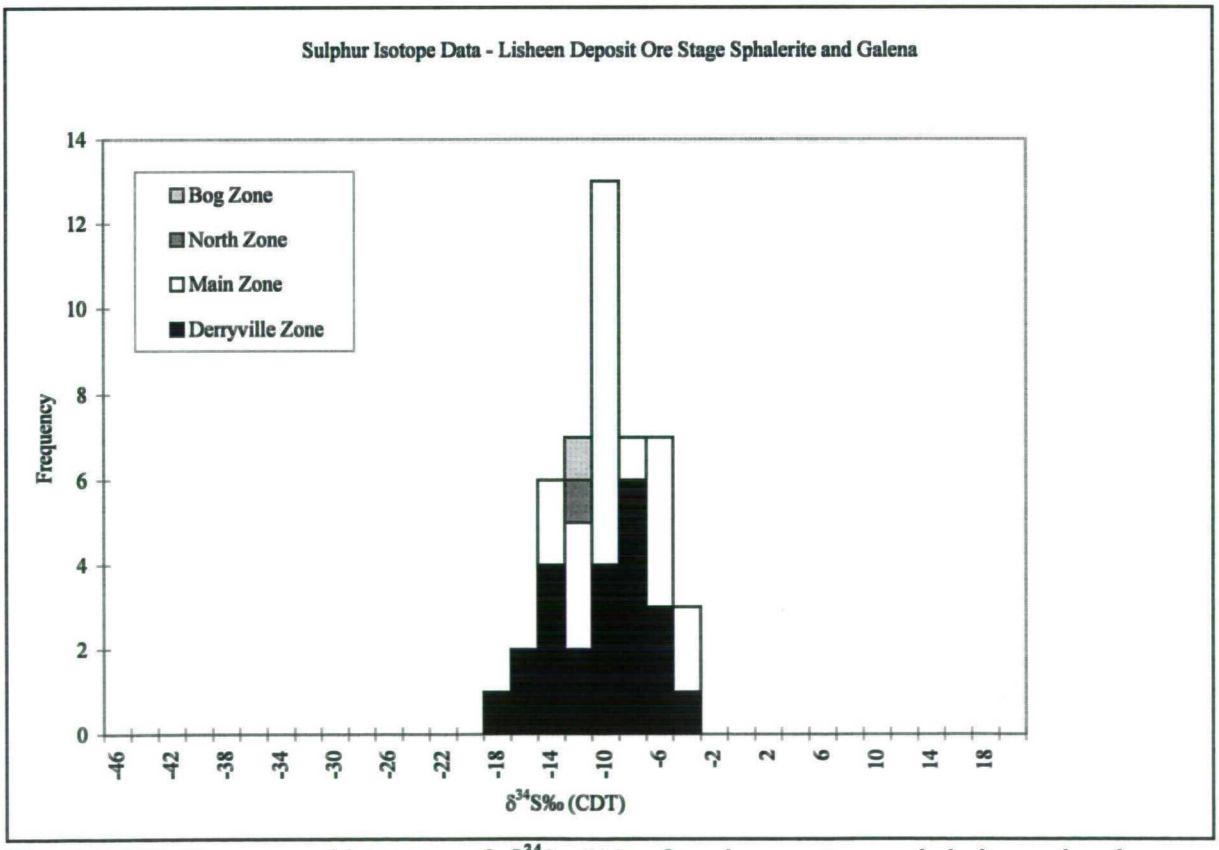


Figure 4.10 Frequency histogram of $\delta^{34}S$ (‰) of main ore-stage sphalerite and galena subdivided according to ore zone at the Lisheen deposit.

that isotopic equilibrium is unlikely to be attained within a low temperature hydrothermal system, where rapid precipitation and fluid mixing may have occurred (Chapter 5) and bacterially reduced sulphur is inferred.

4.2.5 Summary

Two distinct sources of sulphide sulphur are interpreted in the Rathdowney Trend deposits and prospects: (1) a dominant bacteriogenic component derived by the reduction of Lower Carboniferous seawater sulphate; this sulphur is common to all major producing deposits in the Irish Midlands. (2) a subordinate, 'deep-seated' hydrothermal component transported with the ore-forming metals; this sulphur is dominant in the prospects and appears to occur most commonly in the deposits in proximity to major 'feeder' faults and generally later in the paragenesis.

Intermediate isotopic compositions of -10‰ and -12‰ prominent in the major ore zones at Lisheen and Galmoy respectively, suggest mixing of these two distinct sulphur sources.

4.3 CARBON AND OXYGEN

The common approach to stable isotope studies of gangue and alteration phases is through the isotopic analyses of minerals precipitated from or altered by hydrothermal fluids. For example, if an oxygen-bearing mineral is precipitated from solution, the stable isotopic ratio of the mineral is a function of the $\delta^{18}O$ value of the fluid, the temperature of mineral formation and whether isotopic equilibrium is established. Oxygen is a major component of the ore forming fluid in the form of water and is often in equilibrium with the precipitating minerals, however, a variety of species of carbon may be present in the same fluid and these may not be in equilibrium with the minerals deposited (Ohmoto, 1972).

The principal sources of carbon in hydrothermal fluids include marine limestones ($\delta^{13}C \sim 0‰$), deep-seated or average crustal sources ($\delta^{13}C \sim -7‰$), and organic compounds of biogenic origin ($\delta^{13}C \sim -25‰$). Carbon in hydrothermal systems is usually fixed in carbonate minerals and thus the mineralizing fluids must contain some of the oxidized carbon species $CO_{2(aq)}$, HCO_3^- or CO_3^{2-}. The proportions of these species at equilibrium in a hydrothermal fluid will be controlled by a range of factors, primarily pH and temperature. The $\delta^{13}C$ value of the sum of these species (ΣC) can be calculated from the $\delta^{13}C$ of a carbonate mineral using the fractionation factor between the

dolomite (sample 318 450.5) displays $\delta^{13}C$ values as low as -5.79‰. The mean $\delta^{18}O$ value of D5 calcite is 21.50‰ ± 1.31‰, with a wide range in values between 19.29 and 24.06‰.

4.3.2b Galmoy Deposit

A total of 14 analyses on 12 core samples were carried out; 11 analyses on ore-related and post-ore dolomites, and 3 analyses on syn- to post-ore calcites (Appendix, D5). Values for $\delta^{13}C$ in dolomite and calcite range from 0.61 to 3.50‰. Corresponding $\delta^{18}O$ values range from 19.26 to 25.39‰ (Figures 4.18, 4.19, 4.20).

The mean $\delta^{13}C$ and $\delta^{18}O$ values for D2 dolomite are 3.44‰ ± 0.15‰, and 24.23‰ ± 1.28‰ respectively. These values are higher than the corresponding values in D3 dolomites which have mean $\delta^{13}C$ and $\delta^{18}O$ values of 2.20‰ ± 0.52‰, and 21.25‰ ± 1.28‰. D2 and D3 dolomites at Galmoy are virtually identical isotopically to the same phases at Lisheen.

The mean $\delta^{13}C$ and $\delta^{18}O$ values for D5 dolomite are 2.73‰ ± 0.57‰, and 20.06‰ ± 1.31‰ respectively and are isotopically similar to D3 dolomite in the Galmoy deposit. Mean $\delta^{13}C$ and $\delta^{18}O$ values for late D5 calcite are 0.89‰ ± 0.36‰, and 21.39‰ ± 1.19‰ respectively. No D4 dolomite was analyzed at Galmoy.

4.3.2c Rathdowney Trend Prospects

A total of 9 analyses on 7 core samples were carried out; 8 analyses on syn- to post-ore related dolomites, and 1 analysis on post-ore calcite (Appendix D6). Values for $\delta^{13}C$ in dolomite range from 1.96 to 3.03‰. Corresponding $\delta^{18}O$ values range from 20.60 to 24.75‰ (Figures 4.21, 4.22, 4.23).

D4 dolomite generally consists of higher $\delta^{18}O$ values, than those observed in D3 dolomite, however, $\delta^{13}C$ values are very similar. The mean $\delta^{13}C$ and $\delta^{18}O$ values for D3 dolomite are 2.52‰ ± 0.50‰, and 21.10‰ ± 0.71‰ respectively. The mean $\delta^{13}C$ and $\delta^{18}O$ values for D4 dolomite are 2.66‰ ± 0.25‰, and 24.11‰ ± 1.05‰ respectively.

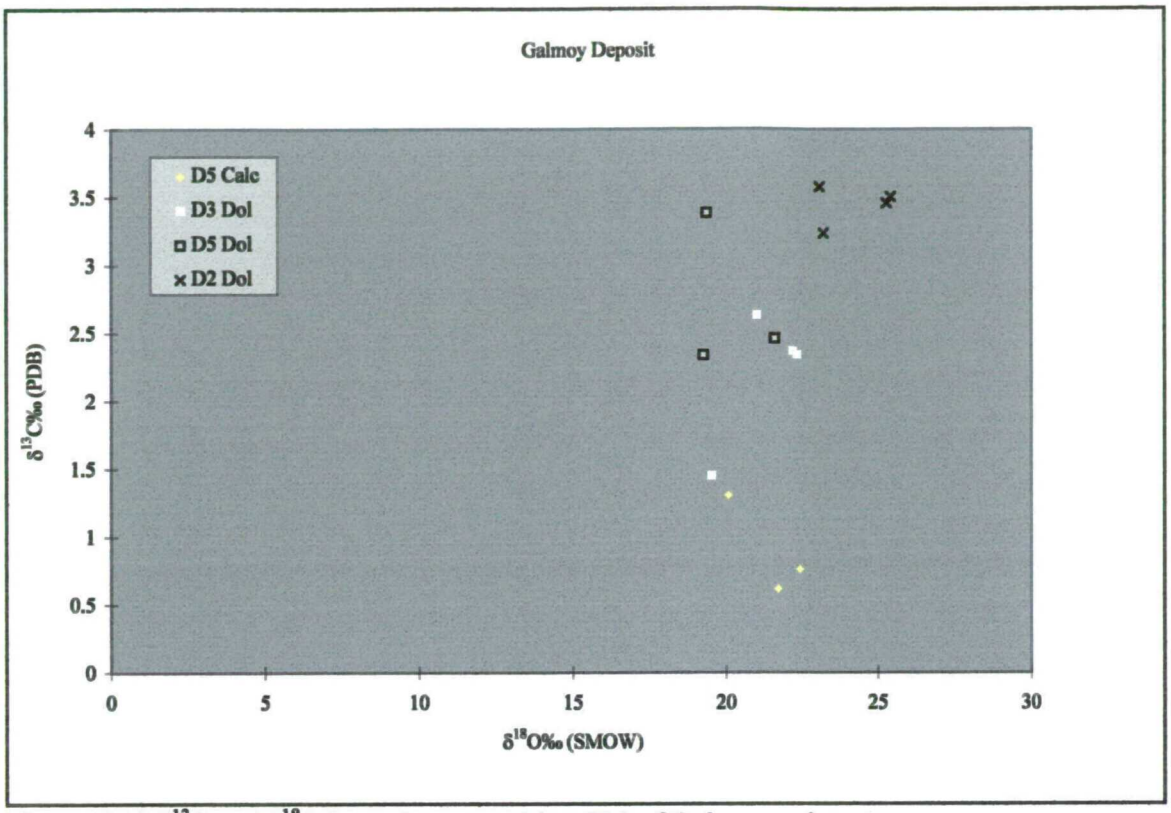


Figure 4.20 $\delta^{13}C$ and $\delta^{18}O$ isotopic composition (‰) of Galmoy carbonates.

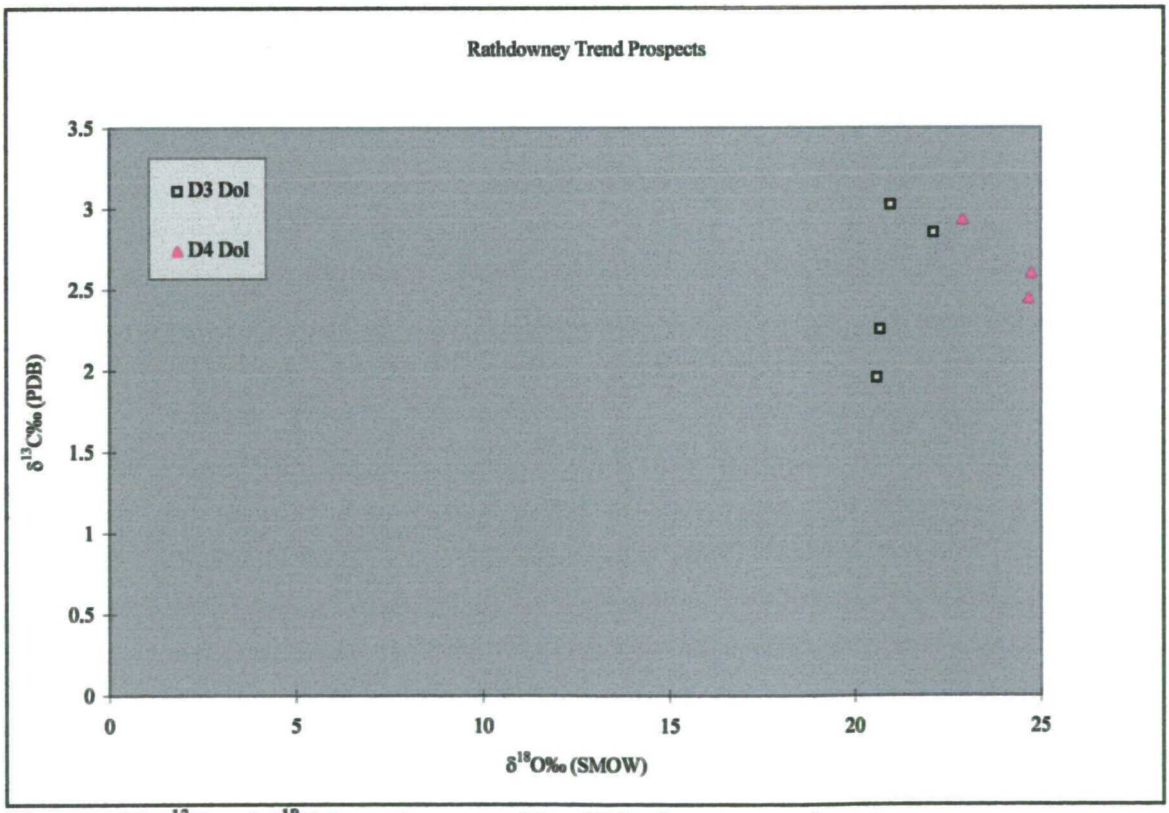


Figure 4.21 $\delta^{13}C$ and $\delta^{18}O$ isotopic composition (‰) of prospect carbonates.

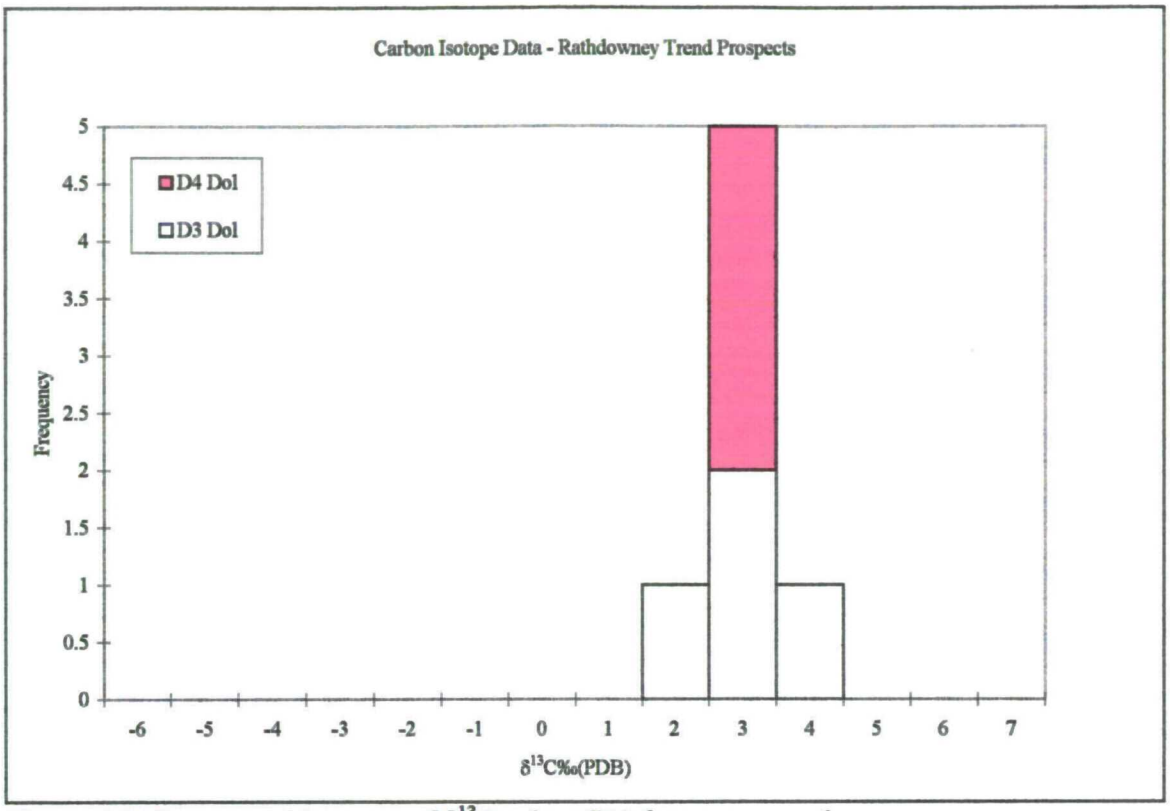


Figure 4.22 Frequency histogram of $\delta^{13}C$ values (‰) for prospect carbonates.

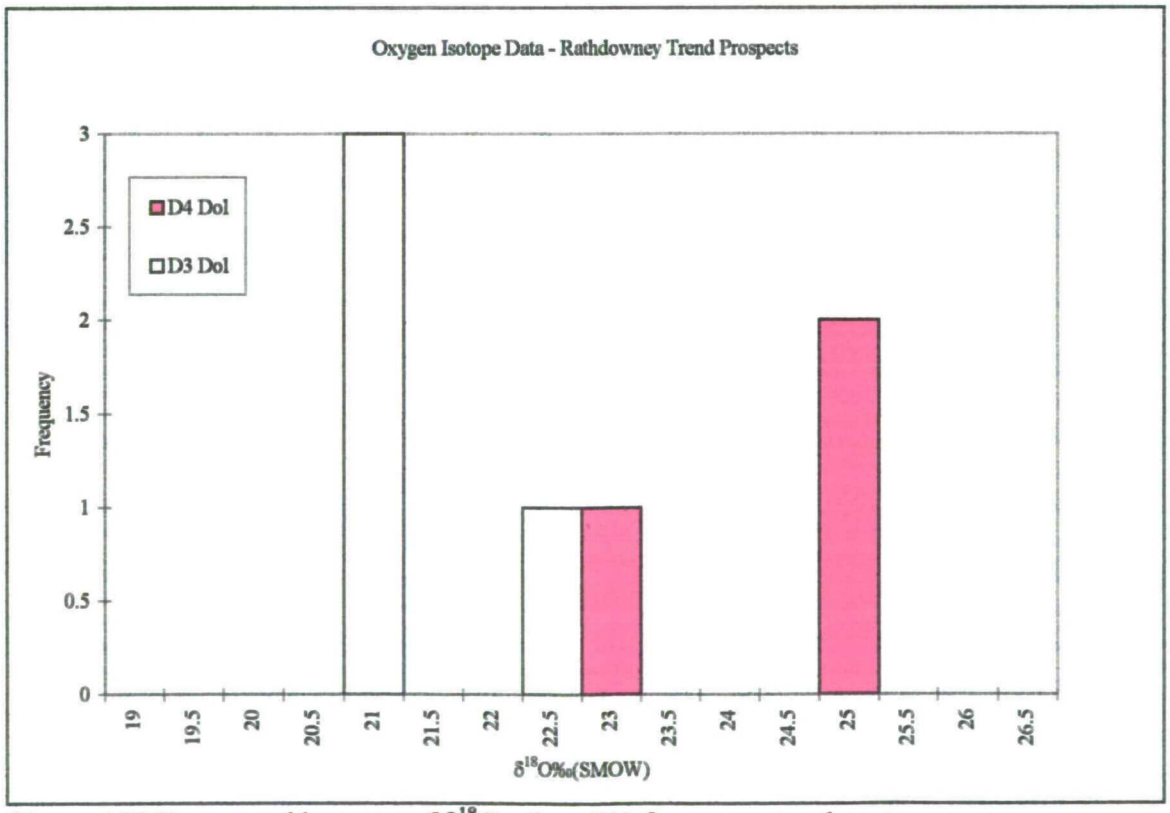


Figure 4.23 Frequency histogram of $\delta^{18}O$ values (‰) for prospect carbonates.

Midlands. This is a similar range to that observed for syn to post ore-stage hydrothermal dolomites in the present study and is therefore considered a likely temperature range for formation of the D2 dolomite. This temperature range coupled with the average $\delta^{18}O$ for D2 dolomite (24.43±1.47‰) gives an estimated $\delta^{18}O_{(H2O)}$ of 9-14‰. At 200°C, the approximate temperature for precipitation of D3, and an average $\delta^{18}O$ value of 20.96±0.78‰, the estimated $\delta^{18}O_{(H2O)}$ is +9.0‰. The temperature of formation of post-ore D4 dolomite is approximately 110°C. With an average $\delta^{18}O$ value of 23.92±0.91‰, this dolomite would have been precipitated at equilibrium from a fluid with a $\delta^{18}O$ value of +4.0‰. At approximately 180°C, the temperature for precipitation of D5 calcite, and a $\delta^{18}O$ value of 21.48‰±1.27‰, the estimated $\delta^{18}O_{(H2O)}$ is +11.0‰. D5 dolomite at the same temperature, with a $\delta^{18}O$ value of 20.32± 0.88‰, would be in equilibrium with an aqueous fluid with a $\delta^{18}O$ of +7.5‰.

4.3.4 Interpretation of Results (Carbon, Oxygen)

In the Lisheen deposit, ore-related D2 dolomite is very similar in $\delta^{13}C$ and $\delta^{18}O$ to Waulsortian regional dolomite, whilst late to post-ore D3 and D4 dolomite are relatively depleted in $\delta^{13}C$ and $\delta^{18}O$. The data exhibit a broad trend toward isotopically lighter compositions with time from the Waulsortian regional dolomite end member. This can be simply interpreted as reflecting decreasing isotopic exchange between an isotopically light infiltrating fluid and the Waulsortian host rock with time, probably due to the increasingly fracture-controlled and less pervasive fluid flow during the later stages of hydrothermal activity. However, Everett *et al.* (1996) showed that this trend could also be produced by a combination of fluid-host rock isotopic exchange and mixing of two fluids with contrasting C/O ratios. Either of these processes can result in a progressive decrease in the $\delta^{18}O$ of the precipitating carbonates and a corresponding increase in the $\delta^{18}O$ of the infiltrating fluid, accounting for the relatively high $\delta^{18}O$ values inferred for the ore-stage dolomitizing fluids. Assuming that the D5 dolomite probably represents the least exchanged infiltrating fluid as it tends to show the most depleted isotopic compositions, the estimated $\delta^{18}O_{(H2O)}$ for this dolomite of +7.5‰ provides an indication of the likely oxygen isotopic composition of the infiltrating fluid. This is consistent with $\delta^{18}O_{(H2O)}$ values of 6-7‰ estimated for inferred Lower Palaeozoic basement-equilibrated fluids (Wilkinson, pers. comm., 1998).

At Galmoy, D2 dolomite is also similar in $\delta^{13}C$ and $\delta^{18}O$ to Waulsortian regional dolomite and late to post-ore D3 and D4 dolomites show a comparable depletion in $\delta^{13}C$ and $\delta^{18}O$ and can be explained by the same general process as at Lisheen. D5 dolomite is isotopically similar to D3

dolomite, suggesting that these white dolomites could be related, albeit occurring in texturally different sites.

Depletion in the heavier isotopes of carbon and oxygen in mineralized carbonates relative to unmineralized host carbonates is common in zinc-lead deposits (Hall and Friedman, 1969; Boast *et al.*, 1981a; Recio *et al.*, 1988). This is due, at least for oxygen, to the relatively heavy isotopic composition of carbonates compared with most crustal fluids which generally have $\delta^{18}O_{(H2O)}$ values of <13‰ (Sheppard, 1986). Hall and Friedman (1969) found a linear relationship between $\delta^{13}C$ and $\delta^{18}O$ in host limestones at increasing distances from ore bodies in a number of MVT deposits. The lightest values were found closest to the deposits where temperatures were highest, clearly suggesting isotopic re-equilibration of limestones with hydrothermal fluids.

The late D5 calcite which clearly postdates D4 dolomite displays anomalously low $\delta^{13}C$ values (Fig. 4.15). The most likely source of isotopically light carbon for these veins is organic matter and, in fact, bitumen has been observed in association with late calcites elsewhere in the Irish Midlands (Gregg, pers. comm., 1998).

4.4 LEAD

Like sulphur, lead isotopic abundances are variable in nature. However, for Pb which has a number of unstable isotopes, this variation results from the addition to existing lead of varying amounts of ^{206}Pb, ^{207}Pb and ^{208}Pb, produced by the radioactive decay of uranium and thorium, over geological time. ^{204}Pb is a stable isotope, and amounts remain unchanged. Therefore, isotopic ratios are usually stated by reference to it, e.g., $^{206}Pb/^{204}Pb$, $^{207}Pb/^{204}Pb$, $^{208}Pb/^{204}Pb$. Two distinct categories of lead, ordinary lead and anomalous lead, have been recognized. Ordinary lead has isotopic ratios that increase steadily with time so long as it remains in uniform source rocks (probably the mantle) in contact with constant amounts of uranium and thorium. Once it has been removed from its source and separated from the elements producing radiogenic lead, its isotopic composition is fixed and if a mathematical model is assumed for the rate of addition of radiogenic leads in the source region then a model lead age can be calculated. Generally, such age determinations are in reasonable agreement with other radiometric age determinations. An additional important point is that when Pb is precipitated in a mineral which contains no U or Th (e.g. galena) then the lead isotopic composition gets fixed at that point in time and no further growth occurs. This is important with regard to the interpretation of galena Pb in Ireland.

Lead isotope ratios provide arguably the strongest evidence of involvement of the Caledonian basement as a source for metals in the Irish-type ore deposits. This origin of lead and other metals in the Zn-Pb deposits was first proposed by Russell (1968). From available data it appears that lead isotopic values for individual deposits depends on geographic location rather than on the style of mineralization or the age of the host rock (Caulfield *et al.*, 1986; O'Keefe, 1986). Lead isotopic ratios are much more variable between, than within, the Irish deposits. LeHuray *et al.* (1987) observed that the lead ratio $^{207}Pb/^{204}Pb$ increases (becomes more radiogenic) from northwest to southeast Ireland. On a $^{207}Pb/^{204}Pb$ versus $^{206}Pb/^{204}Pb$ diagram, the lead isotope data for the deposits plot in a series of en echelon clusters along a linear array (Dixon et al., 1990). The lead isotope data can be contoured across central Ireland. These contours, called 'isoplumbs' (LeHuray *et al.*, 1987), parallel structural and lithologic contacts within the Caledonian basement and cross-cut Carboniferous lithologies. The isoplumbs suggest local derivation of lead from the basement directly beneath individual deposits (LeHuray *et al.*, 1987).

Analysis of lead isotopic ratios in the Lisheen and Galmoy deposits will help to confirm or refute the general geographic variation in lead isotope ratios observed in the Irish deposits, and enable evaluation of the lead source in the southern Irish Midlands.

4.4.1 Sample Selection and Experimental Technique

A total of 10 analyses on 10 galena samples from Lisheen and Galmoy (Appendix D7, D8) were carried out in this lead isotope study. Lead isotope data have been collected from massive ore-stage, and vein-hosted, late to post ore-stage galena.

Galena samples for lead isotope analysis were diamond micro-drilled from hand specimens. Approximately 2-5μg of galena was then dissolved in an excess of 6M HCl. These solutions were directly pipetted on to a single rhenium filament with phosphoric acid and silica gel, as per standard lead loading technique. $^{206}Pb/^{204}Pb$, $^{207}Pb/^{204}Pb$, $^{208}Pb/^{204}Pb$ and other relevant derived ratios were then measured on a VG 54E mass spectrometer, and results were normalized to the NBS 981 standard. The data are corrected for mass fractionation. All errors are quoted to the last decimal places, that is, 15.585±8 is ±0.008.

4.4.2 Results

Lead isotope data are summarized in Table 4.1 and presented in conventional $^{208}Pb/^{204}Pb$ versus $^{206}Pb/^{204}Pb$, and $^{207}Pb/^{204}Pb$ versus $^{206}Pb/^{204}Pb$ plots (Figures 4.25, 4.26).

4.4.2a Lisheen Deposit

A total of 4 analyses on 4 core samples were carried out in the course of this study (Appendix D7).

Sample	$^{206}Pb/^{204}Pb$	$^{207}Pb/^{204}Pb$	$^{208}Pb/^{204}Pb$
416/195.5	18.182±10	15.602±11	38.076±24
262 162.1	18.197±10	15.585±8	38.078±16
179 176.25	18.160±22	15.563±28	38.010±38
431 205.70	18.193±12	15.624±11	38.158±28

Table 4.1 Lisheen deposit - lead isotope ratios in galena

The four analyses yielded mean values of $^{208}Pb/^{204}Pb = 38.080 \pm 0.061$, $^{207}Pb/^{204}Pb = 15.594 \pm 0.026$, and $^{206}Pb/^{204}Pb = 18.183 \pm 0.017$. Pb is isotopically fairly homogeneous within the Lisheen deposit as has been observed for other deposits in Ireland. There is no clear covariance of Pb isotope ratios with $\delta^{34}S$ values in galenas (see Figure 4.25).

4.4.2b Galmoy Deposit

A total of 6 analyses on 6 core samples were carried out in the course of this study (Appendix D8).

Sample	$^{206}Pb/^{204}Pb$	$^{207}Pb/^{204}Pb$	$^{208}Pb/^{204}Pb$
G16-27 366.0	18 204±8	15.597±7	38.084±17
MG18 90.0	18.209±12	15.587±12	38.089±15
MCW13 102.42	18 238±7	15.623±7	38.165±18
GY355 95.0	18.189±31	15.550±23	37.948±52
GY355 78.0	18.226±5	15 604±4	38.121±11
10CW	18.223±9	15.593±10	38.096±20

Table 4.2 Galmoy deposit - lead isotope ratios in galena

The six analyses yielded mean values of $^{208}Pb/^{204}Pb = 38.084 \pm 0.073$, $^{207}Pb/^{204}Pb = 15.592 \pm 0.024$, and $^{206}Pb/^{204}Pb = 18.215 \pm 0.018$. Pb is isotopically fairly homogeneous within the Galmoy deposit. There is no covariance of Pb isotope ratios with $\delta^{34}S$ values in galenas.

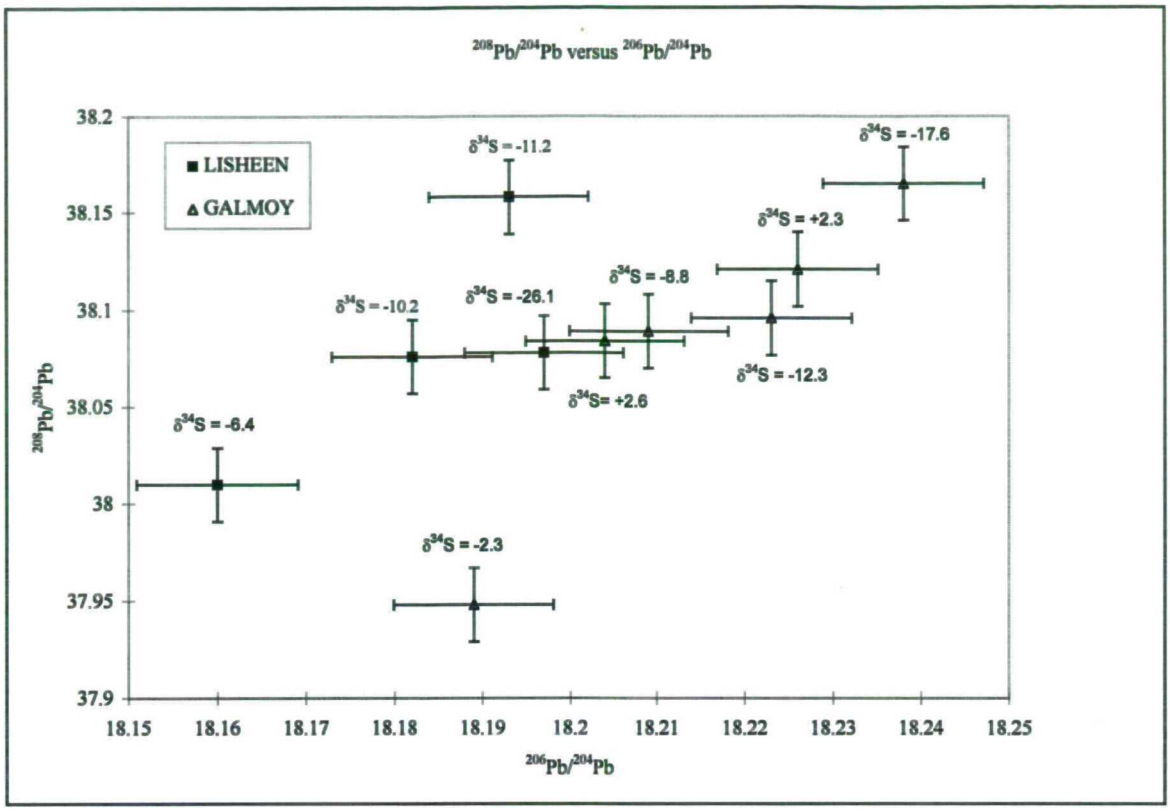


Figure 4.25 Lead isotope ($^{208}Pb/^{204}Pb$ versus $^{206}Pb/^{204}Pb$) ratios for Lisheen and Galmoy galena, with respective $\delta^{34}S$(CDT)‰ values. Error bars represent average analytical error of ~0.05%.

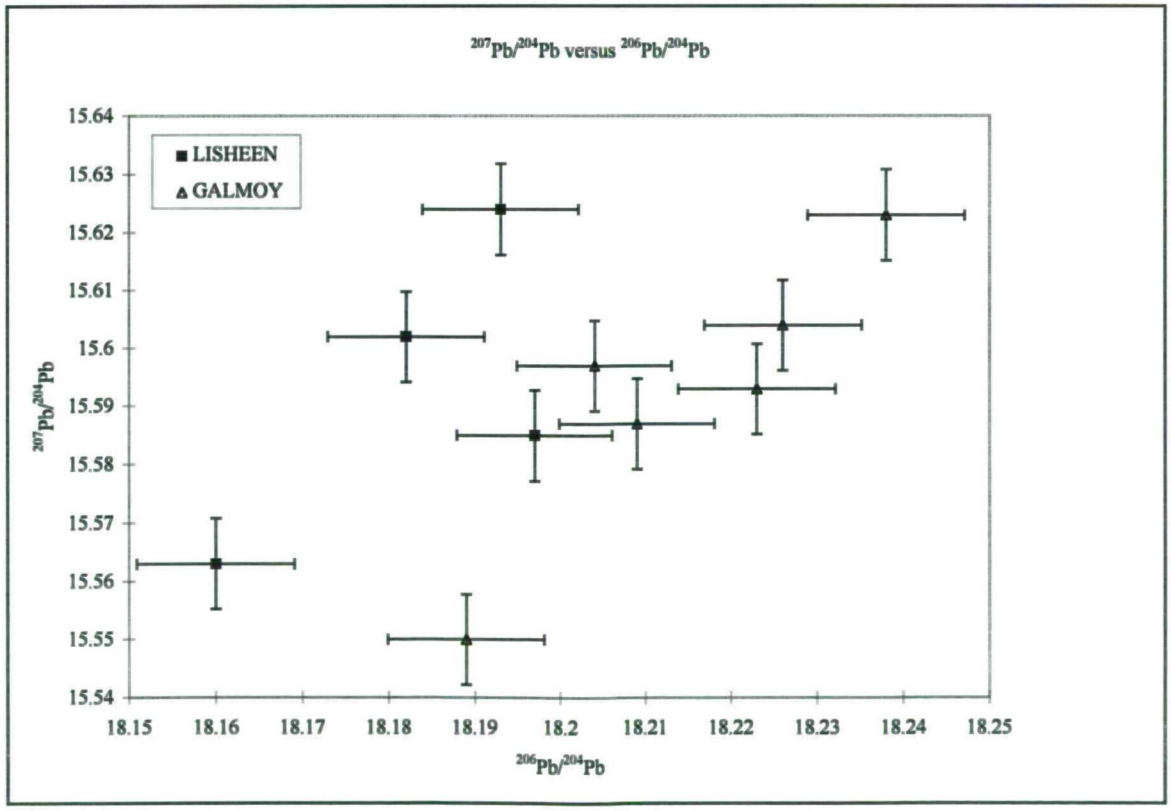


Figure 4.26 Lead isotope ($^{207}Pb/^{204}Pb$ versus $^{206}Pb/^{204}Pb$) ratios for Lisheen and Galmoy galena. Error bars represent average analytical error of ~0.05%.

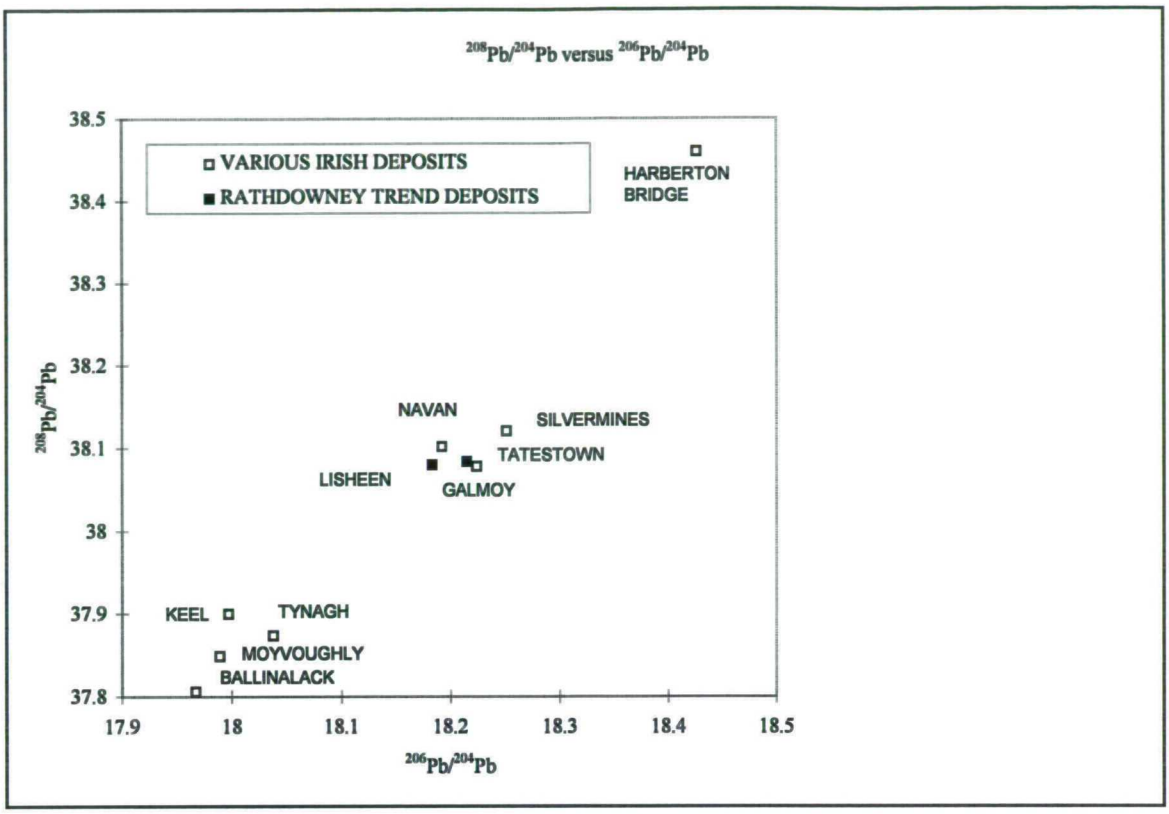


Figure 4.27 Lead isotope ($^{208}Pb/^{204}Pb$ versus $^{206}Pb/^{204}Pb$) ratio of average lead isotopic compositions of Lisheen and Galmoy deposits compared to other Zn-Pb deposits in Ireland.

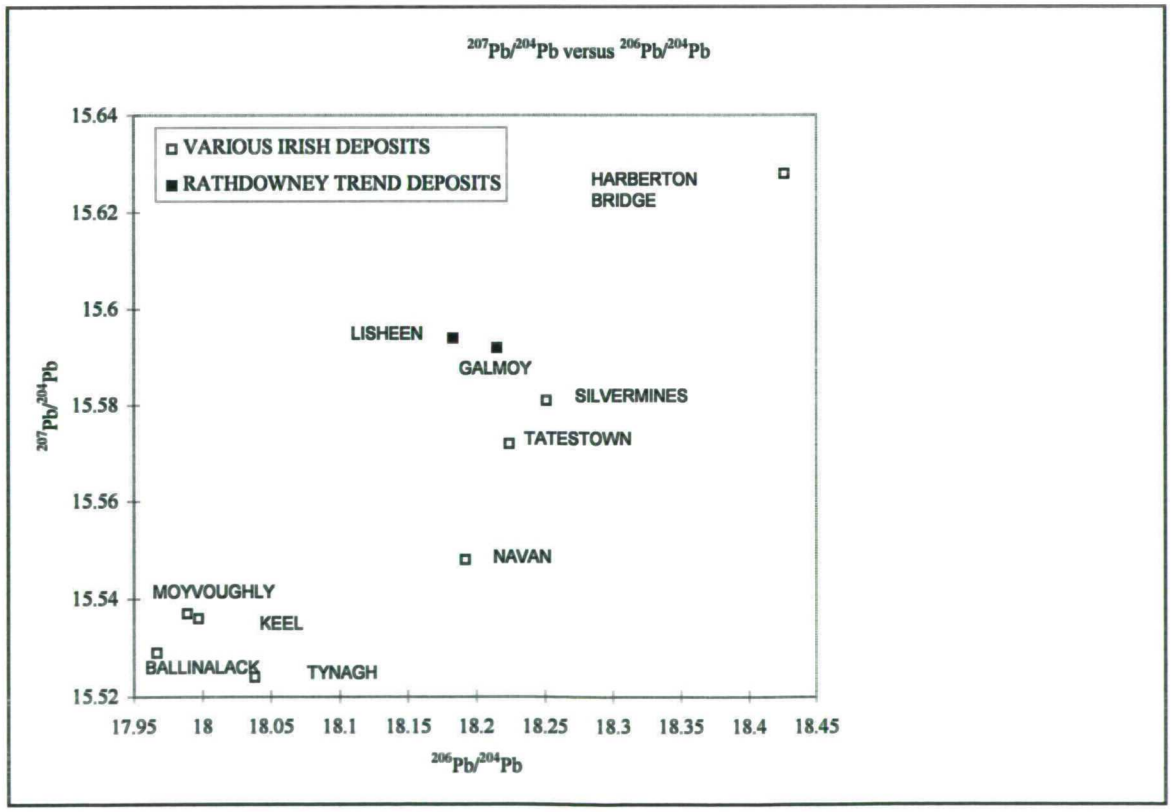


Figure 4.28 Lead isotope ($^{207}Pb/^{204}Pb$ versus $^{206}Pb/^{204}Pb$) ratio of average lead isotopic compositions of Lisheen and Galmoy deposits compared to other Zn-Pb deposits in Ireland.

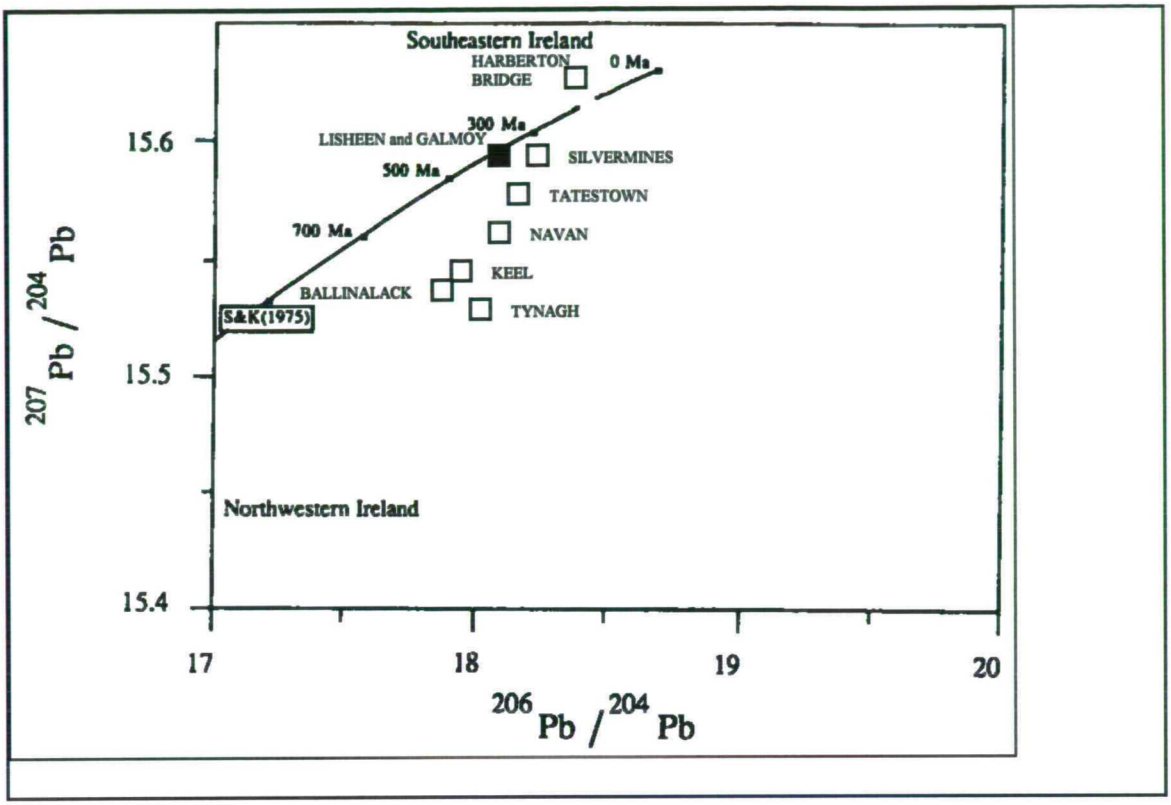


Figure 4.29 Lead isotope ($^{207}Pb/^{204}Pb$ versus $^{206}Pb/^{204}Pb$) ratio diagram showing the average lead isotopic compositions of Zn-Pb deposits in Ireland. Growth curve is that of Stacey and Kramers (1975). Data from this study and Boast *et al.* (1981b), Boast (1983), O'Keefe (1986), LeHuray *et al.* (1987), Gallagher *et al.* (1992), Boyce and Fallick (1995), Caulfield *et al.* (1986).

4.4.3 Interpretation of Results (Lead)

The data from Lisheen and Galmoy are plotted as averages along with data from other deposits in Ireland in Figures 4.27 and 4.28. Data at Lisheen and Galmoy are most similar to Silvermines, implying a similar Pb source. This is perhaps not surprising given the geographic proximity of these deposits (Figure 1.1). However, these data are anomalous as regards the conventional isoplumb theory of LeHuray *et al.* (1987). This indicates that the systematic trend of the isoplumbs does not extend down to the Rathdowney Trend in southern Ireland. This may be because of the structurally complex nature of the terrane south of the Iapetus which comprises a series of fault-bound packages of different geochemistry and origin (Kennan *et al.*, 1987; Murphy *et al.*, 1991).

The data lie slightly to the left of the lead isotope ($^{207}Pb/^{204}Pb$ versus $^{206}Pb/^{204}Pb$) data array for Zn-Pb deposits in Ireland (Figure 4.29). The $^{206}Pb/^{204}Pb$ isotope ratios of 18.20-18.30 are characteristic of Pb from a less radiogenic source than the ORS which shows heterogeneous Pb values in comparison to the Lower Palaeozoic basement which sit to the right of the deposit data array (Everett pers. comm., 1998). The ORS is interpreted as having an external radiogenic component (Everett pers. comm., 1998). This implies that the ORS is unlikely to have contributed significant lead to the Lisheen and Galmoy deposits

The lead isotope ($^{208}Pb/^{204}Pb$ versus $^{206}Pb/^{204}Pb$) ratio diagram (Figure 4.30) shows the average isotopic composition of galenas from Carboniferous- and Caledonian-hosted ore deposits in Ireland. Lisheen and Galmoy data are comparable to other deposits located in or above Silurian rocks. The Silurian rocks beneath the Rathdowney Trend deposits are a mixture of greywackes, siltstones and grits of the Hollyford Formation (Doran, 1974). Dixon *et al.* (1990) indicate how easily Pb is removed from greywackes by cold HCl leaching experiments.

In summary these data confirm the relative homogeneity of Pb isotope data within deposits and support the basement source hypothesis (Russell, 1968; LeHuray *et al.*, 1987) that lead in the base metal deposits of Ireland was principally derived from the local basement rocks. It is unlikely the Pb was sourced from the ORS, which is considered the main candidate for a southern metal source by Hitzman (1995b).

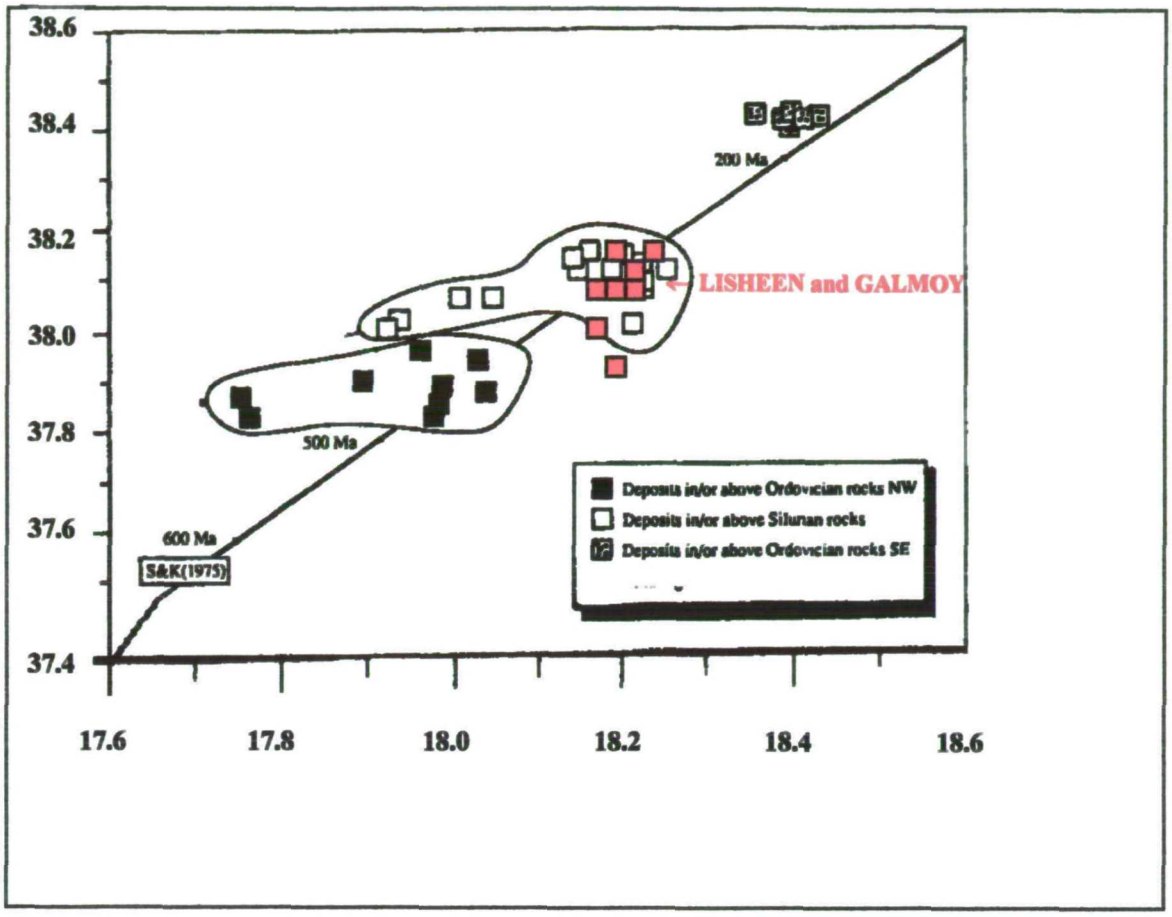


Figure 4.30 Lead Isotope ($^{208}Pb/_{204}Pb$ versus $^{206}Pb/^{204}Pb$) ratio diagram showing the average isotopic composition of galenas from Carboniferous- and Caledonian-hosted ore deposits in Ireland. Growth curve shown is that of Stacey and Kramers (1975). Modified after Dixon *et al.* (1990).

CHAPTER 5: FLUID INCLUSION STUDY

CHAPTER 5: FLUID INCLUSION STUDY

5.1 INTRODUCTION

The objective of this study was to examine and compare the thermal and compositional characteristics of the fluids that have affected the Lisheen and Galmoy deposits and the surrounding sub-economic prospects through a systematic microthermometric study of fluid inclusions from syn-, late, and post ore-stage minerals. Fluid inclusion data can reveal temporal variations in fluid properties if the paragenesis of the host minerals is known, and may reveal spatial variations if there is adequate regional sampling control.

Microthermometric analysis is the most routinely used non-destructive method in the study of fluid inclusions. This technique involves the measurement of the temperature of various phase changes that take place in an individual inclusion upon heating or cooling. Using these measurements reference may be made to simple phase diagrams (one, two, or three component systems), which allow the P-T-X state of the fluids at the time of trapping to be estimated. The main limitation of the technique is the fact that most natural systems are multi-component, so the P-T-X estimates are not truly quantitative (Roedder, 1984). Interpretation of more complex systems is therefore difficult, but the growing body of published theoretical and experimental work facilitates a greater understanding of realistic fluid systems. A detailed review of such studies is beyond the scope of this work and the reader is referred to books by Roedder (1984), Shepherd *et al.* (1985), Hollister and Crawford (1981) and a recent volume of short course notes by De Vivo and Frezzotti (1994).

As with many techniques there are some underlying assumptions made to enable microthermometric interpretation. The first is that the inclusions are representative of the fluid present at a particular time of crystal growth, and the second that the inclusions have behaved as closed systems and have not had material either added or removed since trapping. In the case of the trapping of a homogeneous fluid phase the premise that inclusions are representative of the ambient fluid system is probably a reasonable one. When two or more phases are trapped, it is generally assumed that the phase relations preserved in the inclusions will be the same as in the bulk fluid (Roedder, 1984). However, this may not always be the case (e.g. Ramboz *et al.*, 1988). Small scale heterogeneities due to the precipitation of the host mineral (e.g. boundary layer effect) will also exist but most workers (e.g. Roedder, 1984) consider these effects are probably too small to be of consequence.

The second assumption, that there have been no changes in bulk composition through time, is very important. In general in inclusion studies the problem is often the loss or leakage of material out of (or into) the inclusion. This leakage may occur by the long term and gradual diffusion of material. Unfortunately, the extent of this process is difficult to assess and there is a general lack of experimental evidence on diffusion rates of components from inclusions through various host minerals. It is generally thought that the process is not important but recent work by Sterner *et al.* (1993) suggests that at elevated temperatures and pressures, diffusion of water out of inclusions can occur. Bulk leakage occurs as a result of thermal or mechanical stress and can be recognized by irregular (or cracked) inclusion morphologies, variable degrees of fill within individual inclusion populations and anomalously high homogenization temperatures. A process known as necking-down may also take place where inclusions re-equilibrate to form several smaller more euhedral inclusions. If this occurs after nucleation of one or more new phases during cooling from trapping temperature, variable liquid/vapour or liquid/solid ratios may be preserved in the new inclusions, and they will not be representative of the original fluid.

5.1.1 Sample Selection and Experimental Technique

Forty five samples were selected for fluid inclusion studies from the deposits and prospects. Fluid inclusions were studied in dolomite, sphalerite, calcite, and authigenic quartz. The majority of the sphalerite samples in the deposits were selected from high grade ore zones, but were generally vein and vug-hosted. The high ore-grade replacive mineralization is extremely fine grained and does not contain fluid inclusions suitable for microthermometric study. The dolomite sample suite covers as wide a temporal and spatial distribution as possible throughout the Rathdowney Trend. However, D1 and D2 dolomites have been excluded from this study because very few workable fluid inclusions were found in the representative samples.

Fluid inclusions in D3 dolomite were used to characterize the syn-, to post-ore fluid regime. Inclusions in paragenetically late crystalline sphalerite which occurs in primary vugs preserved through dolomitization and in subsequent fractures with or without associated D5 calcite were used to distinguish late mineralizing ore fluids. Calcite is broadly considered as being partly contemporaneous with but mainly post-dates sphalerite deposition. In some cases very late calcite clearly post-dates D4 pink dolomite. Fluid inclusions in late D5 calcite veins were used to characterize the post-ore fluid regime. Minor authigenic quartz post-dates dolomite and appears to be contemporaneous with syn-, to post-ore calcite.

Fluid inclusions in 100μm thick doubly-polished wafers were analyzed using a Linkam™ THMG 600 heating-freezing stage, employing standard laboratory procedures (Shepherd *et al.*, 1985). Stage calibration was carried out at -56.6°C, 0.0°C, 10.0°C, 30.8°C and 293°C using synthetic H_2O-CO_2 fluid inclusion standards. The calibrated accuracy of the stage is ± 0.2 °C at -60.0 to +30.0°C and ± 0.5°C at >30.0°C. For clearly observable phase changes, measurement precision is ±0.1°C.

5.1.2 Fluid Inclusion Types and Occurrences

Aqueous inclusions are present in most samples examined. Both primary (and pseudosecondary) and secondary types were observed, these can be further classified on the basis of the differing proportions of solids, liquids and vapour present. Two main types have been identified: (1) monophase liquid (L) inclusions (predominantly primary); and (2) biphase liquid and vapour (L+V) inclusions (primary and secondary). The absence of a vapour bubble in the Type 1 inclusions likely indicates low trapping temperature and natural metastability (failure to nucleate a vapour bubble) (Roedder, 1984). Generally, only the primary or pseudosecondary type of biphase inclusions according to the criteria of Roedder (1984) were selected for microthermometric study.

Fluid inclusions in dolomite are commonly small (most are less than 10μm in size) and comprise two phases (L+V) at room temperature. They occur in the cloudy core regions (inherited from replacive dolomite) of the euhedral crystals, the clear rims are generally void of inclusions. Due to the small size and turbid nature of many of the samples studied, problems were encountered in defining the precise point at which the various phase changes take place.

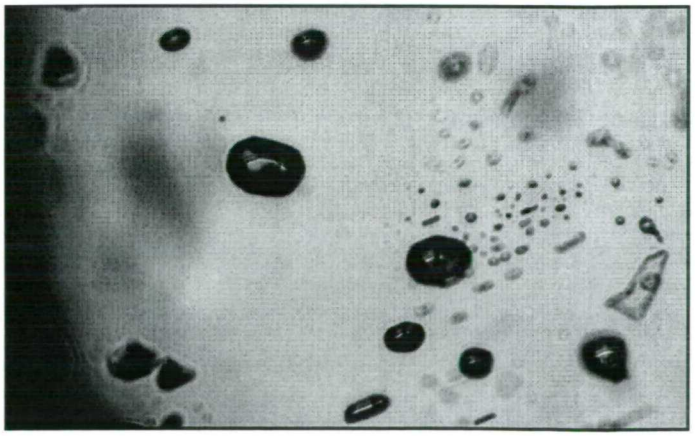


Figure 5.1 Primary and secondary inclusions in sphalerite (Long axis of photomicrograph = 130μm).

Fluid inclusions in sphalerite comprise two phases (L+V) at room temperature. The inclusions occur in clusters, generally lacking fracture control or are isolated. The inclusions are mostly euhedral, and are between 10-30μm in size. Sample 95/335.0 (Figure 5.1) exhibits large, euhedral, biphase, primary inclusions which occur in coarse vein-hosted

sphalerite as well as a plane of flat secondary inclusions on a cross-cutting micro fracture. Fluid inclusions in syn-, to post ore-stage calcites comprise two phases (L+V) and are randomly distributed in three dimensions. Fluid inclusions in Authigenic quartz are rare. They comprise two phases (L+V) and occur in clusters lacking fracture control.

5.1.3 Microthermometric Method

The microthermometric technique uses a heating-freezing stage (see section 5.1.1) and microscope in order to observe and measure the temperature of the phase changes which occur in inclusions upon heating or cooling. As an inclusion cools down from the temperature of trapping to that of observation (room temperature) differential contraction takes place between the solid crystal host and the liquid inclusion resulting in the formation of a vapour bubble. In this study, four phase changes in the presence of this bubble are important: the temperature of first melting (*Tfm*), the temperature(s) of salt hydrate melting (*Tmh*), the temperature of last ice melting (*TmI*), and finally, the liquid-vapour homogenization temperature (*Th*). Ice melting temperatures (*TmI*, where applicable and observable) were measured for approximately 60% of the inclusions for which homogenization temperature data have been obtained.

The temperature of first melting marks the first appearance of liquid upon warming the frozen inclusion and represents the characteristic eutectic temperature of the system. This indicates which dissolved salts are dominant in the inclusion fluid. Identification of the first melting temperature is important as it enables the use of the appropriate phase diagrams for estimation of salinities and element ratios. However, recording the phase change accurately is difficult, as it is marked by the initial formation of tiny amounts of liquid. Roedder (1984) points out that at least 10% melting of a frozen inclusion is generally required for the first melt to be identifiable.

In addition to ice, salt hydrates will normally be present in a frozen inclusion. The temperature at which the last hydrate phase melts is a function of fluid composition and the overall salinity of the trapped fluid. Paired *TmI* and *Tmh* data can be plotted on an appropriate phase diagram (e.g. Oakes *et al.*, 1990) and the ratios of the major solutes in the fluid can be estimated.

The final phase change recorded in this study is the homogenization temperature. This is the temperature at which the inclusion becomes homogeneous, i.e. the vapour bubble disappears into the liquid phase (L) or the liquid phase into the vapour phase (V). This measurement provides a *minimum* constraint on the temperature at which the inclusion formed and must be pressure corrected to give the true trapping temperature of the fluid. Fluid inclusion homogenization

temperatures only provide a minimum constraint on fluid temperature, the difference between T_h and trapping temperature being dependent on the fluid pressure at the time of entrapment. An end-member constraint is provided by the interpretation of the Irish deposits as near seafloor or exhalative systems (Russell, 1978). In this case, fluid pressures would be close to hydrostatic and would essentially depend on seawater depth. Navan shows evidence of shallow water, probably less than a few 10s of metres (Ashton *et al.*, 1992); conversely, the Silvermines area is considered to have been a deeper water basin at the time of mineralization, perhaps 200m (Taylor and Andrew, 1978). This would impart a maximum fluid pressure of ~20 bars. Given that the isochoric dP/dT for moderate salinity fluids is ~20bar $°C^{-1}$, this would yield a maximum correction of +1°C. Alternative models for mineralization invoke moderate burial at the time of mineralization, up to 1km (Hitzman & Beaty, 1996). It is likely that close to hydrostatic conditions would prevail at such depths, giving a maximum estimate of fluid pressures of ~120bars. This implies a maximum temperature correction of +6°C. In both cases, this is markedly less than the range of T_h values observed for individual samples and, particularly with regard to temperature trends in the data, can safely be ignored. This assumption is supported by recent alkali geothermometry which suggest fluid temperatures are close to T_h values in Lower Palaeozoic-hosted veins (Everett *et al.*, in press).

Homogenization temperatures were measured for each selected fluid inclusion in a wafer of sample prior to cooling runs, in order to avoid the possible effects of stretching or leakage caused by fluid freezing (especially problematic for calcite). For monophase fluid inclusions from late gangue phases, however, cooling runs were performed first to force the nucleation of a vapour bubble.

Fluid inclusions commonly behave in a metastable manner, i.e. the inclusion (or phases therein) is not in the equilibrium or most stable state. This behaviour manifests itself in two ways. Invariably, fluid inclusions do not freeze in the temperature range that is expected for a given composition, resulting in a phenomenon known as "supercooling". This occurs because of the absence of suitable nucleation sites for the solid phases. Solidification once started is instantaneous. Superheated ice is a consequence of metastability. This occurs when liquids are metastably stretched to occupy a larger volume at lower density than they would at equilibrium due to the failure of a shrinkage bubble to nucleate. This type of behaviour may be caused by the vapour bubble collapsing due to the growth of ice or natural failure of a vapour bubble to nucleate, and thus, last ice melting occurs in the absence of the vapour bubble. This may lead to ice melting at temperatures above 0°C in dilute inclusions or erroneously high melting

temperatures in more saline inclusions. These and other metastabilty phenomena are discussed at length by Roedder (1984).

5.2 RESULTS

A total of 828 microthermometric measurements on 45 samples were carried out. Homogenization and melting temperatures as well as compositional data calculated from melting temperatures are described for each of the sample locations. Microthermometric data (Appendix E) are presented in frequency histograms and salinity versus homogenization temperature plots. The data are subdivided according to location, mineralogy, and paragenetic stage.

5.2.1 Estimate of Composition and Salinity

In general the first observable melting temperatures fall within the range to -54 to -39°C, however the actual first melting temperatures could be lower than observed. The lower values in this range are characteristic of the $NaCl\text{-}CaCl_2\text{-}H_2O$ system (eutectic at ~ -52°C). The first melting temperatures of such a system are usually within 3°C of the eutectic temperature if stable salt hydrates form during cooling, but may be as low as -80°C if metastable salt hydrates form (Davis *et al.*, 1990). Salinities have been routinely estimated using the $NaCl\text{-}H_2O$ system (Bodnar, 1993) and are referred to as weight percent equivalent NaCl (wt% NaCl eq.). The ternary $NaCl\text{-}CaCl_2\text{-}H_2O$ system was not used for salinity estimations due to insufficient *Tmh* data.

5.2.2 Lisheen Deposit

A total of 548 microthermometric measurements were carried out on sphalerite and gangue samples in the Lisheen deposit (Figures 5.2, 5.3, 5.4, 5.5). Ice melting temperatures (*TmI*), where applicable and observed, were measured for approximately 54% of the fluid inclusions (Appendices E1 and E2).

5.2.2a Dolomites (Syn-, to Post Ore-Stage)

Homogenization temperatures for fluid inclusions hosted by syn-, to post ore-stage D3 dolomite are variable but generally fall within the range 170-210°C. Salinities range from 5-7 wt% NaCl eq. A low temperature, high salinity fluid is present in primary inclusions in the post ore-stage D4 dolomite. Homogenization temperatures indicate a modal temperature of 90-100°C. Salinities

range between 23.0-28.7 wt% NaCl eq. A preliminary study of the homogenization temperatures for fluid inclusions in $D1_C$ dolomite indicate a range within 198-218°C.

5.2.2b Sphalerite (Late Ore-Stage)

Homogenization temperatures for primary fluid inclusions hosted by late ore-stage sphalerite indicate a modal temperature of 170-180°C and a range of 140-210°C. The highest homogenization fluid temperatures (~210°C, with the exception of two outliers) occur in sub-Waulsortian hosted sphalerite (sample 095 335.0) proximal to an E-W trending fault (F291) in the Derryville zone. A small population of lower temperature (70-130°C) secondary inclusions is also present in the sphalerite. Salinities of the higher temperature fluids range from 10.4-18.1 wt% NaCl eq. Salinities of the low temperature fluids range between approximately 24.0-29.0 wt% NaCl eq. Hydrohalite melting occurs prior to ice melting in the sphalerite samples at a temperature of -22.6 ± 0.28°C, indicating NaCl is the dominant solute present.

Homogenization temperatures for fluid inclusions hosted by Main zone sphalerite indicate a modal temperature of 170-180°C (Figure 5.4). Fluid inclusions hosted by North zone and Bog zone sphalerite display slightly higher homogenization temperatures with a modal value of 190-200°C. The highest homogenization temperatures occur in fluid inclusions hosted by Derryville zone sphalerite with a modal value of 200-210°C (Figure 5.4). A moderate temperature (170-200°C), low salinity (~4.5 wt% NaCl eq.) fluid occurs in secondary inclusions in the North zone, but is not observed elsewhere. The low temperature, high salinity fluid present in secondary inclusions in sphalerite is present in all of the ore zones except Main zone.

5.2.2c Calcite and Authigenic Quartz (Late to Post Ore-Stage)

Homogenization temperatures for fluid inclusions in D5 calcite considered contemporaneous with late ore-stage mineralization (D5 Calc (Minz)) indicate a modal temperature of 200-210°C (Figure 5.2). Salinities primarily range between 8-20 wt% NaCl eq. Fluid inclusions hosted by a calcite matrix breccia from within the Derryville ore zone (D5 Calc (Matrix)) display modal homogenization temperatures of 180-190°C. Salinities principally fall within the range 10-18 wt% NaCl eq.

Homogenization temperatures for fluid inclusions hosted by minor authigenic quartz range between 120-150°C, with salinities of 19.0-24.6 wt% NaCl eq. Late D5 calcite, which clearly

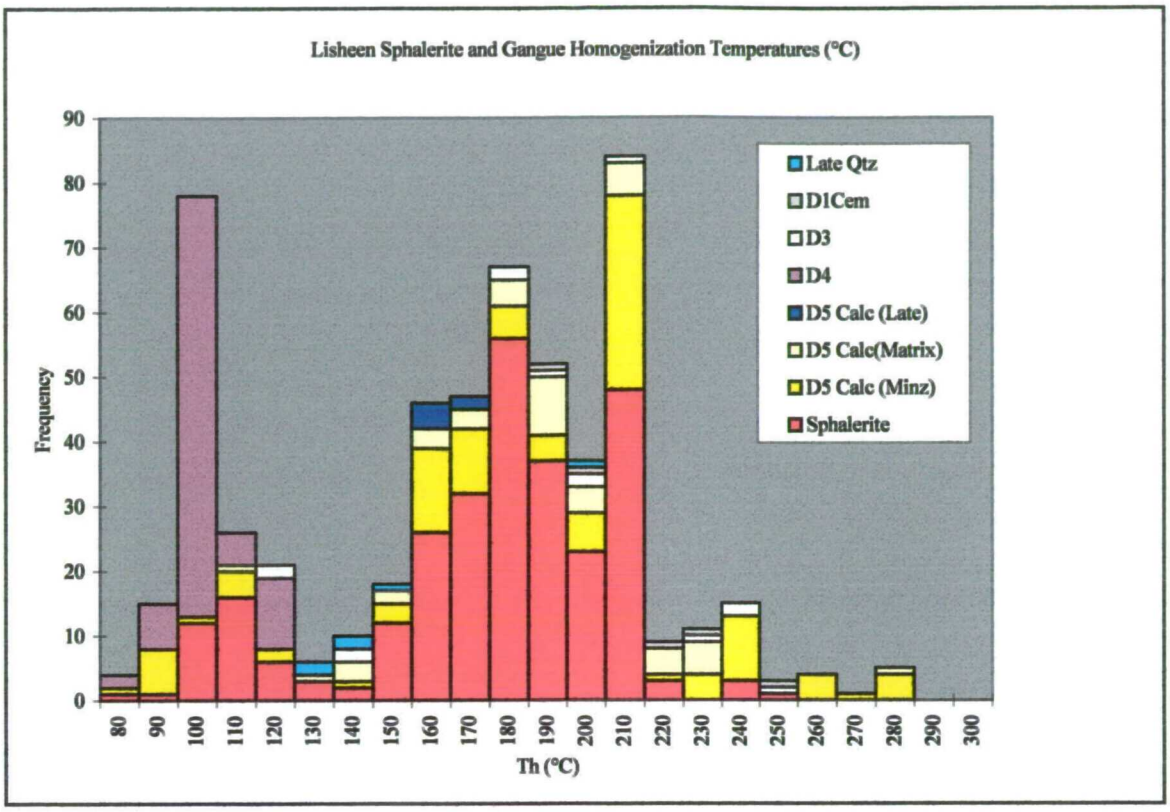


Figure 5.2 Frequency histogram of all homogenization temperatures (°C) at Lisheen.

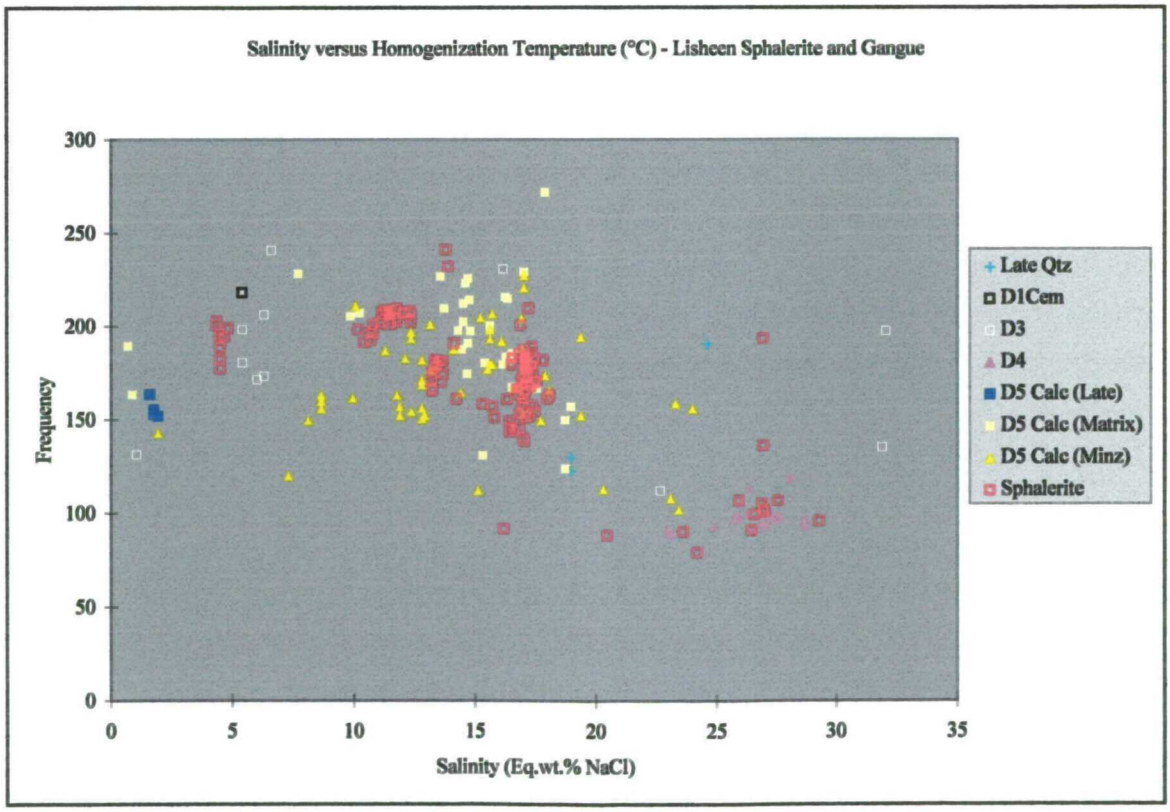


Figure 5.3 Salinity versus homogenization temperature of sphalerite and gangue phases at Lisheen.

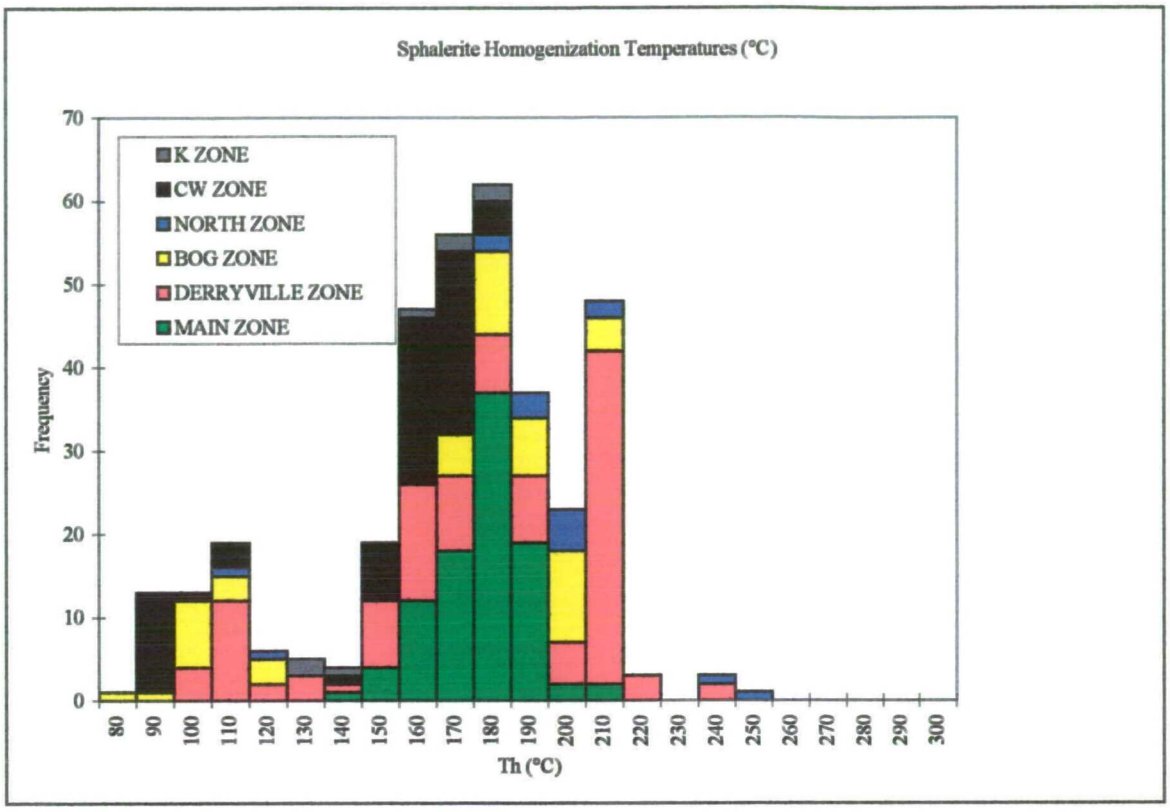


Figure 5.4 Frequency histogram of homogenization temperature in sphalerite, subdivided according to ore zone in the deposits.

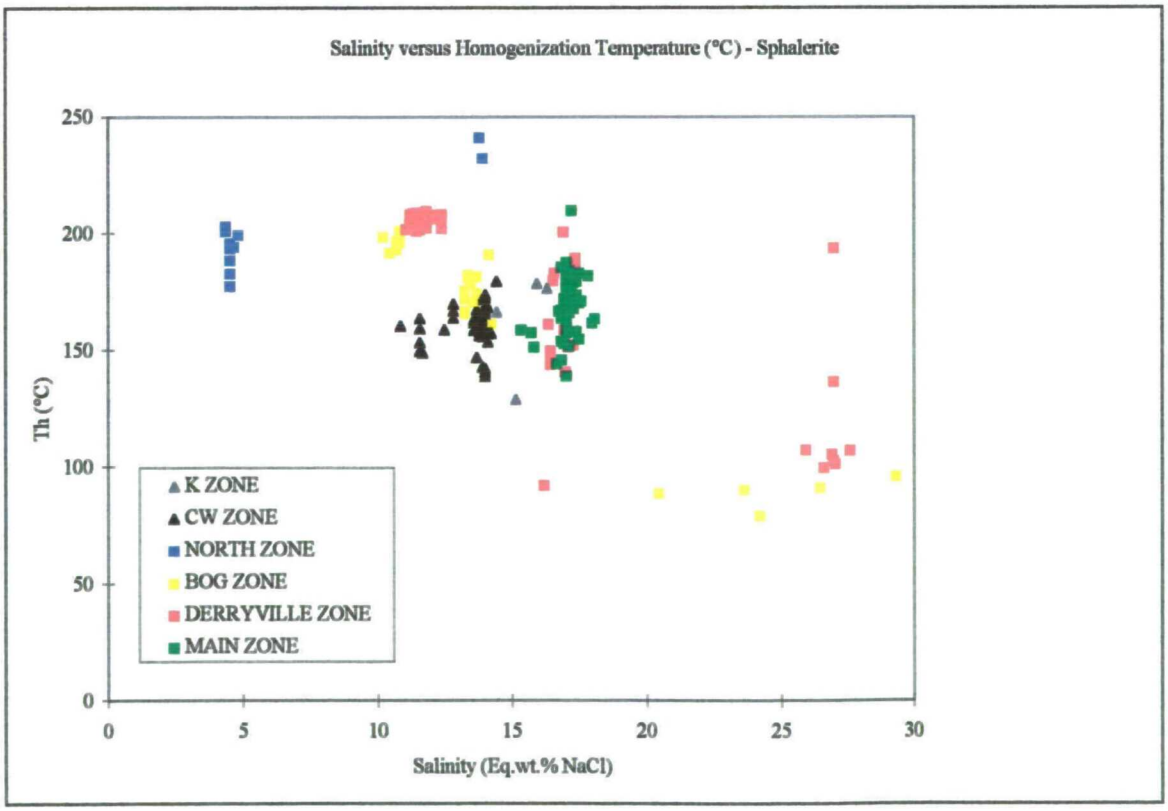


Figure 5.5 Salinity versus homogenization in sphalerite, subdivided according to ore zone in the deposits.

post-dates D4 dolomite, is characterized by homogenization temperatures in the range 150-170°C. Salinities are low ~2.0 wt% NaCl eq.

5.2.3 Galmoy Deposit

A total of 153 microthermometric measurements were carried out on sphalerite and gangue samples from the Galmoy deposit (Figures 5.4, 5.5, 5.6, 5.7). Ice melting temperatures (*TmI*), where observed, were measured for approximately 56% of the inclusions (Appendices E3 and E4).

5.2.3a Dolomites (Syn-, to Post Ore-Stage)

Homogenization temperatures for fluid inclusions hosted by syn-, to post ore-stage D3 dolomite indicate a modal temperature of 180-190°C and range from 130-230°C (Figure 5.6). Salinities range predominantly between 12-16 wt% NaCl eq. In a sub-Waulsortian hosted D5 dolomite vein (G16-27/383.5), moderate temperature (160-200°C), and low temperature (90-130°C) inclusions are present. Salinity data are highly variable.

5.2.3b Sphalerite (Ore-stage to Late Ore-Stage)

Homogenization temperatures for fluid inclusions hosted by ore-stage and late ore-stage sphalerite indicate a modal temperature of 160-170°C (Figure 5.6), lower than homogenization temperatures in late ore-stage sphalerites in the Lisheen deposit. Salinities for the sphalerite are similar to those of the syn-, to post ore-stage D3 dolomite and range between 11 to 16 wt% NaCl eq. A small population of lower temperature (80-110°C) secondary inclusions is also present in the sphalerite, the salinity of which are unknown. A similar low temperature fluid is present in the late ore-stage sphalerites at Lisheen; this fluid has high salinity. Sphalerites show no clear distinction in homogenization temperatures between the CW and K ore zones (Figure 5.4) but salinity values are slightly higher in the K zone (Figure 5.5).

Hydrohalite melting occurs prior to ice melting in the crystalline ore-stage sphalerite (sample 2.0134) at -22.4 ±0.2°C. This is similar to sphalerite at Lisheen and similarly indicates a dominance of NaCl in the fluid.

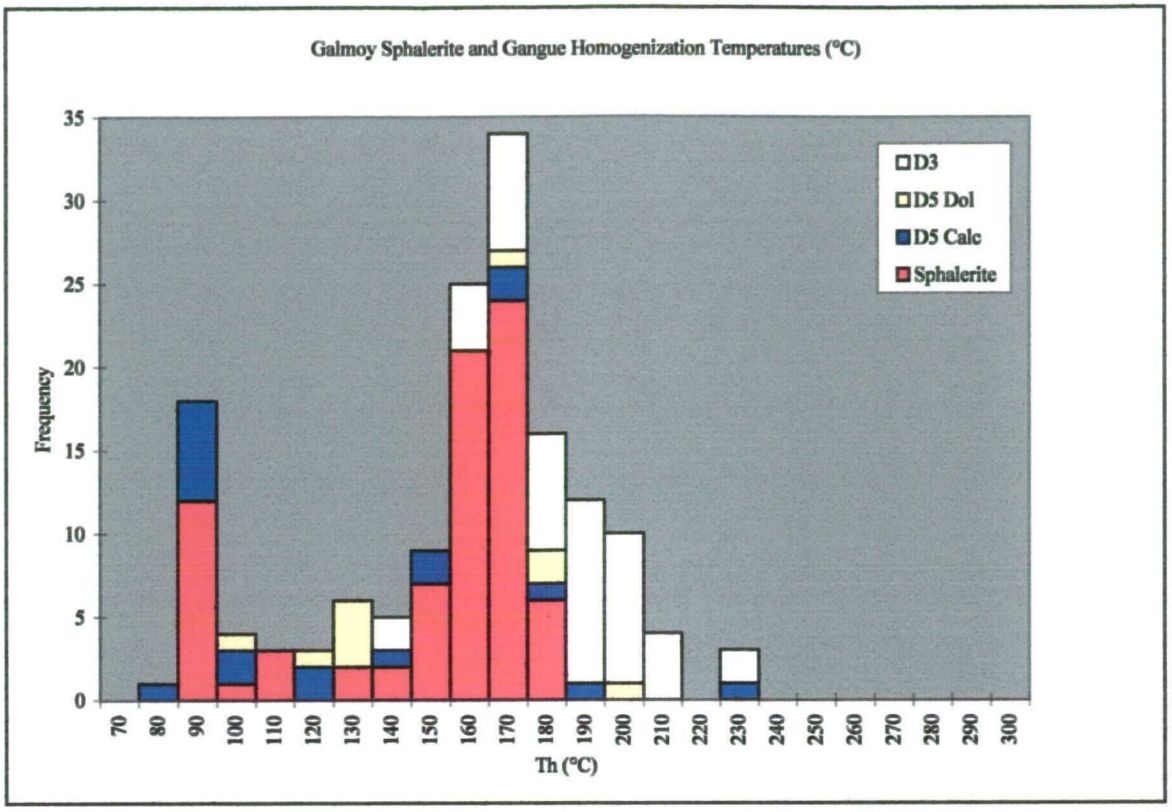


Figure 5.6 Frequency histogram of all homogenization temperatures at Galmoy.

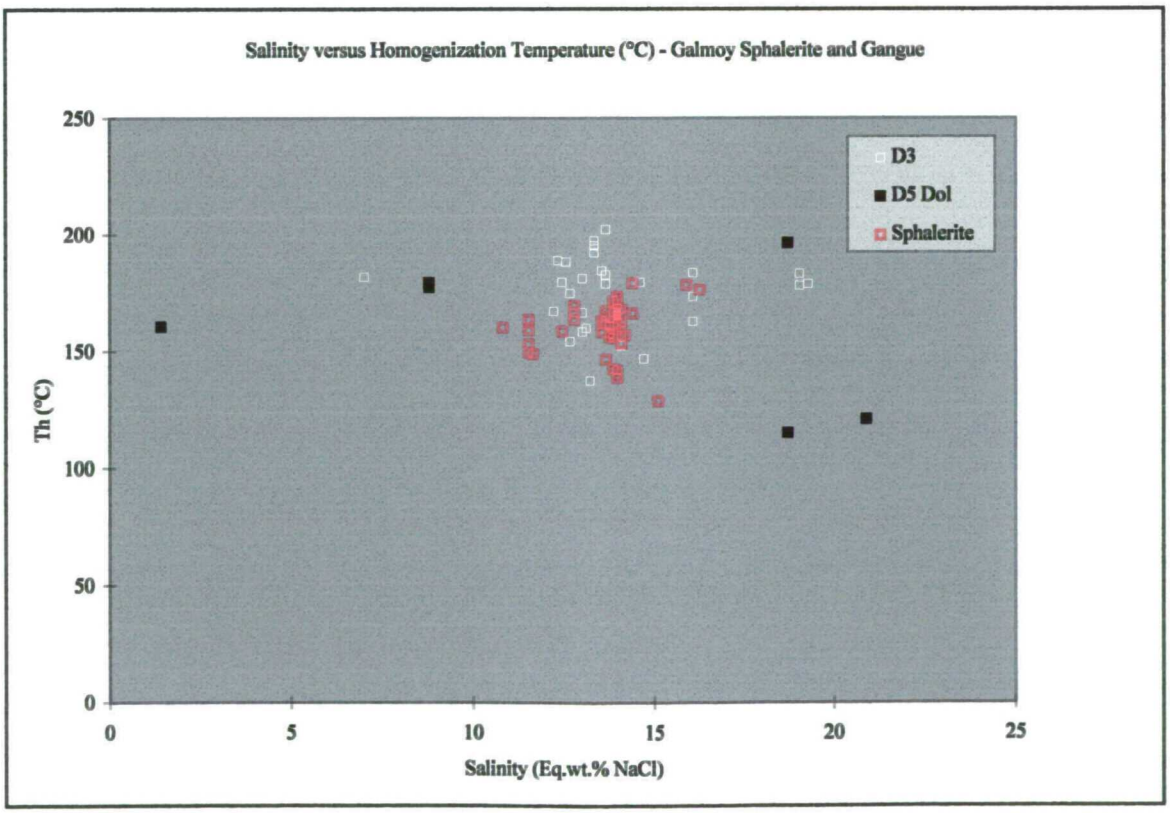


Figure 5.7 Salinity versus homogenization temperature of sphalerite and gangue phases at Galmoy.

5.2.3c Calcite (Post Ore-Stage)

Homogenization temperatures in sub-Waulsortian hosted calcite with trace pyrite from the CW ore zone are highly variable (Figure 5.6). However, as at Lisheen, fluid inclusion populations are present at 90°C and ~160°C. Salinity data are also variable, indicating that variable fluids are present.

5.2.4 Rathdowney Trend Prospects

A total of 127 microthermometric measurements were carried out on sphalerite and gangue samples in the prospects (Figures 5.8, 5.9). Ice melting temperatures (*Tml*) were measured for approximately 70% of the inclusions (Appendices E5 and E6)..

5.2.4a Dolomites (Syn-, to Late stage)

Homogenization temperatures for fluid inclusions hosted by D3 dolomite display a mode at 210-220°C (Figure 5.8). Salinities range principally between 2.0-16.0 Eq.wt.% NaCl. A low temperature (100-130°C), high salinity (~27 wt% NaCl eq.) fluid is present in secondary(?) inclusions in D3 dolomite in the Durrow prospect. An unusually high temperature (240-270°C) population is present in inclusions in D3 dolomite from the Durrow prospect (DUR1/686.5).

Homogenization temperatures for fluid inclusions hosted by post ore-stage D4 dolomite show a mode at 110-120°C, similar to homogenization temperatures in D4 dolomites from Lisheen. However, the range of temperatures in the prospects is much greater (80-160°C). Salinities predominantly fall within the range 21-26 wt% NaCl eq.

Homogenization temperatures for fluid inclusions hosted by D5 dolomite which is contemporaneous with crystalline sphalerite (sample HC5/122.9) in the Holycross prospect, display moderate temperature (170-190°C), and low temperature (90-120°C) populations. These are similar to the fluids identified in the D5 dolomite vein at Galmoy. Salinities in the low temperature inclusions fall in the range 28-29 wt% NaCl eq.

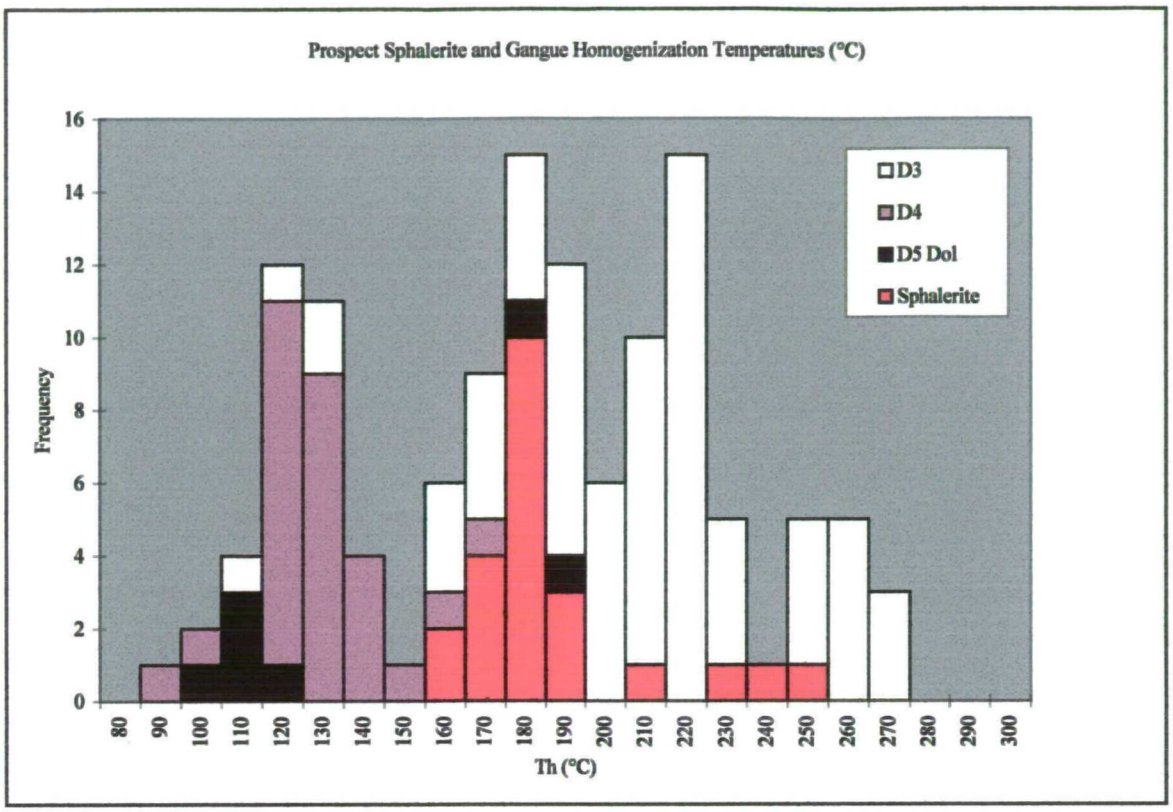


Figure 5.8 Frequency histogram of all homogenization temperatures in the Rathdowney Trend prospects.

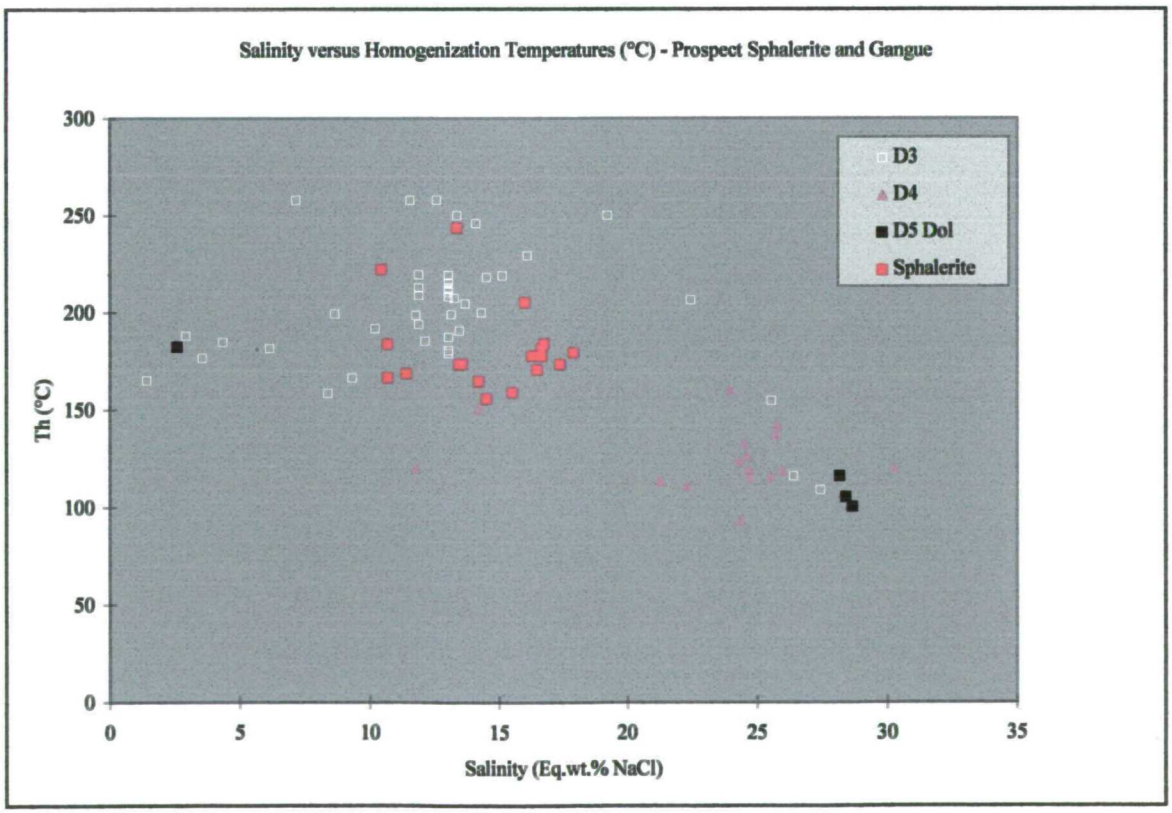


Figure 5.9 Salinity versus homogenization temperature in sphalerite and gangue phases at the Rathdowney Trend prospects.

5.2.4b Sphalerite (Late Stage)

Homogenization temperatures for fluid inclusions hosted by late stage sphalerite (HC5/122.9) at the Holycross prospect display a mode at 170-180°C (Figure 5.8), the same as homogenization temperatures in late ore-stage sphalerites in the Lisheen deposit. However, a small population of higher temperature (220-250°C) primary inclusions is also present in the sphalerite. These show similar salinities to the lower temperature population and may therefore be the result of leakage. Salinities of the moderate temperature fluids range from 10.4-17.9 wt% NaCl eq., the same range observed in the late ore-stage sphalerites at Lisheen, and similar to ore-stage and late ore-stage sphalerites at Galmoy. Hydrohalite melting occurs prior to ice melting in the late stage crystalline sphalerite at -22.7°C, indicative of a NaCl dominated solution.

5.2.5 Interpretation of Results

The microthermometric results suggest that at least two distinct end member fluids have been present during the evolution of the hydrothermal systems of the Rathdowney Trend deposits and prospects. The thermal and compositional characteristics of the fluids in different paragenetic stages and the relationships of the different fluids in each stage are discussed in this section.

According to the relative chronology determined by carbonate petrography (section 3.2), the evolution of hydrothermal systems in the Rathdowney Trend deposits and prospects can be broadly divided into three stages, i.e., syn-, late, and post ore-stages. Fluids present during the mineralization stage are represented by fluid inclusions in sphalerite and cogenetic calcite (D5 Calc) and dolomite (D3, D5 Dol) phases. Fluids post-dating the ore stage are recorded by fluid inclusions in D4 dolomite and late calcite filling vugs. Pre ore-stage fluids represented by fluids in regional dolomite cements have not been studied in detail.

Homogenization temperatures for fluid inclusions hosted by sphalerite and gangue phases in the Rathdowney Trend indicate a modal temperature of 170-180°C (Figure 5.10). Homogenization temperatures for fluid inclusions hosted by late ore-stage sphalerite indicate bimodal populations at 175°C and 205°C (Figure 5.10). From the salinity versus homogenization plot (Figure 5.11) two end member fluids are inferred: (1) a moderate temperature (160-210°C), moderate salinity (9-15 wt% NaCl eq.) fluid in primary gangue and sphalerite inclusions; and (2) a distinctive low temperature (80-140°C), high salinity (22.5-29.0 wt% NaCl eq.) fluid principally occurring in

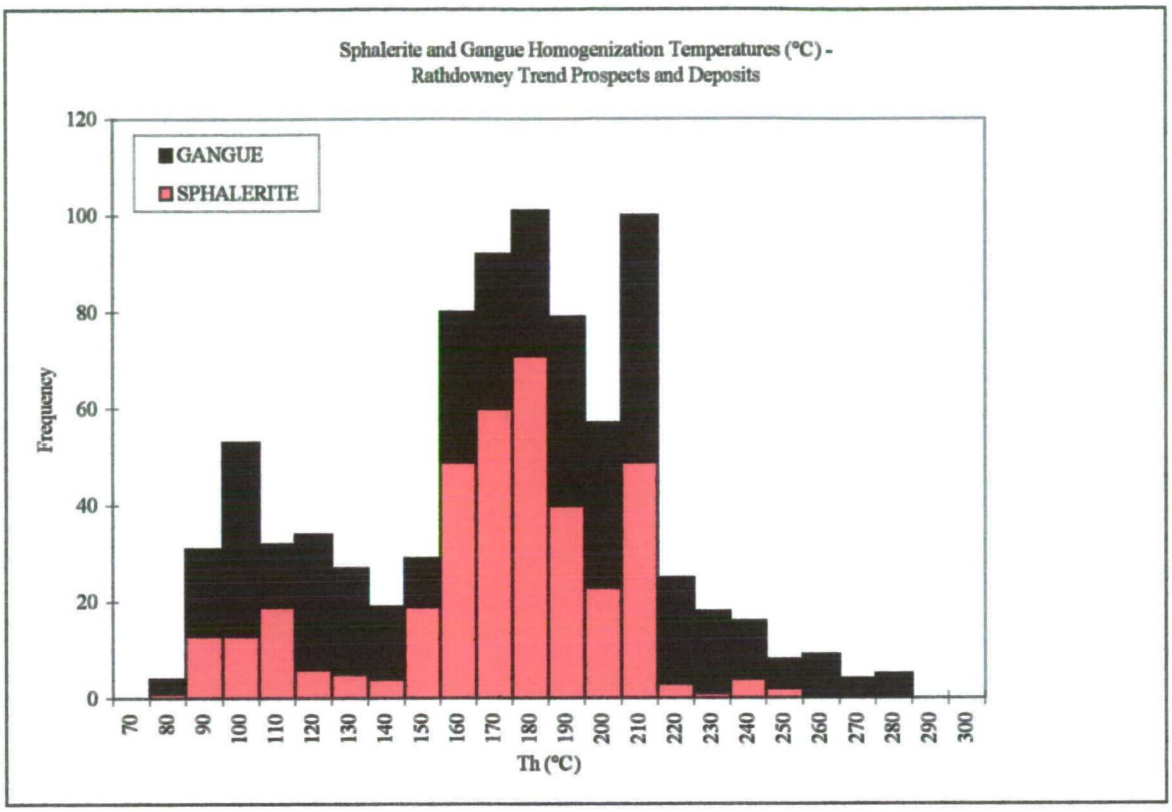


Figure 5.10 Frequency histogram of all homogenization temperatures in the Rathdowney Trend prospects and deposits, subdivided according to mineral phase.

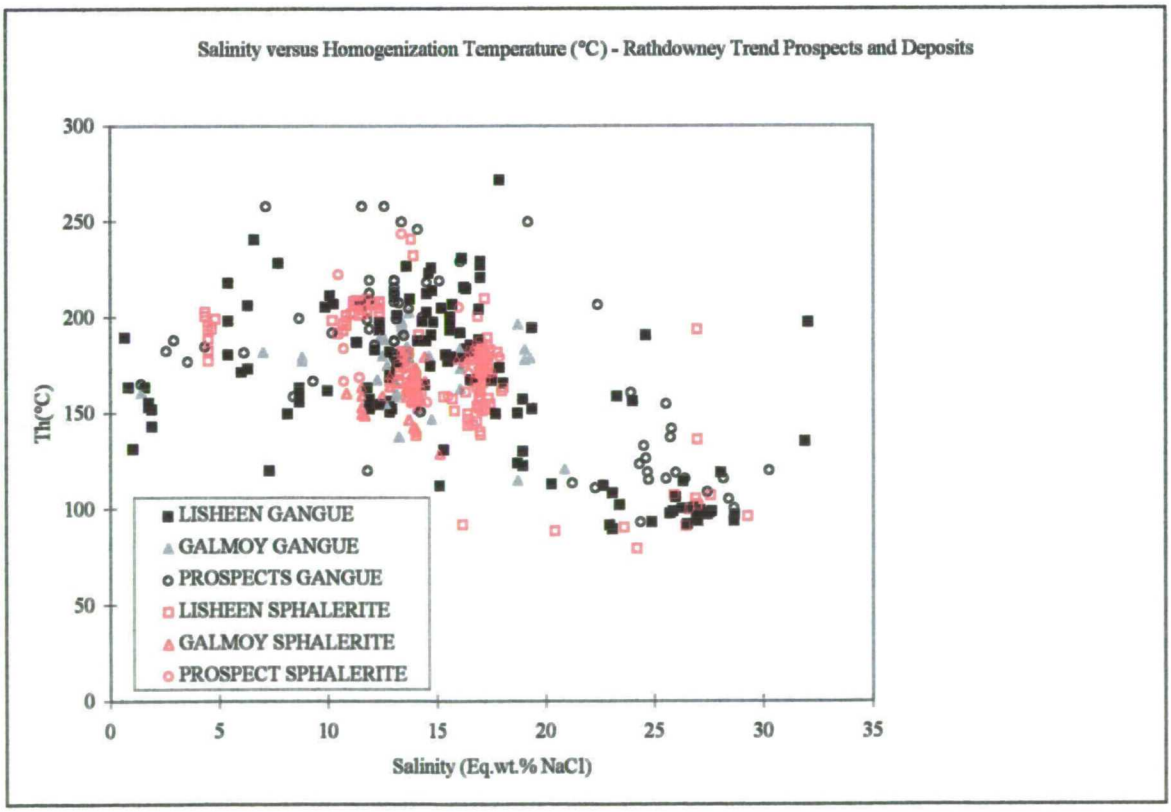


Figure 5.11 Salinity versus homogenization temperature of all sphalerite and gangue phases in the Rathdowney Trend prospects and deposits.

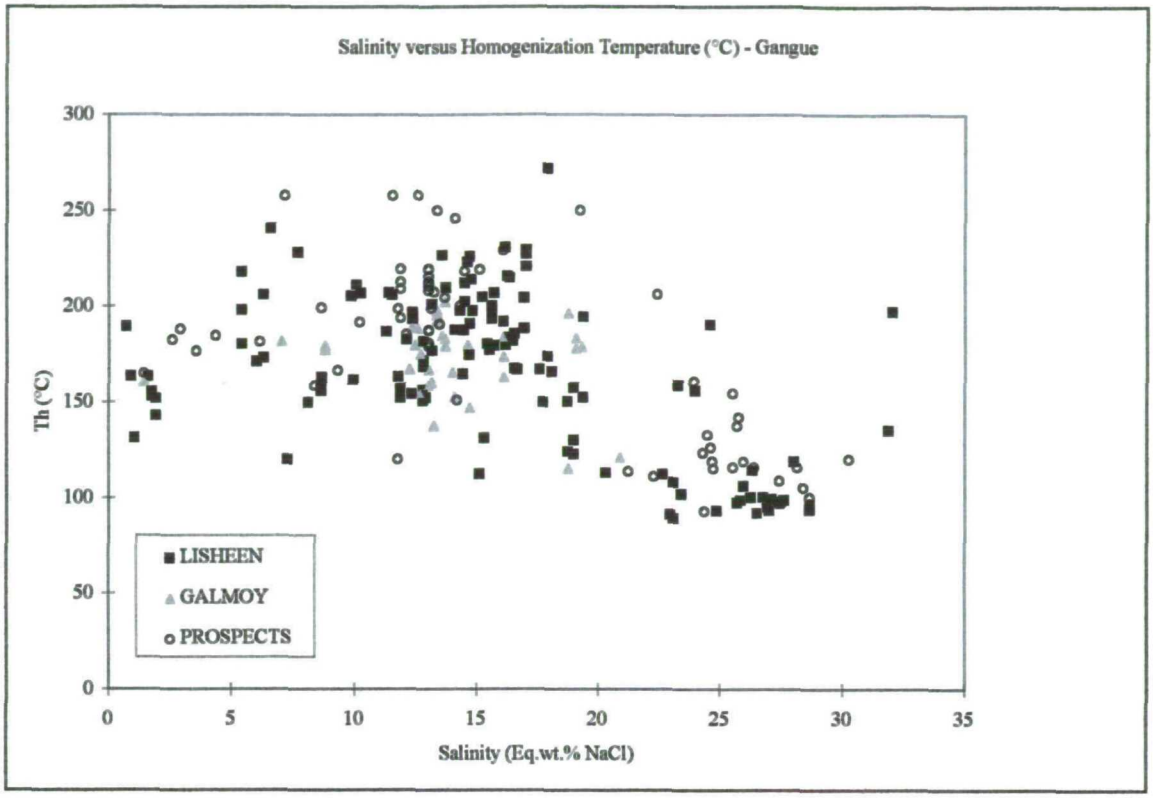


Figure 5.14 Salinity versus homogenization temperature for all gangue inclusions, subdivided according to location.

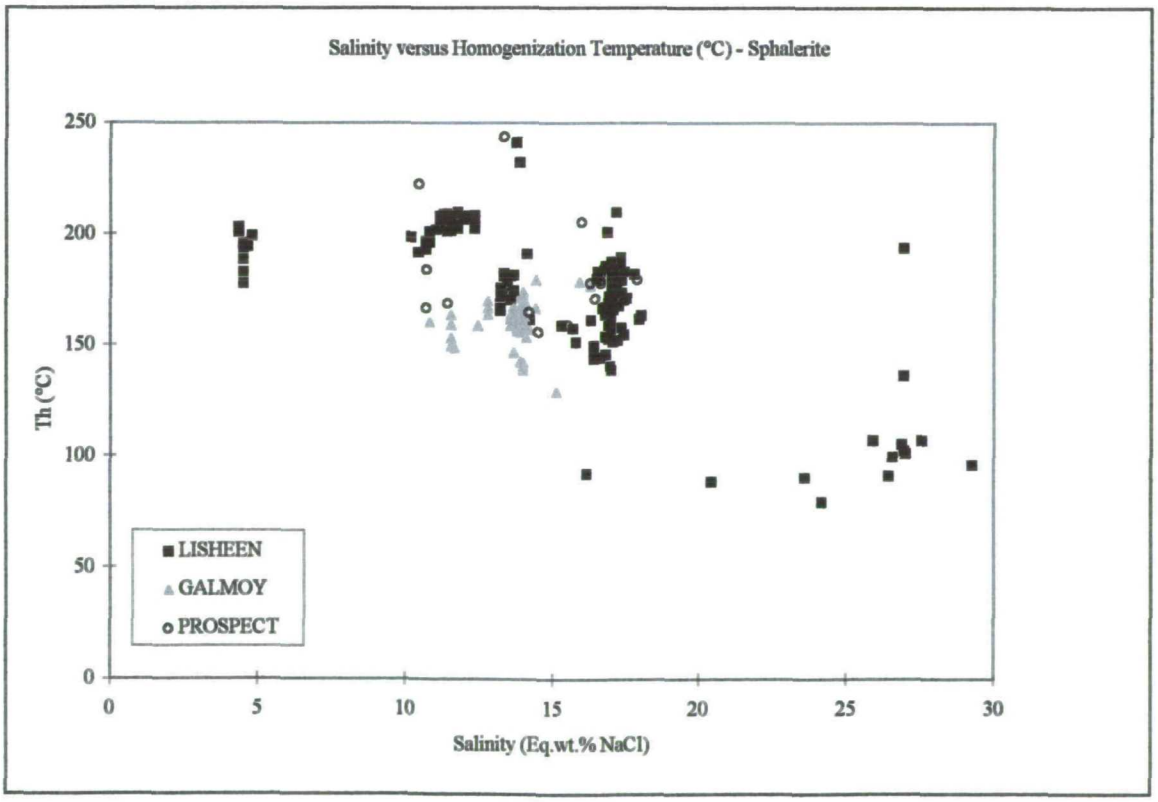


Figure 5.15 Salinity versus homogenization temperature for all sphalerite inclusions, subdivided according to location.

secondary inclusions, but as primary inclusions in post ore-stage D4 pink dolomite. Low temperature phase equilibria indicate that the low temperature end member fluid is of $CaCl_2$-NaCl-H_2O type (Oakes *et al.*, 1990) and is characteristic of MVT epigenetic mineralization.

The homogenization temperatures for $D1_C$ dolomite suggest a possible high temperature regional event was responsible for the pre ore-stage dolomite. The homogenization temperature for fluid inclusions hosted by prospect D3 dolomite (210-220°C) are higher than fluid inclusions hosted by deposit D3 dolomite (~170-210°C), however the range in salinities are comparable, particularly between Galmoy and prospects. Homogenization temperatures for fluid inclusions hosted by post-ore D4 dolomite at Lisheen are slightly lower than fluid inclusions hosted by D4 dolomite at Rathdowney East and Durrow. However, the temperatures fall within the range 90-120°C. Homogenization temperatures for fluid inclusions hosted by D5 calcite and dolomite considered contemporaneous with late ore-stage mineralization are comparable to homogenization temperatures for fluid inclusions hosted by D3 dolomite and fall in the range 170-210°C.

A small population of low temperature (70-130°C), high salinity (20-29 wt% NaCl eq.) inclusions is also present in the D5 gangue samples. These are secondary inclusions, which are also present in D3 dolomites. This low temperature, high salinity fluid end member is present in primary inclusions in the post ore-stage D4 dolomite, therefore its occurrence in both D3 and D5 gangue phases suggest that it represents overprinting. D5 dolomites and calcites broadly considered contemporaneous with mineralization pre-date D4 dolomite (the paragenetic classsification of D5 in this case is slightly misleading). In sphalerite the same type of fluid occurs as secondary inclusions, which suggests that the low temperature, high salinity fluid post-dates the latest phase of mineralization. The very late D5 calcite which occurs in the vugs of D4 dolomite does not contain this low temperature, high salinity fluid. It is characterized by homogenization temperatures in the range 150-170°C and low salinities of ~2 wt% NaCl eq. This late calcite is also characterized by distinct negative $\delta^{13}C$ values (~ -5.5‰).

Homogenization temperatures for fluid inclusions hosted by Lisheen, Galmoy and Holycross sphalerite predominantly fall in the range 150-210°C (Figure 5.10, 5.11). Salinities fall within the range 10.4-18.1 wt% NaCl eq. A small population of low temperature (70-130°C), high salinity (24-29 wt% NaCl eq.) fluids in secondary inclusions occur in the deposit sphalerites.

The general trend of fluid evolution in the Rathdowney Trend may be summarized as follows. During the syn-, to late ore-stage mineralization event, mineralizing fluids had moderate to high

temperatures and moderate salinities. During the post ore-stage of mineralization fluids had lower temperatures and higher salinities than syn-, to late ore-stage fluids.

The wide range of homogenization temperatures and salinities of fluid inclusions in sphalerite and syn-, late, to post ore-stage carbonates in the Rathdowney Trend suggests that more than one fluid has been involved during the precipitation of sphalerite and gangue within the deposits. The spread in the data is noticeably wider and more continuous in the gangue, whilst sphalerite data form distinct clusters (Figure 5.12, 5.13). Variability of fluid inclusion homogenization temperatures and salinities has been reported in many other carbonate-hosted Pb-Zn deposits, e.g., Viburnum Trend in southeast Missouri (Roedder, 1977; Rowan and Leach, 1989), the Nanisivik deposit in Baffin Island (Arne *et al.*, 1991), and the Gays River deposit, Nova Scotia (Chi and Savard, 1995). This variability has been interpreted as evidence for mixing of several fluids during mineralization (e.g., Rowan and Leach, 1989; Shelton *et al.*, 1992).

The moderate temperature, moderate salinity end member fluid observed in primary inclusions within coarse sphalerite probably represents the main mineralizing fluid. These are comparable to basement fluids in the southwest Midlands (Everett *et al.*, in press). However, intermediate temperature and salinity fluids in primary inclusions exist in sphalerite and gangue suggesting that mixing of the higher temperature end member with a second fluid at the site of deposition occurred during the main phase of mineralization. This mixing trend is seen at Galmoy and Lisheen, but is less evident at the prospects (Figure 5.12, 5.13). The second fluid was probably a moderate to low temperature, resident seawater-derived brine, as evidenced by the presence of barite with ore-stage sulphides at Lisheen. A low temperature (68-110°C), high salinity (20-25 wt% NaCl eq.) brine in primary inclusions in barite at Silvermines is consistent with an origin from localized brine pools (Mullane and Kinnaird, 1998). The low temperature, high salinity end member fluid, present in primary inclusions in post ore-stage D4 dolomite in the Rathdowney Trend represents overprinting, and probably postdated the main mineralizing event. This post ore-stage fluid is also observed as an overprint in basement veins (Everett *et al.*, in press).

The mixing trend is evident in both sphalerite and hydrothermal carbonates, but is not as distinct as would be expected. The microthermometric study was primarily restricted to paragenetically late mineral phases (D3 being the exception), therefore the predominant main ore-stage fluid may not be fully represented. If it were represented, a more distinctive trend may be apparent. Cooling arrays are evident in paragenetically late crystalline sphalerite in the Main zone at Lisheen where temperatures range from ~140-220°C, for a moderate to high salinity (~17 wt% NaCl eq.) fluid

(Figure 5.3), evidence that these crystalline sphalerites may represent the waning stages of mineralization.

In the southern Irish Midlands fluid inclusion data from Silvermines (Samson and Russell, 1987) and Tynagh (Banks and Russell, 1992) also indicate the involvement of two distinct fluids in the mineralizing process. A high temperature (~190°C at Silvermines, ~240°C at Tynagh), moderate salinity (8.0-12.0 Eq.wt.% NaCl at Silvermines, 12.0 Eq.wt.% NaCl at Tynagh) fluid mixed with a lower temperature, higher salinity (18.0-22.0 Eq.wt.% NaCl at Silvermines, 21.0 Eq.wt% NaCl at Tynagh) fluid, both within and below the ore zone during mineralization.

5.2.6 Summary

These data for Lisheen and Galmoy are comparable with other deposits and provide a good indication that mineralization in Ireland peaked at ~200°C. These temperatures of formation are significantly higher than for most MVT deposits. Most MVT deposits commonly form at temperatures between 100-150°C (Sangster, 1990).

CHAPTER 6: DISCUSSION

CHAPTER 6: DISCUSSION

6.1 INTRODUCTION

The results of geochemical and isotopic analyses of sulphides and hydrothermal carbonates, and a systematic microthermometric study of fluid inclusions hosted in these paragenetically constrained phases, provide constraints on the sources of components essential to the mineralizing hydrothermal systems and their evolution through time. In this chapter, the processes responsible for generating the observed data are discussed and comparison made between the Lisheen and Galmoy deposits and the weakly mineralized prospects. This can provide an indication of the principal controls on the development of economic mineralization and allow identification of characteristics indicative of the operation of key mineralizing processes. The results of this study are compared primarily to other Zn-Pb deposits in Ireland, to other comparable deposits worldwide, and to the MVT deposits of North America.

6.2 REGIONAL DOLOMITIZATION

The zone of regional dolomite in southern Ireland trends NE-SW from Derrykeam to just south of Lisheen (Hitzman, 1991a). In the Lisheen area, the entire Waulsortian complex as well as relatively non-argillaceous beds within the overlying Crosspatrick Formation and basal portion (Chadian in age) of the Aghmacart Formation are completely dolomitized (Hitzman and Shearley, 1991). However, regional dolomite has not been observed in the Arundian age, upper portion of the Aghmacart Formation (Sheridan, 1977), suggesting that it is pre-Arundian in age. Regional dolomite occurs on both the hanging wall and footwall sides of the main Killoran and Derryville faults in the Lisheen area (Hitzman and Shearley, 1991).

Dolomitization models based on the circulation of normal or slightly modified seawater are favoured for large scale dolomitized sequences. Allan *et al.* (1992) and Shearley *et al.* (1996) proposed that the D1, pre ore-stage, regional dolomite may have originally formed as a result of the flow of pulses of heated, marine derived formation waters, possibly from a foreland basin to the south of the carbonate shelf, during the onset of the Hercynian Orogeny.

However, these dolomites were probably later modified locally by epigenetic dolomitizing/mineralizing fluid(s) responsible for the development of D2 and D3 dolomites. As a result of this modification the original depositional chemistry of these regional dolomites is

indistinct, and dolomitization models for the formation of regional dolomite cannot be easily constrained. This impacts on the proposed model of Allan *et al.* (1992) and Hitzman *et al.* (1998) for regional dolomite in Southern Ireland where the evidence for a marine water/burial origin is based principally on $\delta^{18}O$ analyses (see below).

The regional dolomites are non-stoichiometric; this is atypical of dolomites formed during the slow growth from dilute solutions normally associated with burial conditions. Textural evidence suggests growth of the fine replacive ($D1_R$) dolomite at elevated temperatures and/or high supersaturation. On the basis of petrographic evidence and elemental data the pre-orestage regional dolomites are interpreted as involving both early and late diagenetic or epigenetic dolomitizing fluids. Platform carbonates of the Bonneterre and Davis Formations (SE Missouri) have undergone both early and late diagenetic dolomitization (Gregg and Shelton, 1990).

Oxygen isotope data obtained from coarse white ($D1_C$) dolomite has been interpreted as indicating a low temperature origin (Allan *et al.*, 1992; Hitzman *et al.*, 1998), yet is equally consistent with precipitation at low temperature from a low $\delta^{18}O$ (marine) water (60-110°C for $\delta^{18}O_{(H2O)}$ ~0‰), or precipitation at higher temperature from a high $\delta^{18}O$ "hydrothermal" water (130-220°C for $\delta^{18}O_{(H2O)}$ ~8‰). Comparable $\delta^{18}O_{(H2O)}$ values of 6-7‰ have been estimated for basement-derived fluids in this temperature range (Wilkinson, pers. comm., 1998). Oxygen data alone are clearly ambiguous and more detailed fluid inclusion and chemical analyses will be necessary to distinguish between a putative low temperature "burial" coarse white dolomite and the higher temperature hydrothermal variant which undoubtedly exists.

Preliminary fluid inclusion data from this study indicate a temperature range of approximately 198-218°C in $D1_C$ located approximately 2km northwest of the Lisheen deposit, supporting a possible high temperature regional event. This temperature range coupled with the $\delta^{18}O$ of $D1_C$ (21.50‰) gives an estimated $\delta^{18}O_{(H2O)}$ ~9‰, further supporting possible basement-derived fluid involvement.

The mechanism for fluid movement through the Waulsortian Limestone, from whatever source, is not clearly understood. Diagenetic studies of the Limestone (Miller, 1986) have suggested that its high initial permeability was largely occluded by early diagenetic cementation. Fault conduits may have allowed the fluids responsible for early regional dolomitization to access the Waulsortian Limestone and Crosspatrick Formation, however, there is no direct evidence that these fluids exploited fault-induced permeability (Hitzman *et al.*, 1998). As a result of regional

dolomitization, the increased permeability and porosity may have significantly facilitated the infiltration of later fluids containing ore-forming constituents. The proximity of the Lisheen and Galmoy deposit to the regional dolomite 'front' in the Rathdowney Trend may not just be coincidental and is probably directly related to the significant change in porosity/permeability characteristics of the Waulsortian host rock. The infiltration of ore-forming fluids may well have become concentrated at the dolomite front due to a significant permeability contrast between dolomitized and undolomitized Waulsortian.

Possible evidence for a higher temperature, regional coarse white dolomite is significant. The widespread development of an early regional dolomite from high temperature fluids has important implications for the evolution of the hydrothermal systems in Ireland.

6.3 DOLOMITE MATRIX BRECCIA FORMATION

Widespread faulting during the latest Chadian to mid-Arundian controlled later hydrothermal dolomitization, in particular the formation of D2 and D3 dolomite breccias in areas of complete regional dolomitization at Lisheen, Galmoy and the Rathdowney Trend prospects. The presence of well developed fault structures allowed the channelling of the ore-related dolomitizing fluids into restricted extensional zones. The D2 and D3 dolomite breccias clearly contain regionally dolomitized Waulsortian clasts primarily in the hanging wall of the faults, indicating hydrothermal dolomitization formed after major movement on the faults. In the Lisheen deposit, the D2 dolomite is restricted to zones within several hundred metres of the major faults. The distribution of the D3 dolomite is less well constrained (Redmond, pers. comm., 1996).

At Lisheen and Galmoy the D2 dolomites have been described as *in situ* hydrothermal dolomite breccias by Hitzman *et al.* (1992) and Doyle *et al.* (1992). Hitzman *et al.* (1992) interpret the breccia as having formed by hydraulic fracturing and brecciation, but principally by subsequent *in situ* replacement of dolomitized Waulsortian Limestone. Texturally, however, the contact between D2 dolomite with the regional dolomite precursor is notably sharp, a more diffuse contact might be expected if the process of replacement was pervasive. Further, dissolution and recrystallization of regional dolomite would not be an efficient mechanism in which to create space to allow infiltration and mixing of later ore-forming fluids. Kucha (1989), Hitzman *et al.* (1992), Beaty *et al.* (1991), Shearley *et al.* (1995, 1996) and Hitzman and Beaty (1996), are among those workers who favour a replacive origin for the D2 dolomite breccias at Silvermines and Lisheen.

Johnston (1995c) and Johnston *et al.* (1995) cite the numerical modelling of fluid flow in fractured rock masses of Sanderson and Zhang (1997) to suggest a possible mode of formation for the dolomite matrix breccias. Johnston (1995c) proposes that the breccias are the product of fault related processes, with extensive breccia sheets occurring where the 'parent' fault changes dip. Contrasting rheological behaviour of the massive Waulsortian Limestone with the more ductile sub-Waulsortian argillaceous bioclastic limestones resulted in differential hangingwall subsidence. Displacement continued in the hangingwall beneath the Waulsortian, opening a wedge shaped dilatant zone into which the overlying rocks collapsed (Johnston, 1995c). Under conditions of small differential stresses, such a geometry could result in the generation of extensive, tabular, shallowly dipping zones of dilation without requiring fluid overpressuring (Johnston *et al.*, 1995). This mechanism of formation creates space effectively, allowing the infiltration and mixing of fluids resulting primarily in the precipitation of a dolomite matrix which is replaced at a later stage by sulphides.

The extent of interaction of the dolomitizing fluids with the host rocks is indicated by the C-O isotopic character of the matrix component of the D2 dolomite which is largely inherited from the Waulsortian regional dolomite host. Significant exchange of the incoming fluid with rock has occurred, with the isotope composition of the incoming fluids being shifted toward equilibrium with the host rock. The isotopic character of the matrix component of the D3 dolomite suggests less exchange between the incoming fluid and the surrounding host rock, and an increasing influence of the infiltrating fluid with time. Although broadly consistent with single fluid infiltration, Everett *et al.* (1996) showed how such data could also be produced by a combination of fluid-host rock isotopic exchange and mixing of two fluids with contrasting C/O ratios.

Temperatures of the fluids responsible for the formation of D2 dolomites are thought to be between 150-220°C, whilst temperatures for D3 dolomitization range between 170-210°C. These temperatures are comparable with other deposits and provide a good indication that mineralization in Ireland peaked at temperatures of ~200°C (Figure 6.1). This temperature range, coupled with the average $\delta^{18}O$ for D2 dolomite (24.43±1.47‰), gives an estimated $\delta^{18}O_{(H2O)}$ of 9-14‰. Such high values can only be easily explained by significant interaction of fluids with the Waulsortian dolomite; crustal fluids generally have $\delta^{18}O_{(H2O)}$ values of<13‰ (Sheppard, 1986).

These data support petrographic observations which suggest the D2 dolomite formed by a mechanism involving microfracturing, pervasive fluid-flow, and partial replacement of the regionally dolomitized Waulsortian. This is largely in accord with the models of Hitzman *et al.*

(1992) and others. The D3 dolomite is predominantly a crystalline, open space growth form interpreted to, at least in part, postdate D2 dolomite in the Rathdowney Trend.

The lack of mixing and rotation of the clasts in D2 dolomite at Lisheen and Galmoy suggests that the breccias did not originate as debris flows or by major solution collapse and is hard to reconcile with the tectonic dilation mechanism of Johnston (1995c). However, minimal clast rotation in later D3 dolomites suggests a mode of formation under different conditions in which open space was created.

It is thought that the sequence of dolomite alteration and mineralization stages probably represents pulses of chemically distinct fluids entering the system. However, Hitzman (1995b) has considered the process of a prograding dolomite alteration/mineralization system with sulphides replacing carbonates adjacent to the faults while hydrothermal dolomite breccias were simultaneously formed on the periphery of the system. The D2 dolomite is considered to have developed as an important precursor to sulphide mineralization (Hitzman *et al.*, 1992).

6.4 SOURCES OF MINERALIZING COMPONENTS

6.4.1 Sulphur

Two distinct sulphur sources are interpreted for Rathdowney Trend mineralization: (1) Lower Carboniferous seawater sulphate providing sulphide *via* bacteriogenic reduction and barite-forming sulphate; and (2) a 'deep-seated' hydrothermal component.

The negative $\delta^{34}S$ data from -4 to- 20‰ at Galmoy and Lisheen represents a bacteriogenic fractionation of some 22 to 38‰, typical of naturally occurring open systems (e.g. Goldhaber and Kaplan, 1975). A dominant low $\delta^{34}S$ component attributed to open system bacteriogenic reduction characterizes all the major Irish deposits (Coomer and Robinson, 1976; Boast *et al.*, 1981a; Boyce *et al.*, 1983b; Anderson *et al.*, 1998). Conversely, positive $\delta^{34}S$ values derived predominantly from evaporites characterizes the Gays River and Jubilee deposits of Nova Scotia (Savard *et al.* 1995a), and the Pine Point deposit (Rhodes *et al.*, 1984).

The positive $\delta^{34}S$ data from ~0 to +10‰ at Lisheen and Galmoy is considered to represent a subordinate, 'deep-seated' hydrothermal component, derived from Lower Palaeozoic sediments, transported with the ore-forming metals in line with previous interpretations. This sulphur is

dominant in the prospects and appears to occur most commonly in the deposits in proximity to major 'feeder' faults and generally later in the paragenesis. For the first time, this hydrothermal sulphur component can be directly related to the 'deep hydrothermal fluid' by fluid inclusion data in the paragenetically late crystalline sphalerites.

The presence of barite within massive sulphides at Lisheen with an isotopic composition indistinguishable from contemporaneous seawater sulphate implies that a seawater derived fluid, (probably a brine) penetrated the mineralizing zone. Evidence from fluid inclusions indicates mixing of the 'deep hydrothermal fluid' with a brine during ore-stage mineralization. Fluids carrying seawater sulphate are also noted at Navan, Silvermines and Tynagh (Anderson *et al.*, 1998; Coomer and Robinson, 1976; Boast *et al.*, 1981a; Boyce *et al.*, 1990).

6.4.2 Lead

Several previous workers in Ireland consider that a component of the hydrothermal system responsible for the base-metal deposits must be basement-derived, due to the Pb isotopic composition of contained galena (O'Keefe, 1986; LeHuray *et al.*, 1987). They invoke deep convection cells into the basement underlying the Carboniferous and Devonian sediments to leach metals (cf. Russell, 1978). Analysis of Pb isotopic ratios in galena at Lisheen ($^{208}Pb/^{204}Pb$ – 38.080±0.061, $^{207}Pb/^{204}Pb$ = 15.594±0.026, $^{206}Pb/^{204}Pb$ = 18.183±0.017) and Galmoy ($^{208}Pb/^{204}Pb$ = 38.084±0.073, $^{207}Pb/^{204}Pb$ = 15.592±0.024, $^{206}Pb/^{204}Pb$ = 18.215±0.018) provide evidence in support of a basement contribution to the mineralized system. The Pb was probably derived from the underlying Silurian rocks beneath the deposits in the Rathdowney Trend which comprise greywackes, siltstones and grits. The data, however, are anomalous as regards the conventional isoplumb theory of LeHuray *et al.*, (1987). This indicates that the systematic trend of the deposit isoplumbs does not extend down to the Rathdowney Trend in the southern Irish Midlands.

6.5 EVIDENCE FOR FLUID MIXING DURING MINERALIZATION

Precipitation involving deposition of metals and sulphur from a single hydrothermal fluid would require major fluctuations in either temperature, pH, fO_2 or a combination of these parameters (Ohmoto, 1972; Rye and Ohmoto, 1974). Further, the solubilities of ZnS and PbS in the presence of significant H_2S concentrations are too low to allow transport of ore forming quantities of both metals and H_2S in the same solution (Anderson, 1975; 1983) unless the solution is very acidic (Anderson, 1975). Therefore it is considered unlikely that the spread in both fluid inclusion and

$\delta^{34}S$ data, along with the observed ore textures in this study, can be explained by a single hydrothermal fluid or single sulphur source.

6.5.1 Ore Textures and Sulphur

Textures including dendritic, skeletal, geopetal, colloform, and coarse euhedral growths are interpreted to represent sulphide deposition in open spaces within the carbonate host rock. One of the most effective ways of creating these textural forms is by rapid precipitation of sulphides from supersaturated solutions (Roedder, 1968; Honjo and Sawada, 1982). Abundant colloform textures in sphalerite at the Lisheen deposit suggest it formed from a highly supersaturated solution. Stalactitic and rod-like structures have been produced experimentally by chemical garden growth with rapid precipitation by mixing of an acidic and an alkaline solution (Russell *et al.*, 1984). Sudden supersaturation and rapid precipitation are best explained by mixing of a metal-bearing fluid with a second, sulphur-bearing fluid at the site of ore deposition. However, late ore-stage, coarse euhedral growth forms are indicative of precipitation at low degrees of supersaturation. Thus, the fluid mixing thought to be responsible for ore-stage mineralization may not have occurred in the latest phases of mineralization.

In general there is a close correlation between ore texture, paragenetic stage and $\delta^{34}S$ reflecting the depositional process and the availability of sulphur at the time of deposition. Galena and sphalerite clearly illustrate this correlation in the Lisheen deposit with paragenetically late coarse grained euhedral galena and crystalline sphalerite textures predominantly exhibiting positive $\delta^{34}S$ values, compared with main ore-stage dendritic and skeletal galenas and colloform sphalerite textures which primarily have negative $\delta^{34}S$ values. This clearly shows a shift in the proportions of the two sulphur sources involved in mineralization through time, mirroring fluid inclusion data and C/O data. Fluid inclusion data indicate an increasing dominance of the "deep hydrothermal" component through time. The C/O data exhibit a broad trend toward isotopically lighter compositions with time, simply interpreted as reflecting decreasing isotopic exchange between an isotopically light infiltrating fluid and the Waulsortian host rock, probably due to the increasingly fracture-controlled and less pervasive fluid flow during the later stages of hydrothermal activity.

The occurrence of isotopically mixed sulphides in some samples (e.g 262/162.1 Derryville zone), indicates the probability that ore stage deposition was facilitated through variable mixing of the two sulphur sources. Intermediate isotopic compositions of -10‰ and -12‰ are prominent in the major ore zones at Lisheen and Galmoy respectively. Apparent isotopic disequilibrium

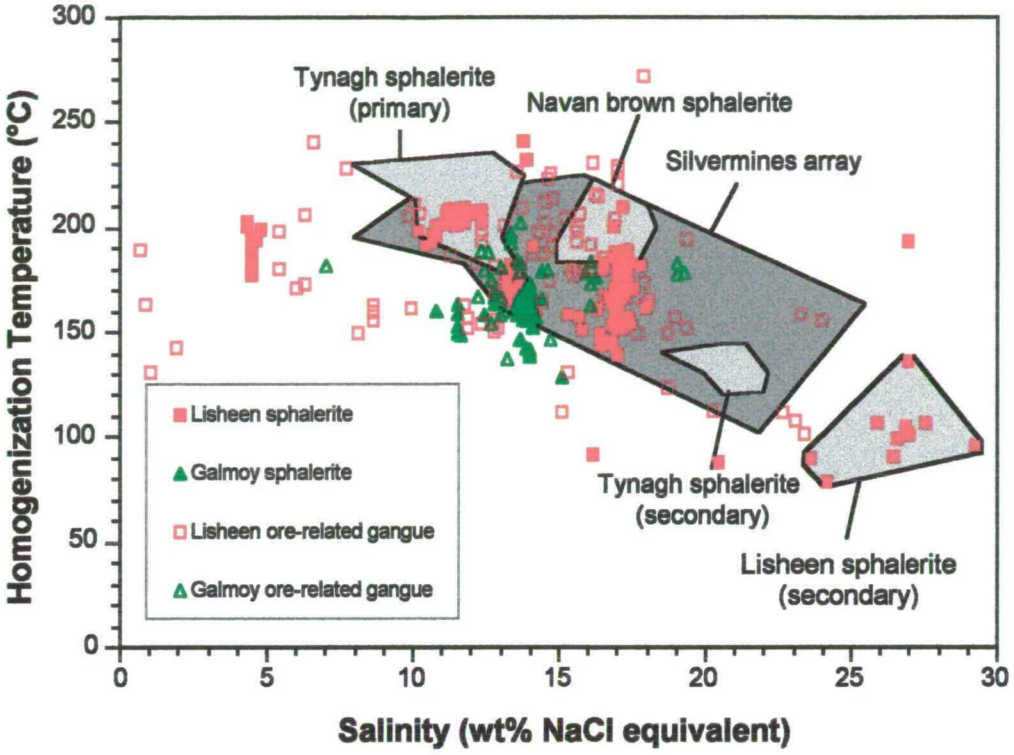


Figure 6.1 Comparison of inclusion data (this study) with other deposits (Silvermines, Tynagh, Navan and Lisheen data from Samson & Russell, 1987; Banks & Russell, 1992; Everett *et al.*, in press).

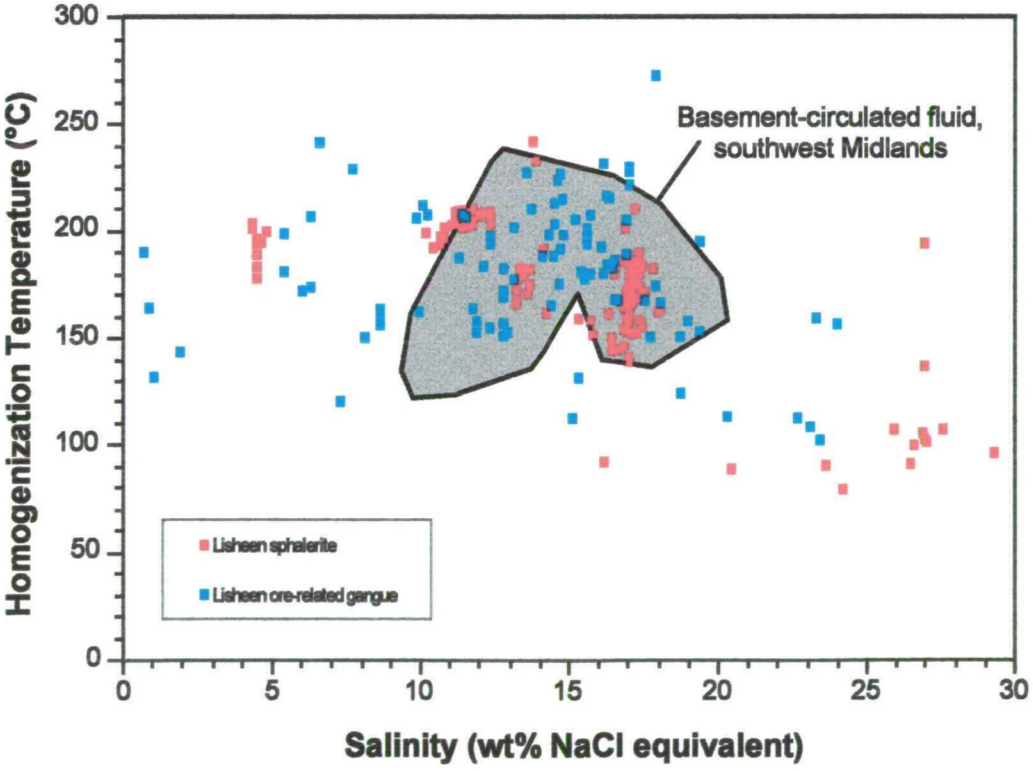


Figure 6.2 Comparison of Lisheen inclusion data with basement-circulated fluids (basement data from Everett *et al.*, in press).

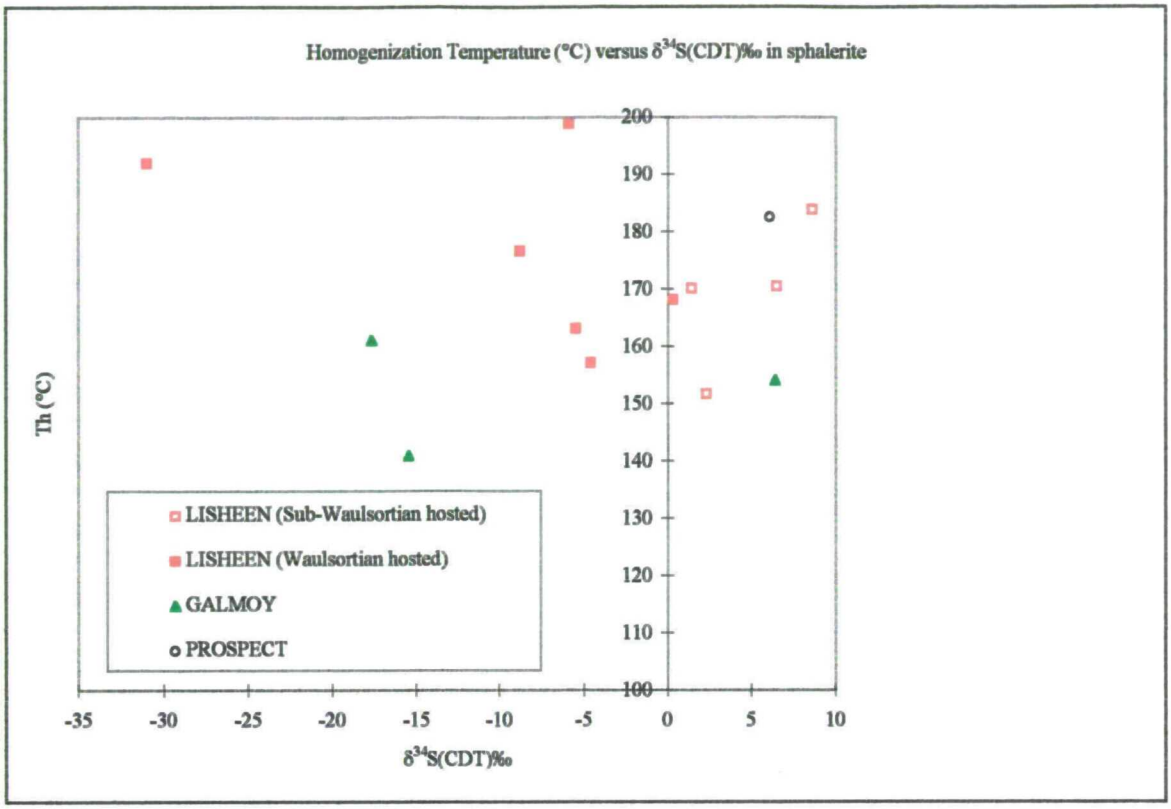


Figure 6.3 Homogenization temperature versus $\delta^{34}S(CDT)‰$ for crystalline sphalerites, subdivided according to location and lithology.

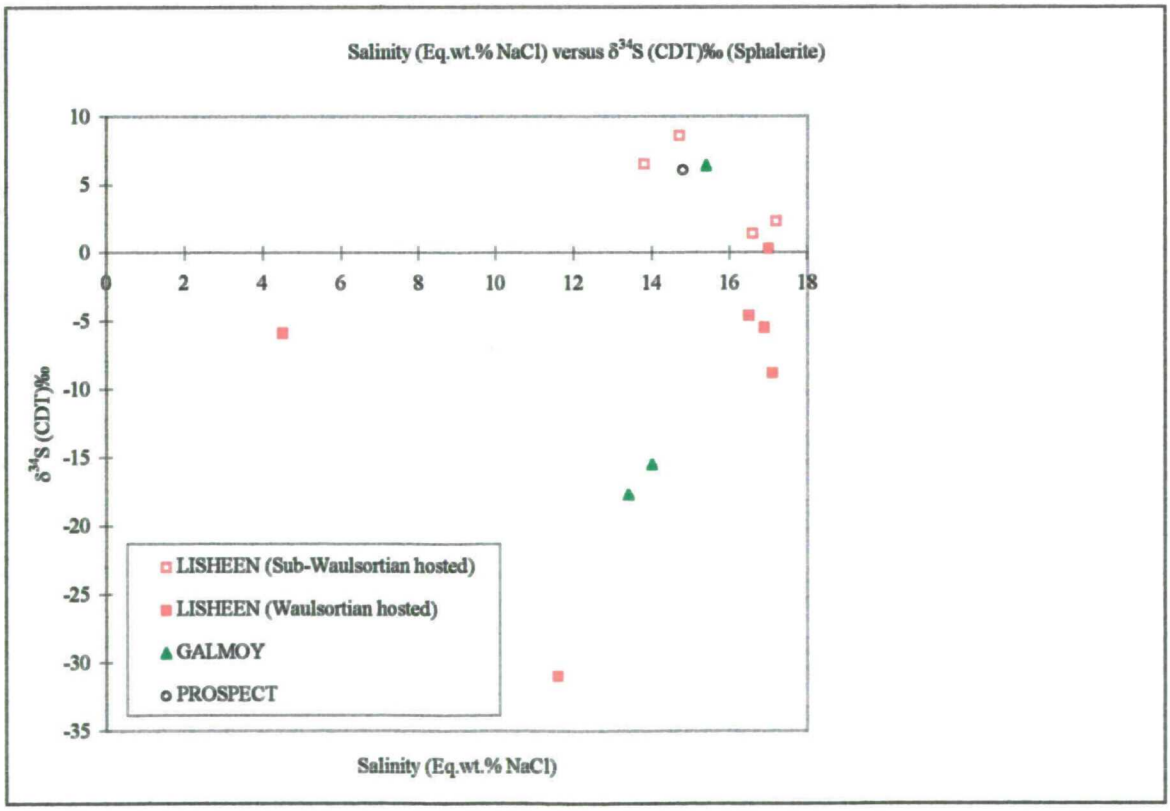


Figure 6.4 Salinity versus $\delta^{34}S(CDT)‰$ for crystalline sphalerites, subdivided according to location and lithology.

relationships are not surprising given that equilibrium is highly unlikely where rapid precipitation and fluid mixing have occurred.

The $\delta^{34}S$ values of ore-stage to late ore-stage crystalline sphalerites have been plotted against salinity and homogenization temperature (Figures 6.3, 6.4). The sphalerites are subdivided according to location and, in the Lisheen deposit, by host lithology. A weak correlation exists between homogenization temperature and $\delta^{34}S$. The sub-Waulsortian hosted sphalerites at Lisheen are characterized by higher $\delta^{34}S$ values and slightly higher homogenization temperatures than Waulsortian hosted sphalerites. The salinity range for the sphalerites are comparable and fall predominantly within the range 13.0-17.5 wt% NaCl eq. However, the higher the $\delta^{34}S$ value in sub-Waulsortian hosted sphalerite the less saline the fluid. This inverse correlation between $\delta^{34}S$ and salinity is consistent with the progressive mixing of two fluids. However, this relationship is not apparent in the Waulsortian hosted sphalerite where the higher the $\delta^{34}S$ value, the more saline the fluid.

6.5.2 Fluid Inclusion Data

The results of the microthermometric study indicate a wide range of homogenization temperatures and salinities of fluid inclusions in sphalerite and syn-, late, to post ore-stage carbonates in the deposits and prospects. This range of data suggests that more than one fluid has been present during the evolution of the hydrothermal systems of the Rathdowney Trend. The microthermometric data for Lisheen and Galmoy are compared to other comparable deposits in the Irish Midlands (Figure 6.1) and to other carbonate-hosted deposits worldwide.

Two end member fluids are inferred: (1) a moderate temperature (160-210°C), moderate salinity (9-15 wt% NaCl eq.) fluid in primary gangue and sphalerite; and (2) a distinctive low temperature (80-140°C), high salinity (22.5-29.0 wt% NaCl eq.) fluid principally occurring in secondary inclusions, but as primary inclusions in post ore-stage D4 pink dolomite.

The higher temperature end member fluid observed in primary inclusions within coarse sphalerite probably represents the main mineralizing fluid. However, intermediate temperature and salinity fluids in primary inclusions exist in sphalerite and gangue suggesting that mixing of the higher temperature end-member with a second fluid at the site of deposition occurred during the main phase of mineralization. Basement-circulated fluids are similar (Everett *et al.*, in press) to the high temperature end-member seen in the deposits (Figure 6.2). The lack of significant

mineralization in the basement may be principally a function of the availability of the reduced sulphur at the site of deposition, but also the absence of an effective deposition mechanism (see 6.6).

The second fluid was probably a moderate to low temperature, resident brine derived from seawater, as evidenced by the presence of barite with ore-stage sulphides at Lisheen. A low temperature (68-110°C), high salinity (20-25 wt% NaCl eq.) brine in primary inclusions in barite at Silvermines is consistent with an origin from localized brine pools (Mullane and Kinnaird, 1998). The low temperature, high salinity fluid present in primary inclusions in post ore-stage D4 dolomite in the Rathdowney Trend represents overprinting, and probably postdated the main mineralizing event.

The mixing trend is evident in both sphalerite and hydrothermal carbonates, but is not as distinct as might be expected. However, for reasons of sample suitability, the microthermometric study was primarily restricted to paragenetically late mineral phases (D3 being the exception), therefore the main ore-stage fluid may not be represented. If it were better represented, a more distinctive trend might have been observed. Apparent cooling arrays are evident in paragenetically late crystalline sphalerite in the Main zone at Lisheen where temperatures range from ~140-220°C for fluids of remarkably constant salinity (e.g. ~17 wt% NaCl eq.). This suggests that these crystalline sphalerites may represent the waning stages of mineralization, or represent precipitation from small batches of cooling fluid subsequent to the bulk of precipitation from an individual mineralizing pulse.

In the southern Irish Midlands, fluid inclusion data from Silvermines (Samson and Russell, 1987) and Tynagh (Banks and Russell, 1992) also indicate the involvement of two distinct fluids in the mineralizing process. A high temperature (~190°C at Silvermines, ~240°C at Tynagh), moderate salinity (8.0-12.0 Eq.wt.% NaCl at Silvermines, 12.0 Eq.wt.% NaCl at Tynagh) fluid is inferred to have mixed with a lower temperature, higher salinity fluid (18.0-22.0 Eq.wt.% NaCl at Silvermines, 21.0 Eq.wt% NaCl at Tynagh), both within and below the ore zone during mineralization. The importance of fluid mixing in the Irish deposits is clear.

Variability of fluid inclusion homogenization temperatures and salinities has been reported in many other carbonate-hosted Pb-Zn deposits, e.g., Viburnum Trend in southeast Missouri (Roedder, 1977; Rowan and Leach, 1989), the Nanisivik deposit in Baffin Island (Arne *et al.*, 1991), and the Gays River deposit, Nova Scotia (Chi and Savard, 1995), Mascot-Jefferson City District, Tennessee (Taylor *et al.*, 1983). This variability has been interpreted as evidence for

mixing of several fluids during mineralization (e.g., Rowan and Leach, 1989; Shelton *et al.*, 1992). Chi and Savard (1995) indicate the mixing of a high temperature (≥ 200°C), high salinity (≥ 27 wt% NaCl eq.) fluid with a lower temperature (107-147°C), lower salinity (24 wt% NaCl eq.) fluid, thought to be a formation water that dolomitized the Early Carboniferous basal Windsor carbonates and saturated their pores before mineralization. A third, lower temperature (<90°C), lower salinity (<20 wt% NaCl eq.) fluid is interpreted as mixing with the two pre-existing fluids.

One of the main differences between the Irish deposits, including Lisheen and Galmoy, and most MVT deposits is that they formed at significantly higher temperatures. MVT deposits commonly form at temperatures between 100-150°C (Sangster, 1990). This contrast is one of the key factors which sets the Irish deposits apart from many other carbonate-hosted base-metal systems.

6.6 MECHANISM FOR MINERALIZATION AND EVOLUTION THROUGH TIME

6.6.1 Syngenetic versus Epigenetic Mineralization

Much of the early literature on Irish deposits suggests that they formed syngenetically or during early diagenesis (Derry *et al.*, 1965). Orebodies at Silvermines, Tynagh and Navan are all considered to have exhalative aspects by Russell and Lewis (1995). An exhalative origin for components of the Silvermines system is supported by the presence of hydrothermal pyrite chimneys, partly surrounded by jasper, proximal to the Main Fault (Larter *et al.*, 1981). The chimneys sometimes contain what are thought to be fossil polychaete worms (Russell, 1983) where epigenetic 'feeder' mineralization interfaces exhalative ore. However, more recent petrographic work (Kucha, 1989; Anderson, 1990; Hitzman *et al.*, 1992; Shearley *et al.*, 1995, 1996; Anderson *et al.*, 1998) supports predominantly epigenetic styles of mineralization noted by earlier workers (e.g. Schultz, 1966a, 1966b; Boast *et al.*, 1981a).

At Tynagh, Derry *et al.* (1965) and Boast *et al.* (1981a) described an initial stage of mineralization of possible synsedimentary or early diagenetic age dominated by colloform and framboidal iron sulphides. This was followed by rapid geopetal precipitation of microcrystalline sphalerite, galena, barite and dolomite within a dilatant fracture system adjacent to the Tynagh Fault. Epigenetic mineralization is dominated by veining and replacement of the host dolomite

and early sulphides by tennantite, chalcopyrite, bornite, arsenopyrite, galena and coarse, sparry barite.

Mineralization in the Lisheen and Galmoy deposits and Durrow prospect exhibit a complex variety of ore textures which are best interpreted predominantly in terms of replacement and open-space growth. Replacement of host carbonates is clearly evidenced by the pseudomorphed bioclasts and allochems. Interpretation of replacement textures clearly has major implications for timing of mineralization relative to host rock lithification.

6.6.2 Distribution and Geometry of Sulphide bodies

The variability in mineral assemblages in space and time, such as the concentration of copper, silver and lead relative to zinc near to fault conduits at Lisheen and Galmoy, is probably a reflection of temperature changes partly caused by mixing of a mineralizing fluid with a second fluid at the site of deposition during the mineralization event. At Ballinalack, Jones and Brand (1986) have described similar sulphide distributions, showing a progressive change in style and complexity both vertically and laterally away from the main Ballinalack Fault.

The sulphur isotope data, sulphide textures and stratiform geometry of the ore bodies can be explained by fluid mixing within the D2 dolomite between a low temperature brine and a higher temperature fluid (Figure 6.5). The former could have been resident within the D2 dolomite or in the porous overlying regional dolomite. Sulphur isotope and fluid inclusion data from veins proximal to the main faults clearly indicate that flow of the latter fluid was focused within the faults (Figure 6.5). Mineral occurrences at Lisheen (Shearley *et al.*, 1993c) and Galmoy (Doyle *et al.*, 1992) thicken and increase in metal grade towards these faults, strongly suggesting that these were where fluid mixing was most effective. The absence of significant amounts of sulphides higher than ~50m above the base of the Waulsortian at Lisheen suggests that the physicochemical reactions occurring as the hydrothermal solutions mixed within the Waulsortian dolomite reservoir were highly effective in precipitation of the majority of contained metals.

6.6.3 Host Rock Replacement and Sulphide Deposition

Much of the data supports a fluid mixing model; somewhat paradoxically, however, the sulphides in the deposits are as much replacive as open-space filling. When carbonate is replaced with sulphide, the molar volumes of the sulphide products are less than those of the dissolved carbonate which results in significant volume reduction and consequent space creation. In

general, the replacement process will persist only if the dominant reactions perpetually produce a negative change in molar volumes between the initial minerals of the host and the later guest minerals.

There are many reactions that are potentially important in this process and they account for replacement textures which can involve a large number of secondary minerals and a wide variety of host rocks. There are at least three classes of reactions that are effective in replacing carbonates by sulphide minerals (Barnes and Gould, 1992). Two of the three reactions are considered here, replacement caused by temperature gradients and acid neutralization.

The effectiveness of carbonate as a concentrator of ore metals commonly results from its ability to neutralize acid and its large solubility in acidic fluids, thereby creating new porosity into which additional hydrothermal fluid flows (e.g., Lu *et al.*, 1992). Very large quantities of acid are generated by reaction schemes where metal-bearing fluid from one source mixes with hydrogen sulphide-bearing fluid from another source; for example, the aqueous $ZnCl_4^{2-}$ in reaction (6.0) is concentrated in one fluid and the H_2S is in another. The precipitation of sulphide minerals as a result of mixing yields hydrogen ions that contributes to wall rock alteration or to creation of open space into which ore precipitates. Acid generated in this way probably contributes to creating open space for ore minerals in MVT deposits (Anderson, 1991; Plumlee *et al.*, 1994).

$$ZnCl_4^{2-} + H_2S\ (aq) \Rightarrow ZnS\ (s) + 4\ Cl^- + 2\ H^+ \qquad (6.0)$$

Decreasing temperature is particularly effective for depositing metals transported as chloride complexes in neutral to weakly acidic solutions containing low H_2S and HS^- concentrations because of the steep temperature dependence of the stabilities of these complexes. As the solution cools, the solubility of base and ferrous metal sulphides decreases and protons are released (i.e., increase in acidity) by reactions such as (6.0). Temperature gradients can readily induce deposition of metal sulphides if these metals are carried in chloride complexes but not if in bisulphide complexes whose stabilities change relatively little with temperature. Furthermore, Hayashi *et al.* (1990) demonstrated that zinc sulphide complexes cannot be responsible for the significant transport of zinc to form economic deposits. Based on preliminary modelling studies of basement-equilibrated fluids in the Irish Midlands, the dominant complex for transport of Zn into the Irish deposits is thought to be $ZnCl_4^{2-}$ (Wilkinson, pers. comm., 1998).

If the pH of the solutions is low enough to cause carbonate dissolution by a reaction such as:

$$CaCO_3\,(s) + 2\,H^+ \Leftrightarrow Ca^{2+} + H_2CO_3\,(aq) \qquad (6.1)$$

then the resulting increase in pH can also cause sulphide deposition (see reaction 6.0). The linked processes of sulphide deposition by fluid mixing, particularly if coupled with cooling of the metal-bearing fluid, and carbonate dissolution can therefore lead to a powerful positive feedback mechanism with the resultant space creation allowing further fluid mixing, thereby promoting extensive sulphide deposition.

6.7 LATE BRINE INFILTRATION

Low temperature, high salinity, post ore-stage fluids characteristic of MVT epigenetic mineralization are observed as secondary inclusions within coarse crystalline sphalerite, and as primary inclusions in D4 pink dolomite. This supports a late stage brine infiltration, which probably post-dated the main ore-stage mineralizing event at Lisheen. This late brine is also observed as an overprint in basement veins (Everett *et al.*, in press).

A significant change in the fluid chemistry is also marked by a dissolution surface between D3 dolomite and D4 dolomite. The striking similarity of CL characteristics and trace element contents in post ore-stage D4 pink dolomite between Rathdowney East and Holycross prospects suggests that a homogeneous regional groundwater flow system is responsible for the formation of the dolomite.

The presence of significant concentrations of Fe in this post ore-stage dolomite implies relatively reducing conditions. However, the lack of iron sulphides in association with the D4 dolomite suggests the fluids were probably sulphur deficient. Land (1980) and Veizer (1983) have indicated that Fe tends to be enriched in later diagenetic dolomites, especially those formed from saline formation waters. Therefore it is considered likely that the D4 dolomite was formed as a result of migration of evolved basin formation waters, possibly during the Variscan orogeny (Figure 6.5).

6.8 COMPARISON OF DEPOSITS AND PROSPECTS

Some significant geochemical and isotopic differences exist between the Lisheen and Galmoy deposits and the weakly mineralized prospects in the Rathdowney Trend. The most distinctive

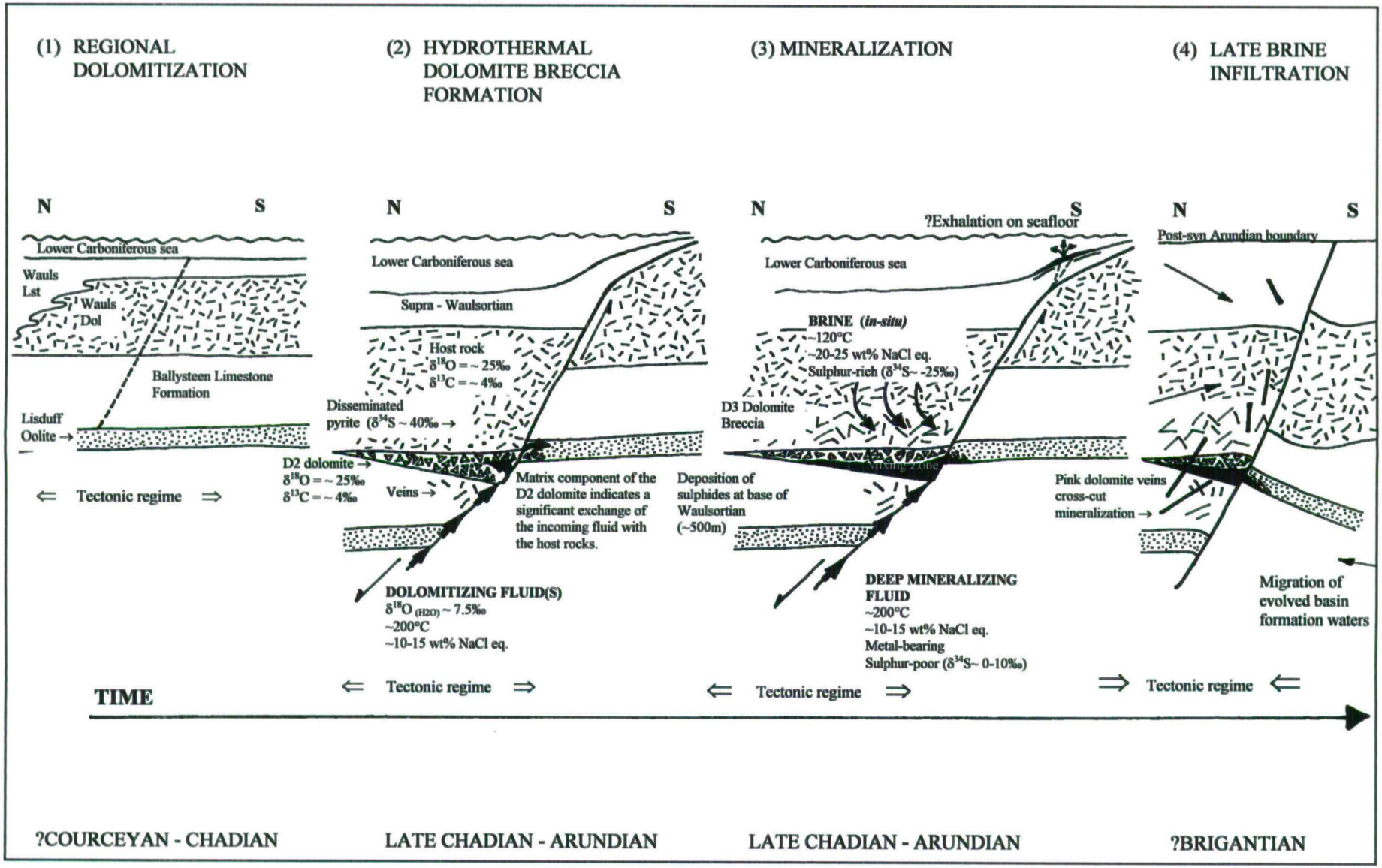


Figure 6.5 Schematic cross-sections illustrating stages of dolomitization and mineralization in the Rathdowney Trend, Ireland: (1) Regional dolomitization of the Waulsortian Limestone; (2) Hydrothermal dolomite breccia formation following widespread faulting; (3) Deposition of sulphides at the base of the Waulsortian by replacement of the dolomite matrix breccia as a result of fluid mixing; (4) Late brine infiltration.

difference is the general lack of a bacteriogenic sulphur component in the prospects. Further, the fluid inclusions show a less well developed mixing trend compared to Lisheen and Galmoy. Therefore the resident, low temperature, sulphur-rich brine inferred to be present in the deposits is probably missing from, or volumetrically insignificant in, the prospects. The prospects are dominated by a 'deep-seated' hydrothermal sulphur component, corresponding to a dominance of the higher temperature, moderate salinity fluid end-member.

Textural differences are evident in the D2 dolomite between the deposits and prospects. The fine crystalline dolomite rhombs within the matrix are noticeably more euhedral in the prospects than deposits. Further, these euhedral rhombs do not exhibit the compositional zoning observed in the dolomite rhombs at both Lisheen and Galmoy. The prospect dolomites in general exhibit elevated Fe and Mn concentrations.

Carbon and oxygen analysis of D2 and D3 dolomites indicates no significant spatial variations between the deposits and prospects. This is somewhat surprising given the inclusion data from D3 dolomites which show a much more pronounced trend toward dilute compositions in the prospects than is observed in the deposits (Figure 5.9).

6.9 TIMING OF MINERALIZATION

The interpretation of replacement textures clearly has major implications for timing of mineralization relative to host rock lithification. Textural evidence (see section 3.5) indicates that sulphides, with the exception of early disseminated pyrite, post-date regional and D2 breccia dolomites, replacing both matrix and regional dolomite clasts. Mineralization must have replaced at least a partially lithified host. Given the occurrence of regional dolomite in Chadian but not Arundian rocks in the Lisheen area, this means that the time of mineralization is constrained to no earlier than the late Chadian, in accord with previous interpretations (Shearley *et al.*, 1996). Mineralization at Navan, the only Irish deposit at which mineralization can be firmly dated stratigraphically, occurred during the late Chadian to Arundian (Ashton *et al.*, 1992).

6.10 GENETIC MODEL

A number of models have been presented for fluid flow associated with Irish-type Zn-Pb ore deposits, in which the mineralizing fluids have been considered as principally either: (1) deeply convected Carboniferous seawater which has reacted significantly with Lower Palaeozoic basement (Russell, 1978, 1986); or (2) are basinal fluids, expelled during Variscan tectonism,

which have migrated laterally within a regional aquifer system (e.g. ORS) (Hitzman and Beaty, 1996). The data reported in this study enable an assessment of these two main competing models by evaluating: (1) Source of mineralizing fluids; (2) source of ore forming constituents; (3) precipitation mechanisms; and (4) fluid pathways. As a result of this, a genetic model can be proposed for the Lisheen and Galmoy deposits in the Rathdowney Trend.

The pre ore-stage regional dolomitization event may have been critical for the later formation of major sulphide deposits at Lisheen and Galmoy. Following early diagenesis, the Waulsortian Limestone had extremely low porosity and permeability. However, as a result of regional dolomite formation, porosity and permeability could have been increased. This permeability and porosity may have facilitated the infiltration of the seawater derived brine which provided the reduced sulphur source at the site of deposition. The sulphur-rich brine may well have become "ponded" at the dolomite front as a result of the permeability contrast with the Waulsortian Limestone. The location of the Lisheen and Galmoy deposits close to the regional dolomite front is therefore unlikely to be coincidental. In weakly mineralized areas throughout the Rathdowney Trend the seawater derived, sulphur-rich brine may not have been sufficiently concentrated in any one area; alternatively it may have been isolated from the favourable mineralization site at the base of the Waulsortian.

Zn-rich, sulphur-poor hydrothermal fluids introduced to the depositional sites along normal faults generated above major, NE trending, reactivated basement structures probably produced distinct thermal anomalies. The low temperature brines in the overlying regional dolomite were probably warmed and set in motion by these thermal anomalies, facilitating circulation of the sulphur-rich brine downwards to the site of deposition at the base of the Waulsortian. The result of mixing at the interface between these two fluids, principally a metal-rich, sulphur-poor fluid with a sulphur-rich fluid resulted in the deposition of ore-stage sulphides in the Lisheen and Galmoy deposits (Figure 6.5). The metal-rich, sulphur-poor, hydrothermal fluids were probably derived from the Lower Palaeozoic basement as suggested by the Pb isotopic composition of precipitated galena, the sulphur isotope composition of sulphides in fault-related veins, and the similarity of basement-circulated fluids to the ore-stage fluids seen in the Lisheen and Galmoy deposits. This suggests that deeply circulated fluids are fundamental to the ore-forming process in the Rathdowney Trend. The ultimate origin of these fluids remains uncertain. Deep circulation is clearly consistent with the models of Russell (1978) and others and, together with Pb isotope data, appears to rule out the ORS as an aquifer and metal source as proposed by Hitzman and Beaty (1996). The presence of fluids of MVT affinity suggests that gravity/topographic driven

fluid-flow models may also be appropriate; however, the evidence from Lisheen currently indicates these relatively late fluids probably post-dated the main mineralizing event.

CHAPTER 7: CONCLUSIONS

CHAPTER 7: CONCLUSIONS

The major conclusions reached following this research are summarized below. In addition, suggestions for further work are proposed.

7.1 PRINCIPAL CONCLUSIONS

- The pre-, syn-, late, and post ore-stage dolomites are all highly non-stoichiometric; this is not typical of dolomites formed under simple burial conditions.

- Fe and Mn concentrations generally increase with time from the earliest pre-ore dolomites to the post-ore dolomites. Irrespective of paragenesis, elevated Fe and Mn concentrations commonly occur in prospect dolomite

- Regional $D1_C$ dolomite and D3 dolomite are texturally similar. Under cathodoluminescence, D3 dolomite exhibits pronounced zonations, due primarily to variations in the Fe/Mn ratio, and not to the absolute concentration of either cation. This zoning is best developed proximal to major mineralized zones.

- Mineralization in the Lisheen and Galmoy Deposits exhibits a variety of ore textures which are best interpreted predominantly in terms of replacement and open-space growth from highly supersaturated solution.

- There is a close correlation between ore texture, paragenetic stage and $\delta^{34}S$, reflecting the depositional process and availability of sulphur at the time of deposition.

- Two distinct sulphur sources are interpreted for Rathdowney Trend mineralization: (1) Lower Carboniferous seawater sulphate providing sulphide *via* bacteriogenic reduction and barite-forming sulphate; and (2) a 'deep-seated' hydrothermal component, probably derived from the Lower Palaeozoic basement.

- Ore-stage sulphides from the base of the Waulsortian at Lisheen and Galmoy always have low $\delta^{34}S$ values (source 1), and fall dominantly within the range $\delta^{34}S$ -4 to -20‰. Late ore-stage sulphides, commonly proximal to major 'feeder' faults, have high $\delta^{34}S$ values in the range ~0 to +10‰ (source 2).

- The Lisheen and Galmoy deposits are dominated by bacteriogenic sulphide; in contrast, the Rathdowney Trend prospects are dominated by the hydrothermal component.

- Intermediate $\delta^{34}S$ isotopic compositions of -10‰ and -12‰, possibly representing mixtures of the two main sulphur sources, are dominant in the major ore zones at Lisheen and Galmoy respectively.

- Isotopic fractionation between sulphide mineral pairs at Lisheen and Galmoy, largely indicate isotopic disequilibrium. This, together with ore textures, supports a fluid mixing model for mineralization.

- The primary fluid associated with ore-stage mineralization was a moderate temperature (160-210°C), moderate salinity (9-15 wt% NaCl eq.) fluid. This is comparable to fluids observed in the Lower Palaeozoic basement.

- At Lisheen and Galmoy, fluid inclusion data imply mixing of the moderate temperature, moderate salinity fluid, with a resident, low temperature, seawater-derived brine at the site of deposition. A less extensive mixing trend is evident at the prospects. Through time the hydrothermal system evolved from a mixing-dominant to a single fluid dominant system.

- Lisheen and Galmoy formed at significantly higher temperatures than most MVT deposits.

- A low temperature (80-140°C), high salinity (22.5-29.0 wt% NaCl eq.) fluid of MVT affinity infiltrated the Lisheen deposit at a late stage, subsequent to the main ore-stage mineralizing event.

- Comparable and correlatable CL zonations in D4 dolomite between Rathdowney East and Holycross prospects indicate a homogeneous regional groundwater flow system at this late stage.

- The $\delta^{13}C$ and $\delta^{18}O$ data exhibit a broad trend toward isotopically lighter compositions with time from the Waulsortian regional dolomite end member

- The $\delta^{13}C$ and $\delta^{18}O$ isotopic character of the matrix component of the D2 dolomite is largely inherited from the regionally dolomitized Waulsortian host, indicative of significant isotopic exchange and supporting a dominantly replacive mode of breccia formation.

- The D5 dolomite represents the least exchanged infiltrating fluid as it shows the most depleted $\delta^{13}C$ and $\delta^{18}O$ compositions. Estimated $\delta^{18}O_{(H2O)}$ for this dolomite of ~+7.5‰ is similar to $\delta^{18}O_{(H2O)}$ values of 6-7‰ estimated for inferred Lower Palaeozoic basement-equilibrated fluids.

- Pb isotopic ratios in Lisheen and Galmoy galenas provide evidence in support of a basement contribution to the mineralizing system in the Rathdowney Trend and confirm the relative homogeneity of Pb isotope data within deposits. The data however, are anomalous as regards the conventional isoplumb theory.

- Pb isotopic ratios in Lisheen and Galmoy galenas are most similar to Silvermines implying a similar Pb source.

- There is no clear correlation of Pb isotope ratios with mineralizing style, paragenetic stage or $\delta^{34}S$.

7.2 FURTHER WORK

Due to the time constraints imposed during the present research, certain aspects of the study could not be fully resolved. Therefore specific areas of further work are proposed. Such additional studies, in combination with the key mineralizing processes in the Rathdowney Trend outlined in this thesis, could further impact on the genesis of, and the exploration for, Irish carbonate-hosted deposits.

7.2.1 Further Work Proposed

Avenues for further work identified during the completion of this project include:

- Identification of characteristics to distinguish between $D1_C$ and texturally similar hydrothermal dolomite.

- Acquisition of further fluid inclusion data on $D1_C$ to confirm or refute a high temperature origin.

- Analysis of fluid inclusion chemistry by crush-leach analysis of sphalerite and, possibly, carbonates.

- Utilization of the above data for modelling ore depositional processes.

- Modelling fluid-rock exchange and fluid mixing effects on carbon and oxygen isotopes.

- More detailed analysis of possible spatial variations in D2 dolomite chemical and isotopic characteristics.

- Analysis of occurrence and distribution of organic matter associated with hydrothermal dolomites.

- Structural analysis of D2 breccia formation.

REFERENCES

REFERENCES

ADAMS, J.E., and RHODES, M.L., 1960. Dolomitization by seepage refluxion: *AAPG Bulletin,* **44**, 1912-1920.

AKANDE, S.O., and ZENTILLI, M., 1984. Geologic, fluid inclusion, and stable isotope studies of the Gays River lead-zinc deposit, Nova Scotia, *Econ. Geol.* **79**, 1187-1211.

ALLAN, J.R., BEATY, D.W., STURTEVANT, R.G., HITZMAN, M.W., and SHEARLEY, E., 1992. The origin of regional dolomite in the Waulsortian of southeast Ireland: Implications for time of ore deposition. *Abstracts of Geological Society of America, annual meeting,* Cincinnati, Ohio, p.A354.

ANDERSON, G.M., 1975. Precipitation of Mississippi Valley-type ores. *Econ. Geol.* **70**, 937-942.

ANDERSON, G.M., 1983. Some geochemical aspects of sulfide deposition in carbonate rocks, *in:* Kisvarsanyi, G., et al., eds., International Conference on Mississippi Valley Type Lead-Zinc Deposits, Proceedings Volume. University of Missouri Rolla, p.61-76.

ANDERSON, G.M., 1991. Organic maturation and ore precipitation in southeast Missouri. *Econ. Geol.* **86**, 909-926.

ANDERSON, G.M., and MACQUEEN, R.W., 1982. Mississippi Valley-Type Lead-Zinc Deposits, *in:* Roberts, R.G., and Sheahan, P.A., eds., Ore Deposit Models. *Geoscience Canada,* Reprint Series 3, 79-90.

ANDERSON, I.K., ANDREW, C.J., ASHTON, J.H., BOYCE, A.J., CAULFIELD, J.B.D., FALLICK, A.E., and RUSSELL, M.J., 1989. Preliminary sulfur isotope data of diagenetic and vein sulphides in the Lower Palaeozoic strata of Ireland and Southern Scotland: implications for Zn+Pb+Ba mineralization: *J. Geol. Soc. London*, **146**, 715-720.

ANDERSON I.K., 1990. Ore depositional processes in the formation of the Navan zinc/lead deposit, Co. Meath, Ireland. *Unpublished PhD Thesis,* Univ. of Strathclyde.

ANDERSON, I.K., ASHTON, J.H., BOYCE, A.J., FALLICK, A.E., RUSSELL, M.J., in press. Ore depositional processes in the Navan Zn+Pb deposit, Ireland. *Econ. Geol.*

ANDERTON, R., BRIDGES, P.H., LEEDER, M.R., and SELLWOOD, B.W., 1992. A Dynamic Stratigraphy of the British Isles: A Study in Crustal Evolution, *Chapman and Hall,* London.

ANDREW, C.J., 1986a. The tectono-stratigraphic controls to mineralization in the Silvermines area, County Tipperary, Ireland, *in:* Andrew, C.J., Crowe, R.W.A., Finlay, S., and Pyne J.F., eds., Geology and genesis of mineral deposits in Ireland: *Irish Association of Economic Geologists,* Dublin, p.377-417.

ANDREW, C.J., 1986b. The geological setting and style of mineralization at Ballyvergin, Co. Clare, *in:* Andrew, C.J., Crowe, R.W.A., Finlay, S., and Pyne J.F., eds., Geology and genesis of mineral deposits in Ireland: *Irish Association of Economic Geologists,* Dublin, p.475-480.

ANDREW, C.J., 1986c. A diagrammatic representation of the Courceyan stratigraphy of the Irish Midlands, *in:* Andrew, C.J., Crowe, R.W.A., Finlay, S., and Pyne J.F., eds., Geology and genesis of mineral deposits in Ireland: *Irish Association of Economic Geologists,* Dublin, p.239-242.

ANDREW, C.J., 1991. Irish zinc deposits - style and process in an orefield context: *Minerals Industry International,* July, 1991, p.9-16.

ANDREW, C.J., 1992. Basin Development Chronology of the Lower-most Carboniferous strata in the north-Central Midlands. In: Bowden, A. A., Earls, G., O' Connor, P.G., and Pyne, J.F., eds., The Irish Mineral industry 1980-1990: *Irish Association for Economic Geologists,* Dublin, p.143-169.

ANDREW, C.J., 1993. Mineralization in the Irish Midlands. *In:* Pattrick, R.A.D., and Polya, D.A., eds., Mineralization in the British Isles. *Chapman and Hall,* London, p.208-269.

ANDREW, C.J., 1995. The Silvermines District, Co. Tipperary, Ireland. *in:* Anderson, K., Ashton, J., Earls, G., Hitzman, M.W., and Tear, S., eds., Irish carbonate hosted Zn-Pb deposits: *Society of Economic Geologists Guidebook Series* **21**, 247-259.

ANDREW, C.J., and ASHTON, J.H., 1982. Mineral textures, metal zoning and ore environment of the Navan orebody, Co. Meath, Ireland, *in:* Brown, A.G., and Pyne, J., eds., Mineral Exploration in Ireland: Progress and Development, 1971-1981. *Irish Association of Economic Geologists,* Dublin, p.35-46.

ANDREW, C.J., and ASHTON, J.H., 1985. The regional setting, geology and metal distribution patterns of Navan orebody, Ireland. *Trans. Inst. Mining Metallurgy (Sect. B: Appl. Earth Sci)* **94**, B66-93.

ANDREW, C.J., and POUSTIE, A., 1986. Syndiagenetic or epigenetic mineralization - the evidence from the Tatestown zinc-lead prospect, Co. Meath, *in:* Andrew, C.J., Crowe, R.W.A., Finlay, S., and Pyne J.F., eds., Geology and genesis of mineral deposits in Ireland: *Irish Association of Economic Geologists,* Dublin, p.281-296.

ARCHER, J.B., SLEEMAN, A.G., SMITH, D.C., 1996. Geology of Tipperary: A geological description of Tipperary and adjoining parts of Laois, Kilkenny, Offaly, Clare and Limerick, to accompany the bedrock geology 1:100,000 scale map series, sheet 18, Tipperary. *Geological Survey of Ireland,* Dublin, pp.76.

ARNE, D.C., CURTIS, L.W., and KISSIN, S.A., 1991. Internal zonation in a carbonate-hosted Zn-Pb-Ag deposit, Nanisivik, Baffin Island, Canada. *Econ. Geol.* **86**, 699-717.

ARTHAUD, F., and MATTE, P., 1977. Late Paleozoic strike-slip faulting in southern Europe and North Africa; results of a right-lateral shear zone between the Appalachians and the Urals, *Geological Society of America,* Bulletin, **88**, 1305-1320.

ASHTON, J.H., DOWNING, D.H., and FINLAY, S.F., 1986. The geology of the Navan Zn-Pb orebody. *In:* Andrew, C.J., Crowe, R.W.A., Finlay, S., and Pyne J.F., eds., Geology and genesis of mineral deposits in Ireland: *Irish Association of Economic Geologists,* Dublin, p.243-280.

ASHTON, J.H., BLACK, A., GERACHTY, J., HOLDSTOCK, M., and HYLAND,E., 1992. The geological setting and metal distribution patterns of Zn-Pb-Fe mineralization in the Navan Boulder Conglomerate. *In:* Bowden, A. A., Earls, G., O'Connor, P.G.,. and Pyne, J.F., eds., The Irish Minerals Industry 1980-1990: *Irish Association of Economic Geologists,* Dublin, p.171-210.

BADHAM, J.P.N., 1975. A new Pb-Zn deposit in the Yukon. *Abstract, Mineral Deposit Studies Group Meeting,* Leicester.

BADHAM, J.P.N., 1982. Strike-slip orogens - an explanation for the Hercynides. *J. Geol. Soc. London,* **139**, 493-504.

BADIOZAMANI, K., 1973. The dorag dolomitization model - Application to the Middle Ordovician of Wisconsin: *Journal of Sedimentary Petrology,* **43**, 965-984.

BANKS, D.A., 1986. Hydrothermal chimneys and fossil worms from the Tynagh Zn-Pb deposit, Ireland, *in:* Andrew, C.J., Crowe, R.W.A., Finlay, S., and Pyne J.F., eds., Geology and genesis of mineral deposits in Ireland: *Irish Association of Economic Geologists,* Dublin, p.441-448.

BANKS, D.A., and RUSSELL, M.J., 1992. Fluid mixing during ore deposition at the Tynagh base- metal deposit, Ireland. *Eur.J. Mineral.,* **4**, 921-931.

BARBANSON, L., TOURAY, J.C., SAULAS, D., VADALA, P., 1983. Distribution at different scales and relative age of the carbonates from Aptian formation of the Santander province (Spain): relation between ferroan halo and Zn-Pb mineralizations of Reocin type. *Chron. Rech. Min.,* **473**, 39-48.

BARKER, A.J., and GAYER, R.A., 1985. Caledonian-Appalachian tectonic analysis and the evolution of related oceans, *in:* GAYER, R.A., ed., The Tectonic Evolution of the Caledonide-Appalachian Orogen. *Earth Evolution Sciences,* Vieweg, Braunschweig, p.126-165.

BARNES, H.L., and GOULD, W.W., 1992. Hydrothermal replacement of calcite by sulfides, *in:* Kharaka, Y.K., and Maest, A.S., eds., *Seventh International Symposium on Water-rock interaction,* Vol., 2. Balkema Press, Rotterdam 1565-1567.

BARTON, P.B., Jr., 1970. Sulfide Petrology. *Mineral. Soc.Am. Spec. Pap.* **33**, 187-198.

BASTIN, E.S., 1950. Interpretation of Ore Textures. *Geological Society of America Memoir,* **45**, pp.101.

BEATY, D.W., ALLAN, J.R., and HITZMAN, M.W., 1991. The relationship of dolomitization and mineralization at the Lisheen deposit, south Central Ireland. *Geological Society of America,* Abstracts with programs, **23**, p.A172.

BERNER, R.A., 1984. Sedimentary pyrite formation, an update: *Geochim. Cosmochim. Acta,* **48,** 605-615.

BERNER, R.A., 1985. Sulfate reduction, organic matter decomposition and pyrite formation. *Philos. Trans. R. Soc. London Ser. A,* **315,** 25-38.

BETHKE, C.M., 1985. A numerical model of compaction-driven groundwater flow and heat transfer and its application to the paleohydrology of intracratonic sedimentary basins. *Journal of Geophysical Research,* **90B**, 6817-6828.

BETHKE, C.M., 1986. Hydrologic constraints on the genesis of the Upper Mississippi Valley mineral district from Illinois basin brines. *Econ. Geol.* **81**, 233-248.

BETHKE, C.M., and MARSHAK, S., 1990. Brine migration across North America: the plate tectonics of groundwater hydrology. *Annual Reviews of Earth Planet. Sciences,* **18**, 287-315.

BISCHOFF, J.L., RADTKE, A.S., and ROSENBAUER, R.J., 1981. Hydrothermal alteration of greywacke by brine and seawater: roles of alteration and chloride complexing on metal solubilization at 200°C and 350°C. *Econ. Geol.* **76**, 659-676.

BOAST, A.M., COLEMAN, M.L., and HALLS, C., 1981a. Textural and stable isotopic evidence for the genesis of the Tynagh base metal deposit, Ireland: *Econ. Geol.* **76**, 27-55.

BOAST, A.M., SWAINBANK, I.G., COLEMAN, M.L., and HALLS, C., 1981b. Lead isotope variation in the Tynagh, Silvermines and Navan base-metal deposits, Ireland. *Trans. Inst. Mining Metallurgy,* **B90**, B115-119.

BOAST, A.M., 1983. Discussions and contributions: *Trans. Inst. Mining Metallurgy,* **92**, Sec. B., 115-119.

BODNAR, R.J., 1993. Revised equation and table for determining the freezing point depression of H_2O-NaCl solutions. *Geochim. Cosmochim. Acta,* **57**, 683-684.

BOYCE, A.J., ANDERTON, R., RUSSELL, M.J., 1983a. Rapid subsidence and early Carboniferous base-metal mineralization in Ireland, *Trans.Inst. Mining Metallurgy,* **B92**, B55-66.

BOYCE, A.J., COLEMAN, M.L., and RUSSELL, M.J., 1983b. Formation of fossil hydrothermal chimneys and mounds from Silvermines, Ireland: *Nature,* **306**, 545-550.

BOYCE, A.J., FLETCHER, T.J., FALLICK, A.E., ASHTON, J.H., and RUSSELL, M.J., 1993. *In:* Fenoll Hach-Al, P., Torres-Ruiz, J., and Gervilla, F., eds., "Current research in Geology Applied to Ore Deposits", Proc. of the 2nd Biennial SGA Meeting, Publ. Univ. of Granada, Spain, p.53-56.

BOYCE, A.J., FALLICK, A.E., FLETCHER, T.J., RUSSELL, M.J., and ASHTON, J.H., 1994. Detailed sulphur isotope studies of Lower Palaeozoic-hosted pyrite below the giant Navan Zn+Pb mine, Ireland: evidence of mass transport of crustal S to a sediment-hosted deposit. *Mineralogical Magazine,***58A**, 109-110.

BOYCE, A.J., and FALLICK, A.E., 1995. Stable and Radiogenic isotopic constraints on genetic models for the Lower Carboniferous carbonate-hosted lead+zinc+barium deposits in Ireland, *in:* Models for carbonate-hosted base metal deposits: *Irish Association of Economic Geologists, Abstracts volume and programme*, p.49-53.

BRADLEY, D.C., 1993. Role of lithospheric flexure and plate convergence on the genesis of some Mississippi Valley-type zinc deposits in the Appalachians: *U.S Geological Survey Bulletin* **2039**, 35-43.

BRAITHWAITE, C.J.R., and RIZZI, G., 1997. The geometry and petrogenesis of hydrothermal dolomites at Navan, Ireland. *Sedimentology,* **44**, 421-440.

BRALIA, A., SABATINI, G., and TROJA, F., 1979. A Revaluation of the Co/Ni ratio in pyrite as geochemical tool in ore genesis problems. *Mineral. Deposita,* **14,** 353-374.

BRENCHLEY, P.J., and TREAGUS, J.E., 1970. The stratigraphy and structure of the Ordovician rocks between Courtown and Kilmichael Point, Co. Wexford. *Proceedings of the Royal Irish Academy,* **69B**, 83-102.

BRINDLEY, J.C., 1969. Caledonian and pre-Caledonian intrusive rocks of Ireland, *in:* Kay, M., ed., North Atlantic Geology and Continental Drift. *AAPG Mem.*, **12**, 336-353.

BRINDLEY, J.C., 1973. The structural setting of the Leinster Granite, Ireland, a review. *Scientific Proceedings of the Royal Dublin Society,* **5A**, 27-36.

BRISKEY, J.A., 1986a. Descriptive model of sedimentary exhalative Zn-Pb. *In:* Cox, D.P., and Singer, D.A., eds., Mineral Deposit Models, *U.S Geological Survey Bulletin,* **1693**, 211-215.

BRISKEY, J.A., 1986b. Descriptive model of southeast Missouri Pb-Zn. *In:* Cox, D.P., and Singer, D.A., eds., Mineral Deposit Models, *U.S Geological Survey Bulletin,* **1693**, 220-221.

BRÜCK, P.M., 1973. Structure of the Lower Palaeozoic greywacke formations west of the Leinster Granite. *Scientific Proceedings of the Royal Dublin Society,* **4A**, 391-409.

BRÜCK, P.M., and REEVES, T.J., 1976. Stratigraphy, sedimentology and structure of the Bray Group in County Wicklow and south County Dublin. *Proceedings of the Royal Irish Academy,* **76**, 53-77.

BRÜCK, P.M., GARDINER, P.R.R., MAX, M.D., and STILLMAN, C.J., 1978. Field guide to the Caledonian and pre-Caledonian rocks of south-east Ireland. *Geological Survey of Ireland Guide series,* 2.

BRÜCK, P.M., COLTHURST, J.R.J., FEELY, M., GARDINER, P.R.R., PENNEY, S.R., REEVES, T.J., SHANNON, P.M., SMITH, D.G., and VANGUESTAINE, M., 1979. South-east Ireland: Lower Palaeozoic stratigraphy and depositional history, *in:* Harris, A.L., Holland, C.H and Leake, B.E., eds., The Caledonides of the British Isles Reviewed. *Geological Society of London Special Publication,* **8**, 533-544.

BRUCKSCHEN, P., BRUHN, F., RICHTER, D.K., 1996. Application of cathodoluminescence to carbonate diagenesis. International Conference on Cathodoluminescence and Related Techniques in Geosciences and Geomaterials, Nancy, Abstracts, p.33-34.

BUELTER, D.P., and GUILLEMETTE, R.N., 1988. Geochemistry of epigenetic dolomite associated with lead-zinc mineralization of the Vibernum Trend, southeast Missouri, *in:* Shukla,

V., and Baker, P.A., eds., Sedimentology and Geochemistry of Dolostones: *SEPM, Special Publication,* **43**, 85-93.

BULLEN, S.B., and SIBLEY, D.F., 1984. Dolomite selectivity and mimic replacement. *Geology,* **12**, 655-658.

CAMPBELL, N., 1967. Tectonics, reefs, and stratiform lead-zinc lead deposits of the Pine Point area, Canada, *Econ. Geol.*Monograph **3**, 59-70.

CARNE, R.C., and CATHRO, R.J., 1982. Sedimentary exhalative (sedex) zinc-lead-silver deposits, northern Canadian Cordillera. *Canadian Institute of Mining, Bulletin,* **75**, No.840, 66-78.

CAROZZI, A.V., 1993. Sedimentary Petrography. *PTR, Prentice Hall Inc.,* New Jersey, pp.261.

CARPENTER, A.B., and OGLESBY, T.W., 1976. A model for the formation of luminescently zoned calcite cements and its implications. *Geological Society of America,* Abstracts with Programs **8**, 469-470.

CATHLES, L.M., and SMITH, A.T., 1983. Thermal constraints on the formation of Mississippi Valley-type lead-zinc deposits and their implications for episodic dewatering and deposit genesis. *Econ. Geol.* **78**, 983-1002.

CAULFIELD, J.B.D., 1986. A model for the genesis of sediment hosted Zn-Pb-Ba deposits in central Ireland based on lead and sulphur isotopic investigations of Keel, Ballinalack, Moyvoughly and Tatestown. *Unpublished PhD Thesis,* Yale University.

CAULFIELD, J.B.D., LeHURAY, A.P., and RYE, D.M., 1986. A review of lead and sulphur isotope investigations of Irish sediment-hosted base metal deposits, with new data from Keel, Ballinalack, Moyvoughly and Tatestown deposits, *in:* Andrew, C.J., Crowe, R.W.A., Finlay, S., and Pyne J.F., eds., Geology and genesis of mineral deposits in Ireland: *Irish Association of Economic Geologists,* Dublin, p.591-615.

CHAMBERS, L.A., and TRUDINGER, P.A., 1979. Microbiological fractionation of stable sulfur isotopes: a review and critique: *Geomicrobiol. J.,* **1**, 249-293.

CHI, G.X., and SAVARD, M.M., 1995. Fluid evolution and mixing in the Gays River carbonate-hosted Zn-Pb deposit and its surrounding barren areas, Nova Scotia. *Atlantic Geology,* **31**, 141-152.

CLAYPOOL, G.E., HOLSER, W.T., KAPLAN, I.R., SAKAI, H., and ZAK, I., 1980. The age curves of sulphur and oxygen isotopes in marine sulfate and their mutual interpretation. *Chem. Geology,* **28**, 199-260.

CLAYTON, G., and GRAHAM, J.G., 1974. Miospore assemblages from the Devonian Sherkin Formation of south-west County Cork, Republic of Ireland. *Pollen et Spores, XVI,* **4**, 565-588.

CLAYTON, G., and HIGGS, K., 1978. The Tournaisian marine transgression in Ireland. *Jour. Earth Sci. Royal Dublin Society,* **2**, 1-10.

CLIFFORD,J.A., RYAN, P., and KUCHA, H., 1986. A review of the geological setting of the Tynagh orebody, Co. Galway. *In*: Andrew, C.J., Crowe, R.W.A., Finlay, S., and Pyne, J.F., eds., Geology and genesis of mineral deposits in Ireland: *Irish Association of Economic Geologists,* Dublin, p.419-439.

COLEMAN, M.L., and MOORE, M.P., 1978. Direct reduction of sulphates to sulphur dioxide for isotopic analysis. *Anal. Chem.,* **28,** 199-260.

COLLER, D.W., 1984. Variscan structures in the Upper Palaeozoic rocks of west central Ireland. *In:* Hutton, D.H.W., and Sanderson, D.J., eds., Variscan Tectonics of the North Atlantic Region. *Geol. Soc. Lond. Spec. Pub.,* **14**, 185-194.

COOMER, P.G., and ROBINSON, B.W., 1976. Sulphur and sulphate-oxygen isotopes and the origin of the Silvermines deposits, Ireland: *Mineral.Deposita,* **11**, 155-169.

COOPER, M.A., and BRÜCK, P.M., 1983. Tectonic relationships of the Leinster Granite, Ireland. *Geological Journal,* **18**, 351-360.

COOPER, M.A., COLLINS, D.A., FORD, M., MURPHY, F.X., and TRAYNER, P.M., 1984. Structural style, shortening estimates and the thrust front of the Irish Variscides, *in:* Hutton, D.H.W., and Sanderson, D.J., eds., Variscan Tectonics of the North Atlantic Region. *Geological Society, London, Special Publication,* No.14, 167-175.

COOPER, M.A., COLLINS, D.A., FORD, M., MURPHY, F.X., and TRAYNER, P.M., and O'SULLIVAN, M., 1986. Structural Evolution of the Irish Variscides. *J. Geol. Soc. London,* **143**, 53-61.

CRAIG, H., 1957. Isotopic standards for carbon and oxygen and correction factors for mass-spectrometric analysis of carbon dioxide. *Geochim. Cosmochim. Acta,* **12**, 133-149.

CRAIG, J.R., and VAUGHAN, D.J., 1981. Ore microscopy and ore petrography. *John Wiley and Sons, Inc,* New York, pp.406.

CROWLEY, J.K., 1986. Visible and near-infrared spectra of carbonate rocks: reflectance variations related to petrographic texture and impurities. *J. Geophys. Res.,* **91**, 5001-5012.

CRIMES, T.P., and DHONAU, N.B., 1967. The Precambrian and Lower Palaeozoic rocks of south-east Co. Wexford, Eire. *Geological Magazine,* **104**, 213-221.

CRIMES, T.P., and CROSSLEY, J.D., 1968. The stratigraphy, sedimentology, ichnology and structure of the Lower Palaeozoic rocks of part of north-eastern Co. Wexford. *Proceedings of the Royal Irish Academy,* **67B**, 185-215.

CROWE, R.W.A., 1986. The stratigraphic and structural setting of Zn-Ba-Pb mineralization at Newtown Cashel, Co. Longford. *In:* Andrew, C.J., Crowe, R.W.A., Finlay, S., and Pyne J.F., eds., Geology and genesis of mineral deposits in Ireland: *Irish Association of Economic Geologists,* Dublin, p.331-340.

CZAMANSKE, G.K., and RYE, R.O., 1974. Experimentally determined sulfur isotope fractionation between sphalerite and galena in the temperature range 600°C to 275°C. *Econ. Geol.* **69**, 17-25.

DAVIS, D.W., LOWENSTEIN, T.K., and SPENCER, R.J., 1990. Melting behaviour of fluid inclusions in laboratory-grown halite crystals in the systems NaCl-H_2O, NaCl-KCl-H_2O, NaCl-$MgCl_2$-H_2O, and NaCl-$CaCl_2$-H_2O. *Geochim. Cosmochim. Acta,* **54**, 591-601.

DE BRIT, T.J., 1989. Timing structural events and basemetal emplacement using extension veins and cements in the Carboniferous of North Central Ireland. *Irish Journal of Earth Sciences* 10, p.13-31.

DERRY, D.R., CLARK, G.R., and GILLATT, N., 1965. The Northgate base metal deposit at Tynagh, Co. Galway, Ireland. *Econ.Geol.* **60**, 1218-1237.

DE VIVO, B., and FREZZOTTI, M.L., 1994. Fluid inclusions in minerals: methods and applications. Short course of the working group " Inclusions in minerals". Virginia Tech., U.S.A. pp. 377.

DEWEY, J.F., 1969. Evolution of the Appalachian-Caledonian Orogen. *Nature,* **222**, 124-128.

DIEHL, P., and KERN, H., 1981. Geology, mineralogy and geochemistry of some carbonate-hosted lead-zinc deposits in Kanchanaburi Province, western Thailand. *Econ.Geol.* **76**, 2128-2146.

DIXON, P.R., LEHURAY, A.P., and RYE, D.M., 1990. Basement Geology and tectonic evolution of Ireland as deduced from Pb isotopes. *J.Geol. Soc.*, **147**, 121-132.

DIXON, P.R., and RYE, D.M., 1991. Fluid flow connections to basement rocks below sedimentary basins: evidence from the base metal deposits in Ireland. *Geophysical Research Letters,* **18**, 943-946.

DORAN, R.J.P., 1971. The Palaeozoic rocks between Tipperary town and Milestone, Co. Tipperary. *Unpublished PhD Thesis*, University of Dublin.

DOROBEK, S.L., 1987. Petrography, geochemistry, and origin of burial diagenetic facies, Siluro-Devonian Helderberg Group (carbonate rocks), Central Appalachians: *AAPG Bulletin*, **71**, 492-514.

DOYLE, E., BOWDEN, A.A., JONES, G.V., and STANLEY G.A., 1992. The Geology of the Galmoy Zinc-Lead Deposits, Co.Kilkenny, *in:* Bowden, A. A., Earls, G., O' Connor, P.G., and Pyne, J.F., eds., The Irish Mineral industry 1980-1990: *Irish Association for Economic Geologists,* Dublin, p.211-226.

DOYLE, E, and BOWDEN, A.A., 1995a. Field Guide to the Galmoy Zinc-Lead Deposits, Co. Kilkenny, *in*: Anderson, K., Ashton, J., Earls, G., Hitzman, M.W., and Tear, S., eds., Irish Carbonate Hosted Zn-Pb Deposits: *Society of Economic Geologists Guidebook series* **21**, 139-145.

DOYLE, E, and BOWDEN, A.A., 1995b. Carboniferous Basin Development in Ireland, Evidence from the Galmoy Area, *in:* Models for Carbonate-Hosted Base Metal Deposits: *Irish Association for Economic Geology, Abstracts Volume and Programme,* p.15.

EBERS, M.L., KOPP, O.C., 1979. Cathodoluminescent microstratigraphy in gangue dolomite, the Mascot-Jefferson City district, Tennessee: *Econ. Geol.* **74**, 908-918.

EL ALI, A., BARBIN, V., CALAS, G., CERVELLE, B., RAMSEYER, K., BOUROULEC, J., 1993. Mn^{2+}- activated luminescence in dolomite, calcite and magnesite: quantitative determination of manganese site distribution by EPR and CL spectroscopy. *Chem. Geol.*, **104**, 189-202.

ELSGAARD, L., ISAKSEN, M.F., and JØRGENSON, B. B., 1994. Microbial sulfate reduction in deep-sea sediments at the Guyamas Basin hydrothermal vent area: influence of temperature and substrates. *Geochim. Cosmochim. Acta,* **58**, 3335-3343.

EVERETT, C.E., RYE, D.M., and DIXON, P.R., 1996. Further evidence for the involvement of deeply circulated fluids in the genesis of Irish base-metal deposits, *Geological Society of America,* Abstracts with Programs, **28**, Denver, Colorado, pA-210.

EVERETT, C.E., WILKINSON, J.J., RYE, D.M., 1997. Brine infiltration of Lower Paleozoic rocks beneath the Navan deposit, Ireland: Implications for the genesis of Irish-type Zn-Pb mineralization. *Geological Society of America,* Abstracts with Programs, No.6, **29**, Salt Lake City, Utah .

EVERETT, C.E., WILKINSON, J.J., RYE, D.M., in press. Fracture-controlled fluid flow in the Lower Palaeozoic basement rocks of Ireland: Implications for the genesis of Irish-type Zn-Pb deposits, *in:* McCaffrey, K., Lonergan, L., and Wilkinson, J.J., eds., Fractures, fluid flow and mineralization. *Geol. Soc. London Special Publication.*

EYRE, S.L., WILKINSON, J.J., STANLEY, C.J., and BOYCE, A.J., 1996. Geochemistry of dolomitization and Zn-Pb mineralization in the Rathdowney Trend, Ireland. *Geological Society of America,* Abstracts with Programs, **28**, Denver, Colorado, p.A-210.

FITZGERALD, E., FEELY, M., JOHNSTON, J.D., CLAYTON, G., FITZGERALD, L.J., and SEVASTOPULO, G.D., 1994. The Variscan thermal history of west Clare, Ireland. *Geological Magazine,* **131**, 545-558.

FOLK, R.L., and LAND, L.S., 1975. Mg/Ca ratio and salinity: two controls over crystallization of dolomite: *AAPG Bulletin,* **56**, 434-453.

FORD, M., 1987. Practical application of the sequential balancing technique: an example from the Irish Variscides. *J. Geol. Soc.London,* **144**, 885-891.

FRANK, M.H., CARPENTER,, A.B., and OGLESBY, T.W., 1982. Cathodoluminescence and composition of calcite cement in the Taum Sauk Limestone (Upper Cambrian), southeast Missouri. *Journal of Sedimentary Petrology,* **52**, 631-638.

FRANK, M.H., LOHMANN, K.C., 1987. Textural and chemical alteration of dolomite: interaction of mineralising fluids and host rock in a Mississippi Valley-type deposit, Bonneterre Formation, Vibernum Trend, *in:* Hagni, R.D., ed., Process Mineralogy IV: Applications to Precious Metal Deposits, Industrial Minerals, Coal, Liberation, Mineral Processing, Agglomeration, Metallurgical Products and Refractories, with special emphasis on Cathodoluminescence Microscopy. *The Metallurgical Society,* Warrendale, Pennsylvania.

FRIEDMAN, I., and O'NEIL, J.R., 1977. Compilation of stable isotope fractionation factors of geochemical interest, *in:* Friedman, I., and O'Neil, J.R., eds., Data of Geochemistry, 6th edition, *Geol. Surv. Am. Prof. Pap.* 440-KK.

GALLAGHER, V., BOYCE, A.J., FALLICK, A.E., and MOHR, P.J., 1992. An isotopic study of the Harberton Bridge Fe-Zn-Pb deposit, County Kildare, and its implication for metallogenesis in Ireland, *in:* Bowden, A. A., Earls, G., O' Connor, P.G., and Pyne, J.F., eds., The Irish Mineral industry 1980-1990: *Irish Association for Economic Geologists,* Dublin, p.261-272.

GALOPIN, R., and HENRY, N.F.M., 1972. Microscopic Study of Opaque Minerals. *W. Heffer and Sons, Ltd.*, Cambridge, England

GARDINER, P.R.R., 1970. Regional fold structures in the Lower Palaeozoics of southeast Ireland. *Geological Survey of Ireland Bulletin,* **1**, 47-51.

GARDINER, P.R.R., and ROBINSON, K.W., 1970. The Geology of Ireland's Eye: the stratigraphy and structure of a part of the Bray Group. *Geological Survey of Ireland Bulletin,* **1**, 3-22.

GARDINER, P.R.R., and MacCARTHY, I.A.J., 1981. The late Palaeozoic evolution of southern Ireland in the context of tectonic basins and their trans-Atlantic significance, *in:* Kerr, J.W., and Ferguson, A.J., eds., Geology of the North Atlantic Borderlands. *Canadian Soc. Petrol. Geol.* Memoir **7**, 683-725.

GARVEN, G., 1985. The role of regional fluid flow in the genesis of the Pine Point deposit, Western Canada sedimentary basin. *Econ. Geol.* **80**, 307-324.

GARVEN, G., and FREEZE, R.A., 1984. Theoretical analysis of the role of groundwater flow in the genesis of stratabound ore deposits: 2. Quantitative results, *American Journal of Science,* **284**, 1124-1156.

GARVEN, G., GE, S., PERSON, M., and SVERJENSKY, D., 1993. The genesis of stratabound ore deposits in the Midcontinent Basins of North America: the role of regional groundwater flow, *American Journal of Science,* **293**, 497-568.

GHAZBAN, F., McNUTT, R.H., and SCHWARCZ, H.P., 1994. Genesis of sediment-hosted Zn-Pb-Ba deposits in the Irankuh District, Esfahan Area, west-Central Iran. *Econ. Geol.* **89**, 1262-1278.

GIBBONS, W., and GAYER, R.A., 1985. British Caledonian terranes, *in*: Gayer, R.A., ed., The Tectonic Evolution of the Caledonide-Appalachian Orogen. *Earth Evolution Sciences,* Vieweg, Braunschweig, p.3-16.

GILL, W.D., 1962. The Variscan foldbelt in Ireland, *in:* Coe, K., ed., Some aspects of the Variscan foldbelt, *Manchester University Press,* Manchester, p.49-64.

GILLIES, D., 1987. Diagenetic history of the Waulsortian carbonate buildups (Dinantian), Craven Basin, NW England, *Unpublished PhD thesis,* University of Edinburgh.

GOLDHABER, M.B., and KAPLAN, I.R., 1975. Controls and consequences of sulfate reduction in recent marine sediments. *Soil Sci.,* **119**, 42-55.

GOLDSMITH, J.R., 1959. Some aspects of the geochemistry of carbonates, *in:* Researches in Geochemistry. Abelson, P.H., ed., *John Wiley*, New York, 336-358.

GONI, J., and REMOND, G., 1969. Localisation and distribution of impurites in blende by cathodoluminescence. *Mineralogical Magazine,* **37**, 153-155.

GOODELL, P.C., and PETERSEN, U., 1974. Julcani mining district, Peru: A study of metal ratios. *Econ. Geol.* **69**, 347-361.

GRAHAM, J.R., 1983. Analysis of the Upper Devonian Munster Basin, an example of a fluvial distributary system. *Special Publications of the International Association of Sedimentology,* **6**, 473-483.

GREGG, J.M., 1985. Regional epigenetic dolomitization in the Bonneterre Dolomite (Cambrian), southeastern Missouri. *Geology,* **13**, 503-506.

GREGG, J.M., 1996. Dolomite: Mineralogy, Sedimentology, and Petrology. *Irish Association for Economic Geology, Short Course, University College Dublin, June 1996.*

GREGG, J.M., 1997. Dolomite cement stratigraphy in Lower Carboniferous carbonates of the Irish Midlands - evidence for regional fluid flow during sulfide mineralization. *Geological Society of America,* Abstracts with Programs, No.6, **29**, Salt Lake City, Utah.

GREGG, J.M., and HAGNI, R.D., 1987. The use of cathodoluminescence microscopy to reveal hidden crystal faces in gangue dolomite cements, Vibernum Trend, southeast Missouri, *in:* Hagni, R.D., ed., Process Mineralogy IV: Applications to Precious Metal Deposits, Industrial Minerals, Coal, Liberation, Mineral Processing, Agglomeration, Metallurgical Products and Refractories, with special emphasis on Cathodoluminescence Microscopy. *The Metallurgical Society,* Warrendale, Pennsylvania.

GREGG, J.M., and SHELTON, K.L., 1989. Minor and trace element distributions in the Bonneterre Dolomite (Cambrian), southeast Missouri: Evidence for possible multiple basin fluid sources and pathways during lead-zinc mineralization. *Geological Society of America Bulletin,* **101**, 221-230.

GREGG, J.M., and SHELTON, K.L., 1990. Dolomitization and dolomite neomorphism in the back reef facies of the Bonneterre and Davis Formations (Cambrian), Southeastern Missouri. *Journal of Sedimentary Petrology,* **60**, No. 4, 549-562.

GREGG, J.M., and KARAKUS, M., 1991. A technique for successive cathodoluminescence and reflected light petrography. *Journal of Sedimentary Petrology,* **61**, No. 4, 613-635.

GREGG, J.M., HOWARD, S.A., MAZZULLO, S.J., 1992. Early diagenetic recrystallization of Holocene (<3000 years old) peritidal dolomites, Ambergris Cay, Belize. *Sedimentology,* **39,** 143-160.

GREIG, J.A., BAADSGARD, H., CUMMING, G.L., FOLINSBEE, R.E., KROUSE, H.R., OHMOTO, H., SASAKI, A., and SMEJKAL, V., 1971. Lead and sulfur isotopes of the Irish base metal mines in Carboniferous carbonate host rocks, *in:* Proc. IMA-IAGOD meetings '70, Joint symposium volume: *Society of Mining Geologists of Japan special issue* ***no.2***, Tokyo, p.84-92.

GUSTAFSON, L.B., and WILLIAMS, N., 1981. Sediment-hosted stratiform deposits of copper, lead and zinc, *in:* Skinner, B.J., ed., Economic Geology, 75th Anniversary Volume 1905-1980, El Paso, *Econ. Geol. Publ. Co.,* p.139-178.

HACKBARTH, C.J., and PETERSEN, U., 1984. Systematic compositional variations in Argentian tetrahedrite, *Ibid.,* **79,** 448-460.

HAGNI, R.D., 1976. Tri-State ore deposits: the character of the host rocks and their genesis, *in:* Wolf, K.H., ed., Handbook of Stratabound and Stratiform Ore Deposits, *New York, Elsevier,* **6**, chap. 10, p.38.

HAGNI, R.D., 1984. Cathodoluminescence microscopy applied to mineral exploration and beneficiation, *in:* Park, W.C., Hausen, D.M., and Hagni, R.D., eds., Applied Mineralogy: Proceedings of the Second International Congress on Applied Mineralogy. *AIME,* New York, p.41-66.

HAGNI, R.D., 1987. Industrial applications of cathodoluminescence microscopy, *in:* Hagni, R.D., ed., Process Mineralogy IV: Applications to Precious Metal Deposits, Industrial Minerals, Coal, Liberation, Mineral Processing, Agglomeration, Metallurgical Products and Refractories, with special emphasis on Cathodoluminescence Microscopy. *The Metallurgical Society,* Warrendale, Pennsylvania.

HAGNI, R.D., and TRANCYNGER, T.C., 1977. Sequence of deposition of the ore minerals at the Magmont Mine, Vibernum Trend, southeast Missouri. *Econ. Geol.* **72**, 451-464.

HALL, W.E., and FRIEDMAN, I., 1969. Oxygen and carbon isotopic composition of ore and host rock of selected Mississippi Valley deposits. *U.S. Geol. Surv. Prof. Pap.* **650-C**, C140-C148.

HALLIDAY, A.N., and MITCHELL, J.G., 1983. K-Ar ages of clay concentrates from Irish orebodies and their bearing on the timing of mineralization: *Transactions of the Royal Society of Edinburgh,* Earth Sciences, **74**, 1-14.

HAMILTON, J..M., DELANEY G.D., HAUSER, R.L., and RANSOM, P.W., 1983. Geology of the Sullivan deposit, Kimberley, B.C. Canada, *in:* Sangster, D.F., ed., Sediment-hosted Stratiform Lead-Zinc Deposits, Short Course Handbook, **8**, 31-83, *Mineralogical Association of Canada,* Victoria.

HANOR, J.S., 1994. Physical and chemical controls on the composition of waters in sedimentary basins. *Marine and Petroleum geology,* **11**, 31-45.

HARDIE, L.A., 1987. Dolomitization: a critical view of some current views: *Journal of Sedimentary Petrology,* **57**, 166-183.

HARRIS, A.L., and PITCHER, W.S., 1975. The Dalradian Supergroup, *in:* Harris, A.L., et al., eds., A correlation of the Precambrian rocks in the British Isles. *Geological Society of London Special Rep.,* p.52-75.

HARRISON, A.G., and THODE, H.G., 1958. Mechanism of the bacterial reduction of sulfate from isotope fractionation studies. *Trans. Faraday Soc.*, **54**, 84-92.

HAYASHI, K., SUGAKI, A., and KITAKAZE, A., 1990. Solubility of sphalerite in aqueous sulfide solutions, at temperatures between 25 and 240°C. *Geochim. Cosmochim. Acta,* **54,** 715-725.

HAYWARD, C.L., 1998. Cathodoluminescence of Ore and Gangue Minerals and it's Application in the Minerals Industry in Ore Geology, *In:* Cabri, L.J., and Jambor, J.L., eds., Modern Approaches to Ore and Environmental Mineralogy. *Mineralogical Association of Canada, Short Course,* **27.**

HAZLETT, T.J., and GARVEN, G., 1995. A hydrogeologic analysis of the role of faults in the genesis of carbonate-hosted Pb-Zn deposits, Midlands Basin, Ireland, *in:* Extended Abstracts, International Field Conference on Carbonate Hosted Lead Zinc Deposits, St Louis Missouri, *Society of Economic Geologists,* p.127-128.

HEYL, A.V., 1983. Geologic characteristics of three major Mississippi Valley-type districts, *in:* Kisvarsanyi et al., eds., Proceedings of the International Conference on Mississippi Valley-type Deposits, *Rolla, University of Missouri,* p.27-59.

HIGGS, K., and RUSSELL, K.J., 1981. Upper Devonian microfloras from southeast Iveragh, Co. Kerry, Ireland. *Bull. Geol. Surv. Ireland.,* **3,** 17-50.

HITZMAN, M.W., 1986. The geology of the Abbeytown mine, Co. Sligo, Ireland, *in:* Andrew, C.J., Crowe, R.W.A., Finlay, S., and Pyne J.F., eds., Geology and genesis of mineral deposits in Ireland: *Irish Association of Economic Geologists,* Dublin, p.341-354.

HITZMAN, M.W., 1991c. Hydrothermal dolomitization of Waulsortian mudbanks at the Silvermines (Magcobar) deposit, *in:* Lower Carboniferous Waulsortian mudbanks: Geometries, Diagenesis, and late dolomitization. *Chevron Mineral Corporation of Ireland Intercompany Technical Group on Carbonates Seminar,* No. LN91000514, Dublin, unpaginated.

HITZMAN, M.W., 1995a. Geological setting of the Irish Zn-Pb-(Ba-Ag) orefield, *in:* Anderson, K., Ashton, J., Earls, G., Hitzman, M.W., and Tear, S., eds., Irish carbonate hosted Zn-Pb deposits: *Society of Economic Geologists Guidebook Series* **21,** 3-24.

HITZMAN, M.W., 1995b. Mineralization in the Irish Zn-Pb-(Ba-Ag) orefield, *in*: Anderson, K., Ashton, J., Earls, G., Hitzman, M.W., and Tear, S., eds., Irish carbonate hosted Zn-Pb deposits: *Society of Economic Geologists Guidebook series* **21**, 25-61.

HITZMAN, M.W., and LARGE, D., 1986. A review and classification of the Irish carbonate-hosted base metal deposits, *in:* Andrew, C.J., Crowe, R.W.A., Finlay, S., and Pyne J.F., eds., Geology and genesis of mineral deposits in Ireland: *Irish Association of Economic Geologists,* Dublin, p.217-238.

HITZMAN, M.W., RECIO, C., CAULFIELD., J.B., BOYCE, A.J., and FALLICK, A.E., 1988. Stable isotopic (S,C,O) study of the Abbeytown Zn-Pb-Ag mine, Co. Sligo, Ireland, abs., *Geol. Soc. America Programs with Abstracts,* **20**, 7, p.A38.

HITZMAN, M.W., and SHEARLEY, E., 1991. Dolomitization at the Lisheen deposit, Rathdowney Trend, Co. Tipperary, *in:* Lower Carboniferous Waulsortian mudbanks: Geometries, Diagenesis, and late dolomitization. *Chevron Mineral Corporation of Ireland Intercompany Technical Group on Carbonates Seminar,* No. LN91000514, Dublin, unpaginated.

HITZMAN, M.W., O'CONNOR, P., ALLAN, J.R., BEATY, D.W., SCHAFFALITZKY, C., SHEARLEY, E., and THOMPSON, T., 1992. Discovery and geology of the Lisheen Zn-Pb-Ag prospect, Rathdowney Trend, Ireland, *in*: Bowden, A. A., Earls, G., O' Connor, P.G., and Pyne, J.F., eds., The Irish Mineral industry 1980-1990: *Irish Association for Economic Geologists,* Dublin, p.227-246.

HITZMAN, M.W., and BEATY, D.W., 1996. The Irish Zn-Pb-(Ba) Orefield, *in:* Sangster, D.F., ed., *Society of Economic Geologists,* Special Publication, No. **4**, 1996, 112-143.

HITZMAN, M.W., ALLAN, J.R., and BEATY, D.W., 1998. Regional dolomitization of the Waulsortian Limestone in southeastern Ireland: Evidence of large scale fluid flow driven by the Hercynian Orogeny. *Geology,* **26,** 547-550.

HOLLAND, C.H., 1981. Cambrian and Ordovician of the Paratectonic Caledonides, *in:* A Geology of Ireland, *Scottish Academic Press,* Edinburgh, p.41-63.

HOLLISTER, L.S., and CRAWFORD, M.L., 1981. A short course in fluid inclusions. *Mineralogical Association of Canada,* Short Course Handbook, **6**, pp.304.

HONJO, H., and SAWADA, Y., 1982. Quantitative measurements on the morphology of a NH_4Br dendritic crystal growth in a capillary. *Journal of Crystal Growth,* **58**, 297-303.

HSÜ, K.J., and SIEGENTHALER, C., 1969. Preliminary experiments on hydrodynamic movement induced by evaporation and their bearing on the dolomite problem: *Sedimentology,* **12**, 11-25.

HUMPHRIES, D.W., 1992. The Preparation of Thin Sections of Rocks, Minerals and Ceramics. Microscopy Handbooks, 24, *Oxford University Press,* pp.83.

HUSTON, D.L., and LARGE, R.R., 1987. Genetic and exploration significance of the zinc ratio (100 Zn/(Zn+Pb)) in massive sulphide systems. *Econ. Geol.* **82**, 1521-1539.

HUTTON, D.H.W., 1982. A tectonic model for the emplacement of the main Donegal Granite, NW Ireland. *J. Geol. Soc.London,* **139**, 615-631.

HUTTON, D.H.W., 1987. Strike-slip terranes and a model for the evolution of the British and Irish Caledonides. *Geological Magazine,* **124**, 405-425.

JACKSON, G.D., and BEALES, F.W., 1967. An aspect of sedimentary basin evolution: the concentration of Mississippi Valley-type ores during late stages of diagenesis. *Canadian Petroleum Geology Bulletin,* **15**, 383-433.

JAMBOR, J.L., and VAUGHAN, D.J., 1990. Advanced Microscopic Studies of Ore Minerals. *Mineralogical Association of Canada, Short Course Handbook,* Volume **17**, pp.426.

JOHNSTON, J.D., 1993. Three-dimensional geometries of veins and their relationship to folds: examples from the Carboniferous of eastern Ireland. *Irish Journal of Earth Sciences,* **12**, 47-63.

JOHNSTON, J.D., 1995a. A Review of the Pre-Devonian Rocks of Ireland, *in*: Anderson, K., Ashton, J., Earls, G., Hitzman, M.W., and Tear, S., eds., Irish carbonate hosted Zn-Pb deposits: *Society of Economic Geologists Guidebook series* **21**, 209-217.

JOHNSTON, J.D., 1995b. Variscan deformation in Ireland, *in*: Anderson, K., Ashton, J., Earls, G., Hitzman, M.W., and Tear, S., eds., Irish carbonate hosted Zn-Pb deposits: *Society of Economic Geologists Guidebook series* **21**, 111-113.

JOHNSTON, J.D., 1995c. A review of the structural controls of Irish carbonate-hosted base metal deposits, *in:* Models for carbonate-hosted base metal deposits: *Irish Association for Economic Geology, Abstracts Volume and Programme,* p.37-39.

JOHNSTON, J.D., REDMOND, P., ZHANG, X., SANDERSON, D.J., 1995. Hangingwall collapse breccias - a mechanism for generation of dolomite matrix breccias. Proceedings of the Irish Geological Research Meeting, Sligo, Abstracts, unpaginated.

JOHNSTON, J.D., COLLER, D., MILLAR, G., CRITCHLEY, M.F., 1996. Basement Structural Controls on Carboniferous-hosted base metal mineral deposits in Ireland, *in:* Strogen, P., Somerville, I.D., and Jones, G.Ll., eds., Recent Advances in Lower Carboniferous Geology. *Geological Society Special Publication* No.**107**, 1-21.

JONES, G.V., and BRADFER, N., 1982. The Ballinalack zinc-lead deposit, Co. Westmeath, Ireland, *in:* Brown, A.G., and Pyne, J., eds., Mineral Exploration in Ireland: Progress and Development, 1971-1981. *Irish Association of Economic Geologists,* Dublin, p.47-62.

JONES, G.V., and BRAND, S.F., 1986. The setting, styles of mineralization and mode of origin of the Ballinalack Zn-Pb deposit, *in:* Andrew, C.J., Crowe, R.W.A., Finlay, S., and Pyne J.F., eds., Geology and genesis of mineral deposits in Ireland: *Irish Association of Economic Geologists,* Dublin, p.355-376.

JONES, G.Ll., SOMERVILLE, I.D., and STROGEN, P., 1988. The Lower Carboniferous (Dinantian) of the Swords area: sedimentation and tectonics in the Dublin Basin Ireland: *Geological Journal,* **23**, 221-248.

JØRGENSON, B.B., ISAKSEN, M.F., JANNASCH, H.W., 1992. Bacterial sulphate reduction above 100°C in deep-sea hydrothermal vent sediments. *Science,* **258,** 1756-1757.

KAMILLI, R.J., and OHMOTO, H., 1977. Paragenesis, zoning, fluid inclusion and isotopic studies of the Finlandia vein, Colqui district, Central Peru. *Econ. Geol.* **72**, 950-982.

KAPLAN, I.R., and RITTENBERG, S.C., 1964. Microbiological fractionation of sulfur isotopes. *J. Gen. Microbiol.*, **34**, 195-212.

KAUFMAN, J., CANDER, H.S., DANIELS, L., and MEYERS, W.J., 1988. Calcite cement stratigraphy and cementation history of the Burlington Keokuk Formation (Mississippian), Illinois and Missouri. *Journal of Sedimentary Petrology,* **58**, 312-326.

KELLY, J., and CSA Geology staff, 1993. Waulsortian and Crosspatrick facies distributions at Lisheen, Co. Tipperary. *C.S.A Report No: 12.93.*

KENNAN, P.S., 1979. Plutonic rocks in the Irish Caledonides. In: Harris, A.L., Holland, C.H and Leake, B.E., eds., The Caledonides of the British Isles Reviewed. *Geological Society of London Special Publication,* **8**, 705-711.

KENNAN, P.S., and KENNEDY, M.J., 1983. Coticules - a key to correlation along the Appalachian Caledonian orogen. In: Schenk, P.E., ed., Regional Trends in the geology of the Appalachian-Caledonian-Hercynian-Mauritanide orogen. *D.Reidel Publishing Co.,* Dordrecht, p.355-361.

KENNAN, P.S., McARDLE, P., GALLAGHER, V., MORRIS, J.H., O'CONNOR, P.G., O'KEEFE, W.G., REYNOLDS, N.A., and STEED, G.M., 1987. A review of recent isotope research on mineralization in Ireland. *Geological Survey of Ireland, Bulletin 1987,* **4**, 1-10.

KERR, J.W., 1977. Cornwallis lead-zinc district: Mississippi Valley-type deposits controlled by stratigraphy and tectonics, *Canadian Journal of Earth Sciences,* **14**, 1402-1426.

KIYOSU, Y., and KROUSE, H.R., 1990. The role of organic acid in the abiogenic reduction of sulphate and the sulphur isotope effect. *Geochem. Jour.* **24**, 21-27.

KOPP, O.C., EBERS, M.L., COBB, L.B., CRATTIE, T.B., FERGUSON, T.L., LARSEN, R.M., POTOSKY, R.A., and STEINBERG, R.T., 1987. Application of cathodoluminescence microscopy to the study of gangue carbonates in Mississippi Valley-type deposits in Tennessee: The search for a "Tennessee Trend", *in:* Hagni, R.D., ed., Process Mineralogy IV: Applications to Precious Metal Deposits, Industrial Minerals, Coal, Liberation, Mineral Processing,

Agglomeration, Metallurgical Products and Refractories, with special emphasis on Cathodoluminescence Microscopy. *The Metallurgical Society,* Warrendale, Pennsylvania.

KREBS, W., 1981. The geology of the Meggen ore deposit, *in:* Wolf, K.H., ed., Handbook of strata-bound and stratiform ore deposits. *Elsevier,* Amsterdam, Part III, p.509-549.

KREBS, W., and MACQUEEN, R., 1984. Sequence of diagenetic and mineralization events: Pine Point lead-zinc property, NWT, Canada, *Canadian Petroleum Geology Bulletin,* **32**, 434-464.

KRETZ, R., 1992. Carousel model for the crystallization of saddle dolomite, *Journal of Sedimentary Petrology,* **62**, 190-195.

KROUSE, H.R., VIAU, C.A., ELIUK, L.S., UEDA, A., HALAS, S., 1988. Chemical and isotopic evidence of thermochemical sulfate reduction by light thermochemical gases in deep carbonate reservoirs. *Nature,* **333,** 415-419.

KUCHA, H., 1989. Macrotextures, microtextures and carbonate-sulfide relationships in stratiform, carbonate-hosted Zn-Pb orebodies of Silvermines, Ireland. *Mineral. Deposita,* **24**, 48-55.

KUCHA, H., and WIECZOREK, A., 1984. Sulphide-carbonate realtionships in the Navan (Tara) Zn-Pb deposit, Ireland. *Mineral. Deposita,* **19**, 208-216.

KUHLEMANN, J., ZEEH, S., 1995. Sphalerite stratigraphy and trace element composition of east Alpine Pb-Zn deposits (Drau Range, Austria-Slovenia). *Econ. Geol.* **90**, 2073-2080.

KYLE, J.R., 1981. Geology of Pine Point lead-zinc district, *in:* Wolf, K.H., ed., Handbook of strata-bound and stratiform ore deposits. *Elsevier,* New York, **9**, 643-741.

KYLE, J.R., 1983. Economic aspects of subaerial carbonates, *AAPG Memoir* **33**, 73-92.

KYLE, J.R., and PRICE, P.E., 1985. Mineralogical investigation of sulfide concentrations in the Hockley Salt-Dome cap-rock, Texas, *in:* Park, W.C., Hausen, D.M., and Hagni, R.D., eds., Applied Mineralogy: Proceedings of the Second International Congress on Applied Mineralogy. *AIME,* New York, p.1065-1082.

LAFLAMME, J.H.G., 1990. The preparation of materials for microscopic study, *in:* Jambor, J.L., and Vaughan, D.J., eds., Advanced Microscopic Studies of Ore Minerals. Short Course Handbook, **17**, *Mineralogical Association of Canada,* Ottawa.

LAND, L.S., 1980. The isotopic and trace element geochemistry of dolomite: The state of the art, *in:* Zenger, D.H., Dunham, J.B., and Ethington, R.L., eds., Concepts and Models of Dolomitization: *Society of Economic Paleontologists and Mineralogists, Special Publication,* **28**, 87-110.

LAND, L.S., 1985. The origin of massive dolomite. *Journal of Geological Education,* **33**, 112-125.

LANDIS, G.P., and RYE, R.O., 1974. Geologic, fluid inclusion, and stable isotope studies of the Pasto Bueno tungsten-base metal ore deposit, Northern Peru. *Econ. Geol.* **69**, 1025-1059.

LARGE, D.E., 1980. Geological parameters associated with sediment-hosted, submarine exhalative Pb-Zn deposits: an empirical model for mineral exploration. *Geol. Jb.,* **40**, 59-129.

LARGE, D.E., 1981. Sediment-hosted submarine exhalative lead-zinc deposits - A review of their geological characteristics and genesis, *in:* Wolf, K.H., ed., Handbook of strata-bound and stratiform ore deposits. *Elsevier,* Amsterdam, **9**, 469-508.

LARGE, D.E., 1983. Sediment-hosted massive sulphide lead-zinc deposits: An empirical model, *in:* Sangster, D.F., ed., Sediment-hosted stratiform lead-zinc deposits, *Mineralogical Association of Canada,* Short Course Handbook, **8**, 1-30.

LARTER, R.C.L., BOYCE, A.J., and RUSSELL, M.J., 1981. Hydrothermal pyrite chimneys from the Ballynoe baryte deposit, Silvermines, Co. Tipperary, Ireland, *Mineral. Deposita* **16**, 309-318.

LEACH, D.L., and ROWAN, E.L., 1986. Genetic link between Ouachita foldbelt tectonism and the MVT lead-zinc deposits of the Ozarks. *Geology,* **14**, 931-935.

LEACH, D.L., and SANGSTER, D.F., 1993. Mississippi Valley-type lead-zinc deposits. *In:* Kirkham, R.V., Sinclair, W.D., Thorpe, R.I., and Duke, J.M., eds., Mineral Deposit Modelling, *Geological Association of Canada,* Special Paper **40**.

LEES, A.J. 1964. The structure and origin of the Waulsortian (Lower Carboniferous) reefs of west Central Eire: *Philosophical transactions of the Royal Society of London,* series **B247**, 483 - 531.

LEES, A.J., NOEL, B., BOUW, P., 1977. The Waulsortian "reefs" of Belgium: a progress report: *Mem. Inst. Geol.* Univ. Louvain, **29**, 289-315.

LEES, A.J., and MILLER, J., 1985. Facies variation in Waulsortian buildups. Part 2. Mid-Dinantian buildups from Europe and North America. *Geol. J.,* **20**, 159-180.

LEHURAY, A.P., CAULFIELD, J.B.D., RYE, D.M., and DIXON, P.R., 1987. Basement controls on sediment-hosted Zn-Pb deposits: A Pb isotope study of Carboniferous mineralization in Central Ireland. *Econ. Geol.* **82**, 1695-1709.

LEVERENZ, H.W., 1968. An introduction to the luminescence of solids. *New York, Dover.*

LEWCHUK, M.T., and SYMONS, D.T.A., 1995. A regional paleomagnetic study of carbonates surrounding MVT orebodies in the Illinois-Kentucky-Tennessee area, *in:* Extended Abstracts, International Field Conference on Carbonate Hosted Lead Zinc Deposits, St Louis Missouri, *Society of Economic Geologists,* p.185-188.

LEWIS, H., COUPLES, G.D., and RUSSELL, M.J., 1995. Characterization of fluid-flow systems for Irish lead-zinc deposits - contributions from mass balance, *Trans. Inst. Mining Metallurgy,* **B104,** 145-155.

LU, C., REED, M.H., and MISRA, K.C., 1992. Zinc-Lead skarn mineralization at Tin Creek, Alaska: fluid inclusions and skarn-forming reactions. *Geochim. Cosmochim. Acta,* **56**, 109-119.

LUMB, M.D., 1978. Luminescence Spectroscopy. *Academic Press,* London.

LYDON, J.W., 1986. Models for the generation of metalliferous hydrothermal systems within sedimentary rocks and their applicability to the Irish Carboniferous Zn-Pb deposits, *in:* Andrew,

C.J., Crowe, R.W.A., Finlay, S., and Pyne J.F., eds., Geology and genesis of mineral deposits in Ireland: *Irish Association of Economic Geologists,* Dublin, p.555-577.

LYDON, J.W., GOODFELLOW, W.D., and JONASSON, I.R.A., 1985. A genetic model for stratiform baritic deposits of the Selwyn Basin, Yukon Territory. *Pap. Geol. Surv. Can.,* 85,/1A, p.651-660.

MacCARTHY, I.A.J., 1995. Devonian and Carboniferous successions of the Munster and South Munster Basins, southern Ireland, *in:* Anderson, K., Ashton, J., Earls, G., Hitzman, M.W., and Tear, S., eds., Irish carbonate hosted Zn-Pb deposits: *Society of Economic Geologists Guidebook series* **21**, 95-102.

MACHEL, H.G., 1985. Cathodoluminescence in calcite and dolomite and its chemical interpretation . *Geoscience Canada,* **12**, 139-147.

MACHEL, H.G., 1987. Saddle dolomite as a by-product of chemical compaction and thermochemical sulfate reduction. *Geology,* **15**, 936-940.

MACHEL, H.G., and MOUNTJOY, E.W., 1986. Chemistry and environments of dolomitization - A reappraisal: *Earth Science Reviews,* **33**, 175-222.

MACHEL, H.G., MASON, R.A., MARIANO, A.N., and MUCCI, A., 1991. Causes and emission of luminescence in calcite and dolomite, *in:* Barker, C.E., and Kopp, D.C., eds., Luminescence Microscopy: Quantitative and Qualitative Aspects: *SEPM Short Course,* **25**, 9-25.

MACHEL, H.G., 1996. Application of cathodoluminescence to carbonate diagenesis. International Conference on Cathodoluminescence and Related Techniques in Geosciences and Geomaterials, Nancy, Abstracts, p.89.

MACQUEEN, R.W., and THOMPSON, R.I., 1978. Carbonate-hosted lead-zinc occurrences in northeastern British Columbia with emphasis on the Robb Lake deposit. *Canadian Journal Earth Science,* **15**, 1737-1762.

MADDEN, W., 1996. The Lisheen zinc/lead mine. *Irish Association for Economic Geology,* Annual Review, 1996, p.73.

MALLON, A..J., 1997. Petrological and mineralogical characteristics of the Old Red Sandstone facies rocks beneath base metal deposits as a guide to the setting of mineralization in the Irish Midlands. *Unpublished PhD Thesis*, University College Cork.

MARFUNIN, A.S., 1979. Spectroscopy, Luminescence and radiation centres in minerals. Translated from Russian by V.V., Schifer, *Springer-Verlag*, Berlin.

MARSHALL, D.J., 1988. Cathodoluminescence of Geological Materials. *Unwin Hyman,* Boston.

MAX, M.D., and RODDICK, J.C., 1989. Age of metamorphism in the Rosslare Complex, SE Ireland. *Proceeding of the Geologists Association,* **100**, 113-121.

McCAFFREY, K.J.W., 1992. Igneous emplacement in the transpressive shear zone: Ox Mountains igneous complex. *J. Geol. Soc. London,* **149**, 221-236.

McCAFFREY, K.J.W., 1994. Magmatic and solid state deformation partitioning in the Ox Mountains granodiorite. *Geological Magazine,* **131**, 639-652.

McCREA, J.M., 1950. On the isotopic chemistry of carbonates and a palaeotemperature scale, *Jour. Chem. Phys.*, **18,** 849-857.

McKEAG, A.H., 1956. Modern applications of luminescent materials. *Industrial Chemist,* **32,** 105-110.

McLIMANS, R.K., 1977. Geologic, fluid inclusion, and stable isotope studies of the Upper Mississippi Valley zinc-lead district, southwest Wisconsin. *Unpublished PhD Thesis,* The Pennsylvania State University.

McQUEEN, K.G., 1989. Sediment geochemistry and base-metal sulphide mineralization in the Quidong area of south-eastern New South Wales, Australia. *Mineral. Deposita,* **24**, 100-110.

MENUGE, J.F., and DALY, S.R., 1990. Proterozoic evolution of the Erris Complex, NW Mayo, Ireland: Neodymium isotope evidence, *in:* Gower, C.F., Rivers, T., Ryan, B., eds., Mid-Proterozoic geology of the southern margin of proto Laurentia - Baltica. *Geological Association of Canada Special Paper,* No. **38**, 41-51.

MEYERS, W.J., 1974. Carbonate cement stratigraphy of the Lake Valley formation (Mississippian) Sacramento Mountains, New Mexico. *Journal of Sedimentary Petrology,* **44**, 837-861.

MEYERS, W.J., 1978. Carbonate cements: their regional distribution and interpretation in Mississippian limestones of southwestern New Mexico. *Sedimentology*, **25**, 371-400.

MILLER, J., 1986. Facies relationships and diagenesis in Waulsortian mudmounds from the Lower Carboniferous of Ireland and N. England, *in*: Schroeder, J.J., and Purser, B.H., eds., Reef Diagenesis: *Springer Verlag,* Berlin, p.311-335.

MILLS, H., HALLIDAY, A.N., ASHTON, J.N., ANDERSON, I.K., and RUSSELL, M.J., 1987. Origin of a giant orebody at Navan, Ireland. *Nature,* **327**, 223-226.

MONTAÑEZ, I.P., READ, J.F., and SINHA, A.K., 1988. Origin of dolomites in cyclic peritidal, Upper Knox carbonates Appalachians: evidence from trace elements, stable and radiogenic isotopes. *Abstracts, SEPM Annual Midyear Meeting,* V, p.38.

MORROW, D.W., 1982. Diagenesis 2. Dolomite - part 2. Dolomitization Models and Ancient Dolostones. *Geosc. Can.* **9**, 95-107.

MORROW, D.W., 1990. Dolomite - Part 2: Dolomitization models and ancient dolostones, *in:* McIlreath, I.A., and Morrow, D.W., eds., Diagenesis, *Geosc. Can. Reprint Series,* **4**, 125-139.

MORTON, J.A., 1993. Re-evaluation of the Geology and Zn-Pb Ore Deposits of the Metaline Mining District, Northeastern Washington, *Washington Geology,* **20**, No. 3.

MUIR, R.J., FITCHES, W.R., and MALTMAN, A.J., 1994. The Rhinns Complex: Proterozoic basement on Islay and Colonsay, Inner Hebrides, Scotland and on Inishtrahull, NW Ireland. *Transactions of the Royal Society of Edinburgh,* **85**, 77-90.

MULLANE, M.M., and KINNAIRD, J.A., 1998. Synsedimentary mineralization at Ballynoe barite deposit, near Silvermines, Co. Tipperary, Ireland. *Trans. Instn. Min. Metall.(Sect.B: Appl. earth sci.,)* **107**, B49-61.

MURPHY, C.P., 1986. Thin Section Preparation of Soils and Sediments, *A. B. Academic Publishers,* Berkhamsted, pp.149.

MURPHY, F.C., 1989. Basement-Cover relationships of a reactivated Cadomian mylonite zone: Rosslare complex, SE Ireland, *in:* Topley, Strachan, Berrinsale and D'Lemos eds., The Cadomian Orogeny. *Geological Society of London Special Publication,* **50**, 329-339.

MURPHY, F.C., ANDERSON, T.B., DALY, J.S., GALLAGHER, V., GRAHAM, J.R., HARPER, D.A.T., JOHNSTON, J.D., KENNAN, P.S., KENNEDY, M.J., LONG, C.B., MORRIS, J.H., O'KEEFE, W.G., PARKES, M., RYAN, P.D., SLOAN, R.J., STILLMAN, C.J., TIETZSCH-TYLER, D., TODD, S.P., WRAFTER, J.P., 1991. An appraisal of Caledonian suspect terranes in Ireland. *Irish Journal of Earth Sciences,* **11**; 1, 11-41.

MURRAY, W.J., 1975. McArthur River H.Y.C lead-zinc and related deposits, *in:* Knight, C.L., ed., Economic Geology of Australia and Papua New Guinea, I. Metals: *Melbourne, Australasian Inst. Mining Metallurgy*, p.329-339.

NAYLOR, D., and JONES, P.C., 1967. Sedimentation and tectonic settings of the Old Red Sandstone of southwest Ireland, *in:* Oswald, D.H., ed., International Symposium on the Devonian System. *Alberta Society of Petroleum Geologists,* p.1089-1099.

NAYLOR, D., SEVASTOPULO, G.D., SLEEMAN, A.G., and REILLY, T.A., 1981. The Variscan fold belt in Ireland, *in:* Zwart, H.J., and Dornstephen, U.F., eds., The Variscan Orogen in Europe. *Geologie en Mijnbouw,* **60**, 49-66.

NAYLOR, D., REILLY, T.A., SEVASTOPULO, G.D., and SLEEMAN, A.G., 1983. Stratigraphy and structure in the Irish Variscides, *in:* Hancock, P., ed., The Variscan fold belt in the British Isles. *Adam Hilger,* Bristol. p.20-46.

NAYLOR, D., SEVASTOPULO, G.D., and SLEEMAN, A.G., 1989. Subsidence history of the South Munster Basin, Ireland, *in:* Arthurton, R.S., Gutteridge, P., and Nolan, S.C., eds., The Role of Tectonics in Devonian and Carboniferous sedimentation in the British Isles. *Occasional Publication, Yorkshire Geological Society,* p.99-109.

NISSEN, A.E., and HOYT S.L., 1915. On the occurrence of silver in argentiferous galena ores. *Econ. Geol.***10**, 172-179.

NOBLE, E.A., 1963. Formation of ore deposits by water of compaction. *Econ. Geol.* **58**, 1145-1156.

NOLAN, S.C., 1986. The Carboniferous Geology of the Dublin area. *Unpub. PhD Thesis,* Univ. Dublin.

NOLAN, S.C., 1989, The style and timing of Dinantian syn-sedimentary tectonics in the eastern part of the Dublin Basin, Ireland. In: Arthurton, R.S., Gutteridge, P., and Nolan, S.C., (eds) The Role of Tectonics in Devonian and Carboniferous sedimentation in the British Isles. *Occasional*

OAKES, C.S., BODNAR, R.J., and SIMONSON, J.M., 1990. The system NaCl-$CaCl_2$-H_20: I. The ice liquidus at 1 atm. total pressure. *Geochim. Cosmochim. Acta,* **54**, 603-610.

O'BRIEN, M.V., 1959. The future of non-ferrous mining in Ireland, *in:* The future of non-ferrous mining in Great Britain and Ireland. *Institute of Mining and Metallurgy,* p.5-26.

O'BYRNE, C.J., 1990. Sedimentology, slump deformation and tectonic evolution of the Middle Cambrian Bray Group, eastern Ireland. *Unpublished PhD Thesis*, National University of Ireland.

O'CONNOR, P.J., KENNAN, P.S., and AFTALION, M., 1988. New Rb-Sr and U-Pb ages for the Carnsore Granite and their bearing on the antiquity of the Rosslare Complex, southeastern Ireland. *Geological Magazine,* **125**, 25-29.

OHMOTO, H., 1972. Systematics of sulfur and carbon isotopes in hydrothermal ore deposits. *Econ. Geol.* **67,** 551-579.

OHMOTO, H., 1986. Stable isotope geochemistry of ore deposits, *in:* Valley, J.E., Taylor, H.P., Jr., O'Neil, J.R., eds., Stable Isotopes in High Temperature Geological Processes. *Mineral. Soc. Am. Rev. Mineral.* **16,** 491-560.

OHMOTO, H., KAISER, C.J., and GEER, K.A., 1990. Systematics of sulphur isotopes in recent marine sediments and ancient sediment-hosted basemetal deposits, *in:* Herbert, H.K., and Ho,

S.E., eds., Stable isotopes and fluid processes in mineralization. *University of Western Australia Publication,* Perth, **23**, 70-120.

OHMOTO, H., and GOLDHABER, M.B., 1997. Sulphur and Carbon Isotopes, *in:* Barnes, H.L., Geochemistry of Hydrothermal Ore Deposits: *John Wiley and Sons, Inc,* New York, p.517-611.

OHMOTO, H., and RYE, R.O., 1979. Isotopes of sulfur and Carbon, *in:* Barnes, H.L., ed., Geochemistry of Hydrothermal Ore Deposits, *John Wiley and Sons, Inc,* New York, p.509-567.

O'KEEFE, W.G.O., 1986. Age and postulated source rocks for mineralization in Central Ireland, as indicated by lead isotopes, *in:* Andrew, C.J., Crowe, R.W.A., Finlay, S., and Pyne J.F., eds., Geology and genesis of mineral deposits in Ireland: *Irish Association of Economic Geologists,* Dublin, p.617-624.

OLSON, R.A., 1984. Genesis of paleokarst and strata-bound zinc-lead sulphide deposits in a proterozoic dolostone, Northern Baffin Island, Canada, *Econ. Geol.* **79**, 1056-1103.

O'REILLY, B.M., READMAN, P.W., and MURPHY, T., (In Press) Gravity lineaments and Carboniferous-hosted base metal deposits of the Irish Midlands. *Gravity and Irish Mineral Deposits.*

ORR, W.L., 1974. Changes in sulfur content and isotopic ratios of sulfur during petroleum maturation - study of Big Horn Basin Paleozoic oils, *AAPG Bulletin,* **58,** 2295-2318.

PERSON, M., and GARVEN, G., 1994. A sensitivity study of the driving forces on fluid flow during continental-rift basin evolution. *Geological Society of America Bulletin,* **106**, 461-475.

PHILCOX, M.E., 1971. A Waulsortian bryozoan reef ('cumulative biostrome') and its off-reef equivalents, Ballybeg, Ireland. *Compte Rendu 6e Congres Intern. Strat. Geol. Carbonif., Sheffield,* 1967, **4**, 1359-1372.

PHILCOX, M.E., 1984. Lower Carboniferous lithostratigraphy of the Irish Midlands. *Irish Association of Economic Geologists,* Dublin, pp.89.

PHILCOX, M.E., 1989. The mid-Dinantian unconformity at Navan, Ireland, *in:* Arthurton, R.S., Gutteridge, P., and Nolan, S.C., eds., The Role of Tectonics in Devonian and Carboniferous

sedimentation in the British Isles. *Occasional Publication, Yorkshire Geological Society,* No.**6**, 67-82.

PHILCOX, M.E., SEVASTOPULO, G.D., MacDERMOT, C.V., 1989. Intra-Dinantian tectonic activity on the Curlew Fault, north-west Ireland, *in:* Arthurton, R.S., Gutteridge, P., and Nolan, S.C., eds., The Role of Tectonics in Devonian and Carboniferous sedimentation in the British Isles. *Occasional Publication, Yorkshire Geological Society,* No.**6**, 55-66.

PHILLIPS, W.E.A., TAYLOR, W.E.G., and SANDERS, I.S., 1975. An analysis of the geological history of the Ox Mountains inlier. *Sci. Proc. R.Dubl. Soc.* **5A**, 311-329.

PHILLIPS, W.E.A., STILLMAN, C.J., and MURPHY, T., 1976. A Caledonian plate tectonic model. *J. Geol.Soc.London,* **132**, 579-609.

PHILLIPS, W.E.A., and HOLLAND, C.H., 1981. Late Caledonian Deformation. *In:* Holland, C.H., ed., A Geology of Ireland: *Scottish Academic Press,* Edinburgh, p.107-119.

PHILLIPS, W.E.A., 1981. The Orthotectonic Caledonides. *In:* Holland, C.H., ed., A Geology of Ireland: *Scottish Academic Press,* Edinburgh, p.17-39.

PHILLIPS, W.E.A., and SEVASTOPULO, G.D., 1986. The stratigraphic and structural setting of Irish mineral deposits, *in:* Andrew, C.J.., Crowe, R.W.A., Finlay, S., Pennell, W.M., and Pyne, J.F., eds., Geology and Genesis of Mineral Deposits in Ireland. *Irish Association for Economic Geologists,* Dublin, p.1-30.

PICKARD, N.A.H., JONES, G.Ll., Rees, J.G., SOMERVILLE, I.D., and STROGEN, P., 1992. Lower Carboniferous (Dinatian stratifraphy and structure of the Walterstown-Kentstown area, Co. Meath, Ireland. *Geological Journal,* **27**, p.35-58.

PICKARD, N.A.H., 1996. Evidence for microbial influence on the development of Lower Carboniferous buildups, *in:* Strogen, P., Somerville, I.D., and Jones, G.Ll., eds., Recent Advances in Lower Carboniferous Geology. *Geological Society Special Publication* No.**107**, 65-82.

PIERSON, B.J., 1981. The control of cathodoluminescence in dolomite by iron and manganese. *Sedimentology,* **28**, 601-610.

PLANT, J.A., 1986. Models for granites and their mineralizing systems in the British and Irish Caledonides, *in:* Andrew, C.J., Crowe, R.W.A., Finlay, S., and Pyne J.F., eds., Geology and genesis of mineral deposits in Ireland: *Irish Association of Economic Geologists,* Dublin, p.121-156.

PLUMLEE, G., LEACH, D., HOFSTRA, A., LANDIS, G., ROWAN, E., and VIETS, 1994. Chemical reaction path modelling of ore deposition in Mississippi Valley-type Pb-Zn deposits of the Ozark region, U.S. midcontinent. *Econ Geol.* **89**, 1361-1383.

POSTGATE, J.R., 1984. The Sulfate-Reducing Bacteria, 2nd edition, *Cambridge University Press,* Cambridge.

POTTS, P.J., 1987. A Handbook of Silicate Rock Analysis. *Blackie*, Glasgow.

POTTS, P.J., BOWLES, J.F.W., REED, S.J.B., and CAVE, M.R., eds., 1995. Microprobe Techniques in the Earth Sciences. *Chapman and Hall,* London.

POUSTIE, A., and KUCHA, H., 1986. The geological setting, style and petrology of zinc-lead mineralization in the Moyvoughly area, Co. Westmeath, *in:* Andrew, C.J., Crowe, R.W.A., Finlay, S., and Pyne J.F., eds., Geology and genesis of mineral deposits in Ireland: *Irish Association of Economic Geologists,* Dublin, p.305-318.

PRICE, C.A., 1988. Some thoughts on the subsidence and evolution of the Munster Basin, southern Ireland, *in:* Arthurton, R.S., Gutteridge, P., and Nolan, S.C., eds., The Role of Tectonics in Devonian and Carboniferous sedimentation in the British Isles. *Special Publication of the Yorkshire Geological Society.*

PRICE, C.A., and TODD, S.P., 1988. A model for the development of the Irish Variscides. *J. Geol. Soc.London,* **145**, 935-939.

RADKE, R.M., and MATHIS, R.L., 1980. On the formation and occurrence of saddle dolomite, *Journal of Sedimentary Petrology,* **50**, No.4, 1149-1168.

RAMAGE,W.E., 1984. The zoning in gangue dolomite from the Vibernum Trend. *Unpublished Senior Thesis, Harvard University,* Cambridge MA.

RAMAGE,W.E., and HOLLAND, H.D., 1984. Chemical zoning of gangue dolomite in lead ores of the Vibernum Trend, Missouri. *Geological Society of America, Abstracts with Programs,* **16,** pp.630.

RAMBOZ, C., OUDIN, E., and THISSE, Y., 1988. Geyser-type discharge in Atlantis II Deep, Red, Sea: evidence of boiling from fluid inclusions in epigenetic anhydrite. *Can., Min.,* **26,** 765-786.

RAMDOHR, P., 1980. The ore minerals and their intergrowths. *Pergamon Press,* Oxford, pp.1207.

RANDELL, R.N., 1994. Geology of the Polaris Zn-Pb Mississippi Valley-type deposit, Canadian Arctic Archipelago, *Ph.D. thesis,* University of Toronto, Toronto, Ontario.

RAVENHURST, C.E., REYNOLDS, P.H., ZENTILLI, M., KRUEGER, H.W., and BLENKINSOP, J., 1989. Formation of Carboniferous Pb-Zn and barite mineralization from basin-derived fluids, Nova Scotia, Canada, *Econ. Geol.* **84,** 1471-1488.

RECIO, C., CAULFIELD, J.D.B., BOYCE, A.J., FALLICK, A.E., and HITZMAN, M.W., 1988. Stable isotopic (S, C, O) study of the Abbeytown Zn+Pb+Ag mine, Co. Sligo, Ireland. Abstracts volume, Mineral Deposits Studies Group Annual Meeting, Egham.

REDMOND, P., 1995. Structural controls on mineralization and dolomitization at the Lisheen zinc-lead deposit, Co. Tipperary, Ireland, *in:* Models for carbonate-hosted base metal deposits: *Irish Association of Economic Geologists, Abstracts volume and programme,* p.16-21.

REDMOND, P., 1992. Cathodoluminescence petrographic study of dolomitization at Lisheen. *C.S.A Technical Report,* 40.92.

REDMOND, P., 1997. *Unpublished MSc Thesis,* Trinity College Dublin.

REED, S.J.B., 1993. Electron Microprobe Analysis, 2nd edn. *Cambridge University Press,* Cambridge.

REED, S.J.B., 1995. Electron Microprobe Analysis, *In:* Potts, P.J., et al., eds., Microprobe Techniques in the Earth Sciences, p.49-89. *Chapman and Hall,* London.

REED, S.J.B., 1996. Electron Microprobe Analysis and Scanning Electron Microscopy in Geology, *Cambridge University Press,* pp.201.

REEDER, R.J., GRAMS, J.C., 1987. Sector zoning in calcite cement crystals: Implication for trace element distribution in carbonates: *Geochim. Cosmochim. Acta,* **51**, 187-194.

RHODES, D., LANTOS, E.A., LANTOS, J.A., WEBB, R.J., and OWENS, D.C., 1984. Pine Point orebodies and their relationship to the stratigraphy, structure, dolomitization, and karstification of the Middle Devonian barrier complex. *Econ. Geol.* **79**, 991-1055.

RIZZI, G., 1993. The sedimentology and petrography of Lower Carboniferous limestones and dolomites; host rocks to the Navan zinc-lead deposit, Ireland. *Unpublished PhD Thesis,* University of Glasgow.

ROBINSON, B.W., and OHMOTO, H., 1973. Sulfur isotope equilibrium during sulfur hydrolysis at high temperatures. *Earth Planet. Sci. Lett.,* **18**, 443-450.

ROBINSON, B.W., and KUSAKABE, M., 1975. Quantitative Preparation of Sulfur Dioxide, for ^{34}S / ^{32}S Analyses, from sulfides by Combustion with Cuprous Oxide. *Analytical Chemistry,* **47**, No.7, 1179-1181.

ROEDDER, E., 1968. The noncolloidal origin of "colloform" textures in sphalerite ores. *Econ. Geol.* **63**, 451-471.

ROEDDER, E., 1977. Fluid inclusion studies of ore deposits in the Viburnum Trend, southeast Missouri. *Econ. Geol.***72**, 474-479.

ROEDDER, E., 1984. Fluid Inclusions, Reviews in Mineralogy, Vol. 12, *Mineralogical Society of America.*

ROSENBAUM, J., and SHEPPARD, S.M.F., 1986. An isotopic study of siderites, dolomites and ankerites at high temperatures. *Geochim. Cosmochim. Acta,* **50,** 1147-1150.

ROWAN, E.L., 1987. Cathodoluminescent zonation in hydrothermal dolomite cements: Relationship to Mississippi Valley-type Pb-Zn mineralization in southern Missouri and northern Arkansas, *in:* Hagni, R.D., ed., Process Mineralogy VI: Applications to precious metal deposits, industrial materials, coal, liberation, mineral processing, aglomeration, metallurgical products, and refractories, with special emphasis on cathodoluminescence microscopy, *The Metallurgical Society,* Warrendale, Pennsylvania. p.89-102.

ROWAN, E.L., and LEACH, D.L., 1989. Constraints from fluid inclusions on sulfide precipitation mechanisms and ore fluid migration in the Vibernum Trend lead district, Missouri. *Econ.Geol.* **84**, 1948-1965.

RUSSELL, M.J., 1968. Structural controls of base metal mineralization in relation to continental drift. *Trans. Inst. Mining Metallurgy,* **77B**, B17-128.

RUSSELL, M.J., 1975. Lithogeochemical environment of the Tynagh base metal deposit, Ireland, and its bearing on ore deposition. *Trans. Inst. Mining Metallurgy*, **84B**, B128-133.

RUSSELL, M.J., 1978. Downward excavating hydrothermal cells and Irish-type ore deposits: importance of an underlying thick Caledonian prism. *Trans. Inst. Mining Metallurgy*, **87B**, 168-171.

RUSSELL, M.J., 1983. Major sediment hosted exhalative zinc-lead deposits: formation from hydrothermal convection cells that deepen during crustal extension, *in:* Sangster, D.F., ed., Sediment-hosted stratiform lead-zinc deposits. *Mineralogical Association of Canada, Short Course Handbook,* **8**, 257-282.

RUSSELL, M.J., 1986. Extension and convection; a generic model for the Irish Carboniferous base metal and barite deposits, *in:* Andrew, C.J., Crowe, R.W.A., Finlay, S., and Pyne, J.F., eds., Geology and genesis of mineral deposits in Ireland. *Irish Association for Economic Geologists,* Dublin, p.545-554.

RUSSELL, M.J., and LEWIS, H., 1995. Hydrothermal solutions feeding the Irish orebodies did probe the basement and did rise to the sea floor: evidence from isotopes, fossils, seismicity, mineralogy and mass balance, *in:* Models for carbonate-hosted base metal deposits: *Irish Association of Economic Geologists, Abstracts volume and programme*, p.54-57.

RYE, R.O., and OHMOTO, H., 1974. Sulfur and Carbon Isotopes and Ore Genesis: A review. *Econ. Geol.* **69**, 826-842.

SAKAI, H., 1968. Isotopic properties of sulfur compounds in hydrothermal processes. *Geochem. Jour.* (Japan), **2**, 29-49.

SALLER, A.H., 1984. Petrologic and geochemical constraints on the origin of subsurface dolomite, Enewetak Atoll: An example of of dolomitization by normal seawater, *Geology,* **12**, 217-220.

SAMSON, I.M., and RUSSELL, M.J., 1983. Fluid inclusion data from the Silvermines Zn+Pb+$BaSO_4$ deposits, Ireland. *Trans. Inst. Mining Metallurgy,* **B92**, 67-71.

SAMSON, I. M., and RUSSELL, M.J., 1987. Genesis of the Silvermines zinc-lead-barite deposit, Ireland: fluid inclusion and stable isotope evidence. *Econ. Geol.* **82**, 371-394.

SANDERS, I.S., DALY, S.R., and DAVIES, G.R., 1987. Late Proterozoic high pressure granulite facies metamorphism in the north-east Ox inlier, north-west Ireland. *Journal of Metamorphic Petrology,* **5**, 69-85.

SANDERSON, D.J., and ZANG, X., 1997. Modelling and prediction of localized flow in fractured rock-masses, with applications to mineral deposits. Structural Controls and Genesis of Economic Resources, the Dave Johnston Memorial Meeting, Trinity College Dublin, Abstracts, unpaginated.

SANGSTER, D.F., 1976. Carbonate hosted lead-zinc deposits, *in:* Wolf, K.H., ed., Handbook of Stratabound and Stratiform Ore Deposits, *Amsterdam, Elsevier,* **6**, 447-456.

SANGSTER, D.F., 1986. Age of mineralization in Mississippi Valley-type (MVT) deposits: a critical requirement for genetic modelling, *in:* Andrew, C.J., Crowe, R.W.A., Finlay, S., and Pyne J.F., eds., Geology and genesis of mineral deposits in Ireland: *Irish Association of Economic Geologists,* Dublin, p.625-634.

SANGSTER, D.F., 1990. Mississippi Valley-type and sedex lead-zinc deposits: a comparative examination. *Trans. Inst. Mining Metallurgy,* **B99**, B21-42.

SANGSTER, D.F., 1993. Evidence for, and implications of, a genetic relationship between MVT and SEDEX zinc-lead deposits, *in:* Mathews, I.G., ed., World zinc '93 International Symposium Proceedings. *Australasian Inst. Mining Metallurgy, Publication Series No.* **7/93**, 85-94.

SANGSTER, D.F., 1995. What are Irish-type deposits anyway? *In:* Irish Association for Economic Geology Annual Review, 1995. *Irish Association of Economic Geology,* Dublin, p.91-95.

SANGSTER, D.F., and LEACH, D.L., 1995. Mississippi Valley-type deposits in the spectrum of sediment-hosted lead-zinc deposits, *in:* Extended Abstracts, International Field Conference on Carbonate Hosted Lead Zinc Deposits, St Louis Missouri, *Society of Economic Geologists,* p.260-263.

SASAKI, A., and KROUSE, H.R., 1969. Sulfur isotopes and the Pine Point lead-zinc mineralization. *Econ. Geol.* **64**, 718-730.

SASAKI, A., 1974. Isotopic data of Kuroko deposits, *in:* Ishihara et al., eds., Geology of Kuroko Deposits. *Soc. Mining Geologists of Japan,* Tokyo, p.389-397.

SAVARD, M.M., 1996. Pre-ore burial dolomitization adjacent to the carbonate-hosted Gays River Zn-Pb deposit, Nova Scotia. *Can. J Earth Sci.* **33**, 303-315.

SAVARD, M.M., CHI, G., KONTAK, D.J., FALLARA, F., 1995a. Ore forming fluids in carbonate-hosted Pb-Zn deposits of the Carboniferous Basal Windsor Group, Nova Scotia, Canada: temperature, chemistry, and water-rock interaction, *in:* Extended Abstracts, International Field Conference on Carbonate Hosted Lead Zinc Deposits, St Louis Missouri, *Society of Economic Geologists,* p.267-269.

SCHULTZ, R.W., 1966a. Lower Carboniferous cherty iron-formation at Tynagh, Ireland. *Econ. Geol.* **61**, 311-342.

SCHULTZ, R.W., 1966b. The Northgate base-metal deposit at Tynagh, County Galway, Ireland - a discussion. *Econ. Geol.* **61**, 1443-1449.

SCOTT, V.D., and LOVE, G., 1994. Quantitative Electron Probe Microanalysis, 2nd edn. *Ellis Horwood,* Chichester.

SCHOLLE, P.A., 1978. A colour illustrated guide to carboante rock constituents, textures, cements and porosities. *AAPG Mem.,* **27**, Tulsa. 10.1, 10.2.1., pp.241.

SEVASTOPULO, G.D., 1981a. Lower Carboniferous, *in:* Holland, C.H., ed., A Geology of Ireland. *Scottish Academic press,* Edinburgh, p.147-172.

SEVASTOPULO, G.D., 1981b. Upper Carboniferous, *in:* Holland, C.H., ed., A Geology of Ireland. *Scottish Academic press,* Edinburgh, p.173-188.

SEVASTOPULO, G.D., 1982. The age and depositional setting of Waulsortian Limestone in Ireland; Symposium on the Environmental Setting and Distribution of the Waulsortian Facies, *El Paso Geological Society and the Univ.Of Texas*, p.65-79.

SEVASTOPULO, G.D., 1991. Thermal maturation history of Upper Palaeozoic rocks in Ireland, *in:* Lower Carboniferous Waulsortian Mudbanks: Geometries, Diagenesis, and Late Dolomitization (LN91000514): *Chevron Mineral Corporation of Ireland Intercompany Technical Group on Carbonates Seminar*, Dublin, Ireland.

SHANNON, P.M., 1978. The stratigraphy and sedimentology of the Lower Palaeozoic rocks of south-east County Wexford. *Proceedings of the Royal Irish Academy,* **78**, 247-265.

SHANNON, P.M., 1979. The tectonic evolution of the Lower Palaeozoic rocks of extreme SE Ireland, *in:* Harris, A.L., Holland, C.H and Leake, B.E., eds., The Caledonides of the British Isles Reviewed. *Geological Society of London Special Publication,* **8**, 281-285.

SHARP, J.M., 1978. Energy and momentum transport model of the Ouachita Basin and its possible impact on formation of economic mineral deposits. *Econ. Geol.* **73**, 1057-1068.

SHEARLEY, E., 1993a. Lithostratigraphy of the Lisheen area. *Compiled by C.S.A, Report No: 84.93*

SHEARLEY, E., 1993d. Mineralization and thickness distribution at Lisheen. *Compiled by C.S.A, Report No: 88.93*

SHEARLEY, E., REDMOND, P., GOODMAN, R., and KING, M., 1995. *In:* Anderson, K., Ashton, J., Earls, G., Hitzman, M.W., and Tear, S., eds., Irish carbonate hosted Zn-Pb deposits: *Society of Economic Geologists Guidebook Series* **21**, 123-137.

SHEARLEY, E., REDMOND, P., KING, M., and GOODMAN, R., 1996. Geological controls on Mineralization and Dolomitization of the Lisheen Zn-Pb-Ag deposit, Co.Tipperary, Ireland, *in:* Strogen, P., Somerville, I.D., and Jones, G.Ll., eds., Recent Advances in Lower Carboniferous Geology. *Geological Society, Special Publication* No.107, London, p.23-33.

SHEARLEY, E., REDMOND, P., GOODMAN, R., DAVIS, R., ROBINSON, H., and KING, M., 1993b. Structural controls on mineralization in the Lisheen area. *Compiled by C.S.A, Report No: 85.93*

SHEARLEY, E., DAVIS, R., GOODMAN, R., ROBINSON, H., and WALTON, G., 1993c. Report on lithology, grade and thickness continuity at Lisheen. *Compiled by C.S.A, Report No: 36.93*

SHELTON, K.L., BAUER, R.M., and GREGG, J.M., 1992. Fluid-inclusion studies of regionally extensive epigenetic dolomites, Bonneterre dolomite (Cambrian), southeast Missouri: Evidence of multiple fluids during dolomitization and lead-zinc mineralization. *Geological Society of America Bulletin,* **104**, 675-683.

SHEPHARD-THORN, E.R., 1963. The Carboniferous limestone succession in north-west Co. Limerick, Ireland: *Proceedings of The Royal Irish Academy,* **62**, No.17, 267-294.

SHEPHERD, T.J., RANKIN, A.H., ALDERTON, D.H.M., 1985. A practical guide to fluid inclusion studies. *Blackie,* London, pp.239.

SHEPPARD, S.M.F., 1986. Characterization and isotopic variations in natural waters, *in:* Valley, J.W., Taylor, H.P, O'Neil, J.R., eds., Stable Isotopes in High Temperature Geological Processes, *Mineralogical Association America,* Reviews in Mineralogy, vol. **16**, 165-183.

SHERIDAN, D.J.R., 1972. The stratigraphy of the Trim No.1 well, Co. Meath and its relationship to Lower Carboniferous outcrop in east-Central Ireland. *Bulletin of the Geological Survey of Ireland,* **1**, 311-334.

SHERIDAN, D.J.R., 1977. The hydrocarbons and mineralization proved in the Carboniferous strata of deep boreholes in Ireland, *in:* Garrard, P., ed., Proceedings of the Forum on Oil and Ore in Sediments, Dept. of Geology, Imperial College, London, U.K., 113-146.

SIBLEY, D.F., 1980. Climatic control of dolomitization, Domi Formation (Pliocene), Bonaire, N.A, *in:* D.H., Zenger, R.J., Dunham, J.B., Ethington, R.L., eds., Concepts and models of dolomitization. *SEPM Spec. Publ.* **28**, 247-258.

SIBLEY, D.F., 1982. The origin of common dolomite fabrics, clues from the Pliocene: *Journal of Sedimentary Petrology,* **52**, 1087-1100.

SIBLEY, D.F., GREGG, J.M., 1987. Classification of dolomite rock textures: *Journal of Sedimentary Petrology,* **57**, No.6, 967-975.

SKALL, H., 1975. The Paleoenvironment of the Pine Point lead-zinc district, *Econ.Geol.***73**, 22-45.

SKYRING, G.W., 1987. Sulfate reduction in coastal ecosystems. *Geomicrobiol. J.* **5**, 295-374.

SLEEMAN, A.G., THORNBURY, B., SEVASTOPULO, G.D., 1986. The stratigraphy of the Courceyan (Carboniferous; Dinantian) rocks of the Cloyne Syncline, west of Cork Harbour. *Irish Journal of Earth Sciences,* **8**, 21-40.

SLEEMAN, A.G. 1990. GSI lexicon entries for formations depicted on the GSI 1:1,000,000 compilation of Rathdowney District. *Unpub. Geol. Surv. Irl* lexicon. 6pp + map.

SLOWEY, E.P., 1986. The zinc-lead and barite deposits at Keel, Co. Longford. *In:* Andrew, C.J., Crowe, R.W.A., Finlay, S., and Pyne J.F., eds., Geology and genesis of mineral deposits in Ireland: *Irish Association of Economic Geologists,* Dublin, p.319-330.

SLOWEY, E.P., HITZMAN, M.W., BEATY, D.W., and THOMPSON, T.B., 1995. The Keel Zn-Pb and Garrycam $BaSO_4$ deposits, Co. Longford, Ireland. *In:* Anderson, K., Ashton, J., Earls, G., Hitzman, M.W., and Tear, S., eds., Irish carbonate hosted Zn-Pb deposits: *Society of Economic Geologists Guidebook series* **21**, 227-241.

SOMERVILLE, I.D., and JONES, G.Ll., 1985. The Courceyan Stratigraphy of the Pallaskenry Borehole, County Limerick, Ireland. *Geological Journal,* **20**, 377-400.

SOMERVILLE, I.D., STROGEN, P., and JONES, G.Ll., 1992. The biostratigraphy of Dinantian limestones and associated volcanic rocks in the Limerick Syncline, Ireland. *Geological Journal,* **27**, p.201-220.

SOMERVILLE, I.D., STROGEN, P., GREGG, J.M., SHELTON, K.L., 1997. Fluid flow, dolomitization and mineralization in Lower Carboniferous carbonate rocks, southern Irish Midlands: a preliminary report, *in:* Hendry, J., Carey, P., Parnell, J., Ruffell, A., and Worden, R., eds., *Geofluids II '97, Extended abstracts volume,* p.209-212.

SOMMER, S.E., 1972a. Cathodoluminescence of carbonates, 1. Characterization of cathodoluminescence from carbonate solid solutions. *Chem. Geol.* **9**, 257-273.

SOMMER, S.E., 1972b. Cathodoluminescence of carbonates, 2. Geological Applications. *Chem. Geol.* **9**, 275-284

SOPER, N.J., and HUTTON, D.H.W., 1984. Late Caledonian sinistral displacements in Britain; implications for a three-plate collision model. *Tectonics*, **3**, 781-794.

SOPER, N.J., WEBB, B.C., and WOODCOCK N.H., 1987. Late Caledonian (Acadian) transpression in northwest England: timing and geotectonic significance. *Proc. Yorks. Geol. Soc.,* **46**, 175-192.

STACEY, J.S., and KRAMERS, J.D., 1975. Approximation of terrestrial lead isotope evolution by a two-stage model. *Earth Planet. Sci. Lett.* **26**, 207-221.

STANTON, R.L., 1972. Ore Petrology. *McGraw-Hill*, New York, pp.713.

STERNER, M.S., HALL, D.L., and WHELLER, J.R., 1993. Post entrapment compositional changes in synthetic and natural fluid inclusions: diffusional re-equilibration of water. *Polska Akad. Nauk, Archiwum Mineralogiczine,* **49**, p.85.

STILLMAN, C.J., and WILLIAMS, C.T., 1978. Geochemistry and tectonic setting of some Upper Ordovician volcanic rocks in east and south-east Ireland. *Earth Planet. Sci. Lett.* **42**, 288-310.

STILLMAN, C.J., 1982. Lower Palaeozoic volcanism in Ireland, *in:* Sutherland, D.S., ed., Igneous rocks of the British Isles, *Wiley, London,* p.113-126.

STROGEN, P. 1973. The volcanic rocks of the Carrigogunnel area Co. Limerick. *Scientific Proceedings of the Royal Dublin Society*, series, A., **5**, 11-26.

STROGEN, P., 1995. Lower Carboniferous Volcanic Rocks of the Limerick Syncline, *in:* Anderson, K., Ashton, J., Earls, G., Hitzman, M.W., and Tear, S., eds., Irish carbonate hosted Zn-Pb deposits: *Society of Economic Geologists Guidebook series* **21**, 75-79.

STROGEN, P., and SOMERVILLE, I.D., 1984. The stratigraphy of Upper Palaeozoic rocks in the Lyons Hill area, Co. Kildare. *Irish Journal of Earth Sciences,* **6**, 155-173.

STROGEN, P., and JONES, G.Ll., 1990. Stratigraphy and sedimentology of Lower Carboniferous (Dinantian) boreholes from west Co. Meath, Ireland. *Geological Journal,* **25**, 103-137.

SVERJENSKY, D.A., 1981. The origin of a Mississippi Valley-type deposit in the Vibernum Trend, southeast Missouri lead district. *Econ. Geol.* **76**, 1848-1872.

SVERJENSKY, D.A., 1984. Oil field brines as ore-forming solutions. *Econ. Geol.* **79**, 23-37.

SVERJENSKY, D.A., 1987. The role of migrating oil field brines in the formation of sediment-hosted Cu-rich deposits. *Econ. Geol.* **82**, 1130-1141.

SWART, P.K., BURNS, S.J., LEDER, J.J., 1991. Fractionation of the stable isotopes of oxygen and carbon in carbon dioxide during the reaction of calcite with phosphoric acid as a function of temperature and technique. *Chem. Geol.* **86,** 89-96.

SYMONS, D.T.A., 1995. Summary of paleomagnetic dating studies of Mississippi valley-type deposits, *in:* Extended Abstracts, International Field Conference on Carbonate Hosted Lead Zinc Deposits, St Louis Missouri, *Society of Economic Geologists,* p.308-310.

TAYLOR, S., 1984. Structural and paleotopographic controls of the lead-zinc mineralistation in the Silvermines orebodies, Republic of Ireland. *Econ.Geol.* **79**, 529-548.

TAYLOR, S., and ANDREW, C.J., 1978. Silvermines orebodies, Co. Tipperary, Ireland. *Trans. Inst. Mining Metallurgy* **87**, sec. B, 111-124.

TAYLOR, M., KESLER, S.E., CLOKE, P.L., KELLY, W.C., 1983. Fluid inclusion evidence for fluid mixing, Mascot-Jefferson City zinc District, Tennessee. *Econ. Geol.* **78**, 1425-1439.

TEN HAVE, T., and HEIJNEN, W., 1985. Cathodoluminescence activation and zonation in carbonate rocks: an experimental appraoch. *Geologie en Mijnbouw,* **64**, 297-310.

THOMPKINS, L.A., PEDONE, V.A., ROCHIE, M.T., and GROVES, D.I., 1994. The Cadjebut deposit as an example of Mississippi Vally-Type mineralization on the Lennard Shelf, Western Australia - single episode or multiple events? *Econ. Geol.* **89**, 450-466.

TIETZSCH-TYLER, D., and PHILLIPS, E., 1989. Correlation of the Monian Supergroup in NW Anglesey with the Cahore Group in SE Ireland. *J.Geol. Soc. London,* **146**, 417-418.

TRUDINGER, P.A., 1992. Bacterial sulfate reduction: current status and possible origin, *in:* Schidlowski, M., Golubic, S., Kimberley, M.M, McKirdy, D.M., Trudinger, P.A., eds., Early Organic Evolution: Implications for Mineral and Energy Resources, *Springer-Verlag,* Berlin, p.367-377.

TUCKER, M.E., 1988. Sedimentary Petrology. *Blackwell Scientific Publications,* Oxford.

TUCKER, M.E., and WRIGHT, V.P., 1990. Carbonate Sedimentology, Blackwell Scientific Publications, London. p.355.

VAIL, P.R. MITCHUM, R.M., TODD, R.G., WIDMIER, J.M., THOMPSON, S., SANGREE, J.B., BUBB, J.N., and HATLELID,W.G., 1977. Seismic stratigraphy and global changes of sea level, *in:* Payton, C.E., ed., Seismic stratigraphy application to hydrocarbon exploration. *AAPG Mem.*,**26**, Tulsa, UK, 49-212.

VAN BREEMEN, O., HALLIDAY, A.N., JOHNSON, M.R.W., BOWES, D. R., 1978. Crustal additions in Late Precambrian times, *in:* Bowes, D.R., and Leake, B.E., eds., Crustal evolution in northwestern Britain and adjacent regions. *Geol. J. Spec. Issue* **10**, 81-102.

VAN LUNSEN, H.A., and MAX, M.D., 1975. The Geology of Howth and Ireland's Eye, Co. Dublin. *Geological Journal,* **10**, 35-58.

VEIZER, J., 1983. Chemical diagenesis of carbonates: theory and application of trace element technique *in:* Arthur, M.A., et al., eds., Stable Isotopes in sedimentary geology. *SEPM Short Course,* **10**, 1-100.

VIETS, J.G., MOSIER,E.L., and ERICKSON, M.S., 1983. Geochemical variation of major, minor, and trace elements in samples of the Bonneterre Formation from drill holes transecting the Vibernum Trend Pb-Zn district of southeast Missouri, *in:* Kisvarsanyi et al., eds., Proceedings of the International Conference on Mississippi Valley-type Deposits, *Rolla, University of Missouri,* p.174-186.

VOSS, R.L., and HAGNI, R.D., 1985. The application of cathodoluminescence microscopy to the study of sparry dolomite from the Vibernum Trend, southeast Missouri, *in:* Hausen, D.M., and Kopp, O.C., eds., Process Mineralogy V, Mineralogy - Applications to the minerals industry*: New York, American Inst. Mining Metallurgical and Petroleum Engineers,* p.51-68.

VOSS, R.L., HAGNI, R.D., and GREGG, J.M., 1989. Sequential deposition of zoned dolomite and its relationship to sulfide mineral paragenetic sequence in the Vibernum Trend, southeast Missouri: *Carbonates and Evaporites*, **4**, 195-209.

WALKER, R.N., GULSON, B., and SMITH, J., 1983. The Coxco deposit - a Proterozoic Mississippi Valley-type deposit in the McArthur River District, Northern Territory, Australia. *Econ.Geol.* **78**, 214-249.

WALLACE, M.W., BOTH, R.A., RUANO, S.M., HACH-ALI, P.F., and LEES, T., 1994, Zebra textures from carbonate-hosted sulphide deposits: sheet cavity networks produced by fracture and solution enlargement. *Econ. Geol.* **89**, 1183-1191.

WALSH, J.J., and WATTERSON, J., 1989. Displacement gradients on fault surfaces: *Journal of Structural Geology*, **11**, p.307-316.

WALTON, G., 1992, Rathdowney South Block, 1992. Renewal Report. P.L.S 3262, 2447, 2448, 2558, 2069. Unpublished Chevron Min. Corp. Ireland/Ivernia West plc report.

WATLING, R.J., 1972. Identification of trace mercury compounds in rocks as a guide to sulphide mineralization at Keel, Eire. *Trans. Inst. Mining Metallurgy* Sect. B, **81**, B47-B48.

WILLIAMS, C.E., and McARDLE, P., 1978. Ireland, *in:* Bowie, S.H.U., Kvalheim, A., and Haslam, H.W., eds., Mineral Deposits of Europe; Volume 1, Northwest Europe. *Institute of Mining and Metallurgy, and the Mineralogical Society,* London, p.319-345.

WILKINSON, J.J., and EARLS, G., in prep. A high temperature hydrothermal origin for black dolomite matrix breccias in the Irish Zn-Pb orefield.

WILLIAMS, B., and BROWN, C., 1986. A model for the genesis of Zn-Pb deposits in Ireland, *In:* Andrew, C. J., Crowe, R.W.A., Finlay, S., Pennell, W.M., and Pyne, J.F., eds., Geology and Genesis of Mineral Deposits in Ireland. *Irish Association for Economic Geology,* Dublin, p.579-590.

WILLIAMS, E.A., BAMFORD, M.F.L., COOPER, M.A., EDWARDS, H.E., FORD, M., GRANT, G.G., MAcCARTHY, I.A.J., McAFFEE, A.M., and O'SULLIVAN, M.J., 1989. Tectonic controls and sedimentary response in the Devonian-Carboniferous Munster and South Munster Basins, *in:* Arthurton, R.S., Gutteridge, P., and Nolan, S.C., eds., The Role of Tectonics in Devonian and Carboniferous sedimentation in the British Isles. *Occasional Publication, Yorkshire Geological Society,* No.**6**.

WILLIAMS. C.T., and SPRATT, J., 1995. Electron Microprobe Techniques in Mineral Analysis. *Journal of the Russell Society,* **6**(1), 5-12.

WINCHESTER, J.A., and MAX, M.D., 1982. The geochemistry and origins of the Precambrian rocks of the Rosslare Complex, S.E Ireland. *J. Geol. Soc. London,* **139**, 309-319.

WU, I., and PETERSEN, U., 1977. Geochemistry of tetrahedrite-tennantite at Casapalca, Peru. *Econ. Geol.* **72**, 993-1016.

YAKOBI, B.G., and HOLT, D.B., 1990. Cathodoluminescence Microscopy of Inorganic Solids. *Plenum Press*, London.

ZEEH, S., and KUHLEMANN, J., 1996. Luminescence and geochemical composition of sphalerite: an example from the alpine lead-zinc deposits (Austria/Slovenia), *in:* International Conference on Cathodoluminescence and Related Techniques in Geosciences and Geomaterials, Abstracts Volume, Nancy.

ZENGER, D.H., 1983. Burial dolomitization in the Lost Burrow Formation (Devonian), east central California, and the significance of late diagenetic dolomitization: *Geology,* **11**, 519-522.

ZENGER, D.H., and DUNHAM, J.B., 1988. Dolomitization of Siluro-Devonian Limestones in a deep core (5,350 m), Southeastern New Mexico, *in:* Sedimentology and Geochemistry of Dolostones, *SEPM* Special Publication No. **43**, 161-173. ISBN 0-918985-77-3.

ZIEGLER, P.A., 1982. Geological Atlas of Western and Central Europe, *Elsevier,* Amsterdam, pp.130.

ZIEGLER, P.A., 1984. Caledonian and Hercynian crustal consolidation of Western and Central Europe - a working hypothesis. *Geologie en Mijnbouw,* **63**, 93-108.

ZIEGLER, P.A. 1988. Evolution of the Arctic-North Atlantic and the western Tethys. *AAPG Mem.,* **43**, pp.198.

ZIEGLER, P.A., 1989. Evolution of Laurussia: A study in Late Palaeozoic Plate Tectonics. *Kluwer Academic Publishers,* Netherlands, pp.102.

ZINKERNAGEL, U., 1978. Cathodoluminescence of quartz and its application to sandstone petrology. *Contributions to Sedimentology,* **8**, E. Schweizerbartsche Verlagsbuchandlung, Stuttgart, Germany.

APPENDICES

APPENDIX A: SAMPLE PREPARATION TECHNIQUES

A1. PREPARATION OF POLISHED BLOCKS

Mounting, Lapping, Polishing

a.) A section approximately 10mm thick is cut from the core sample to fit a 25, 30 or 40mm polyethylene mould.
b.) A prepared epoxy resin (in general use now is the CIBA-GEIGY epoxy resin type NY 753 used with hardener type HY 951 in a 10:1 ratio, and Araldite AY 105 used with hardener HY 932 in a 100:27 ratio) is poured into the mould giving a resin thickness of at least 5mm above the section.
c.) The mounted section is lapped using a slurry of 800 grit, silicon carbide (carborundum) and water.
d.) The section is polished using an automatic polishing machine with 6 or 8" lap. The covered lap is moistened with polishing oil (1:7 ethane diol, distilled water mixture) and charged with approximately ¼ gram of diamond paste (Struers DP diamond pastes, 6-12, 1-5, 0-0.5μm).

A2. PREPARATION OF POLISHED THIN SECTIONS

Mounting, Lapping, Polishing

The procedure used to prepare polished thin sections is similar to that described in A1. However, the reader is referred to Laflamme (1990), Murphy (1986) and Humphries (1992) for further preparation techniques for polished thin sections.

a.) A thin section is finished to an approximate thickness of 50μm using an automatic lapping machine and 600 grit silicon carbide (carborundum) on a glass plate.
b.) A further stage of grinding with 1000 grit silicon carbide, producing a section approximately 35-40μm thick, will give the finer surface finish required before the polishing stage can commence.
c.) Polishing (seeA1, d.).

A3. PREPARATION OF FLUID INCLUSION WAFERS

Mounting, Lapping, Polishing

The procedure used to prepare doubly-polished wafers for thermometric analysis is similar to that described by Shepherd *et al.*, (1985), section 2.5, pp.26-33.

a.) A section is cut from the core sample and trimmed to fit a polyethylene mould (see A1, a.). A cold-setting, clear polyester casting resin encapsulates the section.
b.) Mounted section is removed from the mould and is lapped (see A1, c.)
c.) Lapped surface is polished using a polishing cloth and slurry of 0.3μm grade aluminium oxide powder, water is used as the polishing medium.
d.) Clean polished side is mounted on to a frosted glass slide using a cyanoacrylate bonding medium. The mounted section is trimmed on a diamond saw to 1-2mm thick.
e.) Unpolished side of section is lapped to within 100-200μm of the finished thickness
f.) Second surface of wafer is polished (see A3, c).
g.) Wafer is removed from the glass slide by soaking in acetone for several hours.

A4. STAINING - DICKSON'S METHOD

Reagents

a.) Etching solution - 15ml of 36% HCl dissolved in 500ml distilled water, then topped up to 1000ml with distilled water.
b.) Staining solution part 1 - 0.2g Alizarin red S dissolved in 100ml 1.5% HCl solution.
c.) Staining solution part 2 - 2.0g potassium ferricyanide crystals dissolved in 100ml 1.5% HCl solution.
d.) Mix staining solutions parts 1 and 2 in the ratio 3 of dye to 2 ferricyanide.

Procedure

a.) Immerse thin section (grease free surface) or faced sample in etching solution, for approximately 10-15 seconds at 20°C - for optimum etch (times are approximate, and may vary with grain size, etc).
b.) Immerse specimen in the combined solution for 30-45 seconds. For thin sections, best results are obtained if the stain is warmed.
c.) Wash the specimens gently in two changes of distilled water, for only a few seconds - stains are relatively soluble.
d.) Dry the specimen surface quickly in a stream of warm air (Nb. the stain is a thin surface film and is easily damaged).

Results

Carbonate	**Stain**
Calcite	Varying through very pale pink to red.
Ferroan calcite	Varying through mauve, purple to royal blue with increasing Fe content.
Dolomite	No colour.
Ferroan Dolomite	Pale to deep turquoise with increasing Fe

APPENDIX B: ELECTRON MICROPROBE ANALYSIS - DATA

B1. DETECTION LIMITS - CARBONATES

Operating Parameters: 15kV, 15µA, 15µm

Declare file name	Carbonate												
Beam voltage kV	15												
Beam current (nA)	15												
Beam diameter (µm)	15												
Background (C/S)	Analysis Number	Na	Mg	Si	P	S	K	Ca	Mn	Fe	Sr	Ba	Ce
	#1	5	24.4	18.8	1.3	1.2	5.6	15.2	2.7	3.7	22.3	13.4	14.7
	#2	4.8	17.8	16.4	0.7	1.4	5.2	15.6	1.4	3.1	20.9	11.8	16
	#3	4.2	20.4	17.2	1.8	1.7	5.9	14.2	2.4	2.3	24	12.6	14.5
	#4	4.4	24	20	1.3	1.5	4.8	16.4	2.5	3.5	21.7	10.9	16.9
	#5	3.8	20	17.8	1.7	2.1	6.1	14.6	2.9	3.3	20.5	13.2	15.9
	#6	4.2	21.2	19.6	2.3	1.7	5.5	16	2.6	3.5	23.2	11.9	18.5
	#7	4.8	26.6	15.2	1.2	1.6	5.9	17.8	2.4	3.9	18.9	14.7	16.9
	#8	3.8	23.4	16	1.3	2.1	6	16	2.6	3.8	23.5	14.5	13.9
	#9	4	24.2	20.8	1.2	1.8	4.8	16.2	2.5	2.7	21.9	13.2	16.8
	#10	6.4	22	18.2	1.8	2.6	6.8	16.2	3.3	3.7	20.4	13.5	16.7
	#11	5.2	26.6	20.4	1.2	2.7	5.1	16.6	3	2.7	20.5	14.6	16.9
	#12	6.2	24	21.4	1.6	1	5.8	15.4	2.5	3.8	23.8	11.9	15.1
	#13	5	19.8	18.6	0.9	0.9	5.4	15.6	2.6	3.2	21.1	14	16
	#14	5.6	24.6	19.8	1.2	1.8	5.2	11.8	2.3	3.2	19.8	12.2	16
	#15	5.8	26.4	20.2	2	1.3	5.8	19.4	3	2.8	18.3	11.4	16.9
	Bk C/S/nA												
		Na	Mg	Si	P	S	K	Ca	Mn	Fe	Sr	Ba	Ce
	#1	0.3	1.6	1.3	0.1	0.1	0.4	1.0	0.2	0.2	1.5	0.9	1.0
	#2	0.3	1.2	1.1	0.0	0.1	0.3	1.0	0.1	0.2	1.4	0.8	1.1
	#3	0.3	1.4	1.1	0.1	0.1	0.4	0.9	0.2	0.2	1.6	0.8	1.0
	#4	0.3	1.6	1.3	0.1	0.1	0.3	1.1	0.2	0.2	1.4	0.7	1.1
	#5	0.3	1.3	1.2	0.1	0.1	0.4	1.0	0.2	0.2	1.4	0.9	1.1
	#6	0.3	1.4	1.3	0.2	0.1	0.4	1.1	0.2	0.2	1.5	0.8	1.2
	#7	0.3	1.8	1.0	0.1	0.1	0.4	1.2	0.2	0.3	1.3	1.0	1.1
	#8	0.3	1.6	1.1	0.1	0.1	0.4	1.1	0.2	0.3	1.6	1.0	0.9
	#9	0.3	1.6	1.4	0.1	0.1	0.3	1.1	0.2	0.2	1.5	0.9	1.1
	#10	0.4	1.5	1.2	0.1	0.2	0.5	1.1	0.2	0.2	1.4	0.9	1.1
	#11	0.3	1.8	1.4	0.1	0.2	0.3	1.1	0.2	0.2	1.4	1.0	1.1
	#12	0.4	1.6	1.4	0.1	0.1	0.4	1.0	0.2	0.3	1.6	0.8	1.0
	#13	0.3	1.3	1.2	0.1	0.1	0.4	1.0	0.2	0.2	1.4	0.9	1.1
	#14	0.4	1.6	1.3	0.1	0.1	0.3	0.8	0.2	0.2	1.3	0.8	1.1
	#15	0.4	1.8	1.3	0.1	0.1	0.4	1.3	0.2	0.2	1.2	0.8	1.1
	STDEV	0.1	0.2	0.1	0.0	0.0	0.0	0.1	0.0	0.0	0.1	0.1	0.1
	3*STDEV	0.2	0.5	0.4	0.1	0.1	0.1	0.3	0.1	0.1	0.3	0.2	0.2
	Std.% of element	11.3	60.3	27.8	18.3	17.5	32.9	40.0	100.0	14.6	47.7	78.3	16.8
	C/S/nA on Std.	74.8	842.6	421.5	51.4	44.5	196.6	307.1	228.3	29.3	315.4	292.4	50.9
	C/S/nA/100% Std.	662.8	1396.8	1516.7	280.7	254.7	598.4	766.9	228.3	200.2	661.2	373.2	302.5
	Det. Limit (3s) Wt%	0.03	0.04	0.02	0.03	0.04	0.02	0.04	0.04	0.05	0.05	0.07	0.08
	Det. Limit (3s) Wt% Oxide	0.04	0.07	0.04	0.07	0.08	0.02	0.06	0.05	0.06	0.06	0.08	0.09
	Det. Limit (3s) Mole%	0.07	0.14	0.11	0.18	0.19	0.04	0.1	0.08	0.1	0.08	0.1	0.13

Operating Parameters: 15kV, 15µA, 25µm

Declare file name	Carbonate												
Beam voltage (kV)	15												
Beam current (nA)	15												
Beam diameter (µm)	25												
Background (C/S)	Analysis Number	Na	Mg	P	S	K	Ca	Mn	Fe	Sr	Cd	Ba	Ce
	#1	4.4	30.62	1.6	2.6	5.8	16.2	2.7	4.5	1.47	4.4	10.4	15.67
	#2	3	29.02	1.8	1.2	6.4	12.6	2.3	2.9	1.13	5.33	10.07	15.07
	#3	6	31.22	1.2	1.4	6.8	13.6	2.6	3.6	1.53	4	9.93	16.6
	#4	5.4	33.22	2.6	1.6	6.2	11.8	3.5	1.9	1.53	3.67	10.2	16.33
	#5	3.8	31.22	1.6	1	7.6	13.8	2.1	4.1	1.13	5.4	9.2	16.27
	Bk C/S/nA												
		Na	Mg	P	S	K	Ca	Mn	Fe	Sr	Cd	Ba	Ce
	#1	0.3	2.0	0.1	0.2	0.4	1.1	0.2	0.3	0.1	0.3	0.7	1.0
	#2	0.2	1.9	0.1	0.1	0.4	0.8	0.2	0.2	0.1	0.4	0.7	1.0
	#3	0.4	2.1	0.1	0.1	0.5	0.9	0.2	0.2	0.1	0.3	0.7	1.1
	#4	0.4	2.2	0.2	0.1	0.4	0.8	0.2	0.1	0.1	0.2	0.7	1.1
	#5	0.3	2.1	0.1	0.1	0.5	0.9	0.1	0.3	0.1	0.4	0.6	1.1
	STDEV	0.1	0.1	0.0	0.0	0.0	0.1	0.0	0.1	0.0	0.1	0.0	0.0
	3*STDEV	0.2	0.3	0.1	0.1	0.1	0.3	0.1	0.2	0.0	0.2	0.1	0.1
	Std.% of element	11.28	60.32	18.32	17.45	32.86	40.04	100	100	47.7	77.8	78.33	16.83
	C/S/nA on Std.	76.351	849.281	51.391	54.972	248.186	228.916	226.152	231.443	50.622	151.584	196.026	50.794
	C/S/nA on Std.	676.87057	1407.9592	280.51856	315.02579	755.28302	571.71828	226.152	231.443	106.12579	194.83805	250.25661	301.8063
	Det. Limit (3s) Wt%	0.04	0.02	0.04	0.04	0.02	0.06	0.05	0.09	0.04	0.08	0.04	0.04
	Det. Limit (3s) Wt% Oxide	0.05	0.03	0.09	0.08	0.02	0.08	0.06	0.11	0.05	0.09	0.04	0.05
	Det. Limit (3s) Mole%	0.09	0.07	0.23	0.19	0.04	0.15	0.1	0.19	0.07	0.12	0.06	0.07

Operating Parameters: 15kV, 15µA, 30µm

Declare file name	Carbonate												
Beam voltage (kV)	15												
Beam current (nA)	15												
Beam diameter (µm)	30												
Background (C/S)	Analysis Number	Na	Mg	Al	Si	P	S	K	Mn	Fe	Sr	Ba	Ce
	#1	5.8	11.9	16	21.3	1.1	2.7	7.7	3.1	3.1	24.1	14.8	17.8
	#2	5.9	11.6	16	23.7	1.9	2.3	7.8	3	4.8	25.6	13.9	16
	#3	5.9	11.7	14.9	21.7	1.7	1.9	7.9	2.2	4.5	25.2	16	18.4
	#4	6.4	12.2	17.9	23.1	2.2	2.7	5.6	2.4	4.3	23.4	16.3	18.1
	#5	4.9	10.7	16.2	24	1.4	2.1	8.4	3.1	5	21.3	13.8	18.3
	#6	5.7	10.3	16.2	21.1	2	1.2	6.7	3	5.4	21.3	14.8	18.6
	#7	5.1	13	13.8	21.8	1.3	1.8	7.4	2.9	5	23.7	13.6	15.7
	#8	4.9	9.5	14.4	21.3	1.6	1.7	8	2.7	4	26.1	15.1	16.5
	#9	4.9	10.7	15.7	22.5	1.7	1.1	7.9	3.2	4.1	21.8	14.8	20.7
	#10	5.7	12.9	14.8	19.9	1.8	2.9	7.1	2.7	4.3	24.3	13.7	18.7
	Bk C/S/nA												
		Na	Mg	Al	Si	P	S	K	Mn	Fe	Sr	Ba	Ce
	#1	0.4	0.8	1.1	1.4	0.1	0.2	0.5	0.2	0.2	1.6	1.0	1.2
	#2	0.4	0.8	1.1	1.6	0.1	0.2	0.5	0.2	0.3	1.7	0.9	1.1
	#3	0.4	0.8	1.0	1.4	0.1	0.1	0.5	0.1	0.3	1.7	1.1	1.2
	#4	0.4	0.8	1.2	1.5	0.1	0.2	0.4	0.2	0.3	1.6	1.1	1.2
	#5	0.3	0.7	1.1	1.6	0.1	0.1	0.6	0.2	0.3	1.4	0.9	1.2
	#6	0.4	0.7	1.1	1.4	0.1	0.1	0.4	0.2	0.4	1.4	1.0	1.2
	#7	0.3	0.9	0.9	1.5	0.1	0.1	0.5	0.2	0.3	1.6	0.9	1.0
	#8	0.3	0.6	1.0	1.4	0.1	0.1	0.5	0.2	0.3	1.7	1.0	1.1
	#9	0.3	0.7	1.0	1.5	0.1	0.1	0.5	0.2	0.3	1.5	1.0	1.4
	#10	0.4	0.9	1.0	1.3	0.1	0.2	0.5	0.2	0.3	1.6	0.9	1.2
	STDEV	0.0	0.1	0.1	0.1	0.0	0.0	0.1	0.0	0.0	0.1	0.1	0.1
	3*STDEV	0.1	0.2	0.2	0.3	0.1	0.1	0.2	0.1	0.1	0.3	0.2	0.3
	Std.% of element	11.3	60.3	52.9	23.8	18.3	17.5	32.9	100.0	100.0	47.7	78.3	16.8
	C/S/nA on Std.	77.1	853.9	959.1	421.6	51.4	45.1	247.0	226.3	235.8	29.6	288.8	31.7
	C/S/nA/100% Std.	683.7	1415.6	1812.4	1771.4	280.6	258.5	751.7	226.3	235.8	62.1	368.7	188.5
	Det. Limit (3s) Wt%	0.02	0.02	0.01	0.01	0.02	0.05	0.02	0.03	0.06	0.56	0.05	0.16
	Det. Limit (3s) Wt% Oxide	0.03	0.03	0.02	0.02	0.05	0.1	0.02	0.04	0.08	0.66	0.06	0.19
	Det. Limit (3s) Mole%	0.05	0.07	0.05	0.05	0.12	0.24	0.04	0.06	0.12	0.94	0.07	0.26

B2. DETECTION LIMITS - SULPHIDES

Operating Parameters: 20kV, 20nA, 1-2µm (Sphalerite)

Declare file name	Sphalerite - Salz											
Beam voltage (kV)	20											
Beam current (nA)	20											
Beam diameter (µm)	1											
Background (C/S)	Analysis Number	S	Mn	Fe	Cu	Zn	Ga	Ge	As	Ag	Cd	In
	#1	12.6	12.8	18.4	30.5	51.8	22	19.1	18	9	15.3	24.4
	#2	17.2	15	18.3	31.5	50.6	22.9	17.2	17.7	8.6	17.9	23
	#3	13.2	17.5	19.6	30.2	52	23	17.2	18.3	8.7	15.7	25.5
	#4	12.4	11.9	18.3	31.4	50.4	23.2	19.2	17.8	8.7	14.8	24.5
	#5	12.2	13.8	21.6	32.7	44.4	24.9	18.4	15.7	10.7	18.3	24.6
	#6	14.8	12.7	18.6	31.4	48.4	22.8	18.4	18.2	7.2	16.4	23.9
	#7	19.4	13.2	21.7	32.8	48.6	23.2	22.4	18.2	10	16.7	23.5
	#8	16.8	13.3	21.7	31.6	49.4	26.4	17.3	14.1	9.9	16.8	22.8
	#9	14.4	13.2	21.3	34.1	50	23.1	16	17	9	20.7	21.6
	#10	13.2	13.8	18.6	27.9	43.4	23.8	19	16.8	10.3	17.8	22.5
	#11	13.6	16	19.5	32	53.8	22.6	16.9	16.7	10.2	14.8	22.9
	#12	13	12.5	18.6	33.3	52.6	24	17	20.1	11	15	21.6
	Bk C/S/nA											
		S	Mn	Fe	Cu	Zn	Ga	Ge	As	Ag	Cd	In
	#1	0.6	0.6	0.9	1.5	2.6	1.1	1.0	0.9	0.5	0.8	1.2
	#2	0.9	0.8	0.9	1.6	2.5	1.1	0.9	0.9	0.4	0.9	1.2
	#3	0.7	0.9	1.0	1.5	2.6	1.2	0.9	0.9	0.4	0.8	1.3
	#4	0.6	0.6	0.9	1.6	2.5	1.2	1.0	0.9	0.4	0.7	1.2
	#5	0.6	0.7	1.1	1.6	2.2	1.2	0.9	0.8	0.5	0.9	1.2
	#6	0.7	0.6	0.9	1.6	2.4	1.1	0.9	0.9	0.4	0.8	1.2
	#7	1.0	0.7	1.1	1.6	2.4	1.2	1.1	0.9	0.5	0.8	1.2
	#8	0.8	0.7	1.1	1.6	2.5	1.3	0.9	0.7	0.5	0.8	1.1
	#9	0.7	0.7	1.1	1.7	2.5	1.2	0.8	0.9	0.5	1.0	1.1
	#10	0.7	0.7	0.9	1.4	2.2	1.2	1.0	0.8	0.5	0.9	1.1
	#11	0.7	0.8	1.0	1.6	2.7	1.1	0.8	0.8	0.5	0.7	1.1
	#12	0.7	0.6	0.9	1.7	2.6	1.2	0.9	1.0	0.6	0.8	1.1
	STDEV	0.1	0.1	0.1	0.1	0.2	0.1	0.1	0.1	0.1	0.1	0.1
	3*STDEV	0.3	0.2	0.2	0.2	0.5	0.2	0.3	0.2	0.2	0.3	0.2
	Std.% of element	38.51	100.00	61.49	100.00	67.09	48.20	100.00	51.80	100.00	77.80	49.22
	C/S/nA on Std.	169.98	473.58	300.21	484.53	264.23	252.07	642.52	184.61	167.87	229.89	227.74
	C/S/nA/100% Std.	441.38	473.58	488.23	484.53	393.84	522.97	642.52	356.39	167.87	295.49	462.70
	Det. Limit (3s) Wt%	0.08	0.05	0.04	0.05	0.12	0.03	0.04	0.06	0.10	0.09	0.04

Operating Parameters: 20kV, 20nA, 1-2μm (Galena)

Declare file name	Galena - Salg						
Beam voltage (kV)	20						
Beam current (nA)	20						
Beam diameter (μm)	1						
Background (C/S)	Analysis Number	S	Mn	Ag	Cd	Pb	Bi
	#1	15.2	26.3	16.3	18.6	64.4	36.5
	#2	15.8	25.8	13.9	16.9	56.2	38.3
	#3	18.6	27	13.9	17.8	60.6	36.8
	#4	20.6	25.5	14.5	18.1	59.8	36.1
	#5	15.6	27.4	13.6	17.2	58.8	34.5
	#6	17.8	23.6	11.3	16.1	63.2	37.2
	#7	17.6	25.4	14.1	15.2	61.6	34.3
	#8	20.2	25.6	13.1	18.1	62	34.2
	#9	17.6	25.7	12.3	17.3	63.6	37.8
	#10	16.8	30	13.8	15.8	57.2	37.5
	Bk C/S/nA						
		S	Mn	Ag	Cd	Pb	Bi
	#1	0.8	1.3	0.8	0.9	3.2	1.8
	#2	0.8	1.3	0.7	0.8	2.8	1.9
	#3	0.9	1.4	0.7	0.9	3.0	1.8
	#4	1.0	1.3	0.7	0.9	3.0	1.8
	#5	0.8	1.4	0.7	0.9	2.9	1.7
	#6	0.9	1.2	0.6	0.8	3.2	1.9
	#7	0.9	1.3	0.7	0.8	3.1	1.7
	#8	1.0	1.3	0.7	0.9	3.1	1.7
	#9	0.9	1.3	0.6	0.9	3.2	1.9
	#10	0.8	1.5	0.7	0.8	2.9	1.9
	STDEV	0.1	0.1	0.1	0.1	0.1	0.1
	3*STDEV	0.3	0.3	0.2	0.2	0.4	0.2
	Std.% of element	13.40	100.00	100.00	77.81	86.60	100.00
	C/S/nA on Std.	70.07	471.10	167.28	111.72	100.96	134.28
	C/S/nA/100% Std.	522.93	471.10	167.28	143.58	116.58	134.28
	Det. Limit (3s) Wt%	0.05	0.05	0.12	0.12	0.35	0.17

Operating Parameters: 20kV, 20nA, 1-2µm (Tennantite)

Declare file name	Tennantite - Salt									
Beam voltage (kV)	20									
Beam current (nA)	20									
Beam diameter (µm)	1									
Background (C/S)	Analysis Number	S	Fe	Cu	As	Ag	Sb	Te	Hg	Pb
	#1	13.4	19.3	46.6	21.4	16.9	34.4	38.1	8.3	44.4
	#2	13	19.7	43.8	24	17.6	36.5	37.4	6.8	46.7
	#3	13.4	21.8	46.5	23.8	16.8	33.4	38.5	7	49.5
	#4	12	20.5	47.8	24	17.4	37.4	35.1	7.6	45
	#5	12	19.9	46.4	25.2	17.9	36.8	37.3	7.7	46.5
	#6	17	21.2	42.7	26.6	16.5	37.9	39.4	7.8	47.1
	#7	12.8	22.3	48.6	27.8	17.2	37.4	35.2	7.5	49.7
	#8	15	19.3	48.7	22.8	18.1	38.8	35.5	6.6	47.6
	#9	12.4	19.3	50.3	20.2	16	36.5	38.4	8	53.6
	#10	12.8	19.2	45	24.2	16.6	37.1	35.9	6.5	52.3
	#11	16.4	20.5	44.7	23.4	18.5	37	36.4	7.3	45.9
	#12	13.8	18.4	46.4	22.8	17.1	37.9	36.5	7.2	44.7
	Bk C/S/nA									
		S	Fe	Cu	As	Ag	Sb	Te	Hg	Pb
	#1	0.7	1.0	2.3	1.1	0.8	1.7	1.9	0.4	2.2
	#2	0.7	1.0	2.2	1.2	0.9	1.8	1.9	0.3	2.3
	#3	0.7	1.1	2.3	1.2	0.8	1.7	1.9	0.4	2.5
	#4	0.6	1.0	2.4	1.2	0.9	1.9	1.8	0.4	2.3
	#5	0.6	1.0	2.3	1.3	0.9	1.8	1.9	0.4	2.3
	#6	0.9	1.1	2.1	1.3	0.8	1.9	2.0	0.4	2.4
	#7	0.6	1.1	2.4	1.4	0.9	1.9	1.8	0.4	2.5
	#8	0.8	1.0	2.4	1.1	0.9	1.9	1.8	0.3	2.4
	#9	0.6	1.0	2.5	1.0	0.8	1.8	1.9	0.4	2.7
	#10	0.6	1.0	2.3	1.2	0.8	1.9	1.8	0.3	2.6
	#11	0.8	1.0	2.2	1.2	0.9	1.9	1.8	0.4	2.3
	#12	0.7	0.9	2.3	1.1	0.9	1.9	1.8	0.4	2.2
	STDEV	0.1	0.1	0.1	0.1	0.0	0.1	0.1	0.0	0.1
	3*STDEV	0.2	0.2	0.3	0.3	0.1	0.2	0.2	0.1	0.4
	Std.% of element	38.51	61.49	100.00	51.80	100.00	100.00	38.88	61.12	86.60
	C/S/nA on Std.	169.98	300.21	484.53	184.61	329.08	399.87	130.54	51.20	83.93
	C/S/nA/100% Std.	441.38	488.23	484.53	356.39	329.08	399.87	335.76	83.78	96.92
	Det. Limit (3s) Wt%	0.06	0.04	0.07	0.09	0.03	0.06	0.06	0.10	0.46

Operating Parameters: 20kV, 20nA, 1-2µm (Pyrite)

Declare file name	Pyrite - Sals								
Beam voltage (kV)	20								
Beam current (nA)	20								
Beam diameter (µm)	1								
Background (C/S)	Analysis Number	S	Mn	Fe	Co	Ni	Cu	As	Cd
	#1	23	13.3	25.4	21.6	22.5	25.9	20.8	13.1
	#2	20.2	12.2	31.4	22.6	21.7	24.6	20.1	12.9
	#3	23.4	11.2	28	22.8	21.7	22.7	19.2	16.5
	#4	21.4	12	33.8	22.2	20.2	23.5	20.1	13.7
	#5	16.6	12.6	33.2	18.3	22.1	26.5	22.7	13
	#6	25.2	11	31	20.2	20.6	25.4	21.1	14.2
	#7	23.2	12.5	25.8	23	21.8	25.7	21.2	12.8
	#8	21.2	13.5	27.2	19.8	20.6	24.6	18.2	12.6
	#9	23.8	11.7	29.8	18.5	21.9	27.2	18.6	15.5
	#10	25	11.5	27.8	20.8	19	26.5	20.4	13.9
	Bk C/S/nA								
		S	Mn	Fe	Co	Ni	Cu	As	Cd
	#1	1.2	0.7	1.3	1.1	1.1	1.3	1.0	0.7
	#2	1.0	0.6	1.6	1.1	1.1	1.2	1.0	0.6
	#3	1.2	0.6	1.4	1.1	1.1	1.1	1.0	0.8
	#4	1.1	0.6	1.7	1.1	1.0	1.2	1.0	0.7
	#5	0.8	0.6	1.7	0.9	1.1	1.3	1.1	0.7
	#6	1.3	0.6	1.6	1.0	1.0	1.3	1.1	0.7
	#7	1.2	0.6	1.3	1.2	1.1	1.3	1.1	0.6
	#8	1.1	0.7	1.4	1.0	1.0	1.2	0.9	0.6
	#9	1.2	0.6	1.5	0.9	1.1	1.4	0.9	0.8
	#10	1.3	0.6	1.4	1.0	1.0	1.3	1.0	0.7
	STDEV	0.1	0.0	0.1	0.1	0.1	0.1	0.1	0.1
	3*STDEV	0.4	0.1	0.4	0.3	0.2	0.2	0.2	0.2
	Std.% of element	38.51	100.00	61.49	100.00	100.00	100.00	51.80	77.81
	C/S/nA on Std.	169.98	473.58	300.21	551.85	531.84	484.53	184.61	229.89
	C/S/nA/100% Std.	441.38	473.58	488.23	551.85	531.84	484.53	356.39	295.45
	Det. Limit (3s) Wt%	0.09	0.03	0.09	0.05	0.03	0.04	0.06	0.06

Operating Parameters: 15kV, 20nA, 1-2µm (All Sulphides)

Declare file name	Sulphides															
Beam voltage (kV)	15															
Beam current (nA)	20															
Beam diameter (µm)	1															
Background (C/S)	Analysis Number	S	Mn	Fe	Co	Ni	Cu	Zn	Ga	Ge	As	Ag	Te	Sb	Hg	
	#1	13.8	8.8	15	13.4	17	13.6	23.4	17.1	13.9	14.3	9	19	18.6	5.8	
	#2	12.9	8.4	19	13.3	13.2	14.4	20.4	20.3	15.9	16.2	8.6	19.7	19.2	4.9	
	#3	12.1	7.3	23.6	10.3	17.4	16.8	25.2	20.3	15	15.7	4.8	19.9	16.8	4.5	
	#4	11.8	6.9	21.4	12.9	16.2	17	30.2	20.3	14.6	16.1	7.4	21.1	18.8	5.6	
	#5	11.5	7.8	19.2	13.9	18.8	17.6	26.2	19	15.6	17.8	5.4	19.6	17.4	3.8	
	#6	12.4	10.1	17.4	12.8	16.2	17	29.4	19.4	15.7	15.7	5.2	20.8	16.6	4.9	
	#7	13.3	8.7	18.8	13.4	15.8	14.4	26.2	21.2	13.8	15	3.8	20.3	15.4	5.2	
	#8	12.5	10.1	18.8	11.6	16.4	17.6	21.8	17.5	15.2	15.9	4.8	18.6	19.4	3.4	
	#9	12.2	8.8	20.6	14.6	17.6	19.4	24	20.3	16.4	18.6	5.4	20.1	18.4	3.9	
	#10	10.1	9.8	17.8	11.3	17	16.6	22.6	18.9	15.9	15.5	8	20.2	19.2	5.8	
	Bk C/S/nA															
		S	Mn	Fe	Co	Ni	Cu	Zn	Ga	Ge	As	Ag	Te	Sb	Hg	
	#1	0.7	0.4	0.8	0.7	0.9	0.7	1.2	0.9	0.7	0.7	0.5	1.0	0.9	0.3	
	#2	0.6	0.4	1.0	0.7	0.7	0.7	1.0	1.0	0.8	0.8	0.4	1.0	1.0	0.2	
	#3	0.6	0.4	1.2	0.5	0.9	0.8	1.3	1.0	0.8	0.8	0.2	1.0	0.8	0.2	
	#4	0.6	0.3	1.1	0.6	0.8	0.9	1.5	1.0	0.7	0.8	0.4	1.1	0.9	0.3	
	#5	0.6	0.4	1.0	0.7	0.9	0.9	1.3	1.0	0.8	0.9	0.3	1.0	0.9	0.2	
	#6	0.6	0.5	0.9	0.6	0.8	0.9	1.5	1.0	0.8	0.8	0.3	1.0	0.8	0.2	
	#7	0.7	0.4	0.9	0.7	0.8	0.7	1.3	1.1	0.7	0.8	0.2	1.0	0.8	0.3	
	#8	0.6	0.5	0.9	0.6	0.8	0.9	1.1	0.9	0.8	0.8	0.2	0.9	1.0	0.2	
	#9	0.6	0.4	1.0	0.7	0.9	1.0	1.2	1.0	0.8	0.9	0.3	1.0	0.9	0.2	
	#10	0.5	0.5	0.9	0.6	0.9	0.8	1.1	0.9	0.8	0.8	0.4	1.0	1.0	0.3	
	STDEV	0.1	0.1	0.1	0.1	0.1	0.1	0.2	0.1	0.0	0.1	0.1	0.0	0.1	0.0	
	3*STDEV	0.2	0.2	0.4	0.2	0.2	0.3	0.5	0.2	0.1	0.2	0.3	0.1	0.2	0.1	
	Std.% of element	38.51	100	100	100	100	100	100	48.2	100	51.8	100	38.88	100	61.12	
	C/S/nA/ on Std.	145.554	230.11	242.638	225.95	197.693	163.541	126.914	222.989	526.173	190.408	113.26	87.821	253.155	40.165	
	C/S/nA/ 100% Std.	377.96417	230.11	242.638	225.95	197.693	163.541	126.914	462.63278	526.173	367.58301	113.26	225.87706	253.155	65.714987	
	Det. limit (3s) Wt%	0.04	0.07	0.14	0.09	0.11	0.16	0.37	0.04	0.02	0.05	0.24	0.05	0.08	0.20	

B3. ELEMENTAL CHEMISTRY - LISHEEN CARBONATES

Regional Replacement Dolomites and Carbonate Cements

Element Wt% Oxide. Lisheen Carbonates, November 1995. Operating Parameters: 15kV, 15nA, 25µm.									
Pts. 1-40, D1Cem, 2447-8/13.3.									
	CaO	MgO	FeO	SrO	MnO	BaO	Ce2O3	CO2	TOTAL
#4	30.75	20.07	0.36	0.05	0.07	0.10	0.02	46.36	97.77
#10	30.29	20.45	0.44	0.03	0.07	0.00	0.00	46.42	97.70
#11	30.21	20.17	0.45	0.00	0.00	0.05	0.13	46.06	97.06
#14	30.48	20.31	0.29	0.04	0.02	0.00	0.24	46.40	97.78
#15	30.51	20.61	0.32	0.00	0.00	0.00	0.06	46.66	98.17
#16	30.77	20.52	0.15	0.02	0.00	0.00	0.00	46.64	98.10
#17	31.05	19.84	0.30	0.08	0.01	0.00	0.03	46.26	97.57
#18	30.89	20.62	0.20	0.01	0.02	0.12	0.00	46.93	98.79
#19	31.42	20.41	0.24	0.00	0.03	0.04	0.00	47.11	99.25
#20	30.66	20.58	0.01	0.00	0.02	0.00	0.00	46.55	97.82
#21	30.71	20.60	0.06	0.04	0.00	0.08	0.00	46.67	98.16
#22	30.65	20.42	0.18	0.00	0.05	0.00	0.00	46.49	97.80
#23	30.45	20.79	0.05	0.00	0.04	0.00	0.00	46.65	97.98
#24	30.63	20.49	0.22	0.01	0.07	0.03	0.04	46.62	98.12
#25	30.78	20.46	0.09	0.00	0.03	0.07	0.04	46.60	98.07
#26	30.18	20.56	0.16	0.00	0.09	0.02	0.09	46.32	97.42
#27	30.48	20.66	0.17	0.17	0.01	0.01	0.01	46.66	98.16
#28	30.25	20.58	0.17	0.00	0.02	0.01	0.09	46.36	97.48
#29	30.88	20.65	0.00	0.00	0.00	0.00	0.04	46.80	98.37
#31	30.82	20.48	0.40	0.00	0.10	0.03	0.02	46.86	98.70
#33	31.15	20.40	0.11	0.04	0.00	0.06	0.00	46.82	98.58
#34	30.57	20.78	0.01	0.00	0.05	0.07	0.06	46.75	98.29
#35	30.78	20.54	0.04	0.01	0.01	0.10	0.00	46.64	98.11
#36	31.15	20.51	0.04	0.00	0.00	0.03	0.00	46.87	98.61
#37	30.78	20.49	0.05	0.06	0.00	0.15	0.00	46.62	98.15
#38	31.05	20.18	0.14	0.05	0.04	0.00	0.16	46.58	98.19
#39	30.59	20.28	0.05	0.03	0.01	0.02	0.00	46.20	97.19
#40	30.55	20.65	0.17	0.00	0.01	0.01	0.03	46.65	98.08

Element Wt% Oxide. Lisheen Carbonates, November 1995. Operating Parameters: 15kV, 15nA, 25µm.									
Pts. 61-79, D1Rep, 262/153.6.									
	CaO	MgO	FeO	SrO	MnO	BaO	Ce2O3	CO2	TOTAL
#61	30.71	20.98	0.11	0.00	0.00	0.05	0.00	47.08	98.93
#62	31.08	20.74	0.09	0.02	0.01	0.00	0.08	47.13	99.15
#63	30.96	21.21	0.05	0.01	0.05	0.02	0.00	47.51	99.80
#64	32.11	19.95	0.00	0.02	0.00	0.00	0.00	46.98	99.06
#65	30.94	21.09	0.02	0.04	0.02	0.00	0.00	47.34	99.45
#66	30.70	20.43	0.00	0.00	0.00	0.05	0.10	46.45	97.73
#67	31.11	21.00	0.07	0.00	0.00	0.00	0.00	47.38	99.57
#68	30.69	21.22	0.09	0.09	0.00	0.00	0.00	47.33	99.41
#71	30.97	20.97	0.00	0.10	0.01	0.01	0.03	47.26	99.36
#72	31.14	21.10	0.01	0.02	0.02	0.15	0.00	47.53	99.96
#73	30.59	20.72	0.01	0.02	0.00	0.02	0.00	46.64	97.99
#74	30.55	20.58	0.00	0.05	0.00	0.00	0.08	46.50	97.76
#75	31.05	20.58	0.04	0.00	0.06	0.00	0.00	46.90	98.64
#76	30.91	20.65	0.10	0.03	0.00	0.12	0.01	46.91	98.72
#77	31.68	20.03	0.11	0.08	0.04	0.01	0.00	46.86	98.81
#78	30.92	21.08	0.00	0.00	0.04	0.13	0.00	47.33	99.50

Element Wt% Oxide, Lisheen Carbonates, Various August 1997. Operating Parameters: 15kV, 15nA, 15µm.														
Pts 1-30, D1 Rep, 121/31.4.														
	P2O5	SiO2	SO2	Ce2O3	MgO	CaO	MnO	FeO	SrO	BaO	Na2O	K2O	CO2	TOTAL
#1	0.00	0.01	0.05	0.01	20.25	32.28	0.00	0.00	0.00	0.00	0.03	0.01	47.67	100.32
#2	0.04	0.05	0.02	0.00	20.83	32.63	0.03	0.02	0.01	0.02	0.04	0.00	48.68	102.36
#3	0.04	0.02	0.00	0.07	21.29	31.87	0.07	0.18	0.05	0.00	0.02	0.00	48.66	102.26
#4	0.03	0.01	0.01	0.03	20.82	31.59	0.04	0.08	0.03	0.02	0.05	0.00	47.85	100.56
#5	0.08	0.00	0.02	0.01	21.14	31.54	0.02	0.16	0.07	0.06	0.00	0.01	48.27	101.39
#6	0.02	0.01	0.02	0.00	21.07	32.17	0.01	0.02	0.00	0.00	0.02	0.02	48.48	101.84
#7	0.01	0.05	0.00	0.00	20.99	31.85	0.03	0.00	0.01	0.03	0.04	0.03	48.20	101.26
#8	0.00	0.00	0.00	0.05	21.10	32.19	0.06	0.00	0.05	0.00	0.05	0.03	48.53	102.05
#9	0.03	0.00	0.01	0.00	20.66	32.47	0.00	0.02	0.02	0.00	0.01	0.00	48.23	101.46
#10	0.00	0.04	0.05	0.00	21.13	32.63	0.02	0.01	0.01	0.00	0.01	0.00	48.95	102.85
#11	0.00	0.03	0.00	0.06	21.03	32.53	0.00	0.00	0.04	0.00	0.00	0.01	48.70	102.41
#12	0.01	0.00	0.00	0.05	21.12	32.13	0.05	0.06	0.02	0.04	0.00	0.01	48.50	101.99
#13	0.04	0.04	0.03	0.00	20.51	32.30	0.02	0.04	0.00	0.03	0.00	0.01	48.06	101.07
#14	0.02	0.00	0.00	0.00	20.76	31.89	0.01	0.00	0.05	0.04	0.04	0.00	47.89	100.69
#15	0.05	0.01	0.00	0.00	20.81	32.31	0.01	0.00	0.04	0.00	0.06	0.01	48.36	101.67
#16	0.00	0.00	0.02	0.02	20.90	32.29	0.00	0.00	0.03	0.00	0.00	0.00	48.32	101.59
#17	0.02	0.06	0.04	0.02	21.00	32.25	0.03	0.03	0.05	0.03	0.04	0.02	48.62	102.20
#18	0.07	0.00	0.01	0.08	20.91	32.44	0.02	0.00	0.03	0.00	0.03	0.00	48.60	102.20
#19	0.02	0.04	0.04	0.04	20.62	32.61	0.04	0.00	0.03	0.01	0.01	0.01	48.43	101.90
#20	0.00	0.03	0.03	0.00	21.07	32.00	0.00	0.06	0.05	0.02	0.03	0.01	48.39	101.69
#22	0.07	0.11	0.04	0.04	21.02	32.40	0.00	0.11	0.04	0.00	0.01	0.03	48.91	102.76
#27	0.10	0.52	0.03	0.03	20.80	31.58	0.00	0.05	0.00	0.10	0.04	0.09	48.69	102.01

Element Wt% Oxide, Lisheen Carbonates, Various August 1997. Operating Parameters:15kV, 15nA, 15µm.														
Pts 11-20, D1 Rep, 297/183.3.														
	MgO	Na2O	SiO2	P2O5	SO2	K2O	CaO	MnO	FeO	SrO	BaO	Ce2O3	CO2	TOTAL
#11	21.07	0.01	0.20	0.00	0.01	0.04	32.03	0.01	0.02	0.05	0.09	0.02	48.65	102.20
#13	20.97	0.02	0.41	0.01	0.01	0.10	31.84	0.05	0.00	0.02	0.01	0.00	48.73	102.17
#15	20.93	0.00	0.01	0.04	0.02	0.00	32.53	0.01	0.07	0.02	0.04	0.03	48.68	102.38
#16	20.57	0.02	0.17	0.00	0.05	0.01	32.29	0.02	0.04	0.03	0.00	0.03	48.28	101.50
#19	20.65	0.03	0.44	0.01	0.00	0.08	32.31	0.01	0.04	0.01	0.00	0.03	48.78	102.40
#20	20.33	0.01	0.80	0.04	0.03	0.12	31.78	0.03	0.09	0.00	0.01	0.02	48.66	101.92

Dolomite Matrix Breccias

Element Wt% Oxide. Lisheen Carbonates, November 1995. Operating Parameters: 15kV, 15nA, 25µm.									
Pts 41-60, D2 BMB, 262/153.6.									
	CaO	MgO	FeO	SrO	MnO	BaO	Ce2O3	CO2	TOTAL
#41	31.52	20.12	0.06	0.01	0.02	0.07	0.08	46.80	98.76
#44	30.34	20.28	0.20	0.00	0.02	0.00	0.07	46.11	97.10
#45	30.94	20.78	0.23	0.00	0.00	0.00	0.06	47.13	99.21
#46	30.50	20.88	0.19	0.07	0.08	0.00	0.00	46.93	98.65
#47	30.61	20.86	0.26	0.03	0.01	0.13	0.02	47.01	98.95
#48	30.48	20.85	0.18	0.00	0.00	0.05	0.03	46.82	98.44
#49	31.06	20.81	0.04	0.00	0.00	0.00	0.06	47.15	99.20
#50	30.91	20.80	0.13	0.10	0.05	0.07	0.00	47.13	99.19
#51	30.78	20.71	0.11	0.00	0.00	0.00	0.07	46.87	98.62
#52	30.92	20.83	0.09	0.00	0.05	0.00	0.05	47.11	99.08
#53	31.19	20.63	0.16	0.09	0.07	0.00	0.07	47.20	99.46
#54	30.97	20.47	0.02	0.00	0.04	0.00	0.10	46.73	98.44
#55	31.21	20.43	0.15	0.00	0.00	0.00	0.04	46.91	98.79
#56	33.25	19.35	0.02	0.09	0.01	0.00	0.03	47.30	100.09
#58	30.62	20.61	0.00	0.13	0.00	0.10	0.00	46.62	98.08
#59	30.79	20.70	0.01	0.05	0.03	0.12	0.01	46.84	98.55
#60	31.26	20.82	0.23	0.04	0.00	0.00	0.00	47.41	99.75

Element Wt% Oxide. Lisheen Carbonates, Various August 1997. Operating Parameters: 15kV, 15nA, 15µm.														
Pts. 41-50, D2 BMB, 262/152.3.														
	P2O5	SiO2	SO2	Ce2O3	MgO	CaO	MnO	FeO	SrO	BaO	Na2O	K2O	CO2	TOTAL
#6	0.06	0.18	0.13	0.00	20.50	32.53	0.05	0.14	0.01	0.04	0.00	0.01	48.69	102.33
#7	0.05	0.07	0.03	0.01	20.62	32.44	0.05	0.26	0.04	0.02	0.02	0.03	48.54	102.17
#8	0.01	0.04	0.37	0.00	20.88	32.34	0.00	0.20	0.02	0.00	0.00	0.02	49.01	102.90
#10	0.00	0.38	1.78	0.01	20.10	31.20	0.05	0.21	0.03	0.00	0.11	0.06	49.82	103.75
#11	0.00	0.08	0.29	0.00	20.92	32.35	0.04	0.05	0.04	0.00	0.05	0.00	48.97	102.80
#12	0.06	0.04	0.05	0.00	20.55	32.05	0.00	0.02	0.02	0.00	0.00	0.00	47.93	100.72
#13	0.01	0.00	0.03	0.00	20.70	33.09	0.02	0.04	0.01	0.00	0.00	0.01	48.79	102.70
#14	0.04	0.08	0.07	0.02	20.94	32.38	0.04	0.07	0.06	0.02	0.00	0.04	48.77	102.51
#15	0.01	0.05	0.00	0.04	20.49	32.89	0.03	0.00	0.07	0.03	0.00	0.00	48.44	102.04

Element Wt% Oxide. Lisheen Carbonates, Various August 1997. Operating Parameters: 15kV, 15nA, 15µm.														
Pts. 1-10, D2 BMB, 262/129.8.														
	P2O5	SiO2	SO2	Ce2O3	MgO	CaO	MnO	FeO	SrO	BaO	Na2O	K2O	CO2	TOTAL
#1	0.00	0.50	0.55	0.04	19.93	32.58	0.04	0.20	0.01	0.06	0.05	0.08	49.19	103.24
#2	0.01	0.19	0.55	0.00	20.21	32.40	0.01	0.13	0.00	0.02	0.08	0.06	48.82	102.47
#3	0.00	0.28	0.59	0.01	20.02	32.22	0.04	0.17	0.01	0.05	0.03	0.02	48.64	102.08
#4	0.09	0.27	0.41	0.00	19.91	33.09	0.00	0.14	0.01	0.00	0.04	0.06	49.06	103.09
#5	0.04	0.28	0.93	0.04	20.09	31.60	0.04	0.23	0.03	0.03	0.12	0.05	48.90	102.38
#6	0.00	0.10	0.47	0.04	20.37	32.96	0.05	0.07	0.03	0.00	0.05	0.04	49.16	103.34
#7	0.00	0.15	0.20	0.00	20.13	32.72	0.02	0.22	0.00	0.08	0.02	0.02	48.45	102.02
#8	0.01	0.27	0.07	0.00	20.08	32.70	0.04	0.17	0.00	0.02	0.01	0.04	48.35	101.76
#9	0.01	0.47	0.76	0.00	19.56	31.95	0.15	0.80	0.00	0.00	0.07	0.11	48.95	102.83
#10	0.00	0.18	0.18	0.02	20.46	32.27	0.03	0.14	0.03	0.00	0.08	0.03	48.47	101.88

Element Wt% Oxide. Lisheen Carbonates, Various August 1997. Operating Parameters: 15kV, 15nA, 15µm.														
Pts. 1-10, D2 BMB, 259/222.0.														
	P2O5	SiO2	SO2	Ce2O3	MgO	CaO	MnO	FeO	SrO	BaO	Na2O	K2O	CO2	TOTAL
#1	0.00	0.12	0.04	0.00	21.02	32.14	0.03	0.03	0.02	0.06	0.00	0.04	48.58	102.08
#2	0.01	0.05	0.03	0.01	20.72	32.60	0.05	0.04	0.02	0.04	0.03	0.02	48.56	102.19
#3	0.01	0.06	0.00	0.13	20.54	32.55	0.01	0.00	0.00	0.00	0.07	0.00	48.28	101.64
#4	0.00	0.36	0.00	0.05	20.78	31.42	0.03	0.05	0.00	0.04	0.00	0.08	48.11	100.92
#5	0.04	0.10	0.04	0.06	20.81	33.11	0.00	0.06	0.04	0.00	0.02	0.00	49.15	103.41
#6	0.04	0.58	0.02	0.00	20.52	31.79	0.05	0.05	0.05	0.07	0.01	0.09	48.54	101.80
#7	0.01	0.06	0.00	0.03	20.64	32.30	0.04	0.02	0.08	0.02	0.00	0.03	48.22	101.47
#8	0.00	0.01	0.02	0.01	19.93	33.47	0.02	0.03	0.02	0.01	0.01	0.00	48.23	101.75
#9	0.01	0.04	0.00	0.05	20.79	32.26	0.00	0.08	0.00	0.00	0.02	0.02	48.30	101.58
#10	0.01	0.16	0.01	0.00	20.71	32.40	0.06	0.06	0.03	0.00	0.03	0.04	48.54	102.06

Element Wt% Oxide. Lisheen Carbonates, Various Aufust 1997. Operating Parameters: 15kV, 15nA, 15µm.														
Pts 1-20, D2 BMB, 413/100.5.														
	P2O5	SiO2	SO2	Ce2O3	MgO	CaO	MnO	FeO	SrO	BaO	Na2O	K2O	CO2	TOTAL
#1	0.09	0.39	0.12	0.07	19.34	33.46	0.00	0.17	0.00	0.01	0.04	0.06	48.56	102.31
#4	0.00	0.60	0.14	0.00	19.20	33.49	0.07	0.13	0.00	0.08	0.02	0.13	48.65	102.51
#5	0.19	0.08	0.10	0.01	19.33	34.36	0.01	0.09	0.04	0.00	0.04	0.03	48.85	103.13
#6	0.04	0.41	0.10	0.00	19.33	34.04	0.02	0.10	0.00	0.04	0.01	0.06	48.86	103.03
#7	0.04	0.69	0.08	0.00	19.50	33.81	0.03	0.09	0.05	0.00	0.04	0.17	49.33	103.85
#8	0.05	2.73	0.09	0.06	18.48	32.15	0.03	0.18	0.00	0.00	0.03	0.47	50.11	104.38
#9	0.12	1.11	0.10	0.00	19.25	32.83	0.05	0.18	0.00	0.00	0.06	0.22	49.11	103.02
#10	0.29	1.45	0.06	0.00	19.10	33.11	0.01	0.08	0.03	0.00	0.01	0.26	49.77	104.15
#11	0.05	0.06	0.07	0.02	19.35	34.07	0.02	0.13	0.00	0.00	0.04	0.02	48.38	102.22
#13	0.08	1.60	0.15	0.03	18.95	32.98	0.01	0.12	0.02	0.00	0.07	0.36	49.67	104.04
#15	0.17	0.86	0.09	0.00	19.31	33.55	0.02	0.17	0.07	0.07	0.03	0.19	49.45	103.99
#16	0.03	0.72	0.22	0.04	19.11	33.42	0.05	0.33	0.04	0.00	0.04	0.11	48.94	103.05
#17	0.01	0.13	0.12	0.01	19.51	33.79	0.07	0.16	0.04	0.00	0.05	0.03	48.51	102.42
#18	0.04	0.34	0.11	0.01	19.10	34.09	0.01	0.15	0.02	0.00	0.02	0.06	48.59	102.56
#19	0.04	0.10	0.08	0.00	19.48	34.16	0.03	0.05	0.01	0.00	0.01	0.02	48.58	102.57
#20	0.01	0.61	0.09	0.00	18.76	33.77	0.04	0.09	0.03	0.06	0.04	0.09	48.29	101.88

Element Wt% Oxide. Lisheen Carbonates, Various August 1997. Operating Parameters: 15kV, 15nA, 15µm.														
Pts 1-30, D3 WMB, 538/185.2.														
	P2O5	SiO2	SO2	Ce2O3	MgO	CaO	MnO	FeO	SrO	BaO	Na2O	K2O	CO2	TOTAL
#2	0.06	0.02	0.00	0.01	20.74	32.57	0.02	0.03	0.04	0.04	0.01	0.01	48.51	102.07
#3	0.08	0.01	0.03	0.01	20.84	32.64	0.00	0.01	0.02	0.00	0.00	0.00	48.67	102.30
#4	0.00	0.24	0.08	0.00	20.86	32.21	0.02	0.08	0.01	0.04	0.02	0.00	48.71	102.26
#5	0.06	0.34	0.11	0.03	20.84	32.21	0.00	0.19	0.03	0.00	0.01	0.05	49.04	102.90
#6	0.02	0.01	0.00	0.00	20.83	32.57	0.00	0.00	0.06	0.01	0.02	0.00	48.50	102.02
#7	0.12	0.00	0.05	0.00	21.08	32.18	0.03	0.00	0.01	0.00	0.03	0.01	48.68	102.18
#8	0.00	0.03	0.16	0.03	21.03	32.31	0.02	0.17	0.03	0.05	0.04	0.03	48.91	102.83
#9	0.07	0.35	0.01	0.04	20.58	32.47	0.00	0.01	0.04	0.00	0.00	0.02	48.75	102.35
#10	0.01	0.17	0.01	0.00	21.15	32.05	0.00	0.04	0.05	0.05	0.03	0.02	48.73	102.33
#11	0.00	0.50	0.03	0.00	21.10	31.96	0.02	0.07	0.06	0.01	0.01	0.06	49.13	102.96
#13	0.00	0.36	0.24	0.03	20.69	31.80	0.04	0.21	0.00	0.06	0.05	0.08	48.77	102.33
#14	0.07	0.05	0.00	0.08	21.17	32.24	0.01	0.09	0.00	0.00	0.03	0.01	48.83	102.58
#16	0.04	0.09	0.01	0.00	20.96	32.35	0.04	0.06	0.05	0.00	0.01	0.00	48.68	102.28
#17	0.01	0.14	0.03	0.00	19.85	33.77	0.00	0.00	0.06	0.01	0.06	0.04	48.63	102.60
#18	0.00	0.02	0.03	0.01	19.77	33.64	0.01	0.00	0.04	0.06	0.03	0.00	48.23	101.83
#19	0.05	0.00	0.00	0.04	20.97	32.57	0.07	0.04	0.03	0.00	0.05	0.02	48.79	102.64
#20	0.05	0.02	0.03	0.04	20.57	32.16	0.04	0.05	0.04	0.00	0.03	0.00	48.05	101.06
#21	0.00	0.00	0.01	0.04	20.97	32.01	0.02	0.03	0.00	0.02	0.05	0.00	48.24	101.41
#22	0.04	0.00	0.08	0.00	13.38	41.49	0.00	0.00	0.02	0.00	0.01	0.00	47.46	102.48
#23	0.04	0.04	0.00	0.00	21.24	31.72	0.04	0.02	0.02	0.00	0.00	0.01	48.35	101.49
#24	0.03	0.04	0.00	0.06	21.12	31.97	0.05	0.09	0.00	0.00	0.02	0.00	48.49	101.88
#25	0.01	0.00	0.03	0.04	20.94	31.95	0.03	0.04	0.01	0.02	0.02	0.00	48.19	101.30
#26	0.00	0.03	0.00	0.00	21.35	31.76	0.03	0.15	0.06	0.00	0.00	0.02	48.53	101.93
#27	0.03	0.01	0.02	0.03	21.00	32.27	0.03	0.00	0.04	0.00	0.01	0.01	48.49	101.93
#28	0.01	0.03	0.00	0.03	21.17	32.43	0.00	0.01	0.09	0.10	0.01	0.00	48.81	102.69
#29	0.05	0.00	0.00	0.03	21.28	32.00	0.06	0.07	0.06	0.03	0.02	0.00	48.66	102.26

Element Wt% Oxide, Lisheen Carbonates, January 1998. Operating Parameters: 15kV, 15nA, 15µm.													
Pts 1-20, D3 WMB, 252/174.0.													
	CaO	MgO	Na2O	SO2	K2O	SrO	MnO	FeO	NiO	CdO	BaO	CO2	TOTAL
#1	31.18	20.57	0.00	0.03		0.01	0.14	0.54	0.03	0.04		47.41	99.93
#2	32.08	20.57	0.03		0.01	0.02	0.00	0.20			0.02	47.79	100.72
#3	32.88	20.63				0.01	0.01	0.02	0.06	0.05	0.02	48.40	102.06
#4	32.73	20.30	0.02	0.03	0.03	0.06	0.03	0.00		0.05	0.06	47.99	101.30
#5	32.55	20.41	0.02	0.02	0.00	0.04	0.00	0.02				47.89	100.95
#6	32.56	20.47	0.02		0.01	0.04	0.06	0.08	0.08	0.02	0.06	48.09	101.48
#7	32.98	20.58	0.01	0.01	0.00	0.00	0.02	0.00	0.04	0.02		48.41	102.08
#8	32.57	20.39	0.01	0.00		0.09	0.04	0.03	0.02		0.05	47.93	101.13
#9	32.87	20.40	0.05		0.01	0.06	0.02	0.00	0.08	0.01	0.03	48.19	101.69
#10	32.80	20.39	0.01	0.01		0.03	0.02	0.02				48.06	101.33
#11	32.92	20.43				0.07	0.05	0.02	0.07		0.08	48.27	101.89
#12	32.95	19.95	0.03	0.00		0.05	0.02	0.02		0.02	0.06	47.73	100.83
#13	32.91	20.25	0.02		0.01	0.05	0.04	0.02	0.04		0.03	48.03	101.38
#14	31.89	20.71	0.00	0.02	0.01		0.18	0.35				47.99	101.15
#16	31.52	19.86	0.02	0.01	0.00		0.27	0.72	0.06			47.09	99.55
#17	33.70	18.51	0.05	0.01	0.01	0.02	0.11	0.29		0.05	0.12	47.02	99.89
#18	32.40	19.99	0.01	0.03	0.01	0.08	0.03	0.01	0.02	0.01	0.11	47.39	100.07
#19	33.26	20.27	0.00		0.00	0.07	0.07	0.00	0.01		0.03	48.32	102.02
#20	32.57	20.33				0.07	0.04	0.01	0.03	0.02	0.04	47.85	100.95

Element Wt% Oxide. Lisheen Carbonates, Various August 1997. Operating Parameters: 15kV, 15nA, 15µm.														
Pts 1-10, D3 WMB, 297/183.3.														
	MgO	Na2O	SiO2	P2O5	SO2	K2O	CaO	MnO	FeO	SrO	BaO	Ce2O3	CO2	TOTAL
#1	20.99	0.00	0.05	0.00	0.00	0.01	32.39	0.00	0.00	0.03	0.03	0.01	48.55	102.07
#2	20.88	0.01	0.00	0.00	0.00	0.00	32.94	0.03	0.03	0.03	0.06	0.05	48.85	102.88
#3	21.12	0.00	0.02	0.09	0.03	0.01	32.24	0.00	0.07	0.03	0.06	0.07	48.79	102.53
#4	20.93	0.00	0.03	0.02	0.00	0.02	32.07	0.03	0.12	0.06	0.00	0.00	48.34	101.63
#5	21.05	0.00	0.06	0.03	0.00	0.02	32.52	0.03	0.00	0.01	0.01	0.01	48.78	102.51
#6	21.06	0.01	0.06	0.02	0.00	0.03	32.38	0.03	0.15	0.04	0.02	0.02	48.78	102.59
#7	20.62	0.04	0.05	0.04	0.00	0.03	33.17	0.03	0.04	0.03	0.04	0.02	48.92	103.03
#8	20.53	0.01	0.02	0.01	0.00	0.01	33.21	0.00	0.00	0.04	0.02	0.00	48.65	102.50
#9	20.56	0.01	0.03	0.06	0.02	0.00	32.84	0.04	0.04	0.08	0.00	0.08	48.62	102.37
#10	21.15	0.03	0.00	0.00	0.00	0.00	32.22	0.00	0.06	0.05	0.12	0.03	48.61	102.26

Element Wt% Oxide, Lisheen Carbonates, November 1995. Operating Parameters: 15kV, 15nA, 25µm.									
Pts 1-49, D3 WMB, 121/162.1.									
	CaO	MgO	FeO	SrO	MnO	BaO	Ce2O3	CO2	TOTAL
#1	31.53	21.37	0.28	0.13	0.01	0.10	0.00	48.33	101.74
#2	31.08	21.34	0.28	0.02	0.06	0.05	0.00	47.92	100.74
#3	31.03	21.64	0.35	0.00	0.00	0.00	0.13	48.23	101.37
#4	30.93	21.38	0.12	0.00	0.03	0.00	0.00	47.70	100.17
#5	31.19	21.51	0.13	0.08	0.06	0.00	0.01	48.12	101.10
#6	31.21	21.53	0.23	0.06	0.03	0.02	0.00	48.18	101.25
#7	30.91	21.60	0.36	0.00	0.03	0.00	0.02	48.08	101.00
#8	30.69	21.14	0.35	0.05	0.18	0.17	0.04	47.57	100.18
#9	31.43	21.02	0.12	0.06	0.26	0.04	0.04	47.90	100.87
#10	31.27	20.93	0.00	0.03	0.11	0.14	0.00	47.51	99.98
#11	31.66	20.93	0.04	0.05	0.06	0.07	0.05	47.81	100.67
#12	31.67	20.89	0.00	0.00	0.00	0.05	0.03	47.68	100.32
#13	31.90	20.92	0.09	0.01	0.04	0.17	0.00	48.00	101.12
#14	31.42	20.88	0.00	0.00	0.03	0.00	0.00	47.47	99.79
#15	31.75	20.96	0.07	0.00	0.03	0.00	0.00	47.87	100.68
#16	31.73	21.08	0.10	0.01	0.00	0.09	0.11	48.04	101.16
#17	31.41	20.82	0.00	0.08	0.05	0.00	0.00	47.44	99.80
#18	31.59	21.28	0.00	0.00	0.01	0.00	0.13	48.07	101.08
#19	31.48	21.06	0.04	0.05	0.01	0.00	0.10	47.79	100.53
#20	31.76	20.97	0.07	0.00	0.01	0.10	0.00	47.89	100.79
#21	31.42	20.84	0.16	0.05	0.00	0.05	0.00	47.54	100.05
#22	31.62	20.90	0.02	0.06	0.02	0.00	0.05	47.69	100.36
#23	32.04	21.05	0.01	0.00	0.00	0.00	0.00	48.14	101.24
#24	31.47	21.32	0.00	0.00	0.02	0.19	0.13	48.09	101.23
#25	32.68	20.30	0.00	0.00	0.00	0.00	0.10	47.86	100.95
#26	31.83	20.50	0.01	0.09	0.05	0.00	0.09	47.48	100.06
#27	33.41	19.55	0.00	0.00	0.01	0.05	0.00	47.58	100.60
#28	32.22	20.26	0.05	0.00	0.00	0.00	0.04	47.45	100.02
#29	31.50	21.14	0.07	0.00	0.01	0.04	0.06	47.88	100.70
#30	31.82	21.06	0.01	0.06	0.06	0.00	0.00	48.03	101.03
#31	31.75	20.25	0.00	0.00	0.00	0.00	0.07	47.05	99.12
#32	31.95	20.34	0.10	0.00	0.01	0.00	0.00	47.34	99.73
#33	31.70	20.51	0.23	0.06	0.06	0.00	0.00	47.47	100.04
#34	31.37	20.98	0.17	0.00	0.04	0.14	0.00	47.69	100.40
#35	31.29	21.01	0.00	0.09	0.00	0.07	0.07	47.59	100.13
#36	32.30	20.51	0.09	0.01	0.03	0.09	0.00	47.84	100.87
#37	31.66	20.62	0.05	0.10	0.03	0.01	0.12	47.50	100.09
#38	31.87	20.22	0.00	0.00	0.03	0.07	0.00	47.12	99.31
#39	32.09	19.67	0.04	0.06	0.05	0.00	0.07	46.77	98.75
#40	33.48	19.00	0.12	0.04	0.03	0.00	0.07	47.16	99.90
#41	32.55	20.12	0.00	0.00	0.00	0.11	0.00	47.55	100.34
#42	31.29	20.88	0.00	0.00	0.02	0.05	0.06	47.40	99.70
#43	32.09	20.08	0.10	0.00	0.04	0.03	0.04	47.22	99.61
#44	32.32	20.53	0.15	0.03	0.03	0.13	0.00	47.93	101.12
#45	32.30	20.04	0.00	0.02	0.01	0.00	0.00	47.24	99.61
#46	31.95	20.78	0.13	0.00	0.03	0.01	0.00	47.86	100.77
#47	32.23	20.93	0.11	0.00	0.04	0.17	0.11	48.33	101.93
#48	31.46	20.61	0.06	0.00	0.01	0.08	0.09	47.30	99.61
#49	31.63	20.47	0.08	0.08	0.04	0.00	0.05	47.29	99.64

Pink Dolomite

Element Wt% Oxide, Galmoy Carbonates, August 18, 19th 1997. Operating Parameters: 15kV, 15nA, 15µm.														
Pts 1-14, D4 PINK, 138/225.0.														
	P2O5	SiO2	SO2	Ce2O3	MgO	CaO	MnO	FeO	SrO	BaO	Na2O	K2O	CO2	TOTAL
#1	0.01	0.04	0.00	0.04	20.25	31.54	0.20	1.06	0.01	0.02	0.00	0.02	47.86	101.06
#2	0.01	0.01	0.02	0.00	20.34	31.53	0.20	1.12	0.03	0.02	0.04	0.01	47.99	101.32
#3	0.03	0.02	0.03	0.00	20.33	31.54	0.20	0.91	0.01	0.08	0.01	0.00	47.89	101.05
#4	0.06	0.02	0.02	0.00	20.32	31.21	0.23	0.98	0.02	0.07	0.03	0.01	47.74	100.71
#5	0.00	0.01	0.02	0.00	20.15	32.05	0.27	1.09	0.00	0.06	0.06	0.01	48.22	101.96
#6	0.02	0.01	0.00	0.00	20.36	31.84	0.24	0.97	0.03	0.00	0.01	0.00	48.13	101.60
#7	0.04	0.05	0.02	0.07	20.05	31.48	0.30	1.27	0.03	0.02	0.00	0.01	47.90	101.26
#8	0.00	0.00	0.02	0.05	20.14	31.71	0.20	1.04	0.02	0.05	0.04	0.00	47.84	101.13
#9	0.00	0.02	0.02	0.02	20.15	31.67	0.20	0.94	0.05	0.00	0.00	0.00	47.74	100.80
#10	0.02	0.01	0.03	0.02	20.24	31.16	0.16	0.96	0.03	0.00	0.01	0.01	47.48	100.15

Element Wt% Oxide, Lisheen Carbonates, August 18, 19th 1997. Operating Parameters: 15kV, 15nA, 15µm.														
Pts11-20, D4 PINK, 318/450.0														
	P2O5	SiO2	SO2	Ce2O3	MgO	CaO	MnO	FeO	SrO	BaO	Na2O	K2O	CO2	TOTAL
#11	0.04	0.04	0.01	0.01	20.55	31.53	0.20	0.81	0.04	0.02	0.00	0.02	48.09	101.38
#12	0.07	0.01	0.03	0.01	20.48	31.36	0.24	0.79	0.03	0.02	0.04	0.02	47.92	101.02
#13	0.00	0.02	0.00	0.03	20.56	31.42	0.17	0.72	0.00	0.00	0.00	0.01	47.82	100.76
#14	0.05	0.03	0.04	0.05	20.40	31.48	0.11	0.87	0.04	0.00	0.01	0.00	47.91	101.00
#15	0.03	0.00	0.00	0.00	20.48	31.70	0.17	0.75	0.00	0.05	0.00	0.02	47.97	101.17
#16	0.00	0.02	0.00	0.00	20.61	31.75	0.19	0.82	0.04	0.09	0.02	0.03	48.25	101.83
#17	0.03	0.02	0.02	0.02	20.59	31.72	0.20	0.78	0.00	0.00	0.00	0.01	48.18	101.55
#18	0.03	0.00	0.00	0.00	20.62	31.62	0.19	0.89	0.00	0.04	0.04	0.00	48.18	101.59
#19	0.02	0.00	0.00	0.00	20.54	31.75	0.24	0.97	0.04	0.00	0.02	0.00	48.26	101.85
#20	0.00	0.03	0.03	0.01	19.57	31.35	0.14	0.94	0.00	0.00	0.03	0.00	46.84	98.93

Element Wt% Oxide, Lisheen Carbonates, August 18,19th 1997. Operating Parameters: 15kV, 15nA, 15µm.														
Pts1-10, D4 PINK. 515/173.7.														
	P2O5	SiO2	SO2	Ce2O3	MgO	CaO	MnO	FeO	SrO	BaO	Na2O	K2O	CO2	TOTAL
#1	0.03	0.00	0.02	0.01	20.33	31.52	0.11	0.52	0.04	0.00	0.05	0.01	47.57	100.21
#2	0.02	0.03	0.03	0.02	20.05	31.99	0.29	0.69	0.00	0.00	0.03	0.01	47.87	101.05
#3	0.02	0.04	0.01	0.02	20.05	31.30	0.26	0.69	0.00	0.04	0.03	0.00	47.28	99.73
#4	0.04	0.01	0.01	0.00	20.52	31.80	0.19	0.46	0.05	0.02	0.04	0.00	48.00	101.14
#5	0.01	0.00	0.04	0.00	19.57	32.70	0.17	0.57	0.04	0.03	0.02	0.01	47.70	100.85
#6	0.00	0.03	0.00	0.00	19.70	32.33	0.20	0.71	0.03	0.04	0.09	0.00	47.68	100.82
#7	0.02	0.00	0.01	0.02	19.82	32.20	0.26	0.97	0.00	0.00	0.01	0.01	47.84	101.16
#8	0.04	0.00	0.00	0.00	19.92	31.92	0.27	0.84	0.01	0.00	0.02	0.00	47.66	100.68
#9	0.00	0.03	0.01	0.08	18.82	33.80	0.13	0.39	0.09	0.09	0.05	0.00	47.71	101.22
#10	0.00	0.01	0.03	0.03	19.97	32.40	0.26	0.90	0.03	0.00	0.04	0.01	48.16	101.83

Late, Minor Vein and Vug Dolomite

Element Wt% Oxide, Lisheen Carbonates, Various August, 1997. Operating Parameters: 15kV, 15nA, 15µm.														
Pts 11-20, D5 Dol, 121/319.2.														
	MgO	Na2O	SiO2	P2O5	SO2	K2O	CaO	MnO	FeO	SrO	BaO	Ce2O3	CO2	TOTAL
#11	15.62	0.03	0.01	0.01	0.02	0.00	31.99	0.39	5.56	0.02	0.05	0.01	99.74	99.74
#12	13.17	0.05	0.03	0.06	0.02	0.03	32.07	0.63	8.94	0.04	0.04	0.08	100.97	100.97
#13	13.14	0.07	0.01	0.02	0.06	0.02	32.13	0.76	9.22	0.03	0.00	0.00	101.45	101.45
#14	12.31	0.05	0.05	0.00	0.05	0.02	32.20	0.78	9.55	0.03	0.00	0.00	100.37	100.37
#15	15.99	0.04	0.02	0.00	0.00	0.00	32.60	0.35	5.44	0.03	0.01	0.00	101.26	101.26
#16	15.29	0.06	0.03	0.05	0.02	0.00	32.47	0.32	5.86	0.05	0.00	0.04	100.52	100.52
#17	15.60	0.02	0.00	0.03	0.00	0.03	32.71	0.35	6.03	0.06	0.00	0.10	101.80	101.80
#18	15.41	0.01	0.02	0.01	0.01	0.01	32.53	0.36	5.52	0.01	0.00	0.03	100.07	100.07
#19	15.57	0.05	0.00	0.00	0.00	0.01	32.87	0.42	5.86	0.05	0.01	0.00	101.65	101.65
#20	15.05	0.00	0.08	0.03	0.00	0.00	33.61	0.37	5.13	0.02	0.03	0.01	100.79	100.79

Element Wt% Oxide, Lisheen Carbonates, August 18,19th, 1997. Operating Parameters: 15kV, 15nA, 15µm.														
Pts 1-10, D5 Dol, 517/205.0.														
	P2O5	SiO2	SO2	Ce2O3	MgO	CaO	MnO	FeO	SrO	BaO	Na2O	K2O	CO2	TOTAL
#1	0.04	0.02	0.00	0.04	21.10	32.64	0.01	0.06	0.05	0.00	0.03	0.00	102.95	102.95
#4	0.00	0.04	0.00	0.03	20.07	33.90	0.04	0.00	0.03	0.00	0.03	0.01	102.88	102.88
#5	0.00	0.00	0.00	0.06	21.13	32.61	0.02	0.00	0.01	0.02	0.02	0.00	102.70	102.70
#6	0.04	0.02	0.03	0.00	20.99	32.29	0.02	0.08	0.03	0.03	0.00	0.00	102.10	102.10
#7	0.03	0.03	0.11	0.01	20.86	32.03	0.04	0.00	0.06	0.00	0.02	0.00	101.52	101.52
#8	0.03	0.00	0.00	0.00	21.02	32.29	0.03	0.02	0.04	0.01	0.00	0.01	101.97	101.97
#9	0.03	0.02	0.00	0.01	21.04	32.76	0.08	0.02	0.03	0.00	0.02	0.00	102.97	102.97
#10	0.00	0.04	0.06	0.00	21.15	32.19	0.00	0.07	0.04	0.00	0.03	0.01	102.29	102.29

Late, Minor Vein and Vug Calcite

Element Wt% Oxide, Lisheen Carbonates, Various August, 1997. Operating Parameters: 15kV, 15nA, 15µm.														
Pts 1-10, D5 Calc, 121/319.2.														
	MgO	Na2O	SiO2	P2O5	SO2	K2O	CaO	MnO	FeO	SrO	BaO	Ce2O3	CO2	TOTAL
#1	0.03	0.02	0.01	0.00	0.02	0.01	57.20	0.09	0.07	0.01	0.05	0.03	45.22	102.75
#2	0.27	0.05	0.04	0.04	0.08	0.00	56.57	0.08	0.12	0.12	0.02	0.03	45.25	102.67
#3	0.09	0.04	0.01	0.00	0.00	0.01	57.01	0.09	0.17	0.06	0.07	0.05	45.23	102.83
#4	0.13	0.05	0.00	0.05	0.00	0.00	56.54	0.07	0.10	0.03	0.01	0.05	44.89	101.93
#5	0.09	0.04	0.00	0.00	0.02	0.00	56.77	0.08	0.14	0.08	0.10	0.00	45.03	102.36
#6	0.12	0.00	0.00	0.00	0.02	0.02	56.42	0.04	0.11	0.09	0.01	0.01	44.70	101.53
#7	0.06	0.04	0.01	0.03	0.00	0.01	56.70	0.09	0.08	0.03	0.00	0.03	44.90	101.98
#8	0.13	0.00	0.01	0.03	0.01	0.00	55.81	0.04	0.11	0.05	0.00	0.07	44.27	100.54
#9	0.19	0.00	0.05	0.05	0.03	0.00	57.09	0.02	0.18	0.06	0.00	0.05	45.48	103.20
#10	0.13	0.00	0.03	0.00	0.04	0.00	57.14	0.05	0.02	0.07	0.00	0.03	45.28	102.79

Element Oxide Wt%, Lisheen Carbonates, August 18,19th, 1997. Operating Parameters: 15kV, 15nA, 15µm.														
Pts 1-10, D5 Calc, 318/450.5.														
	P2O5	SiO2	SO2	Ce2O3	MgO	CaO	MnO	FeO	SrO	BaO	Na2O	K2O	CO2	TOTAL
#1	0.05	0.03	0.03	0.00	0.11	57.12	0.10	0.03	0.04	0.00	0.02	0.01	102.90	102.90
#2	0.00	0.00	0.03	0.00	0.08	57.19	0.02	0.04	0.03	0.00	0.04	0.00	102.64	102.64
#3	0.03	0.02	0.03	0.07	0.09	57.33	0.01	0.04	0.04	0.03	0.01	0.00	103.12	103.12
#4	0.00	0.04	0.03	0.02	0.11	57.35	0.01	0.02	0.03	0.04	0.03	0.01	103.10	103.10
#5	0.04	0.02	0.02	0.05	0.16	57.52	0.03	0.00	0.05	0.01	0.00	0.00	103.51	103.51
#6	0.07	0.01	0.01	0.01	0.15	57.26	0.00	0.08	0.03	0.05	0.00	0.00	103.08	103.08
#7	0.00	0.04	0.00	0.01	0.10	57.10	0.00	0.06	0.03	0.00	0.06	0.00	102.60	102.60
#8	0.00	0.00	0.00	0.06	0.14	56.85	0.05	0.03	0.02	0.00	0.03	0.00	102.17	102.17
#9	0.00	0.01	0.01	0.04	0.05	57.27	0.04	0.00	0.05	0.08	0.02	0.00	102.83	102.83
#10	0.08	0.02	0.00	0.03	0.12	57.65	0.07	0.02	0.02	0.06	0.04	0.00	103.89	103.89

Element Oxide Wt%, Lisheen Carbonates, August 18,19th, 1997. Operating Parameters: 15kV, 15nA, 15µm.														
Pts 11-20, D5 Calc, 514/182.5.														
	P2O5	SiO2	SO2	Ce2O3	MgO	CaO	MnO	FeO	SrO	BaO	Na2O	K2O	CO2	TOTAL
#11	0.06	0.03	0.03	0.06	0.10	57.56	0.09	0.01	0.01	0.00	0.01	0.00	103.63	103.63
#12	0.02	0.03	0.02	0.05	0.13	57.71	0.05	0.00	0.11	0.00	0.01	0.01	103.90	103.90
#14	0.01	0.00	0.00	0.02	0.11	57.60	0.02	0.00	0.13	0.02	0.03	0.00	103.49	103.49
#15	0.05	0.00	0.02	0.03	0.03	57.77	0.04	0.03	0.05	0.02	0.00	0.02	103.75	103.75
#16	0.04	0.03	0.00	0.00	0.02	57.36	0.03	0.08	0.04	0.00	0.00	0.01	102.97	102.97
#17	0.05	0.02	0.00	0.00	0.02	57.32	0.04	0.05	0.01	0.04	0.01	0.02	102.90	102.90
#18	0.02	0.06	0.05	0.03	0.14	57.50	0.03	0.05	0.00	0.02	0.01	0.01	103.56	103.56
#19	0.03	0.04	0.02	0.07	0.07	57.48	0.00	0.00	0.02	0.00	0.00	0.00	103.19	103.19
#20	0.02	0.02	0.04	0.03	0.13	58.06	0.04	0.04	0.05	0.00	0.00	0.00	104.44	104.44

Element Oxide Wt%, Lisheen Carbonates, August 18,19th, 1997. Operating Parameters: 15kV, 15nA, 15µm.														
Pts 1-10, D5 Calc, 449/95.5.														
	P2O5	SiO2	SO2	Ce2O3	MgO	CaO	MnO	FeO	SrO	BaO	Na2O	K2O	CO2	TOTAL
#1	0.02	0.01	0.00	0.03	0.17	57.03	0.05	0.23	0.03	0.03	0.00	0.01	102.94	102.94
#2	0.00	0.02	0.00	0.06	0.36	56.40	0.07	0.40	0.01	0.00	0.00	0.00	102.45	102.45
#3	0.06	0.00	0.04	0.03	0.36	56.34	0.10	0.44	0.06	0.00	0.00	0.01	102.69	102.69
#4	0.03	0.00	0.01	0.03	0.39	56.41	0.09	0.34	0.03	0.11	0.00	0.00	102.62	102.62
#5	0.00	0.02	0.00	0.06	0.37	56.92	0.10	0.37	0.04	0.03	0.05	0.02	103.58	103.58
#6	0.04	0.02	0.00	0.04	0.34	56.60	0.11	0.34	0.08	0.03	0.03	0.01	102.98	102.98
#7	0.00	0.00	0.00	0.00	0.30	56.79	0.09	0.39	0.06	0.00	0.06	0.00	103.07	103.07
#8	0.02	0.05	0.00	0.03	0.39	56.66	0.08	0.41	0.07	0.00	0.00	0.00	103.15	103.15
#9	0.04	0.01	0.03	0.00	0.39	56.18	0.09	0.34	0.05	0.02	0.00	0.00	102.19	102.19
#10	0.00	0.01	0.03	0.00	0.39	56.66	0.07	0.35	0.04	0.08	0.01	0.00	103.01	103.01

Element Oxide Wt%, Lisheen Carbonates, August 18,19th, 1997. Operating Parameters: 15kV, 15nA, 15µm.														
Pts 1-10, D5 Calc, 457/212.6.														
	P2O5	SiO2	SO2	Ce2O3	MgO	CaO	MnO	FeO	SrO	BaO	Na2O	K2O	CO2	TOTAL
#1	0.00	0.00	0.06	0.04	0.56	55.93	0.05	0.03	0.02	0.00	0.05	0.00	44.80	101.53
#2	0.03	0.00	0.00	0.00	0.46	56.62	0.05	0.00	0.04	0.07	0.01	0.00	45.17	102.45
#3	0.04	0.02	0.02	0.00	0.47	56.84	0.12	0.03	0.09	0.00	0.01	0.00	45.48	103.12
#4	0.00	0.00	0.02	0.05	0.50	56.59	0.03	0.03	0.04	0.00	0.03	0.00	45.20	102.50
#5	0.03	0.05	0.00	0.00	0.48	56.67	0.03	0.00	0.08	0.00	0.01	0.00	45.30	102.65
#6	0.00	0.03	0.08	0.00	0.33	55.92	0.07	0.02	0.07	0.04	0.02	0.00	44.62	101.21
#7	0.06	0.01	0.02	0.00	0.46	56.46	0.02	0.06	0.05	0.03	0.01	0.00	45.14	102.32
#8	0.08	0.01	0.04	0.00	0.52	56.29	0.06	0.00	0.04	0.03	0.00	0.00	45.11	102.18
#9	0.01	0.02	0.08	0.00	0.28	56.56	0.04	0.06	0.04	0.02	0.00	0.00	45.05	102.17
#10	0.02	0.00	0.02	0.01	0.45	56.61	0.10	0.03	0.04	0.00	0.00	0.02	45.20	102.49

Element Oxide Wt%, Lisheen Carbonates, August 18,19th, 1997. Operating Parameters: 15kV, 15nA, 15µm.														
Pts 1-10, D5 Calc, 463/173.0.														
	P2O5	SiO2	SO2	Ce2O3	MgO	CaO	MnO	FeO	SrO	BaO	Na2O	K2O	CO2	TOTAL
#1	0.00	0.00	0.00	0.05	0.32	55.50	0.11	0.88	0.26	0.04	0.00	0.00	44.76	101.93
#2	0.00	0.06	0.01	0.07	0.29	55.16	0.15	0.96	0.16	0.06	0.02	0.00	44.62	101.55
#3	0.07	0.02	0.00	0.10	0.37	54.25	0.18	1.10	0.16	0.03	0.00	0.00	44.12	100.41
#4	0.01	0.00	0.00	0.00	0.00	0.00	0.00	0.00	0.00	0.00	0.01	0.00	0.03	0.06
#5	0.00	0.02	0.03	0.07	0.41	55.04	0.13	1.19	0.18	0.05	0.03	0.00	44.78	101.95
#6	0.06	0.02	0.04	0.00	0.50	54.64	0.12	1.37	0.21	0.02	0.06	0.01	44.76	101.81
#7	0.05	0.00	0.00	0.07	0.22	55.00	0.04	1.41	0.16	0.05	0.02	0.01	44.61	101.65
#8	0.00	0.01	0.02	0.06	0.38	54.97	0.11	1.21	0.20	0.00	0.00	0.00	44.63	101.60
#9	0.02	0.00	0.03	0.00	0.24	55.22	0.02	1.26	0.16	0.00	0.00	0.00	44.63	101.58
#10	0.01	0.00	0.00	0.07	0.32	55.68	0.10	1.05	0.15	0.10	0.01	0.02	45.02	102.54

Element Oxide Wt%, Lisheen Carbonates, August 18,19th, 1997. Operating Parameters: 15kV, 15nA, 15µm.														
Pts 1-10, D5 Calc, 095/335.0.														
	P2O5	SiO2	SO2	Ce2O3	MgO	CaO	MnO	FeO	SrO	BaO	Na2O	K2O	CO2	TOTAL
#2	0.00	0.03	0.01	0.04	0.08	57.24	0.17	0.14	0.04	0.01	0.00	0.00	103.14	103.14
#3	0.03	0.02	0.06	0.01	0.06	57.79	0.07	0.06	0.04	0.00	0.03	0.00	103.96	103.96
#4	0.03	0.05	0.06	0.01	0.07	57.08	0.08	0.17	0.01	0.02	0.00	0.00	102.95	102.95
#5	0.02	0.05	0.00	0.00	0.04	57.41	0.10	0.09	0.03	0.00	0.00	0.01	103.20	103.20
#6	0.00	0.04	0.01	0.06	0.09	57.90	0.08	0.04	0.00	0.00	0.01	0.00	104.06	104.06
#7	0.01	0.05	0.00	0.05	0.09	57.47	0.13	0.13	0.02	0.00	0.02	0.00	103.56	103.56
#8	0.04	0.03	0.04	0.03	0.10	57.94	0.04	0.01	0.05	0.08	0.02	0.01	104.35	104.35
#9	0.04	0.02	0.02	0.00	0.15	57.22	0.14	0.08	0.02	0.04	0.00	0.00	103.20	103.20
#10	0.01	0.02	0.00	0.05	0.08	57.58	0.14	0.13	0.02	0.09	0.03	0.00	103.82	103.82

Element Oxide Wt%, Lisheen Carbonates, August 18,19th, 1997. Operating Parameters: 15kV, 15nA, 15µm.														
Pts 1-12, D5 Calc, 451/139.10.														
	P2O5	SiO2	SO2	Ce2O3	MgO	CaO	MnO	FeO	SrO	BaO	Na2O	K2O	CO2	TOTAL
#1	0.00	0.02	0.04	0.00	0.27	57.13	0.23	0.10	0.09	0.00	0.00	0.00	45.55	103.41
#2	0.00	0.05	0.00	0.03	0.28	57.97	0.18	0.01	0.05	0.05	0.01	0.01	46.16	104.80
#3	0.05	0.06	0.00	0.05	0.32	56.82	0.26	0.11	0.06	0.00	0.02	0.03	45.52	103.29
#4	0.05	0.00	0.04	0.00	0.20	57.77	0.17	0.10	0.07	0.00	0.01	0.00	46.01	104.42
#5	0.08	0.02	0.06	0.03	0.24	57.70	0.17	0.05	0.02	0.02	0.02	0.00	46.06	104.48
#6	0.01	0.08	0.04	0.08	0.34	56.83	0.11	0.16	0.04	0.02	0.08	0.03	45.57	103.40
#7	0.01	0.00	0.07	0.00	0.22	57.53	0.25	0.05	0.07	0.06	0.05	0.00	45.88	104.18
#9	0.05	0.07	0.01	0.00	0.28	57.57	0.25	0.05	0.03	0.03	0.05	0.01	46.03	104.41
#10	0.03	0.02	0.05	0.00	0.18	58.02	0.16	0.01	0.03	0.03	0.00	0.00	46.11	104.65
#12	0.08	0.02	0.09	0.12	0.09	57.95	0.09	0.04	0.09	0.05	0.00	0.00	46.14	104.75

Element Wt% Oxide, Lisheen Carbonates, August 18,19th, 1997. Operating Parameters:15kV, 15nA, 15µm.														
Pts 1-10, D5 Calc, 529/246.6.														
	P2O5	SiO2	SO2	Ce2O3	MgO	CaO	MnO	FeO	SrO	BaO	Na2O	K2O	CO2	TOTAL
#1	0.01	0.01	0.02	0.04	0.38	56.70	0.07	0.16	0.15	0.00	0.01	0.03	45.31	102.88
#2	0.03	0.00	0.00	0.01	0.29	57.10	0.09	0.08	0.12	0.01	0.04	0.00	45.48	103.26
#3	0.04	0.03	0.00	0.10	0.12	57.62	0.05	0.01	0.03	0.08	0.00	0.00	45.69	103.78
#4	0.00	0.04	0.03	0.08	0.41	56.84	0.05	0.16	0.18	0.00	0.01	0.00	45.51	103.32
#5	0.00	0.00	0.05	0.04	0.16	56.81	0.10	0.00	0.09	0.06	0.00	0.00	45.08	102.40
#6	0.06	0.00	0.01	0.00	0.35	56.78	0.01	0.03	0.15	0.06	0.00	0.00	45.27	102.72
#7	0.00	0.03	0.03	0.03	0.14	57.27	0.11	0.08	0.07	0.05	0.00	0.02	45.48	103.32
#8	0.01	0.04	0.03	0.00	0.32	56.62	0.08	0.12	0.12	0.02	0.00	0.00	45.18	102.52
#9	0.05	0.14	0.02	0.05	0.31	57.04	0.06	0.09	0.14	0.00	0.06	0.03	45.74	103.72
#10	0.03	0.03	0.00	0.03	0.33	56.82	0.06	0.15	0.12	0.02	0.05	0.00	45.38	103.01

B4. ELEMENTAL CHEMISTRY - GALMOY CARBONATES

Regional Replacement Dolomites and Carbonate Cements

Element Wt% Oxide, Galmoy Carbonates, Various August 1997. Operating Parameters: 15kV, 15nA, 15µm.														
Pts 1-10, D1Rep, MG63/97.2.														
	P2O5	SiO2	SO2	Ce2O3	MgO	CaO	MnO	FeO	SrO	BaO	Na2O	K2O	CO2	TOTAL
#1	0.04	1.04	0.02	0.01	19.88	31.80	0.02	0.23	0.02	0.04	0.02	0.14	48.64	101.91
#2	0.00	0.68	0.04	0.00	20.01	32.78	0.02	0.11	0.03	0.05	0.01	0.12	48.90	102.76
#4	0.05	0.76	0.02	0.00	19.60	32.52	0.17	0.87	0.04	0.03	0.03	0.16	49.03	103.27
#5	0.02	0.96	0.02	0.02	19.86	32.71	0.04	0.16	0.02	0.01	0.00	0.14	49.15	103.13
#7	0.00	0.91	0.05	0.03	20.14	32.19	0.01	0.28	0.03	0.00	0.02	0.12	49.02	102.79
#8	0.01	0.43	0.00	0.05	20.36	32.84	0.02	0.18	0.04	0.00	0.00	0.06	48.95	102.94
#9	0.01	0.80	0.09	0.00	20.29	32.51	0.04	0.25	0.03	0.01	0.05	0.15	49.39	103.61
#10	0.06	0.75	0.07	0.00	20.12	32.53	0.05	0.41	0.03	0.01	0.05	0.16	49.31	103.56

Element Wt% Oxide, Galmoy Carbonates, Various August 1997. Operating Parameters: 15kV, 15nA, 15µm.														
Pts 11-20, D1Rep, MG99/100.8.														
	P2O5	SiO2	SO2	Ce2O3	MgO	CaO	MnO	FeO	SrO	BaO	Na2O	K2O	CO2	TOTAL
#12	0.00	0.02	0.01	0.01	20.19	32.23	0.10	0.23	0.06	0.03	0.04	0.00	47.76	100.69
#13	0.05	0.79	0.15	0.00	18.13	34.63	0.00	0.12	0.00	0.04	0.12	0.08	48.72	102.83
#15	0.01	0.44	0.11	0.04	19.07	34.28	0.09	0.06	0.04	0.00	0.03	0.05	48.80	103.00
#16	0.07	0.77	0.09	0.03	18.49	34.62	0.04	0.15	0.03	0.05	0.07	0.15	49.08	103.61
#17	0.09	0.66	0.13	0.09	18.81	34.09	0.09	0.19	0.02	0.00	0.03	0.11	48.97	103.28
#18	0.03	1.80	0.02	0.03	18.80	32.72	0.01	0.15	0.00	0.00	0.04	0.39	49.35	103.36
#20	0.04	0.20	0.07	0.00	18.82	34.72	0.03	0.08	0.01	0.03	0.05	0.02	48.47	102.54

Dolomite Matrix Breccias

Element Wt% Oxide, Galmoy Carbonates, Various August 1997. Operating Parameters: 15kV, 15nA, 15µm.														
Pts1-10, D2 BMB, MG99/100.6.														
	P2O5	SiO2	SO2	Ce2O3	MgO	CaO	MnO	FeO	SrO	BaO	Na2O	K2O	CO2	TOTAL
#1	0.06	0.87	0.18	0.02	18.76	33.76	0.03	0.32	0.00	0.02	0.04	0.16	49.04	103.27
#2	0.02	1.77	0.15	0.05	18.07	33.32	0.07	0.42	0.00	0.02	0.04	0.29	49.31	103.54
#3	0.04	0.17	0.15	0.07	18.75	33.69	0.06	0.22	0.03	0.00	0.04	0.01	47.78	101.01
#5	0.02	3.19	0.48	0.02	17.80	30.79	0.12	0.82	0.01	0.00	0.05	0.61	49.97	103.88
#6	0.00	0.30	0.13	0.04	18.21	34.97	0.02	0.22	0.00	0.03	0.06	0.03	48.28	102.30
#7	0.05	0.42	0.09	0.00	18.82	34.40	0.06	0.21	0.03	0.01	0.03	0.07	48.71	102.90
#8	0.03	0.06	0.15	0.05	18.60	35.03	0.00	0.05	0.06	0.00	0.02	0.03	48.36	102.46
#9	0.03	0.60	0.10	0.07	18.88	34.06	0.02	0.39	0.02	0.00	0.05	0.11	48.90	103.24
#10	0.04	0.55	0.05	0.07	19.01	33.59	0.05	0.47	0.00	0.00	0.02	0.10	48.57	102.53

Element Wt% Oxide, Galmoy Carbonates, Various August 1997. Operating Parameters: 15kV, 15nA, 15µm.														
Pts11-20, D2 BMB, MG63/97.2.														
	P2O5	SiO2	SO2	Ce2O3	MgO	CaO	MnO	FeO	SrO	BaO	Na2O	K2O	CO2	TOTAL
#11	0.02	0.76	0.01	0.06	20.16	32.45	0.07	0.18	0.02	0.05	0.02	0.13	49.02	102.94
#15	0.02	1.45	0.30	0.06	19.71	32.07	0.06	0.63	0.02	0.00	0.04	0.24	49.97	104.57
#16	0.03	0.88	0.05	0.02	19.80	32.70	0.07	0.48	0.04	0.01	0.05	0.17	49.28	103.57
#17	0.05	2.87	0.07	0.04	18.93	31.21	0.08	0.68	0.01	0.10	0.31	0.47	50.63	105.46
#18	0.19	1.44	0.01	0.04	18.13	31.43	0.09	0.65	0.00	0.00	0.03	0.24	47.61	99.87
#19	0.03	0.33	0.07	0.00	19.37	33.84	0.06	0.29	0.03	0.00	0.23	0.07	48.89	103.22

Element Wt% Oxide, Galmoy Carbonates, August 18, 19th 1997. Operating Parameters: 15kV, 15nA, 15µm.														
Pts41-50, D2 BMB, 5.														
	P2O5	SiO2	SO2	Ce2O3	MgO	CaO	MnO	FeO	SrO	BaO	Na2O	K2O	CO2	TOTAL
#41	0.06	0.76	0.02	0.04	20.24	32.29	0.06	0.27	0.00	0.03	0.04	0.11	49.10	103.04
#42	0.02	0.33	0.03	0.06	20.55	32.64	0.03	0.28	0.05	0.00	0.02	0.07	49.00	103.09
#43	0.04	1.59	0.02	0.04	20.06	31.35	0.04	0.36	0.00	0.00	0.02	0.26	49.42	103.20
#44	0.05	0.08	0.02	0.04	20.49	33.03	0.04	0.20	0.03	0.04	0.00	0.02	48.82	102.86
#45	0.07	0.28	0.03	0.01	20.75	32.31	0.02	0.14	0.00	0.00	0.04	0.01	48.83	102.51
#46	0.08	0.39	0.01	0.02	20.21	32.71	0.04	0.25	0.00	0.00	0.03	0.09	48.80	102.63
#47	0.07	0.93	0.04	0.00	20.19	32.07	0.04	0.24	0.02	0.10	0.04	0.18	49.17	103.10
#48	0.03	0.25	0.07	0.08	20.54	32.05	0.01	0.21	0.01	0.01	0.01	0.05	48.41	101.75
#49	0.07	0.91	0.01	0.04	20.23	32.43	0.02	0.14	0.03	0.07	0.02	0.15	49.33	103.44
#50	0.07	1.81	0.00	0.03	19.65	31.61	0.03	0.49	0.00	0.08	0.03	0.34	49.68	103.83

Element Wt% Oxide, Galmoy Carbonates, August 18,19th 1997. Operating Parameters: 15kV, 15nA, 15µm.														
Pts1-10, D3 WMB, GY355/97.0.														
	P2O5	SiO2	SO2	Ce2O3	MgO	CaO	MnO	FeO	SrO	BaO	Na2O	K2O	CO2	TOTAL
#1	0.03	0.03	0.00	0.01	21.42	31.57	0.05	0.00	0.02	0.00	0.00	0.00	48.39	101.51
#2	0.00	0.00	0.04	0.01	21.54	31.72	0.01	0.01	0.00	0.02	0.01	0.01	48.60	101.98
#3	0.03	0.00	0.03	0.00	20.58	32.79	0.02	0.02	0.06	0.04	0.02	0.00	48.47	102.06
#4	0.02	0.02	0.03	0.02	20.92	32.29	0.01	0.02	0.02	0.00	0.04	0.00	48.45	101.84
#5	0.01	0.00	0.03	0.00	20.83	32.57	0.02	0.02	0.00	0.00	0.03	0.00	48.51	102.02
#7	0.00	0.01	0.00	0.00	21.19	32.24	0.04	0.04	0.01	0.00	0.01	0.02	48.63	102.19
#8	0.03	0.02	0.03	0.00	21.19	32.08	0.00	0.00	0.02	0.03	0.03	0.01	48.59	102.05
#9	0.00	0.00	0.00	0.06	20.90	32.27	0.06	0.00	0.02	0.01	0.00	0.01	48.33	101.67
#10	0.00	0.00	0.02	0.05	21.11	32.23	0.00	0.00	0.02	0.04	0.02	0.00	48.54	102.04

Element Wt% Oxide, Galmoy Carbonates, Various August 1997. Operating Parameters: 15kV, 15nA, 15µm.														
Pts 31-40, D3 WMB, MG99/100.8.														
	P2O5	SiO2	SO2	Ce2O3	MgO	CaO	MnO	FeO	SrO	BaO	Na2O	K2O	CO2	TOTAL
#1	0.01	0.02	0.00	0.04	20.58	32.48	0.10	0.07	0.02	0.00	0.01	0.00	48.25	101.58
#2	0.00	0.03	0.04	0.02	20.29	32.09	0.20	0.15	0.02	0.01	0.00	0.00	47.78	100.64
#3	0.00	0.00	0.00	0.01	20.68	31.92	0.18	0.13	0.01	0.10	0.03	0.00	47.99	101.04
#4	0.00	0.02	0.00	0.00	20.74	32.21	0.08	0.00	0.04	0.11	0.03	0.02	48.19	101.46
#5	0.01	0.00	0.01	0.05	20.79	32.73	0.07	0.00	0.01	0.00	0.07	0.00	48.65	102.40
#6	0.04	0.05	0.03	0.04	20.52	32.41	0.03	0.00	0.06	0.00	0.03	0.00	48.19	101.38
#7	0.01	0.00	0.02	0.04	21.15	32.25	0.10	0.00	0.00	0.01	0.00	0.00	48.64	102.22
#8	0.01	0.02	0.00	0.02	20.58	32.18	0.20	0.06	0.05	0.00	0.01	0.00	48.08	101.21
#9	0.03	0.00	0.00	0.05	20.90	32.14	0.08	0.01	0.04	0.06	0.04	0.00	48.34	101.69
#10	0.00	0.01	0.02	0.00	20.80	32.35	0.06	0.00	0.05	0.00	0.02	0.00	48.31	101.62

Pink Dolomite

Element Wt% Oxide, Galmoy Carbonates, August 18,19th 1997. Operating Parameters: 15kV, 15nA, 15µm.														
Pts11-20, D4 PINK, GY355/97.0.														
	P2O5	SiO2	SO2	Ce2O3	MgO	CaO	MnO	FeO	SrO	BaO	Na2O	K2O	CO2	TOTAL
#11	0.06	0.04	0.03	0.00	20.52	31.42	0.22	0.70	0.00	0.08	0.00	0.00	47.94	101.01
#12	0.00	0.00	0.00	0.04	20.68	31.68	0.09	0.82	0.00	0.00	0.01	0.03	48.14	101.49
#13	0.01	0.02	0.03	0.00	20.83	31.21	0.16	0.72	0.02	0.04	0.03	0.00	48.03	101.12
#14	0.06	0.00	0.00	0.00	20.93	31.54	0.18	0.62	0.03	0.06	0.00	0.04	48.35	101.82
#15	0.02	0.01	0.05	0.00	20.46	32.09	0.23	0.70	0.01	0.02	0.00	0.00	48.33	101.94
#16	0.01	0.02	0.02	0.05	20.18	31.13	0.22	0.72	0.04	0.02	0.06	0.01	47.31	99.80
#17	0.01	0.02	0.02	0.00	20.85	31.24	0.13	0.44	0.03	0.01	0.02	0.00	47.84	100.62
#18	0.00	0.00	0.01	0.03	20.39	31.76	0.20	0.55	0.02	0.08	0.03	0.01	47.84	100.93
#19	0.04	0.01	0.00	0.00	20.73	31.70	0.16	0.58	0.00	0.05	0.07	0.03	48.23	101.60
#20	0.05	0.04	0.00	0.00	20.71	31.33	0.10	0.74	0.00	0.01	0.02	0.01	47.97	100.97

Late, Minor Vein and Vug Dolomite

Element Wt% Oxide, Galmoy Carbonates, August 18,19th, 1997. Operating Parameters: 15kV, 15nA, 15µm.															
Pts 1-10, D5Dol, GY333/103.3.															
	P2O5	SiO2	SO2	Ce2O3	MgO	CaO	MnO	FeO	FeO	SrO	BaO	Na2O	K2O	CO2	TOTAL
#1	0.03	0.01	0.00	0.00	0.63	71.43	0.11	0.39	0.39	0.01	0.04	0.01	0.03	29.42	102.51
#2	0.04	0.00	0.05	0.04	15.77	43.09	0.20	3.83	3.83	0.03	0.00	0.00	0.00	33.37	100.26
#3	0.01	0.00	0.02	0.06	15.38	43.45	0.28	5.03	5.03	0.02	0.06	0.00	0.01	32.61	101.95
#4	0.00	0.03	0.03	0.00	15.54	42.93	0.26	4.92	4.92	0.01	0.01	0.00	0.01	32.60	101.25
#5	0.02	0.02	0.01	0.12	15.12	42.97	0.28	5.22	5.22	0.04	0.05	0.01	0.01	32.13	101.22
#6	0.02	0.04	0.02	0.07	15.71	43.86	0.21	3.92	3.92	0.03	0.07	0.00	0.01	33.62	101.49
#7	0.01	0.00	0.03	0.03	15.44	42.84	0.26	5.01	5.01	0.02	0.06	0.04	0.01	32.46	101.23
#8	0.00	0.00	0.02	0.00	15.27	43.19	0.23	4.92	4.92	0.02	0.01	0.00	0.01	32.35	100.95
#9	0.02	0.00	0.04	0.00	15.10	43.04	0.27	5.14	5.14	0.01	0.11	0.00	0.00	32.12	100.98
#10	0.01	0.03	0.03	0.01	15.54	43.72	0.24	4.40	4.40	0.02	0.02	0.01	0.00	33.14	101.56

Element Wt% Oxide, Galmoy Carbonates, August 18,19th, 1997. Operating Parameters: 15kV, 15nA, 15µm.														
Pts 1-10, D5 Dol, G16-27/383.3.														
	P2O5	SiO2	SO2	Ce2O3	MgO	CaO	MnO	FeO	SrO	BaO	Na2O	K2O	CO2	TOTAL
#1	0.03	0.00	0.04	0.04	20.57	31.10	0.25	0.30	0.05	0.05	0.05	0.00	99.98	99.98
#2	0.00	0.02	0.00	0.00	20.90	32.16	0.19	0.11	0.00	0.00	0.00	0.00	101.77	101.77
#3	0.00	0.06	0.05	0.03	20.03	31.21	0.27	1.22	0.02	0.10	0.00	0.01	100.57	100.57
#4	0.05	0.01	0.00	0.06	20.09	31.35	0.24	1.22	0.03	0.02	0.00	0.00	100.75	100.75
#5	0.01	0.04	0.02	0.00	21.14	32.13	0.18	0.00	0.02	0.05	0.01	0.00	102.28	102.28
#6	0.05	0.00	0.00	0.00	20.02	31.37	0.21	0.88	0.05	0.00	0.03	0.01	99.99	99.99
#7	0.00	0.02	0.03	0.01	20.87	32.10	0.22	0.07	0.08	0.02	0.08	0.02	101.97	101.97
#8	0.05	0.00	0.00	0.00	20.41	32.77	0.24	0.01	0.06	0.05	0.01	0.02	102.00	102.00
#9	0.00	0.00	0.05	0.04	20.54	32.68	0.22	0.01	0.03	0.00	0.02	0.00	102.02	102.02
#10	0.04	0.04	0.05	0.00	19.93	32.58	0.21	0.03	0.05	0.03	0.05	0.00	100.85	100.85

Element Wt% Oxide, Galmoy Carbonates, January 1998. Operating Parameters: 15kV, 15nA, 15µm.													
Pts 21-50, D3 Dol, MG63/97.2.													
	CaO	MgO	Na2O	SO2	K2O	SrO	MnO	FeO	NiO	CdO	BaO	CO2	TOTAL
#23	32.02	19.53	0.01	0.02	0.09	0.06	0.03	0.27		0.02	0.11	46.78	98.94
#24	32.08	19.48	0.03	0.07	0.10		0.02	0.22	0.02	0.00	0.07	46.78	98.85
#25	32.26	19.72	0.01	0.04	0.09	0.05	0.08	0.19	0.02		0.00	47.15	99.61
#26	33.02	19.14	0.03	0.07	0.11	0.03	0.04	0.19		0.02		47.13	99.77
#27	31.97	19.61	0.04	0.01	0.12		0.06	0.23			0.02	46.77	98.82
#29	32.55	19.89	0.00			0.02	0.10	0.12			0.04	47.41	100.12
#30	31.38	18.84		0.02	0.03	0.03	0.16	0.25	0.06	0.01		45.52	96.28
#31	32.46	19.46			0.08	0.03	0.18	0.12		0.02	0.03	46.97	99.35
#32	32.64	19.11	0.00	0.01	0.03	0.02	0.10	0.42	0.01			46.84	99.17
#33	32.94	19.31	0.00	0.00	0.01	0.01	0.14	0.35	0.05	0.02	0.07	47.31	100.21
#35	32.08	18.97	0.01	0.01	0.01		0.24	0.77	0.12	0.01	0.04	46.61	98.86
#36	31.96	19.24	0.00	0.01	0.01	0.04	0.25	0.75		0.04		46.75	99.03
#37	32.12	19.18	0.01	0.03	0.00		0.11	0.71			0.02	46.70	98.87
#38	36.17	16.75		0.01	0.00	0.04	0.16	0.48	0.07	0.00		47.14	100.82
#39	32.18	19.10	0.01			0.02	0.15	0.81	0.04		0.04	46.73	99.07
#40	33.27	19.50	0.02		0.01	0.07	0.07	0.15		0.02		47.59	100.71
#42	31.96	19.54	0.02	0.03	0.13		0.06	0.29	0.07	0.02	0.01	46.80	98.93
#43	32.97	18.67	0.01	0.04	0.12	0.00	0.06	0.33				46.62	98.83
#44	31.96	18.86		0.10	0.19	0.01	0.09	0.45	0.00	0.02	0.01	46.24	97.93
#45	32.42	19.52	0.04	0.07	0.12		0.02	0.22			0.06	47.10	99.58
#47	32.44	19.38	0.05	0.04	0.09	0.02	0.03	0.16			0.03	46.88	99.12
#49	32.60	19.00	0.02	0.05	0.07		0.03	0.23	0.04		0.01	46.62	98.66
#50	33.08	19.58	0.03	0.03	0.06		0.07	0.40	0.05	0.05	0.01	47.76	101.12

Element Wt% Oxide, Galmoy Carbonates, August 18,19th, 1997. Operating Parameters: 15kV, 15nA, 15µm.														
Pts 31-40, D5 Dol, 5.														
	P2O5	SiO2	SO2	Ce2O3	MgO	CaO	MnO	FeO	SrO	BaO	Na2O	K2O	CO2	TOTAL
#31	0.02	0.02	0.00	0.01	20.55	32.96	0.08	0.08	0.08	0.01	0.04	0.00	48.63	102.46
#32	0.00	0.00	0.02	0.04	20.54	33.18	0.04	0.07	0.06	0.00	0.01	0.03	48.73	102.71
#33	0.00	0.00	0.00	0.00	20.66	33.21	0.07	0.06	0.05	0.01	0.01	0.01	48.86	102.95
#34	0.02	0.00	0.04	0.07	20.66	33.23	0.00	0.00	0.05	0.08	0.00	0.01	48.90	103.05
#35	0.00	0.00	0.04	0.00	20.36	33.21	0.03	0.00	0.03	0.02	0.05	0.00	48.53	102.28
#36	0.03	0.08	0.03	0.01	20.91	32.81	0.05	0.04	0.03	0.00	0.01	0.01	48.97	102.97
#37	0.00	0.04	0.04	0.04	19.78	33.56	0.10	0.02	0.09	0.00	0.02	0.01	48.30	101.98
#38	0.00	0.01	0.01	0.03	20.13	33.65	0.02	0.06	0.03	0.08	0.00	0.00	48.62	102.64
#39	0.01	0.00	0.01	0.00	20.27	33.75	0.00	0.01	0.04	0.05	0.00	0.00	48.80	102.95
#40	0.02	0.02	0.00	0.01	20.89	32.95	0.09	0.00	0.05	0.02	0.02	0.00	48.94	103.01

Late, Minor Vein and Vug Calcite

Element Wt% Oxide, Galmoy Carbonates, August 18,19th, 1997. Operating Parameters: 15kV, 15nA, 15µm.															
Pts11-20, D5 Calc, GY333/103.3.															
	P2O5	SiO2	SO2	Ce2O3	MgO	CaO	MnO	FeO	FeO	SrO	BaO	Na2O	K2O	CO2	TOTAL
#11	0.00	0.06	0.01	0.05	0.22	71.65	0.09	0.30	0.30	0.02	0.04	0.02	0.00	29.14	101.91
#12	0.01	0.01	0.03	0.01	0.20	71.18	0.09	0.51	0.51	0.03	0.01	0.02	0.00	28.79	101.41
#13	0.00	0.00	0.00	0.03	0.15	71.37	0.09	0.32	0.32	0.00	0.00	0.02	0.02	28.82	101.12
#14	0.07	0.03	0.03	0.08	0.16	71.89	0.11	0.31	0.31	0.05	0.04	0.03	0.02	29.30	102.42
#15	0.00	0.00	0.05	0.05	0.23	71.34	0.04	0.38	0.38	0.03	0.02	0.04	0.01	28.94	101.51
#16	0.00	0.01	0.02	0.00	0.17	71.86	0.13	0.37	0.37	0.03	0.02	0.03	0.01	29.10	102.11
#17	0.05	0.01	0.00	0.05	0.12	72.51	0.09	0.22	0.22	0.02	0.00	0.01	0.00	29.38	102.68
#18	0.00	0.08	0.00	0.04	0.11	71.77	0.17	0.39	0.39	0.02	0.02	0.01	0.01	29.07	102.09
#19	0.01	0.02	0.00	0.02	0.15	71.96	0.07	0.28	0.28	0.04	0.02	0.00	0.00	29.08	101.93
#20	0.04	0.03	0.00	0.05	0.13	72.06	0.08	0.26	0.26	0.05	0.05	0.00	0.00	29.22	102.24

Element Wt% Oxide, Galmoy Carbonates, August 18,19th, 1997. Operating Parameters: 15kV, 15nA, 15µm.															
Pts 21-30, D5Calc, GY333/103.3.															
	P2O5	SiO2	SO2	Ce2O3	MgO	CaO	MnO	FeO	FeO	SrO	BaO	Na2O	K2O	CO2	TOTAL
#21	0.04	0.02	0.00	0.00	0.26	70.14	0.14	0.32	0.32	0.06	0.00	0.00	0.00	28.54	99.85
#22	0.03	0.00	0.01	0.03	0.25	70.82	0.13	0.35	0.35	0.07	0.00	0.02	0.02	28.80	100.87
#23	0.08	0.00	0.02	0.04	0.40	69.71	0.11	0.30	0.30	0.04	0.05	0.04	0.00	28.64	99.74
#24	0.00	0.00	0.00	0.00	0.32	70.32	0.15	0.35	0.35	0.03	0.00	0.00	0.00	28.58	100.11
#25	0.03	0.02	0.01	0.01	0.27	70.34	0.08	0.27	0.27	0.06	0.14	0.00	0.00	28.67	100.17
#26	0.00	0.00	0.00	0.09	0.27	70.82	0.05	0.29	0.29	0.06	0.07	0.01	0.01	28.78	100.76
#27	0.04	0.05	0.00	0.00	0.15	71.74	0.07	0.25	0.25	0.07	0.05	0.03	0.01	29.14	101.85
#28	0.01	0.07	0.03	0.08	0.21	71.19	0.12	0.23	0.23	0.04	0.05	0.01	0.00	29.05	101.31
#29	0.02	0.02	0.04	0.05	0.20	71.15	0.12	0.19	0.19	0.05	0.00	0.01	0.01	29.00	101.07
#30	0.03	0.00	0.03	0.02	0.30	71.61	0.12	0.33	0.33	0.06	0.01	0.00	0.00	29.18	102.02

B5. ELEMENTAL CHEMISTRY - RATHDOWNEY TREND PROSPECT CARBONATES

Regional Replacement Dolomites and Carbonate Cements

Element Wt% Oxide, Prospects Carbonates, Rathdowney East, October 1996. Operating Parameters: 15kV, 15nA, 25µm.														
Pts 44-54, D1Rep, RE24/1625.														
	P2O5	SO2	Ce2O3	MgO	CaO	MnO	FeO	SrO	CdO	BaO	Na2O	K2O	CO2	TOTAL
#44	0.00	0.08	0.00	19.77	33.08	0.13	0.22	0.00	0.04	0.00	0.01	0.13	48.05	101.50
#45	0.01	0.00	0.00	20.04	32.36	0.01	0.25	0.00	0.00	0.00	0.09	0.16	47.69	100.60
#46	0.08	0.04	0.07	19.94	31.51	0.00	0.27	0.07	0.00	0.08	0.04	0.30	47.18	99.58
#47	0.01	0.08	0.05	20.15	32.43	0.11	0.38	0.05	0.00	0.00	0.02	0.00	48.03	101.31
#48	0.00	0.00	0.04	20.16	31.89	0.06	0.19	0.00	0.00	0.03	0.04	0.17	47.43	100.01
#49	0.01	0.08	0.05	20.15	32.43	0.11	0.38	0.05	0.00	0.00	0.02	0.00	48.03	101.31
#50	0.00	0.00	0.04	19.83	32.95	0.03	0.16	0.00	0.03	0.06	0.02	0.13	47.85	101.11
#51	0.00	0.07	0.01	19.36	32.71	0.02	0.35	0.00	0.02	0.05	0.03	0.29	47.41	100.31
#53	0.00	0.06	0.02	19.51	32.08	0.00	0.28	0.02	0.01	0.01	0.00	0.34	47.01	99.34
#54	0.01	0.00	0.02	20.41	32.79	0.04	0.11	0.06	0.00	0.02	0.04	0.05	48.32	101.86

Element Wt% Oxide, Prospects Carbonates, Rathdowney East, October 1996. Operating Parameters: 15kV, 15nA, 25µm.														
Pts 1-10, D1Rep, RE24/1320.														
	P2O5	SO2	Ce2O3	MgO	CaO	MnO	FeO	SrO	CdO	BaO	Na2O	K2O	CO2	TOTAL
#1	0.05	0.01	0.07	20.31	32.05	0.03	0.06	0.00	0.00	0.06	0.02	0.01	47.65	100.33
#2	0.10	0.06	0.03	20.51	31.94	0.00	0.11	0.00	0.07	0.08	0.01	0.02	47.94	100.87
#3	0.00	0.01	0.00	20.77	32.37	0.02	0.03	0.02	0.02	0.01	0.02	0.01	48.26	101.54
#4	0.04	0.04	0.03	20.35	32.72	0.00	0.03	0.02	0.01	0.00	0.07	0.00	48.20	101.52
#5	0.08	0.00	0.00	20.62	31.85	0.02	0.02	0.02	0.00	0.05	0.04	0.00	47.81	100.52
#6	0.01	0.04	0.01	20.42	32.37	0.01	0.00	0.00	0.05	0.00	0.04	0.02	47.92	100.88
#7	0.16	0.00	0.07	20.31	32.02	0.03	0.04	0.00	0.04	0.02	0.03	0.01	47.78	100.51
#8	0.04	0.04	0.00	20.49	32.47	0.04	0.00	0.00	0.05	0.05	0.03	0.01	48.15	101.36
#9	0.14	0.15	0.01	20.28	32.54	0.04	0.08	0.00	0.00	0.00	0.03	0.00	48.31	101.59
#10	0.08	0.00	0.06	20.56	32.37	0.05	0.09	0.00	0.00	0.09	0.06	0.05	48.30	101.72

Element Wt% Oxide, Prospects Carbonates, Rathdowney East, October 1996. Operating Parameters: 15kV, 15nA, 15µm.														
Pts 11-21, D1Cem, RE24/1320.0.														
	P2O5	SO2	Ce2O3	MgO	CaO	MnO	FeO	SrO	CdO	BaO	Na2O	K2O	CO2	TOTAL
#11	0.07	0.00	0.04	20.77	32.50	0.06	0.05	0.00	0.01	0.01	0.00	0.01	48.49	102.01
#12	0.04	0.00	0.12	20.64	32.47	0.01	0.06	0.04	0.00	0.05	0.01	0.00	48.31	101.74
#13	0.01	0.03	0.03	20.49	32.07	0.03	0.00	0.00	0.03	0.00	0.01	0.00	47.74	100.44
#14	0.00	0.01	0.00	20.56	32.32	0.03	0.06	0.04	0.01	0.03	0.00	0.00	48.03	101.11
#15	0.05	0.00	0.02	20.57	32.53	0.08	0.03	0.02	0.01	0.00	0.00	0.03	48.27	101.61
#16	0.05	0.00	0.00	20.83	32.55	0.00	0.07	0.02	0.06	0.02	0.00	0.00	48.56	102.16
#17	0.05	0.01	0.00	20.42	32.83	0.00	0.06	0.00	0.00	0.01	0.02	0.01	48.31	101.71
#18	0.04	0.00	0.09	20.24	32.67	0.00	0.05	0.04	0.00	0.00	0.03	0.00	48.01	101.17
#19	0.08	0.00	0.03	20.53	32.84	0.03	0.00	0.00	0.00	0.04	0.00	0.00	48.47	102.02
#20	0.00	0.00	0.00	20.21	32.28	0.00	0.00	0.02	0.00	0.00	0.06	0.02	47.56	100.15
#21	0.00	0.01	0.07	20.46	32.63	0.05	0.02	0.00	0.02	0.05	0.04	0.00	48.18	101.52

Element Wt% Oxide, Prospect Carbonates, Holycross, September 1996. Operating Parameters: 15kV, 15nA, 30µm.															
Pts 16-30, D1Rep, HC5/122.9.															
	P2O5	SiO2	SO2	Ce2O3	MgO	CaO	MnO	FeO	SrO	CdO	BaO	Na2O	K2O	CO2	TOTAL
#16	0.00	0.04	0.04	0.00	20.28	32.32	0.00	0.10	0.02	0.06	0.02	0.00	0.00	100.69	100.69
#17	0.01	0.02	0.00	0.05	20.50	32.23	0.00	0.18	0.03	0.02	0.03	0.01	0.00	101.08	101.08
#18	0.02	0.00	0.07	0.03	20.50	32.31	0.03	0.07	0.03	0.05	0.03	0.01	0.00	101.24	101.24
#20	0.02	0.25	0.15	0.00	19.96	32.14	0.05	0.35	0.01	0.00	0.00	0.01	0.02	100.95	100.95
#21	0.02	0.08	0.04	0.00	20.16	32.51	0.00	0.05	0.04	0.05	0.04	0.04	0.00	101.00	101.00
#22	0.04	0.08	0.07	0.03	19.50	32.54	0.02	0.06	0.03	0.03	0.00	0.03	0.02	99.77	99.77
#23	0.01	0.51	0.04	0.03	19.25	32.07	0.08	0.67	0.01	0.00	0.02	0.04	0.09	100.48	100.48
#24	0.02	0.06	0.00	0.05	20.01	32.39	0.05	0.09	0.07	0.00	0.00	0.02	0.01	100.43	100.43
#25	0.00	0.21	0.10	0.00	19.95	32.49	0.00	0.23	0.00	0.08	0.01	0.06	0.05	101.27	101.27
#26	0.00	0.00	0.01	0.07	20.26	32.23	0.12	0.15	0.06	0.00	0.04	0.00	0.00	100.72	100.72
#27	0.03	0.00	0.00	0.06	20.12	32.86	0.00	0.00	0.02	0.07	0.00	0.02	0.01	101.18	101.18
#28	0.00	0.18	0.00	0.06	19.88	32.64	0.04	0.01	0.04	0.00	0.05	0.02	0.03	100.76	100.76
#29	0.02	0.37	0.04	0.05	20.31	32.12	0.04	0.07	0.00	0.00	0.00	0.01	0.05	101.31	101.31
#30	0.00	0.20	0.02	0.03	20.42	32.39	0.11	0.13	0.03	0.00	0.05	0.00	0.02	101.74	101.74

Dolomite Matrix Breccias

Element Wt% Oxide, Prospects carbonates, Various August 1997. Operating Parameters: 15kV, 15nA, 15µm.														
Pts 11-20, D2 BMB, HC13/115.3.														
	P2O5	SiO2	SO2	Ce2O3	MgO	CaO	MnO	FeO	SrO	BaO	Na2O	K2O	CO2	TOTAL
#11	0.02	0.03	0.00	0.02	20.76	32.29	0.04	0.02	0.05	0.08	0.00	0.02	48.30	101.63
#12	0.05	0.03	0.00	0.03	20.75	31.86	0.05	0.03	0.01	0.01	0.02	0.03	47.98	100.84
#13	0.04	0.35	0.05	0.00	20.93	31.75	0.02	0.02	0.00	0.03	0.00	0.02	48.57	101.79
#14	0.01	0.95	0.01	0.00	20.52	31.37	0.01	0.02	0.02	0.00	0.03	0.01	48.61	101.57
#15	0.02	0.13	0.01	0.00	18.74	34.90	0.09	0.07	0.03	0.04	0.03	0.01	48.33	102.39
#16	0.00	0.00	0.00	0.02	20.29	32.77	0.03	0.00	0.00	0.00	0.01	0.02	48.02	101.16
#17	0.00	0.11	0.00	0.00	20.70	32.14	0.08	0.08	0.02	0.06	0.01	0.02	48.23	101.45
#20	0.05	0.51	0.02	0.03	20.39	31.92	0.00	0.09	0.03	0.02	0.05	0.04	48.41	101.57

Element Wt% Oxide, Prospect Carbonates, Holycross, September 1996. Operating Parameters: 15kV, 15nA, 30µm.															
Pts 76-88, D2 BMB, HC3569-2/293.1.															
	P2O5	SiO2	SO2	Ce2O3	MgO	CaO	MnO	FeO	SrO	CdO	BaO	Na2O	K2O	CO2	TOTAL
#76	0.00	0.01	0.00	0.10	19.09	30.55	0.30	1.36	0.00	0.09	0.00	0.04	0.00	46.02	97.56
#77	0.00	0.00	0.02	0.01	19.11	30.48	0.23	1.41	0.05	0.07	0.00	0.00	0.00	45.95	97.33
#79	0.00	0.00	0.10	0.02	18.99	30.47	0.37	1.50	0.03	0.03	0.00	0.03	0.00	46.06	97.60
#80	0.02	0.01	0.07	0.02	19.17	31.20	0.23	1.26	0.02	0.00	0.05	0.00	0.00	46.57	98.61
#81	0.06	0.00	0.03	0.02	18.48	31.86	0.17	1.40	0.00	0.04	0.00	0.02	0.00	46.38	98.45
#82	0.07	0.01	0.02	0.00	19.12	30.91	0.28	1.56	0.00	0.00	0.00	0.03	0.01	46.50	98.50
#83	0.04	0.00	0.06	0.01	18.79	30.80	0.31	1.62	0.03	0.00	0.00	0.01	0.00	46.12	97.79
#84	0.00	0.00	0.07	0.04	19.23	30.61	0.27	1.35	0.00	0.00	0.12	0.01	0.01	46.26	97.99
#85	0.02	0.02	0.04	0.00	18.94	30.72	0.25	1.42	0.04	0.00	0.00	0.03	0.00	46.05	97.54
#86	0.01	0.03	0.00	0.01	19.23	30.46	0.27	1.26	0.06	0.11	0.01	0.03	0.02	46.07	97.56
#87	0.05	0.04	0.06	0.00	18.88	30.89	0.28	1.58	0.05	0.10	0.00	0.00	0.00	46.35	98.29
#88	0.02	0.00	0.00	0.07	19.40	30.16	0.10	1.35	0.06	0.00	0.01	0.01	0.00	45.92	97.11

Element Wt% Oxide, Prospect Carbonates, Holycross, September 1996. Operating Parameters: 15kV, 15nA, 30µm.															
Pts 89-98, D4 Pink HC3569-2/293.															
	P2O5	SiO2	SO2	Ce2O3	MgO	CaO	MnO	FeO	SrO	CdO	BaO	Na2O	K2O	CO2	TOTAL
#89	0.00	0.15	0.00	0.08	18.61	30.48	0.34	2.01	0.03	0.00	0.00	0.00	0.03	46.03	97.76
#90	0.02	0.00	0.05	0.00	19.11	30.51	0.34	1.53	0.00	0.06	0.00	0.01	0.00	46.16	97.80
#91	0.04	0.02	0.05	0.06	18.87	30.70	0.30	1.96	0.00	0.01	0.01	0.00	0.01	46.35	98.38
#93	0.00	0.12	0.09	0.05	19.03	30.40	0.28	1.95	0.06	0.03	0.00	0.01	0.02	46.47	98.54
#94	0.09	0.68	0.03	0.01	19.11	30.80	0.31	1.45	0.02	0.00	0.05	0.04	0.10	47.47	100.16
#95	0.01	0.00	0.03	0.00	18.87	30.49	0.30	1.83	0.00	0.04	0.00	0.00	0.02	46.21	97.81
#96	0.04	0.18	0.00	0.00	19.10	30.84	0.27	1.70	0.03	0.03	0.00	0.00	0.02	46.70	98.90
#97	0.02	0.08	0.00	0.02	19.35	30.08	0.32	1.55	0.00	0.00	0.01	0.03	0.01	46.14	97.61
#98	0.08	0.40	0.00	0.03	18.82	30.15	0.31	1.62	0.05	0.00	0.00	0.04	0.06	46.26	97.80

Element Wt% Oxide, Prospects Carbonates, January 1998. Operating Parameters: 15kV, 15nA, 15µm.													
Pts 1-20, D3 WMB, 1/686.5.													
	CaO	MgO	Na2O	SO2	K2O	SrO	MnO	FeO	NiO	CdO	BaO	CO2	TOTAL
#1	30.69	20.73	0.02	0.02	0.00	0.03	0.00	0.06			0.04	46.81	98.40
#4	31.24	20.08	0.01		0.01	0.03	0.03	0.03		0.01		46.50	97.94
#5	31.24	20.03		0.03	0.02	0.04	0.04	0.01	0.07		0.02	46.52	98.01
#6	31.53	19.89	0.02	0.03		0.00	0.01	0.00	0.00			46.52	98.01
#7	31.13	20.18		0.02		0.06	0.01	0.00		0.03	0.03	46.54	98.00
#8	31.02	20.30	0.04		0.00	0.04	0.03	0.00	0.05	0.04	0.07	46.63	98.21
#9	30.47	20.40				0.02	0.05	0.16		0.07	0.04	46.36	97.57
#10	30.95	20.57	0.02		0.01	0.02	0.00	0.01	0.09			46.83	98.50
#11	30.95	20.33	0.04	0.02		0.02	0.02	0.05	0.08		0.02	46.65	98.17
#12	31.78	19.74	0.00	0.03	0.00	0.03	0.00	0.00		0.00	0.03	46.56	98.18
#13	31.38	20.08	0.02			0.02	0.03	0.03	0.01	0.04		46.62	98.22
#15	31.20	20.18	0.00	0.01	0.01	0.03	0.00	0.01		0.04	0.03	46.58	98.10
#16	32.35	19.52	0.02	0.00		0.06	0.03	0.04				46.78	98.80
#18	31.49	19.95	0.01	0.03	0.00	0.04	0.02	0.00	0.04		0.02	46.60	98.21
#19	31.55	19.93				0.06	0.04	0.00	0.04		0.06	46.61	98.29
#20	31.92	20.28	0.03	0.02	0.01	0.03	0.05	0.03	0.03	0.02	0.01	47.32	99.73

Element Wt% Oxide, Prospects Carbonates, January 1998. Operating Parameters: 15kV, 15nA, 15µm.													
Pts 21-40, D3 WMB, 4/365.5.													
	CaO	MgO	Na2O	SO2	K2O	SrO	MnO	FeO	NiO	CdO	BaO	CO2	TOTAL
#21	32.09	17.87	0.02	0.03	0.01	0.03	0.22	1.94	0.01	0.03	0.08	46.13	98.47
#22	32.19	18.33	0.00	0.01		0.06	0.27	2.20			0.02	46.83	99.90
#23	31.76	20.55	0.01	0.00	0.01		0.15	0.35	0.05	0.01	0.08	47.73	100.69
#25	31.76	20.97	0.01	0.03	0.00	0.02	0.08	0.06	0.01		0.02	47.96	100.90
#27	31.46	20.41	0.01	0.02		0.06	0.05	0.23	0.03			47.22	99.49
#28	31.18	20.57	0.00	0.02		0.03	0.04	0.18	0.01			47.10	99.13
#29	31.68	21.08	0.01			0.05	0.00	0.09			0.05	47.97	100.92
#30	31.82	20.61	0.02	0.01		0.00	0.01	0.00			0.06	47.52	100.04
#31	31.91	20.60	0.01	0.03		0.02	0.03	0.05	0.00		0.02	47.65	100.32
#32	31.89	20.58	0.04	0.03		0.03	0.03	0.00	0.09	0.03		47.65	100.36
#33	31.45	20.41		0.02	0.00	0.03	0.00	0.03	0.02		0.02	47.04	99.01
#34	31.73	20.38	0.01	0.01		0.04	0.03	0.18			0.05	47.34	99.79
#35	32.28	20.53	0.01	0.05	0.01	0.07	0.00	0.04	0.01		0.03	47.89	100.91
#36	32.27	20.61	0.02	0.01		0.06	0.02	0.00	0.04	0.01	0.04	47.94	101.04
#37	32.71	20.62		0.02		0.03	0.00	0.04		0.03		48.26	101.71
#38	32.48	20.40	0.01	0.01	0.01	0.01	0.00	0.04		0.02	0.10	47.84	100.91
#39	32.35	20.72		0.02	0.01	0.04	0.00	0.00	0.01	0.04	0.17	48.13	101.50
#40	32.65	20.55	0.03			0.01	0.00	0.04	0.01			48.12	101.41

Element Wt% Oxide, Prospects Carbonates, Various August 1997. Operating Parameters: 15kV, 15nA, 15µm.														
Pts 1-10, D3 WMB, 45/294.6.														
	P2O5	SiO2	SO2	Ce2O3	MgO	CaO	MnO	FeO	SrO	BaO	Na2O	K2O	CO2	TOTAL
#3	0.01	0.00	0.00	0.06	21.25	32.28	0.09	0.11	0.05	0.07	0.03	0.04	48.88	102.87
#4	0.06	0.02	0.01	0.00	21.08	32.57	0.04	0.02	0.03	0.00	0.01	0.00	48.88	102.73
#5	0.06	0.01	0.00	0.00	20.92	32.54	0.04	0.07	0.07	0.00	0.04	0.01	48.73	102.49
#6	0.05	0.05	0.03	0.00	21.13	32.58	0.00	0.00	0.04	0.04	0.00	0.00	48.97	102.90
#7	0.05	0.00	0.03	0.00	20.86	32.54	0.07	0.16	0.03	0.00	0.01	0.00	48.71	102.47
#8	0.02	0.00	0.00	0.02	20.88	32.57	0.02	0.15	0.05	0.03	0.00	0.02	48.65	102.41
#9	0.01	0.00	0.00	0.04	20.95	32.73	0.04	0.00	0.04	0.05	0.00	0.00	48.75	102.60
#10	0.02	0.02	0.00	0.02	21.27	32.21	0.02	0.03	0.01	0.00	0.02	0.04	48.75	102.42

Element Wt% Oxide, Prospects Carbonates, January 1998. Operating Parameters: 15kV, 15nA, 15µm.													
Pts 1-20, D3 WMB, 45/273.0.													
	CaO	MgO	Na2O	SO2	K2O	SrO	MnO	FeO	NiO	CdO	BaO	CO2	TOTAL
#1	32.04	20.89	0.00	0.07		0.04	0.02	0.27	0.05	0.03	0.01	48.27	101.68
#2	32.69	20.47	0.02	0.03		0.01	0.00	0.08	0.03	0.03		48.13	101.47
#3	32.43	20.23	0.02	0.03	0.01	0.06	0.09	0.01		0.01	0.04	47.69	100.62
#4	32.21	20.91	0.04	0.01		0.01	0.00	0.03	0.02		0.04	48.19	101.45
#5	32.47	20.59	0.01	0.05	0.00	0.02	0.04	0.04		0.02	0.04	48.10	101.35
#6	32.38	20.41	0.02	0.04		0.05	0.06	0.04	0.03	0.02	0.04	47.88	100.96
#7	32.00	20.74	0.02	0.05	0.02	0.00	0.02	0.00			0.02	47.85	100.70
#8	32.08	20.50	0.02	0.01	0.01	0.06	0.02	0.08	0.07	0.04		47.72	100.60
#9	31.97	20.19	0.02	0.03	0.01	0.01	0.08	0.02	0.03			47.28	99.64
#10	34.65	18.16	0.03	0.06	0.01	0.06	0.00	0.00	0.02		0.03	47.18	100.20
#11	33.44	20.06	0.01	0.08		0.08	0.04	0.05	0.02			48.35	102.12
#12	32.22	19.56	0.04	0.64		0.02	0.10	1.29	0.05		0.09	48.45	102.45
#13	32.69	20.28		0.00	0.01		0.01	0.02		0.02	0.02	47.83	100.88
#14	32.68	20.40		0.02		0.00	0.07	0.03		0.01	0.05	48.02	101.27
#15	32.05	20.44	0.01	0.02	0.02	0.06	0.01	0.00	0.02	0.06	0.01	47.57	100.25
#16	32.21	20.36		0.02	0.01	0.05	0.03	0.00	0.00	0.02	0.01	47.58	100.27
#17	32.68	19.94	0.00	0.02	0.01	0.07	0.04	0.01	0.08	0.03		47.55	100.41
#18	32.61	20.30	0.01			0.03	0.07	0.00				47.83	100.86
#19	32.31	20.14		0.02	0.01	0.02	0.06	0.00	0.00		0.00	47.43	99.99
#20	32.42	20.44	0.00	0.01		0.04	0.01	0.04	0.05	0.04	0.04	47.87	100.94

Element Wt% Oxide, Prospects Carbonates, January 1998. Operating Parameters: 15kV, 15nA, 15µm.													
Pts 1-20, D3 WMB, HC13/87.5.													
	CaO	MgO	Na2O	SO2	K2O	SrO	MnO	FeO	NiO	CdO	BaO	CO2	TOTAL
#1	33.02	20.74	0.01			0.09	0.01	0.04	0.00		0.02	48.63	102.56
#2	31.95	20.94	0.02	0.03		0.08	0.02	0.08		0.01		48.07	101.19
#3	32.30	20.62	0.02	0.01		0.03	0.03	0.06	0.02	0.02	0.01	47.97	101.10
#4	31.88	20.93	0.01	0.01		0.04	0.07	0.08	0.02			48.02	101.07
#5	32.26	21.22	0.00		0.01	0.05	0.01	0.01	0.09			48.58	102.24
#6	32.63	20.71	0.03		0.01	0.03	0.03	0.01	0.01	0.01		48.28	101.74
#7	32.15	20.73		0.02	0.01	0.01	0.02	0.01	0.10			47.97	101.02
#8	32.42	20.94				0.04	0.02	0.05	0.02	0.02	0.07	48.40	101.97
#9	32.49	20.08	0.02	0.03	0.00	0.04	0.00	0.03				47.52	100.21
#10	31.91	20.96	0.01	0.01		0.04	0.04	0.00	0.05	0.03	0.02	48.03	101.10
#11	32.20	21.31		0.02	0.01	0.04	0.03	0.02			0.04	48.63	102.30
#12	32.51	20.53	0.01	0.02		0.05	0.00	0.00	0.06	0.01	0.05	48.03	101.27
#13	33.02	20.51	0.02	0.01	0.01	0.03	0.06	0.01	0.03	0.04		48.41	102.14
#14	32.15	20.75	0.02	0.01	0.02	0.02	0.04	0.03	0.08	0.03	0.03	48.03	101.21
#15	32.48	20.25	0.01	0.01		0.03	0.05	0.03	0.03	0.06	0.02	47.72	100.67
#16	31.63	21.24	0.02	0.00		0.08	0.04	0.00	0.03		0.03	48.10	101.15
#17	32.26	20.82	0.01			0.01	0.09	0.00		0.04		48.13	101.36
#18	32.18	20.95	0.02	0.01		0.08	0.01	0.09				48.25	101.58
#19	32.08	20.79	0.01	0.01		0.01	0.03	0.07		0.01		47.97	100.97
#20	32.20	20.75			0.02	0.10	0.07	0.13	0.02			48.10	101.38

Element Wt% Oxide, Prospects Carbonates, January 1998. Operating Parameters: 15kV, 15nA, 15µm.													
Pts 1-29, D4 Pink, HC15/200.8.													
	CaO	MgO	Na2O	SO2	K2O	SrO	MnO	FeO	NiO	CdO	BaO	CO2	TOTAL
#1	32.61	18.84	0.00	0.02		0.02	0.16	1.37		0.02		47.13	100.16
#3	33.62	18.04		0.03		0.01	0.16	0.45			0.02	46.51	98.84
#4	33.99	18.90	0.03	0.04	0.01	0.03	0.16	0.32	0.05	0.02		47.72	101.26
#5	33.52	19.01		0.03		0.02	0.21	0.18	0.00		0.06	47.36	100.38
#6	32.05	18.98	0.02				0.23	1.57				46.99	99.85
#7	31.44	19.09	0.03	0.01		0.01	0.26	2.37	0.04		0.08	47.20	100.52
#8	31.60	18.13	0.02	0.03		0.03	0.34	3.20	0.05			46.86	100.25
#9	32.26	19.23	0.02			0.06	0.26	1.00	0.01	0.03		47.13	99.98
#10	32.06	19.40	0.02	0.03	0.01	0.02	0.24	0.93				47.13	99.85
#11	31.28	19.67	0.02		0.01	0.02	0.23	1.06	0.08	0.02	0.03	46.91	99.32
#12	31.05	20.63	0.02		0.01	0.01	0.15	0.80			0.04	47.50	100.21
#13	30.76	20.05	0.01	0.02	0.01	0.02	0.15	1.01		0.01	0.09	46.81	98.94
#14	31.36	19.93		0.01	0.01	0.01	0.18	1.08				47.17	99.75
#15	30.90	20.12	0.01	0.03		0.04	0.17	1.05	0.01	0.08	0.05	47.07	99.51
#17	31.52	19.77	0.02	0.02	0.02	0.04	0.27	1.33			0.00	47.36	100.33
#18	31.48	19.84	0.01	0.02	0.02	0.03	0.18	1.16				47.23	99.95
#19	31.13	19.81			0.00	0.02	0.20	1.12			0.01	46.88	99.17
#20	30.91	20.00	0.03		0.03	0.01	0.17	1.12			0.05	46.94	99.26
#21	31.16	19.63	0.02	0.02	0.01	0.03	0.21	1.13	0.08		0.02	46.80	99.09
#22	31.89	19.91	0.00	0.01	0.02		0.27	1.10		0.01	0.03	47.64	100.87
#23	31.04	19.73	0.11	0.03	0.01	0.01	0.18	1.17	0.08			46.90	99.25
#24	31.24	19.37		0.01		0.03	0.18	1.35	0.03	0.01		46.65	98.87
#26	31.77	19.56	0.09	0.03	0.01	0.04	0.18	1.36			0.07	47.37	100.47
#27	31.67	19.82	0.02			0.04	0.22	1.17	0.00		0.03	47.39	100.36
#28	31.60	19.95	0.07	0.03		0.02	0.20	1.00		0.04		47.43	100.35
#29	31.51	19.63	0.01		0.02	0.05	0.18	1.06	0.03		0.01	46.97	99.46

Element Wt% Oxide, Prospects Carbonates, Rathdowney East, October 1996. Operating Parameters: 15kV, 15nA, 25µm.														
Pts 1-12, D3 WMB, RE24/1674a.														
	P2O5	SO2	CeO	MgO	CaO	MnO	FeO	SrO	CdO	BaO	Na2O	K2O	CO2	TOTAL
#1	0.05	0.00	0.09	20.80	32.76	0.00	0.00	0.00	0.03	0.04	0.02	0.00	48.68	102.47
#2	0.08	0.00	0.02	20.92	32.35	0.00	0.00	0.04	0.01	0.02	0.02	0.00	48.52	102.00
#3	0.02	0.04	0.05	20.93	31.90	0.01	0.00	0.00	0.01	0.00	0.03	0.00	48.12	101.11
#4	0.03	0.03	0.04	20.86	32.49	0.00	0.02	0.04	0.02	0.02	0.03	0.01	48.54	102.13
#5	0.02	0.02	0.06	20.73	32.21	0.01	0.03	0.02	0.00	0.00	0.01	0.01	48.14	101.26
#6	0.06	0.06	0.00	20.67	32.59	0.06	0.05	0.00	0.00	0.08	0.00	0.00	48.51	102.08
#7	0.01	0.02	0.02	19.98	31.99	0.16	1.35	0.00	0.00	0.00	0.00	0.00	48.01	101.54
#8	0.05	0.00	0.01	20.79	32.53	0.04	0.07	0.00	0.00	0.07	0.04	0.02	48.55	102.19
#9	0.04	0.00	0.02	20.65	32.31	0.04	0.08	0.00	0.01	0.02	0.01	0.03	48.19	101.40
#10	0.00	0.05	0.00	20.72	32.77	0.00	0.05	0.05	0.04	0.00	0.06	0.01	48.61	102.35
#11	0.00	0.02	0.05	20.81	31.96	0.08	0.18	0.02	0.06	0.02	0.00	0.02	48.17	101.41
#12	0.04	0.02	0.07	20.74	32.19	0.00	0.04	0.00	0.01	0.04	0.02	0.02	48.21	101.42

Element Wt% Oxide, Prospects Carbonates, Rathdowney East, October 1996. Operating Parameters: 15kV, 15nA, 25µm.														
Pts 109-120, D3? Minz WMB, RE24/1718.0.														
	P2O5	SO2	Ce2O3	MgO	CaO	MnO	FeO	SrO	CdO	BaO	Na2O	K2O	CO2	TOTAL
#109	0.00	0.05	0.01	20.50	33.41	0.07	0.43	0.07	0.01	0.04	0.01	0.03	49.16	103.79
#110	0.00	0.11	0.00	20.08	33.04	0.04	0.62	0.01	0.03	0.01	0.00	0.03	48.54	102.50
#111	0.06	0.08	0.00	19.91	33.56	0.07	0.48	0.00	0.04	0.03	0.05	0.00	48.78	103.07
#112	0.00	0.14	0.00	19.39	32.25	0.07	0.82	0.05	0.00	0.04	0.02	0.17	47.44	100.38
#113	0.07	0.04	0.06	20.59	33.15	0.00	0.03	0.00	0.06	0.00	0.04	0.01	48.87	102.92
#114	0.00	0.00	0.00	20.14	33.16	0.08	0.00	0.07	0.00	0.01	0.01	0.00	48.21	101.68
#115	0.00	0.04	0.01	20.92	33.16	0.05	0.13	0.00	0.00	0.02	0.00	0.00	49.15	103.48
#116	0.00	0.00	0.00	20.35	33.77	0.03	0.05	0.00	0.00	0.00	0.01	0.00	48.88	103.10
#117	0.00	0.01	0.01	20.54	33.52	0.01	0.14	0.03	0.00	0.00	0.03	0.01	48.98	103.28
#118	0.00	0.03	0.02	20.42	33.31	0.05	0.06	0.05	0.00	0.04	0.01	0.02	48.72	102.75
#119	0.00	0.01	0.00	20.31	33.87	0.09	0.04	0.05	0.07	0.02	0.04	0.00	49.04	103.55
#120	0.09	0.19	0.00	20.34	33.36	0.04	0.42	0.00	0.00	0.00	0.00	0.04	49.20	103.67

Pink Dolomite

Element Wt% Oxide, Prospects Carbonates, Rathdowney East, January 1998. Operating Parameters: 15kV, 15nA, 15µm.													
Pts 1-30, D4 PINK, RE24/1625.													
	CaO	MgO	Na2O	SO2	K2O	SrO	MnO	FeO	NiO	CdO	BaO	CO2	TOTAL
#1	31.92	17.78		0.01	0.01	0.00	0.33	3.02	0.02	0.04		46.56	99.69
#2	32.46	19.31	0.04	0.01	0.00	0.03	0.20	0.82	0.07	0.01		47.27	100.20
#3	33.92	19.11	0.01	0.02	0.01	0.02	0.04	0.11	0.04		0.08	47.66	101.02
#4	32.52	18.81	0.01			0.04	0.29	1.31	0.04			47.09	100.11
#5	32.26	18.52					0.23	2.43		0.03		47.17	100.63
#6	31.53	19.52	0.01	0.01		0.02	0.20	1.27	0.04	0.04		47.02	99.65
#7	31.81	19.83	0.04	0.00		0.03	0.20	0.84	0.01			47.29	100.03
#8	31.39	20.04	0.01	0.05		0.03	0.13	0.62			0.07	47.07	99.40
#9	31.57	19.73	0.01	0.01	0.00	0.00	0.15	0.38	0.01		0.00	46.67	98.54
#10	31.71	20.39			0.00	0.03	0.10	0.50	0.01	0.04		47.54	100.31
#11	32.38	19.68	0.01		0.01	0.04	0.13	0.61	0.05		0.02	47.42	100.35
#13	31.80	20.58		0.01	0.01	0.02	0.08	0.32			0.08	47.73	100.63
#14	31.23	20.55	0.01	0.02		0.05	0.15	0.49		0.04		47.41	99.94
#16	31.42	20.37	0.03		0.01	0.03	0.10	0.54				47.32	99.80
#17	31.33	20.41	0.00	0.01	0.01		0.13	0.43			0.04	47.24	99.61
#18	31.48	20.62		0.01		0.03	0.13	0.44		0.04		47.60	100.34
#19	31.07	19.99	0.01	0.02		0.05	0.16	1.15	0.10	0.09	0.01	47.15	99.78
#20	31.30	20.30	0.02	0.02		0.03	0.14	0.79	0.08		0.04	47.40	100.11
#21	31.05	20.36	0.02				0.20	0.77	0.01	0.00	0.07	47.22	99.69
#22	31.00	20.46	0.03	0.02		0.04	0.19	0.78		0.04	0.03	47.35	99.94
#23	31.41	20.47	0.00	0.02	0.01	0.04	0.22	0.78		0.00	0.04	47.68	100.68
#24	31.33	20.38	0.03	0.01		0.07	0.20	0.78				47.50	100.31
#25	31.16	20.29	0.02		0.01	0.04	0.20	0.67	0.04		0.02	47.20	99.64
#26	31.62	20.49	0.02		0.02	0.02	0.24	0.94		0.04	0.00	47.95	101.33
#27	31.38	20.20	0.01	0.02		0.02	0.24	0.87	0.07	0.01		47.44	100.25
#28	31.41	20.37	0.02	0.02	0.01	0.02	0.22	0.82	0.01	0.02		47.58	100.48
#29	30.79	20.27	0.02	0.01		0.01	0.27	1.04	0.04			47.16	99.61
#30	31.17	20.39	0.01	0.02	0.00	0.00	0.14	0.81	0.09		0.01	47.38	100.01

Element Wt% Oxide, Prospect Carbonates, Various August 1997. Operating Parameters: 15kV, 15nA, 15µm.														
Pts11-20, D4 PINK, 2/960.8.														
	MgO	Na2O	SiO2	P2O5	SO2	K2O	CaO	MnO	FeO	SrO	BaO	Ce2O3	CO2	TOTAL
#11	20.76	0.00	0.00	0.01	0.01	0.00	32.37	0.22	0.01	0.02	0.06	0.01	48.39	101.87
#12	20.34	0.02	0.02	0.00	0.02	0.01	32.46	0.27	0.59	0.03	0.05	0.06	48.44	102.30
#13	20.75	0.01	0.00	0.02	0.06	0.01	32.50	0.15	0.04	0.02	0.00	0.00	48.52	102.09
#14	21.06	0.01	0.02	0.02	0.00	0.01	32.59	0.17	0.00	0.04	0.06	0.02	48.91	102.93
#15	21.17	0.02	0.01	0.00	0.01	0.01	31.81	0.15	0.07	0.06	0.06	0.04	48.43	101.85
#16	21.03	0.02	0.01	0.04	0.01	0.00	32.12	0.16	0.02	0.02	0.00	0.00	48.50	101.93
#17	21.08	0.02	0.04	0.04	0.03	0.00	32.23	0.17	0.07	0.03	0.02	0.03	48.79	102.56
#18	21.24	0.01	0.04	0.01	0.01	0.01	32.11	0.15	0.00	0.07	0.00	0.04	48.74	102.43
#20		0.01	0.01	0.05	0.04	0.00	32.63	0.14	0.01	0.05	0.05	0.02	68.96	101.98

Late, Minor Vein and Vug Dolomite

Element Wt% Oxide, Prospect Carbonates, Holycross, September 1996. Operating Parameters: 15kV, 15nA, 30µm.															
Pts 1-15, Minz White Dolomite vein, HC5/122.9.															
	P2O5	SiO2	SO2	Ce2O3	MgO	CaO	MnO	FeO	SrO	CdO	BaO	Na2O	K2O	CO2	TOTAL
#1	0.00	0.00	0.00	0.06	20.09	33.01	0.00	0.03	0.03	0.00	0.00	0.02	0.01	101.26	101.26
#2	0.07	0.02	0.05	0.08	19.11	31.94	0.21	0.69	0.00	0.00	0.03	0.00	0.00	99.08	99.08
#4	0.00	0.00	0.00	0.00	20.77	32.23	0.02	0.06	0.03	0.10	0.10	0.02	0.02	101.56	101.56
#5	0.00	0.00	0.00	0.00	20.74	32.04	0.08	0.02	0.06	0.09	0.01	0.02	0.00	101.12	101.12
#6	0.08	0.00	0.04	0.01	20.93	31.75	0.04	0.03	0.01	0.00	0.00	0.03	0.01	101.09	101.09
#7	0.00	0.05	0.00	0.00	20.53	32.44	0.04	0.01	0.01	0.03	0.04	0.00	0.02	101.31	101.31
#8	0.04	0.02	0.04	0.00	19.67	33.37	0.04	0.02	0.02	0.08	0.00	0.05	0.03	101.40	101.40
#9	0.01	0.03	0.06	0.02	20.07	31.84	0.08	0.77	0.01	0.00	0.00	0.00	0.01	100.60	100.60
#10	0.04	0.02	0.02	0.05	20.33	33.09	0.07	0.05	0.03	0.00	0.14	0.00	0.00	102.37	102.37
#11	0.00	0.04	0.00	0.04	19.96	32.23	0.11	0.00	0.00	0.00	0.11	0.02	0.00	99.91	99.91
#13	0.05	0.05	0.00	0.05	18.83	32.05	0.18	0.75	0.00	0.00	0.01	0.04	0.00	98.59	98.59
#14	0.00	0.03	0.02	0.00	20.30	32.78	0.02	0.08	0.09	0.03	0.14	0.01	0.00	101.73	101.73
#15	0.00	0.00	0.00	0.00	20.35	32.72	0.04	0.00	0.05	0.10	0.07	0.00	0.01	101.45	101.45

B6. ELEMENTAL CHEMISTRY - LISHEEN SULPHIDES

Sphalerite

Element Wt%, Lisheen Sphalerites, July 1997. Operating Parameters: 20kV, 20nA, 1-2µm.												
Pts 1-11, 361/223.4 (brown coloured sphalerite).												
	S	Zn	Cu	Mn	Ga	Ge	Cd	In	Fe	As	Ag	Total
#1	32.11	65.41	0.01	0.01	0.00	0.00	1.21	0.04	0.79	0.10	0.06	99.73
#2	32.10	65.83	0.08	0.03	0.00	0.00	1.32	0.04	0.73	0.04	0.01	100.18
#3	32.53	65.62	0.04	0.00	0.00	0.03	1.24	0.04	0.85	0.02	0.00	100.37
#4	32.43	65.57	0.00	0.02	0.00	0.00	1.36	0.01	0.87	0.00	0.00	100.26
#5	32.71	65.76	0.00	0.02	0.08	0.00	1.25	0.00	0.78	0.06	0.05	100.71
#6	32.46	65.62	0.00	0.01	0.09	0.00	1.39	0.02	0.82	0.06	0.05	100.51
#7	32.77	65.35	0.05	0.00	0.00	0.00	1.31	0.00	0.84	0.00	0.05	100.37
#8	32.24	65.46	0.00	0.03	0.03	0.00	1.34	0.01	0.97	0.06	0.00	100.14
#9	32.22	65.66	0.00	0.04	0.00	0.00	1.25	0.00	1.07	0.02	0.01	100.26
#10	32.45	65.27	0.02	0.01	0.00	0.00	1.36	0.00	1.09	0.05	0.00	100.25
#11	32.43	65.68	0.03	0.01	0.00	0.00	1.17	0.01	1.03	0.06	0.00	100.42

Element Wt%, Lisheen Sphalerites, July 1997. Operating Parameters: 20kV, 20nA, 1-2µm.												
Pts 1-11, 416/195.5 (fine grained, pale to buff coloured, ore grade sphalerite).												
	S	Zn	Cu	Mn	Ga	Ge	Cd	In	Fe	As	Ag	Total
#1	32.34	66.67	0.03	0.02	0.02	0.00	0.08	0.04	0.18	0.00	0.00	99.40
#2	31.92	66.15	0.00	0.00	0.00	0.00	0.13	0.00	0.13	0.01	0.00	98.34
#3	32.57	65.92	0.03	0.00	0.00	0.00	0.08	0.00	0.19	1.11	0.03	99.93
#4	32.37	66.71	0.06	0.00	0.00	0.00	0.10	0.01	0.18	0.00	0.08	99.52
#5	32.52	67.47	0.03	0.02	0.00	0.00	0.16	0.00	0.15	0.07	0.00	100.42
#6	32.54	67.37	0.03	0.03	0.00	0.00	0.05	0.02	0.12	0.00	0.06	100.21
#7	32.14	65.76	0.00	0.02	0.00	0.00	0.13	0.00	0.13	0.04	0.00	98.21
#8	32.19	66.43	0.03	0.02	0.00	0.00	0.08	0.00	0.17	0.05	0.00	98.96
#9	31.90	66.37	0.02	0.04	0.01	0.00	0.10	0.03	0.14	0.05	0.04	98.71
#11	32.58	67.32	0.03	0.03	0.00	0.00	0.07	0.00	0.16	0.09	0.04	100.31

Element Wt%, Lisheen Sphalerites, July 1997. Operating Parameters: 20kV, 20nA, 1-2µm.												
Pts 12-30, 471/210.4 (red-amber coloured sphalerite).												
	S	Zn	Cu	Mn	Ga	Ge	Cd	In	Fe	As	Ag	Total
#12	32.21	66.91	0.02	0.00	0.03	0.00	0.29	0.03	0.34	0.06	0.00	99.88
#13	32.61	67.19	0.08	0.00	0.00	0.00	0.30	0.05	0.15	0.04	0.00	100.43
#14	32.31	66.97	0.00	0.03	0.00	0.00	0.31	0.02	0.11	0.07	0.00	99.82
#15	32.62	67.32	0.00	0.00	0.03	0.00	0.27	0.02	0.07	0.03	0.05	100.41
#16	32.48	67.63	0.00	0.03	0.01	0.00	0.32	0.00	0.05	0.03	0.00	100.55
#17	32.19	67.07	0.01	0.01	0.00	0.00	0.35	0.00	0.08	0.05	0.00	99.74
#18	32.44	67.80	0.03	0.01	0.00	0.00	0.32	0.00	0.06	0.02	0.00	100.69
#19	32.71	67.85	0.01	0.04	0.00	0.00	0.17	0.00	0.02	0.01	0.09	100.90
#20	32.91	68.16	0.02	0.00	0.00	0.00	0.26	0.02	0.04	0.00	0.02	101.42
#22	32.40	68.15	0.04	0.03	0.00	0.00	0.28	0.01	0.09	0.08	0.01	101.08
#23	32.39	66.95	0.01	0.02	0.00	0.00	0.64	0.01	0.47	0.02	0.00	100.51
#24	32.66	66.86	0.03	0.03	0.00	0.00	0.37	0.04	0.36	0.04	0.11	100.49
#25	32.70	67.23	0.04	0.00	0.00	0.00	0.61	0.04	0.42	0.03	0.00	101.08
#26	32.46	68.24	0.04	0.01	0.00	0.00	0.31	0.00	0.09	0.01	0.02	101.18
#27	32.13	67.78	0.05	0.00	0.00	0.00	0.32	0.04	0.09	0.04	0.03	100.47
#28	32.63	67.86	0.01	0.00	0.10	0.01	0.35	0.00	0.10	0.00	0.00	101.08
#29	32.38	67.90	0.02	0.00	0.04	0.00	0.29	0.01	0.21	0.07	0.00	100.91
#30	32.24	66.67	0.00	0.02	0.13	0.00	0.30	0.01	0.53	0.01	0.10	100.02

Element Wt%, Lisheen Sphalerites, July 1997. Operating Parameters: 20kV, 20nA, 1-2µm.												
Pts 15-24, 179/176.25 (fine grained, buff to brown coloured sphalerite).												
	S	Zn	Cu	Mn	Ga	Ge	Cd	In	Fe	As	Ag	Total
#15	32.62	64.74	1.09	0.00	0.00	0.00	0.24	0.00	1.05	0.05	0.01	99.80
#16	32.74	65.89	0.21	0.00	0.01	0.01	0.31	0.00	0.65	0.11	0.01	99.93
#17	32.92	66.16	0.17	0.01	0.00	0.00	0.28	0.03	0.61	0.08	0.02	100.28
#18	32.78	65.80	0.21	0.02	0.00	0.00	0.22	0.00	0.74	0.07	0.00	99.84
#19	33.19	63.83	0.59	0.00	0.00	0.00	0.12	0.02	0.80	0.96	0.08	99.60
#20	32.49	64.07	1.02	0.00	0.00	0.00	0.32	0.01	1.07	0.01	0.00	98.98
#22	32.72	65.62	0.39	0.01	0.00	0.00	0.25	0.02	0.98	0.04	0.04	100.07
#23	32.33	64.91	0.97	0.01	0.00	0.00	0.31	0.00	0.84	0.05	0.00	99.42
#24	32.42	65.99	0.21	0.00	0.00	0.00	0.28	0.00	0.67	0.09	0.00	99.66

Element Wt%, Lisheen Sphalerites, July 1997. Operating Parameters: 20kV, 20nA, 1-2µm.												
Pts 25-39, 095/335.0 (Brown coloured sphalerite).												
	S	Zn	Cu	Mn	Ga	Ge	Cd	In	Fe	As	Ag	Total
#25	32.62	65.19	0.00	0.00	0.00	0.00	0.38	0.02	1.91	0.00	0.00	100.12
#26	31.89	64.95	0.02	0.01	0.00	0.00	0.40	0.01	2.03	0.02	0.09	99.41
#27	32.35	65.08	0.04	0.01	0.00	0.01	0.39	0.01	1.79	0.06	0.00	99.76
#28	32.05	65.41	0.01	0.01	0.00	0.00	0.35	0.00	1.95	0.01	0.01	99.80
#29	32.35	65.21	0.03	0.02	0.00	0.00	0.41	0.00	2.11	0.00	0.00	100.13
#30	32.20	64.89	0.06	0.00	0.00	0.00	0.38	0.02	1.99	0.03	0.04	99.61
#31	32.32	65.31	0.00	0.00	0.00	0.00	0.43	0.03	1.88	0.07	0.04	100.08
#32	32.36	64.79	0.04	0.01	0.00	0.00	0.47	0.02	1.84	0.00	0.00	99.53
#33	32.04	64.94	0.00	0.01	0.00	0.00	0.41	0.01	1.90	0.02	0.03	99.36
#34	31.83	65.13	0.02	0.00	0.00	0.00	0.41	0.05	1.74	0.04	0.00	99.21
#35	32.18	64.69	0.03	0.00	0.00	0.00	0.44	0.00	1.75	0.01	0.00	99.10
#36	32.25	64.73	0.04	0.01	0.03	0.00	0.49	0.03	1.83	0.07	0.00	99.48
#37	32.15	65.17	0.01	0.00	0.01	0.00	0.32	0.05	1.54	0.00	0.01	99.26
#38	31.95	64.77	0.06	0.01	0.00	0.00	0.31	0.01	1.71	0.02	0.00	98.84
#39	32.23	65.89	0.00	0.03	0.00	0.00	0.34	0.00	1.53	0.00	0.00	100.03

Element Wt%, Lisheen Sphalerites, July 1997. Operating Parameters: 20kV, 20nA, 1-2µm.												
Pts 1-10, 515/173.7 (crystalline amber coloured sphalerite in pink dolomite).												
	S	Zn	Cu	Mn	Ga	Ge	Cd	In	Fe	As	Ag	Total
#1	32.81	65.93	0.01	0.00	0.06	0.00	0.79	0.02	0.06	0.00	0.02	99.70
#2	32.19	66.55	0.03	0.00	0.00	0.00	1.14	0.02	0.05	0.03	0.00	100.01
#3	32.48	66.45	0.04	0.00	0.00	0.00	0.92	0.00	0.05	0.04	0.00	99.98
#4	32.42	66.05	0.00	0.00	0.06	0.00	0.96	0.00	0.29	0.02	0.03	99.84
#5	32.91	67.03	0.02	0.02	0.00	0.00	0.42	0.00	0.13	0.05	0.03	100.60
#6	32.54	66.38	0.00	0.02	0.09	0.00	0.98	0.02	0.09	0.03	0.04	100.18
#7	32.55	66.13	0.02	0.01	0.00	0.00	0.26	0.02	0.56	0.03	0.02	99.59
#8	32.76	66.99	0.06	0.00	0.00	0.00	0.35	0.00	0.22	0.02	0.04	100.44
#9	32.68	66.84	0.03	0.00	0.00	0.00	0.36	0.00	0.19	0.09	0.01	100.20
#10	32.67	66.87	0.02	0.02	0.00	0.00	0.60	0.05	0.02	0.00	0.05	100.29

Element Wt%, Lisheen Sphalerites, July 1997. Operating Parameters: 20kV, 20nA, 1-2µm.												
Pts 1-20, 514/182.5 (amber-yellow coloured sphalerite).												
	S	Zn	Cu	Mn	Ga	Ge	Cd	In	Fe	As	Ag	Total
#1	32.19	66.73	0.02	0.02	0.00	0.00	0.03	0.02	0.08	0.00	0.00	99.09
#2	32.28	66.78	0.05	0.01	0.00	0.00	0.03	0.05	0.39	0.00	0.00	99.60
#3	32.52	67.13	0.00	0.00	0.00	0.00	0.06	0.01	0.25	0.02	0.01	100.00
#4	32.66	67.04	0.06	0.00	0.00	0.00	0.10	0.03	0.10	0.06	0.10	100.14
#5	32.46	67.07	0.00	0.00	0.00	0.00	0.02	0.04	0.00	0.05	0.00	99.64
#6	32.47	67.35	0.02	0.03	0.00	0.09	0.02	0.00	0.00	0.05	0.01	100.03
#7	32.58	67.76	0.01	0.03	0.00	0.00	0.00	0.00	0.01	0.02	0.12	100.52
#8	32.53	66.82	0.02	0.00	0.00	0.00	0.00	0.04	0.03	0.04	0.00	99.48
#9	32.66	67.47	0.00	0.01	0.00	0.00	0.01	0.01	0.02	0.04	0.00	100.21
#10	32.84	67.95	0.01	0.00	0.00	0.00	0.00	0.01	0.00	0.01	0.00	100.82
#11	32.10	67.42	0.02	0.03	0.00	0.00	0.00	0.02	0.00	0.01	0.00	99.59
#12	32.44	67.35	0.00	0.00	0.00	0.00	0.03	0.01	0.02	0.00	0.01	99.87
#13	32.59	67.34	0.02	0.03	0.00	0.00	0.00	0.03	0.02	0.03	0.07	100.11
#14	32.64	67.59	0.03	0.00	0.00	0.00	0.02	0.00	0.01	0.04	0.00	100.34
#15	32.54	67.27	0.03	0.00	0.00	0.01	0.06	0.00	0.01	0.05	0.00	99.97
#16	32.62	66.93	0.00	0.01	0.00	0.00	0.03	0.01	0.23	0.02	0.00	99.85
#17	32.61	66.82	0.02	0.00	0.00	0.00	0.01	0.03	0.22	0.00	0.02	99.73
#18	32.45	67.02	0.03	0.00	0.00	0.00	0.05	0.00	0.25	0.03	0.03	99.86
#19	32.90	67.39	0.01	0.01	0.00	0.00	0.05	0.03	0.11	0.02	0.00	100.52
#20	32.09	67.31	0.03	0.01	0.00	0.00	0.02	0.00	0.04	0.12	0.07	99.68

Element Wt%, Lisheen Sphalerites, July 1997. Operating Parameters: 20kV, 20nA, 1-2µm.												
Pts 1-11, 529/246.6 (coarse crystalline, brown coloured sphalerite).												
	S	Zn	Cu	Mn	Ga	Ge	Cd	In	Fe	As	Ag	Total
#1	32.73	64.76	0.00	0.00	0.00	0.00	1.28	0.03	1.44	0.02	0.06	100.31
#2	32.52	64.43	0.02	0.00	0.00	0.00	1.38	0.03	1.70	0.05	0.00	100.14
#3	32.25	64.59	0.01	0.00	0.00	0.00	1.30	0.04	1.62	0.02	0.04	99.88
#4	32.29	64.86	0.00	0.01	0.03	0.00	1.21	0.00	1.43	0.03	0.06	99.90
#5	32.59	65.20	0.00	0.01	0.00	0.00	1.33	0.00	1.16	0.05	0.00	100.34
#6	32.51	65.76	0.00	0.00	0.00	0.04	1.27	0.00	1.15	0.00	0.02	100.76
#7	32.37	65.19	0.01	0.00	0.00	0.00	1.32	0.04	1.35	0.00	0.00	100.27
#8	32.47	65.47	0.04	0.02	0.00	0.00	1.30	0.04	1.35	0.02	0.00	100.71
#9	32.37	65.61	0.00	0.01	0.00	0.00	1.35	0.01	0.96	0.00	0.00	100.30
#10	32.51	65.88	0.03	0.03	0.00	0.00	1.37	0.06	1.10	0.00	0.01	100.97
#11	32.41	65.13	0.00	0.00	0.00	0.00	1.32	0.04	1.00	0.06	0.07	100.01

Element Wt%, Lisheen Sphalerites, July 1997. Operating Parameters: 20kV, 20nA, 1-2µm.												
Pts 1-20, 517/205.0 (crystalline yellow sphalerite - hosted in white dolomite).												
	S	Zn	Cu	Mn	Ga	Ge	Cd	In	Fe	As	Ag	Total
#1	32.34	65.98	0.03	0.00	0.00	0.08	0.27	0.00	0.15	0.05	0.02	98.91
#2	32.29	67.08	0.01	0.00	0.00	0.00	0.20	0.04	0.17	0.06	0.00	99.84
#3	32.08	66.75	0.01	0.00	0.00	0.00	0.33	0.01	0.17	0.08	0.07	99.49
#4	32.40	66.60	0.00	0.00	0.00	0.00	0.34	0.03	0.18	0.00	0.00	99.55
#5	32.37	66.27	0.00	0.02	0.00	0.00	0.23	0.00	0.19	0.00	0.00	99.07
#6	32.41	66.60	0.00	0.00	0.00	0.00	0.18	0.09	0.18	0.02	0.11	99.58
#7	32.07	66.81	0.00	0.01	0.00	0.00	0.33	0.02	0.20	0.03	0.00	99.46
#8	32.55	67.28	0.02	0.00	0.00	0.00	0.19	0.03	0.21	0.03	0.02	100.34
#9	32.38	66.35	0.00	0.01	0.00	0.00	0.23	0.06	0.24	0.03	0.03	99.33
#10	32.53	67.37	0.03	0.00	0.00	0.00	0.16	0.02	0.26	0.03	0.05	100.45
#11	32.25	66.90	0.00	0.03	0.00	0.00	0.22	0.00	0.21	0.05	0.00	99.65
#12	32.23	67.45	0.04	0.01	0.00	0.00	0.21	0.04	0.16	0.06	0.01	100.20
#13	32.18	66.83	0.03	0.00	0.00	0.00	0.28	0.00	0.16	0.00	0.05	99.52
#14	32.19	67.09	0.03	0.03	0.00	0.00	0.15	0.00	0.20	0.01	0.09	99.78
#15	32.56	66.90	0.00	0.02	0.00	0.00	0.18	0.00	0.17	0.02	0.00	99.84
#16	32.60	66.97	0.00	0.01	0.00	0.00	0.28	0.03	0.17	0.00	0.00	100.05
#17	32.41	67.10	0.01	0.01	0.00	0.00	0.33	0.00	0.15	0.03	0.04	100.08
#18	32.39	67.22	0.01	0.00	0.00	0.00	0.27	0.03	0.17	0.03	0.04	100.16
#19	32.65	67.20	0.00	0.00	0.00	0.00	0.16	0.00	0.21	0.00	0.00	100.21
#20	32.13	67.32	0.01	0.01	0.00	0.00	0.22	0.02	0.16	0.07	0.00	99.94

Element Wt%, Lisheen Sphalerites, July 1997. Operating Parameters: 20kV, 20nA, 1-2µm.												
Pts 1-17, 451/139.10 (crystalline dark brown sphalerite).												
	S	Zn	Cu	Mn	Ga	Ge	Cd	In	Fe	As	Ag	Total
#1	32.82	64.33	0.00	0.00	0.00	0.00	0.05	0.01	3.10	0.00	0.00	100.31
#2	32.86	64.22	0.03	0.00	0.00	0.00	0.04	0.00	3.21	0.04	0.07	100.48
#3	32.78	63.95	0.00	0.03	0.03	0.00	0.05	0.06	3.18	0.00	0.09	100.16
#4	32.71	64.16	0.00	0.00	0.00	0.00	0.00	0.02	3.24	0.03	0.00	100.16
#5	32.82	63.89	0.00	0.01	0.00	0.00	0.01	0.04	3.30	0.01	0.00	100.08
#6	32.43	64.54	0.00	0.02	0.00	0.02	0.06	0.02	3.21	0.02	0.00	100.32
#7	32.22	64.41	0.01	0.01	0.01	0.00	0.02	0.02	3.23	0.08	0.03	100.05
#8	32.35	64.13	0.00	0.03	0.00	0.05	0.00	0.04	3.26	0.05	0.01	99.91
#9	32.70	64.46	0.00	0.03	0.01	0.00	0.11	0.04	3.28	0.07	0.01	100.70
#10	32.51	64.35	0.05	0.01	0.00	0.01	0.00	0.01	3.18	0.06	0.07	100.24
#11	32.66	64.70	0.04	0.00	0.07	0.00	0.01	0.03	3.25	0.00	0.00	100.76
#12	32.66	64.10	0.02	0.00	0.03	0.00	0.01	0.00	3.39	0.00	0.00	100.21
#13	32.59	64.98	0.04	0.00	0.01	0.00	0.03	0.04	3.36	0.02	0.00	101.05
#14	32.40	64.17	0.05	0.00	0.08	0.00	0.03	0.00	3.47	0.01	0.00	100.22
#15	32.88	63.88	0.03	0.01	0.00	0.00	0.02	0.00	3.52	0.00	0.06	100.39
#16	32.07	62.38	0.01	0.03	0.00	0.00	0.00	0.02	3.56	0.04	0.03	98.14
#17	32.14	63.56	0.01	0.02	0.00	0.00	0.00	0.03	3.79	0.02	0.04	99.62

Element Wt%, Lisheen Sphalerites, July 1997. Operating Parameters: 20kV, 20nA, 1-2µm.											
Pts 1-11, 325/149.30 (crystalline yellow sphalerite).											
	S	Zn	Cu	Mn	Ga	Ge	Cd	In	Fe	As	Total
#1	32.59	66.57	0.01	0.01	0.00	0.00	0.38	0.00	0.58	0.01	100.14
#2	33.08	67.23	0.00	0.02	0.00	0.00	0.32	0.03	0.52	0.01	101.21
#3	33.53	67.04	0.02	0.00	0.00	0.00	0.32	0.00	0.54	0.04	101.51
#4	32.77	67.62	0.00	0.01	0.00	0.00	0.36	0.02	0.46	0.00	101.24
#5	32.79	67.43	0.04	0.00	0.02	0.00	0.39	0.03	0.45	0.00	101.15
#7	32.61	67.29	0.00	0.03	0.00	0.00	0.32	0.00	0.33	0.03	100.62
#8	32.52	67.72	0.02	0.00	0.00	0.00	0.35	0.00	0.31	0.00	100.91
#9	32.45	67.29	0.00	0.02	0.00	0.02	0.36	0.03	0.34	0.03	100.54
#10	32.60	67.49	0.00	0.00	0.00	0.02	0.32	0.00	0.31	0.01	100.74
#11	32.29	67.76	0.02	0.00	0.00	0.00	0.29	0.00	0.31	0.02	100.68

Element Wt%, Lisheen Sphalerites, July 1997. Operating Parameters: 20kV, 20nA, 1-2µm.											
Pts 1-10, 463/173.0 (Dark brown sphalerite).											
	S	Zn	Cu	Mn	Ga	Ge	Cd	In	Fe	As	Total
#1	32.97	62.30	0.05	0.01	0.00	0.00	0.25	0.03	4.68	0.04	100.33
#2	32.84	61.96	0.02	0.00	0.03	0.05	0.21	0.00	4.72	0.00	99.82
#3	32.81	61.64	0.02	0.00	0.00	0.00	0.22	0.03	4.86	0.00	99.57
#4	33.27	63.64	0.00	0.00	0.00	0.02	0.25	0.02	3.72	0.01	100.91
#5	32.56	62.17	0.04	0.00	0.00	0.00	0.24	0.02	4.54	0.10	99.66
#6	32.95	61.54	0.00	0.00	0.00	0.00	0.30	0.04	4.96	0.07	99.86
#7	32.86	63.28	0.00	0.03	0.08	0.00	0.25	0.04	3.75	0.12	100.41
#8	32.67	64.06	0.04	0.00	0.00	0.00	0.25	0.02	3.31	0.04	100.40
#9	32.41	63.25	0.04	0.03	0.00	0.00	0.23	0.04	3.78	0.00	99.78
#10	32.36	62.25	0.04	0.01	0.03	0.02	0.26	0.00	4.48	0.00	99.46

Element Wt%, Lisheen Sphalerites, Sept 1997. Operating Parameters: 20kV, 20nA, 1-2µm.												
Pts 1-37, 400/205.65a, (Box1). Yellow colloform sphalerite.												
	Zn	S	Cu	Mn	Ga	Ge	Cd	In	Fe	As	Ag	Total
#6	67.53	31.58	0.03	0.01	0.16	0.00	0.10	0.02	0.81	0.07	0.15	100.45
#9	64.74	32.15	0.01	0.02	0.00	0.00	0.15	0.00	1.95	0.11	0.02	99.16
#11	67.33	31.46	0.04	0.04	0.00	0.00	0.41	0.01	0.39	0.02	0.00	99.70
#12	68.24	31.46	0.00	0.01	0.00	0.00	0.36	0.00	0.33	0.03	0.22	100.65
#13	68.57	32.04	0.00	0.00	0.00	0.00	0.10	0.00	0.26	0.12	0.09	101.17
#14	67.70	31.65	0.01	0.00	0.00	0.00	0.20	0.01	0.21	0.09	0.04	99.90
#15	67.41	31.68	0.05	0.00	0.00	0.00	0.25	0.00	0.12	0.01	0.00	99.53
#16	67.46	31.50	0.01	0.04	0.00	0.00	0.22	0.00	0.08	0.00	0.00	99.30
#17	66.61	27.31	0.00	0.00	0.00	0.00	0.29	0.01	0.05	0.04	0.02	94.32
#18	67.26	31.25	0.01	0.00	0.02	0.00	0.30	0.00	0.03	0.08	0.04	98.98
#19	67.57	31.68	0.00	0.00	0.00	0.00	0.14	0.01	0.04	0.01	0.07	99.52
#20	66.45	31.75	0.02	0.00	0.00	0.00	0.23	0.01	0.07	0.05	0.00	98.59
#21	66.01	31.10	0.00	0.01	0.00	0.00	0.31	0.00	0.14	0.04	0.11	97.73
#22	67.09	31.49	0.01	0.01	0.00	0.00	0.23	0.01	0.06	0.06	0.10	99.06
#23	67.98	31.27	0.00	0.01	0.00	0.00	0.30	0.00	0.15	0.02	0.12	99.85
#24	66.89	31.61	0.04	0.01	0.00	0.00	0.31	0.00	0.20	0.09	0.08	99.23
#25	67.39	31.80	0.00	0.02	0.00	0.00	0.26	0.01	0.34	0.00	0.15	99.97
#26	68.16	32.10	0.03	0.00	0.03	0.02	0.28	0.01	0.16	0.01	0.03	100.82
#27	67.70	31.98	0.00	0.00	0.00	0.00	0.32	0.00	0.40	0.02	0.00	100.42
#28	67.24	32.04	0.01	0.00	0.11	0.00	0.27	0.00	0.68	0.01	0.11	100.46
#30	67.25	32.17	0.01	0.00	0.00	0.00	0.24	0.00	0.41	0.03	0.18	100.28
#32	66.93	31.97	0.00	0.02	0.00	0.00	0.23	0.01	0.39	0.06	0.17	99.78
#33	66.76	31.99	0.02	0.03	0.04	0.00	0.20	0.05	0.37	0.05	0.20	99.71
#34	66.42	32.37	0.03	0.00	0.00	0.00	0.23	0.00	0.66	0.01	0.17	99.87

Element Wt%, Lisheen Sphalerites, Sept 1997. Operating Parameters: 20kV, 20nA, 1-2μm.												
Pts 1-47, 400/205.65a, (Box2). Yellow to grey colloform sphalerite.												
	Zn	S	Cu	Mn	Ga	Ge	Cd	In	Fe	As	Ag	Total
#1	66.82	32.21	0.00	0.00	0.00	0.00	0.29	0.01	0.02	0.08	0.00	99.42
#2	67.07	32.13	0.03	0.03	0.00	0.00	0.28	0.01	0.04	0.07	0.00	99.65
#6	66.65	31.46	0.03	0.00	0.00	0.00	0.36	0.03	0.09	0.04	0.08	98.73
#7	68.09	29.87	0.03	0.00	0.00	0.04	0.21	0.00	0.08	0.08	0.13	98.53
#8	67.33	32.18	0.01	0.03	0.00	0.00	0.42	0.06	0.03	0.08	0.05	100.17
#10	67.36	32.09	0.02	0.00	0.00	0.00	0.26	0.01	0.08	0.00	0.04	99.86
#11	66.34	31.75	0.03	0.03	0.00	0.00	0.17	0.00	0.07	0.08	0.06	98.52
#13	66.77	32.07	0.03	0.01	0.00	0.00	0.21	0.02	0.05	0.09	0.10	99.34
#14	67.60	32.46	0.00	0.00	0.00	0.00	0.32	0.02	0.01	0.03	0.14	100.58
#15	67.50	31.54	0.03	0.01	0.00	0.00	0.19	0.00	0.04	0.09	0.10	99.49
#16	66.83	31.91	0.03	0.03	0.00	0.00	0.38	0.02	0.07	0.01	0.00	99.29
#17	67.91	32.32	0.01	0.02	0.00	0.00	0.29	0.04	0.05	0.10	0.05	100.80
#18	67.05	32.24	0.04	0.03	0.09	0.00	0.14	0.05	0.07	0.08	0.12	99.90
#19	67.44	31.76	0.01	0.01	0.00	0.00	0.11	0.07	0.05	0.02	0.00	99.48
#20	66.90	32.21	0.01	0.00	0.06	0.01	0.40	0.00	0.12	0.05	0.06	99.82
#23	67.12	32.29	0.04	0.02	0.01	0.00	0.09	0.00	0.11	0.12	0.00	99.80
#24	67.11	32.23	0.03	0.00	0.00	0.00	0.23	0.01	0.07	0.10	0.03	99.80
#25	67.96	32.39	0.05	0.00	0.00	0.00	0.17	0.00	0.02	0.03	0.00	100.62
#26	66.69	31.85	0.03	0.04	0.00	0.02	0.47	0.00	0.07	0.08	0.02	99.27
#27	67.70	32.44	0.01	0.01	0.03	0.00	0.16	0.01	0.05	0.07	0.04	100.51
#29	68.10	32.37	0.00	0.00	0.00	0.00	0.30	0.00	0.06	0.06	0.04	100.93
#30	67.44	32.25	0.00	0.01	0.00	0.00	0.26	0.03	0.08	0.03	0.00	100.10
#31	68.13	32.03	0.05	0.03	0.00	0.03	0.26	0.00	0.04	0.15	0.12	100.85
#32	67.61	32.49	0.04	0.01	0.00	0.00	0.19	0.05	0.04	0.02	0.09	100.52
#33	67.66	32.11	0.00	0.01	0.00	0.00	0.19	0.02	0.02	0.00	0.09	100.10
#34	67.72	32.57	0.00	0.01	0.03	0.00	0.21	0.01	0.05	0.04	0.10	100.74
#35	68.15	32.58	0.00	0.02	0.00	0.02	0.12	0.02	0.07	0.00	0.08	101.06
#36	67.67	32.41	0.00	0.01	0.00	0.05	0.42	0.04	0.05	0.10	0.06	100.80
#37	67.43	32.20	0.00	0.00	0.00	0.00	0.25	0.00	0.07	0.02	0.10	100.06
#38	67.31	32.17	0.00	0.00	0.00	0.00	0.29	0.00	0.09	0.06	0.06	99.98
#39	67.46	31.90	0.03	0.02	0.00	0.00	0.40	0.01	0.07	0.02	0.11	100.00
#40	67.08	31.85	0.03	0.01	0.00	0.00	0.18	0.00	0.08	0.08	0.03	99.32
#41	67.58	31.89	0.01	0.01	0.00	0.00	0.23	0.02	0.06	0.11	0.21	100.12
#42	68.03	32.61	0.00	0.00	0.00	0.00	0.30	0.00	0.08	0.05	0.06	101.13
#43	67.98	32.67	0.05	0.00	0.00	0.00	0.32	0.04	0.05	0.03	0.00	101.14
#44	67.66	32.22	0.03	0.01	0.00	0.00	0.31	0.05	0.06	0.11	0.02	100.46
#45	67.19	31.89	0.04	0.03	0.00	0.00	0.17	0.00	0.06	0.02	0.06	99.45

Element Wt%, Lisheen Sphalerites, Sept 1997. Operating Parameters: 20kV, 20nA, 1-2μm.												
Pts 1-43, 400/205.65a (Box3). Orange to brown colloform sphalerite.												
	Zn	S	Cu	Mn	Ga	Ge	Cd	In	Fe	As	Ag	Total
#1	66.74	31.74	0.03	0.01	0.00	0.00	0.16	0.00	0.77	0.30	0.05	99.79
#2	67.40	31.94	0.01	0.01	0.03	0.00	0.19	0.02	0.63	0.06	0.05	100.32
#3	68.14	32.46	0.00	0.02	0.00	0.01	0.36	0.00	0.35	0.04	0.00	101.38
#4	65.04	31.85	0.02	0.02	0.00	0.00	0.19	0.02	0.82	0.60	0.00	98.56
#5	68.55	32.16	0.02	0.01	0.00	0.00	0.26	0.04	0.10	0.05	0.06	101.25
#6	68.06	32.30	0.00	0.01	0.10	0.02	0.02	0.02	0.36	0.00	0.00	100.90
#7	66.54	31.62	0.00	0.01	0.00	0.00	0.09	0.00	0.78	0.33	0.12	99.48
#8	65.94	32.14	0.02	0.01	0.00	0.00	0.22	0.01	1.09	0.30	0.08	99.81
#9	67.51	32.17	0.00	0.01	0.00	0.00	0.27	0.04	0.94	0.10	0.02	101.07
#10	66.56	31.55	0.01	0.01	0.00	0.00	0.14	0.00	0.79	0.20	0.14	99.40
#11	67.88	29.78	0.00	0.00	0.00	0.00	0.20	0.00	0.52	0.08	0.09	98.56
#12	67.72	31.90	0.00	0.02	0.00	0.00	0.10	0.00	0.30	0.00	0.04	100.08
#13	67.68	31.95	0.01	0.02	0.00	0.00	0.15	0.00	0.62	0.07	0.05	100.55
#14	66.06	32.53	0.03	0.01	0.00	0.00	0.24	0.00	1.88	0.16	0.00	100.91
#15	65.97	32.08	0.04	0.00	0.04	0.00	0.00	0.05	1.46	0.47	0.05	100.16
#16	66.55	31.63	0.03	0.01	0.00	0.00	0.03	0.00	0.74	0.33	0.00	99.33
#17	66.65	31.00	0.04	0.00	0.00	0.00	0.14	0.01	0.50	0.11	0.11	98.54
#18	67.66	31.97	0.03	0.00	0.00	0.00	0.14	0.00	0.25	0.10	0.00	100.14
#20	67.85	31.51	0.00	0.00	0.00	0.00	0.19	0.00	0.16	0.01	0.00	99.71
#21	67.95	31.92	0.00	0.02	0.00	0.00	0.20	0.00	0.37	0.00	0.02	100.49
#22	64.69	32.05	0.01	0.00	0.00	0.00	0.01	0.02	2.84	0.28	0.00	99.91
#23	66.00	32.04	0.02	0.02	0.01	0.00	0.20	0.03	1.57	0.06	0.00	99.94
#24	67.35	31.70	0.04	0.01	0.07	0.04	0.25	0.00	0.56	0.21	0.03	100.25
#25	67.68	31.93	0.00	0.03	0.00	0.00	0.26	0.00	0.29	0.04	0.00	100.23
#26	67.81	31.80	0.02	0.01	0.00	0.00	0.24	0.00	0.28	0.04	0.00	100.20
#28	65.98	31.95	0.00	0.02	0.00	0.00	0.26	0.05	0.55	0.13	0.03	98.96
#29	66.77	31.70	0.02	0.02	0.04	0.00	0.11	0.02	0.66	0.27	0.24	99.83
#32	67.14	31.82	0.00	0.03	0.00	0.00	0.20	0.03	0.48	0.17	0.00	99.88
#33	67.33	31.67	0.02	0.02	0.00	0.01	0.29	0.03	0.32	0.10	0.00	99.78
#34	66.43	31.64	0.04	0.00	0.06	0.00	0.21	0.03	0.31	0.15	0.08	98.94
#35	67.28	31.44	0.02	0.01	0.00	0.00	0.35	0.02	0.31	0.13	0.11	99.67
#37	67.38	31.46	0.03	0.02	0.00	0.00	0.28	0.02	0.24	0.13	0.14	99.71
#38	71.06	26.52	0.04	0.01	0.00	0.00	0.21	0.02	0.27	0.03	0.03	98.18
#40	67.01	31.30	0.02	0.01	0.00	0.00	0.21	0.04	0.20	0.11	0.08	98.97
#41	67.67	31.42	0.00	0.00	0.06	0.00	0.30	0.00	0.21	0.08	0.09	99.83
#43	67.74	31.66	0.02	0.01	0.13	0.00	0.22	0.04	0.21	0.04	0.03	100.09

Element Wt%, Lisheen Sphalerites, August 1995. Operating Parameters: 20kV, 20nA, 1-2µm.										
Pts 31-60, 262/159.1 (Orange-brown colloform sphalerite - variable colour zonations).										
	Cd	Hg	In	S	Tl	Fe	Cu	Zn	Ga	Total
#30	0.22	0.00	0.03	32.09	0.00	0.42	0.04	66.44	0.00	99.23
#32	0.22	0.04	0.00	31.94	0.13	0.23	0.05	67.42	0.00	100.03
#33	0.18	0.00	0.01	32.36	0.32	0.24	0.03	67.61	0.00	100.75
#34	0.24	0.10	0.05	31.38	0.46	0.24	0.05	67.74	0.00	100.25
#35	0.14	0.02	0.00	31.83	0.09	0.25	0.01	68.45	0.00	100.80
#36	0.23	0.00	0.04	31.97	0.61	0.29	0.08	68.07	0.00	101.28
#37	0.16	0.00	0.00	32.00	0.00	0.23	0.04	67.32	0.00	99.75
#38	0.22	0.00	0.00	32.12	0.18	0.25	0.03	67.76	0.00	100.56
#39	0.14	0.10	0.00	31.64	0.00	0.21	0.04	67.44	0.00	99.58
#40	0.25	0.00	0.08	31.72	0.00	0.23	0.00	67.59	0.00	99.88
#41	0.18	0.16	0.00	31.84	0.00	0.24	0.02	68.01	0.00	100.45
#42	0.20	0.04	0.00	31.31	0.05	0.24	0.07	67.05	0.00	98.97
#43	0.23	0.00	0.09	31.78	0.06	0.28	0.03	67.39	0.00	99.87
#44	0.24	0.00	0.00	31.60	0.00	0.26	0.07	67.53	0.00	99.70
#45	0.17	0.00	0.03	31.51	0.00	0.26	0.04	67.87	0.00	99.88
#46	0.25	0.06	0.00	31.75	0.31	0.23	0.06	67.70	0.00	100.36
#47	0.19	0.05	0.03	31.37	0.23	0.29	0.02	67.64	0.00	99.83
#48	0.17	0.21	0.06	31.29	0.17	0.25	0.01	67.98	0.00	100.13
#49	0.18	0.00	0.05	31.57	0.16	0.25	0.00	68.02	0.00	100.24
#50	0.19	0.00	0.00	31.74	0.13	0.27	0.08	66.97	0.00	99.36
#51	0.12	0.00	0.00	31.40	0.07	0.26	0.09	68.63	0.00	100.57
#52	0.20	0.04	0.04	31.73	0.06	0.26	0.09	67.30	0.00	99.72
#53	0.16	0.11	0.04	31.71	0.32	0.29	0.07	67.35	0.00	100.03
#54	0.13	0.06	0.00	31.58	0.16	0.26	0.11	67.95	0.00	100.25
#55	0.22	0.04	0.02	31.71	0.14	0.24	0.10	67.39	0.00	99.85
#56	0.17	0.00	0.00	31.63	0.17	0.26	0.06	67.58	0.00	99.86
#57	0.26	0.07	0.00	31.19	0.00	0.25	0.07	67.34	0.00	99.17
#58	0.19	0.19	0.04	30.75	0.27	0.23	0.10	67.34	0.00	99.11
#59	0.16	0.00	0.00	31.01	0.04	0.25	0.06	67.50	0.00	99.03
#60	0.15	0.00	0.03	31.26	0.19	0.26	0.02	67.31	0.00	99.22

Element Wt%, Lisheen Sphalerites, December 1996. Operating Parameters: 20kV, 20nA, 1-2µm.								
Pts 1-14, 361/223.4b, (Brown coloured sphalerite - oolite hosted).								
	S	Fe	Zn	Ga	Ge	Cd	In	Total
#2	32.34	0.22	65.97	0.00	0.00	0.65	0.00	99.18
#3	32.21	0.28	64.82	0.00	0.00	1.32	0.04	98.67
#4	32.19	0.10	65.27	0.00	0.00	1.52	0.00	99.08
#5	32.28	0.14	64.28	0.00	0.00	2.08	0.02	98.80
#6	32.76	0.06	65.31	0.00	0.00	1.03	0.03	99.19
#7	32.53	0.13	65.26	0.00	0.00	1.19	0.02	99.11
#8	32.59	0.09	64.45	0.00	0.00	2.48	0.00	99.60
#9	32.84	0.22	64.68	0.00	0.00	1.88	0.05	99.66
#10	32.55	0.09	64.36	0.00	0.00	1.95	0.01	98.96
#11	32.68	0.06	65.94	0.00	0.00	0.85	0.03	99.55
#12	32.65	0.13	65.70	0.00	0.01	1.01	0.02	99.51
#13	32.66	0.11	65.56	0.00	0.00	0.87	0.00	99.20
#14	32.79	0.12	65.76	0.00	0.00	0.67	0.01	99.34

Element Wt%, Lisheen Sphalerites, December 1996. Operating Parameters: 20kV, 20nA, 1-2µm.								
Pts 1-10, 235/167.0 (fine crystalline pale sphalerite).								
	S	Fe	Zn	Ga	Ge	Cd	In	Total
#4	33.20	0.04	64.97	0.00	0.00	0.21	0.00	98.43
#6	32.69	0.04	65.08	0.00	0.00	0.21	0.00	98.03
#7	33.26	0.03	65.07	0.00	0.00	0.21	0.01	98.58
#9	32.74	0.06	65.56	0.00	0.00	0.21	0.00	98.57
#10	33.04	0.02	65.96	0.00	0.00	0.20	0.02	99.23

Element Wt%, Lisheen Sphalerites, December 1996. Operating Parameters: 20kV, 20nA, 1-2µm.								
Pts 1-10, 429/192.1 (orange-brown colloform sphalerite, oolite hosted).								
	S	Fe	Zn	Ga	Ge	Cd	In	Total
#2	32.62	0.82	64.78	0.00	0.00	0.13	0.00	98.35
#3	32.63	0.83	64.80	0.00	0.00	0.12	0.01	98.39
#5	32.74	0.80	64.93	0.00	0.00	0.13	0.01	98.61
#6	32.86	0.83	65.90	0.00	0.00	0.14	0.00	99.73
#9	32.93	0.88	65.17	0.00	0.02	0.13	0.03	99.15
#10	32.59	0.88	64.53	0.00	0.00	0.03	0.03	98.06

Element Wt%, Lisheen Sphalerites, December 1996. Operating Parameters: 20kV, 20nA, 1-2µm.								
Pts 1-10, 359/148.65 (fine crystalline pale sphalerite).								
	S	Fe	Zn	Ga	Ge	Cd	In	Total
#1	33.09	0.26	64.86	0.00	0.04	0.17	0.00	98.43
#2	32.82	0.34	65.15	0.00	0.00	0.11	0.05	98.47
#3	32.67	0.26	65.21	0.00	0.00	0.09	0.00	98.23
#4	32.88	0.21	65.75	0.00	0.00	0.14	0.01	98.99
#6	32.69	0.31	65.71	0.00	0.00	0.14	0.02	98.86
#7	32.77	0.13	65.72	0.00	0.00	0.14	0.00	98.76
#8	32.79	0.18	65.78	0.00	0.00	0.14	0.04	98.93

Element Wt%, Lisheen Sphalerites, December 1996. Operating Parameters: 20kV, 20nA, 1-2µm.								
Pts 1-15, 431/205.70 (fine grained, pale to grey coloured sphalerite.								
	S	Fe	Zn	Ga	Ge	Cd	In	Total
#3	32.81	0.27	65.44	0.00	0.03	0.14	0.05	98.74
#4	32.66	0.06	65.53	0.00	0.00	0.13	0.01	98.39
#5	33.00	0.10	65.58	0.00	0.00	0.16	0.00	98.82
#7	32.59	0.10	65.57	0.00	0.00	0.17	0.00	98.42
#8	32.99	0.02	65.87	0.00	0.00	0.13	0.01	99.01
#10	32.76	0.32	65.80	0.00	0.00	0.14	0.00	99.01

Element Wt%, Lisheen Sphalerites, December 1996. Operating Parameters: 20kV, 20nA, 1-2µm.								
Pts 1-5, 400/205.65b (fine crystalline, yellow sphalerite).								
	S	Fe	Zn	Ga	Ge	Cd	In	Total
#1	33.04	0.17	66.71	0.00	0.00	0.16	0.02	100.10
#2	32.85	0.18	67.38	0.00	0.00	0.21	0.06	100.69
#3	33.11	0.25	66.49	0.00	0.00	0.19	0.06	100.10
#4	32.45	0.30	66.49	0.00	0.00	0.14	0.03	99.41
#5	32.88	0.25	66.92	0.00	0.00	0.15	0.00	100.20

Element Wt%, Lisheen Sphalerites, December 1996. Operating Parameters: 20kV, 20nA, 1-2µm.								
Pts 1-10, 395/194.05 (fine grained pale coloured, sphalerite).								
	S	Fe	Zn	Ga	Ge	Cd	In	Total
#1	33.00	0.03	67.20	0.00	0.00	0.35	0.00	100.57
#2	33.16	0.04	67.08	0.00	0.00	0.31	0.06	100.64
#3	32.78	0.03	67.26	0.00	0.00	0.35	0.00	100.41
#4	32.94	0.04	66.79	0.00	0.00	0.37	0.03	100.18
#5	33.06	0.00	67.22	0.00	0.00	0.44	0.00	100.72
#6	33.14	0.02	66.96	0.00	0.00	0.41	0.02	100.55
#7	33.02	0.00	67.14	0.00	0.00	0.45	0.03	100.63
#8	32.97	0.01	67.08	0.00	0.00	0.48	0.02	100.55
#9	32.71	0.00	67.37	0.00	0.00	0.56	0.00	100.65
#10	32.04	0.13	66.45	0.00	0.00	0.44	0.06	99.11

Element Wt%, Lisheen Sphalerites, December 1996. Operating Parameters: 20kV, 20nA, 1-2µm.								
Pts 1-10, 137/130.0 (Mineralized oolite - fine crystalline buff to pink coloured sphalerite).								
	S	Fe	Zn	Ga	Ge	Cd	In	Total
#1	33.17	0.43	66.19	0.00	0.02	0.20	0.01	100.01
#2	32.97	0.45	65.85	0.00	0.01	0.25	0.00	99.53
#3	33.30	0.67	65.63	0.00	0.02	0.15	0.01	99.78
#4	33.48	0.93	65.80	0.00	0.00	0.18	0.00	100.39
#5	33.13	0.43	66.02	0.00	0.00	0.14	0.02	99.74
#6	33.27	0.47	66.41	0.00	0.00	0.19	0.03	100.37
#7	32.91	0.10	65.41	0.00	0.00	0.10	0.00	98.52
#8	32.93	0.07	66.54	0.00	0.05	0.22	0.02	99.83
#9	33.44	0.13	66.07	0.00	0.00	0.18	0.00	99.81
#10	33.27	0.18	66.00	0.00	0.00	0.14	0.01	99.61

Element Wt %, Lisheen Sphalerite, March 1995. Operating Parameters: 20kV, 20nA, 1-2µm.															
Pts 171-199, 262/159.1 Colloform sphalerite (stage scan).															
	Hg	Cd	Ag	Tl	S	In	Sb	Fe	Zn	Mn	Cu	As	Ga	Ge	Total
#171	0.13	0.27	0.09	0.53	32.13	0.02	0.02	0.19	65.051	0.036	0.024	0.01	0	0	98.494
#172	0.17	0.24	0.00	0.18	32.10	0.00	0.09	0.18	65.269	0	0.008	0.113	0	0	98.346
#173	0.00	0.29	0.08	0.12	31.98	0.01	0.10	0.15	65.319	0.026	0.079	0.069	0	0	98.211
#174	0.00	0.24	0.00	0.54	32.06	0.03	0.00	0.20	65.604	0.02	0	0.048	0	0.002	98.736
#175	0.10	0.22	0.11	0.07	32.13	0.00	0.08	0.24	66.059	0.049	0.049	0.121	0	0	99.234
#177	0.00	0.33	0.01	0.07	32.42	0.00	0.04	0.17	65.747	0.008	0.048	0.125	0	0.058	99.041
#178	0.06	0.23	0.01	0.10	32.23	0.04	0.00	0.21	66.016	0	0.065	0.079	0	0	99.027
#180	0.00	0.29	0.09	0.27	32.11	0.03	0.00	0.17	64.966	0.044	0	0.189	0	0	98.161
#181	0.00	0.18	0.01	0.00	32.05	0.00	0.01	0.20	65.585	0.007	0.045	0.034	0	0	98.12
#182	0.11	0.23	0.10	0.35	32.34	0.07	0.01	0.19	65.715	0.019	0.064	0.082	0	0.07	99.347
#183	0.01	0.25	0.00	0.22	32.42	0.00	0.00	0.15	65.045	0	0	0.016	0	0	98.112
#185	0.06	0.36	0.04	0.16	32.23	0.03	0.00	0.20	65.021	0.024	0.02	0.022	0	0	98.154
#189	0.00	0.27	0.03	0.24	32.27	0.00	0.00	0.17	65.458	0.043	0	0.129	0	0	98.603
#190	0.10	0.24	0.14	0.16	31.93	0.00	0.08	0.12	65.362	0.002	0	0.111	0	0.01	98.24
#192	0.17	0.20	0.05	0.18	32.54	0.03	0.03	0.13	65.043	0.044	0.059	0.022	0	0	98.512
#195	0.12	0.25	0.11	0.49	32.74	0.06	0.01	0.20	65.706	0.026	0	0.078	0	0	99.792
#197	0.00	0.21	0.00	0.13	32.08	0.00	0.02	0.28	65.963	0.027	0.014	0	0	0	98.717
#198	0.00	0.16	0.00	0.36	32.45	0.03	0.00	0.29	65.502	0.02	0.047	0	0	0	98.861
#199	0.00	0.17	0.05	0.16	31.98	0.06	0.00	0.39	65.434	0.047	0.013	0.085	0	0	98.379

Galena

Element Wt%, Lisheen Galena, July 1997. Operating Parameters: 20kV, 20nA, 1-2µm.							
Pts 1-10, 416/195.5.							
	S	Pb	Ag	Bi	Mn	Cd	Total
#1	13.37	87.84	0.04	0.03	0.00	0.17	101.44
#2	13.56	87.26	0.00	0.03	0.03	0.00	100.88
#3	13.27	87.42	0.00	0.00	0.00	0.00	100.69
#4	13.42	86.64	0.01	0.13	0.02	0.00	100.22
#5	13.19	87.50	0.03	0.11	0.00	0.07	100.90
#6	13.40	86.63	0.08	0.02	0.00	0.02	100.15
#7	13.48	87.32	0.04	0.06	0.00	0.07	100.96
#8	13.20	85.94	0.00	0.09	0.01	0.16	99.39
#9	13.42	86.43	0.00	0.12	0.00	0.01	99.97
#10	13.25	87.67	0.01	0.12	0.02	0.13	101.20

Element Wt%, Lisheen Galena, July 1997. Operating Parameters: 20kV, 20nA, 1-2µm.							
Pts 1-10, 361/223.4b.							
	S	Pb	Ag	Bi	Mn	Cd	Total
#1	13.39	86.42	0.01	0.10	0.00	0.00	99.92
#2	13.32	87.31	0.04	0.11	0.04	0.09	100.90
#3	13.01	86.31	0.00	0.05	0.00	0.00	99.37
#4	13.18	86.72	0.00	0.04	0.00	0.04	99.97
#5	13.67	87.05	0.00	0.03	0.02	0.00	100.77
#6	13.30	86.46	0.04	0.03	0.02	0.00	99.85
#7	13.16	86.76	0.00	0.08	0.01	0.05	100.06
#8	13.31	85.74	0.05	0.15	0.01	0.03	99.29
#9	13.42	84.87	0.04	0.00	0.00	0.03	98.37
#10	13.54	86.35	0.01	0.25	0.02	0.00	100.18

Element Wt%, Lisheen Galena, July 1997. Operating Parameters: 20kV, 20nA, 1-2µm.							
Pts 1-10, 262/162.1.							
	S	Pb	Ag	Bi	Mn	Cd	Total
#1	13.37	86.39	0.04	0.02	0.04	0.07	99.92
#2	13.55	86.03	0.00	0.00	0.02	0.00	99.59
#3	13.53	86.68	0.00	0.04	0.01	0.10	100.36
#4	13.40	86.40	0.07	0.13	0.03	0.00	100.02
#5	13.47	86.81	0.02	0.05	0.00	0.01	100.36
#6	13.54	85.97	0.00	0.03	0.04	0.04	99.62
#7	13.60	86.34	0.03	0.27	0.01	0.00	100.25
#8	13.45	86.89	0.04	0.03	0.02	0.00	100.42
#9	13.45	86.37	0.00	0.04	0.00	0.00	99.86
#10	13.48	85.78	0.00	0.21	0.01	0.02	99.50

Element Wt%, Lisheen Galena, July 1997. Operating Parameters: 20kV, 20nA, 1-2µm.							
Pts 11-15, 095/335.0.							
	S	Pb	Ag	Bi	Mn	Cd	Total
#11	13.02	86.00	0.04	0.00	0.00	0.00	99.06
#12	12.85	87.79	0.00	0.10	0.00	0.00	100.74
#13	12.99	88.10	0.03	0.05	0.03	0.05	101.24
#14	13.03	87.86	0.19	0.00	0.01	0.11	101.20
#15	12.77	87.08	0.19	0.00	0.04	0.00	100.08

Element Wt%, Lisheen Galena, July 1997. Operating Parameters: 20kV, 20nA, 1-2µm.							
Pts 1-10, 179/176.25.							
	S	Pb	Ag	Bi	Mn	Cd	Total
#1	13.36	85.83	0.05	0.07	0.03	0.05	99.37
#2	13.42	84.79	0.03	0.05	0.00	0.06	98.35
#3	13.24	87.33	0.00	0.00	0.00	0.00	100.56
#4	13.25	85.68	0.04	0.00	0.02	0.05	99.04
#5	13.45	85.89	0.00	0.02	0.00	0.11	99.48
#6	13.61	86.37	0.06	0.07	0.00	0.15	100.26
#8	13.60	84.96	0.00	0.00	0.01	0.08	98.65
#9	13.23	85.98	0.00	0.09	0.00	0.00	99.30
#10	13.23	86.08	0.02	0.00	0.01	0.20	99.53

Element Wt%, Lisheen Galena, December 1996. Operating Parameters:						
20kV, 20nA, 1-2µm.Pts 1-10, 137/130.0 (Anhedral galena).						
	S	Ag	Tl	Pb	Bi	Total
#1	13.78	0.03	0.09	84.57	0.01	98.46
#2	13.58	0.02	0.00	85.08	0.00	98.68
#3	13.39	0.03	0.18	85.01	0.00	98.60
#4	13.66	0.00	0.19	85.51	0.10	99.46
#5	13.55	0.06	0.00	85.67	0.00	99.28
#6	13.58	0.00	0.00	85.21	0.02	98.81
#7	13.60	0.00	0.10	85.85	0.00	99.55
#8	13.42	0.06	0.00	86.02	0.00	99.49
#9	13.73	0.03	0.00	86.04	0.11	99.90

Element Wt%, Lisheen Galena, December 1996. Operating Parameters:						
20kV, 20nA, 1-2µm.Pts 1-5, 235/167.0.						
	S	Ag	Tl	Pb	Bi	Total
#1	13.34	0.09	0.14	84.77	0.00	98.34
#2	13.51	0.03	0.11	86.18	0.01	99.85
#3	13.74	0.04	0.00	85.98	0.00	99.75
#4	13.54	0.06	0.02	86.10	0.00	99.72
#5	13.40	0.00	0.06	84.97	0.09	98.52

Element Wt%, Lisheen Galena, December 1996. Operating Parameters:						
20kV, 20nA, 1-2µm.Pts 1-5, 361/223.4b.						
	S	Ag	Tl	Pb	Bi	Total
#1	13.34	0.09	0.17	86.40	0.00	99.99
#2	13.47	0.00	0.00	86.87	0.00	100.34
#3	13.44	0.00	0.09	86.20	0.00	99.73
#4	13.78	0.00	0.01	85.98	0.00	99.77
#5	13.64	0.03	0.04	86.18	0.00	99.89
#6	13.56	0.03	0.01	85.33	0.11	99.03
#7	13.59	0.00	0.08	86.14	0.13	99.94
#8	13.59	0.00	0.10	85.60	0.00	99.29
#9	13.61	0.05	0.06	85.92	0.00	99.64
#10	13.44	0.00	0.00	84.74	0.01	98.20

Element Wt%, Lisheen Galena, December 1996. Operating Parameters:						
20kV, 20nA, 1-2µm.Pts 1-5, 400/205.65b.						
	S	Ag	Tl	Pb	Bi	Total
#1	13.64	0.00	0.12	85.31	0.02	99.09
#2	13.63	0.00	0.04	85.81	0.00	99.47
#3	13.57	0.03	0.08	86.38	0.04	100.09
#4	13.58	0.02	0.23	86.32	0.00	100.14
#5	13.62	0.09	0.00	86.03	0.03	99.77
#6	13.34	0.07	0.02	84.88	0.05	98.35
#7	13.33	0.00	0.13	84.66	0.00	98.12
#8	13.57	0.00	0.04	86.88	0.00	100.48
#9	13.36	0.01	0.13	86.19	0.02	99.71
#10	13.34	0.00	0.12	85.58	0.00	99.04

Element Wt%, Lisheen Galena, September 1996. Operating Parameters: 15kV, 20nA, 1-2µm.															
Pts 1-22, 402/196.0.															
	Mn	S	Fe	Cu	Zn	Ga	Ge	As	Ag	Sb	Te	Hg	Pb	Bi	Total
#1	0.00	13.19	0.00	0.00	0.00	0.04	0.00	0.04	0.00	0.02	0.13	0.00	86.19	0.02	99.63
#2	0.05	13.10	0.00	0.00	0.03	0.00	0.08	0.05	0.00	0.12	0.03	0.00	86.13	0.00	99.59
#3	0.00	13.46	0.00	0.10	0.00	0.04	0.02	0.02	0.05	0.00	0.13	0.00	87.02	0.11	100.94
#4	0.02	13.46	0.05	0.22	0.48	0.00	0.01	0.09	0.00	0.03	0.07	0.00	85.26	0.01	99.69
#5	0.11	13.28	0.07	0.02	0.00	0.05	0.08	0.06	0.03	0.00	0.00	0.00	85.29	0.10	99.09
#6	0.00	12.99	0.00	0.02	0.00	0.00	0.02	0.00	0.00	0.00	0.15	0.00	85.69	0.07	98.94
#7	0.00	13.27	0.00	0.17	0.12	0.00	0.08	0.09	0.02	0.00	0.18	0.00	86.00	0.01	99.94
#8	0.10	13.27	0.04	0.05	0.00	0.00	0.00	0.04	0.02	0.06	0.08	0.00	84.76	0.00	98.42
#9	0.07	13.13	0.09	0.00	0.00	0.02	0.09	0.05	0.02	0.02	0.06	0.00	85.26	0.12	98.92
#10	0.00	13.28	0.13	0.00	0.00	0.00	0.03	0.06	0.00	0.00	0.08	0.00	86.81	0.15	100.55
#11	0.08	13.44	0.05	0.21	0.21	0.07	0.00	0.02	0.04	0.03	0.07	0.00	86.62	0.01	100.85
#12	0.07	13.09	0.06	0.07	0.00	0.05	0.05	0.05	0.00	0.02	0.09	0.00	86.66	0.00	100.19
#13	0.05	13.28	0.00	0.00	0.29	0.00	0.02	0.00	0.00	0.00	0.04	0.00	85.02	0.01	98.71
#15	0.05	13.14	0.11	0.09	0.00	0.01	0.03	0.03	0.00	0.01	0.18	0.00	85.80	0.13	99.58
#16	0.00	13.17	0.07	0.01	0.00	0.03	0.02	0.00	0.02	0.00	0.07	0.00	85.39	0.05	98.83
#17	0.00	13.46	0.05	0.04	0.00	0.00	0.13	0.04	0.02	0.01	0.12	0.00	85.25	0.02	99.13
#18	0.00	13.08	0.06	0.00	0.00	0.04	0.06	0.04	0.03	0.02	0.00	0.00	86.17	0.18	99.67
#19	0.00	13.08	0.00	0.18	0.00	0.00	0.00	0.02	0.00	0.02	0.04	0.00	85.54	0.00	98.88
#20	0.22	13.23	0.10	0.00	0.00	0.00	0.00	0.03	0.07	0.00	0.01	0.00	86.05	0.09	99.79
#21	0.09	13.30	0.02	0.00	0.31	0.00	0.06	0.05	0.00	0.08	0.09	0.00	85.31	0.00	99.30
#22	0.00	13.23	0.00	0.12	0.00	0.01	0.01	0.04	0.05	0.09	0.01	0.00	85.19	0.00	98.75

Element Wt%, Lisheen Galena, September 1996. Operating Parameters: 15kV, 20nA, 1-2µm.															
Pts 23-42, 395/194.05.															
	Mn	S	Fe	Cu	Zn	Ga	Ge	As	Ag	Sb	Te	Hg	Pb	Bi	Total
#23	0.13	13.60	0.00	0.22	0.31	0.00	0.02	0.04	0.00	0.00	0.04	0.00	85.79	0.16	100.30
#24	0.07	13.44	0.00	0.03	0.17	0.00	0.05	0.03	0.01	0.01	0.00	0.00	87.03	0.00	100.84
#25	0.04	13.32	0.01	0.00	0.00	0.00	0.05	0.01	0.00	0.00	0.10	0.00	87.04	0.01	100.58
#26	0.00	13.16	0.05	0.04	0.00	0.00	0.02	0.05	0.04	0.00	0.08	0.00	85.81	0.08	99.31
#27	0.00	13.41	0.11	0.15	0.00	0.00	0.11	0.02	0.05	0.02	0.10	0.00	86.99	0.00	100.96
#28	0.11	13.26	0.00	0.08	0.00	0.03	0.00	0.02	0.05	0.00	0.12	0.00	87.60	0.00	101.27
#29	0.05	13.34	0.00	0.15	0.00	0.00	0.02	0.03	0.04	0.09	0.00	0.00	85.94	0.00	99.66
#30	0.15	13.40	0.21	0.01	0.19	0.00	0.02	0.00	0.00	0.00	0.00	0.00	86.64	0.25	100.86
#31	0.00	13.54	0.00	0.21	0.00	0.00	0.00	0.01	0.05	0.00	0.05	0.00	86.57	0.04	100.46
#33	0.04	13.44	0.14	0.00	0.03	0.01	0.03	0.03	0.05	0.02	0.10	0.00	86.21	0.01	100.12
#34	0.12	13.33	0.00	0.00	0.00	0.00	0.00	0.04	0.05	0.03	0.00	0.00	87.20	0.05	100.82
#35	0.06	13.43	0.02	0.09	0.16	0.00	0.03	0.04	0.03	0.00	0.07	0.00	86.43	0.07	100.42
#36	0.00	13.31	0.00	0.03	0.07	0.00	0.04	0.00	0.00	0.05	0.09	0.00	86.08	0.04	99.71
#37	0.09	13.33	0.02	0.03	0.00	0.05	0.02	0.04	0.08	0.04	0.00	0.00	86.23	0.15	100.07
#38	0.04	13.10	0.00	0.03	0.00	0.03	0.00	0.02	0.03	0.01	0.15	0.00	86.38	0.00	99.77
#39	0.01	13.29	0.00	0.18	0.00	0.03	0.09	0.01	0.02	0.00	0.22	0.00	86.69	0.13	100.65
#40	0.00	13.36	0.00	0.24	0.00	0.00	0.04	0.03	0.07	0.00	0.15	0.00	85.58	0.01	99.48
#41	0.03	13.22	0.00	0.00	0.00	0.00	0.07	0.03	0.00	0.00	0.13	0.00	86.86	0.06	100.39
#42	0.01	13.07	0.00	0.00	0.00	0.03	0.04	0.00	0.06	0.11	0.06	0.00	86.32	0.13	99.82

Element Wt%, Lisheen Galena, September 1996. Operating Parameters: 15kV, 20nA, 1-2µm.															
Pts 1-21, 420/190.0.															
	Mn	S	Fe	Cu	Zn	Ga	Ge	As	Ag	Sb	Te	Hg	Pb	Bi	Total
#1	0.00	12.76	0.00	0.01	0.06	0.00	0.03	0.04	0.00	0.00	0.27	0.00	84.77	0.12	98.07
#2	0.00	13.03	0.05	0.14	0.00	0.00	0.00	0.20	0.00	0.07	0.02	0.00	86.12	0.13	99.75
#3	0.00	13.24	0.04	0.00	0.54	0.06	0.05	0.03	0.00	0.02	0.20	0.00	86.14	0.07	100.40
#4	0.00	13.07	0.00	0.01	0.00	0.07	0.00	0.03	0.00	0.00	0.00	0.00	85.60	0.00	98.79
#5	0.00	13.16	0.04	0.10	0.54	0.01	0.04	0.00	0.01	0.00	0.15	0.00	84.17	0.03	98.26
#6	0.00	13.34	0.10	0.00	0.00	0.01	0.03	0.00	0.04	0.02	0.11	0.00	85.50	0.00	99.15
#7	0.00	13.20	0.04	0.00	0.06	0.00	0.01	0.03	0.00	0.00	0.13	0.00	85.33	0.07	98.87
#8	0.00	13.20	0.06	0.17	0.11	0.00	0.04	0.05	0.04	0.01	0.00	0.00	84.92	0.19	98.77
#9	0.10	13.03	0.06	0.03	0.00	0.01	0.07	0.00	0.00	0.01	0.14	0.00	85.41	0.00	98.86
#10	0.00	13.24	0.04	0.00	0.15	0.00	0.00	0.02	0.00	0.00	0.00	0.00	86.00	0.03	99.47
#11	0.00	13.33	0.00	0.00	0.00	0.00	0.02	0.00	0.06	0.00	0.16	0.00	84.88	0.05	98.49
#12	0.00	13.17	0.06	0.10	0.00	0.01	0.05	0.03	0.02	0.00	0.12	0.00	84.95	0.08	98.60
#13	0.00	12.90	0.00	0.00	0.00	0.04	0.06	0.03	0.01	0.00	0.10	0.00	85.40	0.18	98.73
#14	0.00	13.13	0.06	0.00	0.00	0.01	0.07	0.00	0.07	0.04	0.11	0.00	83.15	0.00	96.65
#15	0.18	13.20	0.00	0.39	0.22	0.00	0.00	0.02	0.00	0.13	0.06	0.00	84.37	0.14	98.71
#20	0.06	13.06	0.12	0.15	0.02	0.00	0.05	0.01	0.00	0.00	0.18	0.00	84.56	0.15	98.36

Element Wt%, Lisheen Galena, September 1996. Operating Parameters: 15kV, 20nA, 1-2µm.															
Pts 22-43, 045/215.20.															
	Mn	S	Fe	Cu	Zn	Ga	Ge	As	Ag	Sb	Te	Hg	Pb	Bi	Total
#25	0.09	13.22	0.21	0.23	0.00	0.03	0.05	0.00	0.06	0.11	0.07	0.02	84.93	0.05	99.07
#26	0.00	13.06	0.05	0.00	0.00	0.00	0.03	0.02	0.04	0.06	0.03	0.00	85.60	0.00	98.89
#27	0.10	13.22	0.00	0.00	0.06	0.02	0.06	0.00	0.00	0.01	0.06	0.00	85.06	0.05	98.63
#28	0.14	13.08	0.10	0.23	0.45	0.00	0.02	0.03	0.00	0.05	0.03	0.00	84.82	0.01	98.96
#29	0.00	13.08	0.02	0.00	0.00	0.00	0.03	0.02	0.04	0.03	0.00	0.00	85.40	0.00	98.62
#30	0.16	13.10	0.10	0.03	0.00	0.00	0.00	0.00	0.00	0.03	0.05	0.00	85.03	0.11	98.61
#31	0.00	13.08	0.03	0.14	0.00	0.05	0.02	0.05	0.00	0.00	0.11	0.00	84.56	0.00	98.04
#32	0.00	13.00	0.06	0.00	0.00	0.00	0.08	0.00	0.00	0.00	0.01	0.00	84.94	0.11	98.19
#33	0.07	13.04	0.05	0.14	0.32	0.01	0.07	0.04	0.02	0.00	0.05	0.00	84.52	0.00	98.34
#34	0.04	12.97	0.03	0.00	0.09	0.04	0.02	0.03	0.04	0.00	0.09	0.00	85.37	0.10	98.83
#35	0.05	13.15	0.00	0.20	0.00	0.05	0.06	0.02	0.00	0.00	0.15	0.00	85.14	0.20	99.01
#39	0.13	13.10	0.07	0.15	0.00	0.01	0.00	0.02	0.00	0.04	0.09	0.00	85.32	0.02	98.93
#42	0.20	13.06	0.01	0.00	0.24	0.01	0.02	0.09	0.03	0.00	0.00	0.00	84.71	0.11	98.49
#43	0.03	13.09	0.09	0.25	0.17	0.05	0.06	0.00	0.00	0.05	0.02	0.00	83.91	0.34	98.05

Element Wt%, Lisheen Galena, September 1996. Operating Parameters: 15kV, 20nA, 1-2µm.																
Pts 1-25, 431/199.65.																
	Mn	S	Fe	Cu	Zn	Ga	Ge	As	Ag	Sb	Te	Hg	Pb	Bi	Total	
#1	0.06	13.43	0.07	0.02	0.00	0.01	0.05	0.04	0.02	0.04	0.14	0.00	85.07	0.13	99.08	
#2	0.09	13.29	0.00	0.01	0.00	0.00	0.02	0.00	0.00	0.03	0.10	0.00	85.82	0.16	99.53	
#3	0.08	13.27	0.02	0.00	0.00	0.00	0.03	0.00	0.00	0.00	0.01	0.00	84.90	0.00	98.30	
#4	0.00	13.26	0.07	0.00	0.00	0.01	0.00	0.00	0.00	0.03	0.10	0.00	86.30	0.00	99.76	
#5	0.00	13.36	0.00	0.00	0.00	0.01	0.03	0.03	0.05	0.08	0.00	0.00	85.56	0.08	99.21	
#6	0.00	13.22	0.05	0.00	0.17	0.02	0.07	0.00	0.04	0.00	0.17	0.00	85.82	0.06	99.61	
#7	0.02	13.21	0.07	0.00	0.05	0.06	0.01	0.03	0.00	0.07	0.08	0.00	85.03	0.11	98.73	
#8	0.05	13.05	0.06	0.04	0.00	0.01	0.05	0.06	0.10	0.04	0.13	0.00	86.84	0.00	100.43	
#9	0.00	13.52	0.06	0.00	0.00	0.03	0.03	0.03	0.13	0.05	0.05	0.00	86.23	0.20	100.32	
#10	0.13	13.12	0.03	0.20	0.00	0.01	0.07	0.06	0.00	0.11	0.19	0.00	86.02	0.08	100.02	
#11	0.09	13.32	0.00	0.00	0.27	0.00	0.07	0.00	0.00	0.07	0.02	0.00	86.57	0.07	100.49	
#12	0.00	13.15	0.10	0.07	0.04	0.04	0.06	0.00	0.01	0.00	0.16	0.00	85.82	0.13	99.58	
#13	0.02	13.40	0.00	0.00	0.14	0.00	0.03	0.01	0.00	0.00	0.02	0.00	85.29	0.18	99.07	
#14	0.03	13.54	0.09	0.13	0.49	0.00	0.05	0.01	0.07	0.03	0.05	0.00	84.11	0.06	98.66	
#15	0.04	13.44	0.03	0.08	0.42	0.02	0.00	0.05	0.01	0.04	0.09	0.00	85.70	0.09	100.02	
#16	0.13	13.30	0.00	0.24	0.00	0.04	0.03	0.00	0.04	0.00	0.15	0.00	84.84	0.12	98.89	
#17	0.01	12.98	0.03	0.00	0.31	0.01	0.09	0.00	0.10	0.01	0.19	0.00	86.14	0.25	100.11	
#18	0.00	13.32	0.04	0.05	0.41	0.00	0.09	0.01	0.07	0.00	0.05	0.00	86.24	0.00	100.25	
#19	0.00	13.13	0.08	0.11	0.17	0.00	0.02	0.01	0.04	0.03	0.07	0.00	85.25	0.00	98.91	
#20	0.10	13.47	0.03	0.00	0.00	0.03	0.08	0.00	0.00	0.00	0.13	0.00	85.10	0.00	98.93	
#21	0.13	12.92	0.06	0.00	0.09	0.02	0.00	0.01	0.00	0.01	0.11	0.00	85.46	0.04	98.85	
#22	0.08	13.30	0.09	0.25	0.05	0.00	0.01	0.03	0.07	0.02	0.02	0.00	86.83	0.13	100.86	
#23	0.02	13.21	0.00	0.12	0.68	0.00	0.09	0.03	0.00	0.00	0.07	0.00	84.99	0.00	99.21	
#24	0.00	13.47	0.16	0.00	0.00	0.01	0.09	0.06	0.11	0.13	0.10	0.00	85.62	0.00	99.74	
#25	0.27	12.92	0.00	0.26	0.37	0.00	0.06	0.00	0.00	0.00	0.01	0.00	86.14	0.10	100.11	

Element Wt%, Lisheen Galena, September 1996. Operating Parameters: 15kV, 20nA, 1-2µm.																
Pts 26-44, 359/148.65.																
	Mn	S	Fe	Cu	Zn	Ga	Ge	As	Ag	Sb	Te	Hg	Pb	Bi	Total	
#26	0.04	12.89	0.14	0.08	0.00	0.06	0.02	0.04	0.00	0.02	0.11	0.00	86.33	0.00	99.72	
#27	0.00	13.57	0.02	0.00	2.26	0.00	0.06	0.00	0.00	0.00	0.05	0.00	82.12	0.21	98.27	
#28	0.05	13.14	0.00	0.00	0.13	0.00	0.04	0.03	0.04	0.00	0.02	0.00	86.07	0.01	99.53	
#29	0.04	12.85	0.00	0.00	0.15	0.01	0.06	0.02	0.00	0.00	0.08	0.00	86.15	0.21	99.56	
#30	0.05	13.81	0.00	0.09	1.69	0.05	0.08	0.05	0.05	0.02	0.00	0.00	83.29	0.00	99.19	
#31	0.16	13.45	0.00	0.27	0.39	0.01	0.00	0.00	0.00	0.00	0.06	0.00	85.63	0.08	100.04	
#32	0.00	13.46	0.00	0.00	1.01	0.04	0.08	0.07	0.08	0.01	0.12	0.08	84.56	0.20	99.71	
#33	0.07	13.85	0.00	0.22	2.03	0.02	0.03	0.01	0.00	0.06	0.07	0.00	82.38	0.20	98.94	
#34	0.09	13.07	0.01	0.02	0.24	0.03	0.00	0.00	0.00	0.00	0.14	0.00	87.10	0.06	100.77	
#35	0.00	13.42	0.00	0.16	0.00	0.03	0.03	0.04	0.00	0.04	0.09	0.00	85.27	0.28	99.37	
#36	0.00	13.18	0.01	0.21	0.02	0.00	0.03	0.01	0.00	0.00	0.00	0.00	84.98	0.11	98.56	
#37	0.10	12.94	0.00	0.00	0.12	0.00	0.00	0.00	0.00	0.06	0.07	0.00	86.59	0.07	99.95	
#38	0.00	13.29	0.00	0.00	0.26	0.00	0.01	0.07	0.01	0.06	0.11	0.00	86.12	0.11	100.04	
#39	0.09	12.92	0.00	0.00	0.01	0.01	0.02	0.01	0.00	0.00	0.07	0.00	86.17	0.03	99.33	
#40	0.04	13.17	0.00	0.00	0.00	0.03	0.00	0.00	0.00	0.09	0.01	0.10	0.00	85.65	0.13	99.22
#41	0.09	13.25	0.04	0.00	0.00	0.00	0.00	0.04	0.07	0.07	0.18	0.00	84.57	0.01	98.31	
#42	0.00	13.07	0.00	0.22	0.00	0.00	0.04	0.00	0.02	0.00	0.00	0.00	85.77	0.16	99.28	
#43	0.05	13.40	0.01	0.28	0.01	0.07	0.02	0.04	0.00	0.00	0.00	0.00	86.13	0.04	100.05	
#44	0.00	13.30	0.09	0.00	0.31	0.00	0.09	0.03	0.00	0.03	0.13	0.00	87.29	0.12	101.40	

Pyrite

Element Wt%, Lishen Pyrite, July 1997. Operating Parameters: 20kV, 20nA, 1-2µm.									
Pts 1-10, 471/210.4.									
	S	Fe	Mn	Co	Ni	Cu	As	Cd	Total
#1	53.01	47.87	0.00	0.02	0.00	0.00	0.54	0.01	101.44
#2	52.67	47.62	0.01	0.01	0.00	0.00	0.69	0.02	101.02
#3	52.41	47.62	0.01	0.02	0.02	0.02	1.10	0.00	101.20
#4	52.54	47.69	0.00	0.03	0.03	0.02	1.05	0.02	101.38
#5	52.90	47.90	0.00	0.07	0.00	0.00	0.23	0.00	101.10
#6	53.03	48.08	0.00	0.04	0.02	0.00	0.24	0.04	101.45
#8	52.81	48.27	0.00	0.07	0.04	0.02	0.18	0.07	101.46
#10	52.53	47.91	0.01	0.03	0.02	0.00	0.67	0.01	101.18

Element Wt%, Lishen Pyrite, July 1997. Operating Parameters: 20kV, 20nA, 1-2µm.									
Pts 1-10, 262/153.6.									
	S	Fe	Mn	Co	Ni	Cu	As	Cd	Total
#1	53.02	47.71	0.01	0.05	0.00	0.00	0.11	0.00	100.90
#2	52.33	47.74	0.00	0.05	0.00	0.00	0.79	0.00	100.90
#3	52.36	47.76	0.00	0.05	0.03	0.05	0.62	0.00	100.87
#4	52.26	47.85	0.01	0.06	0.03	0.01	0.50	0.01	100.73
#5	52.44	47.64	0.02	0.05	0.00	0.00	0.75	0.00	100.90
#6	53.19	47.86	0.01	0.02	0.01	0.01	0.10	0.06	101.25
#7	51.90	47.46	0.00	0.07	0.04	0.02	0.72	0.08	100.29
#8	53.05	48.12	0.01	0.02	0.01	0.02	0.16	0.04	101.43
#9	53.17	48.06	0.00	0.01	0.01	0.03	0.16	0.06	101.50
#10	52.60	47.29	0.02	0.01	0.01	0.04	0.49	0.03	100.49

Element Wt%, Lishen Pyrite, July 1997. Operating Parameters: 20kV, 20nA, 1-2µm.									
Pts 11-21, 262/162.1.									
	S	Fe	Mn	Co	Ni	Cu	As	Cd	Total
#11	52.83	47.63	0.00	0.00	0.00	0.02	0.11	0.00	100.60
#12	52.98	47.91	0.01	0.06	0.02	0.04	0.10	0.00	101.11
#13	52.47	47.31	0.01	0.00	0.01	0.02	0.15	0.03	100.01
#14	52.35	47.38	0.01	0.01	0.01	0.00	0.53	0.04	100.33
#15	52.59	47.03	0.04	0.05	0.11	0.00	0.40	0.04	100.26
#16	53.07	47.73	0.02	0.05	0.03	0.03	0.13	0.00	101.06
#17	52.99	47.70	0.02	0.04	0.00	0.15	0.12	0.03	101.05
#18	53.19	47.90	0.00	0.02	0.00	0.00	0.10	0.00	101.21
#19	53.59	47.58	0.00	0.02	0.00	0.05	0.10	0.01	101.36
#20	51.32	47.09	0.00	0.06	0.01	0.03	0.19	0.02	98.72
#21	52.92	47.94	0.01	0.06	0.08	0.00	0.18	0.02	101.20

Element Wt%, Lishen Pyrite, July 1997. Operating Parameters: 20kV, 20nA, 1-2µm.									
Pts 22-31, 095/335.0.									
	S	Fe	Mn	Co	Ni	Cu	As	Cd	Total
#22	52.48	47.39	0.00	0.04	0.35	0.02	0.06	0.00	100.35
#23	52.37	48.04	0.02	0.03	0.00	0.00	0.02	0.00	100.48
#24	52.54	47.61	0.01	0.05	0.00	0.03	0.08	0.00	100.32
#25	52.11	47.89	0.02	0.06	0.02	0.02	0.10	0.05	100.25
#26	52.39	47.72	0.00	0.05	0.02	0.03	0.11	0.02	100.33
#27	52.13	47.36	0.03	0.05	0.11	0.00	0.16	0.00	99.84
#28	51.82	47.41	0.00	0.11	0.09	0.06	0.21	0.04	99.74
#29	51.79	47.54	0.00	0.02	0.04	0.00	0.12	0.02	99.52
#30	51.68	47.46	0.03	0.04	0.03	0.03	0.16	0.06	99.48
#31	51.66	47.11	0.01	0.05	0.01	0.04	0.10	0.00	98.97

Elements Wt%, Lisheen Pyrite, December 1996. Operating Parameters: 20kV, 20nA, 1-2µm.								
Pts 1-14, 431/205.70.								
	S	Mn	Fe	Co	Ni	Cu	As	Total
#1	52.30	0.00	47.41	0.02	0.00	0.00	0.26	99.99
#2	52.95	0.00	47.55	0.00	0.04	0.07	0.34	100.94
#3	52.76	0.01	47.61	0.04	0.01	0.05	0.42	100.89
#4	52.51	0.01	47.54	0.04	0.04	0.00	0.40	100.53
#5	52.72	0.00	47.38	0.07	0.00	0.00	0.44	100.61
#6	52.90	0.00	47.31	0.04	0.01	0.02	0.33	100.60
#7	52.61	0.02	47.67	0.03	0.00	0.02	0.52	100.86
#8	52.62	0.02	47.52	0.01	0.00	0.01	0.34	100.52
#9	53.01	0.00	47.63	0.05	0.03	0.04	0.41	101.16
#10	52.73	0.00	47.58	0.04	0.03	0.01	0.32	100.72
#11	51.00	0.01	44.82	0.04	0.03	0.22	4.05	100.16
#12	52.19	0.00	46.31	0.01	0.00	0.03	1.95	100.49
#13	50.49	0.04	44.25	0.05	0.00	0.12	5.21	100.15
#14	51.57	0.00	45.88	0.05	0.00	0.03	2.97	100.50

Elements Wt%, Lisheen Pyrite, December 1996. Operating Parameters: 20kV, 20nA, 1-2µm.								
Pts 1-5, 395/194.05.								
	S	Mn	Fe	Co	Ni	Cu	As	Total
#2	53.03	0.01	48.36	0.03	0.02	0.00	0.10	101.54
#4	53.09	0.00	47.77	0.02	0.05	0.05	0.05	101.01

Elements Wt%, Lisheen Pyrite, December 1996. Operating Parameters: 20kV, 20nA, 1-2µm.								
Pts 1-10, 235/167.0.								
	S	Mn	Fe	Co	Ni	Cu	As	Total
#1	52.93	0.02	47.31	0.00	0.11	0.05	0.15	100.56
#2	51.86	0.00	46.72	0.08	0.05	0.02	0.16	98.88
#4	52.56	0.02	46.98	0.09	0.13	0.02	0.18	99.98
#5	53.10	0.01	47.24	0.07	0.09	0.04	0.14	100.69
#7	52.46	0.01	46.72	0.07	0.00	0.03	0.11	99.41
#8	52.93	0.01	47.53	0.03	0.11	0.03	0.23	100.86

Elements Wt%, Lisheen Pyrite, December 1996. Operating Parameters: 20kV, 20nA, 1-2µm.								
Pts 1-10, 429/192.1.								
	S	Mn	Fe	Co	Ni	Cu	As	Total
#2	51.31	0.01	45.92	0.44	0.16	0.03	0.48	98.34
#3	50.22	0.01	44.13	0.19	1.92	0.03	3.34	99.84
#4	51.27	0.00	45.78	0.24	0.44	0.05	1.53	99.30
#5	52.60	0.00	46.70	0.09	0.11	0.00	0.24	99.73
#6	52.70	0.01	46.87	0.15	0.14	0.05	0.16	100.06
#8	53.13	0.02	47.10	0.08	0.07	0.00	0.18	100.58
#10	51.70	0.02	46.19	0.10	0.20	0.05	1.78	100.04

Elements Wt%, Lisheen Pyrite, December 1996. Operating Parameters: 20kV, 20nA, 1-2µm.								
Pts 1-10, 137/130.0a.								
	S	Mn	Fe	Co	Ni	Cu	As	Total
#1	51.58	0.00	47.09	0.05	0.00	0.00	2.67	101.39
#2	51.87	0.00	47.41	0.06	0.03	0.00	2.11	101.48
#3	52.71	0.00	47.71	0.05	0.05	0.03	0.95	101.50
#5	52.38	0.00	46.77	0.06	0.00	0.02	1.98	101.21
#7	53.29	0.01	47.63	0.04	0.04	0.00	0.42	101.43

Elements Wt%, Lisheen Pyrite, December 1996. Operating Parameters: 20kV, 20nA, 1-2µm.								
Pts 1-10, 137/130.0b.								
	S	Mn	Fe	Co	Ni	Cu	As	Total
#3	52.63	0.07	47.07	0.01	0.03	0.00	0.98	100.79
#9	53.17	0.04	47.40	0.03	0.00	0.03	0.65	101.32

Tennantite

Element Wt%, Lisheen Tennantite, July 1997. Operating Parameters: 20kV, 20nA, 1-2µm.												
Pts 1-10, 179/176.25.												
	S	Zn	Cu	Mn	Ga	Ge	Cd	In	Fe	As	Ag	Total
#1	28.00	3.62	42.25	0.00	0.00	0.00	0.07	0.00	4.41	20.60	0.19	99.13
#2	28.11	3.57	41.52	0.02	0.00	0.00	0.07	0.03	5.63	20.58	0.32	99.83
#3	27.89	3.68	41.69	0.00	0.00	0.00	0.01	0.04	4.62	21.07	0.19	99.19
#4	28.16	3.77	42.18	0.00	0.00	0.00	0.05	0.00	4.25	20.77	0.25	99.43
#5	28.19	3.91	42.82	0.00	0.00	0.00	0.06	0.01	4.34	20.91	0.15	100.39
#6	28.03	3.66	42.38	0.01	0.00	0.00	0.08	0.04	4.33	20.64	0.25	99.43
#7	28.09	3.76	42.36	0.01	0.00	0.00	0.00	0.02	4.44	20.85	0.13	99.65
#8	28.10	3.61	42.53	0.00	0.00	0.00	0.00	0.00	4.65	20.92	0.26	100.07
#9	27.98	3.72	42.19	0.00	0.00	0.00	0.01	0.05	4.56	21.01	0.17	99.69
#10	28.25	3.75	41.96	0.01	0.00	0.00	0.03	0.02	4.30	20.84	0.05	99.21

Element Wt%, Lisheen Tennantite, March/April 1995. Operating Parameters: 20kV, 20nA, 1-2µm.															
Pts 1-30, 121/192.8b, (salrun2).															
	Hg	Cd	Ag	Tl	S	In	Sb	Zn	Fe	Mn	Cu	As	Ga	Ge	Total
#1	0.00	0.00	0.11	0.22	27.87	0.00	0.01	8.47	1.63	0.00	41.59	21.05	0.14	0.00	101.09
#2	0.06	0.04	0.21	0.05	27.41	0.00	0.02	8.55	1.61	0.00	41.42	21.25	0.09	0.00	100.69
#3	0.00	0.12	0.07	0.03	27.63	0.00	0.01	6.82	1.56	0.00	41.36	21.02	0.00	0.00	98.62
#4	0.00	0.08	0.11	0.41	27.56	0.02	0.00	7.94	1.61	0.03	41.35	21.34	0.00	0.00	100.44
#5	0.00	0.02	0.08	0.12	27.59	0.06	0.13	6.71	1.64	0.00	41.71	21.31	0.00	0.04	99.41
#6	0.07	0.07	0.20	0.36	27.49	0.00	0.00	7.16	1.61	0.03	41.92	21.24	0.06	0.00	100.20
#7	0.01	0.11	0.17	0.32	27.65	0.00	0.00	6.94	1.60	0.02	41.82	21.12	0.03	0.00	99.77
#8	0.00	0.08	0.24	0.00	27.79	0.00	0.00	6.99	1.66	0.01	42.13	21.17	0.01	0.00	100.08
#9	0.09	0.15	0.14	0.22	27.71	0.00	0.02	6.78	1.64	0.02	41.77	21.09	0.00	0.00	99.63
#10	0.18	0.05	0.10	0.37	27.65	0.00	0.05	7.45	1.62	0.02	42.21	21.25	0.05	0.00	101.01
#11	0.00	0.00	0.09	0.00	27.97	0.12	0.01	8.23	1.62	0.02	41.16	21.31	0.00	0.00	100.53
#12	0.01	0.06	0.17	0.00	27.75	0.00	0.00	6.35	1.60	0.00	41.63	21.04	0.00	0.00	98.60
#13	0.12	0.11	0.00	0.17	27.67	0.01	0.03	6.56	1.58	0.05	41.94	21.06	0.04	0.00	99.34
#14	0.02	0.19	0.18	0.11	27.56	0.00	0.08	6.41	1.57	0.03	41.58	21.28	0.17	0.00	99.17
#15	0.00	0.14	0.17	0.07	27.75	0.00	0.01	6.61	1.60	0.01	42.28	21.50	0.00	0.10	100.25
#16	0.14	0.08	0.14	0.00	27.90	0.00	0.00	6.35	1.56	0.00	41.98	21.30	0.03	0.00	99.48
#17	0.03	0.06	0.16	0.23	27.80	0.01	0.04	6.31	1.55	0.00	41.58	21.15	0.13	0.00	99.06
#18	0.06	0.04	0.12	0.17	27.70	0.00	0.07	6.07	1.63	0.02	41.39	20.84	0.12	0.00	98.23
#20	0.05	0.15	0.14	0.15	27.79	0.00	0.07	6.43	1.64	0.00	41.87	20.84	0.00	0.00	99.12
#21	0.04	0.14	0.14	0.45	27.93	0.00	0.02	6.42	1.65	0.04	42.09	20.99	0.04	0.00	99.96
#22	0.00	0.11	0.10	0.11	27.66	0.00	0.06	6.33	1.65	0.01	41.68	21.46	0.00	0.00	99.16
#23	0.00	0.13	0.10	0.21	27.74	0.00	0.00	6.51	1.60	0.06	41.86	21.06	0.00	0.00	99.27
#24	0.02	0.14	0.14	0.28	27.53	0.09	0.07	6.44	1.59	0.02	41.67	21.16	0.05	0.00	99.19
#25	0.20	0.12	0.17	0.00	27.90	0.02	0.05	6.36	1.56	0.00	41.43	21.02	0.05	0.02	98.89
#26	0.00	0.08	0.05	0.10	27.44	0.04	0.07	7.09	1.68	0.04	41.54	21.21	0.00	0.00	99.35
#27	0.14	0.06	0.18	0.32	27.80	0.09	0.02	7.17	1.72	0.00	40.90	21.11	0.10	0.05	99.65
#28	0.01	0.02	0.08	0.07	27.76	0.05	0.02	6.13	1.70	0.01	41.80	21.18	0.02	0.03	98.89
#29	0.14	0.14	0.14	0.00	27.45	0.07	0.00	7.09	1.68	0.00	41.34	20.84	0.03	0.01	98.93
#30	0.01	0.09	0.11	0.20	27.63	0.00	0.03	7.22	1.65	0.00	41.40	20.95	0.03	0.00	99.29

Chalcopyrite

Element Wt%, Lisheen Chalcopyrite, July 1997. Operating Parameters: 20kV, 20nA, 1-2µm.									
Pts 1-10, 361/223.4b.									
	S	Fe	Mn	Co	Ni	Cu	As	Cd	Total
#1	34.10	30.59	0.01	0.04	0.02	34.39	0.05	0.00	99.19
#2	34.00	30.45	0.01	0.00	0.02	34.43	0.05	0.01	98.96
#3	34.67	30.85	0.02	0.00	0.01	34.25	0.05	0.02	99.87
#4	34.17	30.44	0.00	0.00	0.04	34.30	0.10	0.02	99.07
#5	34.38	30.53	0.00	0.03	0.00	34.62	0.07	0.03	99.65
#6	34.26	30.64	0.02	0.03	0.01	34.41	0.04	0.00	99.40
#7	35.08	30.47	0.03	0.03	0.05	34.41	0.10	0.00	100.18
#8	34.28	30.52	0.04	0.02	0.02	34.36	0.06	0.00	99.29
#9	34.64	30.32	0.02	0.01	0.01	34.50	0.10	0.00	99.60
#10	34.48	30.56	0.00	0.00	0.02	34.18	0.08	0.02	99.34

Element Wt%, Lisheen Chalcopyrite, December 1996. Operating Parameters: 20kV, 20nA, 1-2µm.								
Pts 1-10, 235/167.0.								
	S	Mn	Fe	Co	Ni	Cu	As	Total
#1	34.66	0.01	29.58	0.03	0.04	35.82	0.73	100.87
#2	34.97	0.00	30.33	0.05	0.04	36.12	0.03	101.53
#5	34.70	0.03	30.30	0.01	0.02	36.18	0.09	101.33
#7	34.28	0.00	29.40	0.11	0.03	34.16	0.10	98.09
#8	34.81	0.00	29.96	0.03	0.02	36.05	0.21	101.08
#10	34.58	0.02	30.33	0.01	0.01	36.08	0.13	101.16

Element Wt%, Lisheen Chalcopyrite, December 1996. Operating Parameters: 20kV, 20nA, 1-2µm.								
Pts 1-10, 361/223.4b.								
	S	Mn	Fe	Co	Ni	Cu	As	Total
#1	34.56	0.01	30.59	0.05	0.00	36.24	0.03	101.48
#3	34.74	0.01	30.40	0.05	0.02	36.02	0.00	101.23

B7. ELEMENTAL CHEMISTRY - GALMOY SULPHIDES

Sphalerite

Element Wt%, Galmoy sphalerite, July 1997. Operating Parameters, 20kV, 20nA, 1-2µm.												
Pts 1-10, 2(0134) High grade ore, variable coloured crystalline sphalerite.												
	S	Zn	Cu	Mn	Ga	Ge	Cd	In	Fe	As	Ag	Total
#1	32.85	67.92	0.00	0.02	0.00	0.00	0.11	0.02	0.07	0.00	0.03	101.02
#2	32.76	67.48	0.04	0.03	0.00	0.00	0.11	0.00	0.08	0.07	0.04	100.60
#3	32.48	68.17	0.00	0.00	0.01	0.05	0.02	0.00	0.08	0.08	0.01	100.90
#4	32.57	67.90	0.00	0.02	0.03	0.00	0.11	0.01	0.07	0.07	0.00	100.77
#5	32.79	68.09	0.01	0.00	0.00	0.00	0.01	0.04	0.13	0.00	0.00	101.07
#6	32.39	67.83	0.02	0.00	0.00	0.00	0.04	0.00	0.20	0.07	0.04	100.59
#7	32.60	66.79	0.01	0.00	0.00	0.00	0.10	0.05	0.04	0.00	0.00	99.59
#8	32.68	67.46	0.00	0.00	0.00	0.00	0.07	0.02	0.20	0.02	0.04	100.48
#9	32.45	67.83	0.00	0.00	0.09	0.00	0.07	0.03	0.00	0.00	0.00	100.47
#10	32.74	67.80	0.00	0.02	0.00	0.00	0.13	0.00	0.11	0.03	0.01	100.85

Element Wt%, Galmoy sphalerite, July 1997. Operating Parameters, 20kV, 20nA, 1-2µm.												
Pts 1-11, GY382/86.0 (crystalline brown sphalerite).												
	S	Zn	Cu	Mn	Ga	Ge	Cd	In	Fe	As	Ag	Total
#1	32.79	64.80	0.01	0.01	0.00	0.00	0.12	0.00	2.67	0.00	0.11	100.51
#2	33.19	64.95	0.04	0.02	0.00	0.00	0.19	0.01	2.43	0.08	0.05	100.95
#3	32.89	67.58	0.00	0.01	0.00	0.02	0.14	0.02	0.27	0.00	0.02	100.92
#4	32.77	66.09	0.02	0.00	0.00	0.00	0.08	0.00	1.18	0.06	0.07	100.26
#5	32.78	63.79	0.06	0.01	0.00	0.07	0.09	0.00	3.45	0.06	0.04	100.36
#6	32.64	67.58	0.03	0.03	0.00	0.00	0.04	0.04	0.37	0.07	0.02	100.82
#7	32.80	66.57	0.03	0.01	0.00	0.03	0.03	0.01	1.29	0.00	0.00	100.76
#8	32.36	66.89	0.00	0.00	0.00	0.00	0.01	0.01	0.39	0.00	0.06	99.71
#9	32.55	67.10	0.01	0.00	0.00	0.00	0.58	0.01	0.08	0.05	0.00	100.37
#10	32.70	63.70	0.01	0.02	0.00	0.03	0.03	0.00	3.48	0.05	0.12	100.16
#11	32.64	67.15	0.00	0.00	0.03	0.00	0.06	0.05	0.26	0.00	0.02	100.20

Element Wt%, Galmoy sphalerite, July 1997. Operating Parameters, 20kV, 20nA, 1-2µm.												
Pts 12-22, GY382/86.0, (crystalline yellow sphalerite).												
	S	Zn	Cu	Mn	Ga	Ge	Cd	In	Fe	As	Ag	Total
#12	32.27	67.20	0.00	0.03	0.00	0.01	0.71	0.00	0.15	0.03	0.00	100.40
#13	32.87	66.57	0.00	0.00	0.00	0.00	0.54	0.00	0.41	0.06	0.04	100.48
#14	32.47	67.11	0.05	0.02	0.00	0.00	0.63	0.07	0.39	0.00	0.03	100.75
#15	32.64	64.97	0.03	0.00	0.00	0.00	0.14	0.00	2.16	0.08	0.00	100.01
#16	32.56	67.07	0.00	0.00	0.00	0.00	0.51	0.04	0.11	0.04	0.02	100.34
#17	32.48	66.99	0.02	0.02	0.00	0.00	0.23	0.02	0.17	0.00	0.01	99.92
#18	32.51	67.04	0.03	0.05	0.05	0.02	0.50	0.00	0.36	0.04	0.04	100.63
#19	32.64	67.28	0.03	0.00	0.00	0.00	0.54	0.03	0.13	0.05	0.05	100.75
#20	32.41	67.37	0.02	0.01	0.00	0.00	0.06	0.02	1.16	0.03	0.00	101.09
#21	32.68	67.74	0.01	0.00	0.00	0.00	0.49	0.02	0.27	0.00	0.04	101.26
#22	32.82	66.01	0.02	0.02	0.02	0.00	0.32	0.03	1.81	0.07	0.03	101.16

Element Wt%, Galmoy sphalerite, July 1997. Operating Parameters, 20kV, 20nA, 1-2µm.												
Pts 23-32, 10CW (ore grade, crystalline dark yellow sphalerite).												
	S	Zn	Cu	Mn	Ga	Ge	Cd	In	Fe	As	Ag	Total
#23	32.87	67.54	0.01	0.00	0.00	0.00	0.08	0.00	0.05	0.04	0.03	100.62
#24	32.38	66.84	0.00	0.01	0.00	0.03	0.22	0.02	0.55	0.00	0.00	100.05
#25	32.86	67.69	0.03	0.02	0.00	0.00	0.04	0.00	0.39	0.00	0.00	101.04
#26	32.74	67.12	0.03	0.00	0.02	0.01	0.21	0.01	0.59	0.09	0.13	100.94
#27	32.52	67.12	0.03	0.00	0.11	0.01	0.09	0.01	0.44	0.05	0.04	100.41
#28	32.87	66.99	0.03	0.00	0.02	0.00	0.19	0.01	0.50	0.00	0.01	100.63
#29	32.67	67.03	0.01	0.01	0.07	0.03	0.05	0.00	0.41	0.02	0.01	100.30
#30	32.70	66.93	0.02	0.00	0.00	0.00	0.08	0.03	0.45	0.05	0.00	100.25
#31	32.53	66.81	0.01	0.00	0.06	0.00	0.22	0.01	0.64	0.02	0.00	100.28
#32	32.96	67.28	0.02	0.01	0.00	0.00	0.21	0.00	0.56	0.10	0.00	101.13

Element Wt%, Galmoy sphalerite, July 1997. Operating Parameters, 20kV, 20nA, 1-2µm.												
Pts 1-10, MG18/90.0 (fine grained buff coloured sphalerite).												
	S	Zn	Cu	Mn	Ga	Ge	Cd	In	Fe	As	Ag	Total
#1	32.18	65.14	0.17	0.01	0.00	0.00	0.30	0.02	0.42	0.14	0.25	98.63
#2	32.77	65.34	0.04	0.03	0.00	0.00	0.21	0.00	0.49	0.05	0.00	98.93
#4	32.62	66.07	0.06	0.00	0.00	0.00	0.21	0.00	0.28	0.02	0.01	99.27
#6	32.76	67.32	0.07	0.00	0.06	0.00	0.27	0.01	0.31	0.00	0.00	100.80
#7	32.32	66.59	0.08	0.01	0.00	0.00	0.22	0.03	0.33	0.01	0.07	99.66
#8	32.63	67.05	0.00	0.00	0.02	0.00	0.27	0.00	0.28	0.03	0.00	100.27
#9	32.86	66.93	0.05	0.03	0.00	0.00	0.25	0.00	0.32	0.02	0.10	100.56
#10	32.59	66.81	0.02	0.00	0.08	0.00	0.28	0.00	0.57	0.00	0.05	100.39

Element Wt%, Galmoy sphalerite, July 1997. Operating Parameters, 20kV, 20nA, 1-2µm.												
Pts 1-12, GY355/95.0 (Cd rich and As rich sphalerite layers buff to brown coloured sphalerite).												
	S	Zn	Cu	Mn	Ga	Ge	Cd	In	Fe	As	Ag	Total
#1	32.52	66.59	0.01	0.05	0.00	0.00	0.70	0.00	0.11	0.02	0.00	100.00
#2	32.43	66.71	0.02	0.00	0.04	0.00	0.79	0.00	0.07	0.04	0.01	100.10
#3	33.02	66.83	0.03	0.00	0.00	0.00	0.64	0.00	0.04	0.03	0.03	100.62
#4	32.50	65.81	0.02	0.03	0.00	0.00	0.75	0.00	0.16	0.03	0.04	99.34
#5	32.50	67.03	0.00	0.00	0.00	0.00	0.59	0.00	0.05	0.07	0.00	100.23
#6	32.49	66.66	0.01	0.02	0.00	0.00	0.66	0.01	0.09	0.02	0.12	100.08
#7	32.84	66.25	0.00	0.02	0.00	0.00	0.49	0.01	0.19	0.05	0.00	99.86
#8	32.61	67.05	0.01	0.02	0.00	0.00	0.29	0.00	0.08	0.13	0.00	100.19
#9	32.59	66.35	0.00	0.02	0.00	0.02	0.14	0.05	0.61	0.13	0.02	99.93
#10	32.32	65.95	0.05	0.00	0.00	0.00	0.26	0.02	0.64	0.15	0.00	99.38
#11	32.74	65.67	0.00	0.00	0.00	0.00	0.26	0.02	1.09	0.16	0.00	99.94
#12	32.55	66.67	0.00	0.02	0.00	0.00	0.17	0.02	0.43	0.02	0.00	99.87

Galena

Element Wt%, Galmoy Galena, July 1997. Operating Parameters: 20kV, 20nA, 1-2µm.							
Pts 1-10, MG18/90.0.							
	S	Pb	Ag	Bi	Mn	Cd	Total
#1	13.44	86.99	0.01	0.06	0.06	0.00	100.55
#2	13.45	86.48	0.00	0.06	0.00	0.00	99.99
#3	13.47	86.24	0.00	0.14	0.02	0.04	99.91
#4	13.51	85.64	0.01	0.31	0.00	0.04	99.51
#5	13.56	87.66	0.00	0.24	0.03	0.00	101.48
#9	13.38	86.11	0.00	0.00	0.03	0.00	99.52
#10	13.40	85.78	0.04	0.03	0.00	0.00	99.24

Element Wt%, Galmoy Galena, July 1997. Operating Parameters: 20kV, 20nA, 1-2µm.							
Pts 1-10, GY355/95.0.							
	S	Pb	Ag	Bi	Mn	Cd	Total
#1	13.55	87.31	0.00	0.03	0.01	0.00	100.90
#2	13.49	87.24	0.00	0.00	0.01	0.04	100.78
#3	13.29	86.37	0.00	0.05	0.01	0.05	99.76
#4	13.39	86.10	0.00	0.06	0.01	0.03	99.59
#5	13.37	87.22	0.05	0.04	0.00	0.01	100.69
#6	13.42	86.84	0.15	0.04	0.01	0.00	100.46
#7	13.44	86.84	0.02	0.09	0.02	0.12	100.53
#8	13.46	86.20	0.00	0.07	0.04	0.00	99.77
#9	13.66	86.20	0.03	0.00	0.04	0.01	99.94
#10	13.36	87.34	0.00	0.00	0.00	0.14	100.83

Element Wt%, Galmoy Galena, July 1997. Operating Parameters: 20kV, 20nA, 1-2µm.							
Pts 1-10, GY382/86.0.							
	S	Pb	Ag	Bi	Mn	Cd	Total
#1	13.18	86.99	0.12	0.04	0.00	0.06	100.39
#2	13.19	87.23	0.00	0.10	0.01	0.06	100.59
#3	13.28	86.56	0.00	0.00	0.01	0.00	99.85
#4	13.61	87.03	0.00	0.14	0.02	0.00	100.79
#5	13.34	86.95	0.07	0.00	0.01	0.04	100.41
#6	13.23	86.87	0.05	0.00	0.01	0.10	100.25
#7	13.07	86.96	0.12	0.08	0.05	0.00	100.27
#8	13.46	87.36	0.05	0.18	0.03	0.00	101.07
#9	13.22	86.32	0.00	0.06	0.01	0.11	99.71
#10	13.30	87.13	0.01	0.04	0.03	0.05	100.57

Element Wt%, Galmoy Galena, July 1997. Operating Parameters: 20kV, 20nA, 1-2µm.							
Pts 11-20, 10CW.							
	S	Pb	Ag	Bi	Mn	Cd	Total
#11	13.51	87.06	0.00	0.09	0.00	0.00	100.67
#12	13.35	86.87	0.00	0.10	0.02	0.00	100.34
#13	13.49	86.32	0.06	0.00	0.02	0.00	99.89
#14	13.41	86.04	0.00	0.01	0.00	0.01	99.48
#15	13.33	86.97	0.02	0.06	0.04	0.00	100.41
#16	13.26	87.59	0.00	0.12	0.01	0.00	100.98
#17	13.26	86.39	0.00	0.02	0.02	0.06	99.76
#18	13.30	85.83	0.01	0.00	0.01	0.00	99.15
#19	13.27	86.66	0.02	0.15	0.02	0.00	100.12
#20	13.21	86.31	0.05	0.12	0.03	0.00	99.72

Pyrite

Element Wt%, Galmoy Pyrite, July 1997. Operating Parameters: 20kV, 20nA, 1-2µm.								
Pts 1-10, GY355/95.0.								
	S	Fe	Mn	Co	Ni	Cu	As	Cd	Total
#1	52.52	46.77	0.03	0.04	0.00	0.01	1.10	0.00	100.47
#2	52.11	46.53	0.04	0.05	0.02	0.00	1.29	0.03	100.07
#3	52.20	46.08	0.07	0.05	0.02	0.00	1.36	0.00	99.77
#4	52.54	47.99	0.00	0.04	0.00	0.03	0.21	0.00	100.81
#5	52.25	47.13	0.02	0.04	0.00	0.00	0.37	0.03	99.82

Tetrahedrite

Element Wt%, Galmoy Tennantite, September 1997. Operating Parameters: 20kV, 20nA, 1-2µm.											
Pts 1-10, G16-27/383.5.											
	S	Fe	Cu	As	Ag	Sb	Te	Hg	Pb	Zn	Total
#1	23.49	1.05	37.58	2.96	0.40	26.82	0.03	0.00	0.00	7.51	99.84
#2	23.50	1.00	37.48	2.85	0.30	27.20	0.00	0.00	0.00	7.41	99.75
#3	23.29	0.98	37.75	2.71	0.49	27.29	0.08	0.02	0.00	7.47	100.07
#4	23.59	0.99	37.79	3.00	0.46	26.99	0.04	0.06	0.00	7.24	100.16
#5	23.38	0.97	37.48	2.39	0.49	27.88	0.02	0.11	0.00	7.18	99.89
#6	23.44	0.74	37.82	2.44	0.49	27.60	0.07	0.00	0.00	7.37	99.97
#7	23.09	0.82	37.79	2.22	0.51	28.01	0.07	0.06	0.00	7.32	99.89
#8	23.43	0.99	37.66	2.26	0.45	27.86	0.00	0.00	0.00	7.28	99.91
#9	23.39	0.94	37.61	2.38	0.44	28.11	0.07	0.04	0.00	7.14	100.11
#10	23.20	0.99	37.64	2.72	0.40	27.21	0.04	0.00	0.00	7.31	99.49

Chalcopyrite

Element Wt%, Galmoy Chalcopyrite, July 1997. Operating Parameters: 20kV, 20nA, 1-2µm.									
Pts 11-20, G16-27/383.5.									
	S	Fe	Mn	Co	Ni	Cu	As	Cd	Total
#11	34.46	30.61	0.00	0.06	0.01	34.12	0.14	0.00	99.40
#12	34.46	30.64	0.02	0.00	0.00	34.33	0.11	0.00	99.55
#13	34.74	30.73	0.01	0.04	0.06	34.29	0.06	0.00	99.92
#14	34.52	30.53	0.03	0.03	0.00	34.56	0.05	0.00	99.71
#15	34.65	30.74	0.01	0.00	0.03	34.67	0.08	0.00	100.18
#16	34.36	30.52	0.00	0.01	0.02	34.54	0.05	0.03	99.53
#17	34.63	30.70	0.01	0.02	0.00	34.41	0.12	0.05	99.94
#18	34.48	30.36	0.01	0.02	0.03	34.43	0.09	0.02	99.43
#19	34.44	30.53	0.01	0.01	0.01	34.22	0.07	0.04	99.33
#20	34.54	30.57	0.04	0.01	0.00	34.40	0.10	0.00	99.66

B8. ELEMENTAL CHEMISTRY - RATHDOWNEY TREND PROSPECTS SULPHIDES

Sphalerite

Element Wt%, Durrow Sphalerite, February 1996. Operating Parameters: 20kV, 20nA, 1-2µm.
Pts 56-66, 2/960.8 (Sphalerite inclusions in CPY).

	Zn	S	Cd	Mn	Fe	Ni	Co	Cu	As	Ge	Ga	Hg	In	Tl	Sb	Ag	Total
#56	65.84	31.90	0.22	0.00	0.11	0.00	0.00	0.06	0.00	0.00	0.10	0.04	0.02	0.04	0.00	0.00	98.33
#57	65.96	32.11	0.17	0.07	0.04	0.00	0.00	0.14	0.12	0.00	0.13	0.24	0.00	0.19	0.03	0.02	99.22
#58	66.52	32.06	0.24	0.00	0.10	0.04	0.00	0.11	0.00	0.00	0.18	0.00	0.07	0.02	0.00	0.01	99.36
#60	65.92	31.86	0.35	0.17	0.08	0.01	0.00	0.12	0.00	0.00	0.09	0.15	0.04	0.03	0.02	0.00	98.81
#61	65.84	31.96	0.26	0.22	0.12	0.01	0.02	0.14	0.06	0.02	0.13	0.13	0.00	0.14	0.02	0.00	99.07
#62	65.81	32.12	0.32	0.00	0.26	0.00	0.01	0.14	0.00	0.00	0.18	0.03	0.00	0.12	0.05	0.00	99.04
#63	65.69	32.30	0.29	0.02	0.15	0.04	0.01	0.04	0.08	0.00	0.00	0.15	0.03	0.13	0.00	0.08	99.02
#64	65.51	31.71	0.27	0.14	0.14	0.02	0.00	0.15	0.00	0.00	0.00	0.00	0.06	0.00	0.01	0.03	98.05
#65	66.53	32.34	0.23	0.21	0.22	0.00	0.00	0.18	0.00	0.00	0.11	0.00	0.00	0.12	0.01	0.00	99.94
#66	65.35	32.08	0.28	0.13	0.15	0.04	0.00	0.04	0.06	0.00	0.17	0.10	0.05	0.00	0.00	0.00	98.44

Element Wt%, Durrow Sphalerite, February 1996. Operating Parameters: 20kV, 20nA, 1-2µm.
Pts 1-10, 1/910 (6295) Pale yellow sphalerite (see Fe, Cd x-ray distribution map).

	Zn	S	Cd	Mn	Fe	Ge	Ga	Hg	In	Tl	Total
#1	65.16	31.91	0.93	0.17	0.22	0.10	0.06	0.03	0.02	0.23	98.83
#2	65.35	31.63	2.36	0.11	0.19	0.00	0.13	0.13	0.03	0.24	100.15
#3	65.20	32.18	0.94	0.14	0.93	0.00	0.13	0.04	0.00	0.13	99.70
#4	64.74	31.92	1.86	0.00	0.52	0.02	0.14	0.07	0.06	0.01	99.34
#5	65.74	31.88	1.18	0.00	0.08	0.00	0.08	0.10	0.00	0.27	99.32
#6	66.45	31.99	0.76	0.01	0.06	0.00	0.14	0.00	0.04	0.11	99.56
#7	65.95	32.16	0.83	0.03	0.20	0.00	0.08	0.04	0.00	0.22	99.50
#8	66.00	32.17	1.15	0.00	0.07	0.00	0.17	0.11	0.05	0.22	99.93
#9	65.74	31.95	1.16	0.00	0.16	0.00	0.11	0.18	0.02	0.12	99.45
#10	66.23	32.34	0.98	0.00	0.13	0.00	0.04	0.08	0.05	0.18	100.04

Element Wt%, Durrow Sphalerite, February 1996. Operating Parameters: 20kV, 20nA, 1-2µm.
Pts 1-20, 1/910 (6295) Pale yellow sphalerite - associated with pyrite/marcasite assemblage.

	Zn	S	Cd	Mn	Fe	Ni	Co	Cu	As	Ge	Ga	Hg	In	Tl	Total
#1	65.53	31.55	2.11	0.17	0.05	0.00	0.01	0.00	0.08	0.04	0.08	0.04	0.04	0.15	99.85
#2	66.49	32.24	1.17	0.01	0.14	0.01	0.00	0.04	0.07	0.03	0.15	0.14	0.05	0.08	100.62
#3	66.49	32.17	0.25	0.00	0.22	0.00	0.03	0.03	0.05	0.00	0.15	0.12	0.02	0.33	99.87
#4	66.15	32.04	1.14	0.14	0.03	0.00	0.03	0.06	0.02	0.00	0.01	0.05	0.06	0.24	99.97
#5	66.88	32.08	0.68	0.09	0.11	0.00	0.02	0.02	0.07	0.00	0.12	0.00	0.07	0.09	100.25
#6	66.59	32.12	0.81	0.00	0.21	0.00	0.02	0.05	0.00	0.00	0.16	0.09	0.03	0.07	100.16
#7	66.33	31.97	0.73	0.04	0.23	0.00	0.00	0.07	0.04	0.00	0.07	0.20	0.03	0.24	99.95
#8	65.97	32.21	0.87	0.00	0.22	0.04	0.00	0.00	0.02	0.00	0.11	0.01	0.06	0.24	99.74
#9	66.53	32.00	1.02	0.00	0.07	0.00	0.00	0.05	0.00	0.00	0.20	0.01	0.00	0.18	100.04
#10	67.24	32.20	0.76	0.00	0.02	0.00	0.02	0.00	0.12	0.03	0.11	0.06	0.07	0.04	100.67
#11	67.32	32.27	0.05	0.00	0.18	0.00	0.00	0.03	0.08	0.03	0.06	0.00	0.05	0.18	100.24
#12	66.89	31.63	1.23	0.12	0.07	0.05	0.00	0.00	0.07	0.06	0.11	0.14	0.00	0.15	100.52
#13	67.03	31.80	1.45	0.00	0.05	0.03	0.00	0.06	0.01	0.00	0.26	0.11	0.00	0.13	100.93
#14	67.23	31.74	0.98	0.00	0.06	0.02	0.00	0.05	0.10	0.00	0.21	0.00	0.00	0.08	100.46
#15	66.00	32.31	0.95	0.00	0.13	0.03	0.00	0.09	0.00	0.00	0.13	0.00	0.07	0.24	99.94
#16	67.61	31.75	0.34	0.00	0.17	0.00	0.04	0.02	0.00	0.00	0.22	0.00	0.00	0.09	100.24
#17	66.39	32.24	0.76	0.06	0.17	0.01	0.01	0.00	0.08	0.00	0.12	0.10	0.05	0.16	100.13
#18	65.22	31.96	2.15	0.00	0.89	0.00	0.01	0.00	0.00	0.00	0.00	0.00	0.02	0.00	100.25
#19	66.04	32.02	0.76	0.06	0.61	0.00	0.01	0.05	0.01	0.02	0.13	0.00	0.00	0.03	99.73
#20	65.23	31.78	2.11	0.00	0.94	0.03	0.01	0.03	0.00	0.02	0.14	0.00	0.00	0.26	100.55

Element Wt%, Durrow Sphalerite, February 1996. Operating Parameters: 20kV, 20nA, 1-2µm.
Pts 36-50, 1/910 (6295) Colourless sphalerite.

	Zn	S	Cd	Mn	Fe	Ni	Co	Cu	As	Ge	Ga	Hg	In	Tl	Total
#36	66.10	31.58	1.01	0.10	0.00	0.00	0.00	0.09	0.05	0.00	0.16	0.11	0.00	0.32	99.53
#37	66.20	32.35	1.18	0.04	0.03	0.00	0.00	0.05	0.07	0.00	0.16	0.00	0.06	0.11	100.24
#38	66.06	32.15	1.08	0.12	0.01	0.02	0.00	0.03	0.00	0.00	0.16	0.03	0.07	0.17	99.89
#39	66.49	31.96	1.14	0.01	0.09	0.01	0.03	0.00	0.00	0.00	0.01	0.12	0.00	0.02	99.88
#40	66.17	32.26	0.82	0.08	0.01	0.03	0.00	0.00	0.00	0.00	0.20	0.00	0.02	0.13	99.71
#41	66.82	31.76	0.86	0.01	0.02	0.00	0.04	0.00	0.00	0.01	0.08	0.01	0.00	0.13	99.76
#42	66.20	31.50	1.37	0.00	0.04	0.00	0.00	0.06	0.06	0.00	0.20	0.08	0.00	0.22	99.71
#43	66.09	31.74	0.39	0.00	0.01	0.01	0.00	0.00	0.11	0.00	0.14	0.00	0.00	0.12	98.61
#44	66.28	31.87	0.61	0.00	0.03	0.00	0.00	0.07	0.00	0.00	0.19	0.06	0.07	0.11	99.28
#45	66.21	31.98	0.36	0.08	0.04	0.00	0.02	0.04	0.00	0.00	0.11	0.02	0.00	0.36	99.23
#46	66.57	31.95	0.38	0.00	0.00	0.00	0.00	0.01	0.12	0.00	0.20	0.00	0.04	0.04	99.32
#47	65.10	32.09	0.81	0.11	0.67	0.00	0.00	0.00	0.00	0.03	0.14	0.10	0.05	0.11	99.21
#48	66.20	31.84	0.77	0.27	0.17	0.00	0.01	0.05	0.00	0.00	0.12	0.15	0.00	0.13	99.72
#49	66.21	32.07	0.72	0.00	0.12	0.02	0.00	0.00	0.01	0.01	0.16	0.05	0.02	0.05	99.44
#50	66.02	32.26	0.73	0.02	0.16	0.00	0.00	0.02	0.00	0.02	0.13	0.00	0.02	0.18	99.55

Element Wt%, Durrow Sphalerite, February 1996. Operating Parameters: 20kV, 20nA, 1-2µm.
Pts 51-70, 1/910 (6295) Pale-yellow coloured, non-homogeneous sphalerite.

	Zn	S	Cd	Mn	Fe	Ni	Co	Cu	As	Ge	Ga	Hg	In	Tl	Total
#51	65.20	31.58	1.01	0.00	0.04	0.01	0.07	0.00	0.07	0.00	0.10	0.05	0.00	0.21	98.33
#52	65.12	32.17	1.73	0.04	0.12	0.03	0.01	0.04	0.00	0.04	0.13	0.00	0.00	0.09	99.52
#53	66.48	32.16	0.88	0.09	0.04	0.02	0.03	0.00	0.07	0.03	0.04	0.08	0.00	0.14	100.05
#54	65.80	31.62	0.92	0.09	0.08	0.00	0.00	0.06	0.09	0.01	0.02	0.08	0.01	0.17	98.93
#55	65.90	32.07	1.01	0.00	0.13	0.00	0.00	0.00	0.00	0.00	0.17	0.18	0.00	0.11	99.58
#56	64.56	31.57	2.92	0.00	0.16	0.00	0.04	0.11	0.00	0.00	0.09	0.00	0.04	0.10	99.58
#57	65.17	31.43	1.76	0.00	0.42	0.05	0.00	0.00	0.03	0.04	0.00	0.00	0.01	0.03	98.93
#58	65.90	31.95	0.82	0.27	0.16	0.00	0.01	0.00	0.04	0.00	0.03	0.00	0.09	0.20	99.46
#59	65.62	31.17	0.92	0.08	0.10	0.00	0.00	0.01	0.06	0.00	0.14	0.00	0.05	0.12	98.26
#60	66.35	32.00	1.00	0.03	0.11	0.02	0.00	0.00	0.04	0.03	0.16	0.07	0.04	0.24	100.07
#61	65.14	31.40	0.88	0.00	0.09	0.00	0.02	0.04	0.00	0.00	0.13	0.16	0.05	0.11	98.01
#62	66.19	32.21	0.88	0.00	0.06	0.03	0.00	0.06	0.00	0.02	0.26	0.09	0.03	0.08	99.91
#63	65.68	31.31	0.97	0.11	0.04	0.04	0.07	0.03	0.04	0.03	0.15	0.12	0.00	0.11	98.70
#64	65.77	31.85	1.13	0.04	0.11	0.00	0.03	0.05	0.00	0.00	0.21	0.01	0.00	0.09	99.30
#66	65.75	32.39	1.19	0.00	0.12	0.05	0.03	0.03	0.06	0.02	0.02	0.05	0.00	0.15	99.85
#67	66.50	31.82	0.92	0.09	0.04	0.02	0.01	0.00	0.01	0.00	0.10	0.05	0.00	0.10	99.65
#68	66.32	31.98	0.86	0.00	0.14	0.00	0.03	0.09	0.04	0.03	0.11	0.03	0.00	0.08	99.71
#70	66.79	32.11	0.73	0.05	0.01	0.00	0.00	0.00	0.00	0.01	0.10	0.11	0.06	0.08	100.04

Pyrite

Element Wt%, Durrow Pyrite, February 1996. Operating Parameters: 20kV, 20nA, 1-2µm.																
Pts 21-35, 1/910 (6295) Subhedral clear pyrite.																
	Zn	S	Cd	Mn	Fe	Ni	Co	Cu	As	Ge	Ga	Hg	In	Tl	Total	
#21	0.15	52.33	0.08	0.16	48.17	0.02	0.03	0.06	0.07	0.00	0.05	0.02	0.01	0.22	101.35	
#22	0.24	51.53	0.00	0.15	47.33	0.00	0.05	0.01	0.06	0.00	0.05	0.03	0.05	0.17	99.67	
#23	0.15	52.48	0.04	0.15	48.07	0.02	0.00	0.03	0.04	0.00	0.06	0.05	0.02	0.14	101.24	
#27	0.10	52.18	0.00	0.00	48.32	0.03	0.08	0.00	0.05	0.00	0.08	0.03	0.00	0.21	101.08	
#28	0.08	52.79	0.02	0.00	48.12	0.00	0.00	0.00	0.03	0.00	0.09	0.00	0.05	0.13	101.31	
#29	0.20	52.27	0.00	0.05	48.45	0.01	0.01	0.02	0.08	0.00	0.00	0.04	0.00	0.23	101.36	
#30	0.14	52.52	0.00	0.24	48.10	0.00	0.00	0.03	0.06	0.00	0.06	0.09	0.00	0.18	101.42	
#31	0.05	52.11	0.01	0.00	48.43	0.00	0.00	0.01	0.02	0.00	0.03	0.08	0.04	0.19	100.97	
#32	0.00	52.31	0.03	0.02	48.21	0.00	0.03	0.09	0.07	0.00	0.02	0.12	0.02	0.10	101.01	
#34	0.02	52.52	0.00	0.00	48.40	0.06	0.04	0.00	0.03	0.00	0.02	0.06	0.00	0.16	101.30	
#35	0.04	52.20	0.00	0.00	48.55	0.00	0.06	0.00	0.04	0.00	0.04	0.00	0.01	0.20	101.14	

Element Wt%, Durrow Pyrite, February 1996. Operating Parameters: 20kV, 20nA, 1-2µm.																
Pts 71-85, 1/910 (KU3). Euhedral, late pyrite?																
	Zn	S	Cd	Mn	Fe	Ni	Co	Cu	As	Ge	Ga	Hg	In	Tl	Total	
#71	0.03	52.26	0.00	0.00	47.94	0.02	0.07	0.00	0.07	0.00	0.00	0.00	0.00	0.22	100.60	
#72	0.00	52.01	0.03	0.11	48.44	0.03	0.05	0.01	0.06	0.00	0.00	0.07	0.00	0.26	101.08	
#73	0.01	52.07	0.04	0.00	48.10	0.00	0.04	0.04	0.12	0.00	0.03	0.04	0.09	0.13	100.72	
#74	0.05	52.34	0.09	0.00	47.97	0.00	0.02	0.00	0.07	0.00	0.03	0.05	0.00	0.17	100.79	
#75	0.00	52.38	0.00	0.14	48.00	0.00	0.03	0.00	0.03	0.01	0.05	0.07	0.04	0.15	100.91	
#76	0.02	52.49	0.00	0.04	48.24	0.02	0.00	0.04	0.10	0.02	0.00	0.02	0.01	0.28	101.29	
#77	0.06	52.40	0.06	0.16	48.12	0.00	0.02	0.00	0.05	0.00	0.04	0.00	0.00	0.11	101.02	
#78	0.00	52.41	0.01	0.00	48.32	0.00	0.03	0.00	0.12	0.00	0.04	0.00	0.02	0.19	101.13	
#79	0.00	52.06	0.02	0.03	48.07	0.00	0.04	0.02	0.08	0.00	0.06	0.11	0.05	0.09	100.62	
#80	0.00	52.38	0.00	0.24	48.10	0.02	0.06	0.03	0.03	0.00	0.08	0.02	0.04	0.26	101.27	
#81	0.00	52.50	0.03	0.00	48.14	0.00	0.06	0.00	0.00	0.00	0.05	0.05	0.05	0.08	100.95	
#82	0.09	52.16	0.05	0.08	48.29	0.00	0.00	0.05	0.04	0.00	0.02	0.01	0.00	0.23	101.02	
#83	0.08	52.22	0.03	0.00	48.24	0.00	0.06	0.06	0.06	0.00	0.02	0.14	0.04	0.17	101.10	
#84	0.03	52.11	0.00	0.00	48.04	0.04	0.05	0.00	0.06	0.00	0.01	0.00	0.00	0.12	100.46	
#85	0.00	51.99	0.00	0.13	48.11	0.01	0.04	0.03	0.08	0.00	0.00	0.06	0.00	0.02	100.46	

Element Wt%, Durrow Pyrite, February 1996. Operating Parameters: 20kV, 20nA, 1-2µm.																		
Pts 21-35, 2/961.9. Pyrite in vein.																		
	Zn	S	Cd	Mn	Fe	Ni	Co	Cu	As	Ge	Ga	Hg	In	Tl	Sb	Ag	Total	
#21	0.07	52.04	0.09	0.00	47.57	0.00	0.08	0.54	0.10	0.00	0.06	0.00	0.00	0.16	0.00	0.00	100.71	
#22	0.23	49.88	0.11	0.00	45.05	0.64	0.23	1.72	0.87	0.00	0.00	0.00	0.04	0.22	0.02	0.02	99.03	
#23	0.02	50.08	0.11	0.00	45.90	0.05	0.04	0.53	2.13	0.00	0.04	0.01	0.00	0.26	0.46	0.00	99.63	
#24	0.12	51.45	0.00	0.14	47.67	0.10	0.06	0.19	0.09	0.03	0.03	0.00	0.00	0.31	0.00	0.02	100.20	
#25	0.40	50.65	0.02	0.02	45.28	0.03	0.06	3.02	0.86	0.00	0.00	0.12	0.03	0.11	0.15	0.00	100.76	
#26	0.04	51.61	0.03	0.09	47.70	0.03	0.01	0.02	0.06	0.00	0.02	0.11	0.05	0.22	0.00	0.00	99.99	
#28	0.07	51.77	0.02	0.00	47.70	0.04	0.06	0.22	0.12	0.00	0.03	0.07	0.02	0.17	0.00	0.03	100.32	
#29	0.07	52.06	0.03	0.00	47.66	0.01	0.04	0.33	0.17	0.00	0.04	0.00	0.00	0.22	0.00	0.02	100.65	
#30	0.12	52.10	0.00	0.00	46.89	0.09	0.08	1.16	0.06	0.00	0.10	0.14	0.00	0.11	0.00	0.01	100.85	
#31	0.34	50.22	0.00	0.00	46.58	0.02	0.08	1.10	0.08	0.00	0.10	0.09	0.00	0.23	0.01	0.04	98.88	
#32	0.01	51.73	0.01	0.00	47.10	0.05	0.02	0.98	0.12	0.00	0.06	0.08	0.00	0.15	0.00	0.01	100.31	
#33	0.04	51.97	0.00	0.01	47.20	0.24	0.20	0.32	0.08	0.00	0.00	0.05	0.00	0.17	0.00	0.02	100.28	
#34	0.00	51.89	0.00	0.22	46.79	0.19	0.11	0.20	0.05	0.00	0.00	0.00	0.06	0.23	0.04	0.00	99.78	
#35	0.00	34.58	0.00	0.00	29.76	0.01	0.05	35.55	0.08	0.00	0.00	0.00	0.05	0.07	0.02	0.00	100.17	

Tetrahedrite

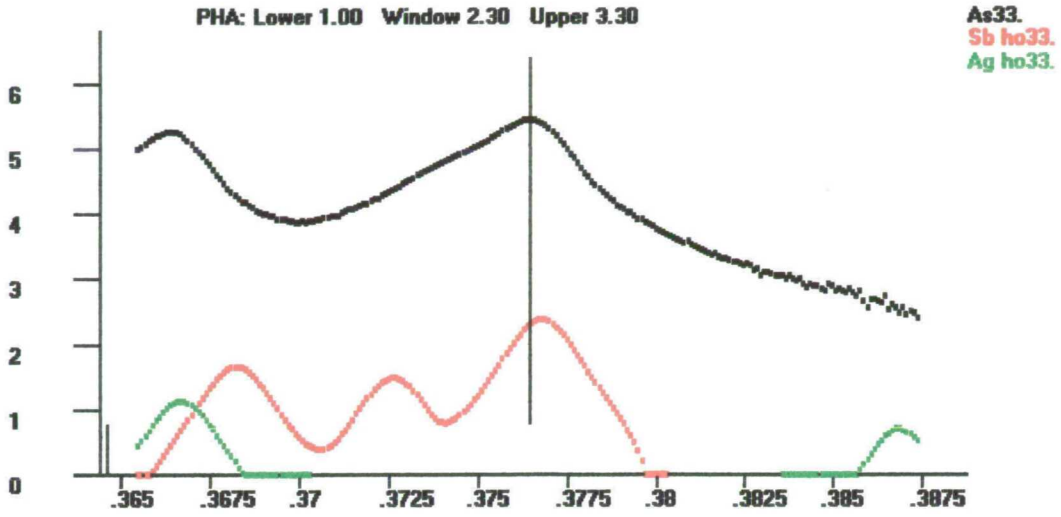
Element Wt%, Durrow Tennantite, February 1996. Operating Parameters: 20kV, 20nA, 1-2µm.																		
Pts 1-20, 2/961.9.																		
	Zn	S	Cd	Mn	Fe	Ni	Co	Cu	As	Ge	Ga	Hg	In	Tl	Sb	Ag	Total	
#3	6.34	24.12	0.01	0.06	1.11	0.00	0.00	39.59	3.49	0.05	0.16	0.25	0.03	0.14	25.56	0.22	101.13	
#5	6.79	24.33	0.13	0.07	1.12	0.00	0.01	40.10	3.73	0.00	0.24	0.00	0.07	0.08	24.51	0.21	101.37	
#8	6.73	24.68	0.10	0.00	0.83	0.00	0.05	39.62	4.45	0.00	0.16	0.39	0.00	0.16	23.89	0.18	101.22	
#15	4.08	23.92	0.07	0.00	2.70	0.00	0.00	39.40	3.30	0.00	0.29	1.30	0.00	0.20	25.94	0.29	101.51	
#18	4.76	24.20	0.23	0.20	2.45	0.05	0.00	39.74	4.36	0.00	0.16	0.34	0.00	0.06	24.58	0.20	101.31	

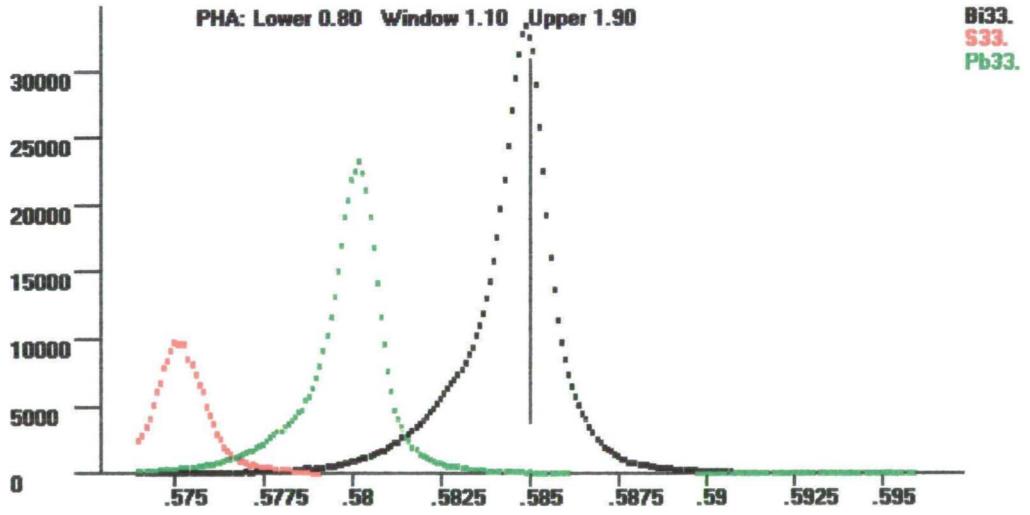
Chalcopyrite

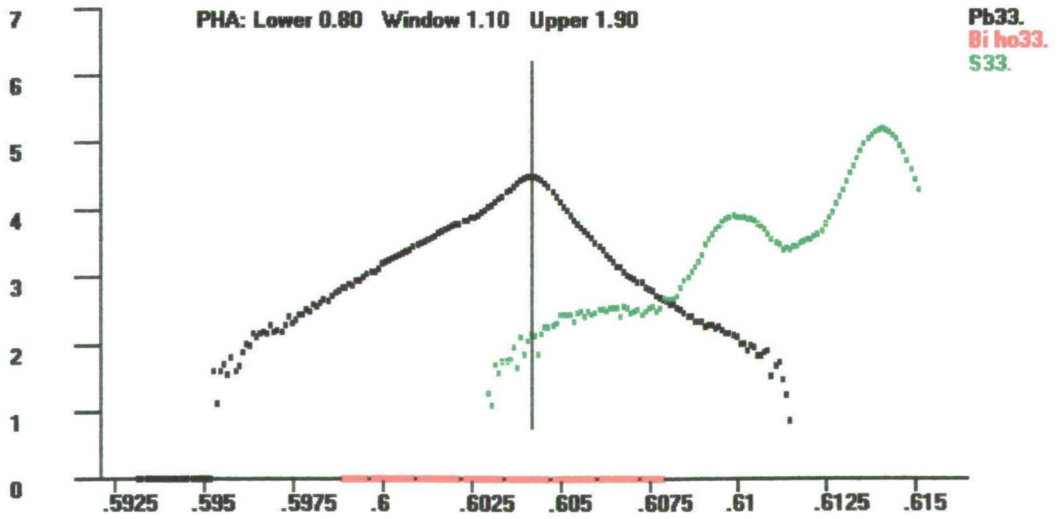
Element Wt%, Durrow Chalcopyrite, February 1996. Operating Parameters: 20kV, 20nA, 1-2µm.																		
Pts 35-55, 2/960.8 (Durrowwt).																		
	Zn	S	Cd	Mn	Fe	Ni	Co	Cu	As	Ge	Ga	Hg	In	Tl	Sb	Ag	Total	
#35	0.00	34.58	0.00	0.00	29.76	0.01	0.05	35.55	0.08	0.00	0.00	0.00	0.05	0.07	0.02	0.00	100.17	
#36	0.07	33.62	0.00	0.06	30.66	0.02	0.00	35.65	0.02	0.00	0.00	0.00	0.00	0.10	0.05	0.00	100.25	
#37	0.00	34.09	0.00	0.01	30.35	0.00	0.01	35.45	0.07	0.00	0.00	0.09	0.01	0.00	0.07	0.03	0.09	100.24
#38	0.00	33.48	0.04	0.00	30.31	0.01	0.03	35.45	0.00	0.00	0.02	0.07	0.04	0.25	0.00	0.00	99.70	
#39	0.05	33.16	0.03	0.00	30.18	0.03	0.03	35.57	0.09	0.05	0.08	0.11	0.00	0.15	0.00	0.00	99.52	
#40	0.00	33.58	0.07	0.06	30.19	0.00	0.03	35.47	0.01	0.00	0.08	0.04	0.00	0.17	0.00	0.00	99.69	
#42	0.00	33.74	0.00	0.00	30.38	0.00	0.04	35.42	0.12	0.00	0.00	0.09	0.01	0.17	0.01	0.02	100.00	
#43	0.00	34.29	0.04	0.05	30.27	0.07	0.04	35.26	0.12	0.00	0.08	0.06	0.01	0.14	0.04	0.04	100.50	
#44	0.04	33.17	0.00	0.00	30.00	0.06	0.03	35.35	0.02	0.00	0.00	0.11	0.00	0.14	0.00	0.02	98.93	
#45	0.04	33.76	0.00	0.00	30.32	0.03	0.04	35.54	0.01	0.00	0.02	0.06	0.00	0.14	0.02	0.04	100.02	
#46	0.00	33.64	0.09	0.06	30.29	0.00	0.03	35.66	0.05	0.00	0.00	0.12	0.00	0.28	0.00	0.03	100.25	
#47	0.11	33.73	0.02	0.00	30.36	0.00	0.00	35.21	0.03	0.00	0.02	0.08	0.00	0.32	0.00	0.02	99.89	
#48	0.07	33.76	0.03	0.05	30.17	0.04	0.03	35.36	0.20	0.00	0.00	0.17	0.06	0.21	0.02	0.00	100.18	
#49	0.06	33.74	0.00	0.16	30.49	0.00	0.00	35.53	0.14	0.00	0.07	0.01	0.06	0.05	0.03	0.00	100.34	
#50	0.03	33.96	0.01	0.03	30.15	0.04	0.02	35.40	0.05	0.00	0.00	0.00	0.00	0.15	0.02	0.00	99.87	
#51	0.08	34.04	0.06	0.00	30.36	0.01	0.03	35.75	0.05	0.00	0.00	0.02	0.00	0.07	0.00	0.00	100.47	
#52	0.02	33.96	0.02	0.00	30.40	0.00	0.00	35.52	0.11	0.00	0.01	0.00	0.00	0.16	0.01	0.00	100.21	
#53	0.00	33.83	0.00	0.00	30.46	0.01	0.03	35.31	0.11	0.00	0.00	0.06	0.00	0.15	0.04	0.04	100.03	
#54	0.03	33.83	0.02	0.00	30.47	0.00	0.04	35.42	0.04	0.01	0.03	0.01	0.09	0.14	0.00	0.07	100.21	
#55	0.00	33.55	0.10	0.00	30.31	0.00	0.02	35.63	0.03	0.01	0.00	0.00	0.00	0.13	0.00	0.01	99.79	

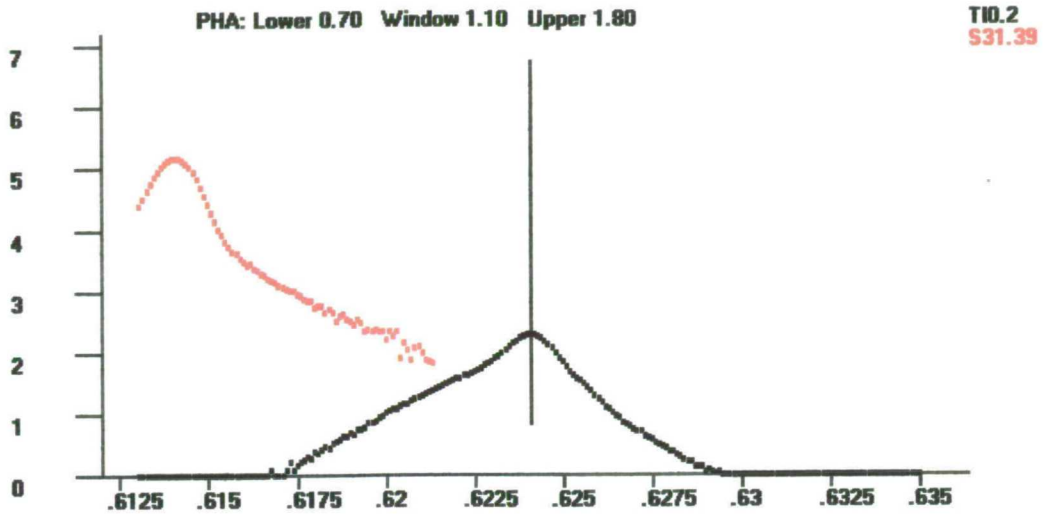
Element Wt%. Darrow Chalcopyrite, February 1996. Operating Parameters: 20kV, 20nA, 1-2µm.																	
Pts 67-80, 2/960.8 (Darrowwt).																	
	Zn	S	Cd	Mn	Fe	Ni	Co	Cu	As	Ge	Ga	Hg	In	Tl	Sb	Ag	Total
#67	0.01	33.88	0.04	0.00	30.13	0.00	0.00	35.73	0.11	0.00	0.09	0.06	0.02	0.16	0.02	0.04	100.28
#68	0.02	34.08	0.00	0.06	30.37	0.03	0.01	35.36	0.06	0.00	0.00	0.02	0.04	0.10	0.01	0.03	100.18
#69	0.09	33.80	0.03	0.02	30.08	0.05	0.02	35.54	0.02	0.01	0.00	0.12	0.00	0.14	0.00	0.10	100.00
#70	0.00	33.93	0.00	0.05	30.37	0.05	0.00	35.59	0.09	0.02	0.05	0.01	0.00	0.20	0.01	0.02	100.38
#71	0.11	33.43	0.05	0.03	30.27	0.01	0.05	35.25	0.11	0.00	0.00	0.11	0.00	0.24	0.08	0.01	99.76
#72	0.01	33.43	0.04	0.03	29.92	0.00	0.04	35.67	0.12	0.00	0.08	0.13	0.00	0.19	0.06	0.05	99.75
#73	0.00	33.90	0.00	0.00	0.78	0.01	0.05	35.63	0.07	0.02	0.00	0.13	0.00	0.22	0.02	0.00	100.83
#74	0.04	33.68	0.00	0.20	0.38	0.00	0.05	35.93	0.11	0.00	0.00	0.00	0.00	0.14	0.01	0.00	100.55
#75	0.06	33.84	0.00	0.00	0.35	0.00	0.04	35.77	0.04	0.00	0.07	0.00	0.00	0.15	0.09	0.00	100.39
#76	0.15	33.63	0.05	0.00	29.90	0.00	0.00	36.12	0.15	0.00	0.03	0.03	0.00	0.17	0.06	0.02	100.32
#77	0.00	33.44	0.00	0.00	30.30	0.04	0.00	35.50	0.04	0.03	0.00	0.00	0.00	0.13	0.04	0.09	99.59
#78	0.06	33.67	0.00	0.00	30.29	0.09	0.00	35.89	0.02	0.00	0.00	0.04	0.06	0.06	0.01	0.02	100.21
#79	0.00	33.90	0.04	0.31	30.54	0.00	0.00	35.61	0.11	0.00	0.01	0.00	0.05	0.19	0.02	0.07	100.84
#80	0.11	33.59	0.04	0.02	30.14	0.00	0.02	35.48	0.08	0.00	0.02	0.12	0.04	0.14	0.03	0.00	99.83

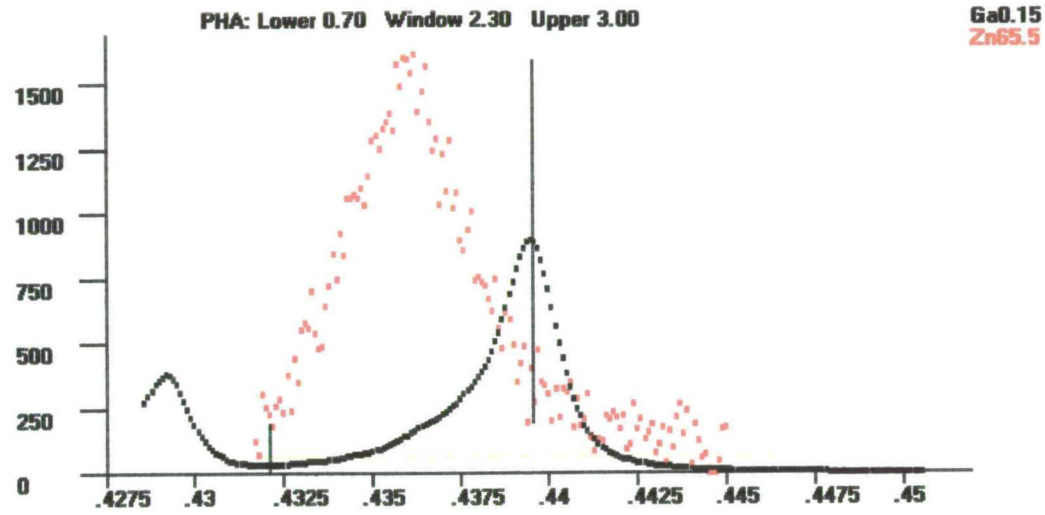
B9. BACKGROUND INTERFERENCE PATTERNS








PHA: Lower 0.70 Window 1.10 Upper 1.80
TI0.2
S31.39
7
6
5
4
3
2
1
0
.6125
.615
.6175
.62
.6225
.625
.6275
.63
.6325
.635


PHA: Lower 0.70 Window 2.30 Upper 3.00
Ga0.15
Zn65.5
1500
1250
1000
750
500
250
0
.4275
.43
.4325
.435
.4375
.44
.4425
.445
.4475
.45

APPENDIX C: RESEARCH TECHNIQUES

C1. CATHODOLUMINESCENCE (CL)

Introduction

Cathodoluminescence is the emission of photons of UV to IR wavelengths stimulated in a material by an incident electron beam due to imperfections in mineral structures. There are many types of defects, which may be categorized in general terms as dislocations and other structural defects; vacancies and non-stoichiometry; substitutional chemical impurities; disorder; and lattice damage. Most observations for geological applications are carried out in the visible region (400-700nm). The technique is extremely sensitive to the most subtle chemical and/or structural variations in a wide variety of ore and gangue minerals, and provides a powerful adjunct to fluid inclusion, isotopic, chemical and conventional petrographic studies.

Commercial microscope mounted CL units have been available since the early 1970's. Many studies prior to the availability of commercial instruments were carried out on SEM or microscope mounted units. A CITL Mark 4 Cold-Cathode System mounted on the stage of a conventional petrological microscope (Leica DM LM, (with X8 ocular and X4, X5, X10 objectives) was used during this research.

The system is relatively cheap and requires only a simple vacuum system. The operator is able to switch rapidly between observation in CL and in plane polarized or cross polarized transmitted or reflected light. It is not necessary to carbon coat samples. The main disadvantage of a cold-cathode system is that it cannot approach the resolution possible with a SEM.

The system is equipped with both manual and automatic control. Automatic vacuum control, brings the beam to current and voltage conditions preset by the operator and these beam conditions are maintained at a constant value indefinitely. All systems operate with vacuums in the region of 0.3-0.7mTorr and have continuously variable beam voltages of 0-30kV and beam currents up to 2mA. The beam voltage is important as this determines which electron transitions are excited (See basic theory section below). Under most operating conditions, the electron beam used in CL actually excites all fluorescent transitions. The current principally affects the intensity of emission. The range of electrons entering the sample from beam voltages of 15-25kV, which are typically used for CL, is approximately 1-3mm in most minerals. Interactions between the photons and mineral structure and the various particles produced by the incident beam will control the CL emitted from the sample. In the present study an operating voltage of 15kV and beam current between 300-400μA is generally employed for the analysis of carbonates. For optimal photographic results a Fuji Provia 400ASA professional colour slide film was used.

Basic Theory

The basic process of luminescence involves the excitation of electrons in a material by an incident energy source and their subsequent spontaneous decay to ground state via one or more transitions with the release of some or all of the excitation energy. The incident energy can be supplied in the form of electrons, ions, neutrons, protons, X-rays, UV, visible light, a chemical reaction, an applied electrical field or mechanical deformation. The excitation energy can be released in a variety of forms, as X-rays, secondary, backscattered and Auger electrons, IR-UV light and phonons. If excitation is via a beam of electrons, the emissions are known as cathodoluminescence. It is the IR-UV, and in particular the visible photons emitted by the sample which are of interest in CL.

A distinction is made between emissions from the sample resulting from decay to the ground state which occurs effectively instantaneously after excitation and emission which persists for longer periods. Those emissions which occur within 10-9 seconds after the cessation of incident excitation are referred to as fluorescence and those which persist for longer periods as phosphorescence. Emissions observed during cathodoluminescence generally consist of a combination of both of these.

Activators, Co-activators and Quenchers

Cathodoluminescence response in carbonate minerals is controlled by the incorporation of trace and minor elements which act as activators, co-activators or sensitizers, and quenchers. Any centre which promotes luminescence is called an activator, while those which inhibit luminescence are known as quenchers. Other centres which appear to facilitate, or enhance the luminescence emitted by activator centres are called co-activators, or sensitizors. In addition to the presence of suitable abundances and types of activation and quenching centres, for luminescence to be observed the luminescent transitions also have to have sufficient probabilities of occurring. These probabilities result from quantum mechanical selection rules for the various possible transitions. These probabilities play a role in determining the efficiency of an activator, which is a function of the number of radiative transitions which occur per unit of incident energy supplied.

Mn^{2+} is the primary 'activator' and produces yellow to red emission in carbonates (Machel *et al.*, 1991). The Mn^{2+} enters both the Ca and the Mg sites, but activation is more efficient at the Ca site than at the Mg site. Sommer (1972a), determined that with increasing substitution of Mn^{2+} into Mg^{2+} rather than Ca^{2+} sites, the colour tends toward red, hence dolomite is characteristically a 'brick-red' colour. Sommer, (1972a) further suggested that dolomite luminescence is made up two components due to Mn on the Ca and Mg sites. El Ali *et al.*, (1993) observed that hydrothermal dolomites were characterized by red CL whereas evaporitic dolomite emitted yellow-orange luminescence. Trace elements such as Sm, Dy, Eu, Er, Ce and Pb act as sensitizors or 'co-activators' facilitating Mn^{2+} activation (Machel, 1985). As little as 10-20 ppm Mn^{2+} in solid solution can produce luminescence, if the total Fe content is less than 150ppm.

Ten Have and Heijnen (1985) found that Miocene dolomites from the Bahamas with only 30-35ppm Mn luminesced. Other possible activators in carbonates include, Ag^{+}, Sn^{2+}, Sb^{3+}, Tl^{+}. Fe^{2+} is the most common 'quencher' ion, although Ni^{2+} and Co^{2+} have similar effects in carbonates. The quencher does not necessarily prevent excitation, but causes low energy, non-radiative (IR) decay transitions of excited electrons. Complete quenching by Fe in dolomite occurs at 15000 ppm, regardless of Mn concentration (Pierson, 1981). Quenching can also occur when activator concentrations rise above certain levels.

Major controls on the uptake of Mn^{2+} and Fe^{2+} in carbonates include the concentration of Mn^{2+} and Fe^{2+} in solution as well as factors which control the effective distribution coefficients for these elements, such as rate of precipitation, super-saturation, face orientation (Reeder and Grams, 1987), temperature and the possible influence of other trace elements. The single most important factor, however is the oxidizing-reducing nature of the mineralizing solution. A model by Carpenter and Oglesby (1976) emphasizes the importance of the oxidation states of Mn and Fe in different regions of an Eh-pH stability field. At high oxidizing potentials, Mn is in the 3^{+} or 4^{+} state and Fe is in the 3^{+} state. These ions are strongly excluded from the carbonate lattice and the characteristic CL is not produced. At lower oxidation potentials, the Mn is reduced to Mn^{2+} and is able to substitute for Ca^{2+}. However, the Fe remains in the 3^{+} state and is not incorporated as a quencher and thus the CL intensity is high. At even greater reducing conditions, Mn and Fe are both in the 2^{+} state and both can substitute for Ca, leading to a dull, partially quenched CL.

A wide variety of CL emissions have been recorded from sphalerites (Goni and Remond, 1969; Marfunin, 1979; Kyle and Price, 1985; Kuhlemann and Zeeh, 1995; Zeeh and Kuhlemann, 1996). However, the complex chemistry of natural sphalerites hinders attempts to relate CL to chemistry. Ag, Ti, W, Fe, Cu, Cd and Mn have been directly identified as activators or implicated in sphalerite luminescence (McKeag, 1956; Goni and Remond, 1969; Marfunin, 1979; Kyle and Price, 1985; Kuhlemann and Zeeh, 1995).

For further detailed information on CL theory, applications and instrumentation, the reader is referred to Leverenz (1968), Lumb (1978), Zinkernagel (1978), Marfunin (1979), Hagni (1984, 1987), Marshall (1988), Yakobi and Holt (1990), Hayward (1997).

C2. REFLECTED LIGHT MICROSCOPY

Introduction

The reflected light microscope is similar to conventional petrographic microscopes in the system of lenses, polarizer, analyzer, and various diaphragms employed, but differs in that it has an incident light source rather than a substage transmitting light source, allowing the examination of polished surfaces of opaque minerals. A Zeiss MC80 reflected light microscope and MC80 microscope camera attachment was used during this research. Observations were made both in air and under oil immersion (n_e = 1.518, n_D = 1.515, 23°C), with a light source set between 8-10 V. For optimal photographic results a Kodak Ektachrome 64T professional colour reversal film was used.

There is a wealth of literature concerning the study of ores in polished section and the interpretation of ore textures, including the standard texts of Bastin (1950), Galopin and Henry (1972), Stanton (1972), Ramdohr (1980), Craig and Vaughan (1981), Jambor and Vaughan (1990).

C3. ELECTRON MICROPROBE ANALYSIS (EMPA)

Introduction

EMPA is a technique for chemically analyzing small selected areas of solid samples, in which X-rays are excited by a focused electron beam (Reed, 1996). The X-ray spectrum contains lines which are characteristic of the elements present, hence a qualitative analysis is easy to obtain by identifying the lines from their wavelengths (or photon energies). By comparing the intensities of these lines with those emitted from standards (pure elements or compounds of known composition) it is also possible to determine the concentrations of the elements (quantitative analysis). The first commercial instrument was manufactured by Cameca in France in 1958; the wavelength-dispersive (WD) analyses in the present study were carried out using a Cameca SX-50 electron microprobe.

Basic Principles

Of fundamental importance in EMPA is the production, identification and measurement of characteristic X-rays produced at a depth of 1-3μm (Figure C3.1). When a high energy electron, generated by an electron microprobe hits the sample, an electron from one of the inner orbital shells of an atom within the sample is ejected. The atom is now in an unstable 'excited' state, an electron from an outer orbital shell will fall into the vacancy created to restore the atom to its 'ground' state. During this process, an amount of energy is released which is equal to the

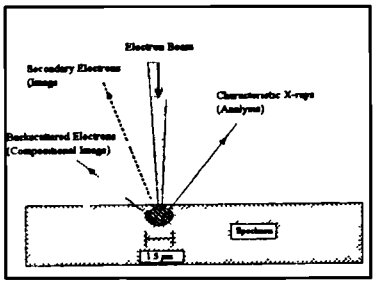


Figure C3.1Electron beam interactions with a mineral specimen (Modified after Williams and Spratt, 1995)

difference in energy between the two orbital shells involved (Figure C3.2). The characteristic X-ray energies emitted are designated by the Roman letter of the electron orbital shell containing the vacancy (i.e. K,L or M), and are suffixed by the Greek letter to denote the group to which the electron belongs (i.e. α,β,γ), and by a number to denote the relative intensities of the emission line (i.e. 1,2,3....). For an electron to be ejected from the atom, the energy of the bombarding electron beam from the microprobe should be at least twice the energy of the emitted X-ray. In practice, elements from Be to Zn are analyzed using the K lines, from As to Hf the L lines, and from Ta to U the M lines.

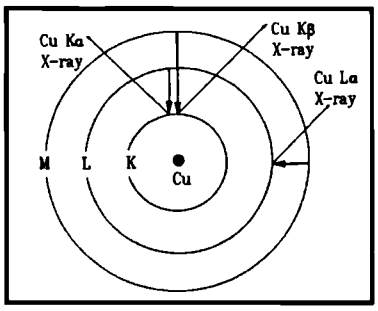


Figure C3.2 Simplified schematic diagram illustrating the emission of a Cu Kα X-ray from an L→K transition, Cu Kβ from an M→K transition, and Cu Lα from an M→L transition. (Modified after Williams and Spratt, 1995).

X-ray Spectrometry - Detection and Measurement

For accurate analysis of minerals by EMPA, the detection and measurement of the characteristic X-rays generated by the mineral sample on bombardment with the electron beam are essential. Two related but distinct methods are employed: analysis on the basis of the energies of the X-rays, i.e energy-dispersive spectrometry (EDS):and analysis on the basis of the wavelengths, i.e. wavelength-dispersive spectrometry (WDS). The wavelength λ (in Ångstroms) is related to energy E (in electron volts) by the expression $\lambda=12396/E$. WD spectrometers give better spectral resolution with fewer peak overlaps than ED spectrometers.

In WDS, the emitted X-rays are first dispersed using a crystal of known structure to isolate the required wavelength. The intensity of the line is then measured using a device called a gas-filled proportional counter. The analyzing crystal reflects X-rays according to the Bragg equation, $n\lambda=2d\sin\theta$, where λ is the wavelength in Ångstroms; *d* the interplanar spacing of the analyzing crystal, in Ångstroms; θ the incident angle with the crystal plane (the Bragg angle); and n the order of reflection (an integer, usually 1). X-rays of differing wavelength are diffracted by differing angles. Four or five spectrometers with different *d*-spacings are needed to cover the complete range of wavelengths required for the analysis of elements from Be to U. The Cameca SX-50 electron microprobe employs four spectrometers.

Spectrometer	SP1	SP2	SP3	SP4
Crystal	PET	PET	LIF	TAP
Elements	Ca	S	Mn	Mg
	Sr	Cd	Fe	Na
	P	Ce		Al
		Ba		

Table C3.1 Element list for carbonate analysis

The PET (pentaerythirtol), LIF (lithium fluoride) and TAP (thallium acid phthalate) crystals consist of different *d*-spacings and cover the necessary range of wavelengths required for the analysis of major and trace elements incorporated in carbonate and sulphide samples (Tables C3.1, C3.2, C3.3, C3.4, C3.5).

Quantitative and Qualitative Analysis

The most important parameters for quantitative analysis procedure are the electron accelerating voltage and beam current. The accelerating voltage must be greater than the excitation potential of the X-ray line of elements present, and preferably should be twice this value to give reasonable

Spectrometer	SP1	SP2	SP3	SP4
Crystal	PET	PET	LIF	TAP
Elements		S	Mn	As
		Cd	Fe	
			Cu	
			Co	
			Ni	

Table C3.2 Element list for sulphide analysis - pyrite

Spectrometer	SP1	SP2	SP3	SP4
Crystal	PET	PET	LIF	TAP
Elements	Ag	S	Mn	Ga
	In	Cd	Fe	Ge
			Cu	As
			Zn	

Table C3.3 Element list for sulphide analysis - sphalerite

Spectrometer	SP1	SP2	SP3	SP4
Crystal	PET	PET	LIF	TAP
Elements	Ag	S	Mn	
	Bi	Cd		
		Pb		

Table C3.4 Element list for sulphide analysis - galena

semi-quantitative analysis.

intensities. Peak intensities and peak to background ratios increase with increasing accelerating voltage. It follows that by operating at a high accelerating voltage better statistical precision can be obtained in a given counting time (or the same precision in a shorter time) and detection limits will be lowered (for a given counting time). These advantages are offset, however, by the increased electron range in the sample, which results in worsened spatial resolution and increased absorption corrections. Balancing these considerations leads to a choice in the range 15-25kV in most cases (Tables C3.6, C3.7). For trace elements, where detectability is more important than the size of the absorption correction, a higher value may be considered. The background regions and potential spectral interferences must also be assessed.

X-ray intensities are, directly proportional to beam current (with other conditions constant). A high current is therefore generally advantageous, but there are some constraints which must be taken into account. Certain types of sample are prone to damage, and show varying degrees of instability under electron bombardment, e.g. carbonates, hydrated minerals, clay minerals and zeolites. This can result in poor analytical precision and accuracy. One way of avoiding this is to use a low beam current or increase the beam diameter, provided the loss of spatial resolution is acceptable. However, the best that can be achieved in these cases is often a

X-Ray Mapping

The spatial distribution of an element can be revealed by recording the intensity of the characteristic X-ray line of that element while scanning the electron beam across the specimen. An X-ray map indicating element distribution is obtained. Such maps provide detailed information on chemical zoning within minerals, textural relationships that are sometimes not apparent from backscattered electron images, or mineral (or zonal) modal analysis.

Digital maps can be produced, in which the intensity of X-rays is recorded at each pixel of a grid equally spaced in the x and y directions and stored in computer memory. The beam is located at each pixel position in turn and resides there for a finite 'dwell time' while X-rays are counted. It is desirable to use a large number of pixels in the interest of image quality, but the dwell time per pixel must then be short, otherwise the total acquisition time is too long. The X-ray maps can be manipulated in a variety of ways using image- processing software. The number of maps obtained simultaneously depends on the number of spectrometers available.

For X-ray maps a resolution of 256 x 256 pixels is adequate and most often used, with a dwell time of the order of 200μs per point (acquisition time is ~4 hours per map). The distance between each point is set at 3μm. In the present study, operating parameters of 15kV, 50-80nA, and a 2μm diameter beam were employed for x-ray mapping.

Spectrometer	SP1	SP2	SP3	SP4
Crystal	PET	PET	LIF	TAP
Elements	Ag	S	Fe	As
	Hg	Sb	Cu	
		Te		
		Pb		

Table C3.5 Element list for sulphide analysis - tennantite, tetrahedrite

Detection limits

The detection limit for a given element is the minimum concentration that can be positively detected, corresponding to a peak which can just be distinguished from statistical background fluctuations. A working definition for a just detectable peak is that its height is greater than three standard deviations of the background count (Reed, 1996). Detection limits for WD analysis are (0.02-0.05 wt%), whereas for routine ED analysis detection limits are (0.2-0.5 wt%).

Electron accelerating voltage (kV)	Beam current (nA)	Beam diameter (μm)
20	20	1-2

Table C3.6 Operating parameters for sulphide analysis

Electron accelerating voltage (kV)	Beam current (nA)	Beam diameter (μm)
15	15	15, 25, 30

Table C3.7 Operating parameters for carbonate analysis

For further detailed information on the theories involved and on various instrumental components, the reader is referred to standard texts, such as Potts (1987), Potts *et al.* (1995), Reed (1993, 1995, 1996), or Scott and Love (1994).

APPENDIX D: ISOTOPE DATA

D1. SULPHUR - Lisheen Deposit

Sample No.	Locality	Line No.	Mineral	Description	Paragenetic Stage	$\delta^{34}S‰$ (CDT)
121/190.2 (1)	Main Zone	SA4049	Pyrite	Disseminated pyrite/marcasite grains.	Early ore-stage	-35.1
121 192.8 (3)	Main Zone	SA4050	Galena	Euhedral galena with associated pale sphalerite rim, in late white dolomite vug.	Late, syn to post ore-stage	-10.5
121 190.2 (4)	Main Zone	SA4051	Pyrite	Disseminated pyrite/marcasite grains.	Early ore-stage	-33.6
121 189.3 (6)	Main Zone	SA4052	Sphalerite	Fine colloform, brown matrix type sphalerite, with minor pyrite.	Main ore-stage	-11.8
121/192.8 (7)	Main Zone	SA4053	Galena	Massive galena - anhedral grains with embayments.	Main ore-stage	-13.9
262 153.6 (9)	Derryville Zone	SA4055	Pyrite	Sub-hedral pyrite grains in black matrix dolomite (post-dated by sphalerite veins).	Early, pre-ore stage	-40.3
262/159.1 (10)	Derryville Zone	SA4057	Sphalerite	Pale brown colloform sphalerite associated with galena grains - late.	Main ore-stage	-10.3
121/189.3 (5)	Main Zone	SA4058	Galena	Euhedral galena associated with late calcite vug.	Late, syn to post ore-stage	-14.8
262 159.1 (11)	Derryville Zone	SA4059	Galena	Euhedral galena, post-dated? By pale brown colloform sphalerite.	Main ore-stage	-10.9
262/152.3 (12)	Derryville Zone	SA4061	Pyrite	Sub-hedral pyrite, hosted in pink dolomite - late/remobilized?	Post ore-stage	-37 9
262 162.1 (20)	Derryville Zone	SA4071	Pyrite	Massive pyrite/marcasite	Early ore-stage	-29.2
262/162.1 (21)	Derryville Zone	SA4072	Pyrite	Massive pyrite/marcasite	Early ore-stage	-27.6
262/162.1 (27)	Derryville Zone	SA4074	Galena	Vein hosted galena associated with tennantite.	Late, post ore-stage	-26.1
262/153.6 (23)	Derryville Zone	SA4075	Pyrite	Fine grained disseminated pyrite, in black matrix dolomite.	Pre-ore stage	-43.7
262 159.1 (24)	Derryville Zone	SA4076	Sphalerite	Dark brown colloform sphalerite with minor pyrite.	Main ore-stage	-9.5
262/162.1 (26)	Derryville Zone	SA4077	Sphalerite	Pale brown colloform sphalerite.	Main ore-stage	-15.1
121 189.3 (27)	Main Zone	SA4078	Pyrite	Pyrite veinlets - stockwork type	Early, ore-stage?	-12.9
121 190.2 (29)	Main Zone	SA4080	Galena	Euhedral galena with associated sphalerite rim, in late white dolomite vug.	Late, syn to post ore-stage	-7.7
121 192.8 (30)	Main Zone	SA4082	Galena	Coarse euhedral galena associated with sphalerite, pyrite and white dolomite.	Late, syn to post ore-stage	-11 9
262 162.1 (22)	Derryville Zone	SA4089	Galena	Dolomite vein hosted galena associated with tennantite.	Late, post ore-stage	-24.9
137 134.9 (17)	Main Zone	SA4090	Pyrite	Massive pyrite - anhedral grains.	Main ore-stage	-17.5
262/159.1 (24) *Repeat*	Derryville Zone	SA4091	Sphalerite	Dark brown colloform sphalerite.	Main ore-stage	-9.3

121 192.8 (28)	Main Zone	SA4095	Pyrite	Massive - banded pyrite.	Main ore-stage	-16.3
121 190.2 (29)	Main Zone	SA4099	Galena	Galena grain in white dolomite vug, pre- and post-dated by sphalerite?	Late, syn to post ore-stage	-5.5
121 189.3 (6) *Repeat*	Main Zone	SA4100	Sphalerite	Fine colloform, brown matrix type sphalerite, with minor pyrite.	Main ore-stage	-10.0
121 192.8 (3) *Repeat*	Main Zone	SA4104	Galena	Euhedral galena with associated sphalerite rim, in late white dolomite vug	Late, syn to post ore-stage	-10.5
262/153.6 (23) *Repeat*	Derryville Zone	SA4105	Pyrite	Fine grained disseminated pyrite, in black matrix dolomite.	Pre ore-stage	-44.1
262/159.1 (14)	Derryville Zone	SA4203	Sphalerite	Dark brown to amber colloform sphalerite	Main ore-stage	-11.6
137 134.9 (17)	Main Zone	SA4206	Pyrite	Massive, fine grained pyrite	Main ore-stage	-16.9
121 319.2 (18)	Main Zone	SA4207	Pyrite	ABL hosted white dolomite vein - minor pyrite.	Late, syn to post ore-stage	-9.7
262 129.8 (21)	Derryville Zone	SA4210	Pyrite	Disseminated fine grained pyrite hosted in black matrix dolomite	Early ore-stage	-39.3
121 194.0 (22)	Main Zone	SA4212	Pyrite	Massive anhedral pyrite	Main ore-stage	-12.8
262/162.1 (22) *Repeat*	Derryville Zone	SA4213	Galena	Dolomite vein hosted galena associated with tennantite.	Late, post ore-stage	-24.2
262/162.1 (23)	Derryville Zone	SA4214	Galena	Vein hosted galena associated with tennantite.	Late, post ore-stage	-26.7
262 159.1 (25)	Derryville Zone	SA4216	Sphalerite	Pale brown colloform sphalerite	Main ore-stage	-14.9
121/189.3 (27)	Main Zone	SA4218	Pyrite	Pyrite veinlets	Main ore-stage	-13.2
121/192.8 (28)	Main Zone	SA4220	Pyrite	Fine grained, banded pyrite	Main ore-stage	-16.7
121/189.3 (31)	Main Zone	SA4221	Sphalerite	Pale pink-brown colloform sphalerite	Main ore-stage	-11.3
121/192.8 (32)	Main Zone	SA4222	Pyrite	Fine grained, banded pyrite	Main ore-stage	-18.4
121/192.8 (33)	Main Zone	SA4223	Pyrite	Massive pyrite	Main ore-stage	-23.9
121/192.8 (34)	Main Zone	SA4224	Galena	Massive, fine grained anhedral galena	Main ore-stage	-14.2
325/135.0 (1)	Derryville Zone	SA4338	Sphalerite	Fine crystalline pale sphalerite	Main ore-stage	-17.2
325 146.2 (2)	Derryville Zone	SA4339	Sphalerite	Fine crystalline pink sphalerite	Main ore-stage	-8.1
325 149.3 (3)	Derryville Zone	SA4340	Galena	Fine grained galena intergrown with pyrite.	Main ore-stage	-9.2
325 149.3 (4)	Derryville Zone	SA4341	Pyrite	Massive pyrite - anhedral grains.	Ore-stage	-19.6
264 172.4 (5)	Derryville Zone	SA4342	Sphalerite	Colloform sphalerite	Main ore-stage	-9 6
264/172.4 (6)	Derryville Zone	SA4343	Pyrite	Pyrite intergrown with sphalerite	Ore-stage	-13.8
275 175.65 (7)	Derryville Zone	SA4344	Galena	Galena intergrown with pyrite in Black Matrix dolomite	Early ore-stage	-19.6
275 175.65 (8)	Derryville Zone	SA4345	Pyrite	Pyrite intergrown with galena in Black Matrix dolomite.	Early, pre ore-stage	-38 5
420 190 70 (9)	Derryville Zone	SA4346	Galena	Vein-hosted galena associated with pale crystalline sphalerite.	Late, syn to post ore-stage	-16.6
420 190.70 (10)	Derryville Zone	SA4348	Pyrite	Fine grained, anhedral pyrite	Ore-stage	-19.4

416 195.5 (11)	Derryville Zone	SA4349	Sphalerite	Fine crystalline pale sphalerite.	Main ore-stage	-6.1
416/195.5 (12)	Derryville Zone	SA4350	Galena	Anhedral galena	Main ore-stage	-10.2
395/194.05 (13)	Derryville Zone	SA4351	Galena	Massive sulphide, coarse subhedral galena	Main ore-stage	-12.2
395 194.05 (14)	Derryville Zone	SA4352	Pyrite	Massive pyrite	Ore-stage	-19.5
394 164.4 (16)	Derryville Zone	SA4353	Galena	Anhedral galena associated with sphalerite.	Main ore-stage	-9 8
394 164.4 (17)	Derryville Zone	SA4354	Sphalerite	Fine crystalline pink sphalerite associated with galena, late?	Ore-stage	-7.5
394/164.4 (18)	Derryville Zone	SA4355	Sphalerite	Colloform sphalerite	Main ore-stage	-12.3
171/172.5 (20)		SA4356	Pyrite	Massive pyrite/marcasite - anhedral grains.	Ore-stage	-14.9
045/215.2 (23)	Main - S Zone	SA4357	Galena	Euhedral galena	Ore-stage	-7.2
179/176.25 (25)	Main - S Zone	SA4358	Chalcopyrite	Massive sulphide - bornite proximal to cpy.	Main ore-stage	-8.3
179/176.25 (26)	Main - S Zone	SA4359	Galena	Massive sulphide - fine grained galena.	Main ore-stage	-6.4
235/167.0 (28)	Main - S Zone	SA4361	Galena	Massive sulphide - fine grained galena.	Main ore-stage	-10.0
137/130.0 (30)	Derryville - S Zone	SA4363	Pyrite	Massive pyrite/marcasite - anhedral grains.	Early ore-stage	-17.2
137/130.0 (31)	Derryville - S Zone	SA4364	Sphalerite	Fine crystalline pink sphalerite.	Ore-stage	-16.1
137/130.0 (32)	Derryville - S Zone	SA4365	Galena	Galena intergrown with pyrite.	Ore-stage	-14.8
361/223.4 (33)	Bog Zone	SA4366	Galena	Fine grained, calcarenite/oolite hosted galena.	Late stage?	+1.6
431/199.65 (37)	Main Zone	SA4371	Galena	Euhedral galena.	Main ore-stage	-10.8
431/199.65 (38)	Main Zone	SA4372	Sphalerite	Fine crystalline pale sphalerite, finely layered.	Main ore-stage	-12.8
431/207.15 (39)	Main Zone	SA4373	Galena	Subhedral to euhedral galena	Main ore-stage	-11.3
431/207.15 (40)	Main Zone	SA4374	Sphalerite	Brown sphalerite	Main ore-stage	-6.4
431/205.70 (41)	Main Zone	SA4375	Galena	Massive colloform galena, sphalerite, pyrite.	Main ore-stage	-11.2
431/205.70 (42)	Main Zone	SA4376	Sphalerite	Massive colloform galena, sphalerite, pyrite.	Main ore-stage	-13.9
431/205.70 (43)	Main Zone	SA4378	Pyrite	Massive colloform galena, sphalerite, pyrite.	Main ore-stage	-14.9
431/191.50 (44)	Main Zone	SA4379	Pyrite	Massive pyrite	Early ore-stage	-26.1
431/210.35 (45)	Main Zone	SA4380	Pyrite	ABL hosted dolomite vein? - minor pyrite.	Late, syn to post ore stage?	-17.4
359/148.65 (46)	Derryville Zone	SA4382	Galena	Galena associated with fine crystalline pink sphalerite.	Main ore-stage	-15.1
359/148.65 (47)	Derryville Zone	SA4383	Sphalerite	Fine crystalline pale sphalerite associated with galena.	Main ore-stage	-7.7
359 133.2 (48)	Derryville Zone	SA4384	Pyrite	Fine grained disseminated pyrite, in Black Matrix dolomite.	Pre ore-stage	-38.1
359 143.6 (49)	Derryville Zone	SA4385	Sphalerite	Masive sulphide - pale yellow, fine crystalline sphalerite.	Ore-stage	-18.7
359 143.6 (50)	Derryville Zone	SA4386	Pyrite	Massive pyrite, intergrown with sphalerite.	Ore-stage	-8.7
451 139.10 (51)	Bog Zone	SA4387	Sphalerite	Coarse crystalline sphalerite in white dolomite vug.	Late, syn to post ore-stage	-31.5

451 139.10 (52)	Bog Zone	SA4388	Galena	Euhedral galena in white dolomite vug.	Late, syn to post ore-stage	-23.2
451 139.10 (53)	Bog Zone	SA4390	Pyrite	Massive pyrite	Late, syn to post ore-stage	-30.0
451 135.65 (54)	Bog Zone	SA4391	Sphalerite	Fine crystalline pale sphalerite.	Ore-stage	-13.6
451 135.65 (55)	Bog Zone	SA4392	Pyrite	Massive pyrite with interstitial fine crystalline pale sphalerite.	Ore-stage	-24.3
400 205.0 (56)	North Zone	SA4393	Pyrite	Fine grained disseminated pyrite, in Black Matrix dolomite.	Pre ore-stage	-40.7
400 205.65 (57)	North Zone	SA4394	Sphalerite	Pale, colloform sphalerite.	Main ore-stage	-13.2
402 196.0 (59)	Derryville Zone	SA4395	Galena	Euhedral galena with associated pale sphalerite rim, in late white dolomite vug.	Late, syn to post ore-stage?	-5.6
095 335.0 (60)	Derryville Zone	SA4396	Pyrite	Coarse grained pyrite associated with late brown sphalerite in white dolomite vug/vein.	Late, syn to post ore-stage	+11.8
095 335.0 (61)	Derryville Zone	SA4397	Sphalerite	Coarse crystalline sphalerite in white dolomite vug/vein associated with pyrite.	Late, syn to post ore-stage	+8.6
171 172.5 (19)	Derryville Zone	SA4401	Barite	White, intergrown with sulphides	Main, ore-stage	+18.1
105/185.65 (22)	Main - S Zone	SA4402	Barite	White	Main ore-stage	+14.5
171/172.5 (19) *Repeat*	Derryville Zone	SA4404	Barite	White, intergrown with sulphides	Main ore-stage	+17.2
105/185.65 (22) *Repeat*	Main - S Zone	SA4405	Barite	White	Main ore-stage	+14.3
045/215 20 (23) *Repeat*	Main - S Zone	SA4409	Galena	Euhedral galena	Ore-stage	-4.9
361 223.4 (33) *Repeat*	Bog Zone	SA4410	Galena	Fine grained, calcarenite/oolite hosted galena.		+3.2
235/167.0 (29)	Main - S Zone	SA4411	Chalcopyrite	Massive sulphide	Main ore-stage	-6.6
179/176.25 (25) *Repeat*	Main - S Zone	SA4412	Chalcopyrite	Massive sulphide	Main ore-stage	-7.4
095/335.0 (60) *Repeat*	Derryville Zone	SA4413	Pyrite	Coarse grained pyrite associated with late brown sphalerite in white dolomite vug/vein.	Late, syn to post ore-stage	+11.7
095/335.0 (61) *Repeat*	Derryville Zone	SA4414	Sphalerite	Coarse crystalline sphalerite in white dolomite vug/vein associated with pyrite.	Late, syn to post ore-stage	+8.6
514 182 5 (35)	Main - S Zone	SA4762	Sphalerite	Very coarse, euhedral, pale yellow sphalerite in calcite vug.	Late, syn to post ore-stage	-8.8
471 210.4 (36)	Main Zone	SA4770	Sphalerite	Red crystalline sphalerite associated with fine grained massive sulphide.	Main ore-stage	-5.5
463 173.0 (37)	Derryville- S Zone	SA4771	Sphalerite	Calcite vein-hosted brown crystalline sphalerite (ABL hosted veins - horizontal).	Late, syn tp post ore-stage	+1.3

517 205.0 (38)	North Zone	SA4772	Sphalerite	Coarse crystalline yellow sphalerite in white dolomite vug.	Late, syn to post ore-stage	-5 8
517 204.9 (39)	North Zone	SA4773	Sphalerite	Coarse crystalline yellow sphalerite in white dolomite vug	Late, syn to post ore-stage	-5.9
529 246.6 (40)	Bog - E Zone	SA4774	Sphalerite	Calcite vein-hosted crystalline brown sphalerite (ABL hosted veins).	Late, syn to post ore-stage	+6.5
475 223.2 (42)	Main Zone	SA4777	Sphalerite	Coarse crystalline yellow sphalerite in white dol/calc?	Late, syn to post ore-stage	+2.3
457 212.6 (43)	Main Zone	SA4778	Sphalerite	Calcite vein-hosted fine crystalline pink-brown sphalerite.	Late, syn to post ore-stage	+0.5
457/212.6 (44)	Main Zone	SA4779	Galena	Vein hosted Galena intergrown with sphalerite	Ore stage?	-0.9
449/95.5 (45)	Bog - S Zone	SA4780	Sphalerite	Calcite vein-hosted fine crystalline sphalerite associated with galena.	Late, syn to post ore-stage	-8.4
449 95.5 (46)	Bog - S Zone	SA4782	Galena	Calcite vein-hosted euhedral galena.	Late, syn to post ore-stage	-1.7
463/173.0 (37) *Repeat*	Derryville- S Zone	SA4784	Sphalerite	Calcite vein-hosted brown crystalline sphalerite (ABL hosted veins - horizontal).	Late, syn to post ore-stage	+1.4
529 246.6 (40) *Repeat*	Bog - E Zone	SA4787	Sphalerite	Calcite vein-hosted crystalline brown sphalerite (ABL hosted veins).	Late, syn to post ore-stage	+6.4
359/152.0 (48)	Derryville Zone	SA4788	Pyrite	ABL vein-hosted pyrite	Late, syn to post ore-stage	-20.2
451/139.10 (1) *Repeat*	Bog Zone	April 98	Sphalerite	Dark brown, coarse (up to 6mm) crystalline sphalerite in late calcite vug with galena.	Late, syn to post ore-stage	-23.0
515 173.7 (2)	Main Zone	April 98	Sphalerite	Crystalline amber sphalerite associated with pink dolomite vug	Late, syn to post ore-stage	+0.3
171 160.0 (3)	Derryville Zone	April 98	Sphalerite	Crystalline brown sphalerite with minor galena, post-dated by white dolomite.	Late, syn to post ore-stage	+2.3
325/149.30 (4)	Derryville Zone	April 98	Sphalerite	Crystalline yellow sphalerite	Ore-stage	-4 5

D2. SULPHUR - Galmoy Deposit

Sample No.	Locality	Line No.	Mineral	Description	Paragenetic Stage	$\delta^{34}S‰$ (CDT)
MG18 89.0 (7)	G Zone (G-NE)	SA4719	Pyrite	Massive, rounded pyrite clasts	Main ore-stage	-8.7
MCW13 102.42 (9)	CW Zone	SA4721	Pyrite	Disseminated pyrite	Pre ore-stage	-35.7
3245-63 103.0 (12)	TT Bog Prospect	SA4727	Pyrite	Massive fine grained pyrite	Early ore-stage	-27.1
3245-63 90.22	TT Bog	SA4728	Pyrite	Massive sulphide -	Ore-stage	-15.3

(13)	Prospect			slightly oxidized		
GY355 100.0 (21)	K Zone	SA4741	Pyrite	Irregular, subrounded pyrite laths in white dolomite	Ore stage	-11.4
GY355 95.5 (22)	K Zone	SA4742	Pyrite	Pyrite banding associated with galena and sphalerite	Ore stage	+0.8
GY355 107.0 (26)	K Zone	SA4752	Pyrite	Disseminated pyrite	Pre ore-stage	-25.9
9. (29)	CW Zone	SA4755	Pyrite	Shale hosted botryoidal pyrite marcasite	Pre ore-stage	-39.9
8. (32)	CW Zone	SA4758	Pyrite	Minor disseminated pyrite	Early ore-stage	-24.0
GY355/95.5 (22) *Repeat*	K Zone	SA4785	Pyrite	Pyrite banding associated with galena and sphalerite	Ore stage	+0.8
G16-27/383.5 (2)	G Zone	SA4715	Chalcopyrite	Lower Ballysteen, dolomite vein-hosted chalcopyrite	Late, syn to post ore-stage	+3.4
G16-27/383.5 (2) *Repeat*	G Zone	SA4786	Chalcopyrite	Lower Ballysteen, dolomite vein-hosted chalcopyrite	Late, syn to post ore-stage	+3.8
G16-27/385.5 (3)	G Zone	SA4716	Galena	Lower Ballysteen, dolomite vein-hosted galena	Late, syn to post ore-stage	+1.1
G16-27/366.0 (4)	G Zone	SA4717	Galena	Lower Ballysteen hosted galena veinlets	Late, syn to post ore-stage	+2.6
3245-63/90.22 (15)	TT Bog Prospect	SA4730	Galena	Massive sulphide intergrown with pinky brown sphalerite and pyrite	Ore-stage	-19.6
GY382/86.5 (17)	K Zone	SA4732	Galena	Vug fill, stromatactic type galena, associated with crystalline zoned sphalerite	Late, syn to post ore-stage	+5.8
GY355/95.0 (18)	K Zone	SA4733	Galena	Galena banding associated with pyrite and sphalerite	Ore-stage	-2.4
GY355/95.5 (23)	K Zone	SA4743	Galena	Galena banding associated with pyrite and sphalerite	Ore-stage	-2.9
GY355/78.0 (28)	K Zone	SA4754	Galena	Minor galena associated with white dolomite	Late, syn to post ore-stage	+2.3
10CW (34)	CW Zone	SA4761	Galena	Euhedral galena associated with crystalline yellow sphalerite	Late, ore-stage	-12.3
MG18/90.0 (5)	G Zone (G-NE)	SA4763	Galena	Anhedral galena intergrown with fine grained pinky brown sphalerite	Main ore-stage	-8.8
MCW13/102.42 (11)	CW Zone	SA4765	Galena	Massive fine grained galena associated with pale grey sphalerite	Main ore-stage	-17.6
3245-28 30.0 (1)	G Zone (G-W)	SA4714	Sphalerite	Massive, pale cream sphalerite with intergrown pyrite - oxidized sample	Main ore-stage	-14.7
MG18 90.0 (6)	G Zone (G-NE)	SA4718	Sphalerite	Fine crystalline sphalerite intergrown with anhedral galena	Main ore-stage	-8.3
MG46 73.0 (8)	G Zone (G-E)	SA4720	Sphalerite	Massive sulphide - fine grained sphalerite associated with fine galena and intergrown with pyrite	Main ore-stage	-18.3
MCW13/102.42 (10)	CW Zone	SA4726	Sphalerite	Very fine grained, pale sphalerite	Main ore-stage	-16.9
3245-63 90.22 (14)	TT Bog Prospect	SA4729	Sphalerite	Massive sulphide - fine crystalline pinky brown sphalerite	Main ore-stage	-12.5

GY382/86.5 (16)		SA4731	Sphalerite	Vug fill, stromatactic type, crystalline zoned sphalerite	Late, syn to post ore-stage	+6.4
GY355 95.0 (19)	K Zone	SA4739	Sphalerite	Sphalerite banding associated with pyrite and galena	Ore-stage	-4.9
GY355 95.5 (24)	K Zone	SA4744	Sphalerite	Anhedral clasts of pale grey, fine grained sphalerite	Main ore-stage	-12.7
GY355 107.0 (25)	K Zone	SA4745	Sphalerite	Pale to colourless sphalerite with minor disseminated pyrite	Ore-stage	-19.2
2. (30)	CW Zone	SA4756	Sphalerite	Massive crystalline, variable coloured sphalerite	Main ore-stage	-17.7
8. (31)	CW Zone	SA4757	Sphalerite	ABL hosted, fine grained, brown sphalerite	Ore-stage?	-20.3
10CW (33)	CW Zone	SA4760	Sphalerite	Coarse yellow sphalerite associated with euhedral galena	Ore-stage	-15.5
GY355/95.0 (19) *Repeat*	K Zone	SA4766	Sphalerite	Anhedral, brown sphalerite clasts	Ore-stage	-5.4
GY355/97.0 (20)	K Zone	SA4767	Sphalerite	Subrounded sphalerite clasts in white-pink dolomite	Ore-stage	-13.3
GY355/78.0 (27)	K Zone	SA4769	Sphalerite	Coarse brown sphalerite in zebra textured white dolomite	Ore-stage	-10.7

D3 SULPHUR - Rathdowney Trend prospects

Sample No.	Locality	Line No.	Mineral	Description	Paragenetic Stage	$\delta^{34}S‰$ (CDT)
2 959.8 (13)	Durrow	SA4062	Pyrite	Fine grained pyrite hosted in dolomitized oolite	Main stage	+3.0
2 960.8 (14)	Durrow	SA4063	Chalcopyrite	Late (pink?) dolomite vug-hosted chalcopyrite.	Late stage	-7.9
2/961.9 (15)	Durrow	SA4064	Tennantite	Late dolomite vein-hosted tennantite.	Late stage	-0.2
1 909.5 (16)	Durrow	SA4066	Pyrite	Fine grained pyrite.	Main stage	-9.0
HC5/122.9 (18)	Holycross	SA4068	Sphalerite	White dolomite vein-hosted pale amber sphalerite with galena inclusions.	Late stage	+6.1
HC5 122.9 (19)	Holycross	SA4070	Pyrite	White dolomite vein-hosted pyrite with galena inclusions.	Late stage	+8.5
1 910.0 (32)	Durrow	SA4084	Pyrite	Replacement pyrite (oolitic ghost extures preserved).	Main stage	-8.9
2 960.8 (14) *Repeat*	Durrow	SA4096	Chalcopyrite	Late dolomite vug hosted chalcopyrite.	Main stage	-7.7
1 909.5 (16) *Repeat*	Durrow	SA4097	Pyrite	Fine grained pyrite.	Main stage	-8.7

1 910.0 (32) *Repeat*	Durrow	SA4101	Pyrite	Replacement pyrite (oolitic ghost textures preserved)	Main stage	-8.6
2 959.8 (13) *Repeat*	Durrow	SA4103	Pyrite	Fine grained pyrite hosted in dolomitized oolite	Main stage	+3.5
HC5 122.9 (18) *Repeat*	Holycross	SA4106	Sphalerite	White dolomite vein-hosted pale amber sphalerite with galena inclusions.	Late stage	+6.4
HC5 122.9 (19) *Repeat*	Holycross	SA4107	Pyrite	White dolomite vein-hosted pyrite with galena inclusions.	Late stage	+8.5
24/1718.0 (1)	Rathdowney East	SA4186	Pyrite	Anhedral to sub-hedral fine grained pyrite with minor gangue inclusions, associated with fine replacive regional dolomite.	Early stage	-39.4
24 1729a. (2)	Rathdowney East	SA4187	Pyrite	Anhedral, fine grained disseminated pyrite, associated with fine replacive regional dolomite.	Early stage	-40.1
24 1729b. (3)	Rathdowney East	SA4188	Pyrite	Anhedral, fine grained disseminated pyrite.	Early stage	-31.4
45/243a. (4)	Derrykeam	SA4189	Pyrite	Anhedral, fine grained aggregate type pyrite	Main stage	-11.8
45 243b. (5)	Derrykeam	SA4192	Pyrite	Anhedral, fine grained disseminated pyrite associated with minor dolomite veinlets.	Late stage	+6.6
45 271.6a. (6)	Derrykeam	SA4193	Pyrite	Anhedral, fine grained pyrite, associated with white dolomite.	Main stage	-9.6
45 271.6b. (7)	Derrykeam	SA4194	Sphalerite	Anhedral, fine grained pale cream sphalerite associated with white dolomite.	Main stage	-20.4
HC13/104.0 (9)	Holycross	SA4196	Pyrite	Stylolitic, fine grained pyrite.	Early stage	-32.5
2 959.8 (11)	Durrow	SA4198	Pyrite	Fine grained pyrite hosted in dolomitized oolite	Main stage	+3.5
2 961.9 (12)	Durrow	SA4199	Tennantite	Late dolomite vein -hosted tennantite.	Late stage	+0.3
2 961.9 (15)	Durrow	SA4204	Chalcopyrite	Late (pink?) dolomite vug hosted chalcopyrite.	Main stage	-7.7
2 960.8 (16)	Durrow	SA4205	Tennantite	Late dolomite vein -hosted tennantite.	Late stage	-0.3
45 243b. (5) *Repeat*	Derrykeam	SA4227	Pyrite	Anhedral, fine grained pyrite associated with minor dolomite veinlets.	Main stage	+6.5
1653-24 (34)	Rathdowney East	SA4367	Pyrite	Fine grained disseminated pyrite	Early stage	-34.9
1650-45 (35)	Derrykeam	SA4369	Pyrite	Fine grained pyrite	Main stage	-22 9
1650-11 (36)	Derrykeam	SA4370	Pyrite	Vug fill pyrite?	Late stage	+8 0
1653-24 (34) *Repeat*	Rathdowney East	SA4406	Pyrite	Fine grained disseminated pyrite	Early stage	-35.0
1650-45 (35) *Repeat*	Derrykeam	SA4407	Pyrite	Fine grained pyrite	Main stage	-22 8
1650-11 (36) *Repeat*	Derrykeam	SA4408	Pyrite	Vug fill pyrite?	Late stage	+8.6

D4. CARBON, OXYGEN - Lisheen Deposit

Sample No.	Locality	Line No.	Mineral	Description	Paragenetic Stage	$\delta^{18}O‰$ (SMOW)	$\delta^{13}C‰$ (PDB)
147 208.6 (4)	Derryville Zone	C14697	Dolomite	Dolomite vein with brown sphalerite.	D5 Dol	21.05	2.27
126 339.45 (5)	Derryville Zone	C14698	Dolomite	Dolomite vug with pale sphalerite.	D5 Dol	19.37	0.16
95 335.0 (8)	Derryville Zone	C14699	Dolomite	Dolomite vug with coarse pyrite, sphalerite and galena.	D5 Dol	20.46	-1.30
517/205.0 (9)	North Zone	C14700	Dolomite	Dolomite vug with coarse crystalline yellow sphalerite.	D5 Dol	20.69	1.99
262 152.3 (24)	Derryville Zone	C14722	Dolomite	Vug fill pink dolomite with pyrite, in well developed Black matrix dolomite.	D4	23.21	2.29
138/225.0 (25)	Main - S Zone	C14723	Dolomite	Coarse pink dolomite, cross-cutting dark dolomite clasts and white dolomite.	D4	24.82	2.69
318/450.5 (26)	Main Zone	C14724	Dolomite	Coarse pink dolomite - deep hole.	D4	23.19	1.94
251 198.3 (38)	Derryville Zone	C14726	Dolomite	Dolomite vug with cubic galena and pale sphalerite.	D5 Dol	20.80	2.67
538 185.2 (40)	North Zone	C14739	Dolomite	White matrix dolomite	D3	20.39	2.39
272 227.6 (41)	Outside ore reserve. Approx 700m north of Derryville Zone.	C14740	Dolomite	White matrix dolomite	D3	20.78	2.28
262/129.8 (51)	Derryville Zone	C14747	Dolomite	Black matrix dolomite	D2	24.36	6.29
275/169.0 (54)	Derryville Zone	C14748	Dolomite	Black matrix dolomite	D2	25.72	3.67
413 100.5 (55)	Outside ore reserve. Approx 200m west of Main Zone.	C14749	Dolomite	Black matrix dolomite	D2	26.27	3.68
259 222.0 (56)	Outside ore reserve. Approx 500m north of Derryville Zone.	C14750	Dolomite	Black matrix dolomite	D2	22.20	3 39

2447-8 13.3 (61)	Regional sample. Approx 2km northwest of Lisheen.	C14755	Dolomite	Regional coarse white dolomite.	D1 Cem	21.50	2.70
147 208.6 (4) *Repeat*	Derryville Zone	C14691	Dolomite	Dolomite vein with brown sphalerite.	D5 Dol	23.09	2.31
126 339.45 (5) *Repeat*	Derryville Zone	C14692	Dolomite	Dolomite vug with pale sphalerite.	D5 Dol	20.90	0.09
95/335.0 (8) *Repeat*	Derryville Zone	C14693	Dolomite	Dolomite vug with coarse pyrite, sphalerite and galena.	D5 Dol	22.83	-1.17
517/205.0 (9) *Repeat*	North Zone	C14694	Dolomite	Dolomite vug with coarse crystalline yellow sphalerite.	D5 Dol	22.18	2.14
252/174.0 (39)	Derryville Zone	C14734	Dolomite	White matrix dolomite	D3	20.84	2.33
297/183.3 (42)	Outside ore reserve. Approx 200m east of Derryville Zone.	C14735	Dolomite	White matrix dolomite		21.13	2.80
121/165.2 (43)	Main Zone	C14736	Dolomite	White matrix dolomite	D3	20.65	2.32
121/146.8 (44)	Main Zone	C14737	Dolomite	White matrix dolomite	D3	20.23	2.45
457/213.6 (1)	Main Zone	C14703	Calcite	Calcite vein with sphalerite, galena	D5 Calc	24.06	0.65
514/182.5 (2)	Main - S Zone	C14704	Calcite	Calcite vug with with coarse crystalline sphalerite.	D5 Calc	21.81	0.47
449/95.5 (3)	Bog - S Zone	C14705	Calcite	Calcite vein with sphalerite and galena.	D5 Calc	20.30	1.03
529/246.6 (6)	Bog - E Zone	C14706	Calcite	ABL hosted? Calcite vein with coarse crystalline brown sphalerite.	D5 Calc	21.44	0.63
95/335.0 (7)	Derryville Zone	C14707	Calcite	Calcite vug with coarse pyrite, sphalerite and galena.	D5 Calc	19.54	-1.09
451/139.10 (10)	Bog Zone	C14715	Calcite	Coarse calcite vug/vein with brown sphalerite, galena and pyrite (proximal to massive sulphide zone).	D5 Calc	21.70	-0.38
420 190.7 (11)	Derryville Zone	C14716	Calcite	Calcite vug with sphalerite.	D5 Calc	23.06	0.77

463 173.0 (12)	Derryville - S Zone	C14717	Calcite	ABL hosted calcite with crystalline brown sphalerite.	D5 Calc	21.45	-0.23
318 450.5 (27)	Main Zone	C14720	Calcite	Very coarse calcite, post-dates pink dolomite.	D5 Calc	21.34	-5.79
121 319.2 (29)	Main Zone	C14727	Calcite	Calcite vein with chalcopyrite.	D5 Calc	22.74	0.37
2258-11/60.8 (31)	Outside ore reserve. Approx 1000m west of North Zone.	C14729	Calcite	Ferroan calcite vein, sub-vertical.	D5 Calc	25.11	2.21
2447-14/190.5 (32)	Regional sample. Approx 3km southwest of Lisheen.	C14730	Calcite	Coarse calcite vein, unmineralized.	D5 Calc	20.99	0.97
264/171.3 (33)	Derryville Zone	C14731	Calcite	Calcite with minor sphalerite clasts.	D5 Calc	22 76	-0 20
262/120.0 (34)	Derryville Zone	C14758	Calcite	Matrix forming white calcite. Dolomite clasts show rotation and have trace pyrite along stylolites.	D5 Calc	22.91	1.87
463/173.3 (30)	Derryville - S Zone	C14760	Calcite	ABL hosted calcite vein - Proximal dolomite vein associated with minor sphalerite.	D5 Calc	20.11	0.16
95/335.0 (7) *Repeat*	Derryville Zone	C14763	Calcite	Calcite vug with coarse pyrite, sphalerite and galena.	D5 Calc	19.29	-1.00
463/173.0 (12) *Repeat*	Derryville - S Zone	C14764	Calcite	ABL hosted calcite with crystalline brown sphalerite.	D5 Calc	20.48	-0.63
318/450.5 (27) *Repeat*	Main Zone	C14765	Calcite	Very coarse calcite, post-dates pink dolomite.	D5 Calc	21.52	-5.22

D5. CARBON, OXYGEN - Galmoy Deposit

Sample No.	Locality	Line No.	Mineral	Description	Paragenetic Stage	$\delta^{18}O‰$ (SMOW)	$\delta^{13}C‰$ (PDB)
G16-27/383.5 (15)	G Zone	C14709	Dolomite	Lower Ballysteen dolomite vein (5mm) thick, associated with cpy.	D5 Dol	19.26	2.34
GY355 97.0 (16)	K Zone	C14710	Dolomite	Crystalline white/pink dolomite with rounded mineralized clasts.	D3	20.99	2.63

GY355 95.0 (17)	K Zone	C14711	Dolomite	White dolomite vug associated with galena.	D5 Dol	21.57	2 46
GY355 100.0 (18)	K Zone	C14712	Dolomite	Crystalline white dolomite associated with pyrite.	D3?	22.30	2.34
GY355 78.0 (19)	K Zone	C14713	Dolomite	Zebra type white dolomite, sphalerite associated.	D3?	19.54	1.45
5. (23)	CW Zone	C14721	Dolomite	Cross-cutting dolomite veins (~2mm) in BMB.	D5 Dol	19.36	3.38
MG99 100.8 (50)	Outside orebody, within deposit.	C14746	Dolomite	Matrix dolomite - white moderately developed.	D3	22.16	2.37
MG99 100.6 (57)	Outside orebody, within deposit.	C14751	Dolomite	Matrix dolomite - black with disseminated pyr.	D2	25.39	3.50
MG63 97.2 (58)	Sub-Economic East of G-NE orebody	C14752	Dolomite	Matrix dolomite - black	D2	23.19	3.24
MG18 87.5 (59)	G Zone (G-NE)	C14753	Dolomite	Matrix dolomite - black	D2	25.27	3.46
5. (60)	CW Zone	C14754	Dolomite	Matrix dolomite - black	D2	23.05	3.58
GY333/103.3 (20)	Sub-Economic East of K orebody	C14718	Calcite	Calcite vein (12mm) in Ballysteen, associated with minor amber sph.	D5 Calc	20.07	1.30
8. (22)	CW Zone	C14719	Calcite	Crystalline calcite in ABL, with trace pyr.	D5 Calc	22.40	0.76
MG99 100.8 (37)	Outside orebody, within deposit.	C14759	Calcite	Calcite proximal to white and black matrix dolomite.	D5 Calc	21.70	0.61

D6. CARBON, OXYGEN - Rathdowney Trend prospects

Sample No.	Locality	Line No.	Mineral	Description	Paragenetic Stage	$\delta^{18}O‰$ (SMOW)	$\delta^{13}C‰$ (PDB)
1 686.5 (45)	Durrow	C14741	Dolomite	White matrix dolomite	D3	20.97	3.03
45 294.6 (47)	Derrykeam	C14743	Dolomite	White matrix dolomite, proximal to minor mineralization.	D3	20.60	1.96
24 1718.0 (49)	Rathdowney East	C14745	Dolomite	White matrix dolomite, proximal to minor mineralization.	D3	20.69	2.26
HC13 87.8 (46)	Holycross	C14767	Dolomite	White matrix dolomite	D3	22.13	2.85
2218-8 34.3 (28)	Rathdowney North	C14769	Dolomite	Pink Matrix dolomite	D4	24.75	2.60
24 1625.0 (36)	Rathdowney East	C14733	Dolomite	Pink matrix dolomite	D4	22 90	2 94
2218-8 34.3	Rathdowney North	C14725	Dolomite	Pink Matrix dolomite	D4	24.67	2 45

D7. LEAD - Lisheen Deposit

Sample No.	Locality	Lab No.	Mineral	Description	$\delta^{34}S$	$^{206}Pb/^{204}Pb$	$^{207}Pb/^{204}Pb$	$^{208}Pb/^{204}Pb$
416 195.5	Derryville Zone	12SE	Galena	Ore-stage anhedral galena	-10.2	18.182±10	15.602±11	38.076±24
262/162.1	Derryville Zone	23SE	Galena	Late ore-stage, vein hosted galena associated with tennantite.	-26.1	18.197±10	15.585±8	38 078±16
179 176.25	Main - S Zone	26SE	Galena	Ore-stage, fine grained galena	-6.4	18.160±22	15.563±28	38.010±38
431 205.70	Main Zone	41SE	Galena	Ore-stage banded, galena associated with sphalerite and pyrite	-11.2	18.193±12	15.624±11	38.158±28
NBS 981 (Std)						**16.945±7**	**15.494±6**	**36.728±16**

D8. LEAD - Galmoy Deposit

Sample No.	Locality	Lab No.	Mineral	Description	$\delta^{34}S$	$^{206}Pb/^{204}Pb$	$^{207}Pb/^{204}Pb$	$^{208}Pb/^{204}Pb$
G16-27/366.0	G Zone	4 SE	Galena	Late ore-stage galena veinlets	+2.6	18.204±8	15.597±7	38.084±17
MG18 90.0	G zone (G-NE)	5 SE	Galena	Ore-stage anhedral galena	-8.8	18.209±12	15.587±12	38.089±15
MCW13 102.42	CW Zone	11 SE	Galena	Ore-stage fine grained galena intergrown with fine grained sphalerite	-17.6	18.238±7	15.623±7	38.165±18
GY355 95.0	K Zone	18 SE	Galena	Ore-stage banded, galena associated with sphalerite and pyrite	-2.3	18.189±31	15.550±23	37.948±52
GY355 78.0	K Zone	28 SE	Galena	Late ore-stage minor galena, associated with white dolomite	+2.3	18.226±5	15.604±4	38.121±11
10CW	CW Zone	34 SE	Galena	Late ore-stage euhedral galena associated with crystalline yellow sphalerite	-12.3	18.223±9	15.593±10	38.096±20
NBS 981 (Std)						**16.945±7**	**15.494±6**	**36.728±16**

All data are corrected for mass fractionation. Mass fractionation factors from SURRC over the period November to end March, 1997:

$^{206}Pb/^{204}Pb = 1.00327$
$^{207}Pb/^{204}Pb = 1.00446$
$^{208}Pb/^{204}Pb = 1.00647$

APPENDIX E: FLUID INCLUSION DATA

E1: FLUID INCLUSIONS - Lisheen Gangue

Sample	Incl. No.	Paragenetic Stage	Classification	Type	Tfm	Tmi	Salinity	Tmh	Th
262/152.3 Pink	16	D4	P	L + V		-30 0	28 7		97 0
"	4	D4	P	L + V	-39 7	-29 0	28 0		118 9
"	5	D4	P	L + V	-39 0	-28 3	27 6	_	98 8
"	11	D4	P	L + V		-27 2	26 9	_	95 2
"	20	D4	P	L + V		-27 3	27 0	_	93 6
"	23	D4	P	L + V	-44 7	-27 5	27 1	_	99 3
"	26	D4	P	L + V	-39 0	-25 2	25 7	_	97 5
"	27	D4	P	L + V	_	-28 1	27 5		98 0
"	2	D4	P	L + V	_	_	_	_	118 1
"	3	D4	P	L + V	_		_	_	96 2
"	4	D4	P	L + V	_	_	_	_	96 2
"	5	D4	P	L + V		_	_	_	91 1
"	6	D4	P	L + V		_	_		83 1
"	7	D4	P	L + V		_	_		97 7
"	8	D4	P	L + V	_	_	_	_	99 6
"	9	D4	P	L + V	_	_	_	_	116 0
"	10	D4	P	L + V		_	_		119 7
"	11	D4	P	L + V	_				97 2
"	12	D4	P	L + V		_	_	_	93 6
"	13	D4	P	L + V	_	_	_	_	79 1
"	14	D4	P	L + V			_	_	88 2
"	15	D4	P	L + V	_	_	_		88 1
"	2a	D4	P	L + V	_	_	_	_	97 4
"	3a	D4	P	L + V		_	_	_	109 8
"	6a	D4	P	L + V	-39 7		_		96 3
"	7a	D4	P	L + V	-38 6	_	_	_	95 8
"	8a	D4	P	L + V	-43 0	_	_		96 9
"	9a	D4	P	L + V		_	_	_	96 9
"	10a	D4	P	L + V	_	_	_	_	96 4
"	17	D4	P	L + V	_	_	_	_	93 8
"	18	D4	P	L + V	_	_	_	_	93 8
"	19	D4	P	L + V	_	_	_	_	96 3
"	21	D4	P	L + V	-39 3		_		96 6
"	24	D4	P	L + V	_	_	_	_	96 8
"	25	D4	P	L + V	_	_	_	_	99 9
"	28	D4	P	L + V					96 3
121/31.4 CW	7	$D1_{Cem}$	P	L + V	_	_	_	_	180.3
"	8	$D1_{Cem}$	P	L + V	_	_	_	_	247 3
"	9	$D1_{Cem}$	P	L + V	_	_	_	_	221 6
121/31.4 QTZ	1	$D5_{Qtz}$	P	L + V	_	-15 4	19 0		122 6
"	5	$D5_{Qtz}$	P	L + V	_	-23 4	24 6		190 5
"	6	$D5_{Qtz}$	P	L + V		-15 4	19.0	_	130 0
"	2	$D5_{Qtz}$	P	L + V	_	_	_	_	135 2
"	3	$D5_{Qtz}$	P	L + V	_	_	_	_	130 5
"	4	$D5_{Qtz}$	P	L + V	_	_	_	_	143 8
325/149.3 Calc	5	$D5_{Calc}$	P	L + V	_	_	_		194 9
"	5a	$D5_{Calc}$	P	L + V	_	_	_	_	230 4
"	6	$D5_{Calc}$	P	L + V		_	_	_	230 7
"	7	$D5_{Calc}$	P	L + V		_	_		232 3
"	8	$D5_{Calc}$	P	L + V	_	_	_	_	232 8
"	9	$D5_{Calc}$	P	L + V		_	_	_	232 3
"	10	$D5_{Calc}$	P	L + V	_				228 2
451/139.10 Calc	2	$D5_{Calc}$	P	L + V	_	-9 3	13 1		201 0
"	3	$D5_{Calc}$	P	L + V	_	-9 3	13 1	_	176 8
"	23	$D5_{Calc}$	P	L + V	_	-8 6	12 4	_	196 9
"	24	$D5_{Calc}$	P	L + V		-8 6	12 4		193 4
"	25	$D5_{Calc}$	P	L + V		-8 1	11 8		163 2
"	26	$D5_{Calc}$	P	L + V	_	-9 0	12 8		181 8
"	27	$D5_{Calc}$	P	L + V		-8 4	12 1	_	182 8
"	28	$D5_{Calc}$	P	L + V	_	-7 7	11 3	_	186 9
"	46	$D5_{Calc}$	P	L + V		-9.1	12 9	_	152 2
"	8	$D5_{Calc}$	P	L + V	-54 0	-7.8	11 4	_	207 0
"	9	$D5_{Calc}$	P	L + V	-54 0	-7 8	11.4	_	207 0
"	22a	$D5_{Calc}$	P	L + V	_	-7 9	11 5	_	205 9
"	1a	$D5_{Calc}$	P	L + V	_		_	_	206 3
"	2a	$D5_{Calc}$	P	L + V	_	_	_	_	206 9
"	3a	$D5_{Calc}$	P	L + V	_	_	_		205 4
"	4a	$D5_{Calc}$	P	L + V		_	_	_	203 0
"	5a	$D5_{Calc}$	P	L + V	_	_	_	_	207 0
"	6a	$D5_{Calc}$	P	L + V	_	_	_	_	207 0
"	7a	$D5_{Calc}$	P	L + V	_	_	_	_	207 0
"	10a	$D5_{Calc}$	P	L + V			_		206 4
"	11a	$D5_{Calc}$	P	L + V					207 0
"	12a	$D5_{Calc}$	P	L + V	_	_	_	_	206 4
"	13a	$D5_{Calc}$	P	L + V	_	_	_	_	206 1
"	14a	$D5_{Calc}$	P	L + V					207 2
"	15a	$D5_{Calc}$	P	L + V					207 2
"	16a	$D5_{Calc}$	P	L + V	_	_	_	_	207 5
"	17a	$D5_{Calc}$	P	L + V					207 2
"	18a	$D5_{Calc}$	P	L + V	_	_	_	_	207 0
"	19a	$D5_{Calc}$	P	L + V			_	_	205 6
"	20aa	$D5_{Calc}$	P	L + V	_	_	_	_	205 6
"	20a	$D5_{Calc}$	P	L + V			_		205 9
"	21a	$D5_{Calc}$	P	L + V	-48 0	_			205 9
"	23a	$D5_{Calc}$	P	L + V	_		_	_	204 6

Sample	Incl. No.	Paragenetic Stage	Classification	Type	Tfm	Tml	Salinity	Tmh	Th
514/182.5 Calc	1	$D5_{Calc}$	P	L + V		_			142
"	2	$D5_{Calc}$	P	L + V					165 2
"	3	$D5_{Calc}$	P	L + V		_			146 6
"	5	$D5_{Calc}$	P	L + V					160 8
"	6	$D5_{Calc}$	P	L + V		_			204 8
"	7	$D5_{Calc}$	P	L + V		_			164 5
"	8	$D5_{Calc}$	P	L + V		_		_	175 8
"	9	$D5_{Calc}$	P	L + V					222 7
"	11	$D5_{Calc}$	P	L + V					164 7
"	12	$D5_{Calc}$	P	L + V		_		_	232 7
"	13	$D5_{Calc}$	P	L + V		_		_	234 2
"	14	$D5_{Calc}$	P	L + V		_			156 1
"	15	$D5_{Calc}$	P	L + V	_	_		_	177 4
"	16	$D5_{Calc}$	P	L + V		_			206 5
"	17	$D5_{Calc}$	P	L + V		_			274 2
"	18	$D5_{Calc}$	P	L + V		_			208 6
"	20	$D5_{Calc}$	P	L + V		_		_	259 7
"	21	$D5_{Calc}$	P	L + V		_	_	_	238 5
"	22	$D5_{Calc}$	P	L + V		_			277 4
"	23	$D5_{Calc}$	P	L + V					267 0
"	24	$D5_{Calc}$	P	L + V					253 9
"	25	$D5_{Calc}$	P	L + V	_	_		_	255 2
"	26	$D5_{Calc}$	P	L + V		_		_	225 4
"	27	$D5_{Calc}$	P	L + V		_		_	221 1
"	28	$D5_{Calc}$	P	L + V				_	238 7
"	29	$D5_{Calc}$	P	L + V		_	_	_	252 4
"	30	$D5_{Calc}$	P	L + V		_		_	212 2
"	32	$D5_{Calc}$	P	L + V		_		_	275 2
"	34	$D5_{Calc}$	P	L + V		_	_	_	274 3
"	35	$D5_{Calc}$	P	L + V				_	235 4
"	2a	$D5_{Calc}$	S?	L + V		_			105 0
"	3a	$D5_{Calc}$	S?	L + V		_		_	87 4
"	5a	$D5_{Calc}$	S?	L + V		_	_	_	93 3
"	6a	$D5_{Calc}$	S?	L + V		_		_	81 2
"	7a	$D5_{Calc}$	S?	L + V	_	_	_	_	81 2
"	8a	$D5_{Calc}$	S?	L + V		_	_	_	102 1
"	14a	$D5_{Calc}$	S?	L + V		_	_	_	78 7
"	15a	$D5_{Calc}$	S?	L + V		_		_	83 4
"	17a	$D5_{Calc}$	S?	L + V	_	_	_	_	82 2
"	19a	$D5_{Calc}$	S?	L + V		_	_	_	86 0
"	20a	$D5_{Calc}$	S?	L + V	_	_		_	100 5
"	22a	$D5_{Calc}$	S?	L + V	_	_			86 4
"	23a	$D5_{Calc}$	S	L + V	_	_	_	_	100 0
529/246.6 Calc	63	$D5_{Calc}$	P	L + V		-5 2	8 1	-21 3	149 7
"	64	$D5_{Calc}$	P	L + V	_	-9 0	12 8	-23 5	168 6
"	67	$D5_{Calc}$	P	L + V		-9 0	12 8		171 5
"	68	$D5_{Calc}$	P	L + V		-8 2	11 9	_	157 1
"	69	$D5_{Calc}$	P	L + V	_	-8 2	11 9	-23 1	152 2
"	70	$D5_{Calc}$	P	L + V		-5 6	8 7		155 8
"	71	$D5_{Calc}$	P	L + V		-5 6	8 7	_	163 1
"	72	$D5_{Calc}$	P	L + V		-6 6	9 9	_	161 7
"	74	$D5_{Calc}$	P	L + V		-5 6	8 7	_	160 0
"	78	$D5_{Calc}$	P	L + V		-10 4	14 4	_	164 6
"	79	$D5_{Calc}$	P	L + V		-13 0	16 9		204 3
"	86	$D5_{Calc}$	P	L + V		-11 2	15 2		204 7
"	95	$D5_{Calc}$	P	L + V		-17 1	20 3		112 9
"	1	$D5_{Calc}$	P	L + V	_	-9 0	12 8	_	156 2
"	7	$D5_{Calc}$	P	L + V		-8 6	12 3	_	154 3
"	8	$D5_{Calc}$	P	L + V		-1 1	1 9	_	142 9
"	9	$D5_{Calc}$	P	L + V	_	-9 0	12 8	_	150 4
"	65	$D5_{Calc}$	P	L + V		_			117 8
"	75	$D5_{Calc}$	P	L + V		_		_	155 3
"	77	$D5_{Calc}$	P	L + V					165 7
"	80	$D5_{Calc}$	P	L + V					188 4
"	81	$D5_{Calc}$	P	L + V					153 0
"	82	$D5_{Calc}$	P	L + V		_		_	196 9
"	83	$D5_{Calc}$	P	L + V		_			197 3
"	84	$D5_{Calc}$	P	L + V					190 2
"	85	$D5_{Calc}$	P	L + V		_			157 0
"	88	$D5_{Calc}$	P	L + V					156 6
"	91	$D5_{Calc}$	P	L + V	_	_	_	_	176 0
121/165.2	1	D3	S?	L + V		-20 4	22 7		112 2
"	2	D3	P	L + V		_			233 2
"	3	D3	P	L + V					228 8
121/146.8	1	D3	P	L + V		-4 1	6 6		240 6
"	2	D3	S?	L + V					113 0
121/162.1	1	D3	P	L + V		-3 9	6 3		206 1
"	3	D3	P	L + V		-3 9	6 3		173 2
"	4	D3		L + V		-35	32 0		197 3
"	5	D3	P	L + V		-3 7	6 0		171 3
"	6	D3	P	L + V		-3 3	5 4		198 2
"	7	D3	P	L + V		-12.2	16 2		230 7
"	8	D3	P	L + V		-3 3	5 4		180 4
"	9	D3	P	L + V		-0 6	1 1		131 2
"	1	D3		L + V	_	-34 8	31 9	_	135 1

Sample	Incl. No.	Paragenetic Stage	Classification	Type	Tfm	TmI	Salinity	Tmh	Th
262/100 Fe Calc	1	$D5_{Calc}$	P	L + V		-12 4	16 5		182 0
"	2	$D5_{Calc}$	P	L + V		-12 4	16 5		182 0
"	3	$D5_{Calc}$	P	L + V		-13	17 0		229 2
"	4	$D5_{Calc}$	P	L + V		-10 2	14 3		197 7
"	7	$D5_{Calc}$	P	L + V	—49 0	-10 4	14 5	-22 8	202 5
"	8	$D5_{Calc}$	P	L + V		-10 4	14 5	_	212 2
"	9	$D5_{Calc}$	P	L + V		-14	17 9		271 8
"	10	$D5_{Calc}$	P	L + V		-12 2	16 3		183 6
"	11	$D5_{Calc}$	P	L + V		-11 2	15 3	_	131 0
"	12	$D5_{Calc}$	P	L + V		-13 6	17 5		166 8
"	13	$D5_{Calc}$	P	L + V		-15	18 7	_	123 8
"	14	$D5_{Calc}$	P	L + V		-11 5	15 6		198 0
"	15	$D5_{Calc}$	P	L + V		-11 3	15 4	_	180 4
"	16	$D5_{Calc}$	P	L + V		-11 5	15 6	_	200 3
"	17	$D5_{Calc}$	P	L + V		-10 5	14 6	_	223 1
"	18	$D5_{Calc}$	P	L + V		-10 6	14 7		190 9
"	19	$D5_{Calc}$	P	L + V		-10 6	14 7	_	225 8
"	20	$D5_{Calc}$	P	L + V		-9 5	13 6	_	226 6
"	21	$D5_{Calc}$	P	L + V		-4 7	7 7	_	228 2
"	22	$D5_{Calc}$	P	L + V		-10 7	14 8		197 5
"	1a	$D5_{Calc}$	P	L + V		-15 4	19 0	_	157 3
"	2a	$D5_{Calc}$	P	L + V		-12 3	16 2		215 7
"	3a	$D5_{Calc}$	P	L + V	_	-10 7	14 7	_	174 6
"	4a	$D5_{Calc}$	P	L + V		-0 4	0 7		189 4
"	8a	$D5_{Calc}$	P	L + V		-15 1	18 7	_	150 0
"	11a	$D5_{Calc}$	P	L + V	_	-12 2	16 2	_	179 6
"	12a	$D5_{Calc}$	P	L + V	_	-10 8	14 8	_	214 0
"	16a	$D5_{Calc}$	P	L + V	_	-12 6	16 5	_	185 6
"	17a	$D5_{Calc}$	P	L + V		-0 5	0 9	_	163 4
"	1b	$D5_{Calc}$	P	L + V	_	-9 8	13 7	_	209 6
"	2b	$D5_{Calc}$	P	L + V		-10 5	14 5	_	187 6
"	4b	$D5_{Calc}$	P	L + V	_	-6 8	10 2	_	206 9
"	5b	$D5_{Calc}$	P	L + V	_	-12 6	16 5	_	167 4
"	8b	$D5_{Calc}$	P	L + V		-12 4	16 3	_	214 8
"	9b	$D5_{Calc}$	P	L + V	_	-6 5	9 9	_	205.4
"	3b	$D5_{Calc}$	P	L + V	_		_	_	150 3
"	6b	$D5_{Calc}$	P	L + V				_	137 4
"	7b	$D5_{Calc}$	P	L + V			_	_	105 1
"	5a	$D5_{Calc}$	P	L + V					176 2
"	6a	$D5_{Calc}$	P	L + V	_	_		_	177 4
"	9a	$D5_{Calc}$	P	L + V	_	_	_	_	183 2
"	10a	$D5_{Calc}$	P	L + V				_	135 4
"	13a	$D5_{Calc}$	P	L + V		_	_	_	142 5
"	14a	$D5_{Calc}$	P	L + V			_	_	150 2
"	15a	$D5_{Calc}$	P	L + V	_	_	_	_	181 5
2447-8/13.3 CW	1	$D1_{Cem}$	P	L + V	_	-3 3	5 4	_	218 1
"	3	$D1_{Cem}$	P	L + V	_	_	_	_	199 0
318/450.5 Calc	6a	$D5_{Calc\ flats}$	P	L + V		-1 1	1 9		151 9
"	9a	$D5_{Calc\ flats}$	P	L + V		-1 0	1 8		155 3
"	10a	$D5_{Calc\ flats}$	P	L + V		-1 0	1 8	_	155 3
"	11a	$D5_{Calc\ flats}$	P	L + V		-1 0	1 8		152 9
"	9	$D5_{Calc\ flats}$	P	L + V		-0 9	1 6	_	163 4
"	8a	$D5_{Calc\ (late)}$	P	L + V		_	_		169 5
318/450.5 Pink	1	D4	P	L + V		-26 9	26 7		100 4
"	2	D4	P	L + V		-21 1	23 1		89 4
"	3	D4	P	L + V		-27 9	27 4	_	97 8
"	4	D4	P	L + V		-28 0	27 4	_	97 1
"	5	D4	P	L + V		-25 4	25 8	_	98 7
"	6	D4	P	L + V		-25 6	26 0	_	106 1
"	7	D4	P	L + V		-26 1	26 3	_	100.2
"	8	D4	P	L + V		-26 2	26 3		114 3
515/173.7 Pink	1	D4	P	L + V		-30 0	28 7		93 8
"	6	D4	P	L + V		-20 9	23 0		91 3
"	7	D4	P	L + V		-23 8	24 9		93 2
"	9	D4	P	L + V		-26 5	26 5	_	92 0
"	12	D4	P	L + V					113 6
463/173.0 Calc	1	$D5_{Calc}$	P	L + V		-13 1	17 0		227 1
"	3	$D5_{Calc}$	P	L + V		-13 1	17 0		220 7
"	4	$D5_{Calc}$	P	L + V		-10 1	14 1	_	187 7
"	5	$D5_{Calc}$	P	L + V		-6 7	10 1	_	211 2
"	6	$D5_{Calc}$	P	L + V		-11 7	15 7	_	179 4
"	7	$D5_{Calc}$	P	L + V		-11 7	15 7		206 7
"	8	$D5_{Calc}$	P	L + V		-11 6	15 6	_	179 4
"	10	$D5_{Calc}$	P	L + V		-11 6	15 6		193 3
"	12	$D5_{Calc}$	P	L + V		-11 5	15 5	_	177 0
"	13	$D5_{Calc}$	P	L + V		-12 1	16 1		191 9
"	11	$D5_{Calc}$	P	L + V	_	_			188 2

Sample	Incl. No.	Paragenetic Stage	Classification	Type	Tfm	Tml	Salinity	Tmh	Th
449/95.5 Calc	1a	$D5_{Calc}$	S?	L + V		-4 6	7 3		120 1
"	2a	$D5_{Calc}$	S?	L + V		-21 6	23 4	_	102 0
"	6a	$D5_{Calc}$	S?	L + V		-21 1	23 1		108 2
"	7	$D5_{Calc}$	P	L + V		-13 0	16 9		188 4
"	8	$D5_{Calc}$	P	L + V		-11 6	15 6	_	198 3
"	9	$D5_{Calc}$	P	L + V		-14 3	18 1		165 7
"	10	$D5_{Calc}$	P	L + V		-12 7	16 6		166 8
"	12	$D5_{Calc}$	P	L + V		-22 4	24 0		156 0
"	13	$D5_{Calc}$	P	L + V		-13 9	17 7	_	149 7
"	14	$D5_{Calc}$	P	L + V		-11 1	15 1		112 2
"	15	$D5_{Calc}$	P	L + V		-21 4	23 3	_	158 7
"	17	$D5_{Calc}$	P	L + V		-15 9	19 4	_	152 3
"	18	$D5_{Calc}$	P	L + V		-15 9	19 4		194 4
"	19	$D5_{Calc}$	P	L + V		-14 1	17 9	_	173 7
"	7a	$D5_{Calc}$	P	L + V				_	173 6
"	6	$D5_{Calc}$	P	L + V				_	188 6
"	11	$D5_{Calc}$	P	L + V				_	208 3
"	16	$D5_{Calc}$	S?	L + V					126 3
"	20	$D5_{Calc}$	S?	L + V					128 0

E2: FLUID INCLUSIONS - Lisheen Sphalerite

Sample	Incl. No.	Paragenetic Stage	Classification	Type	Tfm	Tml	Salinity	Tmh	Th
529/246.6	1	Late ore-stage	PS	L + V		-9 4	13 2	-23 0	173 9
"	2	Late ore-stage	PS	L + V		-9 4	13 2	_	171 8
"	3	Late ore-stage	PS	L + V	_	-9 6	13 6	_	181 2
"	4	Late ore-stage	PS	L + V	_	-17 3	20 4	_	88 5
"	5	Late ore-stage	PS	L + V	_	-9 4	13 3	_	180 8
"	6	Late ore-stage	PS	L + V	_	-9 4	13 3	-23 0	182 2
"	7	Late ore-stage	PS	L + V	_	-9 5	13 5	_	178 4
"	8	Late ore-stage	PS	L + V		-9 5	13 5		178 5
"	9	Late ore-stage	PS	L + V	_	-9 5	13 5		179 8
"	10	Late ore-stage	PS	L + V		-9 7	13 7	_	174 4
"	11	Late ore-stage	PS	L + V		-9 7	13 7	_	181 4
"	12	Late ore-stage	PS	L + V	_	-9 7	13 7	_	174 4
"	14	Late ore-stage	PS	L + V		-9 4	13 2		166 2
"	15	Late ore-stage	PS	L + V	_	-9 4	13 2		166 7
"	16	Late ore-stage	PS	L + V		-9 4	13 2	_	165 5
"	17	Late ore-stage	PS	L + V	_	-9 4	13 2	_	175 6
"	18	Late ore-stage	PS	L + V		9 5	13 5		179 0
"	21	Late ore-stage	S?	L + V		-31 0	29 3		96 1
"	23	Late ore-stage	S?	L + V		-26 4	26 4	_	91 2
"	1a	Late ore-stage	S?	L + V		-22 7	24 2		79 3
"	2a	Late ore-stage	S?	L + V		-21 9	23 6		90 3
"	3a	Late ore-stage	S?	L + V			_		106 5
"	6a	Late ore-stage	S?	L + V					109 0
"	7a	Late ore-stage	S?	L + V					106 5
"	9aa	Late ore-stage	S?	L + V			_		116 6
"	9aa	Late ore-stage	S?	L + V					113 0
"	11a	Late ore-stage	S?	L V					97 2
"	14a	Late ore-stage	S?	L + V			_		95 0
"	15a	Late ore-stage	S?	L + V					117 9
"	16a	Late ore-stage	S?	L + V			_		98 1
"	13	Late ore-stage	S?	L + V			_		161 1
"	20	Late ore-stage	S?	L + V		_	_		180 3
"	22	Late ore-stage	S?	L + V			_	_	96 1
"	24	Late ore-stage	S?	L + V		_	_		96 4
517/285.0	1	Late ore-stage	S	L + V		-2 8	4 7		194 2
"	2	Late ore-stage	S	L + V		-2 8	4 7	_	194 2
"	3	Late ore-stage	S	L + V		-2 9	4 8		199 1
"	4	Late ore-stage	S	L + V		-2 7	4 5		193 3
"	6	Late ore-stage	S	L + V		-2 7	4 5	_	188 5
"	7	Late ore-stage	S	L + V	_	-2 7	4 5		182 6
"	8	Late ore-stage	S	L + V		-2 7	4 5		177 4
"	9	Late ore-stage	S	L + V		-2 7	4 5		195 6
"	10	Late ore-stage	S	L + V		-2 6	4 3		202 9
"	11	Late ore-stage	S	L + V		-2 7	4 5		182 5
"	12	Late ore-stage	S	L + V		-2 6	4 3		200 7
"	4a	Late ore-stage	P	L + V		-9 9	13 9		232 1
"	5a	Late ore-stage	P	L + V		-9 8	13 8		241 0
"	1a	Late ore-stage	P	L + V				_	177 2
"	2a	Late ore-stage	S?	L + V			_	_	105 3
"	3a	Late ore-stage	S?	L + V					111 0

Sample	Incl. No.	Paragenetic Stage	Classification	Type	Tfm	TmI	Salinity	Tmh	Th
514/182.5	3	Late ore-stage	P	L + V		-13 3	17 2		179 1
"	6	Late ore-stage	P	L + V	-52 3	-13 1	17 0	-22 4	177 7
"	11	Late ore-stage	P	L + V		-13 3	17 2	-22 5	177 0
"	13	Late ore-stage	P	L + V		-13 4	17 3	-22 7	179 0
"	14	Late ore-stage	P	L + V	_	-13 5	17 4		173 4
"	15	Late ore-stage	P	L + V		-13 5	17 4	_	179 3
"	16	Late ore-stage	P	L + V	_	-13 4	17 3		179 0
"	17	Late ore-stage	P	L + V	_	-13 2	17 1		172 9
"	18	Late ore-stage	P	L + V		-13 2	17 1	-22 1	165 8
"	19	Late ore-stage	P	L + V		-13 2	17 1		171 9
"	21	Late ore-stage	P	L + V	-50 0	-13 4	17 3	_	167 7
"	22	Late ore-stage	P	L + V	-52 5	-13 5	17 4	-22 7	157 7
"	23	Late ore-stage	P	L + V	~ -50 0	-13 3	17 2	-22 6	209 7
"	27	Late ore-stage	P	L + V		-13 4	17 3	_	179 1
"	28	Late ore-stage	P	L + V	~ -52 0	-13 1	17 0	-22 5	178 6
"	29	Late ore-stage	P	L + V	_	-13 1	17 0	-23 1	177 9
"	30	Late ore-stage	P	L + V	-52 0	-13 1	17 0	-21 9	180 3
"	31	Late ore-stage	P	L + V	_	-13 1	17 0	-22 7	160 9
"	32	Late ore-stage	P	L + V	_	-13 1	17 0	_	176 8
"	33	Late ore-stage	P	L + V		-13 3	17 2	_	179 9
"	34	Late ore-stage	P	L + V	-52 5	-13 2	17 1	-22 5	180 7
"	35	Late ore-stage	P	L + V	-52 5	-13 2	17 1	-22 5	180 7
"	36	Late ore-stage	P	L + V	-52 5	-13 3	17 2	-22 5	180 9
"	37	Late ore-stage	P	L + V	~ -52 0	-13 1	17 0		181 5
"	38	Late ore-stage	P	L + V	-52 5	-13 7	17 5	-23 2	171 0
"	42	Late ore-stage	P	L + V		-13 3	17 2	_	173 9
"	43	Late ore-stage	P	L + V	-52 2	-13 2	17 1	_	177 2
"	46	Late ore-stage	P	L + V		-12 8	16 7		166 4
"	47	Late ore-stage	P	L + V		-13 1	17 0		177 4
"	49	Late ore-stage	P	L + V	~-52 0	-13 1	17 0	-22 6	179 8
"	52	Late ore-stage	P	L + V	-52 2	-13 1	17 0	_	178 4
"	53	Late ore-stage	P	L + V	-52 0	-13 1	17 0	-22 4	172 8
"	54	Late ore-stage	P	L + V	-52 5	-13 6	17 4	_	170 3
"	55	Late ore-stage	P	L + V		-13 6	17 4	_	182 9
"	64	Late ore-stage	P	L + V	-52 0	-13 1	17 0	-22 6	179 7
"	4	Late ore-stage	P	L + V	_	_	_	_	176 6
"	5	Late ore-stage	P	L + V	_	_	_	_	173 4
"	7	Late ore-stage	P	L + V			_	_	166 0
"	8	Late ore-stage	P	L + V					160 7
"	12	Late ore-stage	P	L + V					173 6
"	24	Late ore-stage	P	L + V	_	_	_	_	175 7
"	26	Late ore-stage	P	L + V	_	_		_	175 7
"	40	Late ore-stage	P	L + V	_	_	_	_	173 9
"	41	Late ore-stage	P	L + V	_	_	_	_	173 9
"	44	Late ore-stage	P	L + V	_	_	_	_	166 9
"	48	Late ore-stage	P	L + V	_	_	_	_	180 2
"	50	Late ore-stage	P	L + V		_	_	_	187 8
"	51	Late ore-stage	P	L + V		_		_	173 1
"	56	Late ore-stage	P	L + V	_	_	_	_	184 9
"	57	Late ore-stage	P	L + V	_	_	_	_	195 4
"	58	Late ore-stage	P	L + V	_	_	_	_	165 7
"	59	Late ore-stage	P	L + V					207 1
515/173.7	1a	Post ore-stage?	P	L + V		-12 7	16 6	-22 4	144 1
"	1	Post ore-stage?	P	L + V	_	-12 9	16 8	_	145 7
"	2	Post ore-stage?	P	L + V	_	-12 9	16 8	-22 5	163 5
"	3	Post ore-stage?	P	L + V		-13 2	17 1	-22 8	151 6
"	4	Post ore-stage?	P	L + V	_	-13 0	16 9	_	152 7
"	5	Post ore-stage?	P	L + V		-12 9	16 8	_	153 6
"	7	Post ore-stage?	P	L + V	_	-13 1	17 0	-22 4	164 0
"	8	Post ore-stage?	P	L + V	_	-13 0	16 9	_	171 9
"	9	Post ore-stage?	P	L + V	_	-12 9	16 8	_	166 9
"	11	Post ore-stage?	P	L + V	-52 0	-13 1	17 0	-22 6	184 2
"	12	Post ore-stage?	P	L + V	_	-13 1	17 0		187 5
"	14	Post ore-stage?	P	L + V		-13 1	17 0	-22 9	181 8
"	15	Post ore-stage?	P	L + V	_	-13 1	17 0		169 5
"	16	Post ore-stage?	P	L + V	_	-13 1	17 0	-22 9	182 1
"	18	Post ore-stage?	P	L + V	~-50 0	-13 0	16 9	-22 6	170 2
"	19	Post ore-stage?	P	L + V		-13 2	17 1	_	184 0
"	22	Post ore-stage?	P	L + V	~-53 0	-13 1	17 0	-22 5	176 8
"	24	Post ore-stage?	P	L + V		-13 1	17 0		138 7
"	25	Post ore-stage?	P	L + V	_	-13 1	17 0		178 4
"	26	Post ore-stage?	P	L + V	_	-13 1	17 0	_	161 8
"	21	Post ore-stage?	P	L + V			_	_	188 4
"	22a	Post ore-stage?	P	L + V	_	_	_	_	184 4
"	23	Post ore-stage?	P	L + V	_		_	_	178 4
"	28	Post ore-stage?	P	L + V					191 7
"	29	Post ore-stage?	P	L + V	_		_	_	144 9
"	30	Post ore-stage?	P	L + V	_	_	_		143 7
"	31	Post ore-stage?	P	L + V	_	_	_		183 4
"	32	Post ore-stage?	P	L + V					166 5
471/210.4	46	Main ore-stage	P	L + V		-11 8	15 8	-22 8	151 2
"	47	Main ore-stage	P	L + V	_	-13 1	17 0		157 1
"	49	Main ore-stage	P	L + V	_	-13 6	17 4	-22 5	154 6
"	50	Main ore-stage	P	L + V	_	-11 3	15 3	_	158 6
"	51	Main ore-stage	P	L + V	_	-11 7	15 7	-22 3	157 4
"	55	Main ore-stage	P	L + V	_	-14 0	17 8	-22 4	181 8
"	56	Main ore-stage	P	L + V	_	-12 9	16 8	-23 1	185 5
"	58	Main ore-stage	P	L + V	_	-13 1	17 0	-22 6	178 6
"	59	Main ore-stage	P	L + V		-14 3	18 1		163 3
"	60	Main ore-stage	P	L + V	_	-14 2	18 0	_	161 6
"	61	Main ore-stage	P	L + V		-13 0	16 9		169 8
"	45	Main ore-stage	P	L + V					153 0
"	48	Main ore-stage	P	L + V					151 2
"	53	Main ore-stage	P	L + V	_	_	_	_	153 0
"	54	Main ore-stage	P	L + V	_	_	_	_	169 6

Sample	Incl. No.	Paragenetic Stage	Classification	Type	Tfm	Tml	Salinity	Tmh	Th
463/173.8	32	Late ore-stage	S	L + V		-12.2	16.2		92
"	34	Late ore-stage	P	L + V		-13.0	16.9		158.6
"	35	Late ore-stage	P	L + V		-12.6	16.5		182.9
"	25	Late ore-stage	S	L + V					94.2
"	26	Late ore-stage	S?	L + V					102.6
"	27	Late ore-stage	S?	L + V					100.2
"	28	Late ore-stage	S?	L + V					100.8
"	30	Late ore-stage	S?	L + V					122.1
"	31	Late ore-stage	S?	L + V					109.9
"	33	Late ore-stage	S?	L + V					1.7.8
451/139.10	1	Late ore-stage	P	L + V		-7.0	1.4		191.6
"	4	Late ore-stage	P	L + V		-7.3	10.8	-1.4	195.9
"	5	Late ore-stage	P	L + V		-7.2	10.7	-10.4	196.6
"	8	Late ore-stage	P	L + V		-7.2	10.7		192.9
"	1	Late ore-stage	P	L + V	_	-7.3	10.8		197.9
"	12	Late ore-stage	P	L + V		-7.3	10.8		201.0
"	14	Late ore-stage	P	L + V		-6.8	10.2		198.5
"	16	Late ore-stage	P	L + V		-10.3	14.2		161.2
"	19	Late ore-stage	P	L + V		-10.2	14.1		190.9
"	21	Late ore-stage	P	L + V		-9.7	13.6		170.2
"	6	Late ore-stage	P	L + V	_		_		197.8
"	7	Late ore-stage	P	L + V		_		_	202.7
"	9	Late ore-stage	P	L + V		_			194.9
"	11	Late ore-stage	P	L + V	_	_			203.0
"	13	Late ore-stage	P	L + V					203.5
"	15	Late ore-stage	P	L + V					196.9
"	17	Late ore-stage	P	L + V					180.8
"	18	Late ore-stage	P	L + V					181.5
"	20	Late ore-stage	P	L + V					190.9
325/149.30	1	Late ore-stage	P	L + V		-12.5	16.4		143.7
"	2	Late ore-stage	P	L + V		-12.5	16.4		146.8
"	3	Late ore-stage	P	L + V	~54.5	-12.5	16.4		149.6
"	4	Late ore-stage	P	L + V		-12.5	16.4		145.5
"	14	Late ore-stage	P	L + V	~55.0	-13.1	17.0		140.5
"	11	Late ore-stage	P	L + V		_		_	155.0
"	13	Late ore-stage	P	L + V		_		_	151.3
"	15	Late ore-stage	P	L + V		_	_		169.7
"	16	Late ore-stage	P	L + V	_	_	_	_	146.5
"	17	Late ore-stage	P	L + V	_	_		_	158.1
"	18	Late ore-stage	P	L + V	_				160.5
"	19	Late ore-stage	P	L + V	_	_	_	_	169.1
"	20	Late ore-stage	P	L + V	_	_	_	_	171.1
"	21	Late ore-stage	P	L + V	_	_		_	165.9
"	22	Late ore-stage	P	L + V	_	_			171.7
"	23	Late ore-stage	P	L + V		_	_	_	149.6
"	24	Late ore-stage	P	L + V	_				150.6
"	25	Late ore-stage	P	L + V					166.7
"	26	Late ore-stage	P	L + V					159.1
"	27	Late ore-stage	P	L + V	_				158.1
"	28	Late ore-stage	P	L + V				_	158.6
"	29	Late ore-stage	P	L + V	_		_		156.6
"	30	Late ore-stage	P	L + V		_		_	169.7
"	31	Late ore-stage	P	L + V	_	_			157.1
"	32	Late ore-stage	P	L + V					157.1
"	33	Late ore-stage	P	L + V					156.1
171/167.2	1	Late ore-stage	P	L + V	~55.0	-13.4	17.2		152.1
"	3	Late ore-stage	P	L + V	~55.0	-13.2	17.1		151.4
95/335.0	1	Late ore-stage	S	L + V		-27.3	27.0		101.2
"	2	Late ore-stage	S	L + V	~60.0	-27.2	26.9		102.5
"	4	Late ore-stage	P	L + V	~35.0	-7.6	11.2	-10.7	208.0
"	5	Late ore-stage	P	L + V		-7.8	11.4		207.8
"	6	Late ore-stage	P	L + V		-7.8	11.4		207.1
"	7	Late ore-stage	P	L + V		-7.7	11.3		208.5
"	8	Late ore-stage	P	L + V		-7.8	11.4		206.1
"	9	Late ore-stage	P	L + V		-7.8	11.4		207.8
"	10	Late ore-stage	P	L + V		-7.8	11.4		207.8
"	11	Late ore-stage	P	L + V		-7.7	11.3		208.0
"	12	Late ore-stage	P	L + V	_	-7.8	11.4		208.8
"	14	Late ore-stage	P	L + V	_	-7.9	11.5		208.0
"	16	Late ore-stage	P	L + V		-8.3	12.0		206.4
"	17	Late ore-stage	P	L + V		-8.3	12.0		207.2
"	18	Late ore-stage	P	L + V	~35.0	-8.1	11.8		202.4
"	21	Late ore-stage	P	L + V		-8.1	11.8		204.0
"	24	Late ore-stage	P	L + V	~35.0	-7.5	11.0	_	201.8
"	28	Late ore-stage	P	L + V	_	-7.8	11.4		201.1
"	29	Late ore-stage	P	L + V		-7.9	11.5		203.8
"	31	Late ore-stage	P	L + V	~35.0	-7.6	11.2		202.4
"	32	Late ore-stage	P	L + V	~35.0	-7.6	11.2		202.4
"	33	Late ore-stage	P	L + V		-8.1	11.8		209.5
"	34	Late ore-stage	P	L + V		-8.1	11.8	_	208.9
"	35	Late ore-stage	P	L + V		-8.4	12.1		207.8
"	37	Late ore-stage	P	L + V		-8.1	11.8		208.9
"	39	Late ore-stage	P	L + V		-8.6	12.4		204.7
"	40	Late ore-stage	P	L + V		-8.6	12.4		202.2
"	41	Late ore-stage	P	L + V		-8.6	12.4		207.6
"	42	Late ore-stage	P	L + V		-8.6	12.4		208.1
"	43	Late ore-stage	P	L + V		-7.9	11.5	-12.4	201.4
"	70	Late ore-stage	S	L + V		-25.5	25.9		107.2
"	72	Late ore-stage	S	L + V	~60	-27.2	26.9		19.6
"	79	Late ore-stage	S	L + V		-27.2	26.9		136.4
"	82	Late ore-stage	PS	L + V	~55	13.5	17.3		179.5
"	83	Late ore-stage	PS?	L + V		-13.5	17.3	-20.5	189.3
"	88	Late ore-stage	PS	L + V		-13.3	17.1		176.8
"	90	Late ore-stage	PS	L + V	~55.0	-13.5	17.3	_	185.8
	91	Late ore-stage	PS	L + V	~55	-13.2	17.1		182.9
"	92	Late ore-stage	PS	L + V		-12.6	16.5		179.7
"	94	Late ore-stage	S	L + V	~70	-28.2	27.6		107.1
"	97	Late ore-stage	PS?	L + V		-1.0	16.9		200.6
"	100	Late ore-stage	S	L + V	~70.0	-26.6	26.6	-40.1	99.7
"	103	Late ore-stage	S	L + V	_	-27.1	26.9		105.3

Sample	Incl. No.	Paragenetic Stage	Classification	Type	Tfm	TmI	Salinity	Tmh	Th
	107	Late ore-stage	P	L + V		-7 6	11 2		206 4
"	2a	Late ore-stage	PS	L + V		-12 4	16 3		161 0
"	3	Late ore-stage	S	L + V					98 2
"	20	Late ore-stage	P	L + V			_		20 6
"	23	Late ore-stage	P	L + V					207 1
"	25	Late ore-stage	P	L + V			_		208 7
"	26	Late ore-stage	P	L + V			_	_	189 8
"	27	Late ore-stage	P	L + V		_		_	211 2
"	30	Late ore-stage	P	L + V			_		209 0
"	36	Late ore-stage	P	L + V			_		208 9
"	38	Late ore-stage	P	L + V				_	207 8
"	44	Late ore-stage	P	L + V			_	_	167 7
"	45	Late ore-stage	P	L + V			_		174 6
"	46	Late ore-stage	P	L + V				_	204 9
"	58	Late ore-stage	P	L + V			_	_	182
"	59	Late ore-stage	P	L + V				_	203 4
"	61	Late ore-stage	P	L + V			_	_	211 6
"	62	Late ore-stage	P	L + V			_		197 6
"	65	Late ore-stage	P	L + V				_	209 4
"	66	Late ore-stage	P	L + V				_	213 3
"	69	Late ore-stage	P	L + V		_		_	167 7
"	73	Late ore-stage	S?	L + V					104 4
"	75	Late ore-stage	P	L + V				_	149 5
"	76	Late ore-stage	S?	L + V					118 6
"	77	Late ore-stage	S?	L + V					125 1
"	78	Late ore-stage	P	L + V					177 9
"	85	Late ore-stage	P	L + V		_		_	189 1
"	86	Late ore-stage	S?	L + V				_	123 1
"	87	Late ore-stage	S?	L + V		_			106 4
"	89	Late ore-stage	P	L + V					195 7
"	95	Late ore-stage	P	L + V	_			_	196 3
"	96	Late ore-stage	P	L + V			_		198 9
"	98	Late ore-stage	P	L + V					232 4
"	99	Late ore-stage	P	L + V				_	233 6
"	101	Late ore-stage	S?	L + V			_	_	112 5
"	105	Late ore-stage	P	L + V			_	_	206 7
"	1a	Late ore-stage	P	L + V					183 3

E3: FLUID INCLUSIONS - Galmoy Gangue

Sample	Incl. No.	Paragenetic Stage	Classification	Type	Tfm	TmI	Salinity	Tmh	Th
GY355/97.0	3	D3	P	L + V		-9 3	13 1		160 1
"	4	D3	P	L + V	_	-9 4	13 3	_	197 5
"	5	D3	P	L + V	_	-9 4	13 3	_	192.3
"	7	D3	P	L + V		-9 7	13 7	_	202 4
"	14	D3	P	L + V		-9 4	13 2	_	137 5
"	15	D3	P	L + V		-9 4	13 3		195 3
"	2	D3	P	L + V	_			_	222 1
"	6	D3	P	L + V		_	_	_	205 2
"	8	D3	P	L + V		_			163 5
"	9	D3	P	L + V				_	193 5
"	10	D3	P	L + V			_	_	182 4
"	11	D3	P	L + V	_	_	_	_	193 5
"	12	D3	P	L + V			_	_	193 7
"	13	D3	P	L + V					182 4
G16-27/383.5	2	$D5_{Del}$	S?	L + V		-15 1	18 7	_	115 0
"	6	$D5_{Del}$	S?	L + V		-17 9	20 9	_	120 9
"	8	$D5_{Del}$	P	L + V		-5 7	8 8		177 4
"	9	$D5_{Del}$	P	L + V		-5 7	8 8		179 4
"	11	$D5_{Del}$	P	L + V		-0 8	1 4		160 6
"	12	$D5_{Del}$	PS?	L + V		-15 1	18 7		196 3
"	1	$D5_{Del}$	P?	L + V					122 8
"	5	$D5_{Del}$	P?	L + V					129 3
"	1a	$D5_{Del}$	S	L + V					97 0
"	2a	$D5_{Del}$	P?	L + V	_	_	_	_	121 2
8.Calc	1	$D5_{calc}$	P	L + V					140 7
"	2	$D5_{Calc}$		L + V					<65
"	3	$D5_{Calc}$		L + V	_		_		<65
"	4	$D5_{Calc}$	P	L + V			_	_	112 1
"	5	$D5_{Calc}$	P	L + V					136 7
"	7	$D5_{Calc}$	S	L + V			_		83 0
"	8	$D5_{Calc}$	P	L + V				_	163 5
"	9	$D5_{Calc}$	S	L + V					82 2
"	10	$D5_{Calc}$	P	L + V					163 9
"	11	$D5_{Calc}$	P	L + V			_	_	228 1
"	12	$D5_{Calc}$	P	L + V					145 7
"	13	$D5_{Calc}$	P	L + V					173 5
"	14	$D5_{Calc}$	P	L + V					185 6
"	1a	$D5_{Calc}$	S	L + V					83 2
"	2a	$D5_{Calc}$	S	L + V	_				83 1
"	3a	$D5_{Calc}$	S	L + V					81 2
"	4a	$D5_{Calc}$	S	L + V					81 3
"	5a	$D5_{Calc}$	S?	L + V		_		_	111 2
"	6a	$D5_{Calc}$	S	L + V					98 3
"	7a	$D5_{Calc}$		L + V					<65
"	8a	$D5_{Calc}$	S	L + V		_			78 9
"	9a	$D5_{Calc}$	S	L + V					92 2
"	10a	$D5_{Calc}$		L + V	_	_	_	_	<65
5.Del	3	D ?	P	L + V		-10 7	14 7		147 0
"	4	D3?	P	L + V			_		134 4
"	5	D3	P	L + V					12 8
"	6	D3	P	L + V					128 0
"	7	D3?	P	L + V					121 4
"	8	D3?	P	L + V			_		118 9
"	9	D3?	P	L + V					134 7
"	1	D3	P	L + V	_	_	_	_	1 9 9

Sample	Incl. No.	Paragenetic Stage	Classification	Type	Tfm	Tml	Salinity	Tmh	Th
2. (0134 Del	1	D	P	L + V		-1	4		165 5
"	2	D3	P	L + V	_	-8 9	2 7		154 4
"	3	D3?	P	L + V		-9 2	13 0		158 6
"	4	D3?	P	L + V		-9 7	13 7		179 0
"	5	D3?	P	L + V		-4 4	7 0		181 9
"	6	D3?	P	L + V		-8 9	12 7		175 0
"	7	D3?	P	L + V		-8 5	12 2		167 2
"	8	D3	P	L + V	_	-8 6	12 3		189 0
"	9	D3?	P	L + V	_	-9 2	13 0		166 7
"	10	D3?	P	L + V		-10 6	14 6		179 7
"	11	D3?	P	L + V		-8 7	12 5		179 7
"	12	D3?	P	L + V		-12 1	16 1		183 7
"	13	D3?	P	L + V	_	-9 2	13 0		181 3
"	14	D3?	P	L + V	_	-8 8	12 6		188 5
"	1a	D3?	P	L + V	_	-15 5	19 0		183 2
"	2a	D3?	P	L + V	_	-15 8	19 3	_	178 7
"	4a	D3?	P	L + V	_	-12 1	16 1		162 9
"	5a	D3?	P	L + V		-9 6	13 6		184 6
"	7a	D3?	P	L + V	_	-10 1	14 1		152 5
"	8a	D3?	P	L + V		-15 5	19 0		178 0
"	9a	D3?	P	L + V	_	-9 7	13 7		182 9
"	11a	D3?	P	L + V	_	-12 1	16 1		173 5
"	15	D3?	P	L + V	_				182 7
"	3a	D3?	P	L + V					165 9

E4: FLUID INCLUSIONS - Galmoy Sphalerite

Sample	Incl. No.	Paragenetic Stage	Classification	Type	Tfm	Tml	Salinity	Tmh	Th
GY382/86.0	38	Late ore-stage	P	L + V		-10 0	15 1		128 9
"	39	Late ore-stage	P	L + V	_	-9 9	16 3		176 5
"	42	Late ore-stage	P	L + V	_	-10 0	15 9		178 5
"	44	Late ore-stage	P	L + V	_	-10 0	14 4		166 3
"	36	Late ore-stage	P	L + V	_				129 6
"	37	Late ore-stage	P	L + V		_	_		150 9
"	40	Late ore-stage	P	L + V	_	_	_		134 6
"	41	Late ore-stage	P	L + V					167 7
2. (0134)	1a	Ore-stage?	P	L + V	~-50 0	-10 0	14 0	-22 4	172 3
"	2a	Ore-stage?	P	L + V	_	-10 0	14 0		161 7
"	3a	Ore-stage?	P	L + V	_	-9 9	13 9		171 5
"	4a	Ore-stage?	P	L + V		-9 0	12 8	-22 3	166 7
"	5a	Ore-stage?	P	L + V	~-51 0	-9 0	12 8	_	169 7
"	6a	Ore-stage?	P	L + V	_	-10 0	14 0	-23	173 6
"	7a	Ore-stage?	P	L + V	_	-9 0	12 8	_	163 7
"	1	Ore-stage?	P	L + V	_	-9 7	13 7		146 7
"	2	Ore-stage?	P	L + V	_	-9 9	13 9	-22 2	155 8
"	3	Ore-stage?	P	L + V	_	-7 3	10 8	_	160 3
"	4	Ore-stage?	P	L + V		-9 6	13 6		158 6
"	5	Ore-stage?	P	L + V		-9 7	13 7	-22 2	162 1
"	6	Ore-stage?	P	L + V		-9 7	13 7	_	165 0
"	7	Ore-stage?	P	L + V		-9 9	13 9	-22 4	157 2
"	8	Ore-stage?	P	L + V	~-49 0	-9 8	13 8	-22 4	156 2
"	9	Ore-stage?	P	L + V		-9 8	13 8	-22 4	157 8
"	11	Ore-stage?	P	L + V		-8 7	12 5		158 7
"	12	Ore-stage?	P	L + V		-9 8	13 8	-22 5	158 0
"	13	Ore-stage?	P	L + V		-9 8	1 8		161 2
"	16	Ore-stage?	P	L + V	_	-9 8	13 8	-22 2	158 1
"	18	Ore-stage?	P	L + V	_	-9 8	13 8	_	160 7
"	20	Ore-stage?	P	L + V		-10 1	14 1	_	168 1
"	21	Ore-stage?	P	L + V	_	-10 1	14 1		153 4
"	22	Ore-stage?	P	L + V	_	-10 1	14 1		159 3
"	23	Ore-stage?	P	L + V	_	-10 4	14 4		179 3
"	24	Ore-stage?	P	L + V	_	-10 1	14 1		156 9
"	25	Ore-stage?	P	L + V		-10 1	14 1		162 6
"	26	Ore-stage?	P	L + V		-10 2	14 2		157 1
"	27	Ore-stage?	P	L + V		-7 9	11 5		153 1
"	29	Ore-stage?	P	L + V		-7 9	11 5		149 6
"	33	Ore-stage?	P	L + V	_	-8 0	11 6		148 9
"	34	Ore-stage?	P	L + V	_	-8 0	11 6		148 9
"	35	Ore-stage	P	L + V		-7 9	11 5		159 1
"	36	Ore-stage?	P	L + V		-7 9	11 5	_	163 5
"	39	Ore-stage?	P	L + V		-10 0	14 0		166 3
"	40	Ore-stage?	P	L + V		-9 9	13 9	-22 4	166 7
"	41	Ore-stage?	P	L + V	_	-10 0	14 0		164 0
"	42	Ore-stage?	P	L + V	_	-9 6	13 6		161 8
"	44	Ore-stage?	P	L + V		-9 7	13 7		167 2
"	45	Ore-stage?	P	L + V		-10 0	14 0		168 3
"	46	Ore-stage?	P	L + V		-10 0	14 0		166 9
"	47	Ore-stage?	P	L + V		-9 6	13 6		161 7
"	50	Ore-stage?	P	L + V	_	-9 6	13 6	-22 5	163 2
"	8a	Ore-stage?	P	L + V		_		_	158 1
"	10	Ore-stage?	P	L + V	_				163 1
"	14	Ore-stage?	P	L + V	_				158 5
"	15	Ore-stage?	P	L + V					156 6
"	17	Ore-stage?	P	L + V					158 1
"	19	Ore-stage?	P	L + V					158 1

Sample	Incl. No.	Paragenetic Stage	Classification	Type	Tfm	TmI	Salinity	Tmh	Th
10CW	1	Late ore-stage	P	L + V		-1	14		87
"	2	Late ore-stage	P	L + V		-99	139		1426
"	3	Late ore-stage	P	L + V		-100	140		1419
"	4	Late ore-stage	P	L + V		-100	140		1404
"	6	Late ore-stage	P	L + V				-	1516
"	7	Late ore-stage	S?	L + V			-		871
"	9	Late ore-stage	S?	L + V					874
"	11	Late ore-stage	S?	L + V		-		-	871
"	12	Late ore-stage	S?	L + V		-		-	926
"	13	Late ore-stage	S?	L + V					853
"	14	Late ore-stage	S?	L + V		-			863
"	15	Late ore-stage	S?	L + V					862
"	16	Late ore-stage	S?	L + V		-			896
"	17	Late ore-stage	S	L + V					1006
"	18	Late ore-stage	S?	L + V		-			006
"	19	Late ore-stage	S?	L + V		-			1006
"	20	Late ore-stage	S?	L + V		-			841
"	21	Late ore-stage	S?	L + V			-		860
"	22	Late ore-stage	S?	L + V	-	-			885
"	23	Late ore-stage	S?	L + V		-		-	885
"	24	Late ore-stage	S?	L + V				-	862

E5: FLUID INCLUSIONS - Rathdowney Trend Prospects Gangue

Sample	Incl. No.	Paragenetic Stage	Classification	Type	Tfm	TmI	Salinity	Tmh	Th
HC13/87.8	1	D3	P	L + V		-11 1	15 1		219 1
"	4	D3	P	L + V		-9 2	13 0		219
"	9	D3	P	L + V		-6 1	9 3		166 6
"	11	D3	P	L + V		-20 1	22 4	-22 7	206 3
"	13	D3	P	L + V		-3 8	6 1		181 6
"	14	D3	P	L + V		-9 2	13 0		213 1
"	2	D3	P	L + V		-		-	203 5
"	7	D3	P	L + V		-		-	203 9
"	12	D3	P	L + V					230 0
24/1674	5	D3	P	L + V		-2 6	4 3		184 7
"	6	D3	P	L + V		-5 6	8 7	-	199 3
"	7	D3	P	L + V	-	-5 4	8 4	-	158 6
"	9	D3	P	L + V	-	-2 1	3 6	-	176 7
"	12	D3	P	L + V	-	-6 8	10 2	-	191 7
"	1	D3	P	L + V		-	-	-	178 9
"	2	D3	P	L + V	-	-		-	158 6
"	3	D3	P	L + V	-	-	-	-	178 9
"	4	D3	P	L + V	-			-	168 7
"	11	D3	P	L + V	-	-		-	206 2
"	13	D3	P	L + V					128 0
45/294.6	1	D3	P	L + V		-9 2	13 0		215 5
"	2	D3	P	L + V		-10 5	14 5		218 2
"	3	D3	P	L + V		-9 5	13 5		190 6
"	4	D3	P	L + V		-9 4	13 2		207 5
"	5	D3	P	L + V		-9 2	13 0		208 2
"	6	D3	P	L + V		-0 8	1 4		165 0
"	8	D3	P	L + V		-8 2	11 9		209 0
"	10	D3	P	L + V		-9 7	13 7	-	204 6
"	14	D3	P	L + V		-9 2	13 0	-	187 4
"	16	D3	P	L + V		-9 3	13 1	-	199 1
"	17	D3	P	L + V		-9 2	13 0	-	180 6
"	18	D3	P	L + V		-9 2	13 0		211 9
"	19	D3	P	L + V		-9 2	13 0		211 9
"	23	D3	P	L + V		-9 2	13 0		179 0
"	24	D3	P	L + V		-12 1	16 1		229 3
"	25	D3	P	L + V		-8 1	11 8		198 7
"	26	D3	P	L + V		-9 2	13 0	-	210 4
"	27	D3	P	L + V		-9 2	13 0		211 9
"	28	D3	P	L + V		-10 3	14 3	-	200 1
"	29	D3	P	L + V		-9 2	13 0		219 1
"	30	D3	P	L + V		-9 2	13 0		187 4
"	31	D3	P	L + V		-9 2	13 0		219 1
"	32	D3	P	L + V		-9 2	13 0		219 1
"	33	D3	P	L + V		-9 2	13 0		187 6
"	7	D3	P	L + V		-			221 5
"	9	D3	P	L + V		-			221 5
"	22	D3	P	L + V					216 4
24/1625 Pink	1	D4	P	L + V		-22 4	23 9		160 6
"	2	D4	P	L + V		-8 1	11 8		120 1
"	3	D4	P	L + V		-18 4	21 2		113 6
"	4	D4	P	L + V		-23 0	24 4		93 1
"	8	D4	P	L + V	-	-19 9	22 3		111 0
"	9	D4	P	L + V		-23 5	24 7	-	119 1
"	11	D4	P	L + V		-22 9	24 3	-	123 4
"	12	D4	P	L + V		-23 6	24 7		115 3
"	13	D4	P	L + V		-10 2	14 2		150 8
2/960.8 Pink	1	D4	P	L + V		-24 9	25 5		115 9
"	3	D4	P	L + V		-23 4	24 6		126 3
"	5	D4	P	L + V		-23 2	24 5	-	132 8
"	6	D4	P	L + V	-	-25 3	25 8		141 9
"	7	D4	P	L + V		-25 6	26 0		118 9
"	9	D4	P	L + V		-32 5	30 3		120 1
"	10	D4	P	L + V		-25 2	25 7		137 4
"	2	D4	P	L + V				-	83 9
"	4	D4	P	L + V					125 0
"	8	D4	P	L + V		-		-	131 1
"	11	D4	P	L + V			-		118 9
"	12	D4	P	L + V					123 4
"	13	D4	P	L + V					118 1
"	14	D4	P	L + V					121 6
"	15	D4	P	L + V					121 6
"	16	D4	P	L + V					117 0
"	17	D4	P	L + V					115 9
"	18	D4	P	L + V					134
"	19	D4	P	L + V	-	-	-	-	125 2

Sample	Incl. No.	Paragenetic Stage	Classification	Type	Tfm	Tml	Salinity	Tmh	Th
1 686.5	4	D3	P	L + V		-9 4	13 3		249 9
"	5	D3	P	L + V		-15 7	19 2	_	249 9
"	8	D3	S	L + V		-26 3	26 4	_	115 9
"	9	D3	S	L + V		-28 0	27 4	_	108 9
"	10	D3	PS?	L + V		-24 9	25 5	_	154 6
"	1a	D3	P	L + V		-8 2	11 9	_	212 7
"	2a	D3	P	L + V		-8 2	11 9		193 9
"	3a	D3	P	L + V		-1 7	2 9	_	188 1
"	4a	D3	P	L + V		-8 4	12 1		185 5
"	6a	D3	P	L + V		-10 1	14 1	_	245 8
"	7a	D3	P	L + V		-8 2	11 9		219 4
"	13a	D3	P	L + V		-4 5	7 1	_	257 9
"	14a	D3	P	L + V		-8 8	12 6	_	258 0
"	15a	D3	P	L + V		-7 9	11 5	_	257 9
"	1	D3	P	L + V		_	_	_	161 4
"	2	D3	P	L + V		_	_		120 5
"	6	D3	P	L + V		_	_	_	263 8
"	7	D3	P	L + V		_			258 9
"	8a	D3	P	L + V		_	_		267 4
"	9a	D3	P	L + V					247 1
"	11a	D3	P	L + V					264 3
"	12a	D3	P	L + V					257 7
HCS/122.9	1	$D5_{Dol}$?	P	L + V		-1 5	2 6	_	182 4
"	2	$D5_{Dol}$?	S?	L + V		-29 2	28 2	_	115 9
"	4	$D5_{Dol}$?	S?	L + V		-29 6	28 4	_	105 2
"	6	$D5_{Dol}$?	S?	L + V		-30 0	28 7	_	100 3
"	5	$D5_{Dol}$?	S?	L + V		_	_	_	100 0
"	7	$D5_{Dol}$?	S?	L + V	_		_	_	95 4
"	8	$D5_{Dol}$?	P	L + V	_	_	_	_	173 8

E6: FLUID INCLUSIONS - Rathdowney Trend Prospects Sphalerite

Sample	Incl. No.	Paragenetic Stage	Classification	Type	Tfm	Tml	Salinity	Tmh	Th
HCS/122.9	1	Late stage	P	L + V		- 8	11 4		168 7
"	2	Late stage	P	L + V		-11 5	15 5		159 0
"	3	Late stage	P	L + V		-12 3	16 3		177 8
"	5	Late stage	P	L + V		-7 2	10 7	_	183 9
"	6	Late stage	P	L + V		-12 7	16 6		179 0
"	7	Late stage	P	L + V		-12 7	16 6		181 7
"	8	Late stage	P	L + V		-12 7	16 6		177 6
"	9	Late stage	P	L + V		-12 7	16 6		177 7
"	11	Late stage	P	L + V		12 5	16 5	_	170 8
"	12	Late stage	P	L + V		-9 5	13 5		173 5
"	14	Late stage	P	L + V		-13 5	17 4	_	173 6
"	15	Late stage	P	L + V		-12 0	16 0	_	205 2
"	16	Late stage	P	L + V		-14 1	17 9		179 4
"	19	Late stage	P	L + V		-12 8	16 7	_	184 1
"	4a	Late stage	P	L + V		-7 2	10 7		166 7
"	5a	Late stage	P	L + V		-7 0	10 4	-22 7	222 3
"	6a	Late stage	P	L + V		-10 2	14 2		164 8
"	7a	Late stage	P	L + V		-10 5	14 5		155 8
"	8a	Late stage	P	L + V		-9 4	13 3		243 6
"	9a	Late stage	P	L + V		-9 6	13 6		173 7
"	13	Late stage	P	L + V			_		172 5
"	2a	Late stage	P	L + V					239 0
"	3a	Late stage	P	L + V					168 2

ADDENDUM

SEQUENCE OF ALTERATION AND MINERALIZATION IN THE RATHDOWNEY TREND



1. Regional dolomitization of the Waulsortian Limestone ($D1_R$, $D1_C$)



2. Fault activity - pre/syn dolomite breccia formation

3. Hydrothermal dolomite matrix breccia formation (D2, D3)





4. Sulphide mineralization - syn/post breccia formation



5. Late dolomite (D5 Dol) and calcite (D5 Calc) veins



6. Late crystalline pink dolomite (D4) and vug filling calcite



SCHEMATIC ILLUSTRATION SHOWING THE TEXTURAL RELATIONSHIPS BETWEEN THE VARIOUS CARBONATE GENERATIONS

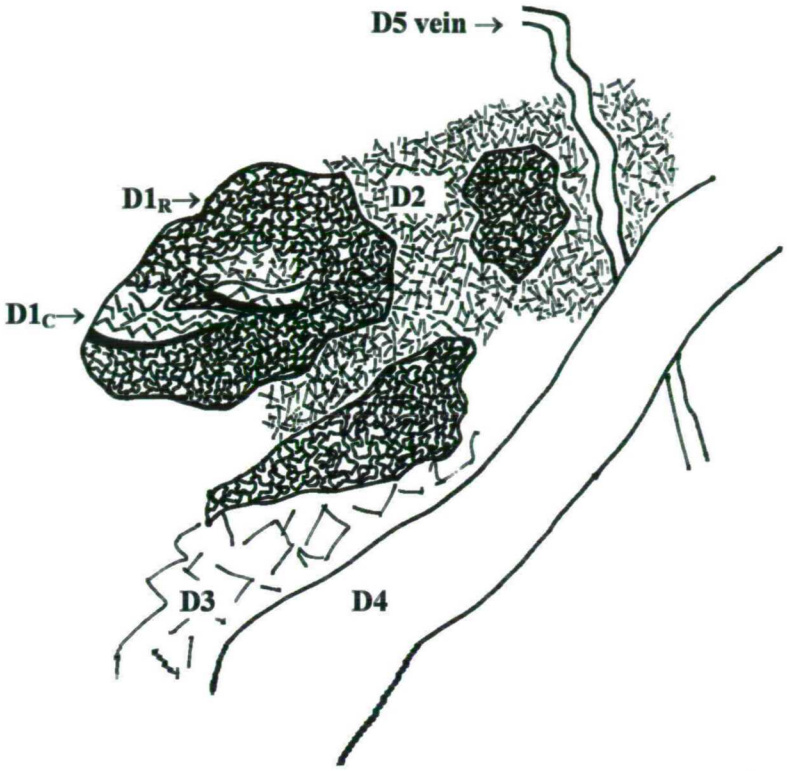


Figure 2A. Regional dolomite clasts consist of fine crystalline grey dolomite ($D1_R$) and coarse crystalline white dolomite ($D1_C$). The clasts occur in black (D2) and white (D3) matrix dolomites. These dolomite phases are post-dated by pink dolomite (D4) and minor dolomite and calcite veins (D5).

TERNARY PLOTS SHOWING THE DIFFERENCES IN MINERAL CHEMISTRY BETWEEN THE DIFFERENT DOLOMITE STAGES

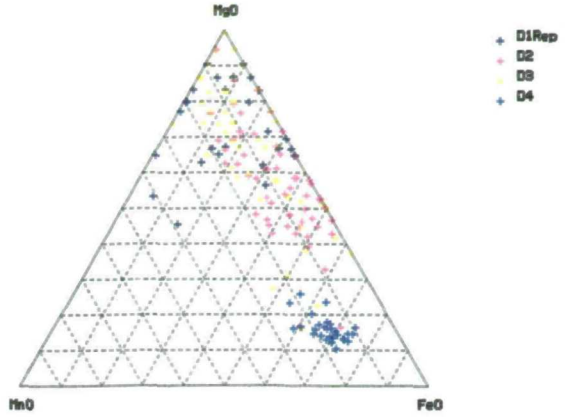


Figure 3A. Covariance of MgO, FeO and MnO wt% in Lisheen dolomites.

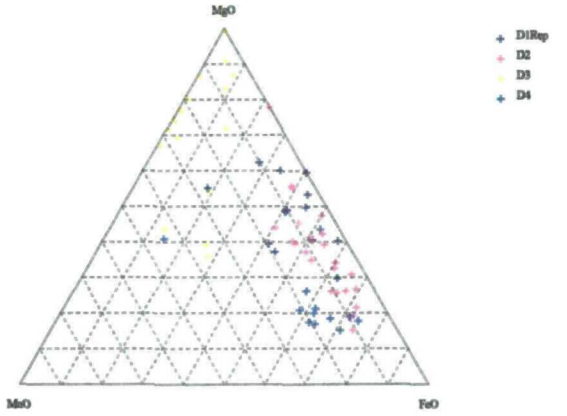


Figure 4A. Covariance of MgO, FeO and MnO wt% in Galmoy dolomites.

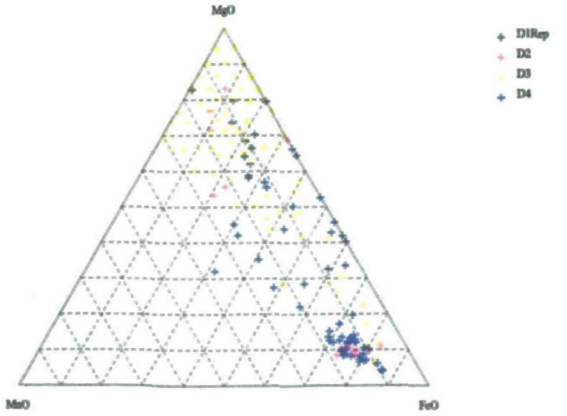


Figure 5A. Covariance of MgO, FeO and MnO wt% in Prospect dolomites.

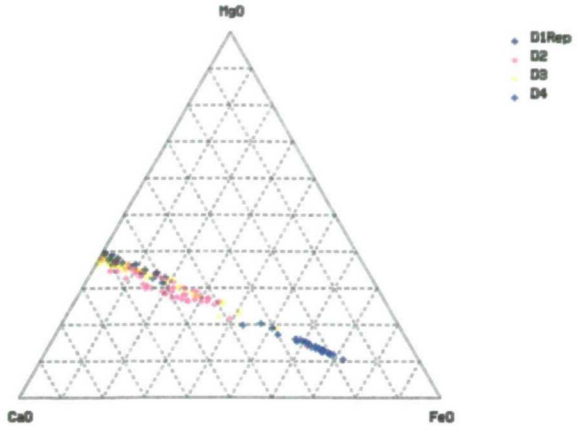


Figure 6A. Covariance of MgO, CaO and FeO wt% in Lisheen dolomites.

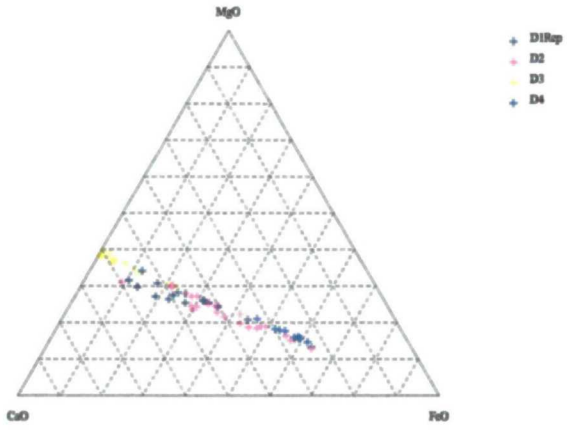


Figure 7A. Covariance of MgO, CaO and FeO wt% in Galmoy dolomites.

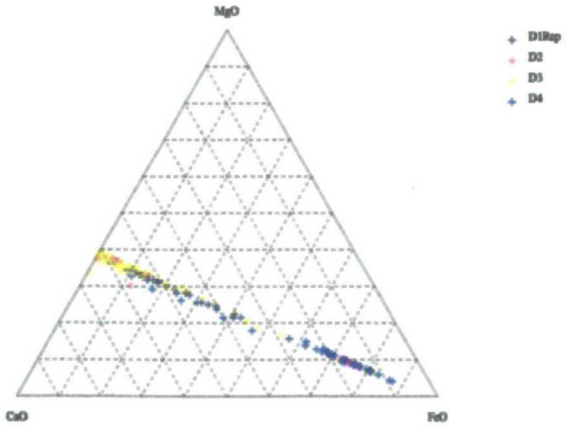


Figure 8A. Covariance of MgO, CaO and FeO wt% in Prospect dolomites.

BIBL. LONDIN. UNIV